Proceedings: **ISSN 2309-0545**
CD-ROM/USB: **ISSN 2309-0553**

ICTPE-2022

CONFERENCE PROCEEDINGS

The 18th International Conference on

Technical and Physical Problems of Engineering

30 October 2022
International Organization of IOTPE

Taba Elm International Institute
Tabriz, Iran
www.tabaelm.com

Seraj Higher Education Institute
Tabriz, Iran
www.seraj.ac.ir

Gazi University
Ankara, Turkey
www.gazi.edu.tr

Istanbul Technical University
Istanbul, Turkey
www.itu.edu.tr

Isik University
Istanbul, Turkey
www.isikun.edu.tr

Van Yuzuncu Yil University
Van, Turkey
www.yyu.edu.tr

Istanbul Rumeli University
Istanbul, Turkey
http://rumeli.edu.tr

Institute of Physics
Azerbaijan National Academy of Sciences
Baku, Azerbaijan
www.physics.gov.az

Azerbaijan Research Institute of Energetics and Energy Design
Azerenerji JSC, Baku, Azerbaijan
www.azenerji.com/en/about/pei.html

Cleaner Production and Energy Efficiency Center
Baku, Azerbaijan
http://cpee.az

Nakhchivan State University
Nakhchivan, Azerbaijan
www.ndu.edu.az

University of Pitesti
Pitesti, Romania
www.upit.ro

University of the Basque Country
Bilbao, Spain
www.ehu.es

Near East University
Lefkosa, Northern Cyprus
www.neu.edu.tr

Ostfold University College
Fredrikstad, Norway
www.hiof.no

The IOTPE Organization is formed by:
- Institute of Physics of Azerbaijan National Academy of Sciences (Baku, Azerbaijan)
- Azerbaijan Research Institute of Energetics and Energy Design, Azerenerji JSC (Baku, Azerbaijan)
- Cleaner Production and Energy Efficiency Center (Baku, Azerbaijan)
- Nakhchivan State University (Nakhchivan, Azerbaijan)
- Seraj Higher Education Institute (Tabriz, Iran)
- Taba Elm International Institute (Tabriz, Iran)
- Gazi University (Ankara, Turkey)
- Istanbul Technical University (Istanbul, Turkey)
- Isik University (Istanbul, Turkey)
- Van Yuzuncu Yil University (Van, Turkey)
- Istanbul Rumeli University (Istanbul, Turkey)
- University of Pitesti (Pitesti, Romania)
- University of the Basque Country (Bilbao, Spain)
- Near East University (Lefkosa, Northern Cyprus)
- Ostfold University College (Fredrikstad, Norway)

Supported, Held and Published by:
International Organization on "Technical and Physical Problems of Engineering" (IOTPE)
URL: www.iotpe.com

Proceedings of the 18th International Conference on
"Technical and Physical Problems of Engineering" (ICTPE-2022)

Proceedings: ISSN 2309-0545
CD-ROM/USB: ISSN 2309-0553

Editorial Production:
General Chair of ICTPE Conference
Prof. Naser MAHDAVI TABATABAEI
Emails: n.m.tabatabaei@gmail.com, iotpe@iotpe.com
URLs: www.iotpe.com, www.iotpe.com/ictpe.html

Chairmen of ICTPE-2022 Conference:
Board of International Organization of IOTPE
E-mails: iotpe@iotpe.com
URL: www.iotpe.com

Printed and Bound by:
The 18th International Conference of ICTPE-2022
International Organization on "Technical and Physical Problems of Engineering" (IOTPE)
www.iotpe.com

CONTRIBUTORS:

- Azerbaijan National Academy of Sciences (ANAS), *Baku, Azerbaijan*
- Azerenerji Joint Stock Company, *Baku, Azerbaijan*
- Ministry of Education, *Baku, Azerbaijan*
- Ministry of Science, Research and Technology (MSRT), *Tehran, Iran*
- Scientific and Technological Research Council of Turkey (TUBITAK), *Ankara, Turkey*
- Ministry of Energy and Natural Resources, *Ankara, Turkey*
- Ministry of Education and Research, *Bucharest, Romania*
- Ministry of Education, Culture and Sports, *Madrid, Spain*
- Department of Education, *Gasteiz, Basque Country, Spain*
- Ministry of Economy and Energy, *Lefkosa, Northern Cyprus*
- Ministry of Education and Research, *Oslo, Norway*

- Atrak Energy Company, *Tehran, Iran*
- Azarbaijan Electric Power Maintenance Company, *Tabriz, Iran*
- Azarbaijan Higher Education and Research Complex, *Tabriz, Iran*
- Azarbaijan Regional Electric Company, *Tabriz, Iran*
- Azerbaijan State Oil Academy, *Baku, Azerbaijan*
- Azerbaijan Technical University, *Baku, Azerbaijan*
- Azarbaijan University, *Tabriz, Iran*
- Baku State University, *Baku, Azerbaijan*
- East Azarbaijan Communication Company, *Tabriz, Iran*
- East Azarbaijan Construction Engineering Organization, *Tabriz, Iran*
- East Azarbaijan Electric Power Distribution Company, *Tabriz, Iran*
- Electric Generation Company Inc. (EUAS), *Turkey*
- Farabi Institute of Higher Education, *Karaj, Iran*
- General Directorate of Electrical Power Resources Survey and Development Administration (EIEI), *Turkey*
- IEEE (Turkey Section), *Ankara, Turkey*
- Institute of Electrical Power Engineering, Wroclaw University of Technology, *Wroclaw, Poland*
- International Ecoenergy Academy, *Baku, Azerbaijan*
- Iran Electrical Industry Syndicate, *Tehran, Iran*
- Iran University of Science and Technology, *Tehran, Iran*
- Iranian Association of Electrical & Electronics Engineers (East Azarbaijan Branch), *Tabriz, Iran*
- Modiran Hamandish Farakhiz Company, *Tabriz, Iran*
- NCE, *Halden*, *Norway*
- Nexans, *Halden*, *Norway*
- Omega Elkraft, *Oslo*, *Norway*
- Sahand University of Technology, *Tabriz, Iran*
- The Chamber of Turkish Electrical Engineers, *Turkey*
- The Chamber of Turkish Electrical Engineers (Ankara Branch), *Turkey*
- TRNC Electricity Authority (KIB-TEK), *Lefkosa, Northern Cyprus*
- Turkey Electricity Distribution Corporation, *Turkey*
- Turkey Electric Trade Substation Corporation (TETAS), *Turkey*
- Turkey Electricity Transmission Corporation, *Turkey*
- University of Tabriz, *Tabriz, Iran*
- World Energy Council, Turkish National Committee, *Turkey*

ICTPE-2022

CONFERENCE PROCEEDINGS

The 18th International Conference on

Technical and Physical Problems of Engineering

30 October 2022
International Organization of IOTPE

www.iotpe.com , www.iotpe.com/ictpe.html
ictpe@iotpe.com , ictpe0@gmail.com

Edited by:

Secretariats of the 18th International Conference of ICTPE-2022

Management Department,
Taba Elm International Institute, Tabriz, Iran
www.tabaelm.com

Electrical Engineering Department,
Seraj Higher Education Institute, Tabriz, Iran
www.seraj.ac.ir

Electrical and Electronics Department,
Faculty of Engineering and Architecture,
Gazi University, Ankara, Turkey, www.gazi.edu.tr

Electrical Engineering Department,
Faculty of Electrical and Electronic Engineering,
Istanbul Technical University, Maslak, Istanbul, Turkey
www.itu.edu.tr

Department of Electrical and Electronics Engineering,
Faculty of Engineering, Isik University,
Sile, Istanbul, Turkey
www.isikun.edu.tr

Department of Electrical and Electronics Engineering,
Faculty of Engineering, Van Yuzuncu Yil University,
Van, Turkey, www.yyu.edu.tr

Faculty of Engineering and Architecture,
International Relations Office,
Istanbul Rumeli University, Silivri, Istanbul, Turkey
http://rumeli.edu.tr

Institute of Physics,
Azerbaijan National Academy of Sciences,
Baku, Azerbaijan
www.physics.gov.az

Azerbaijan Research Institute of Energetics and Energy
Design, Azerenerji JSC, Baku, Azerbaijan
www.azenerji.com/en/about/pei.html

Cleaner Production and Energy Efficiency Center,
Baku, Azerbaijan
http://cpee.az

Physics-Mathematics Faculty,
Nakhchivan State University,
Nakhchivan, Azerbaijan, www.ndu.edu.az

Department of Electrical Engineering,
Faculty of Electronics, Communications & Computers,
University of Pitesti, Pitesti, Romania
www.upit.ro

Department of Applied Mathematics,
School of Engineering,
University of the Basque Country, Bilbao, Spain
www.ehu.es

Electrical and Electronic Engineering Department,
Faculty of Engineering, Near East University, Lefkosa,
Northern Cyprus, www.neu.edu.tr

Electrical Engineering Department,
Faculty of Engineering, Ostfold University College,
Krakeroy, Fredrikstad, Norway, www.hiof.no

The Message of the Conference Organizers to the 18th International Conference on "Technical and Physical Problems of Engineering" (ICTPE-2022) International Organization of IOTPE www.iotpe.com, 30 October 2022

We are honored and pleased to welcome all participants of the **18th** International Conference on "Technical and Physical Problems of Engineering" (**ICTPE-2022**) going to be held in the **International Organization of IOTPE** on **October 30, 2021**.

It is especially pleasant that the organizers of ICTPE conferences from Azerbaijan, Iran, Turkey, Romania, Spain, Northern Cyprus and Norway have decided to organize the successful conferences and hold them every year, in each partner country. We would also like to extend our appreciation to "ICTPE General Chair" for continuing the important scientific activities in a subset framework of the International Organization on "Technical and Physical Problems of Engineering" (IOTPE) and annually holding of ICTPE conferences.

The partners of IOTPE organization are Institute of Physics of Azerbaijan National Academy of Sciences (Baku, Azerbaijan), Azerbaijan Research Institute of Energetics and Energy Design (Azerenerji JSC, Baku, Azerbaijan), Cleaner Production and Energy Efficiency Center (Baku, Azerbaijan), Nakhchivan State University (Nakhchivan, Azerbaijan), Seraj Higher Education Institute (Tabriz, Iran), Taba Elm International Institute (Tabriz, Iran), Gazi University (Ankara, Turkey), Istanbul Technical University (Istanbul, Turkey), Isik University (Istanbul, Turkey), Van Yuzuncu Yil University (Van, Turkey), Istanbul Rumeli University (Istanbul, Turkey), University of Pitesti (Pitesti, Romania), University of the Basque Country (Bilbao, Spain), Near East University (Lefkosa, Northern Cyprus) and Ostfold University College (Fredrikstad, Norway).

The IOTPE organization is a scientific association, founder and holder of International Conferences on "Technical and Physical Problems of *Power* Engineering" (ICTPE) have been held from 2002 to 2012.

The ICTPE Conferences name and topics are improved to International Conference on "Technical and Physical Problems of *Electrical* Engineering" (ICTPE) in 2013 Conference to cover subjects in all fields and topics of Electrical Engineering.

The ICTPE Conferences name and topics are finally promoted to International Conference on "Technical and Physical Problems of *Engineering*" (ICTPE) since 2020 to enlarge topics of the conference in the next editions and have been held till now. The ICTPE Conferences were held biannually till ICTPE-2008 and annually after ICTPE-2009 in the partner universities and institutes.

The ICTPE conferences promote close friendship and scientific collaboration of the scientists and researchers of member countries in electrical engineering development. The importance of holding ICTPE conferences are mutual understanding and recognition between the organizer countries through scientific, social and cultural development which yields increasing international cooperation in scientific areas.

Furthermore, the main subjects of ICTPE conferences are related to the opportunity for researches and scientists from different countries to present and discuss the latest and mutual research achievements and improvements as well as generalization of the internationally obtained results in the area of electrical engineering.

Moreover, the scientific relationship and knowledge expansion in ICTPE conferences bring development of international cooperation in engineering and new technologies. Such scientific activities cause the participating scientists to define and establish joint activities in science, research, technology and industrial fields which positively influence their efforts in creating and disseminating new knowledge, growing the areas of applied science and expansion to international grounds.

The ICTPE conference is registered, cited and indexed in some scientific organization and databases.

Statistics of published papers in ICTPE conferences reveal the most successful growing of quality and quantity of research and international relationships of the participants. We believe that **ICTPE-2022** contains such high quality and quantity expansion regarding the results and solutions to problems of electrical engineering.

It is an honor for us that ICTPE Conferences have the valuable supporting of distinguished international members in the Organizing, Scientific and Executive Committees of the conference, who carry out all the stages of information, reviewing, publishing and programming.

We thank those who were in charge of holding this scientific international conference of the presidents, rectors and directors of the Partners, Organizers as well as the Organizing and Host universities regarding for providing all requirements for the successful holding of the conference, and also wish them success in scientific and executive activities.

We would also like to express our appreciation to the members of the Organizing, Scientific and Executive Committees of the conference from the countries of the world for successfully conducting the related tasks for the conference and wish them great successes in their activities.

Finally, we wish to express our gratefulness to all participants and scientists from all over the world who have scientific papers to be included in the proceedings and hope that the conference will be very successful.

October 30, 2022

ORGANIZING COMMITTEE

Chairmen and General Chair of ICTPE-2022:

Board of International Organization on "Technical and Physical Problems of Engineering" (IOTPE)

Acad. Arif M. HASHIMOV (*Azerbaijan*)
Prof. Naser MAHDAVI TABATABAEI (*Iran*), ***General Chair of ICTPE***
Prof. M. Cengiz TAPLAMACIOGLU (*Turkey*)
Prof. Nicu BIZON (*Romania*)
Prof. Javier J. BILBAO LANDATXE (*Spain*)
Assoc. Prof. Kamil B. GURBANOV (*Azerbaijan*)
Prof. Nariman R. RAHMANOV (*Azerbaijan*)
Prof. Omer USTA (*Turkey*)
Prof. Yorgo ISTEFANOPULOS (*Turkey*)
Prof. Fahreddin M. SADIKOGLU (*Northern Cyprus*)
Prof. Kamil M. DURSUN (*Norway*)
Prof. Naci GENC (*Turkey*)

Rectors / Directors:

Partner Universities and Institutes

Acad. Arif M. HASHIMOV (*Azerbaija*n)
Dr. Balababa H. RZAYEV (*Azerbaijan*)
Prof. Elbrus Saleh ISAYEV (*Azerbaijan*)
Asst. Prof. Hossein NOROUZI (*Iran*)
Prof. Musa YILDIZ (*Turkey*)
Prof. Ismail KOYUNCU (*Turkey*)
Prof. Hasan Bulent KAHRAMAN (*Turkey*)
Prof. Hamdullah SEVLI (*Turkey*)
Prof. Hazim Tamer DODURKA (*Turkey*)
Prof. Dumitru CHIRLESAN (*Romania*)
Prof. Olatz GARCIA (*Spain*)
Prof. Umit HASSAN (*Northern Cyprus*)
Prof. Lars Petter JELSNESS JORGENSEN (*Norway*)

EXECUTIVE COMMITTEE (ICTPE-2022)

SCIENTIFIC COMMITTEE (ICTPE-2022)

Ahrabian, Gh., Asst. Prof. (*Iran*)
Akcam, N., Assoc. Prof. (*Turkey*)
Aksen, A., Prof. (*Turkey*)
Ardehali, M.M., Prof. (*Iran*)
Ari, M., Prof. (*Turkey*)
Banan, Kh., Prof. (*Iran*)
Bay, O.F., Prof. (*Turkey*)
Baysal, U., Prof. (*Turkey*)
Behjat, V., Assoc. Prof. (*Iran*)
Bektas, S., Prof. (*Northern Cyprus*)
Beloiu, R., Assoc. Prof. (*Romania*)
Bilbao, J., Prof. (*Spain*)
Bizon, N., Prof. (*Romania*)
Boushehri, N.S. (*Iran*)
Bravo, E., Prof. (*Spain*)
Bulut, F., Asst. Prof. (*Turkey*)
Camurcu, A.Y., Prof. (*Turkey*)
Can, A., Prof. (*Turkey*)
Chirlesan, D., Assoc. Prof. (*Romania*)
Costea, M., Assoc. Prof. (*Canada*)
Darabi, A., Prof. (*Iran*)
Demiroren, A., Prof. (*Turkey*)
Dursun, K.M., Prof. (*Norway*)
Effatnejad, R., Asst. Prof. (*Iran*)
Eguia, P., Prof. (*Spain*)
Faiz, J., Prof. (*Iran*)
Farsadi, M., Prof. (*Iran*)
Farsangi, M.M., Prof. (*Iran*)
Feizi, M.R., Assoc. Prof. (*Iran*)
Forrisdal, O.K., Assoc. Prof. (*Norway*)
Genc, N., Prof. (*Turkey*)
Ghanbari, E., Prof. (*Iran*)
Gholami, A., Prof. (*Iran*)
Gonzalez, P., Prof. (*Spain*)
Gozde, H., Assoc. Prof. (*Turkey*)
Hardalac, F., Assoc. Prof. (*Turkey*)
Hasanov, E.R., Prof. (*Azerbaijan*)
Hasanova, S.I., Asst. Prof. (*Azerbaijan*)
Hashimov, A.M., Acad. (*Azerbaijan*)
Huseynova, S.A. (*Azerbaijan*)
Hatami, H., Asst. Prof. (*Iran*)
Hernandez, J.R., Prof. (*Spain*)
Huseynov, A., Prof. (*Azerbaijan*)
Ionita, S., Prof. (*Romania*)
Iskanderov, R.A., Prof. (*Azerbaijan*)
Iskender, I., Prof. (*Turkey*)
Istefanopulos, Y., Prof. (*Turkey*)
Izykowski, J., Prof. (*Poland*)
Jadid, Sh., Prof. (*Iran*)
Jafari, A. (*Iran*)
Kalantar, M., Prof. (*Iran*)
Kazemi, A., Assoc. Prof. (*Iran*)
Kenarangui, R., Prof. (*USA*)
Khalin, M., Prof. (*Russia*)
Khalina, T., Prof. (*Russia*)
Khudiev, A.T., Prof. (*Azerbaijan*)
Kocaarslan, I., Prof. (*Turkey*)
Kocabas, D.A., Asst. Prof. (*Turkey*)
Konditi, D.B.O, Prof. *(Kenya)*
Krivova, L.V., Assoc. Prof. (*Russia*)
Kuznetsov, V., Prof. (*Ukraine*)
Mamedov, N.A., Prof. (*Azerbaijan*)
Meral, M.E., Prof. (*Turkey*)
Mokhtarpour, A., Asst. Prof. *(Iran)*
Mordt, H., Assoc. Prof. (*Norway*)
Moradzadeh, M., Assoc. Prof. (*Belgium*)
Mortezaei, S.R. (*Iran*)
Mustafaev, R.I., Prof. (*Azerbaijan*)
Oprescu, B., Prof. (*Romania*)
Oproescu, M., Assoc. Prof. (*Romania*)
Oraee, H., Prof. (*Iran*)
Ozerdem, O.C., Prof. (*Northern Cyprus*)
Pashaei, A., Dr. (*Iran*)
Pavlyuchenko, D.A., Prof. (*Russia*)
Qurbanov, K.B., Assoc. Prof. (*Azerbaijan*)
Rahmanov, N.R., Prof. (*Azerbaijan*)
Rebollar, C., Prof. (*Spain*)
Rodriguez, M., Prof. (*Spain*)
Rosolowski, E., Prof. (*Poland*)
Rostami, A., Prof. (*Turkey*)
Rustamov, R.B., Assoc. Prof. (*Azerbaijan*)
Rzayev, F.T., Dr. (*Azerbaijan*)
Sadikoglu, F.M., Prof. (*Northern Cyprus*)
Saracoglu, R., Assoc. Prof. (*Turkey*)
Sazli, M.H., Prof. (*Turkey*)
Sefa, I., Prof. (*Turkey*)
Senol, M.A., Asst. Prof. (*Turkey*)
Serban, G., Prof. (*Romania*)
Sharifian, M.B.B., Prof. (*Iran*)
Shayanfar, H.A., Prof. (*Iran*)
Shayeghi, H., Prof. (*Iran*)
Stanescu, C., Prof. (*Romania*)
Tabatabaei, Javad M. (*Turkey*)
Tabatabaei, Naser M., Prof. (*Iran*)
Tabatabaei, Nejat M., Asst. Prof. (*Germany*)
Taghizadegan, N., Assoc. Prof. (*Iran*)
Taplamacioglu, M.C., Prof. (*Turkey*)
Tutanescu, I., Dr. (*Romania*)
Usta, O., Prof. (*Turkey*)
Varela, C., Prof. (*Spain*)
Vishtibeyev, A., Prof. (*Russia*)

NUMBER OF PAPERS AND PAGES

CONFERENCE TOPICS NO COUNTRIES	0	1	2	3	4	5	6	7	8
1. Azerbaijan	-	3	7	-	3	-	2	4	-
2. Turkey	-	1	-	-	-	-	-	-	-
3. Spain	-	-	-	-	-	-	-	-	1
4. Northern Cyprus	-	1	-	-	-	-	-	-	-
5. Russia	-	-	-	-	-	-	-	-	1
6. Azerbaijan, Iran	-	-	1	-	-	-	-	-	-
7. Azerbaijan, Canada	-	-	-	-	-	-	1	-	-
8. Azerbaijan, Egypt	-	1	-	-	-	-	-	-	-
9. Azerbaijan, Ukraine	-	-	-	-	-	-	-	1	-
10. Azerbaijan, Venezuela	-	1	-	-	-	-	-	-	-
11. Iran, Denmark	-	-	-	-	-	-	-	1	-
12. Iran, Turkey	-	-	-	-	-	-	-	-	-
13. Turkey, Russia	-	-	-	-	-	-	-	1	-
Number of Papers	-	7	8	-	3	-	3	7	2
Number of Pages	-	39	38	-	13	-	20	40	10

CONFERENCE TOPICS NO COUNTRIES	9	10	11	12	13	14	15	16	Total
1. Azerbaijan	-	-	-	-	-	-	-	-	19
2. Turkey	-	-	-	-	-	-	-	-	1
3. Spain	-	-	-	-	-	-	-	-	1
4. Northern Cyprus	-	-	-	-	-	-	-	-	1
5. Russia	-	-	-	-	-	-	-	-	1
6. Azerbaijan, Iran	-	1	-	-	-	-	-	-	2
7. Azerbaijan, Canada	-	-	-	-	-	-	-	-	1
8. Azerbaijan, Egypt	-	-	-	-	-	-	-	-	1
9. Azerbaijan, Ukraine	-	-	-	-	-	-	-	-	1
10. Azerbaijan, Venezuela	-	-	-	-	-	-	-	-	1
11. Iran, Denmark	-	-	-	-	-	-	-	-	1
12. Iran, Turkey	-	1	-	-	-	-	-	-	1
13. Turkey, Russia	-	-	-	-	-	-	-	-	1
Number of Papers	-	2	-	-	-	-	-	-	**32**
Number of Pages	-	15	-	-	-	-	-	-	**175**

Total Number of Papers = 32
Total Number of Pages = 175
Total Number of Authors = 74

*** The Proceedings of International Conference of ICTPE are supported and indexed in:**

■ **International Organization of IOTPE** supports International Conference of ICTPE,
Indexing address:
www.iotpe.com

■ **Research Bible** Academic Research Index, http://journalseeker.researchbib.com/, since 2016
Indexing address:
http://journalseeker.researchbib.com/view/issn/2309-0545

■ **Scientific Indexing Services (SIS)**, http://www.sindexs.org/, since 2016.
Indexing address:
http://www.sindexs.org/Conflist.aspx?ID=854

Extended versions of the selection accepted papers in the ICTPE-2022 will be published in:

■ **International Journal on "Technical and Physical Problems of Engineering" (IJTPE)**
ISSN 2207-3528, www.iotpe.com/ijtpe.html

*** The issues of IJTPE Journal are registered, cited and indexed in:**

■ **Scopus / Elsevier**, www.scopus.com
The IJTPE is indexed in Scopus / Elsevier since 2019.
Indexing address:
https://www.scopus.com/sourceid/21100913338

■ **Norwegian Directorate for Higher Education and Skils (NDHES)** and **Norwegian Center for Research Data (NSD),** https://www.nsd.no/en/, are under **Norwegian Ministry of Education and Research**
since 2013. Indexing address:
https://kanalregister.hkdir.no/publiseringskanaler/KanalTidsskriftInfo.action?id=480511&request_locale=en

■ **Google Scholar**, http://scholar.google.com/, for searching, exploring, locating, keeping, checking and citing the publications and authors through the libraries and on the web since 2013.
Search for: IJTPE
https://scholar.google.com/citations?hl=da&user=gfWxEhEAAAAJ

■ **Index Copernicus International (ICI)**, https://indexcopernicus.com/index.php/en/, since 2013.
Indexing address:
https://journals.indexcopernicus.com/search/details?id=32511

■ **Research Bible Academic Research Index**, http://journalseeker.researchbib.com/, since 2016.
Indexing address:
http://journalseeker.researchbib.com/view/issn/2077-3528

■ **Scientific Indexing Services (SIS)**, http://www.sindexs.org/, since 2016.
Indexing address:
http://www.sindexs.org/JournalList.aspx?ID=3176

■ **Eurasian Scientific Journal Index (ESJI)**, http://esjindex.org/, since 2018.
Indexing address:
http://esjindex.org/search.php?id=438

■ **Sciamgo Journal & Country Rank (SJR)**, https://www.scimagojr.com/, since 2018.
Indexing address:
https://www.scimagojr.com/journalsearch.php?q=2077-3528

■ **Resurchify**, https://www.resurchify.com/
Indexing address:
https://www.resurchify.com/impact/details/21100913338

■ **Canadian Institute for Knowledge Development (CIKD)**, https://cikd.ca/
Indexing address:
https://ieconferences.cikd.ca/call-for-papers-3rd-ie-conference/

CONTENTS

No	Code	11. CHEMICAL AND PETROLEUM ENGINEERING (11CPE)	Pages

No	Code	12. ENVIRONMENTAL AND GEOLOGICAL ENGINEERING (12EGE)	Pages

No	Code	13. BIOMEDICAL ENGINEERING (13BME)	Pages

No	Code	14. DRAFTING AND DESIGN ENGINEERING (14DDE)	Pages

No	Code	15. AEROSPACE ENGINEERING (15ASE)	Pages

No	Code	16. AGRICULTURAL ENGINEERING (16ACE)	Pages

The 18th International Conference on
"Technical and Physical Problems of Engineering"
30 October 2022
International Organization of IOTPE

ICTPE Conference
www.iotpe.com
ictpe@iotpe.com
ictpe0@gmail.com

ICTPE-2022 Number 01 Code 01PES01 Pages 1-4

NUMERICAL RESEARCH OF OPERATION CIRCUIT BREAKERS WITH PRE-INSERTION RESISTORS AT SWITCHING POWER CAPACITOR BANKS

E. Saafan [1] T. Lazimov [2]

1. Faculty of Engineering, University of El-Mansoura, Mansoura, Egypt, esam_ali_saafan@mans.edu.eg
2. Electro Automatics Department, Azerbaijan State Marine Academy, Baku, Azerbaijan, tahirlazim@gmail.com

Abstract- The article presents results of numerical research of switching (energization and de-energization) power capacitor banks equipped by special switchers which include the sets of pre-insertion resistors with different resistances, in the terms of possible magnitudes of switching transitional voltages (over voltages) and inrush currents, and also the features of the circuit breakers operations with pre-insertion resistors at energization high-voltage (namely 110 kV in the presented article) power capacitor banks. Due to numerous simulations, there were estimated possible ratios of switching overvoltage at switching capacitor banks by SF6 circuit breakers with pre-insertion resistors for all the range of resistances they are equipped, explained the nature of inrush currents spikes at presence of capacitive load (capacitances of connected cable and aerial power transmission lines) on busbar the capacitor banks are connected to. There were stated that, the use of circuit breakers with pre-insertion resistors for switching capacitor banks provide effective mitigation of switching overvoltage (at appropriated pre-insertion times) whereas the ratios of inrush currents at switching-on power capacitor banks by circuit breakers with pre-insertion resistors can reach high values (more than 4.5 amplitude of rated phase current). Right option of resistance and pre-insertion duration can help to reduce the inrush current. Magnitudes of currents at arc repeated restrikes in the capacitor banks switching-off mode can prevail their energization inrush current.

Keywords: Pre-Insertion Resistor, Inrush Current, Pre-Insertion Time, Capacitor Switchers, Back-to-back Arrangement, Wave Impedance.

1. INTRODUCTION

Pre-insertion resistors (PIRs) are mostly used to mitigate transitional voltages at switching high-voltage electrical installations [1, 2]. Initially they were used for the switching-on power transmission lines, so there were produced circuit breakers with resistance of PIR equaled to the aerial power transmission lines' wave impedance i.e., 300-400 Ohms [3].

These resistances of PIR were not appropriated for reliable switching of power capacitor banks since the typical wave impedances of the loops consisting of capacitor banks' capacitance and transformers' inductance are significantly less than aerial power transmission lines' wave impedance. But presently there are produces so called CapSwitchers, the special type of circuit breakers to switch capacitor banks with no high overvoltage and inrush currents due to the wide range of PIR's resistances (37.5-300 ohms) for standard voltages 123-170 kV [4]. Pre-insertion times of these CapSwitchers are 5-10 msec.

The use of these switchers for power capacitor banks, evaluation of switching over voltages and inrush currents, study of the features of the operation circuit breakers with PIRs at switching-on capacitor banks are studied in the presented research. Note here that effectiveness of use the circuit breakers with PIRs have been actively studied in last years, thus some important results concerned to switching-on (energization) of power capacitor banks are presented in [5-9], to energization of aerial power transmission lines. In [10] were considered some peculiarities of switching-off (de-energization) high-voltage power capacitor banks by CapSwitchers.

2. RESEARCH GROUND

A connection circuit and equivalent network of the problem under study are presented below in figure 1. The corresponding numerical values of the parameters used for computer simulation are given in [10]. For implementation the present research there was applied a numerical model described in [11, 12]. In the present research we used both the MATLAB and PSCAD/EMTDC program sets to provide and be confident in obtaining stable solutions for transitional functions. This is conditioned by the nature of such type of the problems belonging to the class of so called "stiff" problems [11-12]. Features of computer simulation "stiff" problems in relation to transient processes in electrical networks are considered in [13-15].

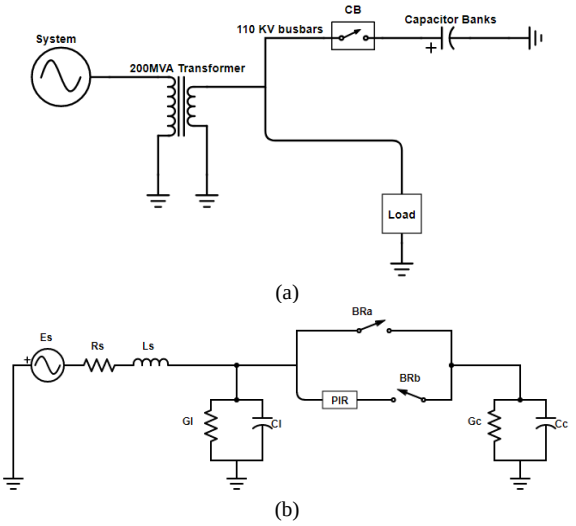

Figure 1. (a) Connection scheme, (b) equivalent network, Case under study for switching-on capacitor bank by circuit-breaker with pre-insertion resistor (PIR)

3. RESULTS AND DISCUSSION

The numerous simulations implemented within this research let us to reveal some features of the process studied. They are presented and considered below.

3.1. Switching-on (Energization) Process

3.1.1. Ratios of Over Voltages and Inrush Currents

In accordance with our results the ratio of overvoltage at switching-on power capacitor banks of 110 kV with no pre-insertion resistors can exceed 1.8-1.9 p.u. This should be taken into consideration at designing substations with power capacitor banks connected to the medial or lower voltage bars of ultra-high voltage (UHV) transformer or autotransformer since the allowable UHV insulation levels are less than 2.0 p.u. [16] and relatively little natural frequencies (about 260 Hz in the case under study) cannot provide effective attenuation at transition to the UHV side.

All the resistances of PIR provide effective mitigation of switching overvoltage in the range of pre-insertion time 5-10 msec. For example, the results of computer simulation at pre-insertion time 6 msec for switching-on the power capacitor bank of 110 kV, 56 MVAr is presented in the table 1. It is seen from this table that, the maximum overvoltage occurred can reach 1.33 p.u (at R_{pir} = 25 ohm, T_{pir} = 6 msec). Moreover, minimum overvoltage occurs at PIR closed to the wave impedance of the circuit consisting of capacitor banks' capacitance and transformers' inductance.

Not all the resistances of PIR provide effective decreasing of inrush currents, e.g., ratios of inrush currents at switching-on capacitor banks of 110 kV, 56 MVAr by CapSwitcher with R_{pir} = 37.5-300 ohms equal to 2.1-4.7 p.u. At that the minimum inrush currents take place at the resistances of PIR approximately equaled to the doubled wave impedance of the switched circuit. In Table 1 standard PIR resistances (37.5, 75, 150, 300 ohms) are used, and the rest (25, 50, 100, 200 ohms) are intermediate resistances for the analysis of the computer simulation results.

The samples of graphs showing temporal dependences of transitional voltages and currents are presented in Figure 2. These graphs are concerned to the case of use pre-insertion resistor of 75 ohm at pre-insertion time 6 msec.

3.1.2. Inrush Current Spikes

As it is seen in the Figure 2 the inrush current has a spike in the very initial period after the switching instant. At that, the magnitudes of these spikes decrease at increasing the PIR's resistance as shown in Table 1.

Table 1. Simulation results for 110 KV, 56 MVAr capacitor bank switching-on at different values of PIRs (T_{pir} = 6 msec)

PIR resistance [ohm]	Voltage on 110 kV bars [p.u]	Inrush current [p.u]	Energy dissipated [kJ]
25	1.33	6.78	1317
37.5	1.18	4.65	930
50	1.16	3.54	718
75	1.20	2.40	493
100	1.23	2.13	375
150	1.26	2.28	253
200	1.26	2.28	196
300	1.24	2.16	126

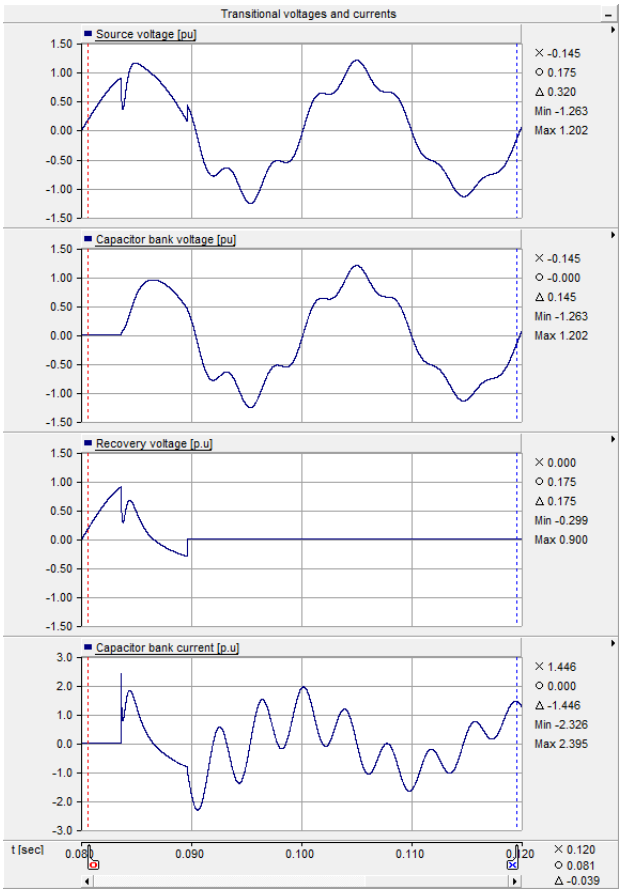

Figure 2. Curves of transitional functions at switching-on 110 kV, 56 MVAr capacitor banks at R_{pir} = 75 ohm and T_{pir} = 6 msec

To clarify the nature of these spikes we implemented some simulations at the case of absence of connections (load) to the 110 kV busbars the switched capacitor banks are connected to. It has turned out that for these cases there are not any inrush currents' spikes at switching-on,

as shown in Figure 3. This phenomenon can be explained due to the known fact of sudden jump of inrush current at switching-on the capacitor banks connected by the back-to-back arrangement at already switched-on another one [4]. These two cases i.e., switching-on capacitor banks connected to the busbars having other connections (e.g., aerial and/or cable power transmission lines, instrument transformers and so on) and switching-on the second capacitor bank in the back-to-back arrangement are physically similar.

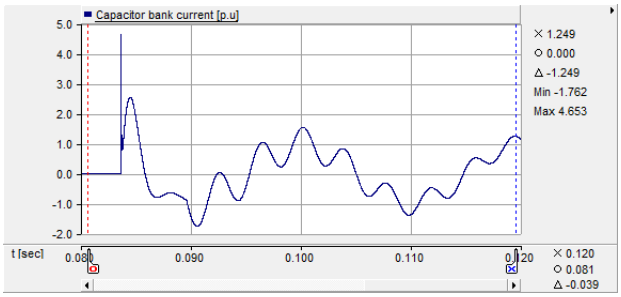

(a)

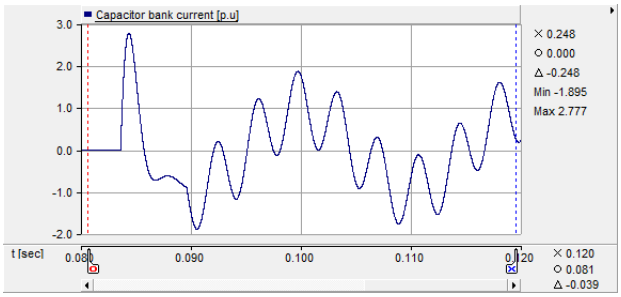

(b)

Figure 3. (a) at presence of capacitances connected to busbars, (b) at absence of capacitances connected to busbars, Curves of inrush currents at switching-on capacitor bank of 110 kV, 56 MVAr at R_{pir} = 37.5 ohm and T_{pir} = 6 msec

3.2. Comparison of Switching-on and Switching-off Processes in the Terms of Inrush Currents' Ratios

Comparing results got in the presented research with ones obtained in the research work [10] devoted to the study of power capacitor banks switching-off (de-energization) we can state the following:

- The ratios of transitional currents conditioned by arcs repeated restrikes at switching-off capacitor banks can notably prevail the ratios of inrush currents at their energization. In our opinion this takes place because of significantly higher magnitudes of intercontact voltages at the arcing instant at switching-off process (recovery voltage can exceed 3.0 p.u), E.g., the calculated current ratios are equalled 2.4 p.u and 3.0 p.u (see [10]) for the cases of switching-on and switching-off capacitor banks of 110 kV, 56 MVAr at PIR resistance 75 Ohm and pre-insertion time 6 msec, respectively.
- Magnitudes of power capacitor banks' inrush currents may have a significant impact on substation's electromagnetic environment and electromagnetic compatibility. In our opinion, use of circuit breakers with pre-insertion resistors can effectively improve electromagnetic environment of substations due to mitigation of inrush currents.

3.3. Energy Dissipated in PIR

Graphs of dependence of the energy dissipated in PIR in all the range of PIR resistances at pre-insertion times 5 msec and 10 msec are presented in Figure 4. All the possible values of the dissipated energy for pre-insertion times between 5 msec and 10 msec lie in the region between the curves given in Figure 4. Note that, the PIR's under consideration were designed for such values of dissipated energy [4]. Fortunately, the energy dissipated in the pre-insertion resistors at switching-off process is quantitatively alike one at switching-on process [10].

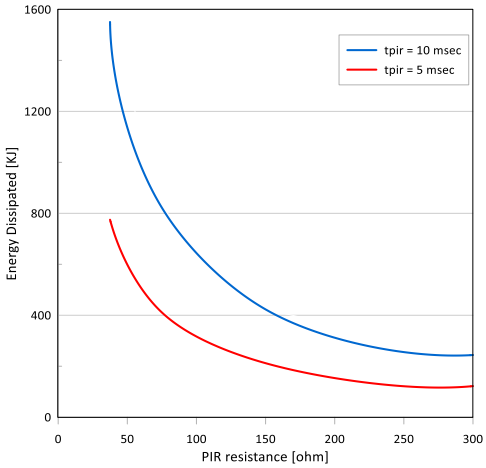

Figure 4. Energy dissipated at switching-on capacitor bank of for 110 KV, 56 MVAr at different values of PIRs resistance and pre-insertion time

4. CONCLUSIONS

The use of circuit breakers with PIR for power capacitor banks leads to effective mitigation of switching overvoltage (at appropriated pre-insertion times), wherein the maximum possible overvoltage that can appear on transformer's higher voltage windings is less than its permissible value for EHV and UHV isolation. Ratios of inrush currents at switching-on power capacitor banks by circuit breakers with PIR can reach high values (e.g., more than 4.5 amplitude of rated phase current for capacitor banks of 110 kV, 56 MVAr). Right option of PIR resistance and pre-insertion time can ensure effective mitigation of inrush current. Splashes of current at arc repeated restrikes in the capacitor banks switching-off mode can prevail switching-on inrush current of the same capacitor banks.

NOMENCLATURES

1. Acronyms

UHV: Ultra-High Voltage
PIR: Pre-Insertion Resistor

2. Symbols / Parameters

R_s: Source resistance
L_s: Source inductance
G_l: Load conductivity
C_l: Load capacitance
G_c: Capacitor bank conductivity
C_c: Capacitor bank capacitance
E_s: e.m.f. of voltage source (rms value)

REFERENCES

[1] R. Smeets, L. Van Der Sluis, M. Kapetanovic, et al., "Switching in Electrical Transmission and Distribution Systems", Wiley, New York, USA, 2014.
[2] D.V. Razevig, "High Voltage Engineering", Khanna Publishers, New Deli, India, 1989.
[3] Gujarat Energy Transmission, "Technical Specifications of 400 kV SF6 Circuit-Breakers with PIR and Spring-Spring Mechanism", April 2013.
[4] S.S. Southern States, "110-170 KV RMS CapSwitcher Sales Brochure", Hampton, GE, 2012.
[5] P.A.A. Pramana, A.A. Kusuma, B.S. Munir, "Inrush Current Investigation of Capacitor Bank Switching for 150 kV Electrical System in Indonesia", High Voltage Engineering and Power Systems (ICHVEPS) International Conference, pp. 259-263, 2017.
[6] L.V. Teli, H.T. Jadhav, "A Review on Protection of Capacitor in Power Quality Industry", Current Trends Towards Converging Technologies (ICCTCT) International Conference, pp. 1-5, 2018.
[7] A.H. Fajariawan, A.I. Fadlika, et al., "A New Switching Control Approach to Reduce Capacitor Bank Inrush Current", Annual International Conference on Renewable Energy (ICORE), University Negeri Malang, Malang, Indonesia, August 9-10, 2019.
[8] V. Kuchanskyy, P. Satyam, O. Rubanenko, et al., "Measures and Technical Means for Increasing Efficiency and Reliability of Extra High Voltage Transmission Lines", Electrotechnical Review, Vol. 96, No. 11, pp. 135-141, 2020.
[9] S.M. Sangeeta, M.S. Sureban, "Effect of Pre-Insertion Resistor on Energization of Long Lines", International Journal of Scientific an Engineering Research, Vol. 10, No. 5, May 2019.
[10] T. Lazimov, E. Saafan, "Transitional Processes at Switching-Off Capacitor Banks with Pre-Insertion Resistors", The MEPS'15 Symposium, pp. 1-4, Wroclaw, Poland, July 2015.
[11] J.C. Butcher, "Numerical Methods for Ordinary Differential Equations", John Wiley and Sons, Ltd., p. 538, New York, USA, 2016.
[12] L.F. Shampine, "Numerical Solutions of Ordinary Differential Equations", Routledge, Oxfordshire, p. 632, England, 2020.
[13] T. Lazimov, E. Saafan, "Influence of Arc Resistance on Transitional Functions, Stability at Computer Simulation of Switching-Off Processes", IEEE PES Asia-Pacific Power and Energy Engineering Conference (APPEEC), pp. 1-4, Hong Kong, 2014.
[14] T. Lazimov, E.A. Saafan, "Computational Features of Numerical Simulation of Some Transitions in Electric Power Systems", The 2019 Modern Electric Power Systems (MEPS), pp. 1-4, 2019.
[15] T. Lazimov, S. Akhundov, "Peculiarities of Transients' Simulation in Electrical Circuits", The Republican Conference on IT, Vol. II, pp. 104-107, Baku, Azerbaijan, 2003.
[16] E. Shim, E. Zaima, "Introduction of Insulation Coordination for UHV AC Systems", Journal of Electrical Engineering and Technology, Vol. 10, No. 3, pp. 1293-1297, May 2015.

BIOGRAPHIES

Esam Saafan was born in El-Mansoura, Egypt in 1977. He received the B.Sc. and M.Sc. degrees in Electrical Engineering from Faculty of Engineering, University of El-Mansoura, Egypt in 2001 and 2007, respectively. He obtained the Ph.D. degree in High Voltage Engineering in 2012 from Azerbaijan Technical University, Baku, Azerbaijan. From 2001 to 2012 he worked in Electrical Engineering Department, University of El-Mansoura, Egypt as a Lecturer Assistant. Since 2012, he has been a Lecturer in the same university. His research areas include transitional processes in power electric systems and their computer simulation, power systems electromagnetic compatibility.

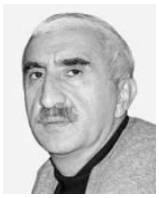

Tahir Lazimov was born in Baku, Azerbaijan in 1955. He received the engineer qualification in electrical engineering from the Azerbaijan State Oil Academy, Baku, in 1977, Ph.D. degree in high voltage engineering from the Tomsk Polytechnic Institute, Tomsk, Russia Federation, in 1989. From 1977 to 2004 he worked in Power Engineering Research Institute, Baku, Azerbaijan. In 2004-2020 he was the head of Electric Power Systems Department in Azerbaijan Technical University, Baku, Azerbaijan. He has been a Professor of Azerbaijan State Marine Academy, Baku, Azerbaijan since 2021. He is the author of about 200 scientific works. His research areas include transitional processes in power electric systems and their computer simulation, power systems electromagnetic compatibility. Prof. T. Lazimov is IEEE Senior member, the member of some scientific councils and editorial boards in Azerbaijan and abroad.

The 18th International Conference on
"Technical and Physical Problems of Engineering"
30 October 2022
International Organization of IOTPE

ICTPE Conference
www.iotpe.com
ictpe@iotpe.com
ictpe0@gmail.com

ICTPE-2022 Number 02 Code 01PES02 Pages 5-8

SOME ISSUES RELEVANT TO MONITORING OF ENERGY SYSTEM

K.A. Suleymanov

Department of Power System Modes, Azerbaijan Research and Design-Prospecting Institute of Energetics, Baku, Azerbaijan, kamran.suleymanov99@gmail.com

Abstract- Over the past decades, there has been a strong increase in the load on transmission networks in the electricity markets. Power transmission systems operate at their technical limits, thus becoming more susceptible to instability and cascading failures than before. The annual increase in power system outages is increasing, so the need for modern tools for monitoring the situation in power systems is becoming the most urgent. Modern systems for regulating the parameters of the operator for online assessment of the state of the system for regulating its operation, considering the forecast, have been developed. This consumption of synchronized vector measurements is becoming a major trend for power system monitoring.

Keywords: Power System, Agent, SCADA/EMS, PMU, MAS, Optimal Placement.

1. INTRODUCTION

Recently, according to the requirements of the socio-economic development of the Republic of Azerbaijan, over the past 30 years, the installed capacity of power plants in its energy system has increased by almost 3000 MW and amounted to 7775.3 MW, incl. traditional power plants 6458.6 MW (without RES). During the same period, the electricity generation increased from 18.71 billion kWh to 26.1 billion kWh. At the beginning of the year, Gobu power plants with a capacity of 385 MW were put into operation, the foundations of 920 MW stations were laid (Yashma CCGT), the implementation of wind farm projects - 240 MW (ACWA Power contract) and solar power plants - 230 MW (Macdar contract).

Azerbaijan has a high renewable energy potential, which is estimated at 26,940 MW (3,000 MW - wind farms, 23,040 MW - solar power plants, 380 MW - bio, 520 MW - mountain rivers), which allows planning the production of electricity based on renewable energy by 2030 at the level of 30 % of total electricity production [1]. Along with this, such factors as the concentrated nature of the network structure of the ES (without extended overhead lines), the presence in the structure of parts of the ES that are redundant and deficient in terms of power, large megacities of production and consumption of electric energy, functioning in the structure of the ES. Association and diversification of technological processes for the production of electric energy (CCGT, GTU, CHPP, HPP, RES-based power plants, MPP with internal combustion engines), development of the principles of distributed generation, the prospect of increasing the share of electricity generation based on RES generate, along with positive factors, also have negative ones: load variability, decrease in the constant inertia of the system, increase in short-circuit currents, ambiguous effect on the generation of higher harmonics, the appearance of low-frequency oscillations, complicating the work of operational dispatch control and conditions operation of RP and PA, etc. This affects the state of operational reliability (RL) of the ES, in particular, such indicators as resilience, controllability and survivability [2].

The above listed features of the network and power structure of the Azerbaijan ES, which determine the requirement for ensuring a high level of the state of the RN, should also include the functioning of the Azerbaijan ES in the structure of the Association: the ES of the Russian Federation (IPS of the SOUTH), Georgia, Turkey, Iran with the prospect of entering the Intercontinental level. The capacities of the listed countries are high: IPS of the South 22,800 MW, Georgia and Turkey 96,439 MW, Iran 85,695 MW, which predetermine the high level of transit of capacities through the I/O structure of the EPS of Azerbaijan and its unpredictable variability.

In the last two decades, in accordance with the requirements of development, two major projects were carried out on the "Modernization of the emergency automatics of the Azerbaijan system using microprocessor technology" in 2010 and 2020, as a result of which the degree of adequacy of the current settings of the emergency automatics in terms of ensuring LV in static and dynamic conditions of the action of disturbances, as well as their sufficiency and location of the UA.

2. OBJECTIVE

At the same time, taking into account the absence of extended overhead lines in the Azerbaijan EPS, the presence of a shortage of reactive power and an imbalance between parts of the EPS, it should be considered the most probable and mutually related indicators of violations: in terms of voltage and current. This affects the state of the launch vehicle and requires the introduction and development of an innovative Smart-Grid control system, which is being implemented in many EPSs of the world.

It implements three main tasks of monitoring and ensuring regime reliability:
- Monitoring;
- Condition assessment;
- Management.

• Monitoring task:
- monitoring the implementation of restrictions on the parameters of the system mode, set by the requirements in accordance with regulatory requirements;
- identification of dangerous mode changes in the direction of violating the boundaries of the permissible area of mode parameters and increasing the emergency.

• With the assessment of the state are carried out:
- formation of the current design scheme according to the ES data;
- analysis of observability;
- detection of gross errors in TI;
- filtering random errors in TI;
- additional calculation of non-measurable parameters.

Based on the data of monitoring and assessment of the state, control actions are formed in accordance with the state of the EPS. At the current stage of development and in the near future, the most important issues for the monitoring of the Azerbaijani HPP are:
1. Real-time monitoring of the status of the ES based on the data in the database.
2. Assess the condition of the ES.
3. Mode visualization.
4. Evaluate the "sensitive" points of the ES.
5. Estimation of transmission capacity of lines and sections.
6. Static stability reserve monitoring.
7. Monitoring of voltage levels.
8. Monitoring the damper characteristics of the system.
9. Monitoring of low-frequency dances and other issues.

The foregoing requires the improvement of the existing PAC system, which at present, against the background of the new properties of the developing Azerbaijan EPS, can show low fault tolerance, lack of adaptability and coordination, interaction, redundancy of primary raw information for the dispatcher in emergency and emergency situations, etc. An analysis of the above, as well as other systemic accidents, shows that if in the initial phase the system operator still manages to influence the processes in the system (by changing generation, limiting flows, disconnecting consumers) and ensuring survivability, then in the next phase the main role should be assigned to the PAH system.

Bringing the PAC system to the new conditions (properties) of the functioning of EPS and their Associations is currently being solved in many EPS and UES of the world on the basis of the implementation of the Concept of intellectualization (Smart Grid) and the creation of Intelligent Power Systems (IES), in which an important place is given to the intellectualization of the PAC system. The latter is implemented on the basis of innovative measuring and control systems, such as SCADA / EMS - WAMS (WAMS, WACS, WAPS) - MAS. The listed systems are integrated and provided based on PMU measurements.

The solution to the problem of preventing these risks in modern EPS is based on the implementation and effective intelligent use of an integrated information-measuring and control system (Smart-Grid) [3]:
- SCADA (EMS, DMS, OMS)
- WAMPAC (WAMS, WACS, WAPS)

The systems are well studied and widely used in the ES of the World and their Associations for the control of stationary (SCADA) and dynamic (WAMPAC) modes. SCADA (EMS) is currently being implemented at the Azerbaijan TPP, covering 7 regional centers of power plants (21) and substations (70) of the Azerbaijan Power Plant. As a result of SCADA/EMS measurements, the following functions are implemented:

$$Y = \left[P_i Q_i P_{ij} Q_{ij} U_i I_i I_{ij} \right] \quad (1)$$

where, P_i, Q_i are active and reactive power in the *i*th node; P_{ij}, Q_{ij} are active and reactive power in the *ij*th branch; U_i is voltage in the *i*th node; and I_i, I_{ij} are currents in the *i*th node and the *ij*th branch, respectively.

As a result of WAMS measurements, the function

$$Y = \left[U_i \delta_i I_{ij} \psi_{ij} \right] \quad (2)$$

where, U_i is the voltage modulus of the *i*th node; I_{ij} is the branch current *ij*th; ψ_{ij} is phase shift; and δ_i is voltage phase of the *i*-th node.

The process of monitoring, control and protection is carried out at a high speed, which is different from SCADA / EMS in Table 1 [4].

Table 1. Process of monitoring

System types	System shut down time	Duration of event
WAMS	Between 100ms-1s	From 100 ms up to several minutes
SCADA	Less than 5s	Less than 1s up to 1 h
EMS	Less than 5s	Less than 1 m up to 1 h

The efficiency of the above-described SCADA/EMS - WAMS system can be significantly increased by using multi-agent technology (MAS) [5, 6], which makes it possible to implement:
- Transition from a centralized to a decentralized (distributed) structure of the PAH system;
- Interaction of elements of the PAC system in the process of ensuring regime reliability;
- Ensuring the prevention and avoidance functions of accidents to a systemic level.

Prevention of the development of system accidents, culminating in a voltage collapse, is solved using multi-agent technology (MAC), which ensures the interaction of emergency management tools in real time. MAC is a distributed network of connected self-regulating regime hardware software agents that work together to achieve a common result and based on which can be built electrical systems with an active-adaptive network. The functioning of the MAC is implemented by agents that are "smart" due to the implementation of such technologies as neural networks, genetic algorithms, fuzzy logic, clustering algorithms, Bayes' theorem, etc.

The operating ARV, RZ, ARS, RPN, etc. are considered as agents with a reactive structure, they are not mutually coordinated. Another type includes interaction based on deliberative behavior in a special language - FIPA (The Foundation for Intelligent Physical Agents). Below, using the example of the simplest system "station-buses-load" (Figure 1), the inclusion and operation of MAC agents and their technology of action are shown [7].

In Figure 1, the Generator Agent (DN) includes information about the generators connected to the power grid. Information about loads is concentrated by means of the Load Agent (ZIPN). The Prime Agent (RN) includes a PMU to monitor and measure system parameters such as current and voltage, as well as network configuration. The RN agent uses voltage and current to identify the fault, and monitors the current state of the network through information from the Y matrix. Protection agent (PR) with built-in equipment and high voltage circuit breaker (CB) provides fault isolation.

For simplicity, all PMUs are assumed located at the nodes of the power system. In this configuration, the group of Node Agents related to every physical unit model is represented by an individual subsystem that is physically linked to others.

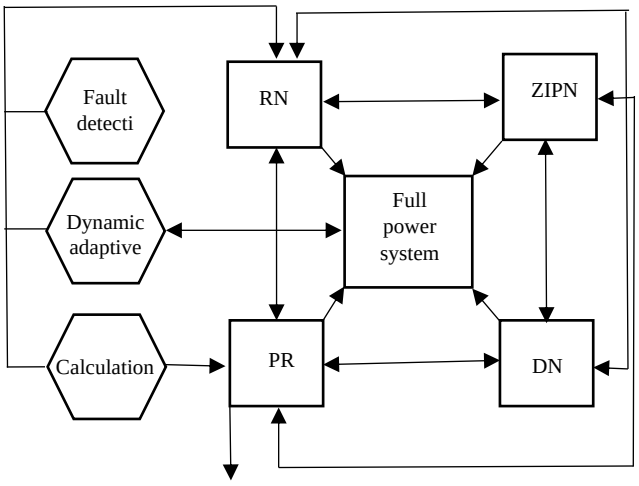

Figure 1. Multi-agents in electrical system diagram "station-line-load"

In Figure 1, there are 4 agents as RN: the main agent that receives information from the PMU, implements the transmission of information, monitoring and its measurements; DN: generator agent; PR: protection agent (RP); and ZIPN is a load agent. Figure 2 demonstrates the interactions of agents under perturbation.

The PMU is the main device that performs synchro phasor measurement and real-time transmission of information to the SCADA / EMS, WAMS system to implement control and monitoring functions. Measurements should be carried out on those elements of the EPS, the parameters of which determine the state of operational reliability. These are "weak", i.e., elements sensitive to disturbances: load nodes (by voltage), high-voltage power lines (by thermal overload), intersystem connections (low-frequency oscillations), SG having a high rate of interphase mutual oscillations, etc. during disturbances.

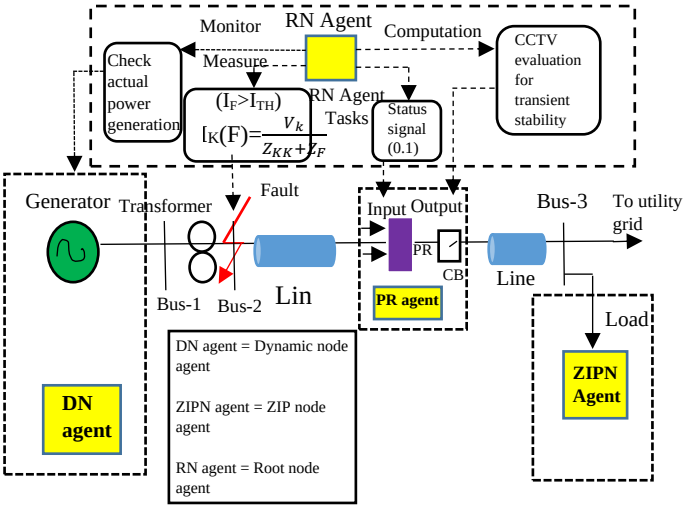

Figure 2. Demonstrates the interactions of agents under

This means that the number of PMUs in a complex ES can be quite large. Given the high cost, including the cost of not only the device itself, but also the cost of information transmission channels, the optimal number of PMUs placed in the ES should be the minimum number that ensures complete observability.

3. METHODS

The CLP method is applied to the 500-330-220 kV electrical network of the Azerbaijan PS, in which there are 36 nodes, incl. 18 nodes in the 500-330 kV network and 18 nodes in the 220 kV network. Decomposition was carried out according to intersystem connections with RF power lines (HVL-330 kV Khachmaz-Derbent), Georgian power plants (HVL-500 kV Samukh-Gardabani, HVL-330 kV Akstafa-Gardabani), Iranian PS (HVL-330 kV Imishli-Parsabad, VL -330 kV Imishli-Tagi Dize) [8].

Those. To ensure full observability, PMUs must be installed in 10 nodes (28% of the total number of nodes) of the ES. In the nodes adjacent to these nodes, the observability is provided by calculations based on measurements of voltages and flows from installed PMUs. If the cost of one channel is 1 cu, then in accordance with the recommendation, the cost of placing a PMU is 48 cu. Observability in the nodes of intersystem communications with the Georgian ES and the Russian ES is provided by calculation (either along the branches from the PMU in the neighboring nodes of the Azerbaijan ES, or the corresponding neighboring ES.

Voltage phase measurements at the ends of the lines of the main sections of the transmitting part allows you to monitor the throughput and static stability margins in real time. Integration of PMU measurement data installed on the voltage busbars of the AzTES-500 kV station, Jenub-220 kV, Shirvan-220 kV, as well as data obtained by calculation on the voltage busbars of the AzTES-330 station kV Sumgayit-220 kV and Shimal-220 kV with information from SCADA/EMS systems in the same nodes makes it possible to monitor dynamic processes under large disturbances.

4. CONCLUSION

An analysis of the network and power structure of the Azerbaijan EPS, the prospects and nature of development, shows that the most likely and significant in the event of a disturbance may be a violation of voltage stability. The structure of both components includes an integrated PAH system: SCADA/EMS-WAMS-MAS fed with information from the PMU synchrophasor measurement device. A recommendation is presented for installing the required number of PMUs in a 500-330-220 kV network that satisfies the requirements for optimality and observability.

REFERENCES

[1] Energy of Azerbaijan, Official Publication, Statistical yearbook 2020, pp. 18-20, Baku, Azerbaijan, 2020.
[2] S.M. Senderov, N.A. Yusifbayli, V.I. Rabchuk, V.K. Nasibov, et al., "Geopolitical Features of Energy Security in Caspian Regions of Russia and Azerbaijan", Geopolitics of Energy, Vol. 41, Issue 1, pp. 5-12, Alberta, Canada, 2019.
[3] A.M. Huseynov, K.A. Suleymanov, "Innovative Information-Measuring System and the Prospect of its Implementation in Azerbaijan Energy System", Magazine of Higher Technical Educational Institutions of Azerbaijan, Vol. 20, No. 6, Issue 116, pp. 67-74, Baku, Azerbaijan, 2018.
[4] J. Hector, A. Ferrer, E.O. Schweitzer, "Modern Solutions for Protection, Management and Monitoring of Electric Power Systems", Schweitzer Engineering Laboratories, p. 361, USA, 2010.
[5] M.C. Artur, E.M. Davidson, V.M. Catterson, "Multi-Agent Systems for Power Engineering Applications - Part I", IEEE Transactions on Power systems, Vol. 22, No. 4, pp. 1743-1752, Manchester, England, 2007.
[6] N.I. Voropay, I.N. Kolosok, D.A. Panasetskiy, "Multi-Agent Technologies in the Study of Electric Power Systems and their Control", ISEM SO RAN, Electronic Resource, Irkutsk, Russia, 2014.
[7] M.S. Rahman, M.A. Mahmud, H.R. Pota, M.J. Hossain, T.F. Orchi, "Distributed Multi-Agent-Based Protection Scheme for Transient Stability Enhancement in Power Systems", Energy Electric Power System, Vol. 76, Issue 8, pp. 117-129, Amsterdam, Netherlands, 2015.
[8] A.M. Huseynov, G.B. Guliyev, K.A. Suleymanov, "Perfection Survivability Monitoring Based on Synchrophasor Measurement Devices", Power Transmission and Distribution of Electricity, Vol. 3, Issue 54, pp. 50-53, Moscow, Russia, May-June 2019.

BIOGRAPHY

Kamran Alipanah Suleymanov was born in Baku, Azerbaijan on September 25, 1990. He graduated from Faculty of Electric Power Engineering, Azerbaijan State Oil and Industry, Baku, Azerbaijan and graduated in 2013 and received the Master's degree. In 2017, he entered the Ph.D. program in the specialty of power plants and power systems at Azerbaijan Research and Design-Prospecting Institute of Energetics (AzR and DPIE), Baku, Azerbaijan. Since 2021, he has been working as a chief specialist in the department of power system modes at the same institute.

The 18th International Conference on
"Technical and Physical Problems of Engineering"
30 October 2022
International Organization of IOTPE

ICTPE Conference
www.iotpe.com
ictpe@iotpe.com
ictpe0@gmail.com

ICTPE-2022 Number 03 Code 01PES03 Pages 9-15

MULTI-STRATEGY OPTIMAL CONTROL FOR COMPENSATING DEVICES IN POWER SYSTEM WITH WIDE RANGE LOAD CONDITIONS

A.M. Hashimov [1] N.R. Rahmanov [2] M.R. Shadmesgaran [1,2,3]

1. Institute of Physics, Azerbaijan National Academy of Sciences, Baku, Azerbaijan, ahashimov@azerenerji.gov.az
2. Azerbaijan Research Institute of Energetics and Energy Design, Azerenerji, Baku, Azerbaijan, nariman@cpee.az
3. Telecommunications Management, East Azarbaijan, Tabriz, Iran, shadmesgaran@yahoo.com

Abstract- Lack of development in the manufacturing sector to meet the growing demand for electrical energy highlighted the need for economical use of the ultimate capacity of current systems in different operating conditions. This paper presents a multi-strategy optimization process organized using modern compensation devices including shunt and series FACTS devices, and demand management program. With the aim of achieve the practical optimal solutions, it is necessary to consider the real system conditions in the optimization process. One of the important conditions affecting the behavior of the power system is the nature of the uncertainty of electrical loads. The multi-strategy optimization process allows the study of load uncertainties on the capacity of the compensating devices and demand response programs as well as the associated costs for a wide range of operating conditions. Also, designing and adopting different strategies for selecting suitable multi-objective functions in the proposed optimization process, ensures the simultaneous improvement of technical and economic indicators of the power system in a competitive market. Another important feature of this article is the analysis of data obtained from optimization processes in making the optimal decision foe perfect management of the power grid. Furthermore, in order to strengthen optimization processes evolutionary algorithm is applied to them. Simulation programs are performed in MATLAB and PSAT environments on the standard IEEE 30-bus test network.

Keywords: Demand Management Program, Shunt and Series FACTS Devices, Economic Optimization, Technical Optimization, Multi-Objective Function, Power Loss, System Loadability, Voltage Static Stability.

1. INTRODUCTION

Uncertainty of electrical loads as an inevitable factor in power grids shows decisive effects on the results of optimization processes. Achieving important economic goals in competitive electricity markets is often impossible without considering the uncertainties conditions of electric loads in optimization processes.

In this regard, organizing the presented multi-strategy optimization process provides the possibility of auditing the effects of load uncertainty over a broad range of operating situations. Thus, the implementation of the multi-strategy optimization process in the presence of a variety of shunt and series FACTS compensators, and demand management program individually and in combination. In addition, assessing the impact of errors and uncertainties in each of these situations, create a strong control system for optimal operation of the power system. Another important aspect of the multi-strategy optimization process is the use of a variety of multi-objective technical and economic functions tailored to the operating conditions of the system. In addition, increased response times of the multi-strategy optimization process to achieve optimal solutions in an acceptable amount of time employs an evolutionary algorithm. The implementation of the evaluation and selection method of the Pareto front is guaranteed.

In reference [1] based on the concept of flexible pricing of demand; the customer benefits from an economic model of price/incentive responsive loads as presented. A combination of flexible alternating current transmission system (FACTS) devices and demand response (DR) were added on transmission lines to manage the power in a restructured market environment [2]. In reference [3] using optimal location and rating of single TCSC in the system, a new optimization method is presented based on an objective to minimizing the device investment cost and maximizing the social welfare. Reference [4] proposes an electricity market strategy under conditions of uncertainty, including distributed generators, renewable power generators, and load support units. The predominant methods for power system operations are to manage the uncertainties caused by large-scale integration of renewable energy and active load demand are discussed [5]. In reference [6], the optimal location and capacity of the demand response program has been determined using multi-objective function. In reference [7], to achieve minimum power losses and maximum voltage static stability, the optimal capacity and location of a TCSC have been targeted.

In reference [8] synthesizing thyristor-controlled phase shifter and flexible AC transmission systems (FACTS) devices, namely, thyristor-controlled series capacitor was applied for solving the optimal power flow (OPF) in the electric power system. In reference [9] the optimal capacity and location of shunt FACTS devices have been determined by the use of genetic algorithm.

In reference [10] the outcomes of uncertainty in prognosticating the wind farm's power output in on location of marginal price in the market have been analyzed. The presented procedure maximizes the social welfare. Simultaneous application of shunt and series FACTS compensators, and demand management program (DR) for purpose of improvement multi-purpose function using evolutionary algorithm is investigated [11].

In reference [12] the importance of demand response program to deal with the out-of-tolerance conditions and control of costs are investigated. The generation capacity expansion in a multi-stage embedded strategic generation companies has been studied using a new framework [13]. In reference [14] a bi-level model including binary variables in both lower and upper levels has been proposed and solved by applying a personalized decomposition and reformulation algorithm. Some ideas for future research have been proposed based on reviewing different research works on DR optimization problems [15].

In [16] new methods for optimal allocation of DR, series and parallel FACTS devices considering both the technical and economic criteria are presented. The impact of the set of lateral conditions on the flexible optimization process is solved in a complex manner considering technical and economic indices for various multi-objective functions. This is according to the current needs of the system [17]. The major purpose of this study is to evaluate the efficiency of shunt and series FACTS compensators, and demand management program to optimizing multi-objective function and comparing them to enhance technical and economic indices for reaching the use of the ultimate capacity of current systems.

In reference [18] the efficiency of shunt and series FACTS devices, and demand management program in optimizing multi-objective function and improvement of technical and economic indices to meet the use of the ultimate capacity of current systems have been evaluated and compared. This paper is arranged as follows. In the next section, optimization approaches are classified according various operating scenarios of the power system. The third section deals with designing of multi-strategy optimization process. In the fourth section, data analysis and recommendations are made. Fifth section presents our conclusions.

2. CLASSIFICATION OF OPTIMIZATION APPROACHES

The approach to solving optimization problems in power systems is highly dependent on the operating conditions and current needs of the system. This includes low load and peak load conditions, normal and fault conditions as well as load uncertainty.

In this way, depending on the mentioned conditions, the targets of the objective function such as reduction of loss, system loadability enhancement, voltage stability improvement and reduction of compensation costs can be selected. In this research, optimization approaches are classified as shown in Table 1. As can be seen from the table, in the case of low load, the approach of loss reduction, voltage stability improvement and costs reduction are targeted.

While in peak load conditions, in order to prevent blackouts, regardless of losses and compensation costs, the approach of system loadability enhancement and voltage stability improvement is a priority. It is worth noting that the choice of compensation equipment or the use of load response program and their individual or group implementation provides the multi-strategy property of the optimization process. Also, all classified approaches and strategies are implemented for normal / fault conditions, as well as fix loads / load uncertainty conditions. In the next section designing and applying of categorized approaches and strategies are described. The most important advantage of these classifications is to help the system operator to make the best decision in order to achieve the maximum potential and benefits of technical and economic opportunities.

Table 1. Approaches Classification

All approach repeated for Normal / fault & fix load / load uncertainty							
	Approaches Classification						
Operation Conditions	Loss reduction	Loadability Enhancement	Series FACTS	Parallel FACTS	Demand Response	Technical Optimization	Technical & Economic Optimization
Low Loads	*	-	*	-	-	-	*
Low Loads	*	-	-	*	-	-	*
Low Loads	*	-	-	-	*	-	*
Low Loads	*	-	*	*	*	-	*
peak Loads	-	*	*	-	-	*	-
peak Loads	-	*	-	*	-	*	-
peak Loads	-	*	-	-	*	*	-
peak Loads	-	*	*	*	*	*	-

3. MULTI-STRATEGY OPTIMIZATION DESIGN

With the aim of achieve the practical optimal solutions, it is necessary to consider the real system conditions in the optimization process. develop the optimization process and to achieve optimal solutions in accordance with the needs of the real power system in all operating conditions, the multi-strategy optimization process is developed. This process provides the possibility of examination and evaluation of the influence of load uncertainty on electric power system effectiveness in various operating scenarios.

Figure 1 shows the block diagram of multi-strategy optimization process. To compare the effect of uncertainty loads on optimal answers; initially the possibility of choosing one of two fixed or uncertain modes for loads is considered. Here the scenario method is used to enter uncertainty conditions in the process.

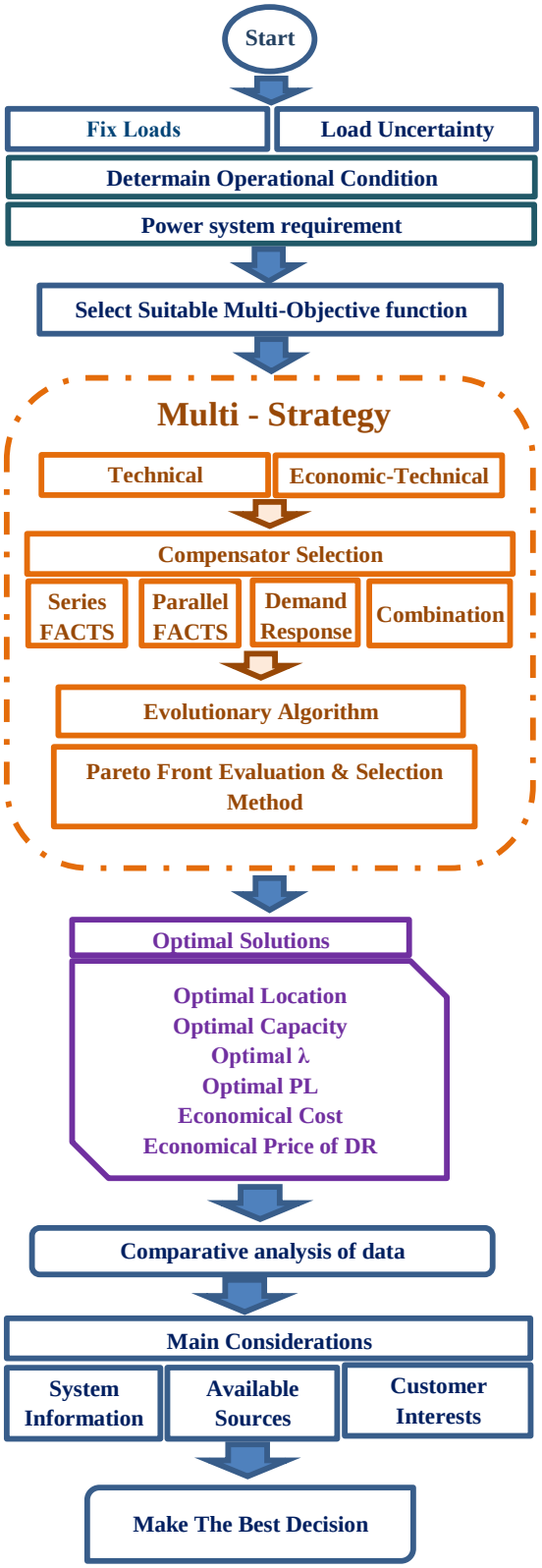

Figure 1. Multi-strategy optimization process flowchart

The mathematical model of the scenario method is performed as Equations (1) and (2).

$$PL_m = \frac{\sum_{i=1}^{n} PL_{OPT}\,(Loads \times KS_i)}{n} \tag{1}$$

$$\lambda_m = \frac{\sum_{i=1}^{n} \lambda_{OPT}\,(Loads \times KS_i)}{n} \tag{2}$$

In the second step for normal or fault operating conditions of system are determined. The choice of fault conditions changes in the network topology. By determining the initial conditions in the third stage; the essential needs of the power system can be defined. In the next step the multi-objective functions are determined based on the operator's interests and power system priorities. Using the multi-objective function ensures the simultaneous improvement of several power system parameters. Also, by defining the objective function and requirements of the power system, the design of the multi-strategy optimization process is initiated. The application of this process outlines various paths to achieve the desired outcome. This provides the possibility of having the most appropriate optimal answers in accordance with the needs of the system. The next stages are based on the initial analysis and the problem-solving approach can be selected between the technical approach and the technical-economic approach.

In the technical optimization approach, regardless of the compensation costs, achieving the maximum improvement of the objectives set by the system operator is desired. As shown in Equation (3), the multi-objective function ensures the simultaneous improvement of important power system parameters.

$$F(\lambda, PL) = (\lambda_{NEW} - \lambda_0)_{\max} \,\&\, (PL)_{\min} \tag{3}$$

In technical-economic optimization, the required improvement of the system index is determined by the operator based on the needs of the network. In this case, reaching the specified set point with the minimum compensatory capacity is carried out. The general form of the multi-objective economic-technical function is represented using Equations (4) and (5).

$$F(PL, C_{Compensator}) = (|PL_{NEW} - PL_{Set}|)_{\min} \,\& \,\&\, (C_{Compensator})_{\min} \tag{4}$$

$$F(\lambda, C_{Compensator}) = (|\lambda_{NEW} - \lambda_{Set}|)_{\min} \,\& \,\&\, (C_{Compensator})_{\min} \tag{5}$$

The multi-strategy optimization process allows the desired results to be achieved utilizing different shunt and series FACTS devices, and demand management program, individually or any desired combination of them. Following stage's locations allow the installation of compensating equipment or demand response program. In addition, the range of capacity change for each the mentioned options are determined. The general figure for determining the range of location changes and the capacity of series compensating devices is shown in Equations (6) and (7), respectively.

The multi-strategy optimization process allows the desired results to be achieved utilizing different shunt and series FACTS devices, and demand management program, individually or any desired combination of them. Following stage's locations allow the installation of compensating equipment or demand response program. In addition, the range of capacity change for each the mentioned options are determined. The general figure for determining the range of location changes and the capacity of series compensating devices is shown in Equations (6) and (7), respectively.

$$L_{Series} = \left\{ L_S \mid 1 \le L_S \le L_{\max} \ , \ L_S \notin \{UPL\} \right\} \quad (6)$$

$$-K_S \times X_{Line} \le X_{Series} \le K_2 \times X_{Line} \quad (7)$$

where, L_{Series} is collection of candidate locations for installation of series compensating devices, L_S is line number of installation place of series compensating devices, $L_{S\max}$ is the largest line number in the network, X_{Series} is range of reactance changes of series compensating devices, X_{Line} is reactance of the desired transmission line, K_1 is fixed coefficient to determine the maximum series compensator reactance in inductance mode, K_2 is constant coefficient to determine the maximum series compensator reactance in capacitive mode and *UPL* is a set of lines in which it is not possible to install series compensating devices

Equations (8) and (9) show the general shape of the range of location and capacity of the parallel compensating devices, respectively.

$$B_{Paralel} = \left\{ B_P \mid 1 \le B_P \le B_{\max} \ , \ B_P \notin \{UPB\} \right\} \quad (8)$$

$$-Q_{\min}^{pu} \le Q_P \le Q_{\max}^{pu} \quad (9)$$

where, $B_{Parallel}$ is a set of candidate buses for the installation of parallel compensating devices, B_P is bus number for installation of parallel compensating devices $B_{\max}$ is the largest bus number in the network, Q_P is range of changes in the capacity of parallel compensating devices, $Q_{\min}$ is maximum parallel compensator capacity in induction mode, $Q_{\max}$ is maximum parallel compensator capacity in capacitive mode and *UPB* is a set of buses in which it is not possible to install parallel compensating devices.

The general figure for determining the range of capacity and location changes of the demand management program is shown in Equations (10) and (11), respectively.

$$B_{Demand\ Response} = \{ B_{DR} \mid 1 \le B_{DR} \le B_{\max} \quad B_{DR} \in \{PQ\} \ , \ B_{DR} \notin \{UPDR\} \} \quad (10)$$

$$0 \le S_{DR} \le K_3 \times S_{BUS} \quad (11)$$

where, $B_{Demand\ Response}$ is a set of candidate buses for implementation of Demand Response program, B_{DR} is bus number for implementation of Demand Response program, $B_{\max}$ is the largest bus number in the network, S_{DR} is range of changes in the capacity of Demand Response program, S_{BUS} is apparent power of the desired bus, K_3 is constant coefficient to determine the maximum capacity of the demand response program and *UPDR* is a set of buses in which it is not possible to implement a demand response program

In the next step a genetic evolutionary algorithm is used to achieve optimal answers in an acceptable time. The loop of multi-objective function optimization the process at each iteration requiring evaluation and arranging multifaceted answers. This is achieved by implementation of the Pareto front assessment and selecting method. Utilizing this method; the output of the multi-strategy optimization process, instead of an optimal solution, a set of optimal solutions are obtained in the form of the Pareto front. Finally, on the basis of the outcomes of comparative analysis, the operator of system makes the best decision taking into account the needs of the power system and predetermined goals.

4. DATA ANALYZING AND MAKE SUGGESTIONS

This paper, provides a robust optimization process for solving electric power system problems in a broad range of loads conditions and system operation. Approaches appropriate to current needs are also identified. In this part, by comparative analysis resulting from optimal solutions for different strategies of improved control of compensators is shown. The following are examples of the calculated results obtained. are presented. Table 2 shows the comparative analysis of the optimal solutions obtained from the technical optimization approach. Simultaneous adaptation of series and parallel FACTS devices along with the demand response program in normal and fault conditions as well as for constant loads and uncertainty loads conditions for eight various approaches are part of the strategy.

As can be seen in Table 2, considering the load uncertainty conditions in all defined methods reveals the range of potentials of the system and causes more power loss reduction and improvement of system loadability and static voltage stability. Also, with adoption of the strategy of simultaneous implementation of three equipment, it is concluded the reduction of losses up to PL = 0.0315 and the increase of system load capacity up to λ = 6.1389. A comparative analysis of the loss reduction index for the simultaneous installation strategy of series and parallel FACTS devices along with load response program for the four most widely used approaches is shown in Figure 2. The blue dashed circle shows the system losses before compensation. As shown in the diagrams, in all adopted approaches, the multi-strategy optimization process ensures reduction of the loss index. The curves also show that the solutions resulting from the optimization of the multi-objective function in the form of Pareto front impose more power losses on the system at peak load conditions while focusing on increasing system loadability. The large range of changes in the loss reduction index proves the applicability of the presented multi-strategy optimization process.

Table 2. Sample strategy of simultaneous implementation of shunt and series FACTS devices along with demand management program

Solution Number	Approaches in accordance with different operating conditions of the system							
	N - Fix - PL	*N - Un - PL*	*N - Fix - λ*	*N - Un - λ*	*E - Fix - PL*	*E - Un - PL*	*E - Fix - λ*	*E - UN - λ*
1	0.0958	0.1007	3.3941	4.1355	0.0434	0.0419	3.0233	3.7529
2	0.202	0.4371	4.0816	5.57	0.0434	0.0349	3.0279	3.6441
3	0.0411	0.2855	2.9152	5.0777	0.2915	0.0452	3.9177	3.8441
4	0.4649	0.4296	4.7638	5.5511	0.2365	0.0422	3.8368	3.7835
5	0.0754	0.099	3.2454	4.1296	0.292	0.0487	3.9968	3.854
6	0.0791	0.3727	3.3069	5.3708	0.4326	0.0741	4.3456	4.1439
7	0.045	0.2769	3.0891	5.0475	0.4375	0.0516	4.3537	3.936
8	0.0802	0.0769	3.378	4.036	0.2241	0.3875	3.7352	5.4523
9	0.2867	0.1563	4.2868	4.4011	0.0961	0.3844	3.4066	5.4206
10	0.1227	0.3224	3.4979	5.1965	0.1534	0.3829	3.6611	5.4196
11	0.051	0.0315	3.2309	3.5847	0.4326	0.051	4.3494	3.9048
12	-	0.219	-	4.8604	0.167	0.2893	3.6842	5.3738
13	-	0.1935	-	4.7744	0.3374	0.3876	4.2638	5.4736
14	-	0.0315	-	3.5835	0.3325	0.2817	4.1123	5.3267
15	-	0.1372	-	4.3374	0.2541	0.0525	3.9072	3.991
16	-	0.107	-	4.2621	0.1074	0.1744	3.4781	4.94
17	-	0.1058	-	4.2563	0.2256	0.0326	3.8008	3.6285
18	-	0.1108	-	4.287	0.4397	0.0497	4.631	3.9024
19	-	-	-	-	0.2931	0.3877	4.0213	5.4744
20	-	-	-	-	-	0.2335	-	5.0259
21	-	-	-	-	-	0.5616	-	6.1389
22	-	-	-	-	-	0.1443	-	4.6347
23	-	-	-	-	-	0.128	-	4.5565
24	-	-	-	-	-	0.1034	-	4.4089
25	-	-	-	-	-	0.2738	-	5.2228
26	-	-	-	-	-	0.0435	-	3.8286
27	-	-	-	-	-	0.0574	-	4.1087
28	-	-	-	-	-	0.0574	-	4.028
29	-	-	-	-	-	0.3868	-	5.4398
30	-	-	-	-	-	0.4443	-	5.6155
31	-	-	-	-	-	0.1297	-	4.5697
32	-	-	-	-	-	0.5103	-	5.8092
33	-	-	-	-	-	0.0737	-	4.1417
34	-	-	-	-	-	0.13	-	4.5827
35	-	-	-	-	-	0.4408	-	5.6002
36	-	-	-	-	-	0.1518	-	4.6772
37	-	-	-	-	-	0.3847	-	5.4225
38	-	-	-	-	-	0.1639	-	4.7402
39	-	-	-	-	-	0.2372	-	5.035
40	-	-	-	-	-	0.0349	-	3.74
41	-	-	-	-	-	0.0743	-	4.2351
42	-	-	-	-	-	0.2723	-	5.1937

The comparative analysis of the optimal solutions for the four main approaches of the power system to improve the loadability index and increase the voltage static stability is shown in Figure 3. Blue dashed circle displays the system loadability index before compensation. As can be seen in the diagram, the multi-strategy optimization process for all approaches strongly increases the loadability index, even during significantly reduction in loss index. Optimal responses in accordance with the change in increasing the system loadability at sharp points of the curves in all approaches are introduced as the best option to prevent global blackouts. Table 3 compares the results obtained for different strategies for the purpose of optimize the multi-purpose function in widely used approaches.

Table 3 shows the optimal capacity and location for the installation of each device and the relevant cost. In this table, the goals of λ = 2.6 and *PL* = 0.0450 are designated by the operator of system in accordance with the needs of the electric power system. As can be seen in Table 3, a specific strategy is not always the best strategy for all approaches. In this way, due to the large difference in costs, the advantage of using the proposed multi-strategy process is confirmed. Another advantage of using the multi-strategy optimization process is determining the optimal location and capacity of the demand response program and its price based on the strategy with lowest obtained cost.

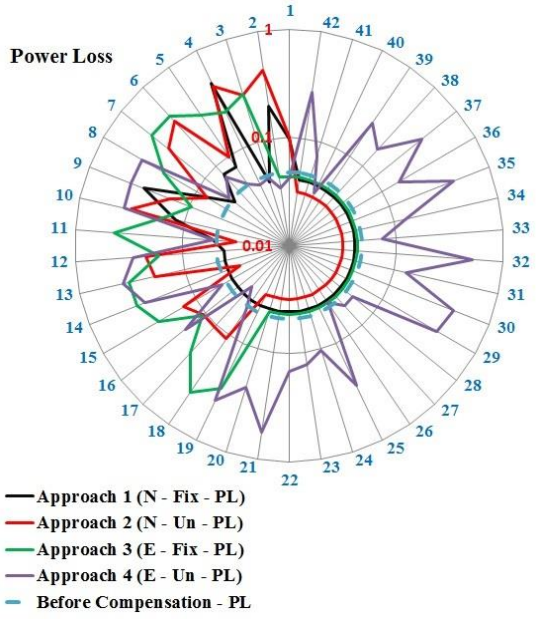

Figure 2. Comparison of loss reduction index in different approaches

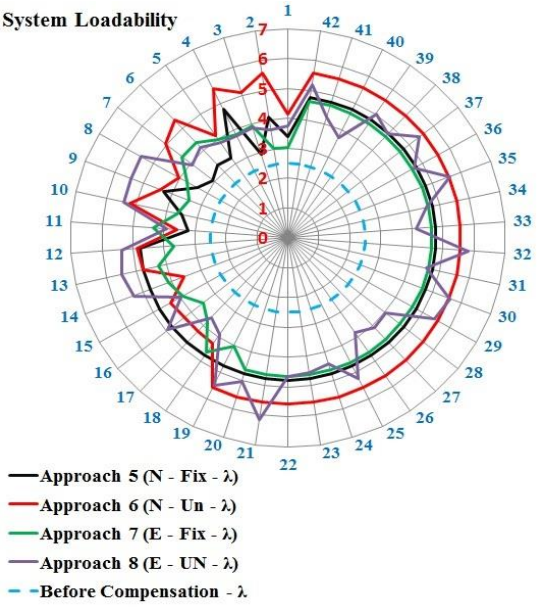

Figure 3. Comparison of system loadability index in different approaches

Table 3. Sample outputs of multi-strategy optimization process

Strategy		Strategy 1			Strategy 2			Strategy 3		
		Series FACTS			Parallel FACTS			Demand Response		
Parameters		Location	Capacity	Cost	Location	Capacity	Cost	Location	Capacity	Cost
Approaches in accordance with different operating conditions of the system	N-Fix-(PL=0.0450)	12	0.28 kvar	43.05	10	10 kvar	1273.8	5	7.18 MVA	43.05
	N-Un-(PL=0.0450)	10	0.5718 Mvar	87681	29	9.43 Mvar	1163400	5	1.04 MVA	87681
	E-Fix-(PL=0.0450)	12	140 kvar	21511	21	10 kvar	1273.8	21	1.72 MVA	1273.8
	E-Un-(PL=0.0450)	10	0.25 Mvar	38393	15	9.77 Mvar	1215700	5	8.52 MVA	38393
	N-Fix-(λ=2.6)	36	2.07 Mvar	315220	23	30 kvar	3821.1	21	2.01 MVA	3821.1
	N-Un-(λ=2.6)	29	4.3 kvar	661	22	110 kvar	14008	2	0.49 MVA	661
	E-Fix-(λ=2.6)	10	1.36 Mvar	207790	9	9.77 Mvar	1215700	21	0.97 MVA	207790
	E-Un-(λ=2.6)	29	4.3 kvar	661	9	10 Mvar	1243590	2	0.41 MVA	661

5. CONCLUSIONS

Different approaches to increase the productivity of power systems were developed and presented based on different operating conditions and a broad range of load changes, utilizing different problem-solving technics in the form of a multi-strategy optimization process. In the technical optimization approach for peak load conditions; the use of the ultimate capacity of current systems regardless of the installation capacity of compensating devices and related costs, the concurrent improvement of the major indicators of the electric power system including loadability enhancement, improvement of voltage static stability and loss reduction was achieved. Also, the results obtained from the technical optimization approach in low load conditions ensured maximum loss reduction while maintaining the system loadability index. The outcomes, denote the advantages of the proposed different strategies in optimization of multi-objective function. In the economic-technical optimization approach, achieving the pre-determined set point by the operator with the least installation capacity of compensating devices and minimum costs are presented by implementing different strategies.

The sharp differences in costs incurred for the different adopted strategies proved the importance of the proposed multi-strategy optimization process. Finally, in this paper, the development of the optimization process and the classification of approaches and strategies provides a model for rising the power system efficiency by considering a broad range of real operational conditions and using other modern compensators.

REFERENCES

[1] M.P. Moghaddam, A. Abdollahi, M. Rashidinejad, "Flexible Demand Response Programs Modeling in Competitive Electricity Markets", Applied Energy, Elsevier, Issue 9, Vol. 88, pp. 3257-3269, 2011.

[2] A. Yousefi, T.T. Nguyen, H. Zareipour, O.P. Malik, "Congestion Management Using Demand Response and FACTS", International Journal of Electrical Power and Energy Systems, Elsevier, Issue 1, Vol. 37, pp. 78-85, 2012.

[3] P.K. Tiwari, "An Efficient Approach for Optimal Allocation and Parameters Determination of TCSC With Investment Cost Recovery under Competitive Power Market", IEEE Transactions on Power Systems, Issue 3, Vol. 28, pp. 2475-2484, 2013.

[4] S. Bose, "On the Design of Wholesale Electricity Markets under Uncertainty", The 53rd Annual Allerton Conference on Communication, Control, and Computing (Allerton), pp. 203-210, Monticello, IL, USA, 29 September -2 October, 2015.

[5] C. Peng, S. Lei, Y. Hou, Wu. Felix, "Uncertainty Management in Power System Operation", CSEE Journal of Power and Energy Systems, Issue 1, Vol. 1, pp. 28-35, 2015.

[6] M.R. Shadmesgaran, A.M. Hashimov, N.A. Yusifbeyli, "Optimal Location and Capacity of Demand Response Program for Simultaneously Power Loss Reduction and Static Voltage Stability Improvement Using Genetic Algorithm", The 11th International Conference on Technical and Physical Problems of Electrical Engineering (ICTPE-2015), pp. 75-79, Bucharest, Romania, 10-12 September 2015.

[7] M.R. Shadmesgaran, A.M. Hashimov, N.A. Yusifbeyli, "Optimal Location of TCSC Due to Power Loss Reduction and Static Voltage Stability Improvement Using Genetic Algorithm", Power Engineering Problems, No. 4, pp. 31-37, Baku, Azerbaijan, 2015.

[8] A. Mukherjee, V. Mukherjee, "Solution of Optimal Power Flow with FACTS Devices Using a Novel Oppositional Krill Herd Algorithm", International Journal of Electrical Power and Energy Systems, Elsevier, Vol. 78, pp. 700-714, 2016.

[9] M.R. Shadmesgaran, A.M. Hashimov, N.R. Rahmanov, "Optimal Location and Capacity of Parallel Facts Devices in Order to Improve Voltage Static Stability and Power Losses Reduction Using Genetic Algorithm", The 12th International Conference on Technical and Physical Problems of Electrical Engineering (ICTPE-2016), pp. 102-106, Bilbao, Spain, 7-9 September 2016.

[10] H. Dehghani, B. Vahidi, S.H. Hosseinian, "Wind Farms Participation in Electricity Markets Considering Uncertainties", Renewable Energy, Elsevier, Vol. 101, pp. 907-918, 2017.
[11] M.R. Shadmesgaran, A.M. Hashimov, N.R. Rahmanov, O. Z. Kerimov, I.I. Mustafayeva, "Technical Analysis of Demand Response Program and FACTS Devices Implementation Using Multi-Objective Optimization", International Journal on Technical and Physical Problems of Engineering (IJTPE), Issue 32 Vol. 9, No. 3, pp. 21-29, September 2017.
[12] R. Sharifi, S.H. Fathi, V. Vahidinasab, "A Review on Demand-Side Tools in Electricity Market", Renewable and Sustainable Energy Reviews, Elsevier, Vol. 72, pp. 565-572, 2017.
[13] J. Valinejad, M. Marzband, M. Funsho Akorede, T. Barforoshi, M. Jovanovic, "Generation Expansion Planning in Electricity Market Considering Uncertainty in Load Demand and Presence of Strategic Gencos", Electric Power Systems Research, Elsevier, Vol. 152, pp. 92-104, 2017.
[14] X. Zhang, D. Shi, Z. Wang, B. Zeng, X. Wang, K. Tomsovic, Y. Jin, "Optimal Allocation of Series FACTS Devices Under High Penetration of Wind Power Within a Market Environment", IEEE Transactions on Power Systems, Issue 6, Vol. 33, pp. 6206-6217, 2018.
[15] A. Rezaee Jordehi, "Optimization of Demand Response in Electric Power Systems, a Review", Renewable and Sustainable Energy Reviews, Elsevier, Vol. 103, pp. 308-319, 2019.
[16] M.R. Shadmesgaran, "Prevail Over Power Electric System Problems by Simultaneous Optimization of Both Technical and Economic Criteria Considering Load Uncertainty", International Journal on Technical and Physical Problems of Engineering (IJTPE), Issue 40, Vol. 11, No. 3, pp. 34-42, September 2019.
[17] M.R. Shadmesgaran, A.M. Hashimov, N.R. Rahmanov, "A Glance at the Effects of System Operating Conditions on both Technical and Economic Multi-Objective Optimization", International Journal on Technical and Physical Problems of Engineering (IJTPE), Issue 46, Vol. 13, pp. 1-10, March 2021.
[18] M.R. Shadmesgaran, A.M. Hashimov, N.R. Rahmanov, "Productivity Comparison of Different FACTS And DR To Enhance Technical Indicators and Economical Operation of Grid", The 2nd International Conference on Electrical, Communication and Computer Engineering (ICECCE), pp. 362-367, Istanbul, Turkey, 14-15 April, 2020.

BIOGRAPHIES

Arif M. Hashimov was born in Shahbuz, Nakhchivan, Azerbaijan on September 28, 1949. He is a Professor of Power Engineering (1993); Chief Editor of Scientific Journal of "Power Engineering Problems" from 2000; Director of Institute of Physics of Azerbaijan National Academy of Sciences (Baku, Azerbaijan) from 2002 up to 2009; and Academician and the First Vice-President of Azerbaijan National Academy of Sciences from 2007 up to 2013. He is laureate of Azerbaijan State Prize (1978); Honored Scientist of Azerbaijan (2005); Cochairman of International Conferences on "Technical and Physical Problems of Power Engineering" (ICTPE) and Editor in Chief of International Journal on "Technical and Physical Problems of Engineering" (IJTPE). Now he is a High Consultant in "Azerenerji" JSC, Baku, Azerbaijan. His research areas are theory of non-linear electrical Networks with distributed parameters, neutral earthing and ferroresonant processes, alternative energy sources, high voltage physics and techniques, electrical physics. His publications are 350 articles and patents and 5 monographs.

Nariman R. Rahmanov was born in Baku, Azerbaijan in 1937. He received the M.Sc. and Ph.D. degrees from Azerbaijan State Oil and Chemistry Institute (Baku, Azerbaijan) in 1960 and 1968, respectively. He received the Doctor of Technical Sciences in Power Engineering from Novosibirsk Electro technical Institute, Russia in 1990. He is a professor since 1990 and Director of Azerbaijan Scientific Research Institute of Energetic and Energy Design (Baku, Azerbaijan) from 2007 up to 2009, and Deputy Director of the same institute and SPII from 2009 up to present. He is Director of Azerbaijan-Norway Center of Cleaner Production and Energy Efficiency (CPEE Center). He is the member of IEEE, Academician of International Eco-Energy Academy (Baku, Azerbaijan), Co-Chairman of International Conference on "Technical and Physical Problems of Electrical Engineering" (ICTPE), member of Editorial Boards of International Journal on "Technical and Physical Problems of Engineering" (IJTPE) and Journal of Power Engineering Problems. His research areas are power systems operation and control, distributed systems, alternative energy sources. His publications are more than 220 articles and patents, and also 3 monographs.

Mohammadreza M. Shadmesgaran was born in Tabriz, Iran, in 1967. He received his M.Sc. degree in electrical engineering from Iran University of Science and Technology, Tehran, Iran in 2008. He is currently a PhD Candidate at ANAS university and works as deputy director of East Azerbaijan Province, Telecommunications Management in Tabriz. Iran. His research interests are increasing efficiency in power systems, demand response, power system dynamics, stability and control and FACTS devices.

The 18th International Conference on
"Technical and Physical Problems of Engineering"
30 October 2022
International Organization of IOTPE

ICTPE Conference
www.iotpe.com
ictpe@iotpe.com
ictpe0@gmail.com

ICTPE-2022 Number 04 Code 01PES04 Pages 16-20

DEVELOPMENT OF A THYRISTOR SYSTEM FOR SWITCHING STATOR WINDING OF A TWO-SPEED ASYNCHRONOUS GENERATOR OF A WIND ELECTRIC INSTALLATION

A.I. Abdulkadyrov N.S. Mammadov G.A. Aliyeva

Electrical Engineering Department, Azerbaijan State Oil and Industry University, Baku, Azerbaijan
aabdulkadirov42@gmail.com, nijatms@gmail.com, gyulnara.alieva-74@mail.ru

Abstract- A calculation method has been developed and the choice of the stator winding of a two-speed asynchronous generator of a wind electric installation has been carried out. The connection diagrams of the stator winding are considered when switching the number of poles in a ratio of 2:1. A thyristor system for switching the stator winding of a two-speed asynchronous generator of a wind turbine has been developed. The use of a three-phase thyristor commutator for switching the stator winding of a two-speed asynchronous generator for starting a wind generator in a motor mode, which becomes necessary at low wind speeds (2.5-3.5 m/s), is proposed. The mechanical characteristics of a two-speed machine with a 2:1 switching of the number of poles at a constant torque and at a constant power are obtained.

Keywords: WEI, TSAG, Thyristor, Switching, Commutation, Starting moment, Modeling, PPCS.

1. INTRODUCTION

The use of wind energy in recent years is the most widespread. Local placement of wind turbines, ease of installation of the mechanism and application are clear advantages over conventional energy sources. A wind electric installation (WEI) or a wind generator is installation that converts the kinetic energy of the wind flow into the mechanical energy of the rotor rotation with further conversion into electrical energy. Wind turbines (or wind power plants - wind turbines) are classified as renewable energy sources. They are distinguished from traditional sources that generate electrical energy by the absence of raw materials and waste, they can operate in a wide range of environmental conditions: 100% humidity and temperatures from -40 to +85 ℃. The only requirement is a high level of wind.

Wind electric installation have number of advantages, which leads to their widespread use. These advantages are:

1. Full renewable energy is used. When the sun influences, there is a constant movement of air flow in the atmosphere, the creation of which does not require extraction, transportation, or combustion of fuel. The source is fundamentally inexhaustible.
2. Under the action of wind turbines, harmful emissions are completely absent. Therefore, this installation is considered environmentally friendly.
3. The use of wind turbines is mainly justified for isolated places.
4. When a WPP is put into operation, the price of a kilowatt-hour of generated electrical energy is significantly reduced.
5. Variable speed wind turbines able to tune into the wind. At the same time, the regulation of the rotation frequency relative to the wind speed is carried out in such a way as to achieve maximum power generation, etc.

To increase the efficiency of wind application, stepwise speed control began to be used. To do this, two windings with a different number of pole pairs are placed in the generator stator. At the lowest wind speed, in order maintain optimal speed, a low speed of rotation of the wind wheel is used and the winding with the largest number of pole pairs is included in the generator. When the wind speed rises above a certain limit, it switches to the smallest value of the number of pole pairs and an increase in rotation speed is allowed.

Two-speed wind electric installations are widely used, so their circuit is quite simpler than circuits with converters [1]. The use of DAG makes it possible to increase the generation of electrical energy at low wind speeds from 3.5 to 5 m/s. Consider the advantages of a two-speed generator used for wind turbines

Advantages:

1) Low noise level
2) Minimal vibration
3) High performance
4) High starting torque
5) Simplicity and reliability of design
6) Ability to work at two speeds

Since the rotation speed depends on the wind, it must be regulated. Step speed control is important for wind turbines. Therefore, at present, two-speed asynchronous generators are widely used in wind electric installations [2].

2. SELECTION OF THE STATOR WINDING OF A TWO-SPEED ASYNCHRONOUS GENERATOR

The case is considered when the number of poles of the stator winding changes in the ratio $2p_1/2p_2 = 8/4 = 2:1$. In this case, each phase of the stator winding consists of two parts, each of which has an equal number of coil groups. When both parts are flowed around by currents in the same direction, a magnetic field arises with large number of poles; when changing the direction of the current in one of the parts, the number of poles is reduced by half.

Such switching of the current direction should be carried out in all phases at the same time, and the switched parts of the winding can be connected in series or in parallel. The winding pitch in the tooth division for both numbers of poles, and the width of the phase zone, which occupies the sides of each coil group, are the same. But since the pole division τ changes twice when the number of poles is switched, the phase zone in electric degrees and the relative pitch of the winding also change. With a small number of poles, the phase zone is α=60°, and with a double number α=120° [3].

The most widely used 2:1 connection scheme (Dahlander's scheme) are shown in Figure 1. Star - double star circuits (Figure 1a, 1b) provide switching at a constant torque, and triangle - double star circuits, which are shown in Figure 1c, 1d at approximately constant power. As can be seen from the diagrams that are shown in Figure 1, when moving from a low speed to a high speed, the direction of the current changes in half of the half-windings of the stator phases. In order for the direction of the field growth to remain unchanged in this case, it is also important to switch the ends of the 2 phases of the winding [4].

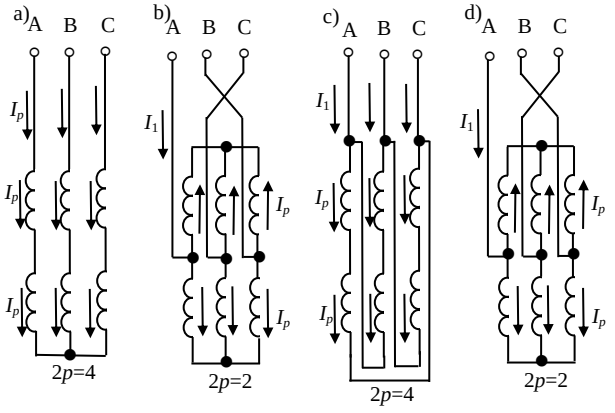

Figure 1. Fundamental schemes of the connection of the stator winding when switching the number of poles in a ratio of 2:1

For these circuits, we can consider the ratios of powers P_2 and moments M in a simplified form (1, 2). Linear voltage U_1, current I_p in each half-winding of the stator phase, efficiency η and cosφ remain constant (3, 4). In this case, for the circuits shown in Figure 1a, 1b, we have:

$$\frac{P_{12}}{P_{11}} = \frac{\sqrt{3}U_l I_{l2}\cos\varphi}{\sqrt{3}U_l I_{l1}\cos\varphi} = \frac{\sqrt{3}U_l 2I_p\cos\varphi}{\sqrt{3}U_l I_p\cos\varphi} = 2 \qquad (1)$$

$$\frac{M_2}{M_1} = \frac{P_{22}}{Q_{22}} = \frac{Q_{21}}{P_{21}} = \frac{P_{12}}{Q_{22\eta}} = \frac{Q_{21\eta}}{P_{11}} = 1 \qquad (2)$$

For the schemes shown in Figure 1c, 1d, we have:

$$\frac{P_{12}}{P_{11}} = \frac{\sqrt{3}U_l I_{l2}\cos\varphi}{\sqrt{3}U_l I_{l1}\cos\varphi} = \frac{\sqrt{3}U_l 2I_p\cos\varphi}{\sqrt{3}U_l \sqrt{3}I_p\cos\varphi} = 1.15 \approx 1 \qquad (3)$$

$$\frac{M_2}{M_1} = \frac{P_{22}}{Q_{22}} = \frac{Q_{21}}{P_{21}} = \frac{P_{12}}{Q_{22\eta}} = \frac{Q_{21\eta}}{P_{11}} = 0.575 \approx 0.5 \qquad (4)$$

In these equations index 1 means lower frequency rotation and index 2 higher frequency rotation. When applying the schemes that are shown in Figure 1c, 1d, as a rule, the same power is indicated for both speeds, i.e., accepted that $P_{12} = P_{11}$ and $M_2 = 0.5M_1$. A variant of a two-speed asynchronous generator is calculated, in which the power ratio is 13/18 kW, as you can see, $\frac{P_{12}}{P_{11}} = 1.385 > 1$, therefore, the stator winding circuit is chosen according to Figure 1a, 1b. Rated linear voltage $U_n = 380\,\text{V}$.

3. CONTACTOR SYSTEM OF SWITCHING IN STATOR WINDING OF A TWO-SPEED ASYNCHRONOUS GENERATOR OF A WIND ELECTRIC INSTALLATION

A contactor is an indispensable device in situations where it is necessary to frequently switch electric current. It allows you to close and open the circuit up to several thousand times per hour. At the same time, the contactor has both electrical and mechanical wear resistance. To perform its function, the contactor must have a simple and reliable design. Of course, some items may differ from model to model. This mainly concerns the number and appearance of contacts and coils. But in general, the internal structure of the contactor has a standard design. So, the main elements of the contactor include:

1) Electromagnetic system;
2) Main contact system;
3) Auxiliary contact system (block contacts);
4) Extinguishing system.

The first circuit is implemented on contactors and is shown in Figure 2. It works in the following way. At the first stage (at wind speeds $5.0 \le v \le 5.5$ m/s), contactors K2 and K3 are off, and contactor K1 is on.

In this case, as can be seen from the figure, two equal parts of the stator winding are connected in series, and terminals A, B, C are connected to the electrical network through the closed contacts of contactor K1. Thus, the asynchronous generator of a wind electric installation generates electrical energy and delivers it to the electrical network to consumers [5].

At the second stage (at wind speeds $v > 5.5$ m/s), the contactor K1 is turned off, its contacts open and the stator winding is disconnected from the electrical network. Following this, commands are given, which are generated by the microprocessor control system of the wind turbine, to turn on the contactor K2, and then the contactor K3. In this case, the conclusions A, B, C are closed to each other. The stator winding circuit of an asynchronous generator takes the form shown in Figure 1b.

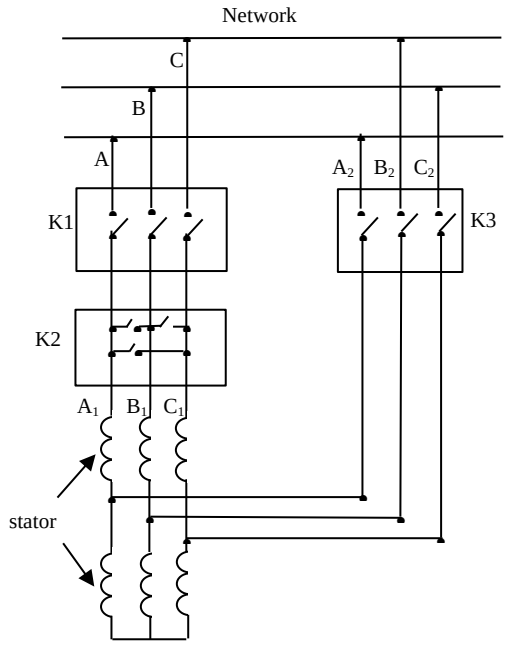

Figure 2. Contactor scheme of switching the stator winding of a two-speed asynchronous generator of a wind electric installation

As a result, the number of stator winding poles is halved. In this case, the rotational speed of the shaft of the asynchronous generator was increased by the wind turbine to the appropriate value, that is, more than 1500 rpm by the amount of slip. It should be noted here that the commands for switching the stator winding of the asynchronous generator and its connection to the electrical network are issued after the generator shaft speed is brought by the wind turbine to the appropriate value (in the first stage, more than 750 rpm, and in the second stage, more than 1500 rpm). Once again, we note that the control commands for switching the stator winding of an asynchronous generator are generated by the wind turbine control system.

4. THYRISTOR SYSTEM OF SWITCHING THE STATOR WINDING OF A TWO-SPEED ASYNCHRONOUS GENERATOR OF A WIND ELECTRIC INSTALLATION

The above contactor scheme for switching the stator winding of an asynchronous generator has a number of disadvantages:
- high cost;
- large dimensions and weight;
- high power of control signals;
- poor compatibility with the microprocessor control system.

The thyristor circuit for switching the stator winding, shown in Figure 3, does not have these disadvantages.

In addition to the functions of switching the stator winding, it can perform a number of new functions. The most important of them is the ability to regulate the voltage in the electrical network. This function can be very useful when the wind turbine is running in motor mode, more specifically when starting the input of the wind turbine. This will be discussed in the following.

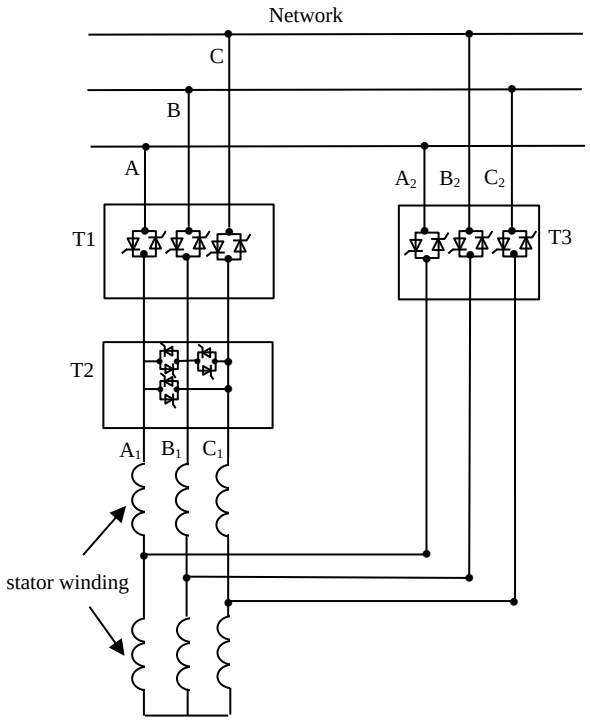

Figure 3. Thyristor scheme of switching the stator winding of a two-speed asynchronous generator of a wind electric installation

The principle of operation of a thyristor pair in phase is known. Each thyristor passes the corresponding half-wave of the AC voltage when the following conditions are met:
- the presence of a positive potential at the anode;
- supply of a pulse with the appropriate parameters to the control electrode.

By placing two back-to-back thyristors in each phase, we will switch a three-phase AC circuit. In addition to switching the stator winding to change the number of poles, the thyristor system according to Figure 3 (we are talking about blocks T1 and T3) can also perform much more effective protection of the stator winding in the event of a short circuit or other damage than the contactor scheme.

5. APPLICATION OF A THYRISTOR SYSTEM FOR SWITCHING THE STATOR WINDING FOR START-UP OF A WIND ELECTRIC INSTALLATION

In practice, at wind speeds of 2.5-3.5 m/s, the wind turbine does not come into rotation. The reason for this is that the torque generated by the wind turbine is not sufficient to overcome the so-called starting torque of the wind turbine. The wind speed range of 2.5-3.5 m/s is observed very often (according to some sources, approximately 30-35% of the annual duration). The generation of electrical energy at these speeds would be very important.

This paper proposes to overcome this shortcoming. It is a so-called motor start-up of a wind turbine. We are talking about the fact that the wind generator is transferred to the motor mode of operation for a very short period of time. When starting off after a certain number of revolutions, the moment of resistance of the

wind turbine abruptly decreases. Thus, as soon as the wind turbine shaft starts to move, the wind turbine picks up the rotation and then starts to work independently in the normal mode.

It is recommended to use the motor mode of operation of the wind generator at a low synchronous frequency of rotation of the generator (in our case, 750 rpm, $2p$ = 8). To do this, in the developed system for switching the number of poles of the stator winding according to Figure 3 thyristor switches T2 and T3 are opened, and T1 is closed. In this case, the mains voltage is applied to the stator winding of the asynchronous generator and the machine starts to rotate [6].

As you know, the initial starting current of an asynchronous motor reaches a value of 5 - 7 rated current. To eliminate the negative value of such a large current surge, it is proposed to reduce the voltage supplied to the stator winding using the T1 thyristor unit, switching it to the voltage regulator mode. To do this, the thyristor unit is equipped with a pulse-phase control system (PPCS).

With the help of PPCS, the thyristor control angle is changed, by selecting the value of which it is possible to limit the starting current to an acceptable value. At the same time, in blocks T2 and T3, the use of such a system is not required [7].

6. SIMULATION RESULTS

Using the program and according to the calculation, Figure 4 shows the mechanical characteristics were.

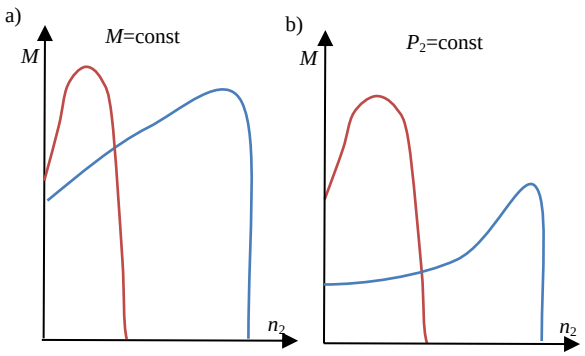

Figure 4. Mechanical characteristics of a two-speed machine with a ratio of 2:1 switching of the number of poles (a) at a constant torque, and (b) at a constant power

7. CONCLUSIONS

The use of a two-speed asynchronous generator in a wind electric installation can significantly increase the wind utilization factor (ultimately, the plant efficiency), which is especially important at low wind speeds. This allows you to significantly increase the annual production of electrical energy. Thanks to the thyristor switching circuit of the stator winding, more effective protection of the stator winding from short circuit is provided. The development of a thyristor system for switching the stator winding of a two-speed asynchronous generator for starting a wind generator in a motor mode improves the operation of a wind turbine at low wind speeds (2.5-3.5 m/s).

APPENDIX

The dependences of current, efficiency and slip on P_2 are called operating characteristics. These quantities can be calculated analytically or found from a pie chart. For analytical calculation, we will use the formulas that are used in determining the nominal values of $r_1, I_1, S, \cos\varphi$ using these formulas, we calculate the values for $0.25P_2$; $0.5P_2$; $0.75P_2$; $1.25P_2$, which we are interested in. İt is necessary to take into account the fact that when calculating additional losses, efficiency values are conditionally taken. The result of the calculation is entered in Tables 1 and 2.

Table 1. Calculation result for 2p=8 characteristics

Conventions	Output power in fractions of the nominal				
	0.25 P_2	0.5 P_2	0.75 P_2	1.0 P_2	1.25 P_2
P_2, kW	3.25	6.5	9.75	13	16.25
I_1, A	7.9	10	12.9	16.1	20.5
cos φ	0.44	0.65	0.75	0.82	0.81
η, p.u.	0.809	0.864	0.870	0.862	0.840

Table 2. Calculation result for 2p=4 characteristics

Conventions	Output power in fractions of the nominal				
	0.25 P_2	0.5 P_2	0.75 P_2	1.0 P_2	1.25 P_2
P_2, kW	4.5	9	13.5	18	22.5
I_1, A	9.7	16.6	24.4	33.2	43.4
cos φ	0.81	0.90	0.93	0.94	0.92
η, p.u.	0.858	0.894	0.893	0.879	0.855

NOMENCLATURES

1. Acronyms

WEI Wind Electric Installation
TSAG Two-Speed Asynchronous Generator
PPCS Pulse-Phase Control System

2. Symbols / Parameters

I_l : The line current value
I_p : The phase current value
M : The moment
P_1 : The value of the power supplied to the machine
P_2 : The value of useful power
S : The full power
n_2 : The rotation frequency
$\cos\varphi$: The power coefficient
η : The efficiency
I_1 : The stator current
U_l : The line voltage
I_{l1} : The line current value of lower rotation frequency
I_{l2} : The line current value of higher rotation frequency
U_n : The nominal voltage
Q : The reactive power

REFERENCES

[1] V.N. Konstantinov, R.S. Abdrakhmanov, "The Choice of Wind Turbines and Evaluation of Their Performance, News of Higher Educational Institutions", Energy Problems, No. 11-12, pp. 48-52, Russia, 2005.
[2] V.V. Shevchenko, Y.R. Kulish, "Analysis of the Possibility of Using Different Types of Generators for Wind Power Plants, Taking into Account the Power Range", Bulletin of NTU, No. 65, pp. 107-117, Russia, 2013.
[3] N.W. Miller, "Frequency Responsive Wind Plant Controls: Impacts on Grid Performance", IEEE Power and Energy Society General Meeting, pp. 1-8, France, 2011.
[4] https://studopedia.su/6_16950_Speed-regulation-of-AM-by-changing-number-of-pole-pairs.html.
[5] W. Cao, Y. Xie, Z. Tan, "Wind Turbine Generator Technologies", INTECH Open Science/Open Minds, p. 44, China, 2012.
[6] A.I. Abdulkadyrov, S.C. Osmanov, N.A. Aliyev, G.A. Aliyeva, "Features of Calculating the Parameters of Special Electric Machines", News of Azerbaijan Higher Technical Schools, No. 5, Issue 87, pp. 55-61, Baku, Azerbaijan, 2013.
[7] J. Mauricio, A. Marano, A. Exposito, J. Ramos, "Frequency Regulation Contribution through Variable Speed wind Energy Conversion Systems", IEEE Trans. Power Systems, Vol. 24, No. 1, pp. 173-180, France, February 2009.

BIOGRAPHIES

Abdulla Ilyas Abdulkadyrov was born in Akhti, Dagestan, Russia on March 26, 1942. In 1962, he graduated from Baku secondary school No. 229 with a gold medal. In 1962-1967, he studied at Azerbaijan Technical University, Baku, Azerbaijan on the specialty "Automation and complex mechanization of the metallurgical industry" (diploma of honors) and received an engineer-electromechanical degree. In 1967-1982, he worked as an engineer, senior engineer, junior researcher and senior researcher at ASRPRE Institute. After passing the competition in 1982, he was appointed to the position of Associate Professor at AOCU, and in 1999, to the position of Professor. So far, he is the author of more than 100 scientific works and more than 10 books. He supervised more than 200 bachelor's and 20 master's studies. He received the state awards, honorary titles: 1) "Inventor of the USSR", 2) Jubilee Medal of the Republic of Azerbaijan. Currently, he works as a Professor at the Department of "Electromechanics" of the Faculty of Energy of Azerbaijan State Oil and Industry University, Baku, Azerbaijan.

Nijat Sabahaddin Mammadov was born in St. Petersburg, Russian on February 23, 1998. In 2003-2015, he received his secondary education at secondary school number 242 of Nizami, Baku, Azerbaijan. In 2015-2019, he received the Bachelor's degree in "Electrical Engineering" from the Electromechanics Department, Azerbaijan State Oil and Industry University, Baku, Azerbaijan. In 2019, he was admitted to the Master's level of the same university. He graduated with honors in 2021. Currently, he is working as a senior laboratory technician at Electromechanics Department, Faculty of Energy of the same university.

Gulnara Alakber Aliyeva was born in Baku, Azerbaijan on August 8, 1974. In 1991, he graduated from secondary school No. 187, Baku, Azerbaijan. In 1992-1996, he received her higher education in "Electrical Engineering" from Energy Faculty, Azerbaijan State Oil Academy (Azerbaijan State Oil and Industry University), Baku, Azerbaijan. Currently, he is working as a senior laboratory technician at Electromechanics, Department, Faculty of Energy of the same university.

The 18th International Conference on
"Technical and Physical Problems of Engineering"
30 October 2022
International Organization of IOTPE

ICTPE Conference
www.iotpe.com
ictpe@iotpe.com
ictpe0@gmail.com

ICTPE-2022 Number 05 Code 01PES05 Pages 21-26

ASSESSING SEQUENCE OF DISTRIBUTION PROBABILITY OF VOLTAGE STABILITY IN A POWER SYSTEM WITH A LARGE SHARE OF RENEWABLE SOURCES INTEGRATION WITH VARIABLE POWER

A.M. Hashimov [1] N.R. Rahmanov [2] A.Z. Mahmudova [2] J.M.B. Morillo [3]

1. Azerenerji JSC, Baku, Azerbaijan, ahashimov@azerenerji.gov.az
2. Azerbaijan Scientific Research and Design Prospecting Power Engineering Institute, Baku, Azerbaijan, ard.nariman@gmail.com, aynur.mahmudova25@gmail.com
3. BRIPCO Engineering and Service, Caracas, Venezuela, julianabricenomorillo@gmail.com

Abstract- The traditional energy infrastructure has been gradually transformed into a modernized framework with a more widespread generation, thanks to the ongoing advancements in renewable energy and microgrid technologies. Since huge amounts of inertia cannot be physically produced by renewable energy source-based systems, these systems require more sophisticated stability considerations. Appropriate explanatory approaches are consequently required for the voltage stability study of renewable-dominated power networks, which contain numerous wind turbines, PV panels, and distributed energy sources. The approach for probabilistically determining the voltage stability limit in a power system that incorporates distributed generation systems with renewable sources and variable generation is suggested in the article. The method is based on repeated solutions of the equations of the constant regimes of the system for a number of random choices of wind power capacities determined as a set of values of its fluctuations corresponding to the average value of wind speed. The process itself of determining the limit of the initial data of the power generation is implemented in the form of a method of sequential loading of the regime according to the P-V function where voltage limit corresponding to the maximum power transfer through the controlled part of the power system network. Modelling on IEEE test diagrams and diagrams of a real power system appeared that the suggested strategy can be utilized to unravel the issues of operational control of the system mode during the characteristic hours of power generation. The obtained estimates of stress limit values for wind speed fluctuations relative to each average wind speed value (determined based on a large number of observations over a long period) make it possible to assess the risks of violation of voltage stability in the system depending on its state (normal circuit, shutdown of its main elements - generators, lines) and the speed of the wind.

Keywords: Wind Power, Variable Generation, Voltage Stability.

1. INTRODUCTION

The development of renewable sources with variable generation, such as wind and solar power plants, creates problems in the central energy system due to the stochastic power generation. These changes in the system require the use of new approaches in managing the power system mode, assessing its normal and critical states. Right now, different approaches are being utilized for the stability analysis of the electric power system, which are widely used in power systems with traditional sources. In studies to determine the limiting regimes, equations are proposed to estimate these regimes by classical methods for identification of the limits of static stability. A large number of works are devoted, including [1], [2] the authors consider the issues of forecasting the stability of a system with a huge share of integrated wind generation. In association with the transformation of the electric power industry, which involves the integration into the power system of a significant proportion of wind and solar PV stations implemented both through distribution PV microsystems and individual PV microsystems, the problem of estimating the stability limit of the system becomes the most relevant. In this regard, the challenge of creating digital models for quick margin determination of static stability of an electric power system with distributed generation networks designed for the dominant use of renewable sources is of great importance. This paper presents one of the possible approaches for stochastic estimation of the limits of voltage stability in a system with developed power generation from wind farms.

This paper's goal is to carry out a voltage stability analysis using an iterative control framework package, to assess the effect of deliberately set wind generators on dispersion frameworks with regard to the basic voltage varieties and collapse edges. This paper concludes with the discussion about criticality points change based on different wind speed and wind power generation.

2. METHODOLOGY

The power flow, voltage profile, and control quality for consumers and power suppliers can all be significantly impacted by wind generators. Recently, there has been a rapid global advancement in the production of wind energy. A significant amount of wind power is entering the power system as wind farms and turbine estimates are growing quickly. The impact of wind turbines on the control quality and voltage stability is becoming more and more important as wind power penetration into the network increases quickly. Because of the erratic nature of the wind and the characteristics of wind turbines, it is widely recognized that a significant increase in the amount of wind power entering a power system may result in serious problems [3].

Power quality problems can become a major concern in smaller facilities connected to flimsy electric grids like medium voltage distribution networks because of the proximity of the generators to the loads. One of the most important power quality issues in distribution networks is the existence of voltage dips. According to estimates, between 75 and 95 percent of industrial sector claims to electric distribution firms in developed nations are connected to issues brought on by this kind of disturbance. Many electrical loads are not built to continue functioning normally after a voltage drop, which causes several problems [3].

Method of Continuation Load Flow study was carried out using the P-V and V-Q Curves. By continuously updating the load flow equation and computing the load flow equation, the convergence issue close to the stable operation limit point can be resolved, and the voltage stability limit may be attained. Additionally, the estimated voltage breakdown point is rounded by the continual prediction and correction procedure. A series of load flow results can be obtained by running the microgrids while altering the load value P or Q of the chosen bus while maintaining the other parameter values. The voltage collapse point, or the boundary between stable and unstable conditions, is the point at which the load flow algorithm fails to converge. In order to conduct the simulation ETAP Software version 19.5.0 has been used.

2.1. Study Area

As a reasonably windy and sunny country with abundant hydro, biomass, and geothermal resources, Azerbaijan offers a considerable untapped potential for renewable energy. The Khizi district in Azerbaijan is chosen in order to use the collected data that are relevant to that location in the proposed method. It is in the country's east and is a part of the Absheron-Khizi Economic Region. Khizi were selected due to the wind potential at these areas and possible construction and operations synergies. According to the information collected from GWA platform, the average annual wind speed in the area reaches 6 m/s.

2.2. Test Scheme

For this study IEEE-30 bus test scheme has been used. The scheme has been selected based on its structural similarities with the selected area electric power system network. The IEEE 30-bus test system has 30 buses, 6 generators, and 6 transformers and 300 MW total demand. The 30-bus test scenario does not have line restrictions, which is important to note. The model places these buses at either 132 or 33 kV. To conduct the study the microgrid with 4 number of wind turbines has been integrated to the scheme.

2.3. Wind Turbine Parameters

The characteristics of the wind turbines selected for installation in the scheme are shown in Table 1. The link between wind speed and the electrical output generated by the selected wind turbine is also shown in Figure 1. There are three stages that need to be discussed, it is obvious. When the wind speed is between 4 and 13.5 m/s, stage 1 begins. When the wind speed fluctuates between the rated (13.5 m/s) and the cutoff speed (25 m/s), stage 2 is reached. When the wind speed reaches the (25 m/s) cut off speed or higher, stage 3 is finally reached.

Table 1. Wind Turbine general specifications

Category	Specification
Rated Power	2 MW
Number of Blades	3
Rotor Diameter	54.4 m
Cut-in Wind Speed	4 m/s
Rated Wind Speed	13.5 m/s
Hub Height	70 m
Cut-out Wind Speed	25 m/s

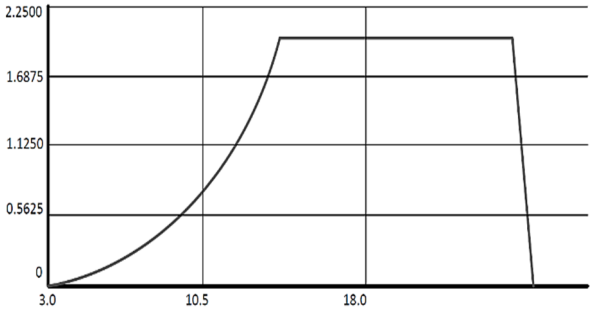

Figure 1. Wind turbine power curve

3. WIND SPEED DATA

The collection and visualization of important wind data was completed after the scheme was structured. For each time step of the year, a one-year time series of average wind speed in meters per second serves as the baseline data. The monthly averages, hourly data, and real data per 100 minutes are displayed in Figures 2, 3, and 4. For more precise wind generation modeling, high resolution (200 meter) data inputs can be found in the Typical Year Virtual Met Mast (TY-VMM) data set.

During the study it has been also investigated the method of generating data for the modeling when the real data is not available. It has been identified that the best method to do this is to use Monte-Carlo modeling to generate the numbers close to the possible wind speed data [4]. Monte Carlo simulation is a powerful statistical analysis tool that is widely used in engineering fields to assess the likelihood of energy system failure.

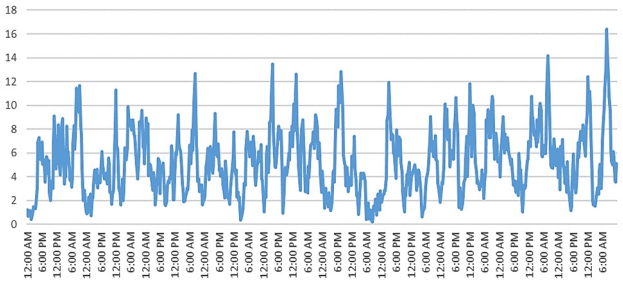

Figure 2. Hourly wind data per month (April)

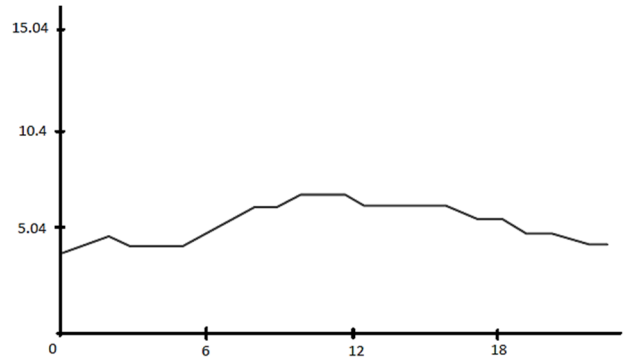

Figure 3. Monthly average wind speed (April)

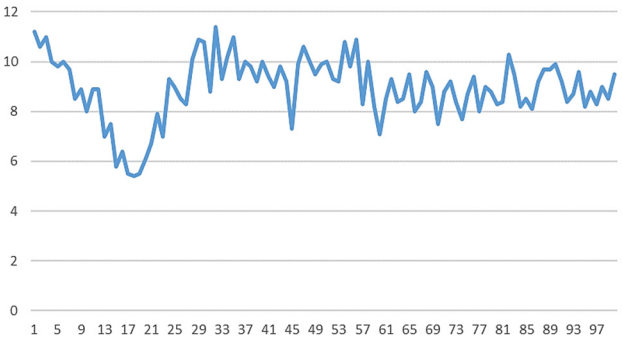

Figure 4. Real data for 100 minutes for a curtain period

This simulation uses random sampling and a large number of computer experiments to display the statistical characteristics of the model outputs to their distributions [5]:

$$x_i = F_x^{-1}\left(u_i\right)\frac{\partial^2\Omega}{\partial v^2} \quad (1)$$

$$\ln x = \lambda_x + \zeta_x \phi^{-1}\left(u_i\right) \quad (2)$$

$$u_i = \phi\left(\frac{\ln\left(X_i - \lambda_x\right)}{\zeta_x}\right) \quad (3)$$

$$x_i = \exp\left(\lambda_x + \zeta_x \phi^{-1}(u_i)\right) \quad (4)$$

where, u_i is random number (0 and 1), and where λ_x and ζ_x are the two parameters of the lognormal distribution. Any random number distribution can be produced by a computer program. In fact, there are numerous computer programs that can produce random numbers for frequently used distributions. The equations given from (1) to (4) can be used to produce a specific distribution if the computer is unable to do so [5].

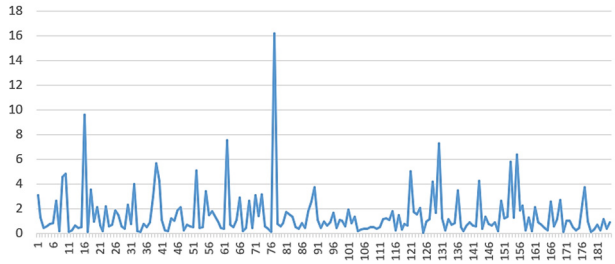

Figure 5. Lognormal variables for Monte-Carlo simulation

4. ALGORITHM OF CALCULATION

Below is the calculation algorithm of the study:

- For real minute measurements of wind speed in a certain period, build the probability distribution. Figure 6 shows the probability density functions for the sample variable from 1 to 25. The function applied to the 100 minutes real data measurements.

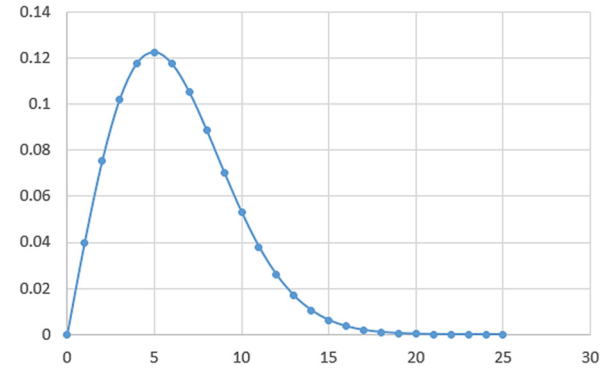

Figure 6. Probability density function (shape factor k=2)

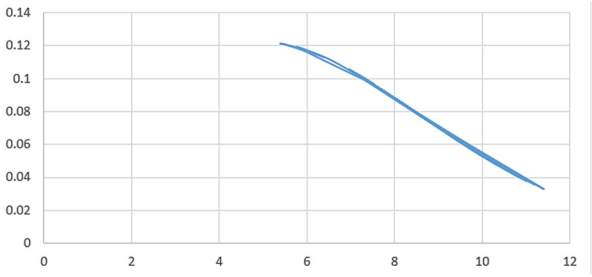

Figure 7. Probability density function for real data

By applying Weibull formula on the data, the most probable wind speed data has been identified. Figure 7, shows that the 5.5 m/s and 6 m/s is the mostly repeated wind speed of the area. The 8-10 m/s is also characteristic to the area, more than 12 m/s is less probable between these 100 minutes of data.

The quantity known as the Weibull k value, also known as the Weibull form factor, represents the width of a distribution of wind speeds. Lower k values are associated with wider distributions of wind speed, demonstrating that winds typically vary over a large speed range. The k number refers to the shape of that distribution. As, k values rise, wind speeds tend to remain within a small range. As a result, a region with strong winds may have a Weibull k value as low as 1.5, whereas a site with strong winds that are relatively constant (such tropical trade wind

conditions) may have a *k* value as high as 3 or 4. We utilize a default Weibull *k* value of 2, which is typical for many

- In the absence of sufficient data on wind speed measurements, they can be simulated using the Monte Carlo method.
- For the most probable interval of repetition of wind speeds, construct the distribution of power generation of wind farms. Figure 8 corresponds to the Figure 6, whereas Figure 8 corresponds to Figure 7 probability function.

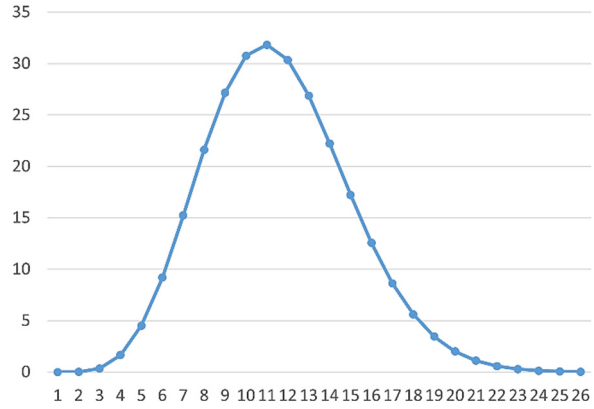

Figure 8. Power density curve based of Figure 6 variables

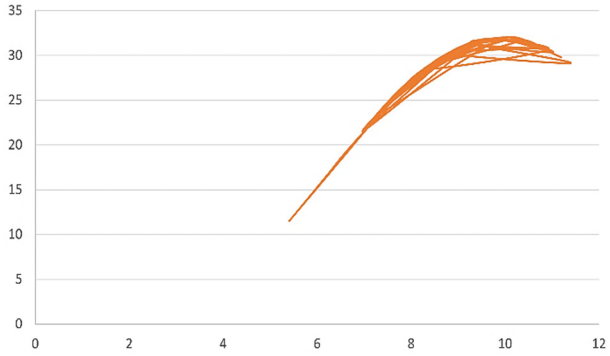

Figure 9. Power density function curve of Figure 7 variables

- For the values of wind speed on 5, ,10, 14 m/s and corresponding power generation, we carry out calculations of the limit of static voltage stability. Several number of wind speed values are considered around the shown numbers. This is due to intermittent and fluctuating character of the wind speed.
- We use the method of maximum network load limit according to the Continuation load flow
- The power of the wind farm is set by the value of the highest output
- A series of calculations of the power load flow is carried out for the load values in the system from the one specified from the daily schedule to those values at which P in one of the transmission lines does not reach the maximum.
- Generate curves P-V and Q-V curves.

5. RESULTS AND DISCUSSIONS

Several load flow analyses were performed beginning with the operational point to obtain the *P-V* curve and *Q-V* curves for wind speeds of 5, 10, and 14 m/s at the power distribution system's common bus.

We obtained a steady-state stability analysis of the system using these simulations. To show each plot, the results were summarized in Figure 10.

It is important to note that as the wind speed and active power of the load increase, so does the current, resulting in higher voltage drops at the cables and an increase in the critical point of the curves (where the system becomes unstable). It can be seen that when the load demand increases, the voltage drops rapidly at the "knee" of the PV curve. Beyond this point, load flow solutions do not converge, indicating that the system has become unstable [6]. When the wind speed reaches 5 m/s, the system reaches a tipping point, with an additional 178 MW load demand and a 26% voltage drop. When the wind speed reaches 10 m/s, the system reaches a critical point, with an additional 175 MW load demand and a 30% voltage drop. When the wind speed reaches 14 m/s, the system reaches a critical point, with an additional 106 MW load demand and a 52% voltage drop. The critical point varies within the area shown in elliptic form. If we combine the critical points with one line we can get the trend of critical points. To show its difference for each wind speed and wind power generation accordingly.

When the wind speed is 14 m/s, the system is less stable in terms of reactive power variation Figure 11 this wind speed is less likely in the study area. Wind speeds of 5-10 m/s, on the other hand, are very typical for the area. Voltage stability is determined by how changes in *Q* and *P* affect the voltages at the load buses. The influence of a device's reactive power characteristics is more obvious in a *QV* connection. It illustrates how bus voltages are sensitive to reactive power injections or absorptions and how they might vary. In typical operation, a rise in *Q* leads to a rise in voltage. Therefore, if the operating point is on the right side of the curve, the system is said to be stable. On the other hand, the functioning points on the left of the graph are thought to be unstable [4, 5].

6. CONCLUSION

The paper presented a method for determining the maximum permissible load in a distribution power system's common bus is presented. The presence of wind power is taken into account in order to assess the impact of this generation on voltage operation and voltage stability limits. For each wind speed and power generation, the voltage stability limit region and a sub-region in which the voltages at the bus are within acceptable ranges are defined. In actual use, the *PQ* curves can be used to identify a system bus's ability to handle an increase in load demand. Of course, the safe voltage limitations must be established in order to satisfy the new demand.

The study concept or design, data collection, analysis, or interpretation for the article, critical revision of the article for significant intellectual content, and approval of the final version for publication have all been significantly influenced by the authors. The authors also contribute in the idea and design of the analysis, data gathering and visualization, resource inquiry, and data curation and then performed the simulation, produced insightful research reports, and contributed to the intellectual and visual aspects of the work.

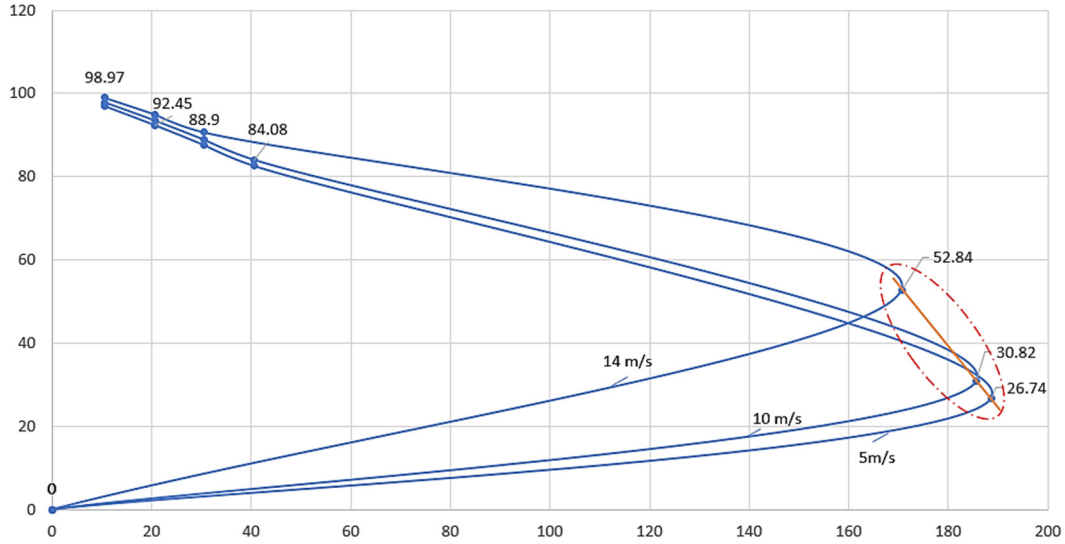

Figure 10. *P-V* curves for 5, 10 and 14 m/s wind speeds

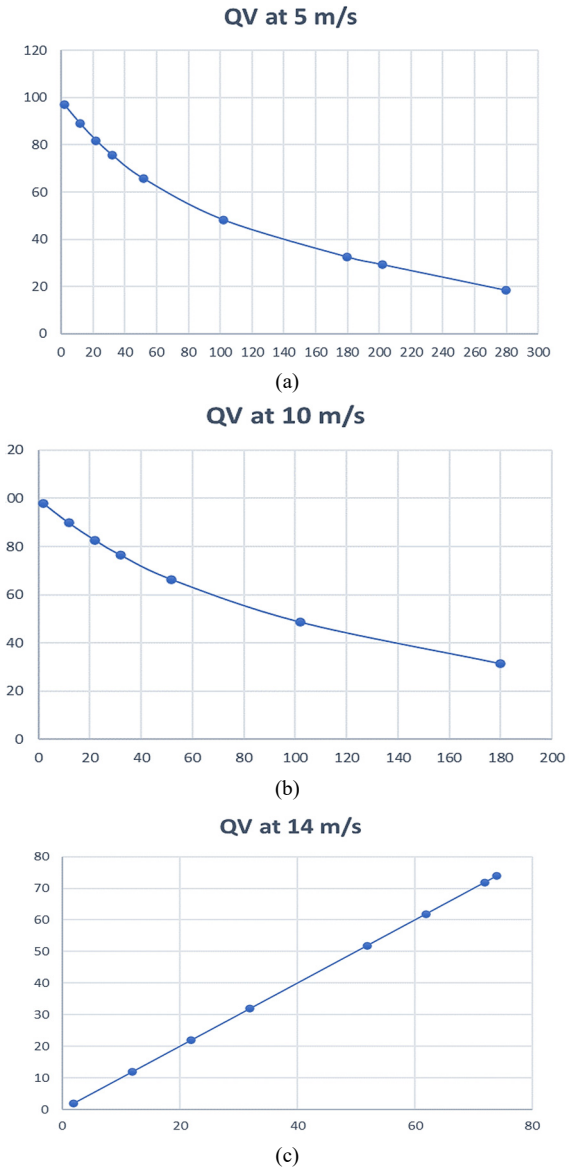

Figure 11. *V-Q* Curves for 5, 10 and 14 m/s wind speeds
(a) Wind speed 5 m/s, (b) Wind speed 10 m/s, (c) Wind speed 14 m/s

REFERENCES

[1] X. Liang, H. Chai, J. Ravishankar, "Analytical Methods of Voltage Stability in Renewable Dominated Power Systems: A Review", Electricity, Issue 1, Vol. 3, pp. 75-107, February 2022.

[2] X. Wu, Z. Yibin, A. Arulampalam, N. Jenkins, "Electrical Stability of Large-Scale Integration of Micro Generation into Low Voltage Grids", International Journal of Electronics, Issue 1, Vol. 4, pp. 1-23, January 2005.

[3] L.N. Tung, "Voltage Stability Analysis of Grids Connected Wind Generators", The 4th IEEE Conference on Industrial Electronics and Applications, June 2009.

[4] R. Gallagher, A.C. Elmore, "Monte Carlo Simulations of Wind Speed Data", Wind Engineering, Vol 33, No. 6, pp 661-673, 2009.

[5] K. Abdusamad, "Wind Energy Reliability Analysis based on Monte Carlo Simulation Method", The First Conference for Engineering Sciences and Technology (CEST-2018), Vol. 2, pp 4-16, September, 2018.

[6] Y. Bulatov, A. Kryukov, V. Senko, K. Suslov, D. Sidorov, "A Stochastic Model for Determining Static Stability Margins in Electric Power Systems", Computation, Vol. 10, No. 67, 2022.

BIOGRAPHIES

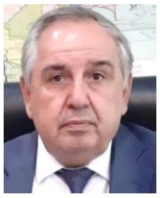

Arif Mamed Hashimov was born in Shahbuz, Nakhchivan, Azerbaijan on September 28, 1949. He is a Professor of Power Engineering (1993); Chief Editor of Scientific Journal of "Power Engineering Problems" from 2000; Director of Institute of Physics of Azerbaijan National Academy of Sciences (Baku, Azerbaijan) from 2002 up to 2009; and Academician and the First Vice-President of Azerbaijan National Academy of Sciences from 2007 up to 2013; and Director of Azerbaijan Research Institute of Energetics and Energy Design from 2014 up to 2020. He is laureate of Azerbaijan

State Prize (1978); Honored Scientist of Azerbaijan (2005); Cochairman of International Conferences on "Technical and Physical Problems of Power Engineering" (ICTPE) and Editor in Chief of International Journal on "Technical and Physical Problems of Engineering" (IJTPE). Now he is a High Consultant in "Azerenerji" JSC, Baku, Azerbaijan. His research areas are theory of non-linear electrical Networks with distributed parameters, neutral earthing and ferroresonant processes, alternative energy sources, high voltage physics and techniques, electrical physics. His publications are 350 articles and patents and 5 monographs.

Nariman Rahman Rahmanov was born in Baku, Azerbaijan on October 29, 1937. He received the M.Sc. and Ph.D. degrees from Azerbaijan institute of Oil and Chemistry (Baku, Azerbaijan) in 1960 and 1968, respectively. He received the Doctor of Technical Sciences in Power Engineering from the Novosibirsk Electro Technical Institute (Russia) in 1990. He is a professor since 1990 and Director of Azerbaijan Power Research Institute of Energy and Energy Design (2007- 2009), and Deputy Director of this institute. He is also a Director of Azerbaijan-Norway Cleaner Production and Energy Efficiency Center, member of IEEE, Co-chairman of International Conference on "Technical and Physical Problems of Engineering", member of Editorial Board on International Journal on "Technical and Physical Problems of Engineering" (IJTPE). His research areas are power systems operation and control, distributed systems, alternative energy sources. He has more than 210 articles, patents and tree monographs.

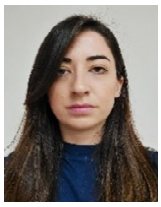

Aynur Zakir Mahmudova was born in Baku, Azerbaijan on January 25, 1991. She graduated as B.Sc. and M.Sc. degrees in electrical engineering. from Azerbaijan State Oil Academy, Baku, Azerbaijan in 2014. Currently, she is a Ph.D. candidate in Azerbaijan Scientific-Research and Design-Prospecting Power Engineering Institute, Baku, Azerbaijan. She is a member of IEEE PES, IAENG, ESOF and Energy Institute. She is working as an Electrical Coordinator within Shah-Deniz-2, CGLP and ACE projects in international oil and gas company. She has participated in the ICTPE and WCE conferences held in different countries. She was a Star Ambassador of IEEE PES YP Powering the Future Summit-2021. She is also a member of Scientific Council working group on Alternative and Renewable energy sources under Azerbaijan National Academy of Sciences, Baku, Azerbaijan.

Juliana Maria Briceno Morillo was born in Maracaibo, Zulia, Venezuela on November 10, 1999. She graduated as Bachelor of Electrical Engineering from University of Rafael Urdaneta, Maracaibo, Venezuela in 2021. She is the member of IEEE Young Professionals, IEEE Industry Applications Society, IEEE Power & Energy Society, IEEE SIGHT and Smart Grid Community. Currently, she is working as Junior Electrical Engineer at BRIPCO Engineering and Service, Caracas, Venezuela carrying out electrical studies of Protection Schemes for Renewable Resources. She is also an Ambassador at IEEE PES YP Powering Future Summit-2021 and IEEE PES YP Humanitarian Activities Liaison-2022.

The 18th International Conference on
"Technical and Physical Problems of Engineering"
30 October 2022
International Organization of IOTPE

ICTPE Conference
www.iotpe.com
ictpe@iotpe.com
ictpe0@gmail.com

ICTPE-2022 Number 06 Code 01PES06 Pages 27-32

AC/DC AND HYBRID MICROGRID CONTROL TECHNIQUES: A REVIEW

S.N. Tackie

Department of Electrical and Electronic Engineering, Near East University, Nicosia, Northern Cyprus
samuel.niitackie@neu.edu.tr

Abstract- Application of renewable energy sources for electric power generation have seen an upward trend in recent year; solar, wind and hydro based power plants lead the pack of renewable energy sources. This has led to renewed research interest and utilization of microgrids. In general, microgrids provides more advantages when compared to microgrids (centralized electric grid), some of these merits are enhanced efficiency, suitable for renewable energy sources which are clean energy, low cost, improves economic growth, provides electric power for hard-to-reach areas, eliminates or reduces transmission losses. Economically it's efficient to cite power generating units close to the consumer. As microgrids continue to evolve, its smooth control has also become a concern. The focus of this paper is to review control techniques for microgrids i.e., dc microgrid, ac microgrid and hybrid microgrids. This review will expose the advantages, disadvantages and implementation challenges of existing control techniques. Selection of appropriate control technique can best be done by comparative analysis focusing on system response to faults, smooth integration of various distributed generation, communication between components, system protection, and whether smart grid or not.

Keywords: Renewable Energy, Control Techniques, DC Microgrid, AC Microgrid, Hybrid Microgrid, Distributed Generation.

1. INTRODUCTION

The demand for energy in the past few years has increased drastically, this can be attributed to population explosion, digitization and industrialization of most economies and improved living standards. Consequently, most conventional power systems are bedeviled with these drawbacks; increased and stretched generation periods, overage systems and less efficient systems and huge transmission losses. Also, majority of these power systems rely on fossil fuels for power generation [1]. Currently, most electric power systems are composed of complex structures such as generating stations, transmission lines and distribution systems. This increases the cost of power system installation and electric power generation, reduce efficiency and also pollutes the environments because of the use of fossil fuels. To address the above problems associated with complex electric power systems, smaller power systems popularly known as distributed generation systems (DGs) have been developed. Distributed generation systems (DGs) are commonly associated with microgrids and renewable energy sources (RES). Grid integration of RES such as PV, wind, hydro etc. together with DGs happen at the distribution level [2].

Although the penetration of DGs in power systems is not on the high side especially in Africa and other third world countries, they will soon phase out complex electric power system because of the numerus benefits they present [3]. Distributed generation system utilizes RES such as PV system, micro turbines, wind generators and mini hydro stations to produce electric power. Power electric converters are required to appropriately condition the generated power for onward transfer to microgrids or national grids. Therefore, power electronic converters are critical devices required for efficient implementation of microgrids [4-5]. Per the type of voltage or power conditioning required, power electronic converters are categorized into four groups; rectifiers (ac-dc conditioning), inverters (dc-ac conditioning) choppers (dc-dc conditioning) and cycloconverters (ac-ac conditioning).

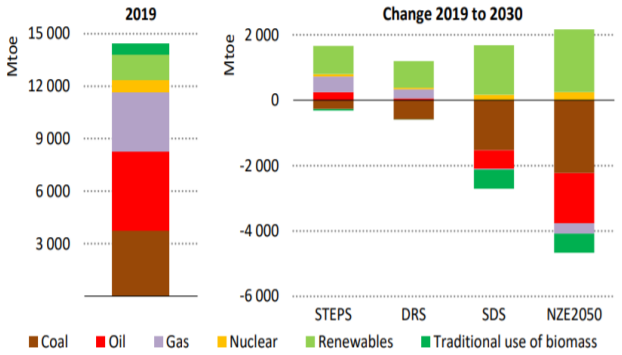

Figure 1. Energy demand and projections from 2019 to 2030 [6]

A microgrid is a small electric power system usually composed a few hundreds of kilometers of transmission lines, generation units, storage systems, control units and loads. Microgrids enable decentralization of power systems, they can be coupled or decoupled from power grids with ease. They therefore boast of the following merits; better power quality, minimized power losses, better system reliability, application of RES and less system cost.

Microgrids can either be a completely dc microgrid, ac microgrid or a hybrid (ac-dc) microgrid. Hybrid microgrid has the advantages of both dc and ac microgrids. Hybrid microgrid is propitious power systems of the future.

RES have become important commodity in the generation of electric power and will soon phase out fossil fuel-based system for electric power generation. Most European countries have set 2030 as the deadline to ban sale of vehicles with combustion engines. Various reports from reputable bodies such as international energy agency (IEA) have shown upward trajectory in the magnitudes of electric power generated from RES. Figure 1 shows a graph of energy (fuel sources) demands for the 2019 and projections from 2019 to 2030. From the graph, it's evident that fossil fuels were the major sources of fuel for the year 2019 to 2022, however, by the end of the year 2030, renewable energy sources will overtake fossil fuel sources as the main source of fuel for electric power generation [6].

The basic topology of the hybrid microgrid is shown in Figure 2, the main components are power electronic converter, dc grid and ac grid. The energy source of a dc microgrid is distributed generations such as PV and wind installations, fuel cells, battery ESS etc. Mostly, the source of generation is DGs. The benefits of microgrids over conventional grids are enormous thus being able to replace it completely at the distribution level [7]. Convectional microgrid response to load disturbances is poor; this pushes the rate of load slew to be restricted to sustain grid stability. On the other hand, microgrids are able to reduce load disturbances, increase power stability and quality by the use of power electronic circuits [8-9]. Due to the importance of microgrids, several researches have been carried out around the world to help solve problems of power quality, stability and efficiency; projects such as CERTS in the USA, the microgrid project in Senegal, Kythnos microgrid in Greece and several other projects in Japan [10].

Investments into DGs construction tend to be higher when compared to conventional power system due the economy-of-scale of the conventional systems. Nonetheless, DGs utility prices tend to be less expensive when compared national grid power prices. Developed countries have instituted hourly prices for electricity; during low price hour, energy can be purchased and stored in batteries and used when prices are high [11].

Hybrid microgrid can be operated in two modes; grid-tied or island modes. A transient transition period occurs during the change in operation mode from either grid-tied to island mode or from island mode to grid-tied. During this transition period, voltage deviations and unbalanced current harmonics are of critical concern to power quality issues. Also, absolute synchronization of phase and voltage between grid-tied and island mode is necessary when switching from island mode to grid-tied [12].

Comprehensive literature research into control methods of dc, ac or hybrid microgrid has revealed a wide variety of control techniques. PI regulators were used by [13] to control microgrids; also [14] used a process known as Optimization-based fuzzy controller incorporated with battery and fly wheel.

Battery technologies control i.e., charging and discharge, storage etc. is proposed by [15-16] and the control of islanded power system using frequency regulation by [27]. Procedures and guidelines are given by [18-19] for optimal battery sizing and efficient battery usage to avoid power fluctuations. [20] Talks about the financial burden of using batteries as storage units. The above control techniques (but not limited to them) can be applied to dc, ac or hybrid microgrid. Our research focus is on hybrid microgrid control. Voltage and frequency (V&F) are the two most easily controlled parameters in a microgrid. Thus, a number of V&F control techniques have been developed. These techniques can be applied in the hybrid microgrid subsystem. In the hybrid microgrid structure, the dc and ac grids are connected by a system of inverters called ILC (interlinking converters). The control strategies for ILC can be based on different methodologies such as communication, droop-based control mechanism [21].

2. STRUCTURE OF MICROGRID

Figure 2 shows a typical structure of a microgrid with power electronic converters. The microgrid is made up of three sources of distributed generations (DG1, DG2 and DG3). The main grid and microgrid are tied together via the PCC (point of common coupling). The static transfer switch (STC), functions as a switch which is able to couple and decouple the microgrid from the main grid usually within half cycle period. An injection transformer is used to stabilize the microgrid power sourced from the main grid or utility. Each DG has ESS and an inverter which inverts dc voltage to ac voltage. To enhance and improve the efficiency of the system, combined heat and power (CHP) unit is also in-cooperated into the supply. The operation of the microgrid can be done in two modes; grid-tied mode or self-sustaining mode which is commonly called islanding mode.

In the grid-tied mode, the utility or main grid provides part of the power together with the DGs. Power is taken from the utility when ESS is completely depleted of energy and during unfavorable weather conditions making RES to under function. CHP plant such as micro-turbine provides power and heat to a close-by load.

On the self-sustaining mode, all power is produced by the DGs and CHP. Due power demand and quality issues, careful calculations are done before installing DGs such that they are able produce the required power at peak loads. When demand exceeds supply, non-critical loads are decoupled or standby gents are powered. Issues of phase angle of voltages and frequencies have to be critical looked at be synchronizing the microgrid and main grid [9].

2.1. Hybrid AC/DC Microgrid Operation

Globally, there's an upsurge in the utilization of renewable energy source and as such distributed generation systems are also gradually becoming the preferred choice. The increase in use of RES and DGs requires innovative ways of control and management; this will make power production, transmission and distribution in microgrids efficient.

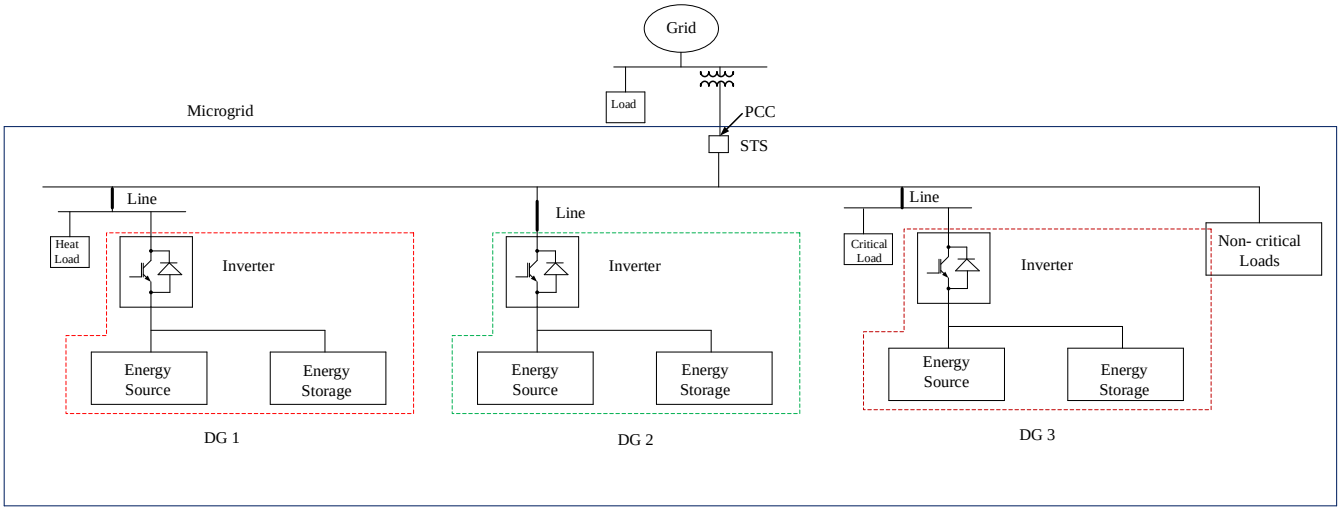

Figure 2. Microgrid structure with multiple DGs

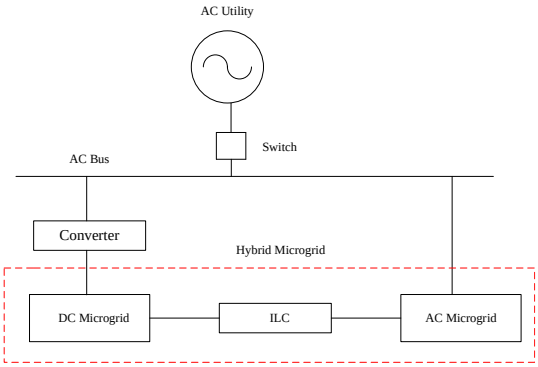

Figure 3. Hybrid microgrid structure

Distributed generation is done on small scale, close to the consumer and to provide the electric power requirements of the consumer. The common components of DGs are photovoltaic power plants, wind farms, energy storage systems, fuel cells and mini-hydro dams. These DG sources when put together constitute a microgrid. Application of RES has tremendous benefits to environment; carbon emissions are reduced thereby minimizing the rate of depletion of the ozone layer. Combining DGs and RES in power generation/microgrid introduces issues of power quality [22]. Figure 3 and Figure 4 shows two structures of hybrid microgrid. Figure 4 shows a hybrid microgrid with power being produced from RES and DGs and also tying the microgrid to utility or main grid, this is beneficial for both the microgrid and utility since power can be transmitted from both ways. In this disposition, the MHP energy and photovoltaic generated power are used efficiently. Thus, the utility becomes backup power as in the case of UPS. In cases where the microgrid cannot provide enough energy to meet the demands of the load, extra power is taken from the grid and when the DGs of the microgrid produces more power than the load needs, the utility absorbs the excess [23]

The hydro and photovoltaic systems are connected to a general direct current bus; this is will reduce the cost of the system, makes it more efficient and thus eliminating complex system structures.

The hybrid microgrid functions as the main power system and the utility acts as a generator to provide power in situations of power shortage in the hybrid system. There are several factors which can account for power deficit in the hybrid microgrid; introduction of new loads, weather conditions in the case of renewable energy sources, system faults etc. in the case of PV system, though power production will be high in summer, system failures/breakdowns will also occur due to high temperatures which is a drawback for semiconductor materials [24].

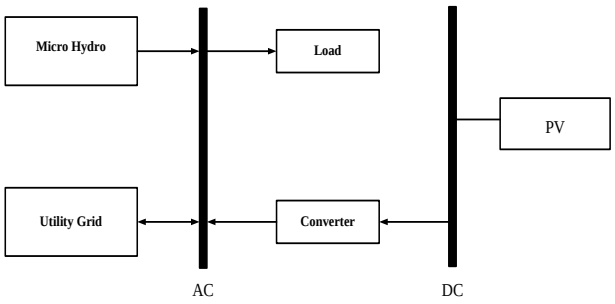

Figure 4. Hybrid microgrid

3. HYBRID MICROGRID OPERATIONS

3.1. Grid-Tied Mode

In the grid-tied mode, the converter should be able to easily switch from ac to dc (rectification) and from dc to ac (inversion), this process also helps in providing or controlling the reactive power. The dc – dc converter maintains the maximum power of the grid. Excess power produced in the microgrid is fed into the main grid. Also with good ESS, excess power can be stored; this methodology is an added cost and not really required since the grid functions as generating set and a storage unit concurrently. Energy storage system will be more useful in islanded mode; ESS will balance the power and provide a stable voltage (voltage stability) [22]. A small ESS will be more useful in the dc sub-grid of the hybrid system to support dc loads and also reduce losses produced by switching.

3.2. Island Mode

In the island or self-sustaining mode, the hybrid microgrid is not tied to main grid or utility. ESS thus becomes an indispensable part of the system by providing voltage stability and maintaining balanced power in the grid. Depending on the load requirements, Buck-boost converter is used to vary the dc voltage; increase or reduce the supply to loads. High quality and stable ac voltage is provided by controlling the main converter with high quality filters [23].

The nature of hybrid microgrids is a complex one; it involves dc power systems and also ac power systems. The control of dc microgrid is relatively easy when compared to ac microgrids. In dc microgrids, there is no need to provide power control because there is no sudden change in power, phase control is not needed because synchronization does not occur in dc power sources, and frequency control is also not an issue. There are fewer power losses in dc microgrids since only one stage conversion is done; thereby increasing the efficiency of the system. All the above advantages are feasible with RES produced dc power making it relatively easy to tie to dc microgrids [6] [25]. Most control methodologies developed are as a result of the use of ac or hybrid microgrids. The next stage of our research is to review the various control strategies employed in dc, ac or hybrid microgrids. The controls of microgrids are done either at the HV or LV levels, at a switchyard or substation.

4. FREQUENCY AND VOLTAGE DROOP METHOD

A very common method known as 'plug and play' is used to control each DG independently; in this method, the terminal voltage of each DG is controlled by using droop control method including the combination of techniques of

i. Real power vs. frequency (P-ω) and

ii. Reactive power vs. voltage (Q-E)

In this method, the reactive and real power flow in a phase connecting nodes (two) isolated by line impedance. Figure 5 shows the droop control method of real power sharing of microgrids. The two voltage values are denoted E_1 and E_2 and the phase angle of E_1 and E_2 is represented by δ. The line resistance R is ignored for pure inductive line impedance. The line impedance Z, real power P and reactive power Q are computed by Equation (1) to Equation (3) [4].

$$Z = R + jX \tag{1}$$

$$P = \frac{E_1}{R^2 + X^2}\left[R\left(E_1 - E_2\cos\delta\right) + E_2\sin\delta\right] \tag{2}$$

$$Q = \frac{E_1}{R^2 + X^2}\left[-RE_2\sin\delta + X\left(E_1 - E_2\cos\delta\right)\right] \tag{3}$$

4.1. Reactive Power Control Algorithm with Improved Accuracy

The reactive power control algorithm with improved accuracy was introduced to solve the problem associated with reactive power control method. The reactive power control mythology is not precise because of the voltage drop which occurs on line impedances. To solve this problem, we ignore voltage drop across the line and understate the effect of the Q-E droop method [26].

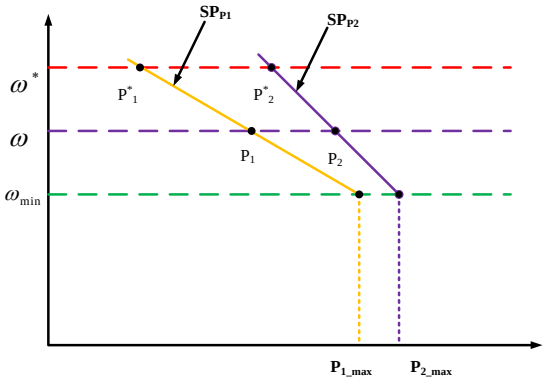

Figure 5. Droop control method of real power sharing

4.2. MG Islanded Control Operation

There are two main scenarios which cause islanded operation of MG; where there's fault in the microgrid and planned maintenance of MG or utility. In this, DG power production and load consumption are made parallel to solve load imbalances in the system. Decoupling MG from utility is done fast to protect loads and this cause microgrid dynamics. In the absence of synchronous machines to stabilize supply and demand via frequency control techniques, switching using inverters are used to control the frequency. The preferred inverter topology is the VSI; voltage source inverter. But this technique only works at the terminals; two other methods which are quick to react to system disturbances are preferred;

a) Single Master Operation: In this method, the voltage source inverter functions as a master and a source to the power supply.

b) Multi-Master Operation: The number voltage source inverters are many and they have an already assigned active power/frequency and reactive power/voltage characteristics.

4.3. Hierarchical Control of Droop Controlled Microgrids

Hierarchical control of droop-controlled hybrid ac-dc microgrid develop a step-by-step control strategy. It applies the top to bottom control method. This idea was borne from ANSI/ISA-95 which is also known as ISA-95; this is a certified international standard control between enterprise and control systems. ISA-95 has six steps multilevel control. The same idea has been established to control MGs. Here, four levels of control strategy have been designed starting from zero;

- Tertiary control (level 3): this is the power/energy production level, and control of energy flow via MG to consumer is done at this level.
- Secondary control (level 2): power quality issues are controlled at this stage. Voltage sag and swell as well other power related problems are controlled or solved.
- Primary control (level 1): this where the actually droop control method is applied. Stability over damped system control is done here.
- Inner control loop (level 0): individual module regulation issues are meshed together at this level. Voltage and current, feed forward and feedback as well as nonlinear

and linear control is done to adjust voltage output value and tune current values although maintaining a stable system. This control strategy can be done in solely ac microgrids, dc microgrids or a hybrid system [3].

4.4. Conventional and Fuzzy-Pi Based Frequency Control

Conventional power system control secondary frequency by the use of proportional integral controllers (PI). The PI operates in a region which is already determined; once the boundary of operation is overcome, the PI becomes obsolete unless it's reprogrammed. [14] uses a popular PI tuning technique called Ziegler-Nichol. Detailed research on PI or PID tuning technique such as Ziegler-Nicholas is presented in [27]. An experimental result is shown by [14] in Table 1 using Ziegler-Nicholas PI tuning technique.

Table 1. Ziegler-Nichols based PI control Magnitude [27]

Controller Parameter	Magnitude
K_p	4.095
K_i	21.84

4.5. Hybrid Mg Control Under Islanding Mode

A new method of controlling hybrid microgrid is proposed by [28], first they control ac grid part separately, and then perform same function for the dc grid after which the hybrid control is done. For the dc control method, two schemes of operation are looked at; central and distributed schemes. In the central control technique, central point of control monitors the whole system and issues commands when necessary, monitoring of various generation sources and distribution system is done via communication devices; this adds extra cost and reduces performance. These disadvantages make the distributed scheme the preferred choice. DC bus signaling (DBS) is the preferred choice of distributed techniques in this paper. In DBS scheme, the bus voltage is considered as the universal index for converter operating levels determination

4.6. Microgrid Control without ESS

The control strategy proposed by [29] is a combination of two factors; power generation control and load control for frequency tuning. The rate of frequency deviation is compared to generation and load frequency variation and the necessary control technique is applied. Artificial neural network (ANN) is applied; the ANN is trained with two target values (voltage); one for maximum power point tracking and the other for 90% power output. With the application of neural network, the system is able predict, detect and offer solutions to help control the frequency of the system.

5. CONCLUSION

Control techniques of microgrids have been reviewed in this paper. Though the principal focus was on control of hybrid microgrid; both dc and ac microgrid control techniques have been investigated. From the conventional droop control method to hierarchical control technique where control is done from the top to bottom approach.

Frequency control was also reviewed and it was established that the use of converters or an inverter enables the application of switching techniques to control the frequency and subsequently provide grid power control.

REFERENCES

[1] O.M. Babatunde, J.L. Munda, Y. Hamam, "A Comprehensive State-of-the-Art Survey on Hybrid Renewable Energy System Operations and Planning", IEEE Access, Vol. 8, pp. 75313-75346, 2020.

[2] X. Gong, F. Dong, M.A. Mohamed, O.M. Abdalla, Z. M. Ali, "A Secured Energy Management Architecture for Smart Hybrid Microgrids Considering PEM-Fuel Cell and Electric Vehicles", IEEE Access, Vol. 8, pp. 47807-47823, 2020.

[3] J.M. Guerrero, J.C. Vasquez, J. Matas, L.G. de Vicuna, M. Castilla, "Hierarchical Control of Droop-Controlled AC and DC Microgrids-A General Approach Toward Standardization", IEEE Trans. Ind. Electron., Vol. 58, No. 1, pp. 158-172, January 2011.

[4] H. Nikkhajoei, R.H. Lasseter, ''Distributed Generation Interface to the CERTS Microgrid", IEEE Trans. Power Del., Vol. 24, No. 3, pp. 1598-1608, July 2009.

[5] N. Hatziargyriou, "Microgrids: Architectures Control", Wiley, Hoboken, NJ, USA, March 2014.

[6] International Energy Agency, "World Energy Outlook 2020, IEA, Licence: Creative Commons Attribution", CC BY-NC-SA 3.0 IGO, 2020.

[7] S. Choe, Y.K. Son, S.K Sul, "Control and Analysis of Engine Governor for Improved Stability of DC Microgrid Against Load Disturbance", IEEE Journal of Emerging and Selected topics in Power Electronics, Vol. 4, No. 4, December 2016.

[8] L. Jian, H. Xue, G. Xu, X. Zhu, D. Zhao, Z.Y. Shao, "Regulated Charging of Plug-in Hybrid Electric Vehicles for Minimizing Load Variance in Household Smart Microgrid", IEEE Trans. Ind. Electron., Vol. 60, No. 8, pp. 3218-3226, August 2013.

[9] Y.W. Li, C.N. Kao, "An Accurate Power Control Strategy for Power Electronics-Interfaced Distributed Generation Units Operating in a Low Voltage Multibus Microgrid", IEEE Trans. Power Electron., Vol. 24, No. 12, pp. 2977-2988, December 2009.

[10] H. Bevrani, F. Habibi, P. Babahajyani, M. Watanabe, Y. Mitani, "Intelligent Frequency Control in an AC Microgrid: Online PSO-Based Fuzzy Tuning Approach", IEEE Transactions on Smart Grid, Vol. 3, No. 4, pp. 1935-1944, December 2012.

[11] H. Lotfi, A. Khodaei, "AC Versus DC Microgrid Planning", IEEE Transactions on Smart Grid, Vol. 8, No. 1, pp. 296-304, January 2017.

[12] S.M. Malik, X. Ai1, Y. Sun, C. Zhengqi1, Z. Shupeng, "Voltage and Frequency Control Strategies of Hybrid AC/DC Microgrid: A Review", IET Gener. Transm. Distrib., Vol. 11, No. 2, pp. 303-313, 2017.

[13] D.J. Lee, L. Wang, "Small-Signal Stability Analysis of an autonomous hybrid renewable energy power Generation/Energy Storage System Part I: Time-Domain Simulations", IEEE Trans. Energy Convers., Vol. 23, No. 1, pp. 311-320, March 2008.

[14] H. Bevrani, F. Habibi, P. Babahajyani, M. Watanabe, Y. Mitani, "Intelligent Frequency Control in an AC Microgrid: Online PSO-Based Fuzzy Tuning Approach", IEEE Trans. Smart Grid, Vol. 3, No. 4, pp. 1935-1944, December 2012.
[15] I. Atzeni, L.G. Ordonez, G. Scutari, D.P. Palomar, J.R. Fonollosa, "Demand-Side Management via Distributed Energy Generation and Storage Optimization", IEEE Trans. Smart Grid, Vol. 4, No. 2, pp. 866-876, June 2013.
[16] D. Kottick, M. Blau, D. Edelstein, "Battery Energy Storage for Frequency Regulation in an Island Power System", IEEE Trans. Energy Convers., Vol. 8, No. 3, pp. 455-459, September 1993.
[17] R. Bhatt, B. Chowdhury, "Grid Frequency and Voltage Support Using PV Systems with Energy Storage", The 43rd North Amer. Power Symp., pp.1-6, Boston, MA, USA, August 2011.
[18] M. Datta, T. Senjyu, A. Yona, T. Funabashi, "Photovoltaic Output Power Fluctuations Smoothing by Selecting Optimal Capacity of Battery for a Photovoltaic-Diesel Hybrid System", Electr. Power Compon. Syst., Vol. 39, No. 7, pp. 621-644, April 2011.
[19] M.R. Aghamohammadi, H. Abdolahinia, "A new Approach for Optimal Sizing of Battery Energy Storage System for Primary Frequency Control of Islanded Microgrid", Int. J. Electr. Power Energy Syst., Vol. 54, pp. 325-333, January 2014.
[20] Z. Xu, X. Guan, Q.S. Jia, J. Wu, D. Wang, S. Chen, "Performance Analysis and Comparison on Energy Storage Devices for Smart Building Energy Management", IEEE Trans. Smart Grid, Vol. 3, No. 4, pp. 2136-2147, December 2012.
[21] P.C. Loh, D. Li, Y.K. Chai, et al, "Autonomous Control of Interlinking Converter with Energy Storage in Hybrid AC-DC Microgrid", IEEE Trans. Ind. Appl., Vol. 49, No. 3, pp. 1374-1382, 2013.
[22] V.Y. Parkavi, R. Vijayalakshmi, et al., "Operation and Control of Hybrid Microgrid", International Journal of Engineering Research and General Science, Vol. 2, No. 6, November 2014.
[23] S. Meshram, G. Agnihotri, S. Gupta, et al., "Modeling of Grid Connected DC Linked Pv/Hydro Hybrid System", AN International Journal (ELELIJ), Vol. 2, pp. 15-20, August 2013.
[24] O.C. Ozerdem, S.N. Tackie, S. Biricik, "Performance Evaluation of Serhatkoy (1.2 MW) PV Power Plant", The 9th International Conference on Electrical and Electronics Engineering (ELECO), pp. 398-402, 2015.
[25] J.M. Guerrero, J.C. Vasquez, R. Teodorescu, "Hierarchical Control of Droop-Controlled DC and AC Microgrids; A General Approach Towards Standardization", Ind. Electron. Conf. (IECON), pp. 4305-4310, November 2009,
[26] J.W. Kim, H.S. Choi, B.H. Cho, "A Novel Droop Method for Converter Parallel Operation", IEEE Trans. Power. Electron., Vol. 17, No. 1, pp. 25-32, January 2002.
[27] H. Bevrani, A. Ghosh, G. Ledwich, "Renewable Energy Sources and Frequency Regulation: Survey and new Perspectives", IET Renew. Power Gener., Vol. 4, pp. 438-457, 2010.
[28] G. Ding, F. Gao, S. Zhang, P.C. Loh, F. Blaabjerg, "Control of Hybrid AC/DC Microgrid under Islanding Operational Conditions", Journal of Modern Power Systems and Clean Energy, Vol. 2, No. 3, pp. 223-232, September 2014.
[29] P.C. Sekhar, S. Mishra, "Storage Free Smart Energy Management for Frequency Control in a Diesel-PV-Fuel Cell-Based Hybrid AC Microgrid", IEEE Transactions on Neural Networks and Learning Systems, Vol. 27, No. 8, pp. 1657-1671, August 2016.

BIOGRAPHY

Samuel Nii Tackie was born in Accra, Ghana in 1988. He graduated from Ho Technical University in 2007 majoring in Electrical and Electronics Engineering. He received his M.Sc. and Ph.D. degrees in Electrical and Electronic Engineering from Near East University, Nicosia, Northern Cyprus in June 2015 and February 2021, respectively. He has been with Department of Electrical and Electronic Engineering, Near East University as a research assistant and a lecturer from 2013 to date. He was promoted to an Assistant Professor in April 2022. His research and teaching interests include power electronics, renewable energy system, power quality and custom power devices.

The 18th International Conference on
"Technical and Physical Problems of Engineering"
30 October 2022
International Organization of IOTPE

ICTPE Conference
www.iotpe.com
ictpe@iotpe.com
ictpe0@gmail.com

ICTPE-2022 Number 07 Code 01PES07 Pages 33-39

L TYPE HALF WAVE MODE ZERO VOLTAGE SWITCHING QUASI RESONANT BOOST CONVERTER FOR PV SYSTEMS

A. Karafil N. Genc

Department of Electrical and Electronics Engineering, Yalova University, Yalova, Turkey
akif.karafil@yalova.edu.tr, naci.genc@yalova.edu.tr

Abstract- High switching loss is one of the most fundamental problems in converters. The occurrence of high switching losses reduces the efficiency of the converters and causes the operating frequency to be low. Zero current switching (ZCS) and/or zero voltage switching (ZVS), which are soft switching techniques, are used to overcome these problems. In this study, a simulation study was carried out in the PSIM program by analyzing L type half wave mode ZVS quasi resonant boost converter with 360 W photovoltaic (PV) panel input power. In the study, maximum power was transferred from the PV panels to the load by using the thinned-out control method.

Keywords: ZVS, Quasi Resonant Boost Converter, MPPT, Thinned-Out Control, PV Systems.

1. INTRODUCTION

The direct conversion of sunlight into electrical energy is provided by PV panels. Depending on the change in solar radiation intensity during the day, the energy obtained from PV panels also changes. In order to extract maximum power from the PV panels, dc-dc converters are widely used as an interface between the PV panel and the load in the system. In order for the dc-dc converter to adapt to changes in the PV panel output power, an appropriate converter topology must be determined. The structure of the converter to be used in the system is determined by the difference between the input voltage obtained from the PV panels and the output voltage of the converter. Conventional dc-dc converters are basically divided into three as boost, buck and buck-boost type [1-5].

The most basic problem encountered in conventional power converters is high switching losses. High switching losses limit the operating frequency of power converters as well as causing low efficiency. In addition, this situation causes the passive circuit elements and the size of the heat sinks to increase; that is, it causes the size of the circuit to increase. All these factors increase the cost of the circuit. Moreover, high values of inrush current and inrush voltage that occur during the switching process cause high-value electromagnetic interference (EMI) noise.

This noise disrupts the signals of all electronic devices operating simultaneously. Soft switching techniques should be used to eliminate all these problems encountered in hard switching [6-8].

In section 2, L type half wave mode ZVS quasi resonant boost converter is analyzed. In section 3, thinned-out controlled MPPT, which is a novel method, is presented. In section 4, simulation results are given and in the last section conclusions obtained in the study are mentioned.

2. ANALYSIS OF L TYPE HALF WAVE MODE ZVS QUASI RESONANT BOOST CONVERTER

2.1. Resonant Switches

Soft switching techniques are generally grouped under two categories as ZCS and ZVS. ZCS is defined as the limitation of the current when the switch is turn-on with the inductor connected in series with the power switch whereas ZVS is a soft switching technique that is achieved by limiting the voltage occurring at the switch ends when the switch is turn-off with a capacitor connected in parallel to the power switch. Figure 1 shows current mode resonant switches, and Figure 2 shows voltage mode resonant switches [9, 10].

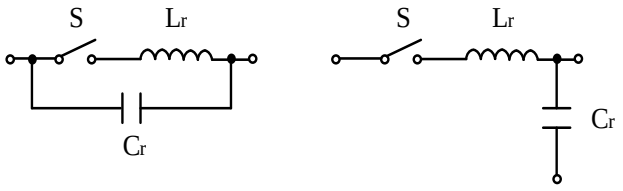

Figure 1. Current mode resonant switches [10]

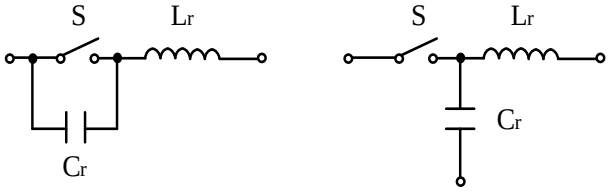

Figure 2. Voltage mode resonant switches [10]

Soft switching conditions are realized with resonant and quasi resonant converter topologies. Quasi resonant converters are obtained when the switch is replaced in conventional converters with one of the resonant switches in Figures 1 and 2. These converters are between conventional converters and resonant converters. A resonant switch consists of a power switch and an inductor and a capacitor, which are resonant elements. Due to the resonant elements, the current or voltage passing through the switch oscillates in the form of a sinusoidal curve, and zero voltage or zero current switching is realized. In general, one of the most important advantages of quasi resonant converters is that high efficiency is provided by the switching element by reducing the conduction loss. In Figure 3, half wave voltage mode resonant switches are presented [11-13].

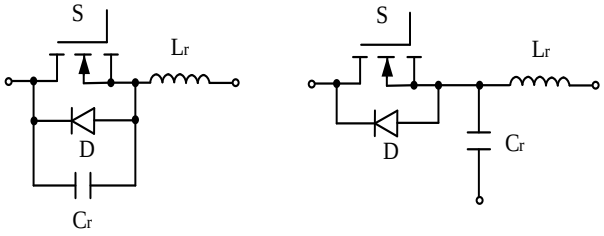

Figure 3. Half wave voltage mode resonant switches [11]

2.2. Modeling of L Type Half Wave Mode ZVS Quasi Resonant Boost Converter

Figure 4 shows the L type half wave mode ZVS quasi resonant boost converter.

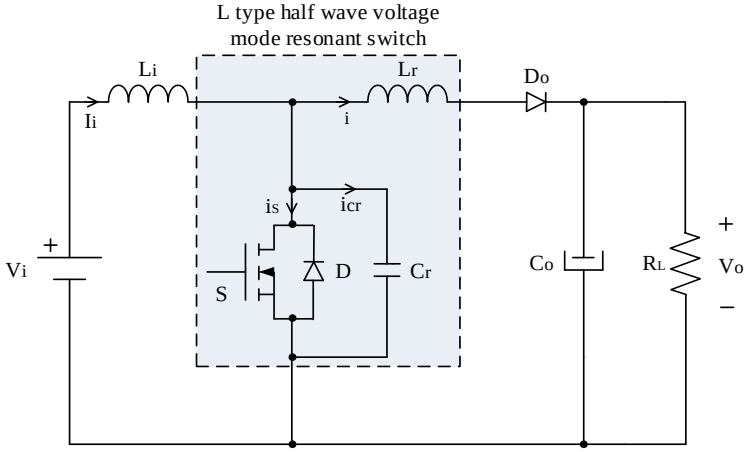

Figure 4. L type half wave mode ZVS quasi resonant boost converter [15]

In order to perform a simple equivalent analysis of the L-type half-wave mode ZVS quasi resonant boost type converter circuit, the L_i inductor value must be much higher than the L_r value of the resonant inductor (L_i>>L_r). Likewise, the C_o output capacitor value should be much higher than the C_r value, which is the resonant capacitor value (C_o>>C_r). In this case, input voltage (V_i) and filter inductor (L_i) can be modeled as constant current source (I_i), and output capacitor (C_o) and load resistor (R_L) can be modeled as constant voltage source (V_o). Under these assumptions, the simple equivalent circuit of the half-wave mode ZVS quasi resonant converter circuit is given in Figure 5 [14, 15].

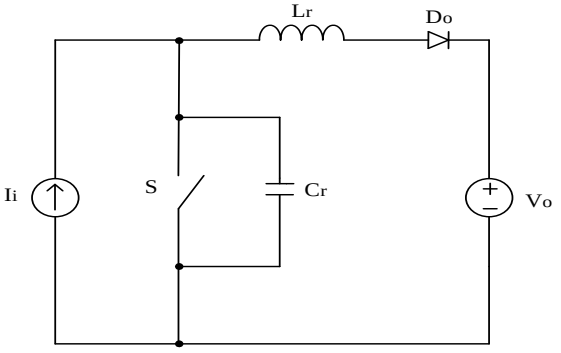

Figure 5. Simple equivalent circuit of half-wave mode ZVS quasi resonant converter circuit [15]

The resonant parameters L_r and C_r values determine the operation and characteristics of the converter. The equations to be used in the analysis of the converter are as follows: voltage conversion ratio (M), characteristic impedance (Z_n), and resonant frequency (f_r) [14].

$$M = \frac{V_o}{V_i} \tag{1}$$

$$Z_n = \sqrt{\frac{L_r}{C_r}} \tag{2}$$

$$f_r = \frac{1}{2\pi\sqrt{L_r C_r}} \tag{3}$$

2.3. Operating States

L type half wave mode ZVS quasi resonant boost converter has four operating ranges depending on the state of the power switch and D_0 diode. The waveforms of the gate-source voltage of the switch (V_{gs}), the voltage of the resonant capacitor (V_{cr}), the current passing through the resonant inductor (i), the current passing through the switch (I_{MOS}) and the current passing through the resonant capacitor (I_{Cr}) related to these time intervals are given in Figure 6 [10].

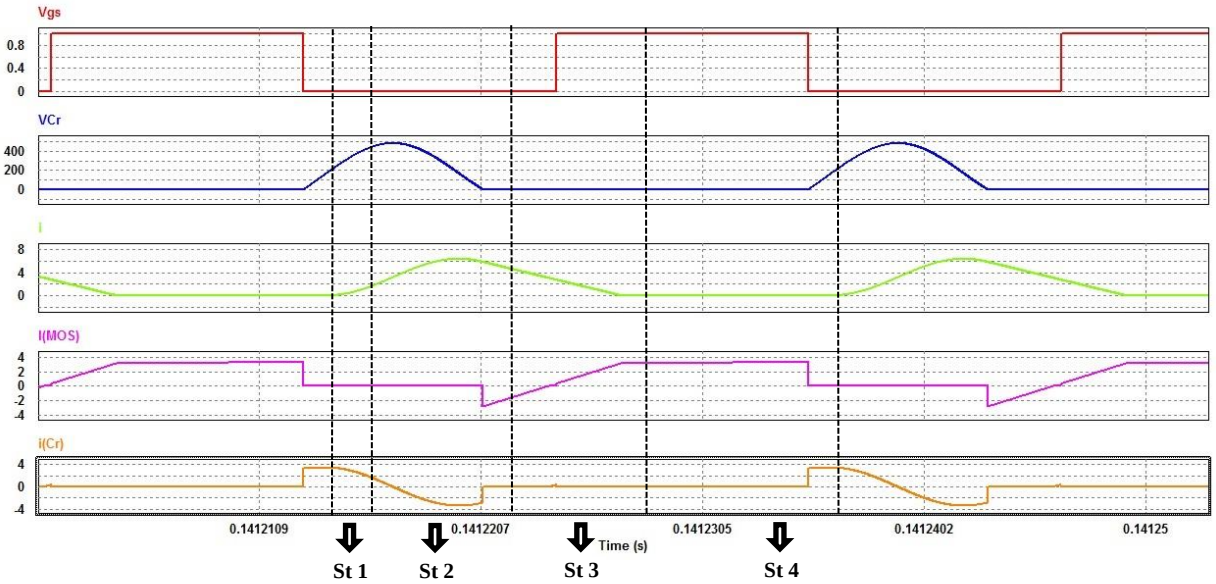

Figure 6. Wave forms of L type half wave mode ZVS quasi resonant boost converter [10]

2.3.1. State 1

This operating state starts when the power switch and diode D_0 are off. The equivalent circuit for State 1 is given in Figure 7. As the resonant capacitor, whose initial value is zero, is charged in this operating range, and the voltage at its terminals increases.

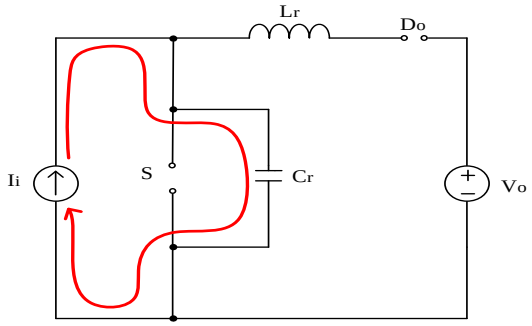

Figure 7. Equivalent circuit of State 1 [10]

2.3.2. State 2

In this operating state, Diode D_0 is on. The inductor and the capacitor work together. In Figure 8, the equivalent circuit for State 2 is presented.

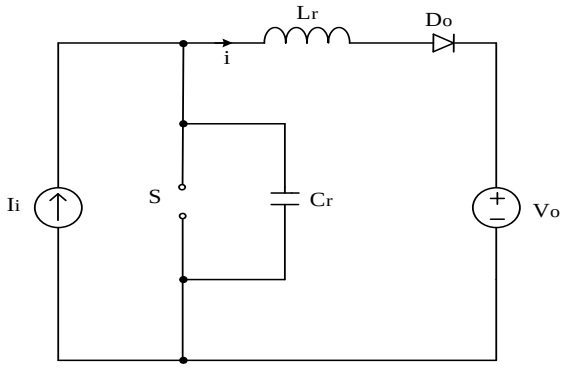

Figure 8. Equivalent circuit of State 2 [10]

2.3.3. State 3

This operating state starts when the capacitor voltage drops to zero. In Figure 9, the equivalent circuit for State 3 is presented. In this operating state, at the end of the period, the inductor current decreases and drops to zero.

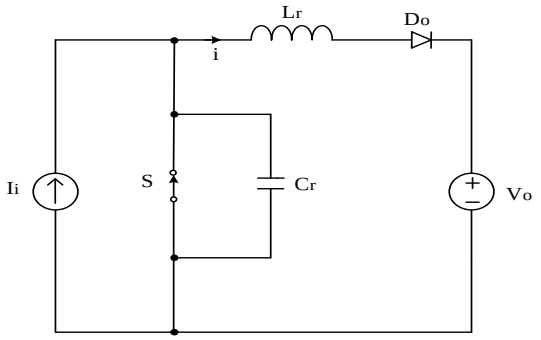

Figure 9. Equivalent circuit of State 3 [10]

2.3.4. State 4

The circuit diagram of State 4 is shown in Figure 10. In this operating state, the D_0 diode is off while the power switch is on. This operating state continues until the switch turns off [10, 15].

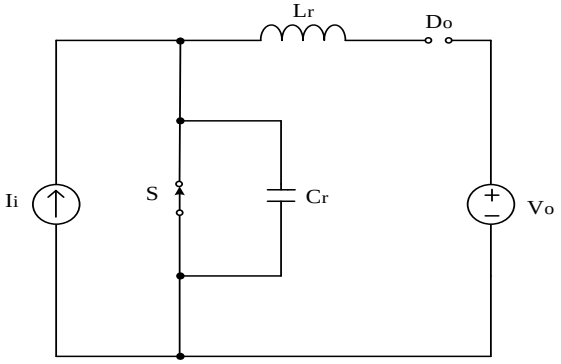

Figure 10. Equivalent circuit of State 4 [10]

3. THINNED-OUT CONTROLLED MPPT

The main drawbacks of PV energy systems are that the efficiency of PV panels is low, atmospheric conditions change during the day and accordingly the power values obtained from PV panels constantly change. Therefore, it is desired that the output power obtained from the PV panels is constantly at the maximum level. In such systems, maximum power point tracker (MPPT) algorithms are used, which continuously tracks the PV panel power and obtains maximum power [16-18].

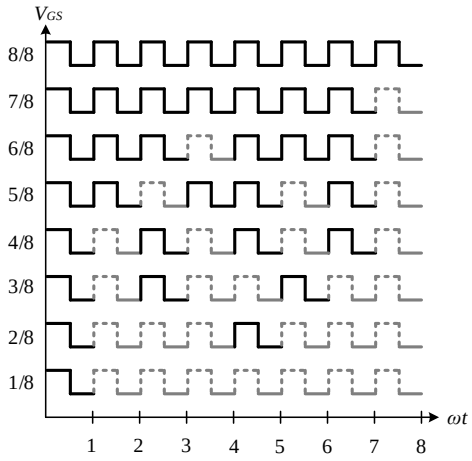

Figure 11. The proposed thinned-out control structure [16]

In this study, power control was provided by thinned-out pulses depending on the change of solar radiation. The proposed thinned-out control structure is shown in Figure 11.

The block diagram of the thinned-out controlled MPPT system is given in Figure 12.

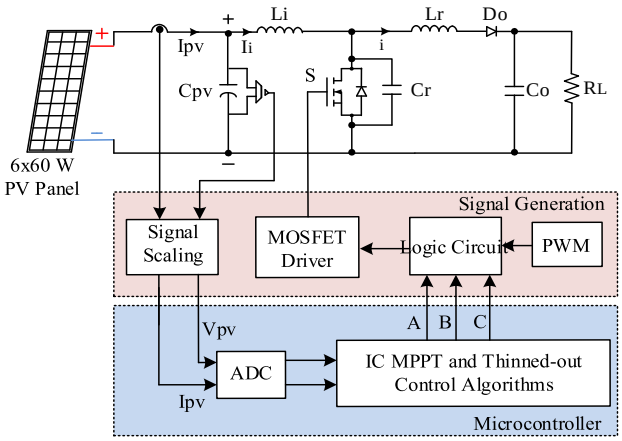

Figure 12. Thinned-out controlled MPPT system

4. SIMULATION RESULTS

The simulation of the L type half wave mode ZVS quasi resonant boost converter was carried out in the PSIM program and is shown in Figure 13.

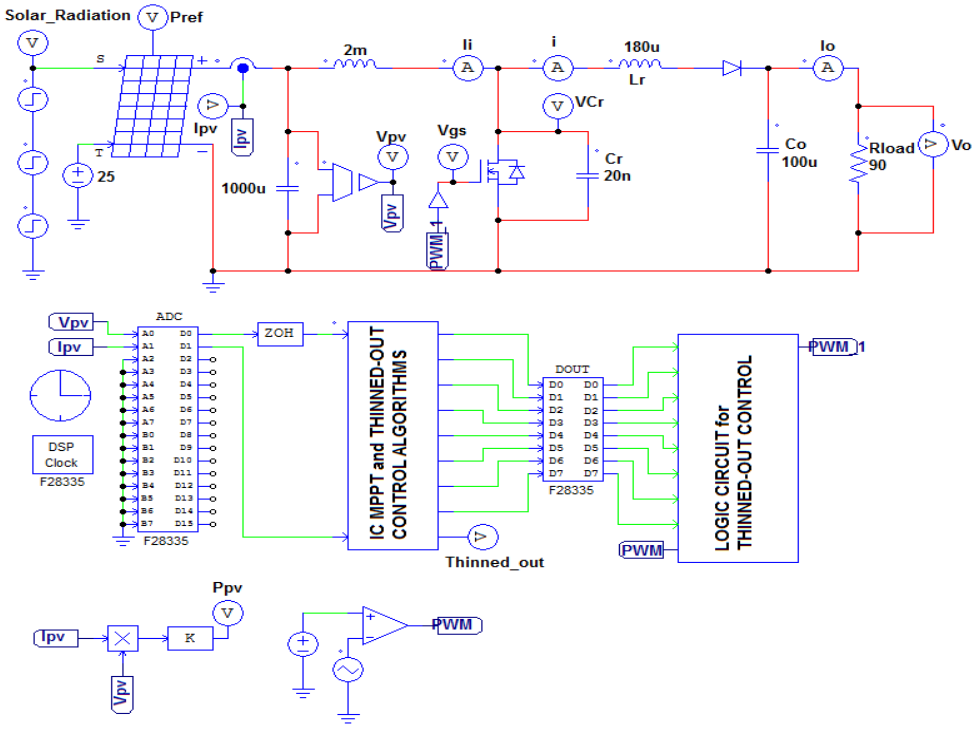

Figure 13. Simulation of L type half wave mode ZVS quasi resonant boost converter

In the study, the power of one PV panel is 60 W, and six panels are connected in series. The maximum input voltage is 102 V. The MPPT efficiency was investigated by changing the solar radiation level of the PV panels to 500-750 and 1000 W/m^2. The switching frequency of the circuit is 45 kHz.

Other parameters of the circuit were determined by calculating as C_{pv}=1000 µF, L_i=2 mH, L_r=180 µH, C_r=20 nF, C_o=100 µF and R_L=90 Ω [19]. The MPPT efficiency of the system is shown in Figure 14. ZVS conditions at values of 500 and 1000 W/m^2 solar radiation are given in Figure 15.

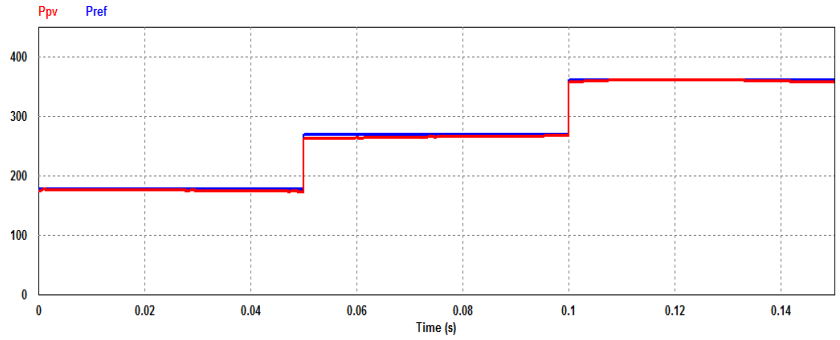

Figure 14. Maximum power tracking

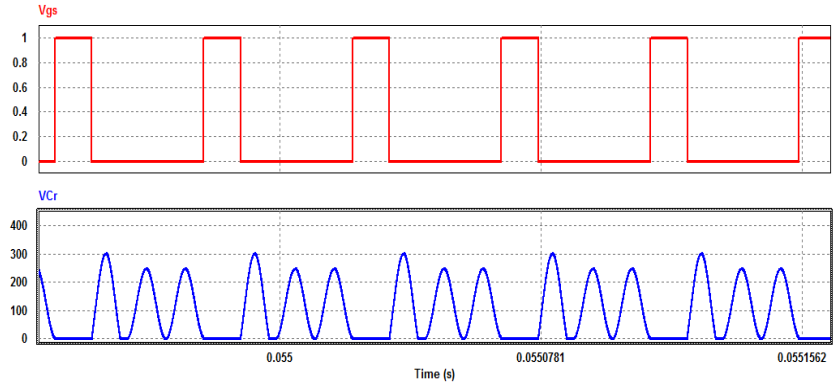

(a)

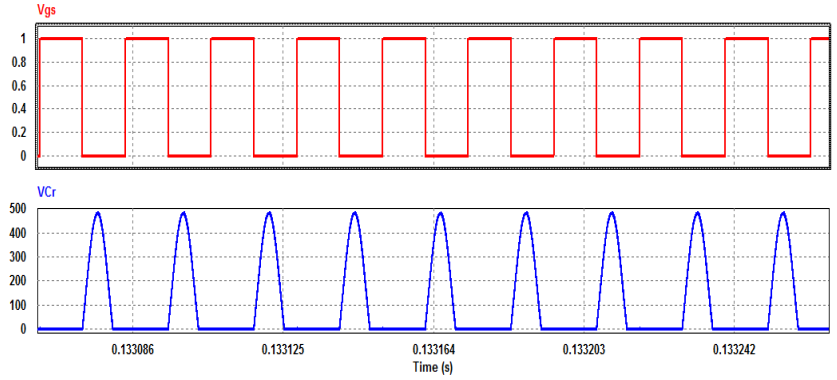

(b)

Figure 15. ZVS conditions, (a) 500 W/m^2, (b) 1000 W/m^2

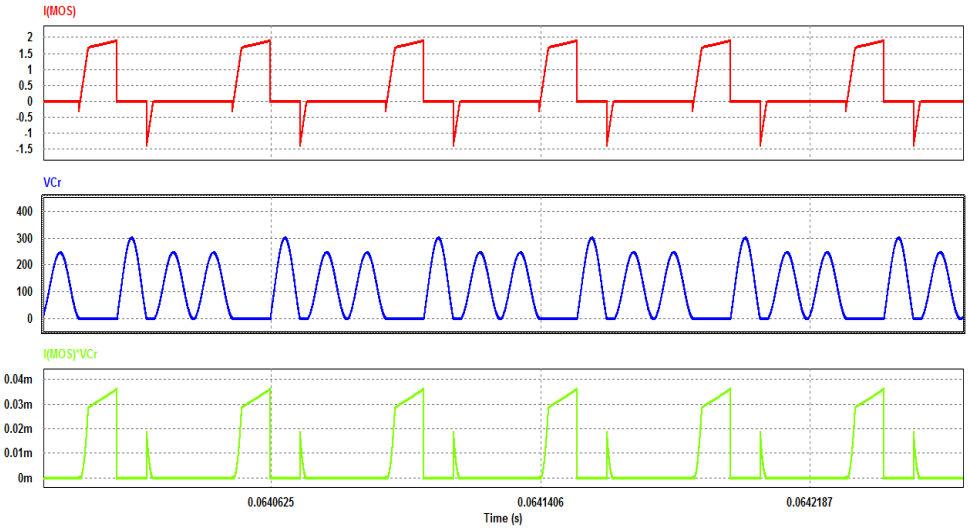

(a)

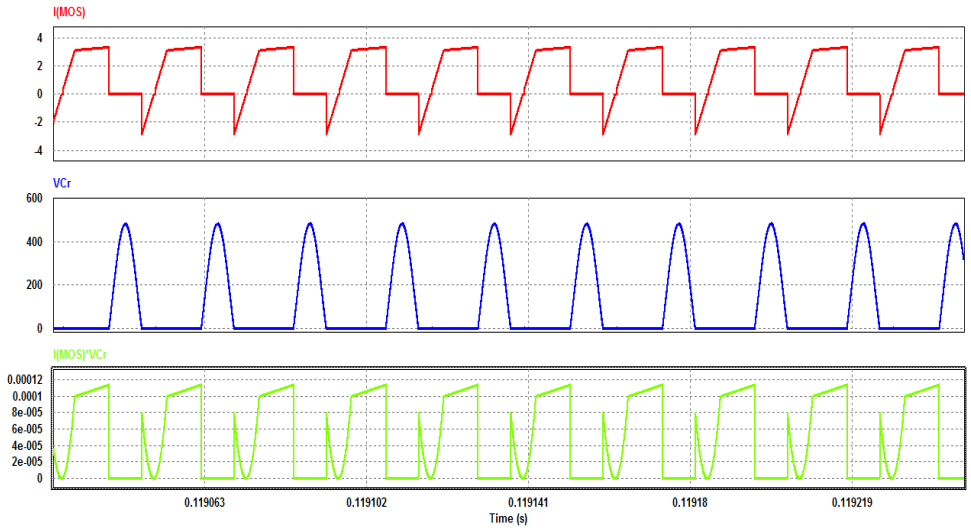

(b)

Figure 16. Current flowing through the power switch, voltage at the switch ends and switching loss, (a) 500 W/m^2, (b) 1000 W/m^2

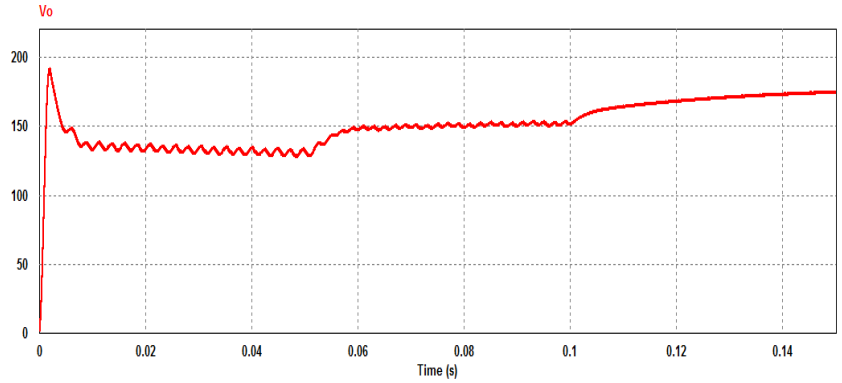

Figure 17. Variation of output voltage

The current passing through the power switch at 500 and 1000 W/m^2 radiation, the voltage at its ends and the switching losses are shown in Figure 16. The variation of the output voltage is given in Figure 17.

5. CONCLUSIONS

In this study, the analysis of the L type half wave mode ZVS quasi resonant boost converter circuit to be used in PV systems was carried out. Maximum power was obtained from the PV panels and transferred to the load by thinned-out of the pulses depending on the change of solar radiation. According to the results obtained, it was seen that while high MPPT efficiency was achieved, switching losses were reduced as a result of ZVS conditions. Reducing the switching losses increases the efficiency of the converter, while at the same time reducing the volume of passive components by providing high frequency operation.

REFERENCES

[1] A. Karafil, H. Ozbay, S. Oncu, "Design and Analysis of Single-Phase Grid-Tied Inverter with PDM MPPT-Controlled Converter", IEEE Transactions on Power Electronics, Vol. 35, Issue 5, pp. 4756-4766, May 2020.

[2] A.N. Karakilic, A. Karafil, N. Genc, "Effects of Temperature and Solar Irradiation on Performance of Monocrystalline, Polycrystalline and Thin-Film PV Panels", International Journal on Technical and Physical Problems of Engineering (IJTPE), Issue 51, Vol. 14, No. 2, pp. 254-260, June 2022.

[3] O.K. Islam, M.S. Ahmed, K. Rahman, T. Tahsin, "A Comprehensive Comparison Between Boost and Buck-Boost Converters in Solar MPPT With ANN", Emerging Technology in Computing, Communication and Electronics (ETCCE), pp. 1-6, Bangladesh, 21-22 December 2020.

[4] A. Pradhan, B. Panda, "Design of DC-DC Converter for Load Matching in Case of PV System", International Conference on Energy, Communication, Data Analytics and Soft Computing (ICECDS), pp. 1002-1007, Chennai, India, 01-02 August 2017.

[5] H. Zhu, D. Zhang, B. Zhang, Z. Zhou, "A Nonisolated Three-Port DC–DC Converter and Three-Domain Control Method for PV-Battery Power Systems", IEEE Transactions on Industrial Electronics, Vol. 62, Issue 8, 4937-4947, August 2015.

[6] S. Oncu, A. Karafil, "Pulse Density Modulation Controlled Converter for PV Systems", International

Journal of Hydrogen Energy, Vol. 42, Issue 28, pp. 17823-17830, July 2017.
[7] N.J. Dahl, A.M. Ammar, A. Knott, M.A. Andersen, "An Improved Linear Model for High-Frequency Class-DE Resonant Converter Using the Generalized Averaging Modeling Technique", IEEE Journal of Emerging and Selected Topics in Power Electronics, Vol. 8, Issue 3, pp. 2156-2166, September 2020.
[8] M. Mohammadi, E. Adib, M.R. Yazdani, "Family of Soft-Switching Single-Switch PWM Converters with Lossless Passive Snubber", IEEE Transactions on Industrial Electronics, Vol. 62, Issue 6, pp. 3473-3481, June 2015.
[9] S.A.Q. Mohammed, J.W. Jung, "A State-of-the-Art Review on Soft-Switching Techniques for DC-DC, DC-AC, AC-DC and AC-AC Power Converters", IEEE Transactions on Industrial Informatics, Vol. 17, Issue 10, pp. 6569-6582, October 2021.
[10] K.H. Liu, F.C. Lee, "Zero-Voltage Switching Technique in DC/DC Converters", IEEE Transactions on Power Electronics, Vol. 5, Issue 3, pp. 293-304, July 1990.
[11] K.H. Liu, R. Oruganti, F.C. Lee, "Quasi-Resonant Converters-Topologies and Characteristics", IEEE Transactions on Power Electronics, Vol. 2, Issue 1, pp. 62-71, January 1987.
[12] S. Lungu, O. Pop, G. Chindris, "Educational Platform for Modeling of Zero-Voltage Switching Quasi-Resonant Boost Converters", The 27th International Spring Seminar on Electronics Technology: Meeting the Challenges of Electronics Technology Progress, pp. 147-152, Bankya, Bulgaria, 13-16 May 2004.
[13] M.A. Ayubirad, S.A. Siavoshani, M.J. Yazdanpanah, "A Robust Passivity Based Control Strategy for Quasi-Resonant Converters", IET Power Electronics, Vol. 14 Issue 7, pp. 1360-1370, May 2021.
[14] E. Tatakis, N. Polyzos, A. Safacas, "Predicting Real Characteristics of Boost Zero-Voltage Switching Quasi-Resonant Converters", The IEEE International Symposium on Industrial Electronics, pp. 759-765, Athens, Greece, 10-14 July 1995.
[15] S. Oncu, S. Nacar, "Soft Switching Maximum Power Point Tracker with Resonant Switch in PV System", International Journal of Hydrogen Energy, Vol. 41, Issue 29, pp. 12477-12484, August 2016.
[16] A. Karafil, "Comparison of the Various Irregular Pulse Density Modulation (PDM) Control Pattern Lengths for Resonant Converter with Photovoltaic (PV) Integration", Journal of the Faculty of Engineering and Architecture of Gazi University, Vol. 36, Issue 3, pp. 1595-1611, 2021.
[17] N. Genc, "PV Based V/f Controlled Induction Motor Drive for Water Pumping", International Journal on Technical and Physical Problems of Engineering (IJTPE), Issue 45, Vol. 12, No. 4, pp. 103-108, December 2020.
[18] T. Hai, J. Zhou, K. Muranaka, "An Efficient Fuzzy-Logic based MPPT Controller for Grid-Connected PV systems by Farmland Fertility Optimization Algorithm", Optik, p. 169636, 2022.
[19] A. Karafil, "Analysis of Voltage Mode L-Type Partial Resonance Amplifier Transducer", The 6th International Engineering Architecture and Design Congress, pp. 970-978, Istanbul, Turkey, 17-18 December 2020.

BIOGRAPHIES

Akif Karafil was born in in Bursa, Turkey on April 19, 1983. He received the B.Sc. degree in Electrical Education from Marmara University, Istanbul, Turkey, in 2007, the M.Sc. degree in Electrical and Electronics Engineering from Karadeniz Technical University, Trabzon, Turkey, in 2011, and the Ph.D. degree in Electrical and Electronics Engineering from Karabuk University, Karabuk, Turkey, in 2018. Currently, he is an Assistant Professor in Electrical and Electronics Engineering Department of Yalova University, Yalova, Turkey. His research interests include pulse density modulation control, resonant converters, soft switching, MPPT, single-phase grid-connected inverters, and PV system applications.

Naci Genc was born in Erzurum, Turkey on October 10, 1977. He received his B.Sc., M.Sc., and Ph.D. from Gazi University (Ankara, Turkey), Van Yuzuncu Yil University (Van, Turkey) and Gazi University in 1999, 2002, and 2010, respectively. Currently, he is a Professor in Electrical and Electronics Engineering Department of Yalova University, Yalova, Turkey. His interests include energy conversion systems, power electronics and electrical machines.

The 18th International Conference on
"Technical and Physical Problems of Engineering"
30 October 2022
International Organization of IOTPE

ICTPE Conference
www.iotpe.com
ictpe@iotpe.com
ictpe0@gmail.com

ICTPE-2022 Number 08 Code 02ELC01 Pages 40-44

INTERNAL AND EXTERNAL INSTABILITY IN TWO-VALLEY SEMICONDUCTORS OF GaAs TYPE

E.R. Hasanov [1,2] S.G. Khalilova [2] R.K. Mustafayeva [1] G.M. Mammadova [2]

1. Baku State University, Baku, Azerbaijan, eldar_hasanov@lenta.ru, ruhi-qrk@mail.ru
2. Institute of Physics, Azerbaijan National Academy of Sciences, Baku, Azerbaijan
shahlaganbarova@gmail.com, gizbesmamedova@gmail.com

Abstract- A theory is constructed in two-valley semiconductors of the GaAs type for internal and external instabilities. An analytical expression is found for the frequency and for the electric field in the case of internal and external instability. When calculating the impedance, ohmic boundary conditions for an alternating electric field were used. In the theoretical calculation, it was taken into account that the transition time from valley a to valley b is much less than the transition time from *b* to *a*, i.e., $\tau_{ab} << \tau_{ba}$. The sample under study is homogeneous and of the electronic type of charge carriers. Therefore, the electron concentration $n = n_a + n_b = \text{const}$. It is taken into account that the current density along the coordinate axes has the form: $j_x' \neq 0$, $j_y' = 0$, $j_z' = 0$. When internal instability appears, analytical expressions are obtained for the oscillation frequency of charge $\omega_0 = -\frac{4E_0 ck}{H_0}$, carriers and the growth increment $\omega_1 = \frac{3}{2}\frac{E_0 ck}{H_0}\frac{\vartheta_2}{kD_2}$. With external instability, the oscillation frequency is a matter variable, and the wave vector is a complex quantity. With the appearance of external instability, analytical expressions for the electric field (33) and the frequency of current oscillations are obtained.

Keywords: Current Oscillations, Growth Rate, Oscillation Frequencies, Sample Impedance, Boundary Conditions, Radiation.

1. INTRODUCTION

The development of semiconductor electronics has created completely new methods for modern technology. First, the low-frequency region was developed. Already in the 50s of the last centuries, new methods were rapidly developing in the field of microwave current oscillations based on semiconductors in multi-valley energy levels. The use of semiconductor devices in microwave technology has led to a significant increase in reliability and a very noticeable reduction in the dimensions of the devices used.

Currently, there are several types of semiconductor microwave devices, tunnel diodes, microwave transistors, avalanche diodes, Gunn diodes. Gunn diodes can operate at frequencies of several tens of gigahertz. Gunn diodes use phenomena in the volume of a homogeneous semiconductor, and this is the advantage of Gunn diodes. In the operation of Gunn diodes, mainly with an increase in the electric field strength, a decrease in the conductivity of the semiconductor occurs, i.e., the current-voltage characteristic has a section of negative differential conductivity and the state of the semiconductor is unstable.

In Gunn diodes, the current-voltage characteristic is N-shaped, i.e., one current value corresponds to several voltage values. In this case, domains appear inside the sample. In Gunn's experiment, the GaAs semiconductor was included ohmic in the circuit. In theoretical works, it was proved that current oscillations in GaAs occur due to the transition of charge carriers under the action of an external electric field from a valley with a lower energy value to a valley with a higher energy value. In this case, the mobility of the current carriers sharply decreases and, in this case, the current decreases. The domains propagate at a speed of 10^7 cm/sec, and the domain transit time is t~10^{-10} sec and generated frequency is ω~10^{10} Hz [1, 2].

Theoretical studies of the Gunn effect without the influence of an external magnetic field *H* were performed in several works. The influence of an external magnetic field on the Gunn effect was first performed by us. In this theoretical work, we will theoretically investigate the influence of an external magnetic field ($\mu H >> c$) on the Gunn effect. When an oscillation occurs inside the sample (but without oscillation in the circuit), the excited waves can grow (instability) or decay. When growing waves appear inside the sample, the oscillation frequency is a complex quantity, the wave vector is a real quantity. When a current oscillation appears in the circuit, the oscillation frequency is a real value, and the wave vector is a complex value [2-7].

In this theoretical work, we will investigate the internal and external instability in two-valley semiconductors of the GaAs type. Let us calculate the real and imaginary parts of the frequency inside the

sample and the critical electric field when oscillations appear inside the sample and when the current oscillates in the external circuit. Let us show that the direction of the external magnetic role plays a significant role for the appearance of oscillations inside the sample and for the appearance of current oscillations in the circuit.

2. BASIC EQUATIONS OF THE PROBLEM

The energy spectrum of charge carriers in GaAs has two minima along the crystal axes [100]. The energy gap between the minima is significant $\Delta\varepsilon = 0.36$ eV. If we designate these valleys as *a* and *b*, then the time of transition is τ_{ab} from valley *a* to valley *b* and the time of transition is τ_{ba} from valley *b* to valley *a* differ, i.e.

$$\tau_{ab} << \tau_{ba} \tag{1}$$

The total concentration n in both valleys is constant due to ohmic contact and due to the absence of recombination and generation processes

$$n = n_a + n_b = \text{const},\ n'_a = -n'_b \tag{2}$$

The continuity equations in the valleys have the form:

$$\begin{aligned} &\frac{\partial n'_a}{\partial t} + \text{div} j_a = \frac{n'_a}{\tau_{ab}} \\ &\frac{\partial n'_b}{\partial t} + \text{div} j_b = \frac{n'_b}{\tau_{ba}} \end{aligned} \tag{3}$$

The j_a and j_b are current flux density in valleys *a* and *b*.

$$\begin{aligned} &\vec{j}_a = n_a\mu_a\vec{E} + n_a\mu_{1a}\left[\vec{E}\vec{H}\right] + n_a\mu_{2a}\vec{H}\left(\vec{E}\vec{H}\right) - \\ &-D_a\nabla n_a - D_{1a}\left[\vec{\nabla}n_a\vec{H}\right] - D_{2a}\vec{H}\left[\vec{\nabla}n_a\vec{H}\right] \end{aligned} \tag{4}$$

$$\begin{aligned} &\vec{j}_b = n_b\mu_b\vec{E} + n_b\mu_{1b}\left[\vec{E}\vec{H}\right] + n_b\mu_{2b}\vec{H}\left(\vec{E}\vec{H}\right) - \\ &-D_b\nabla n_b - D_{1b}\left[\vec{\nabla}n_b\vec{H}\right] - D_{2b}\vec{H}\left[\vec{\nabla}n_b\vec{H}\right] \end{aligned} \tag{5}$$

$$\frac{\partial\vec{H}}{\partial t} = -\text{crot}\vec{E} \tag{6}$$

Choosing the next coordinate system

$$\vec{H}_0 = \vec{i}H_0,\ \vec{E}_0 = \vec{i}E_0 \tag{7}$$

3. THEORY

3.1. Internal Instability

Representing all variable physical quantities in the form of monochromatic waves, i.e.

$\vec{E} = \vec{E}_0 + \vec{E}'$, $n_a = n_{a0} + n'_a$, $\vec{H} = \vec{H}_0 + \vec{H}'$

$\vec{E}' << \vec{E}_0$, $n'_a << n_{a0}$, $\vec{H}' << \vec{H}_0$

From (4), (5), (6)

$$\begin{aligned} &j'_{ax} = \left(\vartheta_{a0} + \vartheta^0_{2a}\right)n'_a - ik\left(D_a + D_{2a}\right)n'_a + \\ &+\left(n_{a0}\mu_{a0}\gamma_a + n_{a0}\mu_{a0} + n_{a0}\mu^0_{2a}\gamma_{2a}\right)E'_x + \\ &+3n_{a0}\mu^0_{2a}\frac{E_0}{H_0}\frac{ck}{\omega}\left(E'_z - E'_y\right) \end{aligned}$$

$$j'_{ay} = n_{a0}\mu_{a0}E'_y + n_{a0}\mu^0_{2a}\frac{E_0}{H_0}\frac{ck}{\omega}\left(E'_x - E'_z\right) - D_a ikn'_a$$

$$\begin{aligned} &j'_{az} = n_{a0}\mu_{a0}E'_z + n_{a0}\mu^0_{1a}\frac{E_0}{H_0}\frac{ck}{\omega}\left(E'_x - E'_z\right) - \\ &-n_{a0}\mu^0_{1a}E'_y + n_{a0}\mu^0_{2a}\frac{E_0}{H_0}\frac{ck}{\omega}\left(E'_y - E'_x\right) - \\ &-ik\left(D_a - D_{1a}\right)n'_a \end{aligned}$$

$\gamma_{1a} = 2\dfrac{d\ln\mu_{1a}}{d\ln E_0^2}$, $\gamma_{2a} = 2\dfrac{d\ln\mu_{2a}}{d\ln E_0^2}$, are obtained.

Considering that $D_{1a} >> D_a$, $\mu_{2a} >> \mu_{a1}$ from

$$j'_{ay} = j'_{az} = 0 \tag{8}$$

is obtained

$$E'_y = AE'_x,\ E'_z = BE'_x \tag{9}$$

Substituting (9) to j'_{ax} the following dispersion equations are obtained

$$\begin{aligned} &\left(\vartheta_2 - ikD_2\right)\phi_1^2 + \mu E_{char}\phi_1^2\left(ik\vartheta_2\tau + k^2D_2\tau\right) + \\ &+3\mu E_{char}\frac{\Omega}{\omega}\left(\frac{\mu H}{c}\right)^2\left(1-\frac{\Omega}{\omega}\right)\phi_1 - 3\left(\frac{\mu H}{c}\right)^2\frac{\Omega}{\omega}\mu_{1a}E_{char}\phi \\ &\left[\phi_1\left(ik\vartheta_2\tau + k^2D_2\tau\right) - 3\frac{\Omega}{\omega}\left(\frac{\mu H}{c}\right)^2\left(1-\frac{\Omega}{\omega}\right)\right] + \\ &+3\frac{\Omega}{\omega}ikD_a\left(1-\frac{\Omega}{\omega}\right)\left(\frac{\mu H}{c}\right)^2\phi\phi_1 = 0 \end{aligned}$$

where,

$$\phi = 2\left(\frac{\Omega}{\omega}\right)^2 + \frac{\Omega}{\omega},\ \phi_1 = 1 + \left(\frac{\mu H}{c}\right)^2\left(\frac{\Omega}{\omega}\right)^2 - \left(\frac{\mu H}{c}\right)^3\frac{\Omega}{\omega}$$

$\Omega = ck\dfrac{E_0}{H_0}$, where, k is wave vector.

$$E_{char} = \frac{i}{k\mu_2\tau}\cdot\frac{1}{\dfrac{3\mu_2}{\mu}\dfrac{\Omega}{\omega}\left(\dfrac{\mu H}{c}\right)^3\dfrac{\phi}{\phi_1} - 1} \tag{10}$$

At $\phi_1 = \alpha\dfrac{\Omega}{\omega}\dfrac{\mu H}{c}\phi$, here $\alpha = 3\left(\dfrac{\mu H}{c}\right)^2$. From (10) relatively ω the dispersion Equation (11) is obtained.

$$\omega^2 + \Omega\left(-1+\phi\right)\omega + 2\phi\Omega^2 = 0 \tag{11}$$

From solution (11)

$$\omega_1 = \frac{E_0ck}{H_0}\left(-4 - i\frac{\vartheta_2}{kD_2}\right) + \frac{5}{2}i\frac{E_0}{H_0}ck\frac{\vartheta_2}{kD_2} \tag{12}$$

$$\omega_2 = \frac{E_0ck}{H_0}\left(-4 - i\frac{\vartheta_2}{kD_2}\right) - \frac{5}{2}i\frac{E_0}{H_0}ck\frac{\vartheta_2}{kD_2} \tag{13}$$

are obtained.

It can be seen from (12) and (13) that a wave with a frequency is incremental.

$$\omega = -\frac{4E_0ck}{H_0} + \frac{3}{2}\frac{iE_0ck}{H_0}\frac{\vartheta_2}{kD_2} \tag{14}$$

and increment is $\omega_1 = \dfrac{3}{2}\dfrac{E_0ck}{H_0}\dfrac{\vartheta_2}{kD_2}$.

Thus, for internal instability (i.e., $\omega = \omega_0 + i\omega_1$), the value of the radiation frequency $\omega_0 = -\frac{4E_0 ck}{H_0}$ is the rise impedance ω_1. These values (ω_0 and ω_1) are obtained if the external electric field

$$E_0 >> \frac{1}{5}\frac{2\pi T}{eL} \tag{15}$$

where, L is the size of the sample, e is the elementary charge, T is the temperature in ergs.

Estimation (15) shows that under experimental conditions $E_0 >> 100$ V/cm this value corresponds to the experiment in GaAs where it was obtained for

$$E_0 \sim 2\times 10^3 \text{ V/cm} \tag{16}$$

3.2. External Instability (Impedance Instability)

When the current density j'_{ax} appears in the external circuit (i.e., current fluctuations) the impedance of the sample (GaAs) becomes a complex quantity. This occurs at the complex value of the wave vector (k) and at the real value of the current oscillation frequency (ω_0). For sample impedance calculation, the boundaries (i.e., $l = 0$ and $l = l_x$) are the main factor, i.e., boundaries can be ohmic and injecting. In the Gunn experiment, the GaAs boundaries were ohmic;

$$\begin{aligned} &E'_x(0) = 0 \quad \text{at} \quad l = 0 \\ &E'_x(l) = 0 \quad \text{at} \quad x = l \end{aligned} \tag{17}$$

An alternating electric field will be sought in the following form;

$$E'_x(x) = c_1 e^{ik_1 x} + c_2 e^{ik_2 x} + \frac{j'_x}{\sigma} \tag{18}$$

where, $\sigma = en\mu$.

The complex wave vectors k_1 and k_2 are calculated from the dispersion equation respect to k from (11), i.e.

$$k^4 + \left(\frac{H_0}{E_0}\frac{\omega}{2c} + i\frac{\vartheta_2}{D_2}\right)k^3 + \frac{iH_0}{E_0}\frac{\omega\vartheta_2}{cD_2}k^2 - \\ -\frac{H_0}{E_0}\frac{\omega}{cD_2\tau_1}k + \frac{\omega^2}{2c^2 D_2\tau_1}\left(\frac{H_0}{E_0}\right)^2 = 0 \tag{19}$$

$$k_{char}^4 = \left(\frac{H_0}{E_0}\right)^2 \frac{\omega^2}{2c^2 D_2\tau_1}$$

$$\frac{1}{\tau_1} = \frac{1}{\tau_{ab}} - \frac{1}{\tau_{ba}}$$

We introduce $\frac{k}{k_{char}} = y$ from (19) at $y = y_0 + iy_1$, $y_1 << y_0$, for determining y_0 and y_1 the Equations (20) and (21);

$$y_0^4 + \alpha_0 y_0^3 - 3\alpha_1 y_0^2 y_1 - 2\beta y_0 y_1 - \gamma y_0 + 1 = 0 \tag{20}$$

$$4y_0^3 y_1 + 3\alpha_0 y_0^2 y_1 + \alpha_1 y_0^3 + \beta y_0^2 - \gamma y_1 = 0 \tag{21}$$

are obtained.

Analysis of (20), (21) shows that;

$$y_0^{(1,2)} = -\frac{\alpha, u}{2} \pm \left(1 - \frac{2\beta}{\alpha_1^2 u}\right)$$

$$\beta = \frac{4}{5}\alpha_0\alpha_1, \ \alpha_0 = \frac{H_0\omega}{2cE_0 k_{char}}, \ \alpha_1 = \frac{\vartheta_2}{D_2 k_{char}} \tag{22}$$

$$y_1 = \frac{y_0^3 + \alpha_0 y_0^2 - \gamma}{3\alpha_1 + 2\beta}$$

From Equations (20)-(21)

$$\begin{aligned} y_0^{(1)} &= -\alpha_0 \\ y_0^{(2)} &= -\frac{3}{2}\alpha_0 \end{aligned} \tag{23}$$

are found.

Substituting (23) to (22)

$$y_1 = -\frac{2\beta}{\alpha_1 u} + i\frac{4\alpha_0^4\beta^2}{3\alpha_1^9} = y_{10} + iy'_1$$

$$y_2 = -\alpha_1 u - \frac{1}{3}\alpha_1^2 u^3 = -y_{20} + iy'_2$$

$$u = \frac{\vartheta_2}{k_{xar}D_2}\left(\frac{2k_{xar}E_0 c}{H_0\omega}\right)^2 = \left(\frac{E_0}{E_1}\right)^3$$

$$\alpha_0 = \frac{H_0\omega}{k_{xar}E_0 2c} = \frac{E_2}{E_0}$$

$$\alpha_1 = \frac{\vartheta_2}{k_{xar}D_2} = \frac{E_0}{E_3}$$

are found.

Substituting the boundary conditions for the electric field (17) into (18), the constants c_1 and c_2

$$c_1 = -\frac{J'}{\sigma}\cdot\frac{e^{iy_2} - 1}{e^{iy_2} - e^{iy_1}}$$

$$c_1 = -\frac{J'}{\sigma}\cdot\frac{e^{iy_2} - 1}{e^{iy_2} - e^{iy_1}}$$

are found.

Pattern's impedance

$$Z = \frac{1}{\sigma J'}\int_0^l E'(x)dx \tag{24}$$

$$J' = j'_{ax}S$$

Substituting $E'(x)$ constants c_1 and c_2 to (24) after integrated:

$$Z = \frac{l}{\sigma S}\left[-\frac{\left(e^{iy_1} - 1\right)\left(e^{iy_2} - 1\right)}{e^{iy_2} - e^{iy_1}}\cdot\frac{i\left(y_2 - y_1\right)}{y_1 y_2}\right] \tag{25}$$

are obtained.

Substituting y_1 and y_2, to (25) for the impedance the following complex values.

$$Z = \frac{l}{\sigma S}\left\{1 - \left[1 + A\cdot\left(\cos\phi'_2 + i\sin\phi'_2\right)\right]\times\frac{a + ib}{a_1 + ib_1}\right\} \tag{26}$$

$$A=\frac{1}{\phi_3 E_0^{9/2}},\ a=\left(\frac{\vartheta_2}{D_2 k_{char}}\right)^3\left(\frac{2cE_0k_{char}}{H_0\omega}\right)^2,$$

$$b=\left(\frac{\vartheta_2}{D_2 k_{char}}\right)^8\left(\frac{2cE_0k_{char}}{H_0\omega}\right)^3,\ a_1=\left(\frac{E_0}{E_1'}\right)^4,$$

$$b_1=\frac{8}{3}\left(\frac{E_0}{E_2}\right)^{9/2}$$

are obtained.

Separating the imaginary and real parts of the impedance from (26) we obtain;

$$\mathrm{Re}\,Z=-Z_0A\frac{aa_1+bb_1}{a_1^2+b_1^2}\cos y_2'+Z_0A\frac{ba_1-ab_1}{a_1^2+b_1^2}\sin y_2' \quad (27)$$

$$\mathrm{Im}\,Z=-Z_0A\frac{ba_1-ab_1}{a_1^2+b_1^2}\cos y_2'-Z_0A\frac{aa_1+bb_1}{a_1^2+b_1^2}\sin y_2' \quad (28)$$

From (27)-(28) shows that at

$$y_2'=\frac{1}{3}\alpha_1^2u^3=\pi \quad (29)$$

$$\mathrm{Re}\,Z=-Z_0A\frac{aa_1+bb_1}{a_1^2+b_1^2} \quad (30)$$

$$\mathrm{Im}\,Z=-Z_0A\frac{ba_1-ab_1}{a_1^2+b_1^2} \quad (31)$$

are obtained. Denoting

$$\psi=Z_0A\frac{aa_1+bb_1}{a_1^2+b_1^2},\ \psi_1=Z_0A\frac{ba_1-ab_1}{a_1^2+b_1^2}$$

From (30)-(31)

$$\frac{ba_1-ab_1}{aa_1+bb_1}=\frac{R_1}{R} \quad (32)$$

is obtained.

From (29)

$$E_0=H_0\left(\frac{2}{27}\frac{eH_0}{k_{xar}T}\right)^{1/2}\left(\frac{\omega}{k_{xar}c}\right)^{3/2} \quad (33)$$

the value of the electric field is obtained.

In deriving (33), the inequality $R_1>\sqrt{3}R$ is used, where, R is ohmic resistance, R_1 is capacitive or inductive resistance. In deriving the electric field (33), the inequality

$$E_0>\left(\frac{9}{2}\right)^{1/5}\frac{E_3^{9/5}E_1^{1/5}}{E_2} \quad (34)$$

is used.

Substituting (34) to (33)

$$\omega>k_{char}c\frac{k_{char}T}{eH},\quad k_{char}c=\omega_{char},\quad \omega>\omega_{char}\frac{k_{char}T}{eH}$$

interval change in frequency of current oscillation is obtained.

4. CONCLUSION

Thus, we have constructed a theory of internal and external instability when the external magnetic field is directed along the external electric field. The magnetic field is strong, i.e., $\mu H>c$. With internal instability, an analytical formula for the oscillation frequency and the electric field at which internal unstable waves are excited are obtained, and the growth rate of the oscillation inside the crystal is found. When the current begins to oscillate in the external circuit, the sample (i.e., GaAs) emits energy at a certain frequency. The limit of change in the frequency of current oscillations in the external circuit, as well as the value of the electric field at the beginning of radiation, are calculated.

From $\frac{\omega_0^{external}}{\omega_0^{internal}}$

$$\frac{\omega_0^{external}}{\omega_0^{internal}}\sim\frac{1}{2}\cdot10^{-4}<<1$$

is found. Thus, the frequency and electric field are decreased.

From the relation $\frac{E_0^{internal}}{E_0^{external}}$ electric field is

$$\frac{E_0^{internal}}{E_0^{external}}=\frac{5\times10^{-12}\times10^{-11}}{\pi\times10^{-14}}\sim10^{-7}$$

As the electric field decreasing, in external current circuit the oscillation frequency of current increases.

REFERENCES

[1] B.K. Ridley, "Specific Negative Resistance in Solids", Proc. Phys. Soc., Vol. 82, p. 954, 1963.

[2] J. Copeland, "Stable Space Charge Layers in Double-Valley Semiconductors", J. Appl. Phys., Vol. 37, No. 9, p. 3602, 1966.

[3] B.K. Ridley, T.B. Watkins, "The Possibility of Negative Resistance in Semiconductors", Proc. Phys. Soc., Vol. 78, p. 293, 1961.

[4] J.B. Gunn, "Characteristics of the Electron Transfer Effect Associated with Instabilities in GaAs", Proc. Int. Conf. Phys. Semicond., p. 505, Kyoto, Japan, 1966.

[5] E.R. Hasanov, S.G. Khalilova, G.M. Mammadova, "Determination of Frequency in Two Valley Semiconductors Such as GaAs", AJP FIZIKA Vol. XXVII, No. 3, pp. 12-15, Baku, Azerbaijan, 2021.

[6] E.R. Hasanov, S.G. Khalilova, G.M. Mammadova, "Multi-Valley Semiconductors in a Strong Magnetic Field (μH>C)", Institute of Physics, Azerbaijan National Academy of Science, No. 5, pp. 60-67, Baku, Azerbaijan, 2021.

[7] E.R. Hasanov, S.G. Khalilova, G.M. Mammadova, E.O. Mansurova, "Excitation of Unstable Waves in Impurity Semiconductors with Two Types of Charge Carriers in External Electric and Weak Magnetic Fields", International Journal on Technical and Physical Problems of Engineering (IJTPE), Issue 47, Vol. 13, No. 2, pp. 94-97, June 2021.

[8] E.R. Hasanov, S.G. Khalilova, R.K. Mustafayeva, G.M. Mammadova, "Oscillation of Current in Two-Valley Semiconductors in a Strong Electric Field", Advanced Studies in Theoretical Physics, Vol. 15, No. 3, pp. 145-152, Bulgaria, 2021.

BIOGRAPHIES

Eldar Rasul Hasanov was born in Azerbaijan, 1939. He graduated from Azerbaijan State University, Baku, Azerbaijan. Currently, he is working in Institute of Physics, Azerbaijan National Academy of Sciences, Baku, Azerbaijan. He is the Head of Laboratory. He is the author of 200 scientific paper.

Shahla Ganbar Khalilova was born in Baku, Azerbaijan on November 18, 1977. She received the B.Sc. in Physics from Baku State University, Baku, Azerbaijan in 2005, and the M.Sc. degree in heat physics and molecular physics from the same university. She is with Institute of Physics, Azerbaijan National Academy of Sciences, Baku, Azerbaijan as Scientific Researches (2006) and as Postgraduate Student (2011-2015). She received the Doctor of Philosophy (Ph.D.) in 2019. Her research interests are in development theoretical foundations of electrophysical methods used in technological processes. Investigation of electrical properties of composite materials based on polymer dielectrics.

Ruhiyya Karam Mustafayeva was born in Azerbaijan on February 05, 1977. She received the B.Sc., M.Sc. and Ph.D. degrees in Physics from Department of Solid-State Physics, Faculty of Physics, Baku State University, Baku, Azerbaijan in 1998, 2000 and 2018, respectively. She was a teacher in the same university since 2018. Her research interests are Semiconductor physics, solid state physics.

Gizbes Mannad Mammadova was born in Barda, Azerbaijan, 1964. She is graduated in Physics from Baku State Pedagogical University, Baku, Azerbaijan in 1985. Currently, she is an Engineer at Institute of Physics, Azerbaijan National Academy of Sciences, Baku, Azerbaijan.

The 18th International Conference on
"Technical and Physical Problems of Engineering"
30 October 2022
International Organization of IOTPE

ICTPE Conference
www.iotpe.com
ictpe@iotpe.com
ictpe0@gmail.com

ICTPE-2022 Number 09 Code 02ELC02 Pages 45-49

RADIATION OF ENERGY FROM A MULTI-VALLEY SEMICONDUCTOR OF THE GAAS TYPE IN AN EXTERNAL ELECTRIC AND STRONG (MH>C) MAGNETIC FIELDS

E.R. Hasanov [1,2] S.G. Khalilova [2] G.M. Mammadova [2] E.O. Mansurova [2]

1. Baku State University, Baku, Azerbaijan, eldar_hasanov@lenta.ru
2. Institute of Physics, Azerbaijan National Academy of Sciences, Baku, Azerbaijan
shahlaganbarova@gmail.com, gizbesmamedova@gmail.com, esmira85mansurova@gmail.com

Abstract- Using the Boltzmann kinetic equation, the frequency of the current oscillation in multi-valley semiconductors, in an external electric and strong magnetic fields, has been calculated. It has been proven that for the excitation of current oscillations in multi-lobe semiconductors, the sample size must be certain. It was found that the critical value of the electric field when the current oscillation appears almost does not differ from the value of the electric field obtained by the experiment of Gunn. It is shown for the first time that the appearance of unstable oscillations in two-valley semiconductors of the type GaAs size along the coordinate axes of the sample must have a certain value. Application of the Boltzmann kinetic equation leads to consistent values for the electric field and the frequency of current oscillations in the specified semiconductor. The obtained theoretical formulas were evaluated using the Gunn experiment in a semiconductor GaAs and numerical values were obtained for the current frequency and the critical value of the electric field.

Keywords: Oscillations, Frequency, Distribution Function, Electric Field, Magnetic Field, Current-Voltage Characteristic, Multi-Line Semiconductors.

1. INTRODUCTION

In theoretical works, current oscillations in two-valley semiconductors of the GaAs type in an external electric field, and in an external electric and strong magnetic fields are investigated by solving the Boltzmann kinetic equation. In these works, the critical values of the electric and magnetic fields were calculated from the condition

$$\frac{dj}{dE} = \sigma_d = 0 \qquad (1)$$

The j is the current flux density, E is the electric field, σ_d is the differential conductivity. However, from condition (1) it is impossible to determine the frequency of the current oscillation.

Therefore, it is of great interest to determine the current fluctuation in the presence of condition (1). In this theoretical work, we will calculate the frequency of current oscillation and the critical value of the electric and magnetic fields by applying the Boltzmann kinetic equation [1-4].

2. THEORY

Let's develop a mathematical model of three-phase two-pole synchronous motors with permanent magnets, which is shown in Figure 1. Here, there is a falling section on the current-voltage characteristic.

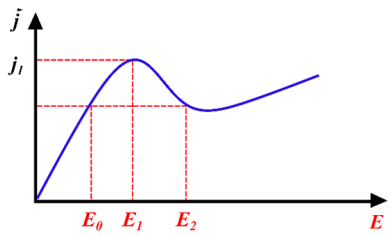

Figure 1. The dependence of the current density on the electric field in two-valley semiconductors of GaAs type is an N-shaped characteristic

The field strength is a multivalued function of the current density at certain range of currents $j_2 < j < j_p$. In this current range, the system can be in one of three spatially homogeneous states. The Gunn effect is associated with an N-shaped characteristic. With negative differential conductivity, electric charges in the system are distributed unevenly, i.e., spatial regions with different values of charges appear in the system (i.e., electrical domains appear). One of the mechanisms for the appearance of domains is the Ridley-Watkins-Hillsum mechanism. In electronic gallium arsenide GaAs, the dispersion law is as follows [5, 6].

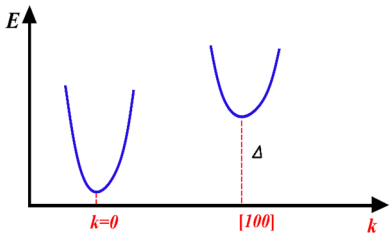

Figure 2. Electron energy versus wave vector in GaAs

Since the energy distance between the minima is relatively large ($\Delta = 0.36$ eV, $\Delta >> T_p, T_p$ is the lattice temperature) under conditions of thermodynamic equilibrium, the presence of upper valleys (minima) practically does not affect the statistics of electrons.

Some of the electrons go to the upper minimum when heated sufficiently. In this case, the effective mass of electrons in the lower valley m_a is much less than the mass of electrons in the upper valley m_b. Therefore, the electron mobilities in the corresponding valleys are related by the relation

$$\mu_b >> \mu_a \tag{2}$$

If we designate the concentrations in the valleys n_a, n_b we can write an expression for the current in the form;

$$\vec{j} = en_a\mu_a\vec{E} + en_b\mu_b\vec{E} \tag{3}$$

$$n = n_a + n_b = const \tag{4}$$

The diffusion current due to $eEl >> k_0T$, where e is the elementary charge, as the electron mean free path which are neglected.

In works, without taking into account the intervalley scattering (it is considered small in comparison with the intravalley one), by solving the Boltzmann equation, more specific conditions for the appearance of current oscillations were obtained. In the scientific literature, there are no works devoted to theoretical studies of the Gunn effect taking into account the intervalley scattering based on the solution of the Boltzmann kinetic equation. We will theoretically analyze the influence of a strong magnetic field on the Gunn effect, taking into account the above [5-6].

3. BASIC EQUATIONS OF THE PROBLEM

Under the action of external forces, the state of charge carriers is described by the distribution function $f(\vec{k},\vec{r})$, the value that is necessary when considering transport phenomena, $f(\vec{k},\vec{r})$is the probability that an electron with a wave vector $\vec{k}$ (quasi-momentum $h\vec{k}$) is located near the point $\vec{r}$. We consider stationary processes, then $f(\vec{k},\vec{r})$ is clearly independent of time. The distribution function is found from the kinetic Boltzmann equation. It is known that the distribution function changes under the influence of external factors and under the influence of collisions with lattice vibrations (phonons) and crystal defects. In the considered stationary state, the influence of these factors mutually compensates each other.

$$\left(\frac{\partial f}{\partial t}\right)_{external} + \left(\frac{\partial f}{\partial t}\right)_{coll} \tag{5}$$

In external electric and magnetic fields, Equation (5) has the form [7]

$$\vec{\vartheta}\nabla_{\vec{r}} f + \frac{e}{h}\left\{\vec{E} + \frac{1}{c}\left[\vec{\vartheta}\vec{H}\right]\right\}\nabla_{\vec{k}} f = \left(\frac{\partial f}{\partial t}\right)_{coll} \tag{6}$$

where, $\vec{\vartheta} = \frac{1}{h}\nabla_k\varepsilon(\vec{k})$ is the electron velocity, $\nabla_{\vec{k}}$ and $\nabla_{\vec{r}}$ is the wave vectors and the gradient in the space of coordinates.

When solving the problem, we neglect the anisotropy. The fact that no orientation dependence was found in studies of the Gunn effect on GaAs samples speaks in favor of this assumption. We will assume that for the lower valley the intervalley scattering prevails over the intravalley one, and for the upper valley, the intravalley scattering prevails over the intervalley one. Then the Boltzmann equation for the lower valley can be written in the form

$$\left(\frac{\partial f^a}{\partial t}\right)_{internal} + \left(\frac{\partial f^a}{\partial t}\right)_{intervalley} \tag{7}$$

And for the upper valley - in the form

$$\left(\frac{\partial f^b}{\partial t}\right)_{internal} + \left(\frac{\partial f^b}{\partial t}\right)_{intervalley} \tag{8}$$

Davydov [8] showed that in a strong electric field the distribution function has the form:

$$f = f_0 + \frac{\vec{p}}{p}\vec{f}_1 \tag{9}$$

where, f_0 is the equilibrium distribution function, is the momentum of charge carriers. It is clear that you can write

$$f^a = f_0^a + \frac{\vec{p}}{p}\vec{f}_1^a,\ f^b = f_0^b + \frac{\vec{p}}{p}\vec{f}_1^b \tag{10}$$

Distribution function f^b found from Equation (8) in [8]

$$f_0^a = Be^{-\alpha_a(\varepsilon-\Delta)^2} \tag{11}$$

$$f_1^a = -\frac{em_bl_b}{p}\vec{p}\frac{\partial f_0^b}{\partial p} \tag{12}$$

where,

$$l_b = \frac{\pi h^4\rho u_0^2}{D^2m_b^2k_oT} \tag{13}$$

$$\alpha_a = \frac{3D^4m_b^5k_0T}{e^2\pi^2h^8\rho^2u_0^2} \tag{14}$$

It is clear that for the valley "a" you can write similar Equations (13)-(14) replacing "a" with "b". The l_b is the mean free path, D is the deformation potential, T is the temperature of the lattice, ρ is the density of the crystal, and u_0 is the speed of sound in the crystal.

Let's calculate the total current;

$$\vec{j} = \vec{j}_a + \vec{j}_b \tag{15}$$

$$\vec{j} = \frac{2e}{(2\pi)^3}\int_0^\infty \frac{\vec{p}}{p}\vec{f}\vec{\vartheta}d\vec{k} \tag{16}$$

Davydov [8] showed that in the case of intravalley scattering f_1^b in an external electric and magnetic field f_1^b has the following form

$$f_1^b = -\frac{el_b m_b}{p}\frac{\partial f_0^b}{\partial p}\cdot\frac{\vec{E}+\left(\frac{el_b}{cp}\right)\left[\vec{E}\vec{H}\right]+\left(\frac{el_b}{cp}\right)^2\vec{H}\left(\vec{E}\vec{H}\right)}{1+\left(\frac{el_b}{cp}\right)^2\vec{H}^2} \tag{17}$$

$$\alpha_a = \frac{3D^4 m_b^5 k_0 T\left[1+\left(\frac{el_b}{cp}\right)^2\vec{H}^2\right]}{e^2\pi^2 h^8\rho^2 u_0^2\left[E^2+\left(\frac{el_b}{cp}\right)^2\left(\vec{E}\vec{H}\right)^2\right]} \tag{18}$$

where, f_1^a and α_a are obtained if we replace "b" with "a" in (17)-(18). After an easy calculation of the current density j_a and j_b from (16) we get:

$$\vec{j}_a = \frac{e^2 l_a \alpha_a A}{12\pi^2 h^2 m_a^2}\left\{\vec{E}\frac{c^2}{e^2 l_a^2 H^2}\left(\frac{4m_a^2}{\alpha_a}\right)^2 + \right.$$
$$\left. +\left[\vec{E}\vec{H}\right]\frac{c\Gamma\left(\frac{7}{4}\right)}{el_a H^2}\left(\frac{4m_a^2}{\alpha_a}\right)^{\frac{7}{4}} + \vec{H}\left(\vec{E}\vec{H}\right)\frac{\Gamma\left(\frac{3}{2}\right)}{H^2}\left(\frac{4m_a^2}{\alpha_a}\right)^{\frac{3}{2}}\right\} \tag{19}$$

After calculating the total current by the formula;

$$\vec{j} = \vec{j}_a + \vec{j}_b \tag{20}$$

$$j_z' = \frac{8nc^2 m_a^{\frac{1}{2}}}{3\sqrt{2}\Gamma\left(\frac{3}{2}\right)l_a}\cdot\frac{E_z'}{H^2}\cdot\frac{\alpha_a^{-\frac{1}{4}}}{1+\gamma^{-\frac{3}{2}}Z^{\frac{3}{4}}\beta}\left\{1+t\gamma_z^{-2}\beta + \right.$$
$$\left. +\frac{e^2 l_a^2 \alpha_a^{\frac{1}{2}}}{2c^2 m_a}H^2\Gamma\left(\frac{3}{2}\right)\left[1+t\gamma^{-1}z^{\frac{1}{2}}\beta\right]\right\} \tag{21}$$

where, $A = t\gamma^{-1}z^{-\frac{1}{2}} = \frac{m_b}{m_a}$, $\gamma = \frac{m_a}{m_b}$, $z = \frac{\alpha_a}{\alpha_b}$, $t = \frac{l_b}{l_a}$,

$$e^{-a\alpha^{\Delta^2}} = e^{-\left(\frac{E_x}{E}\right)^2} = \left(1-\frac{E_x}{E}\right)^2;$$

$$E_x^2 = \frac{3D^4 m_0 m_a^3 k_0 T}{e^2\pi^2 h^8\rho^2 u_0^2} \tag{22}$$

We write (21) in the following form

$$\vec{j} = \sigma\vec{E} + \sigma_1\left[\vec{E}\vec{h}\right] + \sigma_2\vec{h}\left[\vec{E}\vec{h}\right] \tag{23}$$

where, $\vec{h}$ is unit vector in the magnetic field. Comparing (23) with (21), one can easily write the expressions $\sigma+\sigma_1$, σ_1, σ_2.

When obtaining an expression for the current density j_z' using (21), then we direct the electric field and the magnetic field H_0 as follows

$$\vec{E}_0 = \vec{h}E_0,\ \vec{H}_0 = \vec{h}H_0 \tag{24}$$

The E_x value is obtained from the following condition;

$$\frac{dj_z'}{dE_z'} = 0 \tag{25}$$

when, estimating E_x^2 for GaAs, the value

$$E_x^2 = 43.84\left(\frac{\text{V}}{\text{cm}}\right)^2 \tag{26}$$

For all strong electric fields,

$$E >> E_x \tag{27}$$

It is quite satisfied. Now let's calculate the frequency of the current oscillation. When an alternating electric field E' is excited inside the medium, an alternating magnetic field H' arises, which satisfies Maxwell's Equation (28);

$$\frac{\partial\vec{H}'}{\partial t} = -\text{crot}\vec{E}' \tag{28}$$

The current density in the presence of electric and magnetic fields has the form;

$$\vec{j} = \sigma\vec{E} + \sigma_1\left[\vec{E}\vec{H}\right] + \sigma_2\vec{H}\left[\vec{E}\vec{H}\right] \tag{29}$$

Let us direct the external electric and magnetic field as follows.

$$\vec{E}_0 = \vec{h}E_0,\ \vec{H}_0 = \vec{h}H_0 \tag{30}$$

where, $\vec{h}$ is the unit vector in z. We find the variable value j_x', j_y', j_z' from (29) taking into account (28-30), then we get.

$$j_x' = \sigma\left(1-\frac{\mu k_z E_0}{\omega}\right)E_x' + \sigma_1\left[\left(1+\frac{ck_x E_0}{\omega H_0}\right) - \right.$$
$$\left. -\frac{2\sigma_2 ck_z E_0}{\omega H_0}\right]E_y' + \frac{2\sigma_2 ck_y E_0}{\omega H_0}E_z' \tag{31}$$

$$j_y' = -\sigma_1 E_x' + \left(\sigma - \frac{\sigma_1 ck_z E_0}{\omega H_0}\right)E_y' + \sigma_1\left(1+\frac{ck_y E_0}{\omega H_0}\right)E_z' \tag{32}$$

$$j_z' = (\sigma+\sigma_2)E_z' - \frac{2\sigma_2 ck_y E_0}{\omega H_0}\left(E_x' + E_y'\right) \tag{33}$$

Equating $j_x' = 0$ and $j_y' = 0$ to zero, we find E_z' and E_y' from (31)-(32) and supplying E_z', E_y' in (33), we obtain for j_z' the following expressions.

$$j_z' = \left[\sigma_2 + \frac{2\sigma_2 ck_x E_0}{\omega H_0}\left(1+\frac{c}{\mu H}\frac{ck_z\mu E_0}{\omega} + \right.\right.$$
$$\left.\left. +\frac{c}{\mu H_0}\frac{ck_y k_z \mu E_0}{\omega^2}\cdot\frac{E_0}{H_0} - \frac{ck_y}{\omega}\frac{c}{\mu H_0}\right) + \right.$$
$$\left. +\frac{2\sigma_2 ck_y E_0}{\omega}\cdot\frac{E_0}{H_0}\left(\frac{ck_y}{\omega} + \frac{ck_y k_z c\mu E_0}{\omega^2}\right)\frac{E_0}{H_0}\right]E_z' \tag{34}$$

When deriving expression (34), we used the conditions of a strong magnetic field $\mu H_0 \gg c$. Equating expressions (34) and (21), we obtain the following dispersion equation for determining the frequency of current oscillation.

$$\left(\sigma_2 - \tilde{\sigma}\Phi\right)\omega^3 + \frac{2\sigma_2 c k_x E_0}{H_0}\left(1+\frac{E_0}{H_0}\right)\omega^2 + \frac{2\sigma_2 c k_x E_0}{H_0}\omega + \\ + \frac{\sigma_2 c k_x E_0}{H_0} c k_y \mu k_z E_0\left(\frac{c}{\mu H_0}\cdot\frac{E_0}{H_0} + 2\frac{E_0}{H_0}\right) = 0 \tag{35}$$

where, $\tilde{\sigma} = \dfrac{8nc^2 m_a^{\frac{1}{2}} \alpha_a^{-\frac{1}{4}}}{3\sqrt{2}\Gamma\left(\frac{3}{2}\right) l_a H^2}$,

$$\Phi = \frac{1}{1+\gamma^{-\frac{3}{2}} Z^{\frac{9}{4}}\beta}\left[1 + t\gamma^{-2} Z\beta + \right. \\ \left. + \frac{e^2 l_a^2 H^2 \alpha_a^{\frac{1}{2}}}{2c^2 m_a}\Gamma\left(\frac{3}{2}\right) + \left(1 + t\gamma^{-1} Z^{\frac{1}{2}}\beta\right)\right] \tag{36}$$

Equating $\sigma_2 = \tilde{\sigma}\Phi$, $\left(\dfrac{H_x}{H_0}\right)^0 = 1$.

$$H_x = H_0 = \left[\frac{8c^2 m_a^{\frac{1}{2}} \alpha_a^{-\frac{1}{4}}}{3\sqrt{2}\Gamma\left(\frac{3}{2}\right) l_a e\mu}\right]^{\frac{1}{2}} \tag{37}$$

is obtained.

Putting the values of $\alpha_a^{-\frac{1}{4}}$ in (37)

$$H_0 = \left[\frac{8}{3\sqrt{2}\Gamma\left(\frac{3}{2}\right)}\right]^2 \cdot \left(\frac{k_0 T}{3m_0 u_0^2}\right)^{\frac{1}{8}} \cdot \left(\frac{c^2 m_a^{\frac{1}{2}}}{\mu}\right)^{\frac{1}{2}} \times \left(\frac{1}{el_a}\right)^{\frac{1}{4}} E_0^{\frac{1}{4}} \tag{38}$$

are obtained.

From (38), we get;

$$E_0 = \left(\frac{\mu}{c^2 m_a^{\frac{1}{2}}}\right)^2 el_a \left(\frac{H_0}{\varphi}\right)^4$$

$$\varphi = \left[\frac{8}{3\sqrt{2}\Gamma\left(\frac{3}{2}\right)}\right]^{\frac{1}{2}} \cdot \left(\frac{k_0 T}{m_0 u_0^2}\right)^{\frac{1}{8}} \tag{39}$$

Thus, the value of the electric field is obtained during current fluctuations in the above two-valley semiconductors of the GaAs type. In [8], it was obtained that taking into account (26).

$$E_0 = E_{kr} = 1500\ \frac{\text{V}}{\text{cm}} \tag{40}$$

Supplying (40) to (39), it is easy to see that $\mu H_0 >> c$, from the solution of the dispersion Equation (35), we easily obtain.

$$\omega_{1,2} = -\frac{c k_z E_0}{2H_9} \pm i\frac{c k_z E_0}{H_0}\left(\frac{L_z}{L_y}\right)^{\frac{1}{2}} \tag{41}$$

For growing fluctuations;

$$\omega = -\frac{c k_z E_0}{2H_0} + i\frac{c k_z E_0}{H_0}\left(\frac{L_z}{L_y}\right)^{\frac{1}{2}} = \omega_0 + i\gamma \tag{42}$$

From (42), it is seen that in the crystal.

$$L_y > 4L_z \\ \gamma << \omega_0 \tag{43}$$

Thus, with the size (43) (L_x can be any), current oscillations (i.e., instability) are excited under an electric field (39) In the calculation, we direct E_0 along H_0. Of course, any orientation of the electric and magnetic fields could be chosen. For other orientations, it is necessary to obtain expressions (21) and (34) in the same orientations, and then find the vibration frequencies in the same orientations.

4. CONCLUSION

In valley semiconductors of the GaAs type, current oscillations occur under the influence of an external electric and strong ($\mu H_0 >> c$) magnetic field. The frequency of this oscillation ω_0 (42) is close to the frequency of the Gunn effect, i.e., $\omega_0 \sim 10^7 \div 10^9$ Hz. This proves that the application of the Boltzmann equation is quite valid, although the Boltzmann equation in strong fields is not always applied. By directing $E_0 = \vec{i}E_0$, $E_0 = \vec{j}E_0$, $H_0 = \vec{i}H_0$, $H_0 = \vec{j}H_0$ one can carry out a theoretical calculation and determine the critical value of the electric field (including the magnetic field) and the frequency of current oscillation. Of course, with such calculations, conditions (43) will most likely change. Theoretical analysis of current fluctuations in multi-valley semiconductors of the GaAs type shows that the sample size at current fluctuations is significant. This fact was confirmed in the experiment of Gunn.

REFERENCES

[1] E.R. Hasanov, A.R. Hasanova, S.G. Khalilova, R.K. Mustafayeva, "Current Oscillations in Semiconductors with Deep Traps in Strong Electric and Magnetic Fields", IOSR Journal of Applied Physics, Vol. 11, Issue 1, No. 1, pp. 13-18, India, 2019.

[2] E.R. Hasanov, S.G. Khalilova, Z.A. Tagiyeva, S.S. Asadova, "Oscillation of Current in Electric and Magnetic Fields", The 15th International Conference on Technical and Physical Problems of Electrical Engineering (ICTPE-2019), pp. 103-107, Istanbul, Turkey, 14-15 October 2019.

[3] E.R. Hasanov, J.J. Mustafayev, "Non-Linear Fluctuations of Concentration of Charge Carriers and Electrical Field in Semiconductors", International Journal

on Technical and Physical Problems of Engineering (IJTPE), Issue 32, Vol. 9, No. 3, pp. 39-43, September 2017.
[4] E.R. Hasanov, V.M. Hajiyeva, A.S. Rikani, "Radiation Doped Semiconductors with Certain Impurities", The 14th International Conference on Technical and Physical Problems of Electrical Engineering (ICTPE-2018), pp. 1-5, Nakhichevan, Azerbaijan, 15-17 October 2018.
[5] B.K. Ridley, T.B. Watkins, "The Possibility of Negative Resistance Effects in Semiconductors", Proc. Phys. Soc., Vol. 78, p. 293, 1961.
[6] C.H. Hilsum, "Transferred Electron Amplifiers and Oscillators", Proc. IRE, Vol. 50, p. 185, 1962.
[7] A.I. Anselm "Introduction to the theory of semiconductors", International Congress of Mathematicians, p. 418, Moscow, Russia, 1962.
[8] A.B. Davydov, "On the Theory of the Motion of Electrons in Gases and in Semiconductors", ZhETF, Issue 7, p. 1069, Russia, 1937.

BIOGRAPHIES

Eldar Rasul Hasanov was born in Azerbaijan, 1939. He graduated from Azerbaijan State University, Baku, Azerbaijan. Currently, he is working in Institute of Physics, Azerbaijan National Academy of Sciences, Baku, Azerbaijan. He is the Head of Laboratory. He is the author of 200 scientific paper.

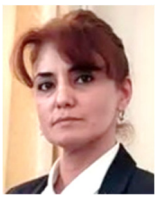

Shahla Ganbar Khalilova was born in Baku, Azerbaijan on November 18, 1977. She received the B.Sc. in Physics from Baku State University, Baku, Azerbaijan in 2005, and the M.Sc. degree in heat physics and molecular physics from the same university. She is with Institute of Physics, Azerbaijan National Academy of Sciences, Baku, Azerbaijan as Scientific Researches (2006) and as Postgraduate Student (2011-2015). She received the Doctor of Philosophy (Ph.D.) in 2019. Her research interests are in development theoretical foundations of electrophysical methods used in technological processes. Investigation of electrical properties of composite materials based on polymer dielectrics.

Gizbes Mannad Mammadova was born in Barda, Azerbaijan, 1964. She is graduated in Physics from Baku State Pedagogical University, Baku, Azerbaijan in 1985. Currently, she is an Engineer at Institute of Physics, Azerbaijan National Academy of Sciences, Baku, Azerbaijan.

Esmira Omer Mansurova was born in Baku, Azerbaijan on September 21 1985. She works at Institute of Physics, Azerbaijan National Academy of Sciences (Baku, Azerbaijan) since 2009. Her research interests are semiconductor physics and solid state physics.

The 18th International Conference on
"Technical and Physical Problems of Engineering"
30 October 2022
International Organization of IOTPE

ICTPE Conference
www.iotpe.com
ictpe@iotpe.com
ictpe0@gmail.com

ICTPE-2022 Number 10 Code 02ELC03 Pages 50-54

ELECTRICAL PROPERTIES OF INTERCRYSTALLITE BOUNDARY AND MECHANISMS OF CONDUCTIVITY IN A ZnO VARISTOR WITH IMPURITIES

S.M. Ahadzade A.M. Hashimov T.K. Nurubeyli V.M. Hajiyeva S.A. Huseynova S.S. Ahadova

Institute of Physics, Azerbaijan National Academy of Sciences, Baku, Azerbaijan
ahadzade79@mail.ru, vefa86haciyeva@gmail.com

Abstract- The article describes the electrical properties of the intercrystallite boundary and mechanisms of conductivity in a ZnO varistor with impurities. The study shows the properties of the reagents used in the synthesis of the ZnO varistor, as well as the composition of the substances used to provide the varistor effect. The article also presents the energy diagrams of the crystallite boundary in the ZnO varistor, the equivalent circuit diagram and the energy diagram of micro varistors, respectively. It has been established that conductivity is possible during physical processes both at the intercrystallite boundary and through a potential barrier. And also, the dependence of conductivity on frequency and temperature was shown. It turned out that in the low-frequency region, the electrical conductivity increases monotonically, and then strongly increases with increasing frequency. In this case, the electrical conductivity σ changes according to the law $\sigma \approx f^{0.8}$. The resulting dependence $\sigma \approx f^{0.8}$ indicates a hopping mechanism of charge transfer over states localized in the vicinity of the Fermi level [1]. Dependence of conductivity on temperature, it can be said that the charge transfer in the varistors under study is carried out by hopping conduction of electrons with a variable hopping length over localized states lying in a narrow energy band near the Fermi level. These states in a varistor can be created by extended defects, intercrystallite boundaries and dislocations.

Keywords: ZnO Varistors, Impurities, Potential Barrier, Crystallite, Reagents, Diffractogram, Non-Linearity, Electrical Conductivity, Frequency, Temperature.

1. INTRODUCTION

It is known that that semiconductor materials are of great importance for power engineering due to their non-linear conductivity. The use of such materials provides attenuation of harmful voltage waves, which can be amplified during power surges on high voltage lines and half stations. It should be noted that SiC and ZnO materials with symmetrical current-voltage characteristics are mainly used for this purpose in modern electrical engineering. The material based on these elements (at operating voltages) as a dielectric has a high resistance. With a sharply decreasing resistance, it has a conductive property, i.e., varistor property. If we connect such an element, for example, a transformer, in parallel to our protective device, then the sharply rising waves will decrease, and the device will not detect high transient voltages [13].

Numerous experimental results show that the formation of the varistor effect in these materials is directly related to the presence of a potential barrier at the boundaries of the crystallite-amorphous phase [2]. Such a structure of ZnO causes bipolar conductivity in the specified material and the ability to change the resistance sharply at certain voltages.

One of the factors that distinguishes ZnO ceramics from a varistor is the wide variation in its basic electrophysical parameters due to the introduction of a small number of impurities into them. It should be noted that one of the most promising areas for the development of protective devices and elements is the creation of two-phase and multiphase composite materials based on a ceramic varistor [7-16].

2. METHOD OF ANALYSIS

For the manufacture of varistors, a ceramic charge of the composition (mol.%) 96.5ZnO + $0.5Bi_2O_3$ + $0.5Co_3O_4$ + $0.5MnO_2$ + $0.5B_2O_3$ + $1Sb_2O_3$ + $0.5ZrO_2$ in an amount of 100 g is weighed and crushed in a ball mill to a particle size of 60 microns or less [4]. Then, granules are prepared from this mixture, which are pressed under a force of 40-ton force to obtain samples in the form of washers 10 mm high and 20 mm in diameter. After that, the samples are placed in an electric furnace for synthesis: heating to a temperature of 900°C is carried out at a rate of 150 °C/h, and to a temperature of 1250 °C at a rate of 200 °C/h.

The properties of the reagents used and the composition of the varistor samples are shown in Tables 1 and 2. Synthesis of pressed washers takes place in atmospheric air, and the washers are annealed at a temperature of 1200 °C for 2 hours.

After turning off the oven, the samples are cooled for 7-8 hours. These surfaces are vacuum-deposited with a thin layer (3-4 mm) of aluminum to provide electrical contact. The height of the intergranular barrier $\varphi_0 = 0.8$ eV in ZnO oxides with surface-active ions (Bi, Co, Mn). The addition of ZnO to these ions complicates its structure.

Table 1. Properties of reagents used [4]

Properties	ZnO	Bi_2O_3	Co_3O_4	Sb_2O_3	MnO_2	Ni_2O_3	CrO_3	H_3BO_3
Quan. of main component, mas. %	99.96	99.97	99.97	99.96	99.95	99.3	99.93	9.96
Degree of dispersion, μm	0.3	5-10	0.5-2	0.2-1	0.3-3	0.5-4	0.5-2	0.5-3
Density 10^3 kg/m^3	5.6	8.9	5.68	5.2	5.18	7.45	4.98	3.2
Melting points, °C	1975	817	1805	655	1785	1957	break	break
Cation radius, mm	0.074	0.098	0.072	0.090	0.080	0.069	0.052	-
Type of electrical conductivity	N	p	p	p	p	p	p(Cr_2O_3)	p

Table 2. Composition of varistor samples [4]

Ingredient	Sample No. 1		Sample No. 2		Sample No. 3	
	mol%	Quantity in 500 g	mol%	Quantity in 500 g	mol%	Quantity in 500 g
ZnO	97	91.6	96.5	90.76	95.5	89.577
Bi_2O_3	0.5	2.7	0.5	2.69	0.5	2.6845
Sb_2O_3	1	3.4	1	3.368	1	3.359
Co_3O_4	0.5	1.398	0.5	1.392	0.5	1.3887
B_2O_3	0.5	0.41	0.5	0.404	0.5	0.403
MnO_2	0.5	0.51	0.5	0.502	0.5	0.4955
Cr_2O_3	-		0.5	0.878	0.5	0.876
Ni_3O_2	-	-	-	-	0.5	0.522
SiO_2	-	-	-	-		0.692

For example, when trivalent Ca is added to ZnO, adsorption surfactant centers are formed. The resulting this structure can localize free electrons [Ca^{3+}-O_2^-] Numerous experimental results show that the potential crystal barrier in ZnO stabilizes only in the range of 350-400 °C, regardless of the type of impurity. In general, it is necessary to determine the mechanism of physical processes in bipolar conduction devices, to ensure the use of varistor materials for various purposes, and the stability of their properties [8].

When choosing various functional varisters made of semiconductor ceramic materials (for example, ZnO, SiC), it is necessary to take into account their crystalline conductivity, band gap, electrical conductivity of electric charges, and potential amplitudes at the interface between amorphous and crystalline phases. Consider the process of moving charge carriers in ZnO, which differs from a number of other semiconductor materials.

The process of moving electric charges in polycrystalline semiconductor ceramics based on ZnO is divided into two groups:

- the movement of electrons through a potential barrier;
- along the border of a potential barrier.

The first mechanism is the conversion of electrical carriers from crystallites to crystalline ones, and the second mechanism is breakthrough displacements. Despite the differences in voltage ranges and types of materials, the only working element of all ceramic varistors with a fuzzy structure is the crystallite boundary.

At present, ZnO-based varistors are widely used in high voltage technology to limit the increase in voltage (current) caused by various reasons. The non-linearity (β) of the current-voltage voltage (U_{op}) of ZnO-based cells varies in the range of 50-70. This high non-linearity makes ZnO varistors indispensable compared to other semiconductors [4]. The ZnO varistors are connected in series and placed in a dielectric coating. One of the most important factors in the application of varistors is the stability of their parameters. To do this, electro thermal wear of the varistor is carried out: under the influence of an electric field, the barriers are heated to 403-423 K, and then cooled to room temperature. To protect them from the environment, the surface of the electrodes is varnished. This process is repeated until the varistor opening voltage (U_{op}), non-linearity factor (β) and resistance (ρ) to the opening voltage stabilize. It is important that the varistor settings are protected from moisture in order for them to remain stable. The last operation of varistors is to place electrodes on their surface. The process is carried out as follows: the surface of the elements is chemically cleaned, silver pastes are placed on the surface and fired. To protect the electrodes from the environment, their surface is polished. ZnO is a semiconductor compound and is type A^2 B^6 [3].

The corresponding parameters of SiC, its band gap is larger than that of other semiconductors. Therefore, the non-linearity of the original ZnO must be greater after its opening voltage, since its coefficient of non-linearity is smaller. However, despite the band gap, due to the lack of oxygen during the firing process, the stoichiometry of ZnO is distorted and therefore has an n-type semiconductor. A very thin insulating region is formed among the ZnO crystallites, which ensures the formation of the varistor effect. The ZnO varistor, with a cross section of 1 cm^2, has a constant amplitude of several kA and can withstand high voltage surges up to the operating voltage [11].

When studying the transport characteristics of inhomogeneous materials, an important role is given to the analysis of the dispersion of the dielectric parameters of the material (dielectric permittivity, dielectric losses, etc.). The dependences of the effective values of the permittivity and the dielectric loss factor on frequency are sensitive to the relationship between the electrical parameters of the dispersed phase and the matrix, as well as to the shape of the inclusions and their orientation in an external electric field [5].

Despite the wide range of applications in various fields of physics and chemistry [6, 10, 15], theoretical studies of the dispersion of the permittivity of heterogeneous media are hindered for a number of reasons, among which the following should be noted.

Analytical calculations of the effective parameters of multi component systems, which are of independent importance and are an integral part of the theory of dispersion of inhomogeneous dielectrics, are in themselves a complex mathematical problem that can be solved only in individual cases.

The frequency dependence of the dielectric parameters, namely, the components of the complex permittivity, is a characteristic of the material and is determined for each substance not only by the properties of the material's molecules, but by the presence and composition of impurities [4, 10, 13]. Note that the addition of ZnO with additives of various composition directly affects their crystal structure and physical properties. Therefore, the determination and comparison of structure-sensitive physical properties and crystal structure, which are important for semiconductors, is one of the important issues [6, 17].

It should be noted that the study of electrical conductivity is one of the main methods used to determine the purity of materials, mainly metals and semiconductors. In addition, electrical conductivity makes it possible to clarify the dynamics of current carriers in a macroscopic object, the features of their interaction with each other and the object with other objects. The mechanism of electrical conductivity in dielectric materials is more complex than in semiconductor materials. This is due to the fact that the movement of electric charge carriers (electrons, holes) in these materials is hindered by various factors, for example, defects in the crystal lattice, including deep and shallow traps of energy levels in its band gap, scattering of the lattice crystal from thermal vibrations, etc. d. available [13]. Figure 1 shows the conductance as a function of frequency.

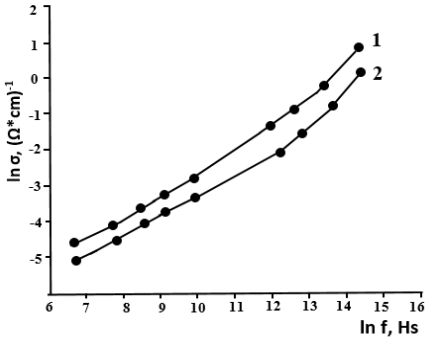

Figure 1. Dependence conductivity from frequency (ZnO with impurities) 1-303K, 2-344K [5]

Figure 1 shows that in the low-frequency region, the electrical conductivity increases monotonically, and then increases strongly with increasing frequency. In this case, the electrical conductivity σ changes according to the law $\sigma \approx f^{0.8}$. The dependence $\sigma \approx f^{0.8}$ obtained indicates a hopping mechanism of charge transfer over states localized in the vicinity of the Fermi level [1]. Note that at the temperatures under study, the $\sigma=F(f)$ dependence has the same character [5]. Figure 2 shows the temperature dependence of conductivity at f=10 kHz.

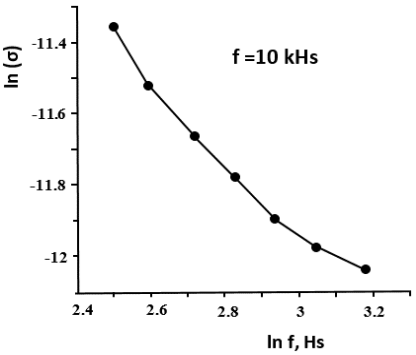

Figure 2. Conductivity versus temperature at f=10 kHz (ZnO with impurities) [5]

It can be seen from the experiments and Figure 2 that the conductivity decreases with the temperature dependence. Note that the frequency dependence of the dielectric parameters, namely, the components of the complex permittivity, is a characteristic of the material and is determined for each substance not only by the properties of the material's molecules, but by the presence and composition of impurities [5].

3. CONCLUSIONS

The article describes the electrical properties of the intercrystallite boundary and mechanisms of conductivity in a ZnO varistor with impurities. It has been established that conductivity is possible during physical processes both at the intercrystallite boundary and through a potential barrier. And also, the dependence of conductivity on frequency and temperature was shown. It was found that the frequency dependence of the dielectric parameters is a characteristic of the material and is determined for each substance not only by the properties of the molecules of the material, but by the presence and composition of impurities.

ZnO ceramic varistors with all these advantages, proven in experiments, are synthesized with polymers to produce high-quality composites for the energy field and are successfully applied [7-16].

REFERENCES

[1] N. Mott, E. Davis, "Electronic Processes in Non-Crystalline Substances", Mir, p. 472, 1974.

[2] Kharbeka, "Polycrystalline Semiconductors - Physical Properties and Applications", Mir, p. 341, Moscow, Russia, 1989.

[3] N.M. Livanova, Y.I. Lyakin, A.A. Popov, V.A. Shirinev, "Structure of the Interfacial Layer and Properties of Cross-Linked Heterophase Mixtures of Butadiene-Nitrile and Ethylene-Propylene Diene Elastomers", High-Molecular Compounds, Vol. 49, No. 3, pp. 465-472, 2007.

[4] A.M. Hashimov, K.B. Kurbanov, S.M. Hasanli, R.N. Mehdizadeh, S.M. Azizova (Ahadzade), K.B. Bayramov, "Varistor", State Agency for Standardization, Metrology and Patent of Azerbaijan, Vol. 60, No. I, 2007.

[5] F. Kharirchi, S.M. Hasanli, S.M. Azizova (Ahadzade), J.J. Khalilov, "Spectroscopy of Dielectric Parameters of ZnO-Based Varistors", Electronic Processing of Materials, Vol. 48, No. 1, pp. 58-62, 2012.

[6] F.L. Souza, J.W. Gomes, P.R. Bueno, et al., "Effect of Addition of ZnO Seeds on the Electrical Properties of ZnO Based Varistors", Materials Chemistry and Physics, Vol. 80, p. 512, 2003.
[7] S.M. Azizova (Ahadzade), "Electrophysical Properties of the Polymer-ZnO Composite used in Electric Gas Discharge", Problems of Energy, No. 1, pp. 72-76, 2009.
[8] S.M. Azizova (Ahadzade), "Determination of Main Parameters of ZnO Substitutes and Optimization of the Synthesis Process", Problems of Power Engineering, No. 4, pp. 22-29, 2021.
[9] A.M. Hashimov, K.B. Kurbanov, S.M. Hasanli, R.N. Mehdizadeh, S.M. Azizova (Ahadzade), K.B. Bayramov, "Method of Preparation of Composite Varistors of Thin Layers", State Agency for Standardization, Metrology and Patent, Azerbaijan, Vol. 172, No. I, 2007.
[10] A.M. Hashimov, S.M. Hasanli, R.N. Mehtizadeh, S.M. Azizova (Ahadzade), K.B. Bayramov, "The Nonlinear Resistor on the Basis of a Composition Polymer - Ceramics", JTF, Vol. 77, No. 8, pp. 127-130, 2007.
[11] S.M. Ahadzade, A.M. Hashimov, "Variation of the Main Parameters Composite Varistors Based on ZnO", The 16th International Conference on Technical and Physical Problems of Engineering (ICTPE-2020), Rumeli University, pp. 99-101, Istanbul, Turkey, 12-13 October 2020.
[12] S.M. Ahadzadeh A.M. Hashimov S.G. Khalilova, "Research of the Electrical Properties of Composite Varistors Based on ZnO-polymer", The 17th International Conference on Technical and Physical Problems of Engineering (ICTPE-2021), Rumeli University, pp. 86-89, Istanbul, Turkey, 18-19 October 2021.
[13] A.M. Hashimov, S.M. Hasanli, R.N. Mehtizadeh, K.B. Bayramov, S.M. Azizova (Ahadzade), "Zinc Oxide and Polymer Based Composite Varistors", Physical Status Solidi (PSS), No. 8, pp. 2871-2875, 2006.
[14] S.M. Ahadzadeh A.M. Hashimov, "Possibility Varistor Effect of Different Properties in Polymers", The 12th International Conference on Technical and Physical Problems of Power Engineering (ICTPE-2016), University of the Basque, pp. 181-183, Bilbao, Spain, 7-9 September 2016.
[15] M.A. Kurbanov, S.M. Ahadzadeh, I.S. Ramazanova, Z.A. Dadashov, I.A. Farajzade, "Varistor Effect in Highly Heterogeneous Polymer-ZnO Systems", FTP, Vol. 51, Issue 7, pp. 992-997, 2017.
[16] S.M. Ahadzadeh, A.M. Hashimov, S.G. Khalilova, "Research of the Electrical Properties of Composite Varistors Based on ZnO-Polymer", International Journal on Technical and Physical Problem of Engineering (IJTPE), Issue 50, Vol. 14, No. 1, pp. 166-171, March 2022.
[17] V.S. Pershenkov, V.D. Popov, A.V. Shalnov, "Surface Radiation Effects in ICs", Energy Publishing House, p. 256, Moscow, Russia, 1988.

BIOGRAPHIES

Shafaq Mirbaba Ahadzade was born in Shirvan, Azerbaijan on February 16, 1979. She graduated from Electrical Engineering Faculty, Azerbaijan Technical University, Baku, Azerbaijan in 2000 and received the Master's level from the same university 2002. In 2010, she defended his thesis on the topic "Varistor effect of composite materials based on polymer and zinc oxide ceramic with various impurities" and received Ph.D. in Physics in 2017. She is an Associate Professor since 2017. She has participated in a number of national and international scientific conferences, published about 38 scientific articles, and has 2 patents. She currently works as a leading researcher in Physics and Techniques of High Voltages Laboratory, Institute of Physics, Azerbaijan National Academy of Sciences, Baku, Azerbaijan. Her research interests are mechanism of the formation of the varistor effect in composites based on polar and nonpolar polymers and zinc oxide ceramics with various impurities.

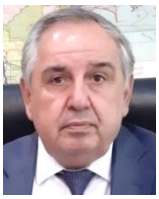

Arif Mamed Hashimov was born in Shahbuz, Nakhichevan, Azerbaijan on September 28, 1949. He is a Professor of Power Engineering (1993); Chief Editor of Scientific Journal of "Power Engineering Problems" from 2000; Director of Institute of Physics of Azerbaijan National Academy of Sciences (Baku, Azerbaijan) from 2002 up to 2009; and Academician and the First Vice-President of Azerbaijan National Academy of Sciences from 2007 up to 2013; and Director of Azerbaijan Research Institute of Energetic and Energy Design from 2014 up to 2020.From 2021 up to now he is Director of Institute of Physics of Azerbaijan National Academy of Sciences (Baku, Azerbaijan). He is laureate of Azerbaijan State Prize (1978); Honored Scientist of Azerbaijan (2005); Cochairman of International Conferences on "Technical and Physical Problems of Power Engineering" (ICTPE) and Editor in Chief of International Journal on "Technical and Physical Problems of Engineering" (IJTPE). He is also a High Consultant in "Azerenerji" JSC, Baku, Azerbaijan. His research areas are theory of non-linear electrical Networks with distributed parameters, neutral earthing and ferroresonant processes, alternative energy sources, high voltage physics and techniques, electrical physics. His publications are 350 articles and patents and 5 monographs.

Tarana Kamil Nurubeyli was born in Baku, Azerbaijan on February 17, 1978. She graduated in Master degree in Honours from Baku State University, Baku, Azerbaijan in 2001. Since 2004 she was a research assistant of Institute of Physics, Azerbaijan National

Academy of Sciences, Baku, Azerbaijan. Since 2011, she was a candidate of physics-mathematical sciences (Ph.D.). Her scientific interests are design of mass analyzers, estimation of assembly and designing of time-of-flight energy-mass analyzers, carrying out of tests of developed devices, planning and carrying out of scientific researches with a chromatograph mass spectrometer. She is a member of Russian Mass-Spectrometry Society.

Vafa Musa Hajiyeva was born in Azerbaijan on 18, August 1986. She received the B.Sc. and M.Sc. degrees in Physics from Azerbaijan State Pedagogical University, Baku, Azerbaijan in 2005, 2017, respectively. Currently, she is an engineer at Institute of Physics, Azerbaijan National Academy of Sciences, Baku, Azerbaijan.

Sabina A. Huseynova was born in Baku, Azerbaijan, on July 24, 1977. She received B.Sc. and M.Sc. degrees from Azerbaijan State Oil Academy, Baku, Azerbaijan in 1998, 2002 respectively. Currently, she is a scientific researcher in Physics and Techniques of High Voltages Laboratory, Institute of Physics, Azerbaijan National Academy of Sciences, Baku, Azerbaijan. Her areas of expertise are various types of heaters, including industrial carbon, butyl rubber, and electric heater.

Sevil Sedireddin Ahadova was born in Gabala, Azerbaijan, on October 16, 1962. She is a High-Laborant at Institute of Physics, Azerbaijan National Academy of Sciences, Baku, Azerbaijan.

The 18th International Conference on
"Technical and Physical Problems of Engineering"
30 October 2022
International Organization of IOTPE

ICTPE Conference
www.iotpe.com
ictpe@iotpe.com
ictpe0@gmail.com

ICTPE-2022 Number 11 Code 02ELC04 Pages 55-58

PROPERTIES OF PHOTOCONDUCTIVITY AND VOLTAMMETRY IN HETEROJUNCTION WITH n-InTe/p-$TlGaTe_2$ STRUCTURE

M.S. Hasanova C.I. Abilov N.T. Huseynova

Azerbaijan Technical University, Baku, Azerbaijan, mhsh28@mail.ru, cabilov@yahoo.com, nigar.huseynova@aztu.edu

Abstract- A thin-layer heterojunction with n-InTe/p-$TlGaTe_2$ structure was created, its photoelectric, volt-ampere and other characteristics were studied, energy diagram of the transition was constructed. Based on finding the maximum value of photoconductivity, it was proposed to use the generated heterojunction a sensitive recording device at near infrared wavelengths. It is shown that at low voltage values, the current flow in the heterojunction is determined by the equilibrium conductivity. Based on the value of some parameters, it was determined that the volume of injection current of the n-InTe layer is limited by space loads. It is shown that the exponential distribution of local conditions in the restricted zone is the result of the process of straight tunneling of the main carriers from the p-$TlGaTe_2$ layer to the epitaxial n-InTe layer.

Keywords: Heterojunction, Photoconductivity, Voltammeter, Energetic Diagram.

1. INTRODUCTION

The photoelectric properties of heterojunction can be divided into two major groups. One is the generation of a photocurrent as a result of the absorption of photons, and the other is the emission of photons as a result of the excitation of electrons. There are different mechanisms of photon absorption depending on the wavelength of light that affects the structure. Both of these processes are important. The first is the process of generating free electrons and holes, that is, the presence of photo-excitation of additive conditions or conditions at on the border of separation. The second is the process that leads to the generation of an electron-hole pair (excitation of an electron from the valence band to the conduction band). Namely, the generation of free charge carriers at contact at the separation boundary or within the diffusion length causes a photocurrent to form in the heterojunction. The generation of free charges can occur not only through the absorption of photons, but also under the influence of an electric field. Radiative recombination of generated free charge carriers leads to the emission of photons.

2. EXPERIMENTAL PART

The creation of the heterojunction was carried out in accordance with the technology given in [1]. However, in this case, the following is taken as a basis. Depending on the type of conductive type of condensed material, in order to obtain a stoichiometric composition, the substances in the source of tellurium and indium tellurides were completely evaporated and precipitated on the substrate (single crystal of $TlGaTe_2$ compound 0.8-1 mm thick). The surface of the $TlGaTe_2$ compound used as a substrate was electrochemically treated, smoothed and cleaned. When a thin layer of InTe is obtained separately, the contacts are made of pure In and Ni elements. The lower and upper contacts of the n-InTe/p-$TlGaTe_2$ structure have always been made of indium. It should be noted that when a thin layer of pure InTe was formed, the temperature of the sources of indium and tellurium was ~1373 K in the in part and ~1253 K in the tellurium part. When the thin layers were formed from pre-synthesized InTe and In_2Te_3 compounds, the evaporator source temperature was ~1473 K (when InTe was obtained) and ~1453 K (when In_2Te_3 was obtained). Thus, the deposition of indium tellurides on the substrate was carried out by evaporation of both individual elements and evaporation of dual indium telluride compounds. The voltammeter characteristic and the spectral dependence of the photoconductivity in the generated heterojunction were performed according to the method given in [2].

3. RESULTS AND DISCUSSION

It is known that the volt-ampere characteristic of a heterojunction changes its position when the structure is exposed to photons. As a result, this change is characterized by the following formula:

$$I = I_S = \left[\exp\frac{qU}{kT} - 1\right] - I_R \qquad (1)$$

where, I_S is the dark reverse saturation current density, I_R is the photocurrent density, and U is the applied voltage. In the absence of generation and recombination of carriers in the decontaminated area, the I_R value does not depend on the voltage and is equal to the short-circuit current (I_{SC}). In the open circuit (I=0), the free-flow voltage (V_{ff}) in heterojunction depends on photocurrent density and dark saturation current as follows;

$$V_{ff} = \frac{kT}{q}\ln\left(1+\frac{I_R}{I_S}\right) \quad (2)$$

In general, the I_R depends on the geometric dimensions of the heterojunction, on the physical properties' semiconductor materials of the heterojunction, and the direction of irradiation. In practice, the heterojunction is mainly affected by a large semiconductor zone (perpendicular to the transition), which is blocked by light rays.

In this case, high-energy hotons are absorbed in a material with a large band gap, while small energies pass through this material and are absorbed near the contact boundary of the small bandwidth material. This phenomenon is known in the literature as the "window effect", and it causes the growth of the photo response. If the F_0 photon flux falls on the front of a material with a large band gap, then the I_R current associated with the absorption of photons will consist of two components I_{R1} and I_{R2}, which are also associated with the recombination of electron-hole pairs from broad and narrow band bands, respectively. Since these processes do not exclude the occurrence of these processes in the n-InTe/p-$TlGaTe_2$ heterojunction created by us, the structure was illuminated by p-$TlGaTe_2$ and the dependence of the wavelength of light acting on the photocurrent was studied. When measuring photoconductivity, voltage was also applied to the heteroconductor.

Figure 1 shows the spectral characteristics of the generated heterojunction at different values of applied voltage. As can be seen, as the value of the applied voltage increases, the photosensitivity increases. The maximum dependence is found at each value of the voltage. In each case, the maximum in the characteristics corresponds to a wavelength of ~0.93 μm. However, the value of the width of the forbidden zone of the material was calculated using the value of 1.05 μm of spectral attenuation formed after the maximum. In this case, a value of ~1.18 eV was obtained for the width of the restricted zone, which is well consistent with the energy parameter of the $TlGaTe_2$ compound. Reaching the maximum value of photoconductivity indicates that the resulting n-InTe/p-$TlGaTe_2$ heterojunction can be used as a near-infrared wavelength sensitive sensor.

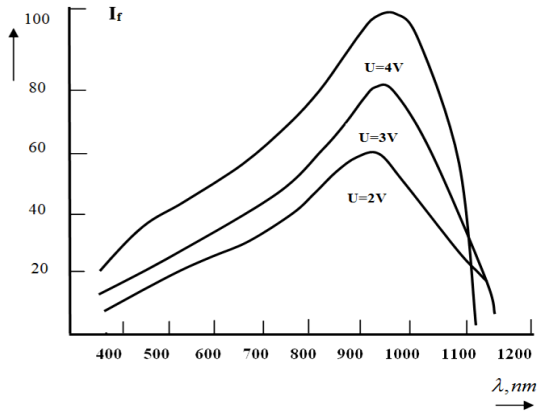

Figure 1. Spectral dependence of photoconductivity at different values of applied voltage in a heterojunction

The voltampere characteristic of the created n-InTe/p-$TlGaTe_2$ structured heterojunction was measured at room temperature. Because ohmic contacts are indium, it has not been possible to study voltampere characteristic at higher temperatures. An energy diagram of the heterojunction created according to the model proposed in, without taking into account the surface electrical conditions (Figure 2) [3]. The diagram is based on the values of the energy parameters of the InTe and $TlGaTe_2$ compounds derived from literature and our own research. There are, $E_c = \chi_1 - \chi_2 = 1.11$ eV and $E_V = \Delta E(TlGaTe_2) - \Delta E(InTe) = 0.24\ \text{eV} \cdot \Delta\chi$ quantity the quantities found for the average value of the electronegativity of the elements in the compounds in contact.

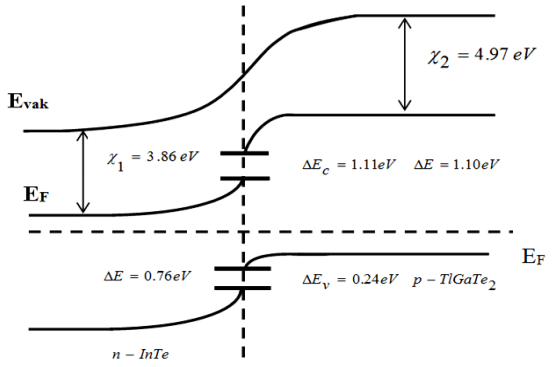

Figure 2. n-InTe/p-$TlGaTe_2$ energy diagram of the heterojunction (E_{vak} is vacuum level, E_F is Fermi level, electron greedy)

And some of the data was derived from studies in the case. For example, the energy of the Fermi level E_F, in the previous paragraphs, $\log\sigma \sim f(10^3/T,K)$ is assumed to be equal to the activation energy of the additives (for example in accordance with the [4, 5] methodology). That is, its distance to the passage zone is 0.01 eV in the InTe combination. To calculate the thickness of areas weakened by additives in the InTe and $TlGaTe_2$ compounds, the following statements can be used in [6].

$$d_n = \sqrt{\frac{2\varepsilon_0 N_A \varepsilon_n \varepsilon_p \varphi_0}{eN_D\left(\varepsilon_n N_D + \varepsilon_p N_A\right)}}$$
$$d_p = \sqrt{\frac{2\varepsilon_0 N_D \varepsilon_n \varepsilon_p \varphi_0}{eN_A\left(\varepsilon_n N_D + \varepsilon_p N_A\right)}} \quad (3)$$

where, e is the load of the electron; ε_0 is dielectric constant (8.85×10^{-12} Fm^{-1}); ε_n and N_D are relative dielectric constant and concentration of donors; ε_p and N_A are relative dielectric constant and concentration of acceptors; and φ_0 is the height of the potential fence.

From the measurement of the stationary voltammetric characteristics of the resulting solid structure, it was found that the heterojunction n has the ability to straighten. The value of the correction factor in the heterojunction is small (k=3÷10). The direction of current discharge is compensated by the positive values of the external slip of the base. As can be seen from Figure 3, the dark voltampere characteristic of the heteroconductor generated at low voltages is symmetrical.

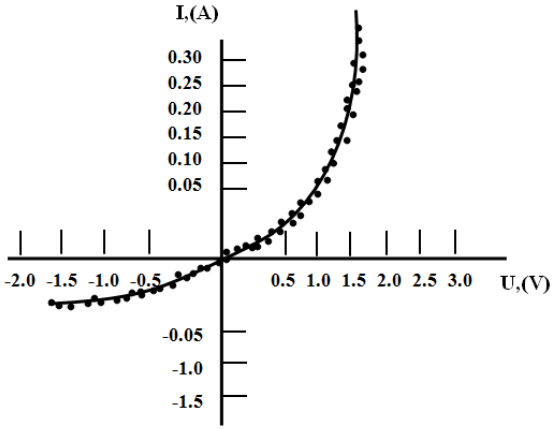

Figure 3. Volt-ampere characteristic of a heterojunction with n-InTe/p-$TlGaTe_2$ structure

This shows that the value of current at low voltages is determined not by injection, but by equilibrium conductivity. At currents up to 2V, the exponential part of the voltampere characteristic corresponds well to the expression $I = I_0 \exp \frac{eV}{\beta kT}$.

In here β=1.2-2.0 which indicates that a generation-recombination process has taken place in the field of volumetric loads. It was determined that the voltage separating the current from the linear part of the voltampere characteristic has a value of V_d = 0.98 V. In the opposite direction, at relatively low values of voltage (U<3V), the voltampere characteristic of the resulting solid structure obeys the linear law.

However, at large prices of the reverse voltage, there is a gradual hole that indicates that the reverse voltage is based on tunnel mechanism. At zero voltage values, the dark saturation current from the rectilinear part of the voltampere characteristic in the direction of current discharge did not exceed 10^{-6}A/sm^2. This value indicates that the concentration of equilibrium carriers involved in the conduction is not large. At values of voltage higher than V_d, the straight arm of voltampere characteristic is explained by the law $I=B\cdot U_m$(Figure 4). Here, B is the coefficient of proportionality, and m is the composite indicator of the voltage and takes values of m=1.4-1.6.

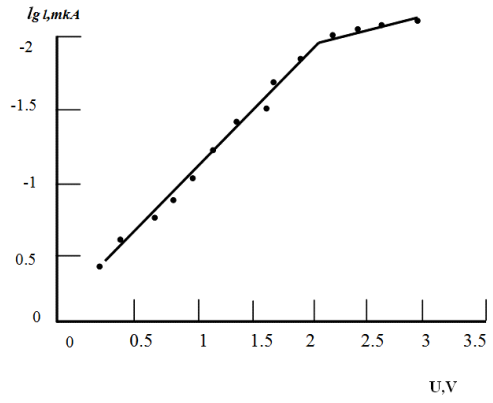

Figure 4. The straight arm of the voltampere characteristic is on the semi-logarithmic scale of the n-InTe / p-$TlGaSe_2$ heterojunction

According to the literature, such dependence may be due to the fact that the volume of injection current in the n-InTe layer is limited by space loads. There is also an exponential distribution of local conditions in the no-go zone. In this connection, it can be assumed that the process of straight tunneling of the main carriers from p-$TlGaTe_2$ to the n-InTe layer takes place. At values $V < V_d$, there is also thermal activation of the carriers in the valence band. At voltages higher than V_d, the process of regulating the current in the n-InTe layer with volumetric space loads takes place.

REFERENCES

[1] M.S. Hasanova, C.I. Abilov, N.T. Huseynova, "Elaboration of Solid-State Structure n-In_2Te_3 p-$Cu_2Ga_4Te_7$", Book of Abstract, The 31st International Physical Congress, p. 339, Bodrum, Turkey, 21-24 July 2014.

[2] L.P. Pavlov, "Methods for Measuring the Parameters of Semiconductor Materials", Higher School, p. 240, Moscow, Russia, 1987.

[3] B.L. Sharma, R.K. Purohit, "Semiconductor Heterojunctions", Elsevier, Vol. 5, 2015.

[4] M.S. Hasanova, "Physico-Chemical and Electrophysical Properties of Crystals of the In_2Te_3-Fe_2Te_3 System", Dissertation of the Degree of Candidate of Physical and Mathematical Sciences, p. 183, Baku, Azerbaijan, 1997.

[5] S.A. Zeynalov, "Electrical and Thermal Properties of Systems In_2Te_3 - Cr_3Te_4 and In_2Te_3 - Co_3Te_4 / Abstract of Dissertation for the Degree of Cand", Physical and Mathematical Sciences, p. 22, Baku, Azerbaijan, 2003.

[6] A. Ferenbrukh, R. Bube "Solar Cells Theory and Experiment", Energoatomizdat, p. 360, Moscow, Russia, 1987.

BIOGRAPHIES

Mehriban Shirin Qizi Hasanova was born in Tovuz, Azerbaijan, on February 28, 1964. In 1998 she defended her thesis on the specialty Solid State Physics on theme Physical-chemical and electrical-physical properties of In_2Te_3-Fe_2Te_3 system crystals" and received the Ph.D. degree in physics and mathematics. She completes work on her doctoral thesis "Physical and chemical fundamentals of technology of new materials based on indium tellurides and their electronic and thermal properties". Currently, she engaged in research of high thermal efficiency based on Fe_2Te_3, nature of the phase stability in semiconductor systems, study of electrical characteristics, galvanomagnetic and thermal properties of the materials of complex composition. She has 130 publications.

Chingiz Ildirim Abilov was born in Shusha Azerbaijan, on December 5, 1945. In 1980 he defended his thesis on specialty Technology of semiconductors and electronic materials and received the Ph.D. degree in Technology. In 1994 he defended his doctoral thesis on the specialty Technology of semiconductors and electronic materials and received the title of Doctor of Technical Sciences. In 1996 he was awarded the title Associate Professor. He is currently a Professor at Electronics Department of Azerbaijan Technical University, Baku, Azerbaijan. In 2011, he has been awarded "Progress" medal. His scientific research fields are AIIIBVI, A2VB3VI and AIVBVI type compounds and solid solutions based on them, the study of their physicochemical, electrophysical properties, the development of technology of thermo- and photovoltaic converters. He is an author of 265 publications, including 10 copyright certificates, 1 handbook, 2 monographs, 5 textbooks.

Nigar Tarkhan Huseynova was born in Baku, Azerbaijan, on April 9, 1963. She defended her dissertation in the specialty of Electrophysics on the topic "The features of ageing of ethylene-α-olefine copolymers affected by the electric charges" in 2007 and received the Ph.D. degree in physics and mathematics. Her research interests are mechanism of electrical aging of polymer dielectrics by determining the relationship between the structure of ethylene copolymers with α-olefins formed by varying the composition, quantity and geometric dimensions of the comonomer and changes in their electrical and physical-mechanical properties under the action of partial discharge plasma. She has 69 publications.

The 18th International Conference on
"Technical and Physical Problems of Engineering"
30 October 2022
International Organization of IOTPE

ICTPE Conference
www.iotpe.com
ictpe@iotpe.com
ictpe0@gmail.com

ICTPE-2022 Number 12 Code 02ELC05 Pages 59-62

CLASSIFICATION OF SMALL-ANGLE X-RAY SCATTERING REFLECTIONS ON ORIENTED POLYMER SYSTEMS

A.M. Hashimov [1] K.B. Gurbanov [1] Z.A. Tagiyeva [1] S.V. Bayramov [2] L.C. Suleymanova [2] N.M. Tabatabaei [3]

1. Institute of Physics, Azerbaijan National Academy of Seances, Baku, Azerbaijan, tzenfira@mail.ru
2. Mingachevir State University, Mingachevir, Azerbaijan, suleymanovalc@mail.ru
3. Electrical Engineering Department, Seraj Higher Education Institute, Tabriz, Iran, n.m.tabatabaei@gmail.com

Abstract- The work involves the categorization of small-angle X-ray patterns discovered through the investigation of orientated, amorphous-crystalline polymers. The suggested one-dimensional model may be utilized to analyze the shape of various small-angle reflections, according to an examination of the work done.

Keywords: Polymer, X-ray, Reflex, Classification, Intensity, Small-Angle X-ray Patterns, Macromolecule, Texture, Crystallization.

1. INTRODUCTION

Numerous studies have been conducted (both domestically and internationally) on small-angle X-ray scattering on oriented polymers of different types that are produced and processed under a variety of different circumstances. This research resulted in the identification of numerous types of small-angle X-ray diffraction patterns. [1-5]. Figures 1 and 2 show diagrams of the most common types of such X-ray diffraction patterns characteristic of polymers. Of course, it is not possible to describe all the small-angle radiographs observed so far within the framework of this article: this would require compiling an entire album (which, undoubtedly, could be one of the handbooks for specialists in this field). Consideration of a large number of small-angle X-ray patterns allowed D. Ya. Tsvankin [1] to classify them for the first time and distinguish two groups of reflections.

Figures 1 and 2 schematically show the small-angle X-ray diffraction patterns that are typically seen in the investigation of materials with a high degree of orientation. Figure 1a shows a reflex in the shape of a stroke that intersects the meridian of the X-ray diffraction pattern, with the meridian itself acting as the stroke's point of highest intensity. This is the simplest reflection possible because the macromolecules' axes and the sample's texture axis are in line with one another. This reflection is particularly common in orientated samples with a C-texture. The term "four-point" refers to a small-angle radiograph that is formed when the intensity maxima are symmetrically situated on both sides of the meridian and are moved from it.

The term comes from the fact that there are a total of four reflexes seen on the x-ray. The literature has a sufficient number of references to these radiographs. The existence of planes inclined with respect to the texturing axis in the structure is the most common theory used to explain the four-point radiograph. There are yet further structural interpretations of the four-point, several of which conflict with one another. We will discuss this issue in more detail in the next article, but already now we can express the opinion that due to the ambiguity of the existing interpretations of four-point radiographs, the four-point problem requires further research.

A rarer case is when instead of four reflections on a small-angle X-ray pattern, only two centrally symmetric reflections are formed, the centers of which are displaced from the meridian.

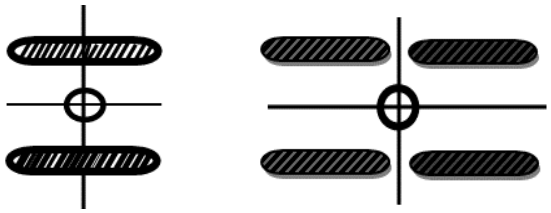

Figure 1. Schemes of tangential reflexes, (a) dashed reflex, (b) four-dot

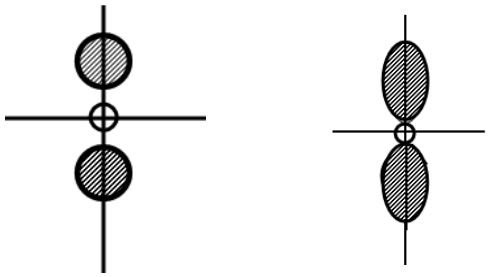

Figure 2. Schemes of radial reflections

In the works, a radiograph of this type is called a two-point radiograph or "two-point". Two-spot radiographs are obtained from samples subjected to shear deformations.

All reflections are situated on layered lines, which is a characteristic shared by the two kinds of small-angle X-ray diffraction patterns schematically depicted in (Figure 1) shows that these layer lines are usually located perpendicular to the meridian of the small-angle radiograph. If the sample has a complex texture, the axes of which are pointing in the direction of the X-ray pattern, the layer lines may also be positioned at an angle to the meridian.

This radius must be simultaneously the axis of the sample texture. Therefore, a stroke, a four-point and a two-point are called tangential reflections, meaning their location tangentially relative to any radiograph radius. Along with such maxima, X-ray diffraction patterns often reveal reflections that have a completely different form.

Frequently, maxima on a small-angle radiograph's meridian take the shape of a "circle" or "drop," stretched toward the radiograph's center (Figure 2). During the annealing of orientated samples, this sort of diffraction maxima develops.

These reflexes have a high level of intensity. Particularly strong circular reflections have tremendous intensity. The strength of this particular collection of reflexes is typically focused close to the radiograph's meridian or another radius that extends to its center. The equatorial diffuse scattering, which appears in cold drawing at the equator and is angled perpendicular to the texture axis off the sample, has to be distinguished from these radial reflections.

Figure 3. Small angle radiographs of high-pressure polyethylene (LDPE) stretched at room temperature after orientation at *T*=1000 °C

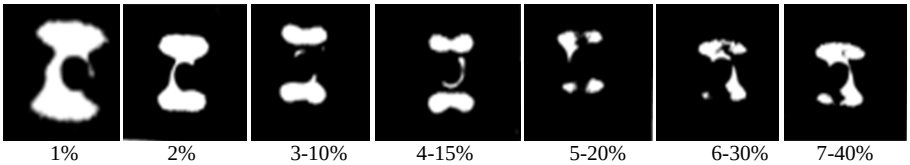

Figure 4. Small-angle radiographs of LDPE oriented at room temperature (1) then free-shrunk at *T*=100 °C (2), re-stretched at room temperature (3)-(7)

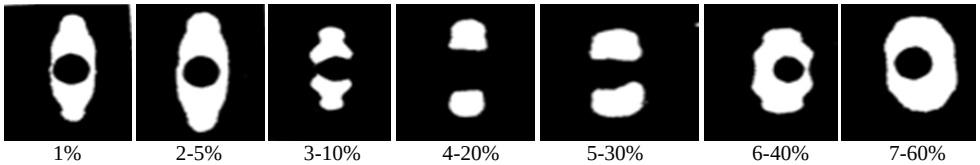

Figure 5. Small angle X-ray patterns of medium pressure polyethylene PESD lightly irradiated (*nγ* radiation) in the reactor at *T*=200 °C, stretched at *T*=1600 °C and crystallized at *T*=600 °C

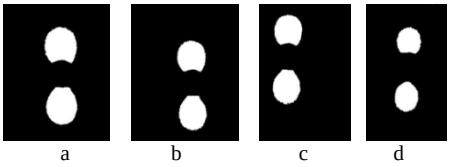

Figure 6. Patterns of small-angle X-ray diffraction of samples of polyamide 6, annealed in the free state at *T*=850 °C and deformed at room temperature

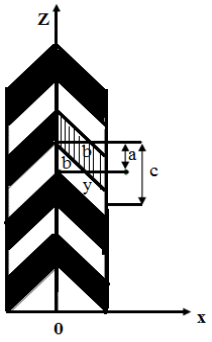

Figure 7. Scheme of the longitudinal section of the model of fibrils with sinuous layers

Issues related to four-spot radiographs, indicating that there are diagonal grating planes that are tilted with respect to the texture axis, are also considered in a model in which elementary fibrils are more independent of each other, i.e., independent to such an extent that they can move relative to each other. In this case, as shown in Figure 9, it is easy to imagine how inclined lattice planes can be formed if the crystalline regions of neighboring fibrils are not located at the same level. Indeed, such an arrangement of crystalline regions should be considered normal, because, due to steric hindrances, the location of such regions in planes perpendicular to the texture axis is very unlikely [4].

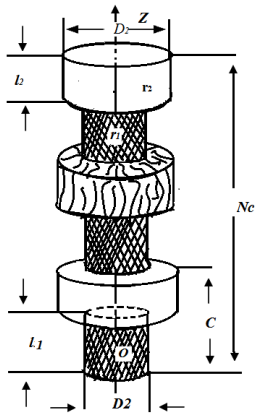

Figure 8. Schematic representation of fibrils with antinodes

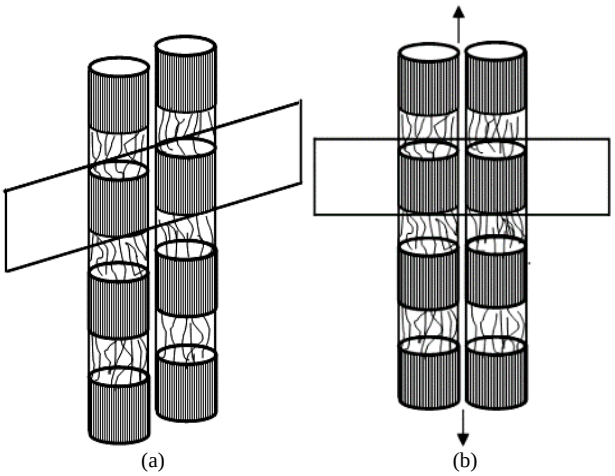

(a) (b)

Figure 9. The elementary cylinders were moved in such a way that the distortion vanished in the following diagram showing changes in the supramolecular structure during stretching of the three samples: (a) initial state, (b) sample will stretch

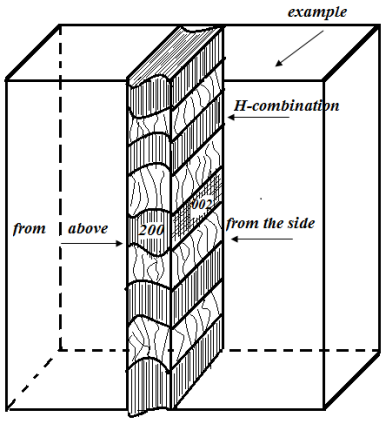

Figure 10. Scheme of the supramolecular structure of an oriented polyamide 6 film annealed in a free state

A more thorough interpretation of four-point X-ray patterns is contained in the work of D.Y. Tsvankin [1], where a new model of oriented systems is proposed. A feature of the model is that it contains crystallites in the form of oblique parallelepipeds adjacent to the transition zones and monotonically changing density. The model has a lateral smooth surface.

The suggested fibril model and an oblique crystallite are shown in Figure 7. With the use of the suggested model, small-angle scattering can be calculated, and its origins can be explained for different kinds small-angle X-rays patterns. The intensity distribution in the full reciprocal space for different values of the parameters describing the shape and dimensions of the oblique crystallite may be calculated by using the general formula for the form factor that was deduced in the study under review [1]. The author of [2] shown through an analysis of the form factor formula that the parameter bt/a is the primary parameter representing the impact of the crystallite shape on the intensity distribution. The calculations carried out and the intensity distribution graphs built on their foundation demonstrate that the occurrence of small-angle reflections of different sorts may be explained by a simple the bt/a value was increased from 0.6 to 2.0.

When it comes to axial textures, there is a progressive change from a dash to a four-dot and finally to an X-ray diffraction pattern of the "oblique four-dot" type as bt/a rises. When bt/a1.7-2.0 has large values, a radial-type reflex that is angled toward the meridian occurs. Because of this, it can be shown from the findings in [3] that the suggested one-dimensional model may be used to categorize and explain the form of different small-angle reflections. According to a review of the data from the literature, most experts believe that the four-point small-angle X-ray diffraction pattern is what causes the structure's planes to be inclined with respect to the texturing axis. Thus, the results presented in [1] show that the proposed one-dimensional model can be used to classify and interpret the shape of various small-angle reflections. An analysis of the literature data shows that most researchers explain the four-point small-angle X-ray diffraction pattern by the existence of planes inclined with respect to the texture axis in the structure.

REFERENCES

[1] D.Y. Tsvankin, "Long Periods in Oriented Polymers", Dis. for the Competition Uch. Doc. Degree, F.M. Sciences, M: Izs., Russia, 1970.

[2] S.L. Bazhenov, A.V. Efimov, A.V. Bobrov, "Conditions for the Adiabaticity of the Stretching Process of Homogeneously Deforming Polymers", High Mollusks Connection, Vol. 60, No. 5, Series A, pp. 426-430, 2018.

[3] V.A. Gerasin, B.F. Shkyaruk, M.A. Guseva, "Orientation Crystallization During Stretching of Ultra-High Molecular Weight Polyethylene, the Effect of Thermal Fixation", High Mollusks Connection, Vol. 63, No. 3, pp. 163-174, 2021.

[4] A.M. Hashimov, N.M. Tabatabaei, K.B. Gurbanov, L.C. Suleymanova, Z.A. Tagiyeva, "Structure Interpretations of Polymers Properties", International Journal on Technical and Physical Problems of Engineering (IJTPE), Issue 35, Vol. 10, No. 2, pp. 34-38, June 2018.

[5] K.B. Gurbanov, "Some Issues of X-ray Diffraction on Oriented Amorphous-Crystalline Polymer Systems", Ph.D. Thesis, Leningrad, Russia, 1974.

BIOGRAPHIES

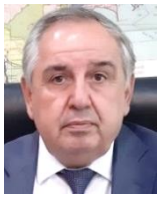

Arif Mamed Hashimov was born in Shahbuz, Nakhichevan, Azerbaijan on September 28, 1949. He is a Professor of Power Engineering (1993); Chief Editor of Scientific Journal of "Power Engineering Problems" from 2000; Director of Institute of Physics of Azerbaijan National Academy of Sciences (Baku, Azerbaijan) from 2002 up to 2009; and Academician and the First Vice-President of Azerbaijan National Academy of Sciences from 2007 up to 2013; and Director of Azerbaijan Research Institute of Energetics and Energy Design from 2014 up to 2020. From 2021 up to now he is Director of Institute of Physics of Azerbaijan National Academy of Sciences (Baku, Azerbaijan). He is laureate of Azerbaijan State Prize (1978); Honored Scientist of Azerbaijan (2005); Cochairman of International Conferences on "Technical and Physical Problems of Power Engineering" (ICTPE) and Editor in Chief of International Journal on "Technical and Physical Problems of Engineeing" (IJTPE). Now he is a High Consultant in "Azerenerji" JSC, Baku, Azerbaijan. His research areas are theory of non-linear electrical Networks with distributed parameters, neutral earthing and ferroresonant processes, alternative energy sources, high voltage physics and techniques, electrical physics. His publications are 350 articles and patents and 5 monographs.

Kamil Bakhtiyar Gurbanov was born in Agdam, Azerbaijan on December 9, 1942. He is Candidate of Physical-Mathematical Sciences in the field of "physical mathematical sciences of polymers". He defended his dissertation at the Scientific Council of Institute of High Molecular Compounds, Academy of Sciences of RF, St-Petersburg, Russia in 1974. He is a Leading Researcher of the Institute on Physics, Azerbaijan National Academy of Sciences, Baku, Azerbaijan. He is a specialist on investigation of the physical-chemical processes in the conditions of action of the electrical discharges. Under his supervision the investigations on study of the processes of oxidation and modification of materials with the use of actions of the electrical discharges are carried out and also the high effective methods of solution of the ecological problems are developed.

Zenfira Adikhan Tagiyeva was born in Baku, Azerbaijan, on December 3, 1974. She received the B.Sc. and the M.Sc. degrees from Azerbaijan State Oil Academy (Baku, Azerbaijan). Currently, she is a Scientific Researcher at Laboratory of High-Voltage Physics and Engineering, Institute of Physics, Azerbaijan National Academy of Sciences (Baku, Azerbaijan).

Shahin Vagif Bayramov was born in Mingachevir, Azerbaijan, on July 4, 1979. He defended his dissertation on "Neighborhood Policy of the European Union and the problems of integration into the economic space of Azerbaijan" and received the scientific degree of Doctor of Philosophy in Economics.

Liliya Chingiz Suleymanova was born in Yevlakh, Azerbaijan on November 8, 1978. She works as a teacher at Mingachevir State University, Mingachevir, Azerbaijan.

Naser Mahdavi Tabatabaei was born in Tehran, Iran, 1967. He received the B.Sc. and the M.Sc. degrees from University of Tabriz (Tabriz, Iran) and the Ph.D. degree from Iran University of Science and Technology (Tehran, Iran), all in Power Electrical Engineering, in 1989, 1992, and 1997, respectively. Currently, he is a Professor in International Organization of IOTPE (www.iotpe.com). He is also an academic member of Power Electrical Engineering at Seraj Higher Education Institute (Tabriz, Iran) and teaches power system analysis, power system operation, and reactive power control. He is the General Chair and Secretary of International Conference of ICTPE, Editor-in-Chief and member of Editorial Board of International Journal of IJTPE and Chairman of International Enterprise of IETPE, all supported by IOTPE. He has authored and coauthored of 10 books and book chapters in Electrical Engineering area in international publishers and more than 200 papers in international journals and conference proceedings. His research interests are in the area of power system analysis and control, power quality, energy management systems, microgrids and smart grids. He is a member of the Iranian Association of Electrical and Electronic Engineers (IAEEE).

The 18th International Conference on
"Technical and Physical Problems of Engineering"
30 October 2022
International Organization of IOTPE

ICTPE Conference
www.iotpe.com
ictpe@iotpe.com
ictpe0@gmail.com

ICTPE-2022 Number 13 Code 02ELC06 Pages 63-66

EFFECT OF COMPLEXING AGENT ON OPTICAL PROPERTIES OF CdSe THIN FILMS OBTAINED BY CHEMICAL BATH DEPOSITION (CBD)

M.H. Huseynaliyev L.N. Ibrahimova

1. Institute of Natural Resources, Nakhichevan Department of Azerbaijan National Academy of Sciences, Nakhichevan, Azerbaijan, mamedhuss@mail.ru, leyla.ibrahimova.1992@bk.ru

Abstract- At room temperature cadmium selenide (CdSe) thin films are deposited onto glass substrate employing chemical bath deposition (CBD) method. A comparative analysis of the optical properties of CdSe thin films deposited from a solution containing four components (cadmium chloride, ammonium hydroxide, triethanolamine (complexing agent), and sodium selenesulphate) and from a solution containing three components (cadmium chloride, ammonium hydroxide and sodium selenesulphate) was carried out. A shift in the band gap of a CdSe thin film obtained from a three-component solution towards higher energies was observed.

Keywords: Complexing Agent, CdSe, Chemical Bath Deposition, Sodium Selenosulphate, Thin film, Optical Absorbtion Spectrum, Tauc Equation, Band Gap.

1. INTRODUCTION

Cadmium selenide (CdSe) is considered a promising compound for use in solar energy converters due to its high optical absorption coefficient and optimal band gap. The semiconductor compound CdSe can crystallize in two different structures: zinc blende (cubic- optical band gap ~1.71 eV) and wurtzite (hexagonal- optical band gap ~1.80 eV). This compound can be used as window material, buffer layer and absorber in solar cells. The nanostructured thin CdSe films, depending on the size of the nanostructure, acquire new interesting properties that differ significantly from their bulk compounds. In addition, it is possible to control the electronic and optical properties of a nanostructured CdSe thin film by simply changing the size of nanocrystals, which allows it to be used as solar cells, high-performance thin-film transistors, photodetectors, and light-emitting diodes [1-4].

CdSe is used as an active medium in semiconductor lasers [5], liquid crystal displays, gamma-ray detectors and gas analyzers [6]. In addition, Cadmium selenide is a promising compound for the creation of photoresistors and light-emitting diodes [7, 8], highly efficient thin-film transistors [9], optical amplifiers, photocatalysts and materials for photocatalytic systems [10].

The widespread use of this material dictates the need to develop new methods of synthesis or improve old ones. More accessible are hydrothermal methods [11], spray pyrolysis [12, 13], ion layering (SILAR) [14], electrochemical [15, 16] and hydrochemical deposition [17-18].

In the present investigation a comparative analysis of the optical properties of CdSe thin films obtained by chemical bath deposition method from a solution containing four components (cadmium chloride, ammonium hydroxide, triethanolamine, and sodium selenesulphate) and from a solution containing three components (cadmium chloride, ammonium hydroxide and sodium selenesulphate) was carried out.

2. EXPERIMENTAL METHODS

The chemical bath deposition (CBD) method was used to obtain CdSe thin films. Equal volumetric amounts (each 13 ml) of 0.5M cadmium chloride ($CdCl_{2x2.5}H_2O$), 13.4M (25%) ammonia (NH_3OH), 7.4 M triethanolamine ($C_6H_{15}NO_3$) and 0.2 M sodium selenosulfate (Na_2SSeO_3) were mixed in a 60 ml beaker. Sodium selenosulfate (Na_2SeSO_3) was prepared in the laboratory by dissolving an appropriate amount of selenium powder in 100 ml of sodium sulfite (Na_2SO_3) aqueous solution at 90 °C for 7 hours. After the undissolved selenium particles were filtered off, a clear solution of sodium selenosulfate was obtained [19].

Before the amorphous glass substrates (38×26×1 mm) were put into the solution, they were soaked in diluted acid, rinsed in deionized water and then dried in air. The substrates were put in glass vessels vertically. Chemical baths have waited for 48 hours at room temperature (27 °C) and this regime turned out to be the most optimal for obtaining a high-quality thin film. When the solutions are mixed, a white precipitate first forms at the bottom of the beaker. Over time, this precipitate and solution acquire a dark yellow color, and then a red color corresponding to CdSe. After deposition substrates were removed from the beaker, washed with distilled water and dried.

In the three-component (in the absence of triethanolamine) case, the chemical process was carried out completely according to the technology corresponding to the four-component case described above, that is, mixture of cadmium chloride, ammonium hydroxide and sodium selenosulfate was prepared while maintaining all

of the above conditions. As a result, in both cases a red and homogeneous CdSe thin film was obtained on the glass substrate, with good adhesion. CBD film has thickness of around 200 nm.

3. RESULTS AND DISCUSSION

In Figure 1 is shown the X-ray spectrum of a thin CdSe layer obtained for the four-component case. This spectrum shows that the resulting thin layer is polycrystalline in nature. The two theta peaks at 25.3, 42 and 49.8 are the result of reflections from the (111), (220) and (311) planes, respectively. The (111) plane is considered the main direction of CdSe, which crystallizes in a zinc blende (cubic) crystal structure (JCPDS No. 190191).

The optical absorption measurement was carried out in the wavelength range of 200 ÷1100 nm, by using a U-5100 Spectrophotometer. Figure 2 shows optical absorption spectrum CdSe thin films obtained from four-component and three-component solutions by chemical bath deposition method.

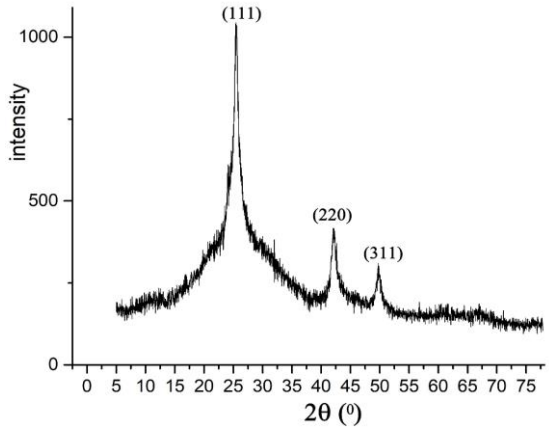

Figure 1. X-ray spectrum of CdSe thin film obtained by chemical bath deposition from a solution containing four components

In Figure 3, dependences $\alpha(h\nu)$ for CdSe thin films obtained from four-component and three-component solutions by chemical bath deposition were plotted.

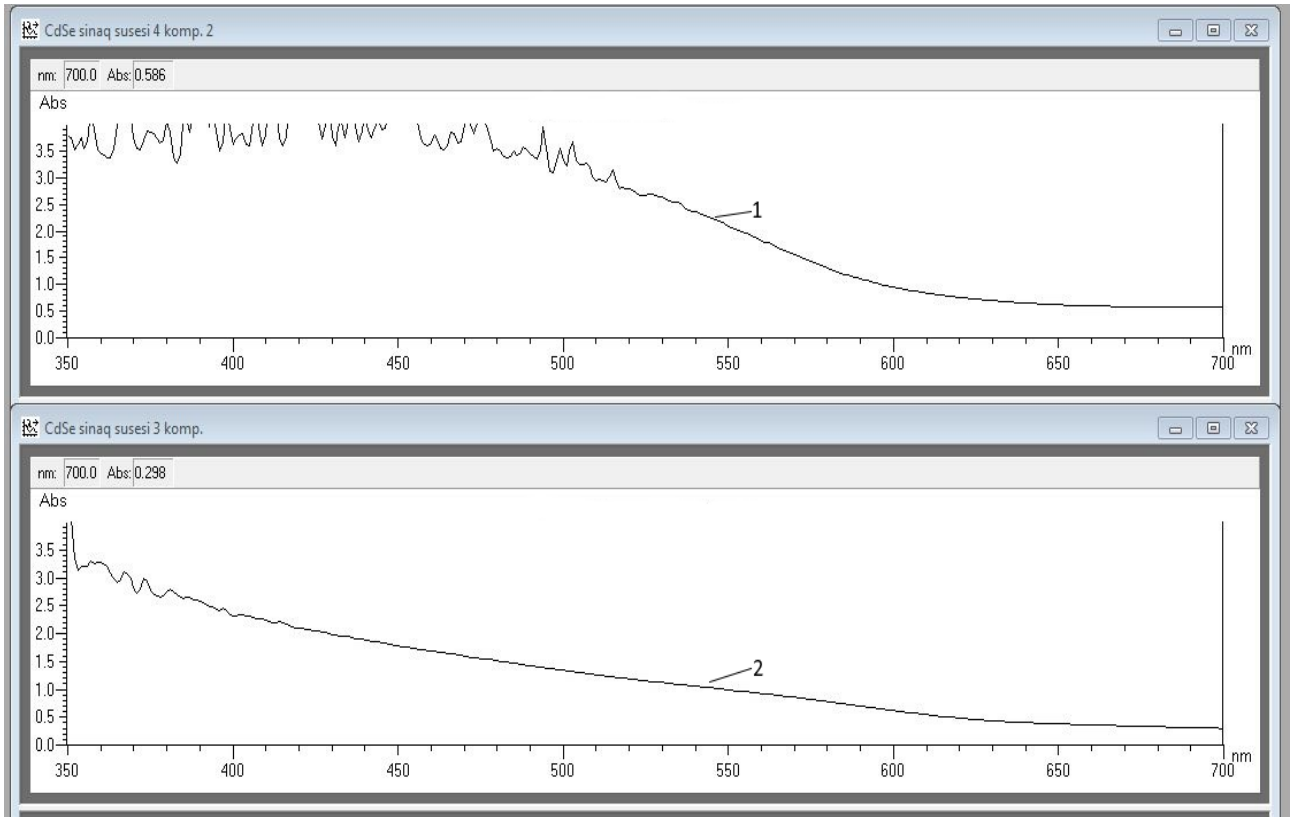

Figure 2. Optical absorption spectra of CdSe thin films obtained by chemical bath deposition from four-component (1) and three-component (2) solutions

As we know, the Tauc equation is used to calculate the width of the band gap of semiconductor [17]:

$$(\alpha h\nu)^{\frac{1}{n}} = A(h\nu - E_g) \quad (1)$$

where, A is a constant and E_g is band gap of semiconductor, and ($h\nu$) is the energy of the photon. The values that n can take in this expression depend on the type of transition and can take on the following values [20]:

- for an allowed direct transition $n = \frac{1}{2}$
- for an allowed indirect transition $n = 2$
- for a forbidden direct transition $n = \frac{3}{2}$
- for a forbidden indirect transition $n = 3$

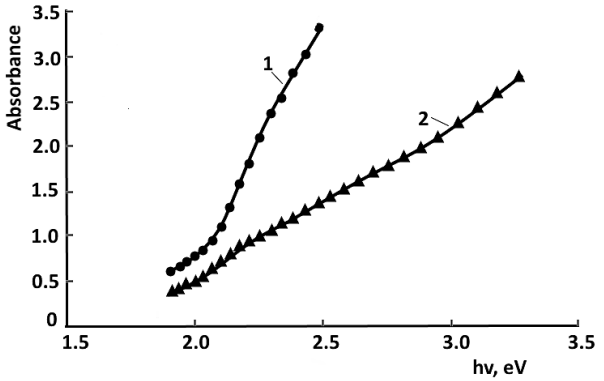

Figure 3. $\alpha(h\nu)$ dependences of thin CdSe films obtained by chemical bath deposition from four-component (1), three-component (2) solutions

As it was reviewed in [21] the CdSe thin films have an optical transition corresponding to the first case near fundamental absorption edge, so for spectral dependence of absorption coefficient can be applicable a formula;

$$(\alpha h\nu)^2 = A(h\nu - E_g) \quad (2)$$

Constructing $(\alpha h\nu)^2$ as a function of $(h\nu)$ according to an optical absorption spectrum of CdSe thin films, obtained by CBD given in Figure 4.

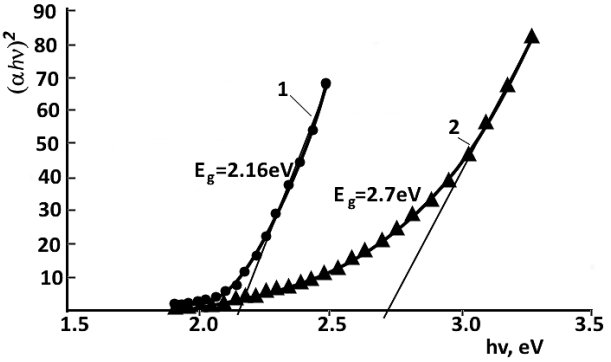

Figure 4. Plots of $(ah\nu)^2$ versus $(h\nu)$ for CdSe thin films obtained by chemical bath deposition from four-component (1) and three-component (2) solutions

The estimated value E_g for CdSe thin films obtained by chemical bath deposition from four-component and three-component solutions correspond E_g=2.16 eV and E_g=2.7 eV respectively, i.e., a shift in the band gap of a CdSe thin film obtained from a three-component solution towards higher energies was observed.

4. CONCLUSIONS

Optical absorption spectra of CdSe thin films obtained by the CBD method at room temperature are measured for two regimes: in the presence of triethanolamine in solution and without it. Using the Tauc equation, the widths of band gaps of CdSe thin films were determined. The estimated values E_g for CdSe thin films obtained from four-component (in the presence of triethanolamine) and three-component (without triethanolamine) solutions correspond E_g= 2.16 eV and E_g=2.7 eV, respectively.

REFERENCES

[1] L. Zhao, L. Hu, and X. Fang, "Growth and Device Application of CdSe Nanostructures", Adv. Funct. Mater., Vol. 22, pp. 1551-1566, 2012.

[2] A.V. Shaikh, R.S. Mane, O.S. Joo, et al., "Electrochemical Deposition of Cadmium Selenide Films and their Properties: A Review", J Solid State Electrochem, Vol. 21, No. 9, pp. 2517-2530, 2017.

[3] A.S. Khomane, "Structural and Optical Characterizations of Chemically Deposited Cadmium Selenide Thin Films", Mater. Res. Bull. Vol. 46, pp. 1600-1603, 2011.

[4] O.I. Olusola, O.K. Echendu, I.M. Dharmadasa, "Development of CdSe Thin Films for Application in Electronic Devices", J. Mater. Sci. Mater. Electron, Vol. 26, pp. 1066-1076, 2015.

[5] S. Wageh, "Raman and Photoluminescence Study of CdSe Nanoparticles Capped with a Bifunctional Molecule", Physica E: Low-Dimensional Systems and Nanostructures, Vol. 39, pp. 8-14, 2007.

[6] R.A. Potyrailo, A.M. Leach, "Selective Gas Nano Sensors with Multisize CdSe Nanocrystal/Polymer Composite Films and Dynamic Pattern Recognition", Appl. Phys. Lett., Vol. 88, p. 134110, 2006.

[7] F. Li, W.N. Li, S.Y. Fu, et al., "Formulating CdSe Quantum Dots for White Light-Emitting Diodes with High Color Rendering Index", J. Journal of Alloys and Compounds, Vol. 647, pp. 837-843, 2015.

[8] X. Dai, Z. Zhang, Y. Jin, et al, "Solution-Processed, High-Performance Light-Emitting Diodes Based on Quantum Dots", Nature., Vol. 515, p. 96, 2014.

[9] F.Y. Gan, I. Shih, "Preparation of Thin-Film Transistors with Chemical Bath Deposited CdSe and CdS Thin Films", IEEE Transactions on Electron Devices, Vol. 49, Issue 1, 2002.

[10] A. Kubacka, M. Fernandez Garcia, G. Colo, "Advanced Nanoarchitectures for Solar Photocatalytic Applications", Chem. Rev., Vol. 112, pp. 1555-1614, 2012.

[11] J. Li, Y. Nia, J. Liua, et al., "Preparation, Conversion, and Comparison of the Photocatalytic Property of $Cd(OH)_2$, CdO, CdS and CdSe", Journal of Physics and Chemistry of Solids, Vol. 70, pp. 1285-1289, 2009.

[12] A.A. Yadav, M.A. Barote, E.U. Masumdar, "Studies on Nanocrystalline Cadmium Sulphide Thin Films Deposited by Spray Pyrolysis", Materials Chemistry and Physics, Vol. 12, pp. 53-57, 2010.

[13] M.M. Betkar, G.D. Bagde, "Structural and Optical Properties of Spray Deposited CdSe Thin Films", Materials Physics and Mechanics, Vol. 14, pp. 74-77, 2012.

[14] K.B. Chaudhari, G.M. Narayani, N.G. Deshpande, et al., "Chemical Synthesis and Characterization of CdSe Thin Films Deposited by SILAR Technique for Optoelectronic Applications", Journal of Science: Advanced Materials and Devices, Vol. 1, pp. 776-481, 2016.

[15] H. Bayramoglu, A. Peksoz, "Electrodeposition of in CdSe Precursor Thin Films in Aqueous Electrolytes Including Different Selenous Acid Concentrations as Se

Source", Materials Science in Semiconductor Processing, Vol. 60, pp. 13-19, 2019.
[16] R. Choudhary, R.P. Chauhan, "Nitrogen Ion Implantation Effects on the Structural, Optical and Electrical Properties of CdSe Thin Film", Journal of Materials Science: Materials in Electronics, Vol. 29, pp. 12595-12602, 2018.
[17] S. Singh, A.K. Shrivastava, S. Tapdiy, "Synthesis and Characterization of Mn Composition Effect on CdSe Thin Films", Advanced Materials Proceedings, Vol. 2, pp. 367-370, 2017.
[18] M.P. Deshpande, N. Garg, V. Sandip, et al., "Photoluminescence Behavior in the Synthesized CdSe Thin Films Deposited on ITO Substrates", Mater. Sci. Process, Vol. 16, pp. 915-922, 2013.
[19] T.R. Kumar, M. Vedamalai, "Deposition of ZnSe Thin Film by Chemical Bath Deposition and for Photovoltaic Application", International Journal of Pure and Applied Mathematics, Vol. 119, No. 12, pp. 6665-6675, 2018.
[20] J. Tauc, "Amorphous and Liquid Semiconductors", Plenum Press, p. 441, New York, USA, 1974.
[21] V.I. Qavrilenko, A.M. Qrekhov, D.V. Korbutyak, et al., "Optical Properties of Semiconductors", Handbook, Naukova Dumka, p. 602, Kiev, Ukraine, 1987.

BIOGRAPHIES

Mammad Huseynali Huseynaliyev was born in Nakhichevan, Azerbaijan, 1952. He graduated from Physical Faculty, Azerbaijan State University (Baku, Azerbaijan) in 1974. He received the degree of Candidate of the Physical-Mathematical Sciences on 2009. Currently, he is working as chief of Physical Investigations Laboratory at Institute of Natural Resources at Nakhchivan Department, Azerbaijan National Academy of Sciences, Nakhichevan, Azerbaijan. His basic research areas are symmetry problems and problems of production and study of perspective semiconductor materials used in solar energy converters.

Leyla Nadir Ibrahimova was born in Nakhchivan city, Nakhchivan, Autonomus Republic, Azerbaijan, 1992. She graduated from Physical Faculty in Nakhchivan State University in 2013. She got master degree and graduated in 2016. She is a Ph.D. student in Nakhchivan Branch of National Academy of Sciences of Azerbaijan. Her research area is the production and study of semiconductor materials used in solar energy converters.

The 18th International Conference on
"Technical and Physical Problems of Engineering"
30 October 2022
International Organization of IOTPE

ICTPE Conference
www.iotpe.com
ictpe@iotpe.com
ictpe0@gmail.com

ICTPE-2022 Number 14 Code 02ELC07 Pages 67-73

BROADBAND FREQUENCY DEPENDENT RESISTOR

T.R. Mehdiyev A.M. Hashimov S.N. Aliyeva I.F. Yusibova

Institute of Physics, Azerbaijan National Academy of Sciences, Baku, Azerbaijan
jophphysics@gmail.com, shahla-aliyeva22@rambler.ru, yusibova78@mail.ru

Abstract- The spectra of micro powders and nano thin films of $Ni_{1-x}Zn_xFe_2O_4$ ferrospinels in the region of super high frequencies, including terahertz frequencies, have been studied with the aim of their specific practical application in the structure of the shell of a frequency-dependent resistor to eliminate high-frequency over voltages in networks and devices in power engineering, electronics, computer systems for receiving/processing information, etc. The interpretation and analysis of the research results confirm the effectiveness of the use of Ni-Zn ferrites as an element of the absorbing shell of a frequency-dependent resistor for filtering high-frequency over voltages that occur in the high and super high frequencies.

Keywords: Ferrospinel, Super High Frequency, FD-Resistor, Overvoltage, Domain Wall.

1. INTRODUCTION

The perspective of using frequency-dependent resistors for filtering external and internal high-frequency interference arising from external, natural, or other factors leading to the occurrence of high-frequency over voltages in power networks and systems, in circuits of electronic modules, systems for receiving/transmitting and processing information, etc., as studies have shown, stimulated the study of electrical, thermal, magnetic, optical and other properties, the role of geometric factors, the presence of a layered structure of the ferromagnetic layer, the quality of the surfaces of the layers, etc. resistors of this type [1-10].

Already the first experimental studies and subsequent analysis of the processes of electric current flow through a frequency-dependent resistor under conditions of high-frequency interference were carried out in the framework of computer simulation based on the percolation model of the resistor shell, created on the basis of [11] indicated that the resistive properties and features of the flow of alternating current in the resistor are determined, first of all, the frequency dependence of the magnetic permeability of the ferromagnetic shell, the observed skin effect, the ratio of the concentrations of components in the structure, the grain sizes of micro- and nano powders of ferrite used in the shell of the resistor.

The promising materials for the shell of frequency-dependent resistors include $Ni_{1-x}Zn_xFe_2O_4$ ferrites, which, as studies have shown, intensively absorb electromagnetic radiation in the frequency range from 10 MHz to 1000 MHz. The absorption of electromagnetic radiation in these ferrites in the frequency range above 300 MHz is determined by ferromagnetic resonance. The results of studying the EPR spectra and AFM profiles of $Ni_{1-x}Zn_xFe_2O_4$ ferrites, published earlier in [12-14], established the presence of features associated with changes in spin concentrations in the octahedral and tetragonal sublattices in various compositions of $Ni_{1-x}Zn_xFe_2O_4$ and the temperature range (3-300 K). The observed effects were determined by the occupation of tetrahedral and octahedral positions by Zn, Ni, and Fe ions, that is, by changes in the sublattice magnetization. The absence of the identity of the $Ni_{1-x}Zn_xFe_2O_4$ sublattices causes non-zero total mechanical and magnetic moments and, since the values of the g-factors of the sublattices are different, the compensation points for the magnetic and mechanical moments do not coincide with each other. Thus, at the points of intersection of the dependences of the spin concentrations of the magnetic sublattices, in all probability, compensation points were observed. The conducted studies allowed us to establish that the reason for the spin reorientation observed in the EPR spectra of $Ni_{1-x}Zn_xFe_2O_4$ ferrites, as well as the generation of 26.4 THz (880 cm^{-1}) terahertz radiation observed in Raman scattering, is the appearance of magnetic inhomogeneities and a non-collinear magnetic structure as a result of the influence temperature on the concentration and orientation of spins of Fe^{3+} ions in canted and superparamagnetic states. The value of the energy gap equal to 0.10914 meV agrees in value with that found in experiments on small-angle neutron scattering.

The results of studies of the Raman scattering spectra [15] in $Ni_{1-x}Zn_xFe_2O_4$ nano powders and thin films made it possible to assume the presence of magnetic inhomogeneities in them localized in the surface layer of the ferrite film, the thickness of which is comparable to the length of the exchange spin waves. This assumption was based on a physical model of the coexistence of two subsystems in magnetite: one associated with cations (Fe^{2+} and Fe^{3+}) and the second with hopping 3d electrons between cations $Fe^{2+} \rightleftarrows Fe^{3+}$, leading to magnetic ordering.

In addition to the strong electrostatic interaction between cations, the theoretical description of the effect included taking into account the influence of the

Vonsovskii s-d exchange interaction, which, in the case of a positive s-d exchange, took into account the magnetopolaron states, and in the case of a negative s-d exchange, not only the localization of conduction electrons but also partial screening of the magnetic moments of atoms as a result of the orientation of the spins of conduction electrons antiparallel to these moments. An analysis of the MFM profiles of (Zn-Ni) ferrites' thin films [14] confirmed the presence of magnetic clusters in them, the size of which depended on the composition of the ferrites. Note that the assumption about the presence and nature of magnetic excitations in $Ni_{0.4}Zn_{0.6}Fe_2O_4$ ferrite was previously expressed by the authors of [16], who performed an energy analysis of small-angle neutron scattering.

In the compositions x(Zn) = 0.60; 0.68; 0.75, at low temperatures, a high-field susceptibility characteristic of a noncollinear magnetic structure, as well as the occurrence of intensive small-angle scattering, were detected. The results of the above studies were reflected in the implementation of various types of shells for frequency-dependent resistors operating in the optical, low-frequency (up to 1 MHz), terahertz ranges. This publication presents the results of microwave studies (from 1 MHz to 20 GHz) of $Ni_{1-x}Zn_xFe_2O_4$ ferrites, the purpose of which was to expand the frequency range of operation of frequency-dependent resistors.

2. EXPERIMENTAL METHODS AND TECHNIQUE

Synthesis of micro powders and thin films of the compositions $Ni_{1-x}Zn_xFe_2O_4$, where, x = 0.0; 0.25; 0.4; 0.5; 0.6; 0.75; 1.0, with their further annealing at a temperature of 960 °C was carried out according to the high-temperature technology published in [14, 15, 17], the quality of which was controlled by X-ray diffraction patterns. The surface quality of $Ni_{1-x}Zn_xFe_2O_4$ films, where x=0.25,0.4,0.5,0.6,0.75 deposited on high-quality surfaces of leucosapphire substrates 2 mm thick and 12 mm in diameter, were studied on SmartSPM confocal and atomic force microscopes with an AIST-NT measuring head (Tokyo Instruments, Japan) [14]. The Raman spectra of $Ni_{1-x}Zn_xFe_2O_4$ micro powders and thin films were studied on a 3D Laser Raman Micro spectroscopy System Nano finder 30 Raman spectrometer (Tokyo Instruments, Japan) [15,17]. The excitation source was a YAG Nd laser (λ=532 nm), with the possibility of changing the radiation power from 0.1 mW to 10 mW. Note that these spectra already refer to high terahertz frequencies. EPR data obtained with the aid of a ELEXSYS E500 spectrometer (Bruker, Germany) at 300 K and down to 4K [14].

The high-frequency spectra of ferrites were studied using a "Deepace KC901V" vector network analyzer by the coaxial method in a short-circuited line. Granular thin films consisting of nano- or submicron magnetic particles embedded in the technological process in an immiscible, non-conductive or metallic matrix represent a special class of artificially structured materials that, due to the possibility of modeling and forming microstructures with a predetermined geometry that provides the necessary spatially modulated magnetic and electrical profiles, high coercivity, giant magnetoresistance, spin-orientation transitions, and other macroscopic quantum effects, turned out to be promising for new technical solutions. At the same time, the rigidity of the bond between the particles and the matrix turned out to be an important factor in the stability of the created structure. As it turned out, the tendency to conglomerate free particles over time led to the degradation of some key properties of granular magnetic systems, which significantly depended on the volume fraction x_v and sizes $2r$ of embedded magnetic particles, where the parameter x_v can continuously vary from 0 to 1, and the parameter $2r$ has the value, only for small values of x_v. The evolution of the granular microstructure with a change in the x_v parameter can be represented as follows: for any granular systems with a uniform dispersion of ferrite fillers, there is a so-called percolation volume fraction x_p, whose values lie in the range of 0.5-0.6. Isolated ferrite beads exist at $x_v<x_p$, and a continuous network of interacting beads appears at $x_v>x_p$.

In a real granular system, the particles are not spherical. If the average distance between particles is of the order of the particle size, then giant magneto-transport properties appear. In granular systems, the single-domain behavior of magnetic particles is observed at low volume concentrations ($x_v<x_p$), and the usual magnetic properties appear at $x_v>x_p$. In this case, all magnetic moments are coaxial and rotate synchronously with the external field as one giant moment, which corresponds to extreme ferromagnetic characteristics. Granular $Ni_{0.5}Zn_{0.5}Fe_2O_4$ (one of the Ni-Zn ferrites) embedded in a fused quartz matrix exhibits superparamagnetic properties even after being heated at 1100 °C for 2 hours. In the (Ni-Zn-ferrite/SiO_2) system, magnetic properties can be changed in a wide range by changing the volume fraction and diameter of ferromagnetic particles. At x<34%, the formation of pure stoichiometric Ni-Zn ferrite in the SiO_2 matrix is observed. Note that a characteristic feature of Ni-Zn ferrites is the presence of electronic transitions in those initiated by super exchange interaction of the $Fe^{2+}\rightarrow O^{2-}\rightarrow Fe^{3+}$ type.

The combination of various concentrations of Ni-Zn ferrite and its heat treatment made it possible to obtain samples with a saturation magnetization from 1.3 to 68 emu/g and a coercive force from 0 to 123 Oe, a value that is higher than the coercivity of bulk Ni-Zn ferrite. It was also found that $NiFe_2O_4$ films ($Ni_{1-x}Zn_xFe_2O_4$ composite at x=0) deposited on a sapphire substrate had a high coercive force, which was ~32.5 mT in out-of-plane and in-plane geometries. The calculation of deformations at the film-substrate interface, taking into account the parameters of crystal lattices and elastic coefficients C_{11}=174 GPa and C_{12}=67 GPa, showed that: coercive field, during compression: in-plane - 32.5 mT and out-of-plane - 32.5 mT; in tension: in-plane - 0 and out-of-plane - 25 mT. Magnetization: when compressed: in-plane - 10 G and out-of-plane - 5 G; in tension: in-plane - 26 G and out-of-plane - 23 G. Thus, in thin $NiFe_2O_4$ films, there are coercive fields in the out-of-plane geometry and there is anisotropy of the "easy" plane type, which is characteristic of two-dimensional layers.

On the other hand, the technology of obtaining ultrathin films by high-temperature evaporation of the initial components in a vacuum chamber is very difficult. That is why it was decided to use PLD (pulsed laser deposition) - a method in which granular ferrite microstructures with spatially modulated magnetic and electrical profiles are created by the action of pulsed laser radiation on submicron $Ni_{0.4}Zn_{0.6}Fe_2O_4$ powder particles deposited on a glass substrate (optical glass K8, a similar glass produced by the German company Schott AG, is designated as BK7).

It has been established [18], that the thin films of ferrite obtained by deposition were observed to overlap the crystalline islands with an amorphous phase. The subsequent annealing of the obtained films led to their texturing and enhancement of the magnetic properties, and despite the fact that the magnetization of the films was close to the magnetization of the bulk ferrite, the value of the coercive magnetic field in the films was greater than in the bulk material, i.e. confirms the conclusion of the authors of the publication [19] that this feature is associated with the anisotropy of crystallites observed in the microstructure of the film of this ferrite. The scheme of the experiment is shown in Figure 1a. Modification of $Ni_{0.4}Zn_{0.6}Fe_2O_4$ ferrite nano powder was carried out by radiation from a wavelength-tunable Spectra-Physics Tsunami laser. With irradiation parameters: radiation wavelength 1.064 μm, pulse duration 10 ns, and energy density 480 mJ/cm^2 were obtained, shown in Figure 1, photomicrographs of areas of the substrate with particles of ferrite powder without exposure (b) and under exposure to a constant magnetic field (c, d), with a resolution better than 250 nm. Under the action of laser pulses with a duration of ~10 ns, conglomerates of submicron particles melted and combined into drop-like structures.

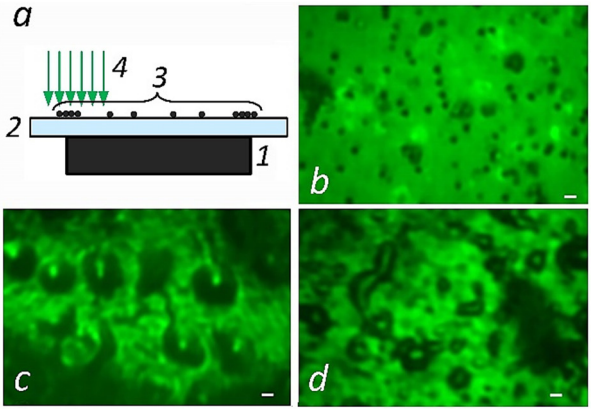

Figure 1. Experimental scheme, (a) 1. permanent magnet, 2. glas substrate; 3. submicron powder particles $Ni_{0.4}Zn_{0.6}Fe_2O_4$, 4. laser radiation, (b) radiation without influence, (c) at the influence of magnetic field, scale = 1 μm [19]

Analysis of the microcrystalline structure shown in Figure 1 showed that the nano thin ferrite film is formed by spheroids of various sizes, unevenly distributed in a fine-crystalline granular mass with rare crystallographically irregular, isometric inclusions. A complete AFM analysis of the resulting nanofilms was published in [14, 19].

Technological control of the process, previously published in [19], was carried out to achieve the desired effect for the reproducibility of parameters and the efficient operation of devices. It can be considered established that the melt of this ferrite wets the glass surface. This fact is easy to explain if you pay attention to the property of the components that make up the ferrite composition to react with silicon dioxide, namely:

Reaction $SiO_2 + 2Fe_3O_4 \rightarrow 3Fe_2SiO_4 + O_2$, in which SiO_2 is an acid and Fe_3O_4 - alkali, passes with the formation of iron orthosilicate, that is, the mineral fayalite:

$2O^{-II} - 4e^- \rightarrow 2O^0$ (oxidation)

$6Fe^{8/3} + 4e^- \rightarrow 6Fe^{II}$ (recovery)

On the other hand, this reaction is reversible;

$3Fe_2SiO_4 + O_2 \rightarrow 2Fe_3O_4 + 3SiO_2$

Similarly, the reaction $2NiO + SiO_2 \rightarrow Ni_2SiO_4$ of the interaction of nickel oxide with SiO_2 leads to the formation of nickel silicate, and the reaction $ZnO + SiO_2 = ZnSiO_3$ leads to the formation of zinc metasilicate. At about 1200 °C, all three ferrite components react with SiO_2 Detailed studies of the strength characteristics of wetting with Ni-Zn-ferrites in junctions with glasses, published in [19], indicated that in the case of, for example, permalloy (i.e., Fe-Ni alloy) or zinc-nickel ferrite, the maximum stress compensation was achieved at glass thicknesses and permalloy 1-1.5 μm and 0.5-0.75 μm, respectively.

The parameters of the optimal mode for obtaining junctions were set, namely: temperature rise to 900 °C at a rate of 10 °C/min, cooling from 900 °C to 500 °C at a rate of 10 °C/min., at a temperature of 500 °C isothermal exposure 40 min. With subsequent cooling of the junction at a rate of 3 °C/min. The influence of an external magnetic field on the nature of the change in macros tresses and the role of the mutual orientation of the domain and external magnetic fields were also established. Thus, it becomes obvious that the created ferrite microstructures, due to the chosen geometry of the macrostructure, will have specific spatially modulated magnetic and electrical profiles.

3. EXPERIMENTAL RESULTS AND THEIR DISCUSSION

As stated in [20], in the frequency range up to 300 MHz, domain wall resonance plays an important role. The condition for the occurrence of domain wall resonance is their rigid fixation at grain boundaries, pores, or other defects, which ensures their displacement relative to the equilibrium position. The frequency of natural oscillations of domain walls is determined by the stiffness coefficient of the quasi-elastic force, reduced to a unit of the effective mass of the domain wall. In a real ferrite, there are many domain boundaries of various sizes, and each such boundary has its own oscillation frequency, so the dispersion region μ'' is composed of many peaks of resonances of individual boundaries. The resonance frequency of the boundary depends on its type. The harder and shorter the boundary, the higher the resonance frequency. Thus, the resonance frequency of domain walls is determined by the grain sizes of ferrite micro powders, and the actual spread of ferrite grain sizes will lead to an increase in the width of the domain wall resonance curve.

Assuming grains of ferrite spherical diameter d, the mass of the domain wall m can be determined from (1) Equation [21]

$$m = \frac{d^2}{2\gamma^2}\left[\frac{2kT_C}{aK}\left(1+\frac{\mu_0 H_A}{I_0}\right)\right]^{-1/2} \quad (1)$$

where, γ is the gyromagnetic ratio, k is the Boltzmann constant, a is the lattice constant, K is the crystallographic anisotropy constant, T_C is the Curie temperature of $Ni_{1-x}Zn_xFe_2O_4$ ferrites , H_A is anisotropy field, which is related to the natural ferromagnetic resonance frequency ω_{EFMR} by the $H_A = \omega_{EFMR} / \gamma$. The value of the stiffness coefficient or quasi-elastic coefficient from the Dering Equation $\xi = \frac{4\pi r I_0^2}{3\mu\mu_0} + 2\pi\sigma$.

The I_0 is saturation magnetization = 0.2÷0.3 Tl; $2r$ is major axis of the ellipsoid of revolution; μ is initial magnetic permeability; surface tension force $\sigma = \left(\frac{2kT_C K}{a}\right)^{\frac{1}{2}}$.

The δ_ω is domain wall thickness $\sigma_\omega = \sqrt{\frac{2kT_C}{aK}}$ and the natural frequency of oscillations of domain walls ω_0 is expressed in terms of the effective mass and the generalized quasi-elastic coefficient by the expression: $\omega_0 = \sqrt{\frac{\xi}{m_{eff}}}$.

In Figures 2 and 3 show the calculated (within the framework of the percolation model) and experimental spectra of the frequency dependences of the imaginary and real parts of the magnetic permeability for $Ni_{0.5}Zn_{0.5}Fe_2O_4$ in the range from 1 to 20000 MHz. As can be seen, the region of the spectrum caused by the vibrations of the boundaries has

the form of a wide frequency decay band μ' and its corresponding resonant maximum μ'', the high-frequency "tail" of which can reach frequencies much higher than the frequency of the natural resonance of the boundaries. The nature of these spectra is obviously influenced by the processes of super exchange interaction, etc. [20], which lead to recessions μ' and maxima μ'' at frequencies coinciding with their relaxation frequencies, and for $1/\tau$ close to the oscillation frequency of the boundaries ω_0, an expansion of the resonance region is observed, and for $1/\tau \leq \omega_0$ a relaxation maximum μ'' and the corresponding decline μ′ form a separate area [20]. An estimate of the oscillation frequency of domain walls ω_0 for $Ni_{0.5}Zn_{0.5}Fe_2O_4$ ferrite micro powder gives a value of 280 MHz.

As is known, the conductivity of $Ni_{1-x}Zn_xFe_2O_4$ ferrites is associated with the presence in them of two and three-charged ions of the transition elements of iron and nickel. In the conduction process, the participation of nickel is difficult, while, between iron ions of different valence, the process of electron hopping through the intermediate oxygen ion (indirect exchange) is observed.

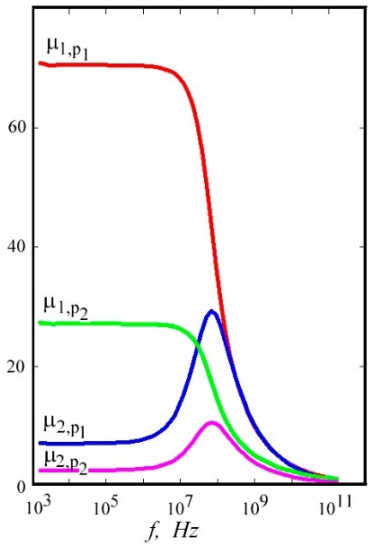

Figure 2. Calculated frequency dependences of the imaginary and real parts of the magnetic permeability of the control percolated medium with filling factors p= 0.5 and 0.8, particle radius an equal to 2·10-3 cm, magnetic permeability of the ferromagnetic substance (100-10 j), electrical conductivity σ= 105 $Om^{-1}cm^{-1}$, Filler: $Ni_{0.5}Zn_{0.5}Fe_2O_4$

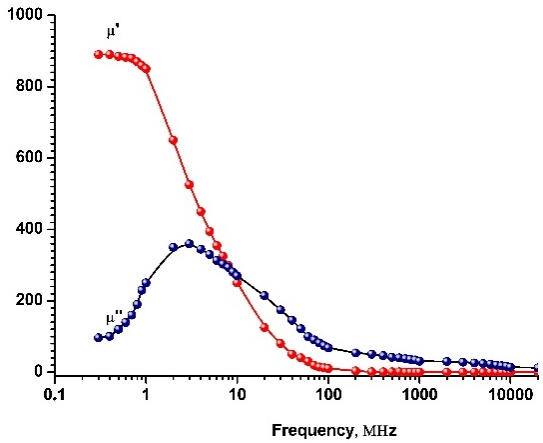

Figure 3. Experimental frequency dependences of the imaginary and real parts of the magnetic permeability of $Ni_{0.5}Zn_{0.5}Fe_2O_4$

The predominant directions of electron hopping can be caused by the precession of magnetization, which is associated with the fact that ions of different valence occupy crystallographically nonequivalent positions, and there are four types of such octahedral knots in spinels. Their local axes form different angles with the magnetization, and the energy of the system depends on where, at what site, at a given moment of time, the "extra" electron is located. Thus, during the precession of the magnetization, the angles of the moment vector with the local axes and the energy levels of the system corresponding to the doubly charged iron ion change, providing the preferential directions of transitions with the frequency of precession.

And, taking into account that the transitions of electrons between octahedral sites may lag behind the change in energy, the energy will be transferred from the magnetic subsystem to the subsystem of ions with variable valence, and from it to the crystal lattice with which the ions are associated.

$$\tau = \tau_0 \exp\frac{W}{kT} \qquad (2)$$

where, W is the activation energy (constant value); for spinels: $\tau_0 \sim 10^{-14}$, $W \sim 0.25$ eV and usually, the achievement of relaxation time to $1/\omega$ occurs at temperatures of 300-400 K. As can be seen, this maximum in the compositions x=0.5 and 0.75 is reached at a temperature of 200 K.

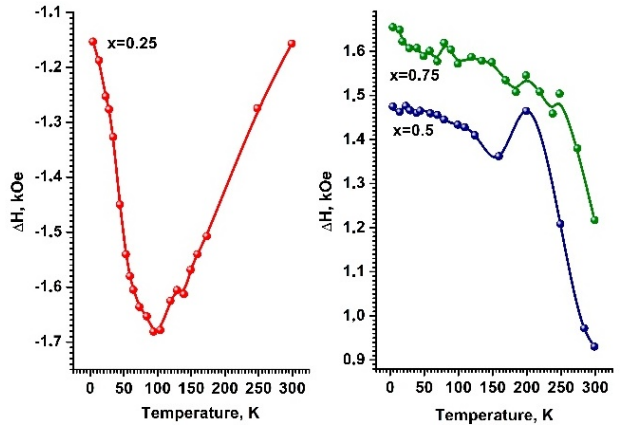

Figure 4. Experimental temperature dependences of the resonant field of $Ni_{1-x}Zn_xFe_2O_4$ (x=0.25; 0.5; 0.75) micro powders

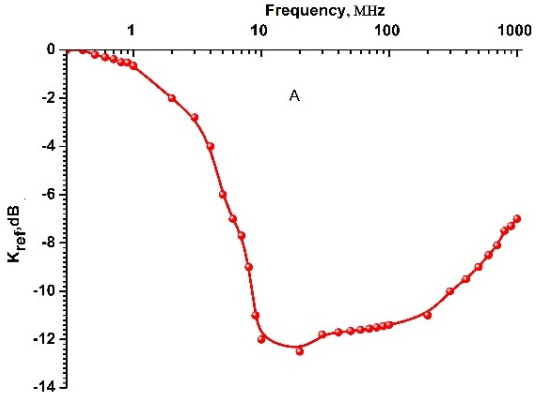

Figure 5. Reflection coefficient spectrum of $Ni_{0.5}Zn_{0.5}Fe_2O_4$ at T=300 K in the range from 1 to 1000 MHz

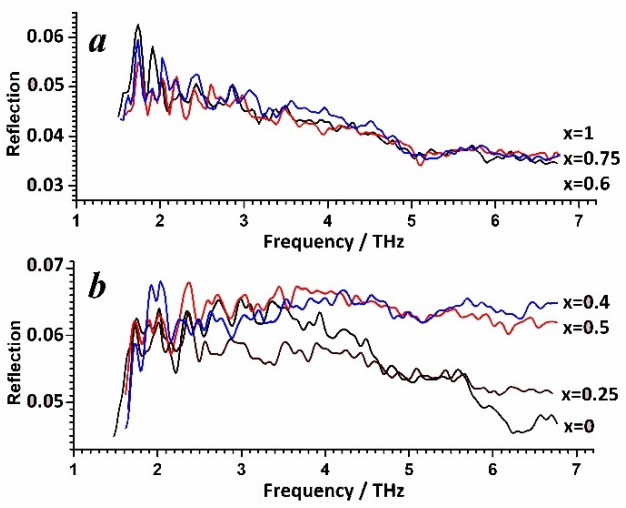

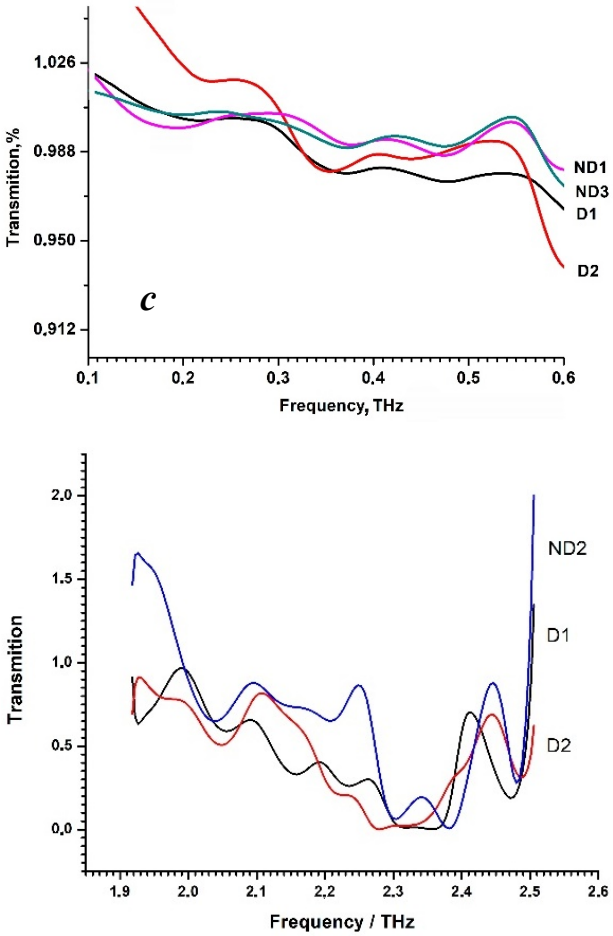

Figure 6. Terahertz reflection spectra, (a, b) $Ni_{1-x}Zn_xFe_2O_4$ ferrite nano powders in the 1-7 THz region, (c) transmission of the $Ni_{0.4}Zn_{0.6}Fe_2O_4$ granular film in the range of 0.1-2.5 THz [19, where, D1, D2 are sections of the film that differ in density (dense), ND2 is a section of low density (not dense)

For the composition, the relaxation frequencies of the excited states of Fe^{3+} are such that one can assume very fast energy transfer from the lattice and magnetic sublattices, and it is natural that ions strongly bound to the magnetic subsystem will be excited during its vibrations. The temperature dependences of resonant fields are determined by the temperature dependences of relaxation times and equilibrium populations. The relaxation time usually decreases rapidly according to the law (2). Note that the theory of Clogston [20] even in a rough approximation confirms the observed frequency and temperature dependences of the resonance curves and dynamic shifts of the resonance field, which are shown in Figure 4 for various compositions of $Ni_{1-x}Zn_xFe_2O_4$ (x=0.25; 0.5 and 0.75) ferrites.

An analysis of the absorption of the THz spectra (Figures 5 and 6) of a frequency-dependent resistor made in the form of thin granular films of $Ni_{0.4}Zn_{0.6}Fe_2O_4$ ferrite confirmed their possibility of using interference in the terahertz frequency range [19]. Observed split sequences: (0.343 and 0.483; 0.571 and 0.727; 0.815 and 0.967; 1.05 and 1.211; 1.288 and 1.444; 1.516 and 1.680; 1.763 and 1.955; 2.012 and 2.131; 1.35; 2; 14 THz) correlates with acoustic modes with intervals: ~0.24 THz (0.9 meV),

within the group ~0.15 THz (0.6 meV), between the limits ~0.08 THz (0.33 meV). The positions of the maxima in the THz spectra of granular $Ni_{0.4}Zn_{0.6}Fe_2O_4$ ferrite films of different thicknesses practically do not change, which, as indicated in [19, 22], can occur due to unlimited acoustic phonon modes.

As noted in [19], in the range from 0.4 to 2 THz, the absorption of electromagnetic radiation in magnetite due to spin ordering is extremely low, since the frequency of spin reorientation in a magnetic material does not exceed 0.02 THz [22]. Thus, the process of absorption of electromagnetic radiation in the THz range is mainly associated with dielectric losses. The transmission spectra of the selected sections of the $Ni_{0.4}Zn_{0.6}Fe_2O_4$ films in the THz region show oscillations associated with acoustic modes. The change in transmission demonstrates a weak dependence on the frequency of the terahertz field. Comparing the results of terahertz studies with the data of [23], it is easy to notice their similarity, indicating the possibility of studying ferrites in all $Ni_{1-x}Zn_xFe_2O_4$ compositions in the THz frequency range of the $Fe^{2+} \rightarrow O^{2-} \rightarrow Fe^{3+}$ super exchange interaction.

Analyzing the results of research in the field of microwave frequencies, as well as the practical use of Ni-Zn ferrites as an effective absorbing sheath of a frequency-dependent resistor for filtering high-frequency over voltages, it is pleasant to note a new confirmation - the publication of [24] confirming the complete suppression of the Ni-Zn ferrite absorber. distortion at frequencies of 10, 2.4, 3.65, and 5 GHz.

ACKNOWLEDGEMENTS

The work is carried out in limits within the framework of the Azerbaijan-Belorussian project at financial support of Belorussian and Azerbaijan Funds of fundamental investigations (project Ф18АЗ-003 Belarus) and (projects: EIF-2013-9(15)-46/05/1-M-12 and EIF-BGM-3-BRFTF-2^+/2017 Azerbaijan.

REFERENCES

[1] A.M. Hashimov, T.R. Mehdiyev, N.R. Babayeva, "Possibilities for Limiting High-Frequency Surges When Using a Frequency-Dependent Resistor", International Conference Energy of Moldova 2005, pp. 265-269, Chisinau, Moldova, 21-24 September 2005.

[2] A.M. Hashimov, T.R. Mehdiyev, N.R. Babayeva, "Frequency Dependent Resistor", International Conference Physics 2005, pp. 613-617, Baku, Azerbaijan, 7-9 June 2005.

[3] A.M. Hashimov, T.R. Mehtiyev, N.R. Babayeva, "Effect of Magnetic Multi-Layer to Resistive Properties of Frequency-Dependent Resistor", The 3rd International Conference on Technical and Physical Problems in Power Engineering (ICTPE-2006), pp. 604-606, Ankara, Turkey, 29-31 May 2006.

[4] A.M. Gashimov, T.R. Mehtiyev, N.R. Babayeva, "On the Appropriateness of Use of Frequency-Dependent Resistor at Limitation of High-Frequency Over Voltages", MEPS'06, pp. 379-382, Wroclaw, Poland, 6-8 September 2006.

[5] N.R. Babayeva, A.M. Hashimov, E.V. Dmitriyev, T.R. Mehdiyev, "Study of the Skin Effect and Thermal Modes of Operation of a Frequency-Dependent Resistor", AJP Fizika, Vol. XIII, No. 1-2, pp. 102-107, 2007.

[6] H. Habibzadeh, T.R. Mehdiyev, A.M. Hashimov, E.V. Dmitriyev, N.R. Babayeva, "Influence of Concentration and the Sizes of Ferromagnetic Granules on Electrical and Magnetic Properties of FD-Resistor Shell", International Journal for Knowledge, Science and Technology, Vol. 1, No. 1, pp. 49-56, 2009.

[7] E.V. Dmitriev, A.M. Hashimov, T.R. Mehdiyev, N.R. Babaeva, "Thermal Parameters and Mode of Operation of a Frequency-Dependent Resistor", Collection of Reports of the Scientific Conference, Electro Physics of Materials and Installations, Siberian Energy Academy, p. 316, Novosibirsk, Russia, 2006.

[8] S.M. Korobeynikov, L.I. Sarin, A.A. Chelaznov, "Resistor with Frequency Dependence for Over Voltage Reduction", The Second All-Russian Scientific Tech. Conf. Surge Limitation and Neutral Grounding Modes of 6-35 kV Networks, pp. 52-59, Novosibirsk, Russia, 15-17 October 2002.

[9] S.M. Korobeynikov, L.I. Sarin, A.A. Chelaznov, A.P. Drozhzhin, "One of the Ways to Reduce the Energy Absorbed by the Surge Arrester when Exposed to Lightning", All-Russian Scientific Technical Meeting Scientific Aspects and Current Problems of Development, Testing and Application of OPN, St. Peterburg, Russia, October 8-10, 2001.

[10] S.M. Korobeynikov, A.P. Drozhzhin, L.I. Sarin, "Skin Effect in Composite Materials", Electricity, No. 7, pp. 2-9, 2004.

[11] A.A. Habibzadeh, S.N. Aliyeva, N.R. Babyeva, T.R. Mehdiyev, "Peculiarities of Current Flow within the Framework of the Percolation Model of a Frequency-Dependent Resistor", AJP Fizika, Vol. XVII, No. 3, pp. 23-28, 2011.

[12] S.N. Aliyeva, S.I. Aliyeva, "SHF-Magnetic Properties of ((Ni-Zn)-Ferrite)-Dielectric-Metal", Academic Journal Eurasion Universities Union, Vol. 1, No. 2, pp. 31-44, 2012-2013.

[13] S.N. Aliyeva, S.I. Aliyeva, "SHF Magnetic Properties of FD Resistor Shell", International Journal on Technical and Physical Problems of Engineering (IJTPE), Issue 14, Vol. 5, No. 1, pp. 119-126, March 2013.

[14] S.N. Aliyeva, Y.N. Aliyeva, A.I. Nadjafov, I.S. Hasanov, E.K. Huseynov, T.R. Mehdiyev, "EPR and SPM Studies of Zn-Ni Ferrites", Phys. Status Solid (c), Vol. 12, No. 6, pp. 615-619, 2015.

[15] S.N. Aliyeva, S. Babayev, T.R. Mehdiyev, "Raman Spectra of $Ni_{1-x}Zn_xFe_2O_4$ Nano Powders", J. Raman Spectrosc., Vol. 49, pp. 271-278, 2018.

[16] Y.G. Chukalkin, A.E. Teplykh, "Magnetic State of Nickel-Zinc Ferrites at High Zinc Concentrations", Physics of the Solid State, Vol. 40, No. 8, pp. 1503-1504, 1998.

[17] S. Aliyeva, T. Mehdiyev, "Peculiarities of Magnetic Interaction in $Ni_{1-x}Zn_xFe_2O_4$ Nano Dimensional Ferrites", Smart Nanocomposites, Vol. 8, pp. 149-153, 2017.

[18] O.F. Caltun, "Pulsed Laser Deposition of Ni-Zn Ferrite Thin Films", Journal of Optoelectronics and Advanced Materials, Vol. 7, No. 2, pp. 739-744, April 2005.
[19] T.R. Mehdiyev, A.M. Hashimov, S.N. Aliyeva, I.F. Yusibova, A.V. Agashkov, B.A. Bushuk, "Luminescent and Optical Properties of (Ni, Zn) Ferrites", International Journal on Technical and Physical Problems of Engineering (IJTPE), Issue 46, Vol. 13, No. 1, pp. 81-90, March 2021.
[20] A.G. Gurevich, "Magnetic Resonance in Ferrites and Antiferromagnets", M. Nauka, Moscow, Russia, 1973.
[21] J. Smith, H. Wen, "Ferrites, Physical Properties and Practical Application" M. Publishing House of Foreign Literature, Moscow, Russia, 1962.
[22] B.T. Draine, A. Lazarian, "Magnetic Dipole Microwave Emission from Dust Grains", Astrophys. J., Vol. 512, pp. 740-754, 1999.
[23] E. Baldini, C.A. Belvin, M. Rodriguez Vega, et al., "Discovery of the Soft Electronic Modes of the Trimeron Order in Magnetite", Nature Physics, Vol. 16, pp. 541-545, 2020.
[24] M. Derakhshani, E. Taheri Nassaj, M. Jazirehpour, S. M. Masoudpanah, "Structural, Magnetic, and Gigahertz-Range Electromagnetic Wave Absorption Properties of Bulk Ni-Zn Ferrite", Sci. Rep., Vol. 11, p. 9468, 2021.

BIOGRAPHIES

Talat Rzaqulu Mehdiyev was born in Baku, Azerbaijan, on June 1944. He is head of "Resonance Spectroscopy of Ferromagnetic Materials" laboratory at Institute of Physics, Azerbaijan National Academy of Sciences (Baku Azerbaijan, Doctor of Physics-Mathematical sciences, the experience is 55 years, a specialty in physics of semiconductors and dielectrics (optics, roentgen diffractometer, magnetic and electric properties and etc); applied and system programming, electronics, calculative technique. At the same time, he is editor of the Azerbaijan Journal of Physics. He has authored or coauthored several papers (over to 150) local and international conference proceedings.

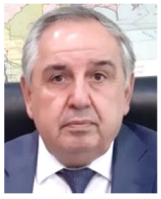

Arif Mamed Hashimov was born in Shahbuz, Nakhichevan, Azerbaijan on September 28, 1949. He is a Professor of Power Engineering (1993); Chief Editor of Scientific Journal of "Power Engineering Problems" from 2000; Director of Institute of Physics of Azerbaijan National Academy of Sciences (Baku, Azerbaijan) from 2002 up to 2009; and Academician and the First Vice-President of Azerbaijan National Academy of Sciences from 2007 up to 2013; and Director of Azerbaijan Research Institute of Energetics and Energy Design from 2014 up to 2020. From 2021 up to now he is Director of Institute of Physics of Azerbaijan National Academy of Sciences (Baku, Azerbaijan). He is laureate of Azerbaijan State Prize (1978); Honored Scientist of Azerbaijan (2005); Cochairman of International Conferences on "Technical and Physical Problems of Power Engineering" (ICTPE) and Editor in Chief of International Journal on "Technical and Physical Problems of Engineering" (IJTPE). He is also a High Consultant in "Azerenerji" JSC, Baku, Azerbaijan. His research areas are theory of non-linear electrical Networks with distributed parameters, neutral earthing and ferroresonant processes, alternative energy sources, high voltage physics and techniques, electrical physics. His publications are 350 articles and patents and 5 monographs.

Shahla N. Aliyeva was born in Baku, Azerbaijan in May 1985. She received the M.Sc. degree from Baku State University (Baku, Azerbaijan) in 2007 and Ph.D. degree on Physics from Electronicsin "Magnetic properties of $Ni_{1-x}Zn_xFe_2O_4$ micro powders and thin films" in 2016. She is a leading scientific researcher, Doctor of Philosophy on Physics. She has authored or coauthored of several papers (more than 35) in journals and international conference proceedings. Her research interests are electronics, magnetic, electric and optic properties of ferrites.

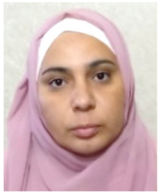

Ilhama F. Yusibova was born in Baku, Azerbaijan, on September 5, 1978. She received the B.Sc. and M.S.E. degrees in Physics in 2006 and 2008, respectively. She works in Institute of Physics, Azerbaijan National Academy of Sciences (ANAS), Baku, Azerbaijan since 2009. Currently, she is a Ph.D. student and works at Laboratory of Resonance Spectroscopy of Ferromagnetic Materials of the same institute. Her research interests are magnetic, electric and optical properties of ferrite materials, and semiconductors.

The 18th International Conference on
"Technical and Physical Problems of Engineering"
30 October 2022
International Organization of IOTPE

ICTPE Conference
www.iotpe.com
ictpe@iotpe.com
ictpe0@gmail.com

ICTPE-2022 Number 15 Code 02ELC08 Pages 74-77

INFLUENCE OF SILVER NANORODS ON DIELECTRIC PROPERTIES OF NEMATIC LIQUID CRYSTAL 5CB

A.R. Imamaliyev G.A. Muradova

Institute of Physics, Ministry of Science and Education, Baku, Azerbaijan
rahimoglu@mail.ru, gunayagayeva2013@mail.ru

Abstract- The influence of silver nanorods on the dielectric and conductivity properties of the nematic liquid crystal 4-pentyl-4′-cyanobiphenyl experimentally studied. Adding the particles decreases the dielectric constant's longitudinal component ($\varepsilon_{\parallel}$) of the liquid crystal, while increases its transversal component ($\varepsilon_{\perp}$). Silver nanorods shift the dispersion of $\varepsilon_{\parallel}$ towards higher frequencies, but dispersion of $\varepsilon_{\perp}$ towards low frequencies. Both electrical conductivity components ($\sigma_{\parallel}$ and $\sigma_{\perp}$) increase by 1-2 orders of magnitude and approach each other. Qualitative explanations of the obtained results are given.

Keywords: Liquid Crystals, Silver Nanorods, Dielectric Permittivity, Electric Conductivity.

1. INTRODUCTION

When talking about liquid crystal (LC), the liquid crystal display (LCD) immediately comes to mind [1], although there are numerous applications of LCs outside of displays [2]. The competition of LCDs with other types of displays (plasma, LED etc.) requires a continuous improvement in the exploitation parameters of operating LC used in display, for which many material parameters of LC should be optimized. In recent years, researchers have been trying to solve this problem by adding nanoparticles of different nature (carbon nanotubes, fullerenes, ferro-electric and ferromagnetic nanoparticles, semiconductor nanowires and nanodots, metal nanoparticles etc.) to LC based on the idea that a constructive combination of the properties of two functional materials can lead to an improvement in some properties, and sometimes to qualitatively new effects [3-5]. A review of works devoted to the properties of liquid crystal colloids based on nanoobjects has been collected in a recently released two-volume book edited by Lagerwall and Scalia [6].

Metal nanoparticles in a liquid crystal medium are also of interest in another aspect. The phenomenon localized surface plasmon resonance (LSPR) occures in metal particles (mostly in noble metals, such as gold and silver) nanoparticles distributed in a dielectric medium, accompanied by light absorption in a certain wavelength range [7].

At the same time, the absorption maximum is very sensitive to the properties of the medium, which is used in the development of various biological sensors [8]. There are a number of other uses for LSPR such as surface-enhanced Raman scattering [9], fluorescence enhancement [10], refractive index (RI) measurement [11] etc. The range of these applications can be extended by varying the shape and size of the particles, as well as by modifying their surface [12]. Even greater opportunities will arise if the passive dielectric medium is replaced by a liquid crystal, the property of which is easily controlled by an external influence such as electric and magnetic field, mechanical stress etc. [13].

As mentioned above, the addition of metal nanoparticles to a LC can affect the electro-optical characteristics by changing its material properties [14]. Therefore, the study of the influence of the type, shape and size of a metal particle on the material properties of LC is of great practical interest. In this work, using the low frequency dielectric spectroscopy method we studied the effect of silver nanorods on the dielectric constant and conductivity components of the classical LC 5CB.

2. EXPERIMENT

The liquid crystal 4-cyano-4′-pentylbiphenyl (5CB) has a structure;

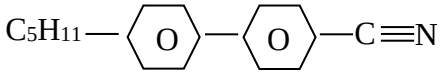

The nematic phase exists in the temperature range of 22.5-35.6 °C. The 5CB has positive dielectric anisotropy: $\Delta\varepsilon = \varepsilon_{\parallel} - \varepsilon_{\perp} = 19.7 - 6.7 + 13$ [15].

AgNRs was in the form of cylinders with diameters in the range of 2-5 nm and lengths in the range of 10-20 nm uniformly dispersed in ethanol in a weight amount of 5%. This colloid mixes easily with 5CB. The resulting mixture (5CB, ethanol and AgNRs) is shaken in a NATO CD-4800 ultrasonic disperser for 6 hours at 40 °C until the ethanol is completely evaporated, which is controlled using an ADAM PW 124 balance. In the finally obtained colloid of 5CB+AgNRs, the amount of AgNRs, was 0.2% w. The corresponding volume fraction of silver particles is 1.8×10^{-4}.

The dielectric properties of the LC were measured at 36 °C in an electro-optical cell. The electro-optic cell has a sandwiched structure and consists of two parallel plate glasses separated by a 30 μm Teflon spacer. A thin (0.1 μm) metallic transparent layer of ITO (indium teen oxide) was deposited on the inner surfaces of these plates. Homeotropic alignment (rod-like molecules of LC are perpendicular to the electrodes' surface) is obtained spontaneously, i.e., without surface treatment. Polyimide was used as a planar aligning (LC molecules are parallel to the electrodes' surface) material [16].

The process of filling of the electro-optical cell was carried out by a capillary method in the isotropic state of the LC. The IET-1920 LCR-meter was used in experiment, allowing to measure the electrical capacitance (C) and resistance (R) of the filled electro-optic cell in the frequency range from 20 Hz to 1 MHz. The amplitude of the AC test signal was 0.25 V.

The dielectric constant of the LC was determined by the expression $\varepsilon = \frac{C}{C_0}$, where C_0 is the capacitance of the empty electro-optic cell, and C is the capacitance of the filled cell. The homeotropic alignment of the LC molecules in the cell, gives us the dielectric constant's longitudinal component ($\varepsilon_{\parallel}$) was measured, and the case planar alignment of the LC molecules gives the transversal components ($\varepsilon_{\perp}$).

The formulae

$$\varepsilon' = \frac{\varepsilon}{\sqrt{1+D^2}} \quad (1)$$

and

$$\varepsilon'' = \varepsilon' D \quad (2)$$

allow us to calculate the real and imaginary parts of the dielectric constant [17].

$$D = \frac{1}{2\pi f CR} \quad (3)$$

is the dissipation factor or loss angle tangent and f is AC voltage frequency. Electric conductivity was calculated from formula [17]

$$\sigma = 2\pi f \varepsilon_0 \varepsilon'' \quad (4)$$

where, $\varepsilon_0 = 8.85 \frac{\text{pF}}{\text{m}}$ is the electric constant.

3. RESULTS AND DISCUSSIONS

The results of our experimental measurements are shown in Figures 1-3. Figure 1 show the dependences of the real ($\varepsilon'_{\parallel}$) and imaginary ($\varepsilon''_{\parallel}$) parts of the longitudinal component of the dielectric constant of pure LC 5CB and colloid 5CB+AgNRs on AC testing frequency corresponding to homeotropic alignment. Similar, Figure 2 shows the dependences of transversal component parts ($\varepsilon'_{\perp}$ and $\varepsilon''_{\perp}$) corresponding to planar alignment. Figure 3 shows the frequency dependences of conductivity components ($\sigma_{\parallel}$) and ($\sigma_{\perp}$) of pure LC and colloid.

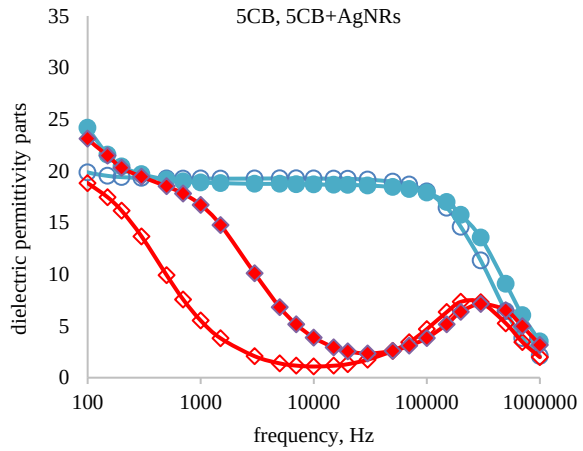

Figure 1. Frequency dependence of real (circles) and imaginary (rhombs) parts of dielectric constant of pure 5CB (empty figures) and 5CB+AgNRs colloid (filled figures) in the case homeotropic alignment

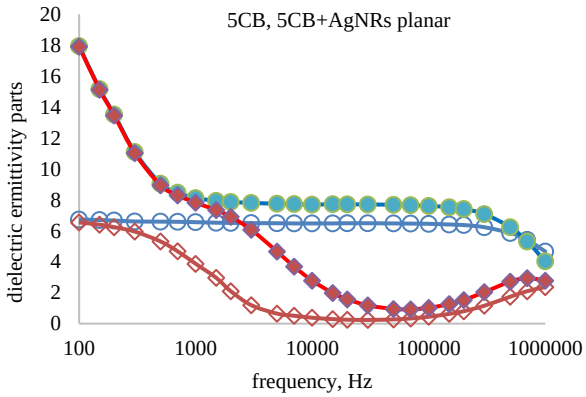

Figure 2. Frequency dependence of real (circles) and imaginary (rhombs) parts of dielectric constant of pure 5CB (empty figures) and 5CB+AgNRs colloid (filled figures) in the case planar alignment

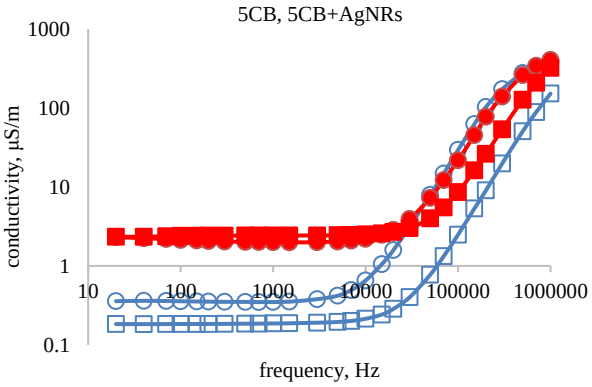

Figure 3. Frequency dependence of conductivityreal (circles) and transversal (rhombs) components of conductivity of pure 5CB (empty figures) and 5CB+AgNRs colloid (filled figures)

From the analysis of these graphs, some regularities can be established. Adding silver particles to the liquid crystal 5CB to the following changes in its properties:

1) The dielectric constant longitudinal component ($\varepsilon_{\parallel}$) slightly grows, while the transversal component ($\varepsilon_{\perp}$) is getting lower. As a result, the anisotropy of the dielectric permittivity ($\Delta\varepsilon$)significantly decreases.

2) The dispersion of dielectric constant longitudinal component ($\varepsilon_{\parallel}$) shifts towards higher frequencies (from 200 kHz to 300 kHz), but the dispersion of transversal component ($\varepsilon_{\perp}$) shifts towards low frequencies (from 1.2 MHz to 700 kHz).
3) Starting from 1 *kHz* a decrease in frequency leads to a sharp increase in both parts ($\varepsilon_{\parallel}$ and $\varepsilon_{\perp}$) of the dielectric permittivity.
4) Both electrical conductivity components ($\sigma_{\parallel}$ and $\sigma_{\perp}$) increase by 1-2 orders of magnitude and approach each other.

It was noted above that, in the absence of treatment, 5CB molecules are oriented normally to the metal (ITO) surface, so there takes place a weak polar anchoring. Similar should take place in the case of AgNRs. In the case of weak anchoring of LC molecules to the surface of AgNPs ($W \propto 10^{-6}\ \frac{\mathrm{N}}{\mathrm{m}}$), the extrapolation length $\tilde{l} = \frac{K}{W}$ is of the order of 10^{-6} m, $K \propto 10^{-12}$ N is the elastic constant of liquid crystal. Simple calculations show that for our sample the average distance between AgNPs is also of the order of 10^{-6} m. As is known [18], under such conditions, the particles interact weakly (of the quadrupole-quadrupole type), slightly distorting the director field of LC. Distortion of homogeneity by AgNPs reduces the degree of orientation (the value of the effective order parameter). As a result, according to the Mayer-Meyer theory [19], the dielectric constant longitudinal component ($\varepsilon_{\parallel}$) of the 5CB+ AgNRs colloid has a smaller value compared to the pure 5CB liquid crystal (Figure 1). According to the same theory, the dielectric constant transverse component ($\varepsilon_{\perp}$) of the colloid will be increased in comparison with the pure liquid crystal (Figure 2).

A weak distortion of the nematic director also alleviates the rotation of rod like liquid crystal molecules around its' short axis, which leads to a shift in the frequency dispersion of the longitudinal component ($\varepsilon_{\parallel}$) towards higher frequencies. Similarly, the frequency shift of the dispersion of the transversal component ($\varepsilon_{\perp}$) to the low frequencies region shows that in the LC structure distorted by silver particles, the rotation of LC molecules around the long axis is difficult.

The closeness of the values of the electrical conductivity components upon the addition of AgNRs to the 5CB liquid crystal indicates the dominant role of silver particles in the conductivity of the 5CB + AgNRs system. The strongly overestimated value of the electrical conductivity of the colloid as compared to pure 5CB is due, in our opinion, to the percolation effect [20]: concentration used in our experiment (volume fraction is 1.8×10^{-4}) of silver particles is above the percolation threshold.

4. CONCLUSION

The addition of silver nanorods to a nematic liquid crystal disorder the homogeneity of the nematic structure due to the anchoring of LC molecules to the surface of silver particles. As a result of a decrease in the effective degree of orientation (order parameter), the dielectric constant components change, and in different directions: the longitudinal component decreases, and the transversal component increases. A decrease in the order parameter also affects the rotation of LC molecules around both the long and short axes. Since the rotation of LC molecules around the short axis becomes easier, the dispersion of the dielectric constant longitudinal component shifts towards higher frequencies. Difficulty in the rotation of molecules around the long axis leads to the fact that the relaxation of the dielectric constant transversal component is shifted to the low-frequency region.

Measurement results show that in the conductivity of the 5CB+AgNRs colloid, the dominant role is played not by LC impurities, but by silver nanorods. This is confirmed by the fact that the longitudinal and transversal components of electrical conductivity are close in value. In addition, the conductivity of is of a percolation nature, since its electrical conductivity of the colloid is at least one order of magnitude higher than that of a pure LC.

REFERENCES

[1] R.H. Chen, "Liquid Crystal Displays: Fundamentals, Physics and Technology", John Wiley and Sons Inc., p. 497, Hoboken, New Jersey, USA, 2011.
[2] Q. Li, "Liquid Crystals Beyond Displays: Chemistry, Physics and Applications", John Wiley and Sons, Inc., p. 573, Hoboken, New Jersey, USA, 2012.
[3] T.D. Ibragimov, A.R. Imamaliyev, G.F. Qanizade, "Effect of Fullerenes C 60 on Dielectric Properties and the Threshold Voltage of Smectic a Liquid Crystal", Molecular Crystals and Liquid Crystals, Vol. 691, Issue 1, pp. 27-34, December 2019.
[4] A.R. Imamaliyev, S.A. Humbatov, M.A. Ramazano, "Effect of Ferroelectric $BaTiO_3$ Particles on Threshold Voltage of a Smectic a Liquid Crystal", Beilstein Journal of Nanotechnology, Vol. 9, pp. 824-828, 2018.
[5] R. Basu, "Soft Memory in Ferroelectric Nanoparticle Doped Liquid Crystal", Physics Reviews: E, Vol. 89, pp. 022508-1 - 022508-5, 2014.
[6] J.P.F. Lagerwal, G. Scalia, "Liquid Crystals with Nano and Microparticles", Series in Soft Condensed Matter, World Scientific Publishing Co, Vol. 7, p. 920, Singapore, 2017.
[7] V. Amendola, R. Pilot, M. Frasconi, O.M. Marago, M. A. Iati**, "**Surface Plasmon Resonance in Gold Nanoparticles: A Review", Journal of Physics: Condensed Matter, Vol. 29, pp. 203002-203049, 2017.
[8] A. Loiseau, V. Asila, G. Boitel Aullen, M. Lam, M. Salmain, S. Boujday, "Silver-Based Plasmonic Nanoparticles and Their Use in Biosensing, Biosensors**,** Vol. 9, No.78, pp. 2-40, 2019.
[9] C.Y. Chen, E. Burstein E, "Giant Raman Scattering by Molecules at Metal-Island Films", Physics Reviews Letters, Vol. 45, No. 15, pp. 1287-1291, 1980.
[10] K. Sokolov, G. Chumanov, T.M. Cotton, "Enhancement of Molecular Fluorescence Near the Surface of Colloidal Metal Films", Analytical Chemistry, Vol. 70, No. 18, pp. 3898-3905, 1998.
11. J. Zeng, D. Liang, Z.X. Cao, "Applications of Optical

Fiber SPR Sensor for Measuring of Temperature and Concentration of Liquids", Proceeding SPIE, Vol. 5855, pp. 667-670, 2005.
[12] J. Becker, A. Trugler, A. Jakab, U. Hohenester, C. Sonnichsen, "The Optimal Aspect Ratio of Gold Nanorods for Plasmonic Bio-Sensing", Plasmonics, Vol. 5, pp. 161-167, 2010.
[13] H.M. Wang, A. Vial, "Plasmonic Resonance Tunability and Surface-Enhanced Raman Scattering Gain of Metallic Nanoparticles Embedded in a Liquid Crystal Cell", Journal of Physical Chemistry, Vol. 117, pp. 24537-24542, 2013.
[14] Y. Sakai, N. Nishida, H. Shiraki, Y. Shiraishi, T. Miyama, N. Toshima, S. Kobayashi, "Dielectric Properties of Twisted Nematic Liquid Crystal Displays Fabricated by Ping Ag-Pd Metal Nanoparticles Having a Long-Term Stability", Molecular Crystals and Liquid Crystals, Vol. 441, No. 1, pp. 143-152, 2005.
[15] L.M. Blinov, V.G. Chigrinov, "Electrooptic Effects in Liquid Crystal Materials", Springer, Science and Business Media, New York, USA, p. 464, 1996.
[16] J. Cognard, "Alignment of Nematic Liquid Crystals and Their Mixtures", Gordon and Breach Science Publishers, p. 77, 1982.
[17] L.M. Blinov, "Structure and Properties of Liquid Crystals", Springer, p. 458, 2011.
[18] Y. Reznikov, "Ferroelectric Colloids in Liquid Crystals", Liquid Crystals Beyond Displays: Chemistry, Physics, and Applications, Edited by Quan Li, John Wiley and Sons, Inc., pp. 402-426, Hoboken, New Jersey, USA, 2012.
[19] D. Dunmur, K. Toriyama, "Dielectric Properties of Liquid Crystals", Handbook of Liquid Crystals, (Eds.) D. Demus, J. Goodby, G.W. Gray, H.W. Spiess, V. Vill, Vol. 1, pp. 231-253, Fundamentals, Wilay-Vch Verlag, 1998.
[20] J.P. Clerc, G. Giraud, J.M. Laugier, J.M. Luck, "The Electrical Conductivity of Binary Disordered Systems, Percolation Clusters, Fractals and Related Models", Advanced Physics, Vol. 39, No. 3, pp. 191-309, 1990.

BIOGRAPHIES

Abbas R. Imamaliyev was born in Vardenis, Armenia on March 14, 1960. He graduated from Baku State University (Baku, Azerbaijan) in 1981. He received Ph.D. degree in 1992. In 1994-2013 worked in Baku State University. Since 2013 at present, he is a senior researcher at Institute of Physics, Azerbaijan National Academy of Science (Baku, Azerbaijan). His area of scientific interests are liquid crystals and polymer gels. He is the author of 112 scientific works, including 61 articles and 1 monograph.

Gunay A. Muradova was born in Jalilabad, Azerbaijan on July 27, 1989. She received the B.Sc. degree from Baku State University (Baku, Azerbaijan) and the M.Sc. degree from Sumgait State University (Sumgait, Azerbaijan) both in the Physics in 2006 and 2010, respectively. Currently, she is a Scientist at Institute of Physics, Azerbaijan National Academy of Sciences (Baku, Azerbaijan). Her area of scientific interests are liquid crystals and polymer physics. She is the author of 7 scientific works, including 4 articles.

The 18th International Conference on
"Technical and Physical Problems of Engineering"
30 October 2022
International Organization of IOTPE

ICTPE Conference
www.iotpe.com
ictpe@iotpe.com
ictpe0@gmail.com

ICTPE-2022 Number 16 Code 04CIT01 Pages 78-82

SYNTHESIS OF NITIHF ALLOY BY USING MACHINE LEARNING METHODS

M.B. Babanli C.A. Imamalizade

Azerbaijan State Oil and Industry University, Baku, Azerbaijan, pr.asoiu@asoiu.edu.az, cimamelizade@gmail.com

Abstract- It is known that nitinol is a promising functional material that is used in aerospace, bioengineering, medicine and other fields of modern high technologies. In this work, the dependence of the transition temperature on the processing conditions during the synthesis of NiTiHf alloy, a modification of nitinol, which has a wide application field, was investigated by using Machine Learning (ML) methods, and certain theoretical results were obtained. In addition, suggestions were made to improve the obtained results.

Keywords: Nitinol, Machine Learning, Deep Learning, Regression, Python.

1. INTRODUCTION

Over the past 30 years, materials science has made significant development in the field of data generation. As a result, huge amounts of data are collected in different data sources related to material science [1-6]. To manage and use this data effectively Big Data term was added. ML (Machine learning) is a field which can deal with big data and meets requirements of scientists and engineers in modern world. Machine learning is science where different regression, classification or statistical algorithms is developed depends on given target and data. ML methods play an important role in solving actual problems in the field of materials science [7-11]. One of these problems is the synthesis of new types of alloys based on finding an effective relationship between various characteristics of alloys. For instance, ML is used to detect and develop alloys with narrow thermal hysteresis in parallel with the optimization of thermal hysteresis and transition temperatures.

ML methods consist of 2 main categories: Shallow Learning and Deep Learning. Shallow learning methods belong to classic ML methods and are designed to work with relatively small amounts of data. Shallow learning methods include algorithms such as Linear Regression, Logistic Regression, Random Forest, Support Vector Machine (SVM) and Gaussian process regression. Deep learning methods refer to methods based on modified artificial neural networks and are designed to work with large-scale data. Deep learning methods include algorithms such as Convolutional Neural Network (CNN), Recurrent Neural Network (RNN), Deep Belief Network (DBN) [12-16].

Shape memory alloys belong to alloys that can recover their original shape and size during phase transformation. One of the most common shape memory alloys is NiTi (nitinol) and NiTi-based alloys. Nitinol consists of approximately equal amounts of Ni and Ti elements and is widely used in the development of cardiovascular stands, micro activators and in the fields related to damping instruments. Interest to Nitinol started in 1972 when William Bulher and Frederick Wang found shape memory effect in NiTi based alloys during working in military laboratory [17, 18]. Nitinol has two unique properties: thermal shape memory and super elasticity which makes it promising for use in various industries [19-22]. Mechanism of shape memory effect is shown on Figure 1, while mechanism of super elasticity is presented on Figure 2 [19].

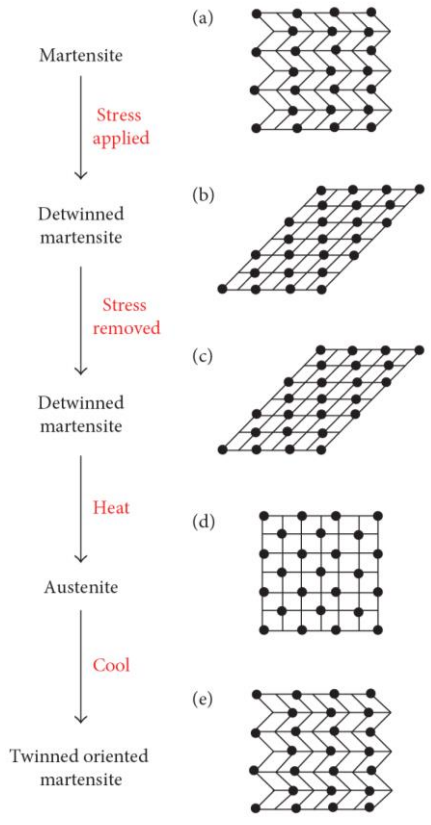

Figure 1. Mechanism of shape memory effect [19]

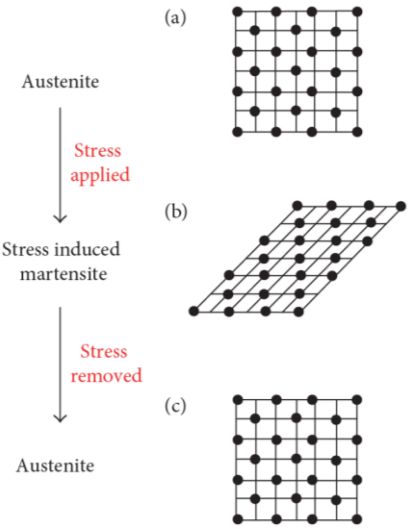

Figure 2. Mechanism of super elasticity [19]

Many scientific works and articles have been published in the field of synthesis of nitinol and its alloys by ML methods [23-27]. Analyzing the research conducted in this field in recent years, it can be concluded that the most important characteristics during the synthesis of nitinol are transition temperatures and thermal hysteresis. Numerous works and researches devoted to this field show that the transition temperatures during the synthesis of nitinol are affected not only by the composition of the alloy, but also by its processing conditions. Gauss Process Regression was used for the synthesis of NiHiHf in [28]. Pearson correlation method was applied to find correlation between input features and temperatures. Then thermal hysteresis and average transition temperatures were predicted with higher accuracy by using not only structural but also processing features of alloy and confirmed by physics-informed feature engineering. High results were obtained taking into account the processing parameters of NiHiHf using artificial neural network in [29]. Unlike previous work, most of the input data features consist of processing condition and just atom pencent of elements in NiTiHf alloy were used in calculation. High accuracy was gained by Neural Network as regression algorithm. Shallow learning algorithms were applied to find transition temperatures of NiTiHf [30]. Results of each method were compared among each other and discussed [30].

2. EXPERIMENTAL PART

In this work, the dependence of processing conditions on the transition temperatures in an alloy based on nitinol was studied using classical ML methods. The calculations were carried out on the Jupyter Notebook online platform based on Python 3.9.1. In parallel with the classical methods of ML, the expediency of using deep learning methods (Deep Learning) is proposed. To determine the dependence of the transition temperature on the processing parameters, the data were divided into 70% (training sample for calculating the dependence) and 30% (test sample for applying the found dependence). The data used to run the algorithms are taken from [20].

The accuracy measure of algorithm is demonstrated with R^2 and MAE (mean absolute error) which calculation formula given by [14, 28]:

$$R^2 = 1 - \frac{\sum_{i=1}^{n}(y_i - \hat{y}_i)}{\sum_{i=1}^{n}(y_i - \bar{y}_i)} \quad (1)$$

and

$$MAE = \frac{\sum_{i=1}^{n}(y_i - \hat{y}_i)}{n} \quad (2)$$

where, $\hat{y}_i$ predicted value, y_i actual data and $\bar{y}_i$ is the mean value of output data, i amount of data used in samples.

Based on experimental and predicted data, Figure 3 represents graphical results of regression algorithms used in train sample, while Figure 4 illustrates graphical results of regression algorithms used in test sample. Linear Regression between processing conditions and transition temperature shows R^2=83.5% accuracy and 20.06 K MAE for train data and R^2=68.4% accuracy and 41.36 K MAE for test data (Figure 3a and Figure 4a).

Gauss Process Regression between processing conditions and transition temperature shows R^2 =80.4% accuracy and 22.67 K MAE for train data and R^2 =78% accuracy and 31.55 K MAE for test data (Figure 3b and Figure 4b). Support Vector Regression between processing conditions and transition temperature shows R^2=81.8% accuracy and 19.45 K MAE for train data and R^2=74.5% accuracy and 34.82 K MAE for test data. Linear kernel was used during regression because of higher accuracy compared to other kernel algorithms (Figure 3c and Figure 4c).

From the computed results we can see that the higher accuracy in train sample belongs to Linear Regression. However, in test sample accuracy decreased from R^2=83.5% to R^2=68.4% and MAE from 22.67 K to 41.36 K which worst results among compared algorithms.

Similar to Gauss Process Regression, Support Vector Regression, shows nearly the same accuracy in both train and test samples R^2=81.9%, 19.45 K MAE and R^2=74.5%, 34.82 K MAE respectively. Obtained higher accuracy by using linear kernel emphasize that both train and test samples can be linearly separable.

Gauss Process Regression shows nearly the same accuracy in both train and test samples R^2=80.4%, 22.67 K MAE and R^2=78%, 31.55 K MAE, respectively. As a result, this algorithm is preferable than others. The obtained results show the necessity for further research in this field.

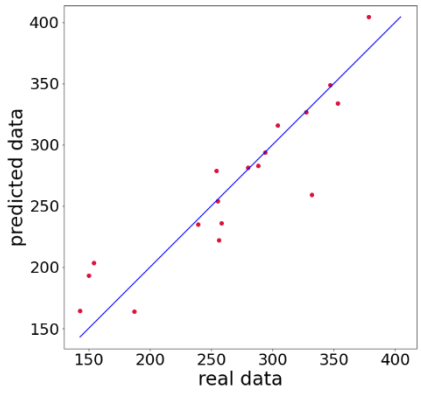

(a)

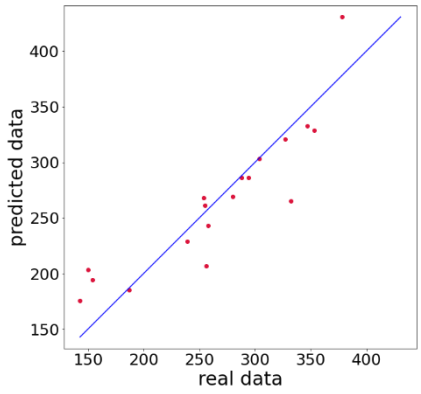

(b)

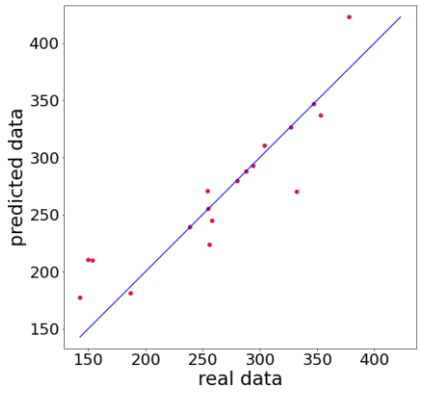

(c)

Figure 3. Regression graphs of used algorithms (train sample), (a) Linear Regression, (b) Gauss Process Regression, (c) Support Vector Regression

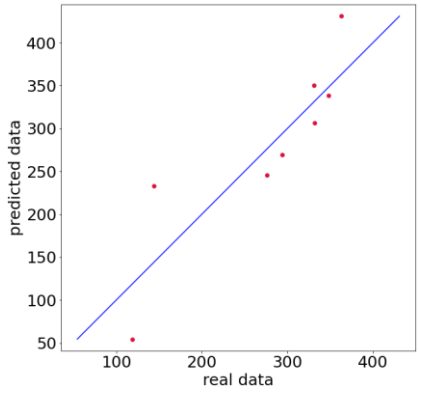

(a)

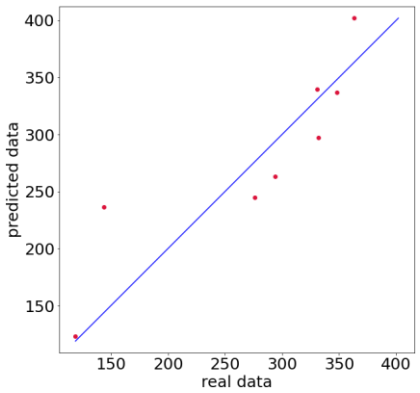

(b)

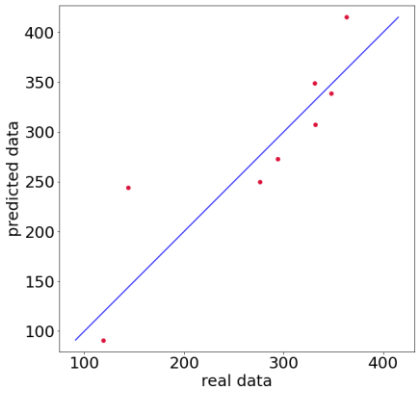

(c)

Figure 4. Regression graphs of used algorithms (test sample), (a) Linear Regression, (b) Gauss Process Regression, (c) Support Vector Regression

3. CONCLUSIONS

In this work, influence of processing conditions to transition temperature of NiTiHf alloy, was investigated by using Machine Learning (ML) methods, and gained results was compared among each other. The results can be used during manufacturing of NiTi based alloys which show shape memory and super elasticity properties.

REFERENCES

[1] D. Packwood, L.T.H. Nguyen, P. Cesana, G. Zhang, A. Staykov, Y. Fukumoto, D.H. Nguyen, "Machine Learning in Materials Chemistry: An Invitation", Machine Learning with Applications, Vol. 8, No. 11, p. 100265, 2022.

[2] R. Armiento, "Database-driven High-Throughput Calculations and Machine Learning Models for Materials Design of Machine Learning Meets Quantum Physics", Lecture Notes in Physics, Eds.: K.T. Schutt, S. Chmiela, O.A. von Lilienfeld, A. Tkatchenko, K. Tsuda, K.R. Muller, Springer, Vol. 968, p. 484, Cham, Switzerland, 2020.

[3] J.E. Hein, "Machine Learning Made Easy for Optimal Reactions", Nature, Vol. 590, pp. 40-41, 2021.

[4] J. Schmidt, M.R.G. Marques, S. Botti, M.A.L. Marques, "Recent Advances and Applications of

Machine Learning in Solidstate Materials Science", NPJ Computational Materials, Vol. 5, p. 83, 2019.
[5] R. Barta, "Machine Learning from Diverse Data Sources", Nature, Vol. 589, pp. 524-525, 2021.
[6] N.S. Johnson, P.S. Vulimiri, A.C. To, X. Zhang, C.A. Brice, B.B. Kappes, A.P. Stebner, "Invited Review: Machine Learning for Materials Developments in Metals Additive Manufacturing", Additive Manufacturing, Vol. 36, pp. 101641-101650, 2020.
[7] B.D. Ripley, "Spatial Statistics", The 1st Ed., John Wiley and Sons, 1981.
[8] O. Scabenberger, C.A. Gotway, "Statistical Methods for Spatial Data Analysis", CRC Texts in Statistical Science, Chapman and Hall, 2004.
[9] C.J. Long, J. Hattrick Simpers, M. Murakami, R.C. Srivastava, I. Takeuchi, V.L. Karen, X. Li, "Rapid Structural Mapping of Ternary Metallic Alloy Systems Using the Combinatorial Approach and Cluster Analysis", Review of Scientific Instruments, Vol. 78, Issue 9, p. 072217, 2007.
[10] C.J. Long, D. Bunker, X. Li, V.L. Karen, I. Takeuchi, "Rapid Identification of Structural Phases in Combinatorial Thin-Film Libraries Using X-ray Diffraction and Non-Negative Matrix Factorization", Review of Scientific Instruments, Vol. 80, No. 11, p. 103902, 2009.
[11] A.G. Kusne, T. Gao, A. Mehta, L. Ke, M.C. Nguyen, K.M. Ho, V. Antropov, C.Z. Wang, M.J. Kramer, C. Long, I. Takeuchi, "On-The-Fly Machine-Learning for High-Throughput Experiments: Search for Rare-Earth-Free Permanent Magnets", Scientific Reports, Vol. 4, pp. 6367-6373, 2015.
[12] J. Wei, X. Chu, X.Y. Sun, "Machine Learning in Materials Science", InfoMat, No. 1, pp. 338-358, 2019.
[13] A. Agrawal, A. Choudhary, "Perspective: Materials Informatics and Big Data: Realization of the "Fourth Paradigm" of Science in Materials Science", APL Materials, Vol. 4, No. 11, pp. 053208-1053208, 2016.
[14] D. Xue, D. Xue, R. Yuan, Y. Zhou, P.V. Balachandran, X. Ding, J. Sun, T. Lookman, "An Informatics Approach to Transformation Temperatures of NiTi Based Shape Memory Alloys", Acta Materialia, Vol. 125, pp. 532-541, 2017.
[15] P. Baldi, "Deep Learning in Biomedical Data Science", Annu. Rev. Biomed. Data Sci., No. 1, pp. 181-205, 2018.
[16] M. Wainberg, D. Merico, A. Delong, B.J. Frey, "Deep Learning in Biomedicine", Nature Biotechnology, Vol. 36, No. 9, pp. 829-838, 2018.
[17] W.J. Buehler, J.V. Gilfrich, R.C. Wiley, "Effect of Low-Temperature Phase Changes on the Mechanical Properties of Alloys Near Composition TiNi", Appl Phys, Vol. 34, pp. 1475-1477, 1963.
[18] G.B. Kauffman, I. Mayo, "The Story of Nitinol: The Serendipitous Discovery of the Memory Metal and Its Applications", The Chemical Education, Vol. 2, No. 2, pp. 1-21, 1996.
[19] A. Wadood, "Brief Overview on Nitinol as Biomaterial", Advances in Materials Science and Engineering, Article ID 4173138, 2016.
[20] P. Novak, H. Moravec, P. Salvetr, F. Prusa, J. Drahokoupil, J. Kopecek, M. Karlik, T.F. Kubatik, "Preparation of Nitinol by Non-Conventional Powder Metallurgy Techniques", Materials Science and Technology, Vol. 31, No. 15, pp. 1886-1893, 2015.
[21] J.J. Mohd, M. Leary, A. Subic, M.A. Gibson, "A Review of Shape Memory Alloy Research, Applications and Opportunities", Mater Design, No. 56, Vol. 113, p. 1078, 2014.
[22] H. Sehitoglu1, Y. Wu1, L. Patriarca, G. Li, A. Ojha, S. Zhang, Y. Chumlyakov, M. Nishida, "Super elasticity and Shape Memory Behavior of NiTiHf Alloys", Shap. Mem. Superelasticity, No. 3, pp. 168-187, 2017.
[23] M. Mehrpouya, A. Gisario, M. Nematollahi, A. Rahimzadeh, K.S. Baghbaderani, M. Elahinia, "The Prediction Model for Additively Manufacturing of NiTiHf High-Temperature Shape Memory Alloy", Materials Today Communications, Vol. 26, No. 8, p. 102022, 2021.
[24] W.J. Song, S.G. Choi, E.S. Lee, "Prediction and Comparison of Electrochemical Machining on Shape Memory Alloy (SMA) Using Deep Neural Network (DNN)", J. Electrochem. Sci. Technol., Vol. 10, No. 3, pp. 1-8, 2019.
[25] J.W. Mwangia, L.T. Nguyena, V.D. Buia, Th. Bergera, H. Zeidlera, A. Schubert, "Nitinol Manufacturing and Micromachining: A Review of Processes and Their Suitability in Processing Medical-Grade Nitinol", Journal of Manufacturing Processes, No. 38, pp. 355-369, 2019.
[26] D. Kapoor, "Nitinol for Medical Applications: A Brief Introduction to the Properties and Processing of Nickel Titanium Shape Memory Alloys and Their Use in Stents", Johnson Matthey Technol Rev, Vol. 61, No. 1, pp. 66-76, 2017.
[27] D. Hodgson, S. Russell, "Nitinol Melting, Manufacture and Fabrication", Min lnvas Ther and Allied Techno1, Vol. 9, No. 2, pp. 61-66, 2000.
[28] B. Liu, B. Kappes, B.A. Ahmadi, "Physics-Informed Machine Learning for Composition Process Property Design: Shape Memory Alloy Demonstration", Applied Materials Today, Vol. 22, p. 100898, 2021.
[29] H. Abedi, K.S. Baghbaderani, A. Alafghani, "Neural Network Modeling of NiTiHf Shape Memory Alloy Transformation Temperatures", Research Squrae, pp. 1-29, 2021.
[30] M. Nematollahi, G. Toker, S.E. Saghaian, "Additive Manufacturing of Ni-Rich NiTiHf20: Manufacturability, Composition, Density, and Transformation Behavior", Shape Memory and Super Elasticity, Vol. 5, No. 5, pp. 113-124, 2019.

BIOGRAPHIES

Mustafa B. Babanli was born in Saatli, Azerbaijan on February 21, 1968. He defended his doctoral thesis for technical sciences in 2008. Since 2015 to the present, he has been the Rector of Azerbaijan State University of Oil and Industry, Baku, Azerbaijan. He is a Professor at the same university. He has 124 scientific and scientific-methodological works, 8 patents, 50 materials for international and republican scientific-technical conferences, 4 textbooks, 4 manuals and 6 monographs.

Chingiz A. Imamalizade was born in Baku, Azerbaijan on 19 January, 1995. He received Bachelor degree from Baku Engineering University, Baku, Azerbaijan in 2017 and Master degree from Azerbaijan State University of Oil and Industry, Baku, Azerbaijan in 2019. Currently, he is a Ph.D. student in material science field at Azerbaijan State University of Oil and Industry.

The 18th International Conference on
"Technical and Physical Problems of Engineering"
30 October 2022
International Organization of IOTPE

ICTPE Conference
www.iotpe.com
ictpe@iotpe.com
ictpe0@gmail.com

ICTPE-2022 Number 16 Code 04CIT02 Pages 83-86

ANALYSIS OF CYBER SECURITY CHALLENGES IN SMART CITY ENVIRONMENT

M.A. Hashimov

Institute of Information Technology, Azerbaijan National Academy of Sciences, Baku, Azerbaijan
mamedhashimov@gmail.com

Abstract- One of the new ways proposed to solve various urban problems during the last decade is the smart city concept. A smart city is presented as a concept that uses advanced technologies, applies innovations and offers a high quality of life. A smart city analyzes the situations happening in the city, offers technological solutions to improve the urban development and quality of life. The presented article provides information on the current state and further prospects of the smart city concept. It highlights the benefits of the services covering the smart city environment for citizens and government institutions. The article also analyzes cyber security problems arising during the use of smart city services.

Keywords: Smart City, Internet of Things, Cyber Security, Cyber-Attacks.

1. INTRODUCTION

The Department of Economic and Social Affairs of the United Nations (DESAP) conducted a study in 2018 and revealed that about 30% of the total population of the world lived in cities in the 1950s. This number increased to 55% in 2014. According to these studies, 60% of the total population of the world is predicted to live in modern cities by 2030, and 70% by 2050 [1].

The rapid growth of cities exacerbates many problems associated with an urban living (public safety, traffic management, waste management, noise, air and water pollution, etc.).

Experts believe that "it will be impossible to prevent urbanization". The arrival of people to the city will continue as usual. Therefore, it is necessary to make the lifestyle easier. In such a situation, the only way out will be "smart cities". In recent years, cities are tending to use more information and communication technologies and to become smarter. New technologies enable the cities to make better use of their resources, save money and provide superior services to citizens. A concept of smart city aims to integrate "smart" systems that manage information about factors that influence the positive development of the city, such as economic, social, environmental quality of life [2].

The quality of life and services delivered for citizens, as well as the city environment are significantly improved by smart cities. They monitor physical things in real time and ensure citizens with intelligent information about transportation, healthcare, smart buildings, public safety, smart parking, road system, smart agriculture, etc.

Due to the growing number of people the countries are investing profoundly in smart city projects. China, for instance, is engaged in 200 projects under the smart city framework [3]. Technologies related to smart city concept enable the municipalities of the cities to control daily operations to ease the people's lives. Many devices and interconnected systems that offer various applications such as smart healthcare, smart transportation, smart parking, smart traffic system, smart agriculture, and smart homes for people are included into the smart city infrastructure.

The report predicts the smart city market to grow gradually and reach 1 trillion USD in the near future [4]. In fact, the states are committed to attracting huge funds for the realization of smart city concept. The massive concept indicated involves deploying numerous sensor nodes across the urban environment for ensuring the people with real-time information on various services such as public transport, traffic flow, water and energy consumption levels.

However, the management and analysis of large amounts of confidential data raises concerns about how to protect sensitive data from unauthorized parties, along with a number of security and confidentiality issues. Therefore, identifying cyber security problems in the smart city environment and developing the ways to combat them are currently one of the most urgent issues. This article aims to identify the further research fields to address various security and privacy issues in smart city environment. In this regard, the article provides an overview of the cyber security issues arising when using smart city services.

2. SMART CITY SERVICES

The main idea of the smart city concept is to connect and manage all service areas and facilities of the city in one system. Smart cities also aim to benefit residents in various characteristics which are strictly associated to their living standard, e.g., energy, environment, industry, life and services. Some of these services include [5-7].

2.1. Smart Government

Smart government is of great importance for a smart city. Smart government aims to offer a better service to its residents and brings together information, entities, judicial processes, including physical infrastructure through ICT. Furthermore, smart governance allows residents to involve in public decision-making, urban scheduling, and consequently expand information transparency as well as efficiency.

For example, it ensures the use of e-services by citizens (choice of school, reservation of public catering facilities, library services, etc.), access of citizens to official documents and participation in decision-making processes. Smart government is the next step towards e-government. Smart government uses real-time information to increase situational awareness, respond efficiently and effectively to accidents, examine emergencies, and reduce crime.

2.2. Smart Mobility

Smart mobility is designed to make smarter use of transportation systems. In particular, smart transport networks may deliver advanced service to the population and increase safety, speed and reliability. Urban residents may effortlessly set daily plans, look for location of buses or trains by using transport-oriented mobile applications, detect traffic jams in real time, find the most economical and fastest routes. Smart parking is the use of information and communication technologies to assist drivers to find parking spaces more efficiently. Smart parking involves monitoring of parking spaces for residents and visitors, informing the drivers about the availability of vacant spaces, detecting parking violations and online parking payment.

2.3. Smart Environment

Smart environment may significantly provide its contributions for the creation of a sustainable society. In particular, applying technical organizational means, energy consumption, air quality, structural reliability of buildings and traffic density can be managed through a smart city, it can also effectively combat pollution or waste. For example, smart waste management solutions use sensors embedded in containers to measure the fill levels of cans and alert municipal waste collection services when the containers are ready to be emptied. Over time, data collected by sensors can be used to optimize driver routes and schedules and reduce operating costs.

New environmental sensor networks used in smart city environments can further even predict and detect natural disasters.

Smart cities may reduce excessive consumption of resources, e.g., water, gas, electricity, advance economic development and provide its contribution to environmental protection through smart utilities. For the control of distributed energy resources, smart grids widely apply smart metering. Smart grid refers to a data transmission network that offers an intelligent tactic to traditional energy generation, storage, transmission, distribution and demand management to improve reliability and achieve better power quality. It also refers to an intelligent monitoring system which manages the electricity passing through this network. It applies the tools capable of bidirectional communication to measure and determine the electricity to be produced and consumed. Later, the information is sent to users and operators as well as automatic devices to monitor and make decisions about any changes in the condition of power grids.

Smart water technology controls the entire water supply chain, from freshwater storage to wastewater collection and treatment. Various sensors are widely used in smart water resource management. Using data generated by sensors at various points in the water supply chain, smart meters and monitoring centers measure water consumption in real time, help identify overuse and waste points, adjust usage patterns, and forecasts future consumption.

2.4. Smart Services

Smart services offer multiple benefits to the residents. Smart healthcare applications for instance are capable to control people's health in real time through wearable devices and medical sensors. As a healthcare service, Smart Health connects people, healthcare facilities, and other related entities using various techniques, for example through wearable devices, the IoT, and the mobile Internet. Smart health includes several key elements such as doctors, patients, hospitals and medical research institutions. It also includes multiple aspects such as disease prevention, patient monitoring, diagnosis and treatment, hospital management, healthcare decision making and medical research. remote monitoring can be performed through wireless connection of smart devices with healthcare centers and data analysis system.

A comfortable, intelligent and environmentally-friendly living can be created through many smart services for example by controlling household appliances remotely. Finally, social media, entertaining, smart shopping and other smart services have greatly enhanced the ease of daily lives of the population.

Although the smart city is considered to be a promising solution to provide efficient services to citizens using information and communication technologies, it is vulnerable to various security threats. One of the most important problems related to the wide spread and implementation of the smart city concept is cyber security.

3. SECURITY CHALLENGES IN SMART CITY

Security issues in a smart city are viewed as one of the main reasons why many people are skeptical of Smart city projects. IoT devices are inherently security vulnerabilities. Since smart cities enable a large number of devices to connect to the Internet, security becomes a critical issue. The number of smart city devices are predicted to reach 1 billion by 2025. These devices connected to the Internet are estimated to generate large amounts of data in real time.

HP company estimates that approximately 70% of Smart City IoT devices are at risk of attack due to significant vulnerabilities such as insufficient authorization, insufficient software protection, and poorly encrypted communication protocols [8]. Hackers, viruses, "Trojan" and other threats have a great potential to disrupt services and interfere with the entire system (banking, transportation, etc.), which can result in huge losses [4]. These vulnerabilities can lead to mass cyber-attacks in smart cities. Malicious attackers may generate false information while manipulating sensitive data, which can result in loss of control over highly intelligent systems. For example, in 2015, a power outage caused by a denial-of-service (DoS) attack on a smart grid (SG) in Ukraine affected 230,000 people [9].

Various application scenarios have recently suffered from significant problems. residents' privacy, as well as their behaviors and working hours for instance, can be monitored by smart metering infrastructure in smart grids. Correspondingly, device producers and service providers may see sensitive data in terms of smart homes and smart health. Additionally, a huge volume of trajectory data sensed by smart mobility apps may be applied to suppose a user's location and movement outlines. For example, no encryption or authentication is performed for the communication between traffic control systems and traffic lights in intelligent transportation management, which may lead to alteration and falsification of information by an attacker. Moreover, they cause massive traffic jams that can last for hours by breaking traffic light control systems and their sequencing, road signs and speed limit signs.

Many car companies have recently begun to pay more attention to creating autonomous vehicles targeting to reduce the road crashes. Serious security and privacy threats still remain at the background of all advantages of the introduction of this technology. As a result, the security of citizens and the protection of data privacy in smart cities remain under threat. In particular, attackers may take advantage of these security vulnerabilities for performing attacks at a distance, e.g., braking, engine shutdown, and steering. Furthermore, access to huge personal data sensed by autonomous vehicle computer system can lead to serious privacy issues.

Hacking the wireless sensors used in a smart city environment is the easiest way to perform remote cyber-attacks on a city's critical infrastructure. False data from various sensors is another potential threat in urban environments; for example, by interfering with the sensors installed to detect earthquakes, floods, etc., cybercriminals use them to perform false warnings and cause public fear. On the other hand, by simulating destruction of tunnel or bridge, shooting, etc., they can cause a general state of panic through alarms [10]. Attackers can perform malicious attacks by tampering with waste collection and management systems by spoofing odor or litter level sensors on empty bins to cause them to waste time and resources.

Cyber-attacks compromise the safety gaps in smart city applications. These security gaps are the attacks as follows: passive and active. Passive attack aims to attain and use various system data without changing any resources. They mainly aim to study the system configuration, behavior and architecture. These attacks are difficult to detect because the data does not change here. Therefore, more attention should be paid to preventing such attacks. Eavesdropping is a passive attack, defined as an illegal interception of communications without the consent of the communicating parties. Snooping is a hazardous attack that compromises the privacy and integrity of the network in smart cities, as well as causing personal and financial setbacks. This attack can be used to capture the behavior of network traffic and trace communication channels to obtain a network map [11].

Alternatively, attackers perform active attacks for affecting and altering the system functioning by modifying the information and entering false information to the system. An attacker disrupts the regular functioning of IoT devices and networks. Denial-of-service attacks (DoS) of various types, such as resource exhaustion and overload, are active attacks. A smart city has tens of thousands of IoT devices and sensors, which are vulnerable to different cyber security levels. Attackers take advantage of this vulnerability and create a malicious botnet by hacking sensors and IoT devices in smart cities, thereby launching DDoS attacks. Attackers use simple communication protocols to send numerous requests to IoT devices to deplete their resources, thus causing the device to stop working. Since most of the devices connected to the IoT network do not authenticate each other, a DoS attack becomes easy to be performed. Cybercriminals also perform Distributed Denial of Service (DDoS) attacks, which are very similar to DoS attacks, but performed by multiple computers. In some cases, attackers apply both methods at the same time. For example, they first hijack the target node or nodes through virus programs, and then perform DoS or DDoS attacks through the hijacked node or nodes. By doing so, they may cause the usual transmission of data, its reception, infect numerous IoT devices, smart city sensors, then disrupt services there [12].

Man-in-the-middle attack, another type of attack, has two main types, passive and active ones. The attacker performing a passive attack is only interested in the data transmitted. In this attack, an attacker stands between users and servers to eavesdrop and steal useful information without the awareness of legitimate users. A man-in-the-middle attack is an internal attack, where data from a source node comes to an attacker before reaching the destination node, with both the source and receiver thinking that data is being exchanged directly. In an active attack, the attacker manipulates the received packets before forwarding them to the destination node. A man-in-the-middle attack can be performed based on the communication protocols used in the network. Devices used in a smart city environment cannot use secure communication protocols due to limited number of resources [13].

4. CONCLUSIONS

The services covering the smart city concept are of critical importance, therefore special requirements are specified on their security and reliability. This article analyzed cyber security problems during the use of smart city services and highlighted some cyber-attacks that may damage the privacy of users. In order to solve the above-mentioned problems, the following issues should be solved in the further research work:

• Development of methods and algorithms for detection of unauthorized nodes (devices) connected to smart city systems.

• Development of methods and algorithms for protection of smart city services from DoS attacks.

• Development of methods for identifying man-in-the-middle attacks of network infrastructure of smart city systems.

The vulnerability of a smart city is that it lacks a centralized infrastructure, which poses a security challenge in terms of cyber-attacks. Attackers are difficult to control. Therefore, the attack scenarios and their effects for each smart city service should be studied, and different types of solutions should be implemented to prevent each attack.

REFERENCES

[1] UN Press release, www.population.un.org/wup/ Publications/Files/WUP2018- PressRelease.pdf.

[2] K. Ayca, K. Ondrej, K. Attila, M. Fatih T., "Future Trends and Current State of Smart City Concepts: A Survey", IEEE Access, Vol. 8, pp. 86448-86467, 2020.

[3] P. Liu, Z. Peng, "China's Smart City Pilots: A Progress Report", Computer, pp. 72-81, 2014.

[4] S.S. Abbas, S.S. Daniel, K. Anup, E. Adel, "IoT in Smart Cities: A Survey of Technologies, Practices and Challenges", Smart Cities, Vol. 4, pp. 429-475, 2021.

[5] Z. Andrea, B. Nicola, C. Angelo, V. Lorenzo, Z. Michele, "Internet of Things for Smart Cities", IEEE Internet of Things Journal, Vol. 1, No. 1, pp. 22-32, 2014.

[6] K. Zhang, J. Ni, K. Yang, X. Liang, J. Ren, X. Shen, "Security and Privacy in Smart City Applications: Challenges and Solutions", IEEE Communications Magazine, Vol. 55, Issue 1, pp. 122-129, 2017.

[7] C. Ma, "Smart City and Cyber-Security; Technologies Used, Leading Challenges and Future Recommendations", Energy Reports, Vol. 7, pp. 7999-8012, 2021.

[8] M. Yasir, A. Farhan, Y. Ibrar, A. Asma, I. Muhammad, G. Sghaier, "Internet-of-Things Based Smart Cities: Recent Advances and Challenges", IEEE Communications Magazine, Vol. 55, No. 9, pp. 16-24, 2017.

[9] A. Goudarzi, F. Ghayoor, M. Waseem, S. Fahad, I. Traore, "A Survey on IoT-Enabled Smart Grids: Emerging, Applications, Challenges, and Outlook", Energies, Vol. 15, Issue. 19, pp. 2-32, 2022.

[10] A. Alibasic, R. A. Junaibi, Z. Aung, W.L. Woon, M.A. Omar, "Cybersecurity for Smart Cities: A Brief Review", Lecture Notes in Computer Science Book Series, 2017.

[11] O. Saber, T. Mazri, "Smart City Security Issues: The Main Attacks and Countermeasures", The 6th International Conference on Smart City Applications, Turkey, pp. 465-472, 27-29 October 2021.

[12] M. Kalinin, V. Krundyshev, P. Zegzhda, "Cybersecurity Risk Assessment in Smart City Infrastructures", Machines, Vol. 9, Issue 4, pp. 2-19, 2021.

[13] J.C. Lee, J.H. Kim, J.T. Seo, "Cyber Attack Scenarios on Smart City and their Ripple Effects" International Conference on Platform Technology and Service (PlatCon), Jeju, South Korea, pp. 1-5, 28-30 January 2019.

BIOGRAPHY

Mammad Arif Hashimov was born in Baku, Azerbaijan on January 30, 1986. He graduated in Automation and Control from Azerbaijan Technical University, Baku, Azerbaijan in 2006. He received his Master's degree in Automation and Control from the same university in 2010. He received his Ph.D. degree in Computer Sciences from Institute of Information Technology, Azerbaijan National Academy of Sciences, Baku, Azerbaijan in 2016. He is leading researcher in the same institute. His research interests include various areas in internet of things, cloud computing, data processing, computer networks, virtual computing, particularly in the area of cloud technology applications.

The 18th International Conference on
"Technical and Physical Problems of Engineering"
30 October 2022
International Organization of IOTPE

ICTPE Conference
www.iotpe.com
ictpe@iotpe.com
ictpe0@gmail.com

ICTPE-2022 Number 18 Code 04CIT03 Pages 87-90

CLOUD COMPUTING: MODELS, SERVICES AND PROBLEMS

R.G. Alakbarov O.R. Alakbarov

Institute of Information Technology, Azerbaijan National Academy of Sciences, Baku, Azerbaijan
rashid.alakberov@gmail.com, oqtayalakbarov@yahoo.com

Abstract- Cloud computing enables the computer technology infrastructure to be directly built in a networked environment and allows users to benefit from computing resources. This technology help to the users store their software on cloud servers, processed and the results are delivered to the user. This article analyzes the architectural-technological principles of cloud computing. Moreover, various cloud computing models and services are extensively analyzed. Advantages, disadvantages and problems of cloud computing are studied. It is suggested to use edge computing to reduce network delays.

Keywords: Cloud Computing, Models, Cloud Services, Computing Resources, Edge Computing.

1. INTRODUCTION

Despite the increase in the technical capabilities of mobile devices in recent times, problems arise in using them with software applications that require large computing and memory resources. The mentioned problems can be overcome by using new paradigm cloud technologies. Thus, by providing mobile devices with higher computing and memory resources through cloud technologies, limitations in computing and memory resources can be overcome. Cloud technologies provide mobile users with sufficient computing and storage resources by running their issues on a cloud platform [1, 2]. The CC technologies provide clustering and virtualization of computing and memory resources of data processing centers. This technology allows users to access high computing and memory resources, and simultaneously, a user is not interested where these resources are located and configured. The first cloud computing systems, namely Amazon Simple Storage Service and Amazon Elastic Compute Cloud, were created in 2007 by Amazon.

The idea of using computing and memory resources as a service was first proposed in 1960 by John McCartney, a professor at the Massachusetts Institute of Technology. He believed that in the near future, computing resources will be used as utilities (as in the electricity, gas and water supply systems).

2. CLOUD COMPUTING ARCHITECTURE AND MODELS

The concept of CC technology is the creation of computer technology infrastructure and software in a direct network environment. CC technology enables the migration of computing and memory resources and software from enterprise server computers to the cloud, i.e., they are grouped together. Experts believe that large companies using this technology have reduced the financial costs of purchasing software and hardware and electricity by five times.

Noted that this technology allows customers to get the necessary resources in a short time and easily. In general, this technology consists of two main parts: cloud platform and cloud services. The cloud platform is a provider that mainly provides a customer with the required resources (computing and memory, web access, etc.). The cloud platform provides a user with any software and virtual machine, and additional hardware or software are not needed. Through this platform, a service provider builds a virtual machine on cloud servers at the customer request and makes it available for use. The user simply creates the applications he/she needs and runs them in a virtual machine.

The main criteria attracting users in CC technology [5] may include:

- fast provision of demand for computing and memory resources;
- resource scalability in any volume;
- lack of large costs for resource access;
- high availability;
- offering a wide range of Internet services;
- payment for the actual service.

Cloud service platforms refer to the structures implementing the services offered. Here, data processing centers provide access to a part of their resources for a certain amount of money. These services are delivered by cloud platforms, through which different users get access to certain remote data and services. The customer uses the Internet to connect to server and can access any software [6]. The CC conceptual model is shown in Figure 1 [7]:

- Private cloud;
- Community cloud;
- Public cloud;
- Hybrid cloud.

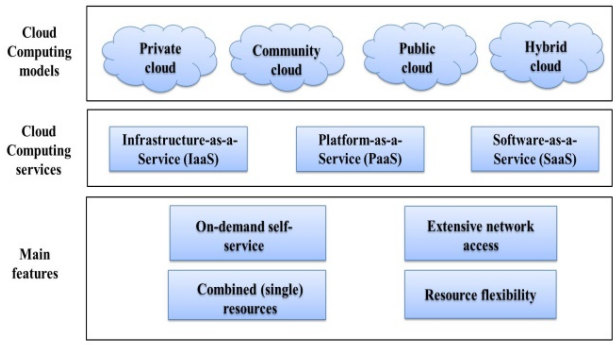

Figure 1. Conceptual model of cloud computing

Private Cloud is created for use by only one company. It can be placed within an organization or in a provider's data processing center. Private cloud provides the highest security and resource control. The key moment is to allocate the cloud infrastructure to one consumer, thus, although virtual resources are shared between internal units of the organization, they are still used by one consumer. Operating costs are more expensive than other cloud models, as the creation, expansion and management of private cloud infrastructure are carried out by the organization. However, data security in private clouds is higher than in other clouds.

Community cloud is a cloud infrastructure that provides cloud services to a specific group (community) of consumers created to solve common problems within an organization. In this model, the information center is owned by one or more organizations, managed by either a third party or only one community organization.

Public cloud provides the creation of virtual infrastructures for a large number of customers. In public clouds, company's data, along with data from other organizations, are stored on a physical server, securely stored, and isolated (with the cloud provider intervention). In fact, in this case, a set of physical resources of the provider's data processing center is divided into several virtual data processing centers used by cloud service customers. Users are not informed on what specific technical devices their data is stored. The main advantages of the public cloud are that the service is cheap and these services are accessible to a wide range of customers. Data security in public clouds is provided by cloud providers.

Hybrid cloud. As the name suggests, hybrid cloud is a combination of public and private cloud infrastructures. Typically, customers host critical applications on their servers that require more secure and reliable control, while the rest of the applications are hosted on servers offered by the cloud provider. In hybrid clouds, part of the service is performed in private clouds created by the organization, whereas another part is performed in the public cloud offered by cloud providers.

3. CLOUD COMPUTING SERVICES

Currently, users take advantage of three main cloud computing services (IaaS, PaaS, SaaS) more widely (Figure 2) [8].

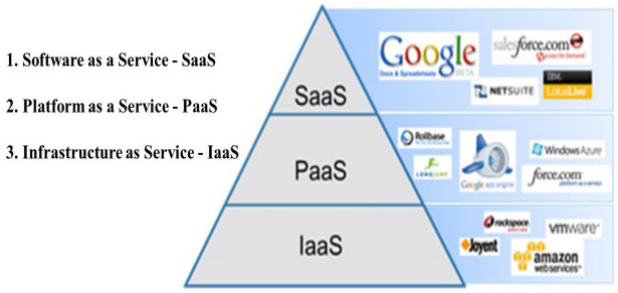

Figure 2. Cloud Computing services

IaaS (Infrastructure-as-a-Service). This service is one of the most common services. It provides the customers with computing resources rented as a virtual infrastructure. The service provides users with computer infrastructure (computing and memory resources). The IaaS service allows the user to use the cloud infrastructure to manage processing, storage, networking and other key computing resources. This service provides users with direct access to computing resources (devices) and allows them to configure these resources and run operating systems and software as they wish.

PaaS (Platform-as-a-Service). This service is also one of the main services and allows the customer to get a full-fledged virtual platform consisting of various tools and services. The customer can customize such a platform according to own needs and perform software testing. This type of service is particularly popular among software providers. The service provides users with a computer platform with the operating system installed. Customers create their own applications, and this service provides a set of operating systems, programming languages, and software tools so that they can use trials in test mode. PaaS allows users to use cloud-based software platforms, operating systems, DBMS (database management systems) and test newly created applications.

SaaS (Software-as-a-Service). This cloud service is also considered to be the most popular at the moment, since almost all users with Internet access use this service. It allows the customer to access any software product via the Internet. For example, Gmail mail service or 1C cloud version. This service provides users with software. Users solve their problems using applications and software applications hosted on cloud computing servers.

The cloud services market is constantly evolving and offering new cloud services to businesses to reduce costs and increase business agility. Recently, the cloud service market has many different services for all segments. Currently, EaaS/XaaS (Everything as-a-Service) service is widely used [9].

Thus, the EaaS service provides the user with all kinds of services, from software and hardware to workflow management, including interaction between

4. ADVANTAGES AND CHALLENGES OF CLOUD COMPUTING

The features distinguishing CC technologies from other information technologies are as follows [10]:

• On-demand self-service. When a user requests a virtual machine to process and store tasks, he/she gets it without

an interaction between users and service providers. Users can set and change the amount of computing and memory resources required as needed, without informing the provider;

• Extensive network access. Customers can access the computing and memory resources of cloud servers anytime and anywhere using a variety of devices (laptops, smartphones, tablets, etc.);

• Resources accessibility. Cloud resources can be accessed by multiple users. The user does not know where the resources are provided by the service provider;

• Combined (single) resources. The shared resources are used by multiple users by combining the provider's computing and memory resources under a single umbrella;

• Resource flexibility (scalability). The customer accesses the resources on demand and able to increase or decrease them.

Advantages of CC technologies [11]:

• user access to information via the Internet;

• solving users' tasks requiring high large computing and memory resources through cloud computing services;

• providing users with unlimited computing and memory tools;

• ensuring fast data processing;

• when documents are stored in cloud, users can use them anytime and anywhere;

• when data is stored in cloud, duplicates are automatically stored on the servers of many data processing centers on different continents.

• constant updating of used programs;

• computing resources are unlimited, scalable and flexible, i.e., resources are provided in that amount as the user needs.

Problems in the effective use of CC services [10]:

• locating cloud servers away from the user;

• Internet overload;

• network delays;

• interruptions in communication channels;

• low bandwidth of communication channels;

• online running software applications (Aps);

• late delivery of information and results to the user;

• deployment of software applications on remote servers;

• use of various connection technologies to connect to the network;

• building continuous communication channels;

• use of computers with different technical capabilities in the network;

• optimal placement of user queries on virtual machines;

• and etc.

Recently, border computing systems (cloudlets, edge, fog computing, etc.) based on the infrastructure of cloud computing systems are used to solve the above-mentioned problems. Edge (peripheral) computing systems are established in the vicinities where data is generated or in mobile devices. Fog computing systems expand the boundaries of cloud computing by directing computing resources to the nearest point where tasks (applications) occur [12].

Fog computing is presented as a paradigm expanding the CC platform. The use of fog technology together with cloud technologies helps reduce the data center loading. Local servers process the data and send only the most important data to the data center. Fog computing is closer to the user, so data processing and transmission time is reduced. This reduces latency in the use of Internet services and improves QoS services.

Therefore, fog computing is more suitable for geographically dispersed enterprises. In fog computing, the data is processed on servers close to the user, which in turn eliminates delays in the Internet network infrastructure. Fog computing aims to increase efficiency by processing data where they are located and to reduce the amount of data transmitted to remote cloud servers [13]. This improves security concerns in the network infrastructure. Many users have processed applications on remote servers, and the results are not transmitted efficiently. Fog computing provides faster data processing and prevent network overload. Fog counting systems are very suitable for control systems requiring direct data processing, analytical analysis and rapid decision-making at the place where the data is generated.

5. CONCLUSIONS

The article shows the use of cloud technologies to enable the use of software applications that require large computing and memory resources on mobile devices. The advantages, disadvantages and problems of CC were analyzed. Features distinguishing cloud-computing technologies from other information technologies were analyzed. The problems arising in the efficient use of cloud computing services were analyzed and proposals were made for their solution. It was proposed to use edge-computing systems to eliminate network delays in CC.

REFERENCES

[1] G. Reese, "Cloud Application Architectures", International Journal of Information Management, Vol. 30, Issue 5, p. 208, 2010.

[2] P. Srivastava, R. Khan, "A Review Paper on Cloud Computing", International Journals of Advanced Research in Computer Science and Software Engineering, Vol. 8, Issue 6, pp. 17-20, 2018.

[3] D. Sood, H. Kour, S. Kumar, "Survey of Computing Technologies: Distributed, Utility, Cluster, Grid and Cloud Computing", Journal of Network Communications and Emerging Technologies (JNCET), Vol. 6, No. 5, pp. 99-102, 2016.

[4] M.N. Birje, P.S. Challagidad, R.H. Goudar, M.T. Tapale, "Cloud Computing Review: Concepts, Technology, Challenges and Security", Int. J. Cloud Computing, Vol. 6, No. 1, pp. 32-57, 2017.

[5] M. Armbrust, A. Fox, R. Griffith, A.D. Josep, "Above the Clouds: A Berkeley View of Cloud Computing", www.eecs.berkeley.edu/Pubs/TechRpts/2009/EECS-2009-28.html.

[6] K.G. Bakde, B.M. Patil, "Survey of Techniques and Challenges for Load Balancing in Public Cloud", International Journal of Technical Research and Applications, Vol. 4, No. 2, pp. 279-290, 2016.

[7] T. Diaby, B.B. Rad, "Cloud Computing: A review of the Concepts and Deployment Models", I.J. Information Technology and Computer Science, Vol. 6, pp. 50-58, 2017.
[8] S. Khurana, A.G. Verma, "Comparison of Cloud Computing Service Models: SaaS, PaaS, IaaS", International Journal of Electronics & Communication Technology, Vol. 4, No. 3, pp. 29-32, 2013.
[9] K. Kaur, "A Review of Cloud Computing Service Models", International Journal of Computer Applications, Vol. 140, No. 7, pp. 15-18, 2016.
[10] M.F. Mushtaq, U. Akram, I. Khan, S.N. Khan, A. Shahzad, A. Ullah, "Cloud Computing Environment and Security Challenges: A Review" International Journal of Advanced Computer Science and Application, Vol. 8, No. 10, pp. 183-195, 2017.
[11] T. Diaby, B.B. Rad, "Cloud Computing: A review of the Concepts and Deployment Models", I.J. Information Technology and Computer Science, No. 6, pp. 50-58, 2017.
[12] D. Dalan, "An Overview of Edge Computing", International Journal of Engineering Research & Technology, Vol. 7, Issue 05, pp. 1-4, 2017.
[13] K. Shenoy, P. CCokare, U. Pai, "Fog Computing Future of Cloud Computing", International Journal of Science and Research, Vol. 4, No. 6, pp. 55-56, 2015.

BIOGRAPHIES

Rashid G. Alakbarov was born in Masis, Armenia on February 2, 1953. He graduated from Automation and Computer Engineering Faculty, Azerbaijan Polytechnic University, Baku, Azerbaijan in 1975. In 2006, he defended his dissertation on the topic of Development of models and algorithms for the synthesis of computing environment based on distributed computer networks and received the Ph.D. degree in the field of Analysis, Management and Data Processing. He is Head of Department at Institute of Information Technology, Azerbaijan National Academy of Sciences, Baku, Azerbaijan since 2002. Since 2010, he has been leading the development of "AzScienceNet" infrastructure. In 2011, he was appointed as the Deputy Director of the same institute. He is a member of the International Electrical and Electronic Engineers. His research interests include various areas in cloud computing, data processing, computer networks, virtual computing, particularly in the area of distributed computing.

Ogtay R. Alakbarov was born in Sumgait, Azerbaijan on October 24, 1988. He graduated from Chemistry Faculty, Baku State University, Baku, Azerbaijan in 2006. He received his Master's degree in Information Technology Management from Qafqaz University, Baku, Azerbaijan. He graduated in the field of System Analysis from Institute of Information Technology, Azerbaijan National Academy of Sciences, Baku, Azerbaijan, in 2022. His research interests include various areas in cloud computing, data processing, computer networks, virtual computing, particularly in the area of cloud technology.

The 18th International Conference on
"Technical and Physical Problems of Engineering"
30 October 2022
International Organization of IOTPE

ICTPE Conference
www.iotpe.com
ictpe@iotpe.com
ictpe0@gmail.com

ICTPE-2022 Number 19 Code 06RES01 Pages 91-98

DEVELOPMENT OF ECOAGROROBOT POWERED BY SOLAR PANELS

Z.A. Hasanov [1] T.D. Jafarov [1] S.A. Khanahmadova [2] S.K. Gasimov [3]

1. Azerbaijan State Oil and Industry University, Baku, Azerbaijan, zakir.hasanov@asoiu.edu.az, samira1009@mail.ru
2. State Oil Company of Azerbaijan (SOCAR), Baku, Azerbaijan, tahircafarov50@gmail.ru
3. Sumgait Technological Park (STP), Baku, Azerbaijan, sahibgasimov@gmail.com

Abstract- A wheeled ecoacrorobot powered by photoelectric panels and carrying out agricultural work has been proposed. The linear motion and maneuverability of ecoacrorobot is achieved by adjusting and reversing the speed of the two leading wheels. The other two wheels are of the "royal" (passive) type and do not generate traction. An algorithm for maneuvering and bypassing of obstacles of ecoagrorobot was developed, calculation of parameters of solar panels and selection of other devices were introduced.

Keywords: Wheeled Robot, Solar Panel, Smart Village, Frequency Inverter.

1. INTRODUCTION

In the scientific works dedicated to the wheeled robots [4-13] and their precise movement trajectories, stability, dynamic modes were studied in detail. These robots are fed from an autonomous energy source. The renewable energy sources should be used for agricultural robots to use energy sources more economically and efficiently. For this purpose, this article focuses on the development of an ecoagrorobot (EAR) that fed by solar panels and performs agricultural works within the framework of the "smart village" project in Karabakh. Functional scheme of the proposed EAR shown in Figure 1.

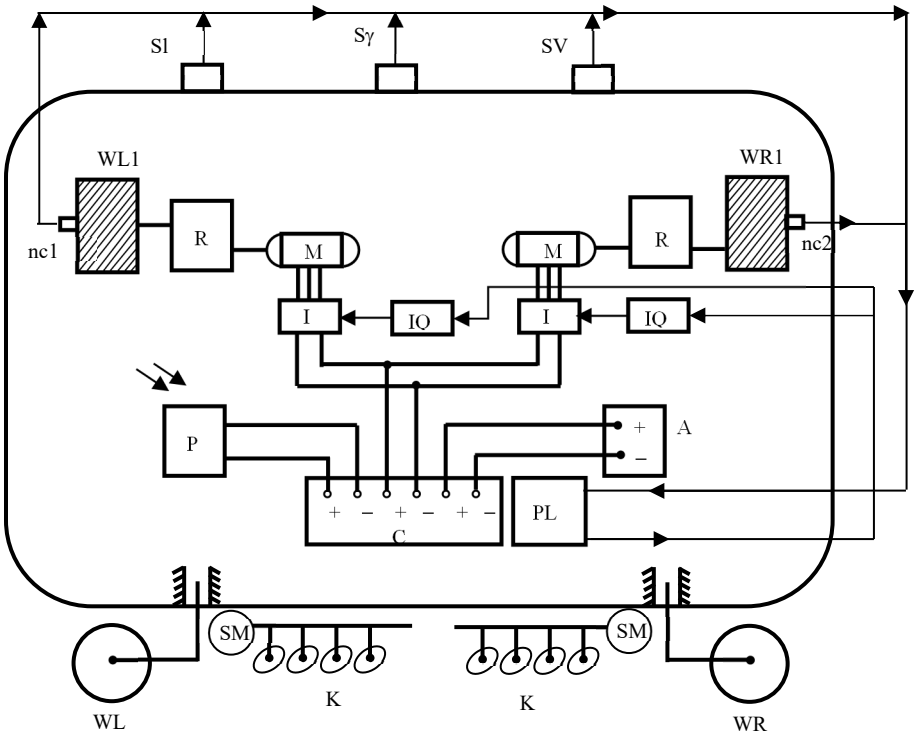

Figure 1. Functional diagram of the proposed EAR

In Figure 1, WL1 and WR1 are leading wheels, using which the robot's speed can be changed and its movement direction can be reversed, WL2 and WR2 are "royal" (passive) type wheels, M1 and M2 are alternating current electric motors, R1 and R2 are reduction gears, I1 and I2 are Frequency Inverters which changes the value and frequency of direct current, IQ1 and IQ2 are control panels for inverters, PV is solar panels, AK is accumulators, C is a controller, K is an agricultural mechanism for cultivation, SML and SMR are servomotors that performs

the movement of the agricultural mechanism along the width and length of the EAR, nd and nc2 are the encoders that determine the angular velocity of the wheels, and sγ, sv and sl are the sensors of the road, the course, and the linear speed of the EAR, respectively. The PLC is a logic controller that manages the work of EAR on in accordance with the developed program.

2. THE WORKING PRINCIPLE OF EAR

The electricity generated by the PV panels not only drives the EAR but also recharges the batteries. The charging of the AK, power supply from PV to AK, or to the consumers (I1, I2) is controlled by the controller (C). Operating of EAR starts when the solar radiation intensity is high (12:00-17:00). Until 12:00 and after 17:00 the power from PV charges only the AK.

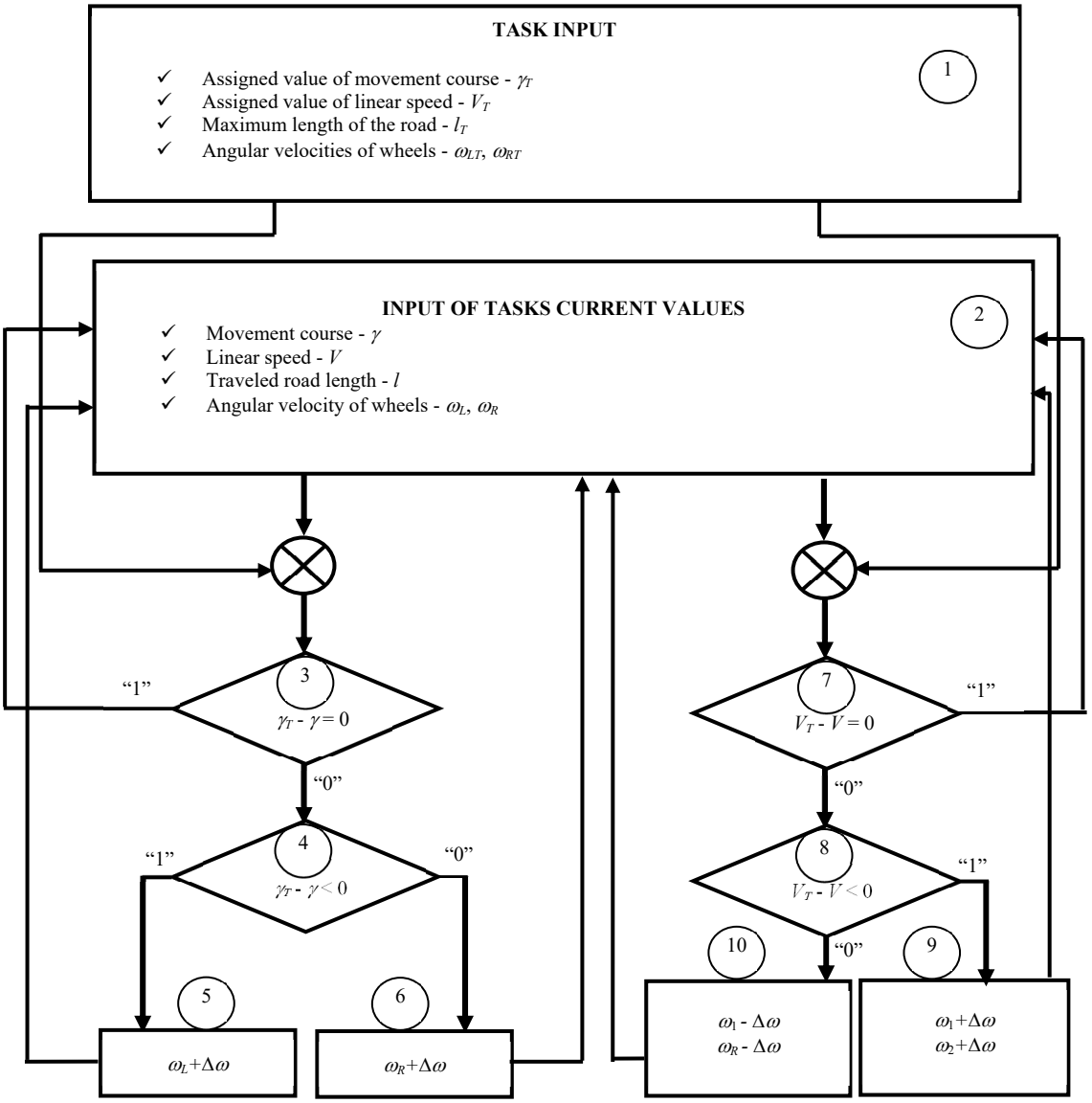

Figure 2. Block diagram of movement program of EAR according to course

Before starting operation of EAR the following parameters, which determine the operating mode of the EAR, are set to PLC:

- Assigned value of movement course of EAR - γ_T;
- Assigned value of linear speed of EAR's platform according to the technological process - V_T;
- The maximum length of the cultivated road when moving in one direction - L_T;
- Assigned values of angular velocities of *WL*1 and *WR*1 wheels - ω_{LT}, ω_{LT}.

The current values of these parameters are measured by sensors $s\gamma$, sv, sl, nc1 and nc2 and entered into the PLC. The algorithm shown in Figure 2 is implemented during movement of the EAR on the course. The 1st block is input of task values γ_T, V_T, L_T, ω_{LT}, ω_{RT} to the PLC, and the 2nd block is input of the current values of the γ, V, L, ω_L and ω_R parameters from the sensors to PLC.

The 3rd block checks the course of EAR $(\gamma_T - \gamma)$. If the course rate of EAR is equal to the set value, i.e., $\gamma_T - \gamma = 0$, then checking process continues. Otherwise,

the direction of the course is determined. The 4th block increases or decreases the angular velocities of the left (WL1) or right (WR1) wheels, depending on whether the EAR turns to the left or to the right. The blocks 5 and 6 continue these operations until they the set value of the course is reached. After the EAR moves along the assigned course, its linear speed is checked (block 7). If the current value of the linear speed (V) is less than the set value (block 8), then the angular velocities of the left and right wheels are increased (block 9). Otherwise, the angular velocities of the left and right wheels are reduced (block 10). This check is continued until the condition $V_T = V$ is satisfied (block 7).

After crossing the L_T path EAR stops. Then *SM*1 and *SM*2 servo motors start moving the cultivating devices forward and outward from the center. The purpose of these operation is that the cultivation works can be carried out on far side of the strip when EAR moves back. In this case, the previously cultivated soil layer is not damaged by EAR wheels. Moving on to opposite direction the EAR approaches to the next lane with maneuvering mode after reaching the initial position. EAR resumes its work by switching to the program "movement course in new lane".

It should be noted that the steering control of the EAR, both during move on with determined course and in maneuver mode, in contrast to the steering control mode of the wheels [1], is performed only by changing the angular velocities of the wheels WL1 and WR1. The wheels WL1 and WR1 are rotated by M1 and M2 engines independently from each other around their axes referring to EAR platform.

Let's determine varying of the steering angle of EAR platform referring to the difference of angular velocity of the wheels WL1 and WR1. Figure 3 illustrates the angular velocities $(\omega_{L1},\ \omega_{R1})$ of the WL1 and WR1 wheels in the fixed OXY coordinate system referring to the EAR platform, the linear velocities of the wheel axes referring to the ground $(V_{L1},\ V_{R1})$ and the angular velocity of platform (ω) referring to the instantaneous center of speed (O1).

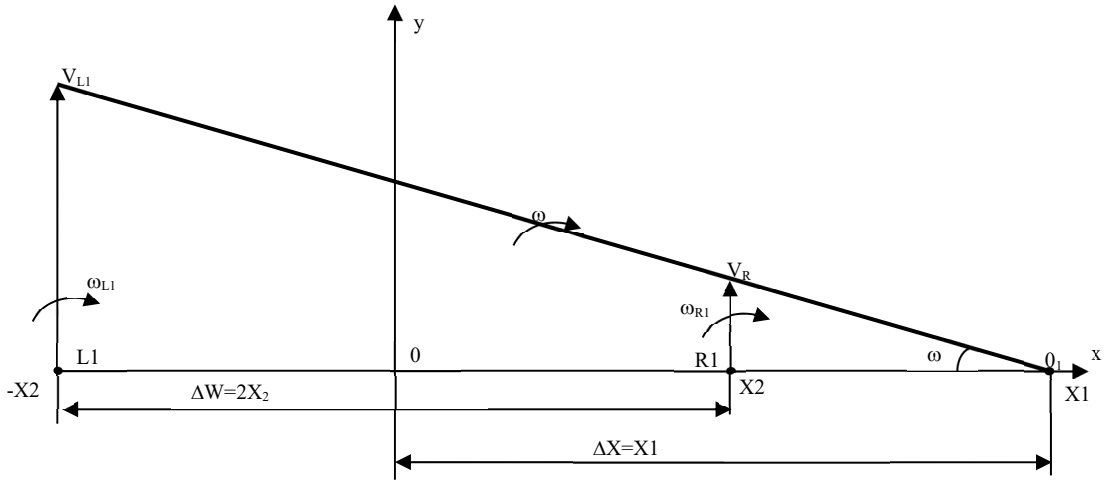

Figure 3. Angular $(\omega_{L1}, \omega_{R1}, \omega)$ and linear velocities (V_{L1}, V_{R1}) in the fixed OXY coordinate system referring to the EAR platform

The coordinates of L1, R1 and O_1 as follows: $\mathrm{L1}(-X2;0)$, $\mathrm{R1}(X2;0)$, $\mathrm{R1}(X2;0)$, $\mathrm{O_1}(X1;0)$. The distance between rotational axes of wheels is $\Delta W = L1 \times R1 = X2 - (-X2) = 2X2$.

The distance between coordinate start and instantaneous center of velocity [1, 4]: $\Delta X = \mathrm{O\text{-}O1} = X1$. The following expressions can be written for the specified parameters:

$$\begin{aligned} V_{L1} &= \omega(\Delta X + 0.5\Delta W) \\ V_{R1} &= \omega(\Delta X - 0.5\Delta W) \end{aligned} \quad (1)$$

If the radius of the wheels WL1 and WR1 are denoted by *r,* then we can write for velocities V_{L1} and V_{R1},

$$\begin{aligned} V_{L1} &= \omega_{L1} r \\ V_{R1} &= \omega_{R1} r \end{aligned} \quad (2)$$

Since the left side of Equations (1) and (2) are equal:

$$\begin{aligned} \omega_{L1} r &= \Delta X + 0.5\Delta W \\ \omega_{R1} r &= \Delta X - 0.5\Delta W \end{aligned} \quad (3)$$

We divide these expressions side to side:

$$\frac{\omega_{L1}}{\omega_{R1}} = \frac{\Delta X + 0.5\Delta W}{\Delta X - 0.5\Delta W} \quad (4)$$

where, $K_\omega = \dfrac{\omega_{L1}}{\omega_{R1}}$ if we accept this substitution:

$$K_\omega = \frac{\Delta X + 0.5\Delta W}{\Delta X - 0.5\Delta W} \quad (5)$$

or;

$$\Delta X = 0.5 \times \Delta W \frac{K_\omega + 1}{K_\omega - 1} \quad (6)$$

we get this expression and $\Delta X - K_\omega$ characteristic is shown in Figure 4.

The analysis of this characteristic shows that when $K_\omega = 1 \times \Delta X$ approaches to infinity [2, 3]. This means that the wheels WL1 and WR1 rotate in the same direction at the same angular velocities, the EAR moves towards straight line and the instantaneous speeds center is at infinity.

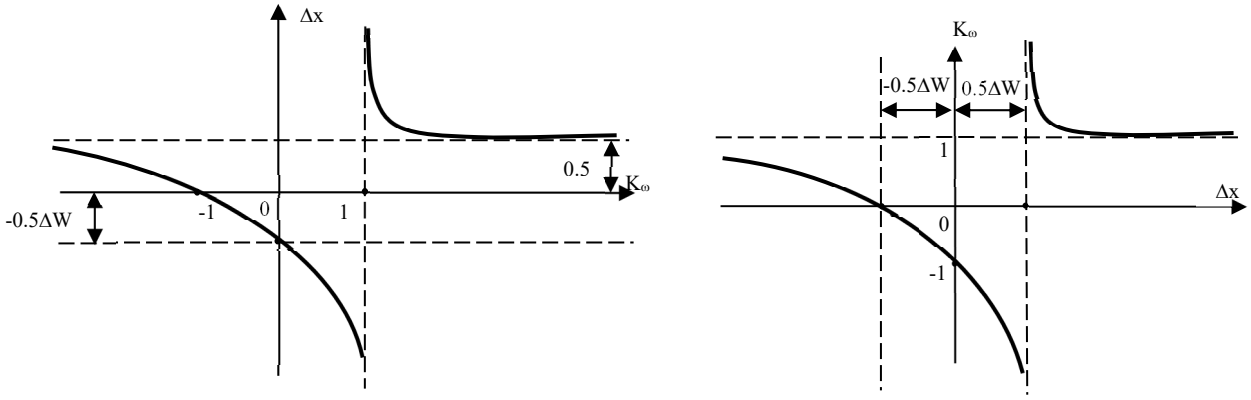

Figure 4. $\Delta X - K_\omega$ and $K_\omega - \Delta X$ characteristics

In Figure 4, $K_\omega = -1$, $\Delta X = 0$. That is, if ω_{L1} rotates in the forward direction, ω_{R1} rotates in the reverse direction, and the absolute values of the angular velocities of the wheels are equal to each other, then the EAR will rotate around the midpoint "O" of an axle connecting the centers of rotation of the wheels. This is used in maneuver mode when EAR moves to a new lane. Diagram of EAR's transition to a new lane illustrated in Figure 5. The figure shows the positions "a", "b", "c" and "d" of the EAR during the transition from the first lane to second lane

At position "a", EAR moves back to a distance of $0.5\Delta W$ from the boundary line of the cultivated lane (S1–S1), then the wheels WL1 and WR1 rotate in opposite directions to each other at equal speed $K_\omega = -1$ turns 90° clockwise around the point "O".

At position "b", already turned 90° EAR moves at a certain speed V in a straight line to the right along the boundary line (S1–S1). The EAR crosses the lane boundary line (S2 – S2) and stops by moving point "O" to a distance of $0.5\Delta W$ from that boundary line.

After stopping EAR in the position "c" at a distance of $0.5\Delta W$ from the boundary line (S2–S2) the wheels WL1 and WR1 rotate at the same speed in opposite directions to each other and rotate 90° anticlockwise around the point "O".

At position "d", already turned 90° EAR moves at a certain speed V in a straight line along the boundary line (S2–S2). When the EAR reaches the border line (S1–S1) activates the agricultural mechanism (K) which carrying out the cultivation works and starts cultivating in the second lane. The EAR continues moving, avoiding the obstacles encountered while moving on the defined course.

Figure 6 is a graphical description for determining the parameters of the EAR performing this process. In the figure, there is an element of M as obstacle that has entered the lane as far as Δl distance.

The parameters of the obstacle element are determined by a camera installed in the EAR. Let determine the coordinates of EAR's instantaneous turn centre (O1) and the turning radius (R) of EAR around that point to bypass the obstacle element. For this purpose, the point WL1 is connected to the point M1 by a straight line. From point M1 straight line is drawn at an angle equal to the angle M1WL1O (α_1). The point O1 where this straight line intersects the OX axis will be the instantaneous turning center, and the straight line M1O1 will be the turning radius (R). Based on the distances $M1WL1 = l_2$ and Δl,

$\sin\alpha_2 = \dfrac{\Delta l}{l_2}$ and $\alpha_2 = \arcsin\dfrac{\Delta l}{l_2}$.

$$R = \frac{l_2}{2\cos\alpha_1} = \frac{l_2}{2\sin\alpha_2} \tag{7}$$

parameters are calculated. Since the radius R is:

$$R = \frac{\Delta W}{2} + \Delta X \tag{8}$$

then, according to (7) and (8):

$$\frac{\Delta W}{2} + \Delta X = \frac{l_2}{2\sin\alpha_2}$$
$$\Delta X = \frac{l_2}{2\sin\alpha_2} - \frac{\Delta W}{2} \tag{9}$$

After determining the coordinates of the instantaneous turning center, according to Equation (5) is calculated.

$$K_\omega = \frac{\Delta X + 0.5\Delta W}{\Delta X - 0.5\Delta W} \tag{10}$$

Taking the values V_{L1} or $\omega_{L1} = V_{L1}/r$ from Equation (11)

$$K_\omega = \frac{\omega_{L1}}{\omega_{R1}} = \frac{V_{L1}}{V_{R1}} \tag{11}$$

$V_{R1} = \dfrac{V_{L1}}{K_\omega}$ or $\omega_{R1} = \dfrac{\omega_{L1}}{K_\omega}$ is defined.

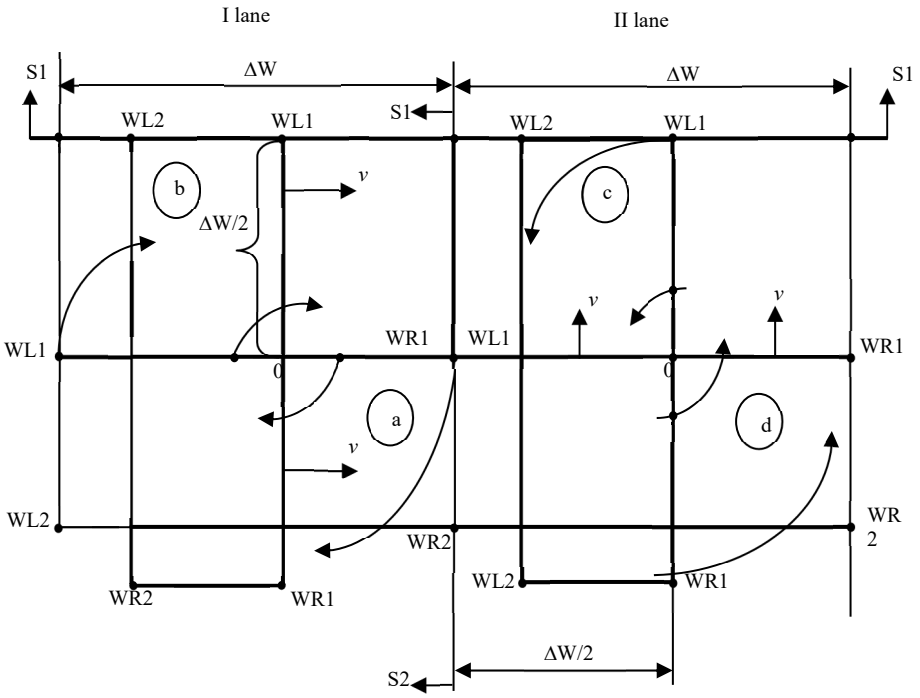

Figure 5. Diagram of EAR moving to new lane

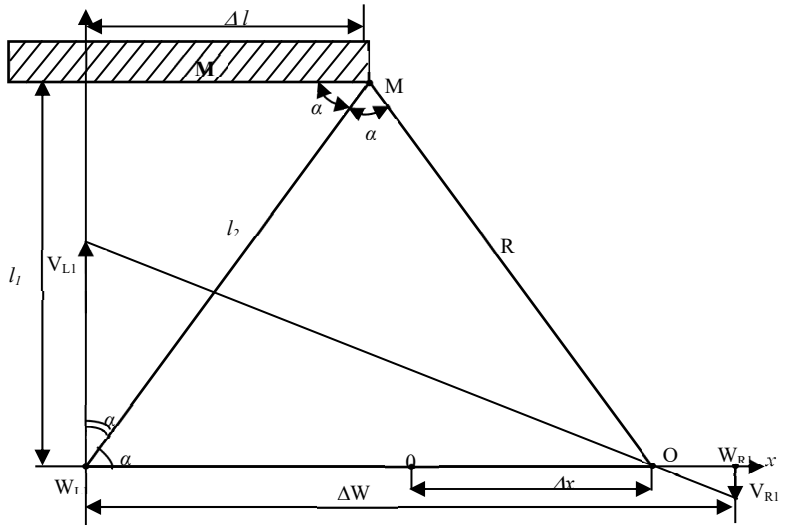

Figure 6. Graphical illustration of the parameters of EAR to continue its defined course, bypassing the obstacle

• Example 1: Determine the equipment and parameters of the EAR to carrying out cultivation work in the area with dimensions (250×100) m. The dimensions of the EAR platform are (2×6) m (Figure 7). First, we define the energy needed to cultivate the area. Agricultural machines that cultivate one hectare (ha) area and run-on diesel fuel consume 17 liters of diesel fuel on soil with a specific mechanical resistance of about 40 kPa [2]. Considering that the specific combustion heat of one kg of diesel fuel is 10031 kcal and its specific weight is 0.8 kg /dm^3, the specific combustion heat of 17 liters of diesel fuel is 17×0.8×10031 = 136421.6 kcal.

Taking into account that 1 kWh = 860 kcal, then 136421.6 kcal = 158 kWh. Assuming the efficiency of diesel engines η=0.4, then 158 kWh × 0.4 = 63.2 kWh of energy is required for the movement and cultivation of the unit per one hectare. Part of this energy ≈80% will be spent on the unloaded movement of the traction unit, and part ≈20% will be spent to the mechanism performing cultivation works. Thus, the EAR which cultivates one hectare area will consume 63.2 kWh × 0.2 = 12.64 kWh energy. Since the given area is (250×100) m = 25000 m^2 = 2.5 ha, 2.5×12.64=31.6 kWh of energy is required for the cultivation of that area.

Dividing this area into 6 meters wide strips (according to the dimensions of the EAR) and 250 meters long, we get 17 strips. Energy to be used for cultivation in each strip becomes:

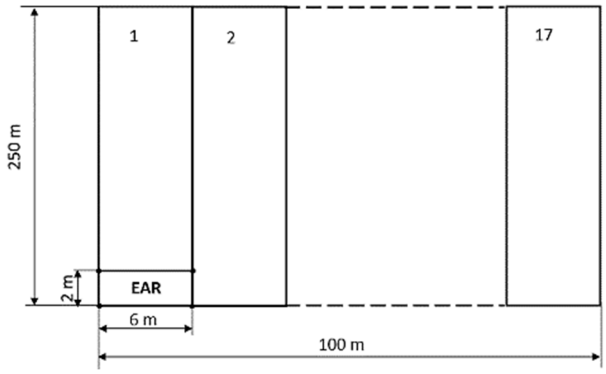

Figure 7. Dimensions of EAR platform and cultivated area

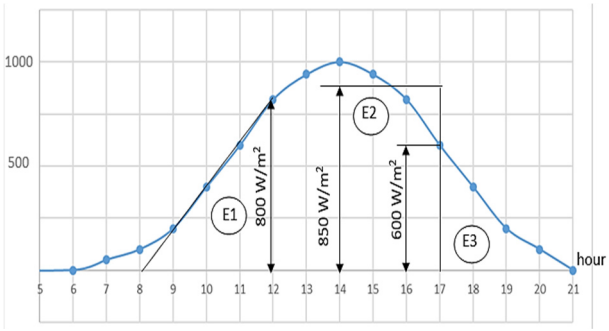

Figure 8. Intraday graph of average solar radiation intensity in July for Karabakh and Aran zones of Azerbaijan

$$E_z = \frac{31.6}{17} = 1.86 \text{ kWh} \qquad (12)$$

Figure 8 shows the average daily intensity of solar radiation in July for the Karabakh and Aran zones of Azerbaijan [1]. According to this schedule, solar energy falling per square meter from 8:00 to 12:00 is, $E_1 = \frac{800(12-8)}{2} = 1600$ Wh/m^2.

Solar energy falling per square meter from 12:00 to 17:00 is, $E_z = 850(17-12) = 4250$ Wh/m^2.

Solar energy falling per square meter from 17:00 to 20:00 is, $E_z = \frac{600(20-17)}{2} = 900$ Wh/m^2.

Finally, the average value of falling solar energy per square meter for July during the day (8:00-20:00) becomes:

$E = E_1 + E_2 + E_3 = 1600 + 4250 + 900 = 6750$ Wh/m^2.

Since the area of the EAR platform is S=2×6=12 m^2, the area which can receive solar energy during the day becomes $E_p = E \times S = 6750 \times 12 = 81000$ Wh or 81 kWh.

The 6 number of "Sila Solar" solar panels can be placed on the EAR platform. The parameters of this panel are shown in the Table 1 and the wiring diagram is shown in Figure 9.

Table 1. Parameters of PV panels

Type of panel	Capacity, W	Dimensions W×L×D mm	Weight kg	Efficiency %
Sila Solar	460	2094×1038×35	2.5	22.5

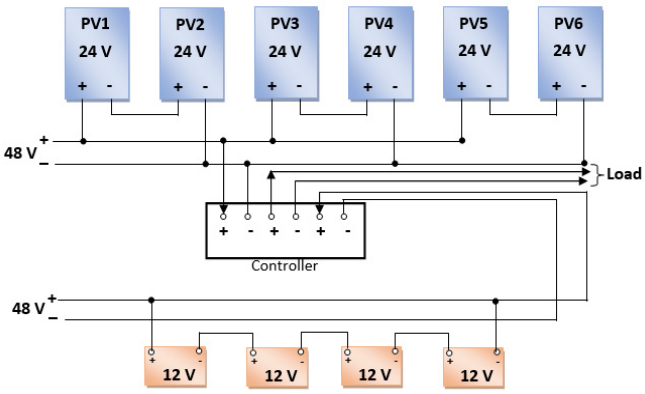

Figure 9. Wiring diagram of 6 numbers "Sila Solar" type solar panels and accumulators

According to this table the area of 6 *PV* panels is, S_g=6×2.094×1.038=13 m^2. Since the area of all *PV* panels is, S_g=13m^2 the solar energy that EAR panels can receive during the day becomes:

$E_p = E \times S_g = 6750 \times 13 = 87750$ Wh or ≈ 88 kWh

Since the efficiency of selected solar panels is 0.225 the electricity generated from solar energy during the day will be:

$E_e = E_g \times 0.225 = 88 \times 0.225 = 19.8$ kWh ≈ 20 kWh

According to (12), only E_a=1.86 kWh of energy is consumed for cultivation in each lane. If we accept the efficiency of EAR η=0.5, then, $E_{EAR}=E_Z/\eta$=3.72 kWh of energy will be required for EAR cultivating in one lane. So, the ratio of electrical energy per day (E_e≈20 kWh) generated from solar panel to the electrical energy consumed EAR in one lane is: $\frac{E_l}{E_{EAR}} = \frac{20}{3.72} \approx 5.4$.

This means that EAR can cultivate 5 lanes a day consuming solar energy. While EAR moves along the lane, it will be cultivated at about 3 m in front of the lane width, and in the opposite direction at about 3 m on the other side of the lane width. Thus, EAR will cross the road in 5 lanes, $L = 5 \times 2 \times 250 = 2500$ m.

Assuming that the cultivation time during the day is t=5 hours (12.00-17.00), the linear speed of the EAR will be, $V = \frac{L}{t} = \frac{2500}{5} = 500 \frac{\text{m}}{\text{hour}} = 0.014 \frac{\text{m}}{\text{sec}}$.

So, EAR will complete the cultivation work in 17/5≈4 days in a field dimensioning (100×250) m with an area of 2.5 hectares. We choose 4 number of Volta GST 12/200 SOLAR batteries to accumulate part of the electricity generated by PVs. These batteries will be connected in series and will have parameters 48 V, 200 Ampere · hour (Figure 9). The energy that batteries can store will be, $E_A = V \times Ah = 48 \times 200 = 9600$ Wh=9.6 kWh.

For normal operation of the battery, 50% of the energy stored in it (9.6×0.5=4.8 kWh) can be used. Therefore, E_t=4.8 kWh of energy can be accumulated to the selected batteries per day. Assuming that the electricity produced per day is E_e=20 kWh and the cultivation time for one lane is extended to 5 hours, the capacity of the electric motor

that drives the EAR will be, $P_m = k_m \times \frac{20}{T} = 1.5 \times \frac{20}{T} = 6$ kW, where k_m=1.5 is the coefficient foreseen for rapid maneuvering modes. In this case, inverters with a power greater than 3 kW must be selected for each motor.

• Example 2: Determine the linear and angular velocities of the WL1 and WR1 wheels to overcome the obstruction encountered during the linear motion of the EAR. The radius of the wheels to be accepted as r=0.25 m.

Let's perform the calculation according to the parameters noted in Figure 6 with the values shown below: l_1= 3 m; Δl = 2 m; ΔW=6 m.

Let's define the parameters l_2 and $\sin\alpha_2$ using the following expressions:

$$l_2 = \sqrt{l_1^2 + \Delta l^2} = \sqrt{3^2 + 2^2} = 3.61 \text{ m}$$

$$\sin\alpha_2 = \frac{\Delta l}{l_2} = \frac{2}{3.61} = 0.554$$

Let's define turning radius of EAR platform according to (7): $R = \frac{l_2}{2\sin\alpha_2} = \frac{3.61}{2 \times 0.554} = 3.258$ m.

Let's define the coordinates of instantaneous turning center according to (9):

$$\Delta X = \frac{l_2}{2\sin\alpha_2} - \frac{\Delta W}{2} = 3.258 - 3 = 0.258 \text{ m}.$$

According to (10) the ratio of the angular velocities of the wheels WL1 and WR1 is,

$$K_\omega = \frac{\Delta X + 0.5\Delta W}{\Delta X - 0.5\Delta W} = \frac{0.258 + 3}{0.258 - 3} = -1.188$$

Using Equation (11), $K_\omega = \frac{\omega_{L1}}{\omega_{R1}} = \frac{V_{L1}}{V_{R1}}$, and accepting the value of the linear velocity of one of the wheels, e.g., $V_{L1} = 1.5\frac{\text{m}}{\text{sec}} = 5.4\frac{\text{km}}{\text{hour}}$, then will be, $V_{R1} = \frac{V_{L1}}{K_\omega} = \frac{1.5}{-1.188} = -1.26\frac{m}{\text{sec}}$.

According to Equation (2):

$$\left.\begin{aligned} V_{L1} &= \omega_{L1} \times r \\ V_{R1} &= \omega_{R1} \times r \end{aligned}\right\}$$

From this, $\omega_{L1} = \frac{V_{L1}}{r} = \frac{1.5}{0.25} = 6\frac{1}{\text{sec}} = 57.3\frac{\text{per}}{\text{sec}}$;

$$\omega_{R1} = \frac{V_{R1}}{r} = \frac{-1.26}{0.25} = -5.04\frac{1}{\text{min}} = -48.2\frac{\text{per}}{\text{sec}}.$$

Thus, $V_{L1} = 1.5\frac{\text{m}}{\text{sec}}$; $\omega_{L1} = 6\frac{1}{\text{sec}}$; $V_{R1} = -1.26\frac{\text{m}}{\text{sec}}$; $\omega_{R1} = -5.04\frac{1}{\text{sec}}$.

3. CONCLUSION

1. An eco-agrorobot was proposed to perform ecologically clean cultivation works fed from solar panels. This eco-agrorobot performs agricultural work using the energy source more economically and efficiently.

2. It was shown that the EAR maneuvering process is performed by changing and reversing the speeds of the two wheels. Because of the maneuvering process is performed in simple way here, the reliability of the mechanical part of the EAR increases.

3. To perform the maneuvering process of EAR the calculation of the parameters was given. A parameter calculation was shown to bypass the obstacle encountered by the EAR also. Here, the speeds and directions of the wheels were determined depending on the dimensions of the obstacle.

4. The relationship between the capacity of energy-carrying facilities and the cultivated field has been identified. The main conditions that determine these dependencies has been indicated.

REFERENCES

[1] A.M. Shelemetyev, Y.V. Shelemetyeva, A.V. Smirnov, "Development of a Wheeled Vehicle Control System Based on the Difference in the Speeds of Rotation of the Control Wheels", Bulletin of the Chuvash University, pp. 259-312, Chuvashia, Russia, 2016.

[2] State Land and Mapping Committee, "National Atlas of Azerbaijan", pp. 132, Baku, Azerbaijan, 2014.

[3] E. Kayacana, E. Kayacanb, H. Ramona, W. Saeysa, "Towards Agrobots: Identification of the Yaw Dynamics and Trajectory Tracking of an Autonomous Tractor", pp. 1-17, 15 April 2021, https://arxiv.org/pdf/2104.06833.pdf.

[4] H. Fang, L. Dou, J. Chen, R. Lenain, B. Thuilot, P. Martinet, "Robust Anti-Sliding Control of Autonomous Vehicles in Presence of Lateral Disturbances", Control Engineering Practice, Vol. 19, pp. 468-478, May 2011.

[5] J. Backman, T. Oksanen, A. Visala, "Navigation System for Agricultural Machines: Nonlinear Model Predictive Path Tracking", Computers and Electronics in Agriculture, Vol. 82, pp. 32-43, 2012.

[6] D. Piyabongkarn, R. Rajamani, J.A. Grogg, J.Y. Lew, "Development and Experimental Evaluation of a Slip Angle Estimator for Vehicle Stability Control", IEEE Transactions on Control Systems Technology, Vol. 17, pp. 78-88, 2009.

[7] E. Kayacan, E. Kayacan, H. Ramon, W. Saeys, "Modeling and Identification of the Yaw Dynamics of an Autonomous Tractor", The 9th Asian Control Conference (ASCC), pp. 1-6, 2013.

[8] E. Kayacan, E. Kayacan, H. Ramon, W. Saeys, "Towards Agrobots: Identification of the Yaw Dynamics and Trajectory Tracking of an Autonomous Tractor", Computers and Electronics in Agriculture, Vol. 115, pp. 78-87, April 2015.

[9] A. Khalaji, S. Moosavian, "Robust Adaptive Controller for a Tractor-Trailer Mobile Robot", Mechatronics, IEEE/ASME Transactions on, Vol. 19, No. 3, pp. 943-953, June 2014.

[10] M. Michalek, M. Kielczewski, "The Concept of Passive Control Assistance for Docking Maneuvers with n-Trailer Vehicles", Mechatronics, IEEE/ASME Transactions on, Vol. 20, No. 5, pp. 2075-2084, Moscow, Russia, October 2015.

[11] J.B. Derrick, D.M. Bevly, "Adaptive Steering Control of a Farm Tractor with Varying Yaw Rate Properties", Journal of Field Robotics, Vol. 26, No. 6-7, pp. 519-536, 2009.
[12] M. Karkee, B.L. Steward, "Study of the Open and Closed Loop Characteristics of a Tractor and a Single Axle Towed Implement System", Journal of Terramechanics, Vol. 47, No. 6, pp. 379-393, 2010.
[13] H. Li, W. Yan, "Model Predictive Stabilization of Constrained Underactuated Autonomous Underwater Vehicles with Guaranteed Feasibility and Stability", IEEE/ASME Transactions on Mechatronics, Vol. 22, No. 3, pp. 1185-1194, June 2017.

BIOGRAPHIES

Zakir Alikram Hasanov was born in Haji-Qabul, Azerbaijan in 15 October 1948. He received a Master degree in the field of electrical signal and automation of industrial installations" in 1971. He entered the postgraduate course of Department of Electric Machines in 1974, and was Candidate of Technical Sciences since 1984. He defended dissertation on the topic "Asynchronous electric drive of the crane mechanism controlled by the frequency of the resistance of the rotary circuit". He was the Associate Professor in Department of Electromechanics, Azerbaijan State University of Oil and Industry, Baku, Azerbaijan since 1986. His research interests are control of asynchronous electric drives, and use of alternative energy sources. He is the author of 85 scientific articles, 16 publications, 4 patents and earned 3 awards.

Tahir Damir Jafarov was born in Samux, Azerbaijan, in 10 May 1950. He received the Master degree education in the field of electrical engineering in 1972. He was the Head of Mingachevir Regional Department of State Energy Control (1980), Director of Mingachevir electric grid (1989), and Head of Energy Department of Ministry of Industry and Energy (2006) all in Azerbaijan. He worked as a chief power engineer at State Agency for Alternative and Renewable Energy Sources, Baku, Azerbaijan since 2013, after retiring. He worked as a technical director for development of drafts of new laws and codes with the participation of European experts on the formation of the country's energy policy and the implementation of reforms in this area in accordance with European directives. He is technical specialist at State Oil Company of Azerbaijan (SOCAR). His current research interests are the role of pumped storage power plants in the integration of renewable energy sources into the energy system, and electric power industry on the verge of existence and non-existence, He also published the book of "Electric Power Industry - Reforms and Intellectual Market", and author of the articles on improving the efficiency of energy system, introduction of modern technologies in energy sector, safety of SES, use of renewable energy sources, and scenario of reforms in energy sector. He performed the lectures on energy issues to teaching and student staff of Azerbaijan State Oil and Industry University, Baku, Azerbaijan. He is author of 1 patent and 3 awards.

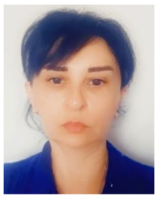

Samira Alkhadi Khanahmedova was born in Baku, Azerbaijan on 9 October, 1967. She received Master degree in electrical engineering in 1990. He hired as a senior laboratory assistant at Department of Electrical Equipment and Automation of Industrial Installations in 2004. She was a dissertation student at Azerbaijan State Oil and Industry University, Baku, Azerbaijan in 2007-2012. She defended her Ph.D. dissertation in the field of "Design and research of electromechanical elements on board autonomy moving objects" in 2014. She has worked as an assistant at Department of Electrical Equipment and Automation of Industrial Installations since 2015. She worked as an Associate Professor at Department of Electromechanics of the same university since 2016. Her research interests are control of asynchronous electric drives, the use of alternative energy sources, and management of various technological processes using programmable logic controllers. She is the author of 54 scientific articles, and 14 publications.

Sahib Kamal Gasimov was born in Baku, Azerbaijan on 23 March 1965. He received the Master degree in the field of "Electrical drive and automation of industrial installations" from Elektromechanics Faculty, Azerbaijan State Oil and Chemical Institute (Azerbaijan State University of Oil and Industry), Baku, Azerbaijan in 1990. He worked as project electrical engineer for development of Holcim Azerbaijan Cement Plant, Azerbaijan in 2000-2003. He worked as project electrical engineer for quality control at the construction of Sangachal Oil Terminal, Azerbaijan in 2003-2006. He worked as Director of Factory "GBS" which specialized building of electrical switchboards, Baku, Azerbaijan in 2007. He worked as project electrical engineer for 4000t/day Dry Kiln Project of Holcim Azerbaijan in 2008-2014. He worked as Head Project Control Department at Baku Metropolitan CJSC, Azerbaijan in 2014-2018. He worked as Director of Baku Metroproject Institute, Baku, Azerbaijan in 2018-2021. Since 2021, he works as Chief Power Engineer at Sumgait Technological Park (STP), Baku, Azerbaijan. In 2018, he started his Ph.D. work. His research interests are control of asynchronous electric drives, the use of alternative energy sources which is applied in Eco-agrorobot. He is the author of 4 scientific articles.

The 18th International Conference on
"Technical and Physical Problems of Engineering"
30 October 2022
International Organization of IOTPE

ICTPE Conference
www.iotpe.com
ictpe@iotpe.com
ictpe0@gmail.com

ICTPE-2022 Number 20 Code 06RES02 Pages 99-103

HIGH EFFICIENCY SOLAR CELL SYSTEMS - ACHIEVEMENTS AND CHALLENGES

S.Z. Celik [1] R.B. Rustamov [2]

1. Chemical Engineering Department, University of Rovira i Virgili, Toronto, Canada, szeynepcelik@gmail.com
2. Institute Physics, Azerbaijan National Academy of Science, Baku, Azerbaijan, r_rustamov@hotmail.com

Abstract- There is no source of energy more plentiful than our Sun and the sunlight reaching the Earth has the potential to fulfil the world's needs, via solar panels made up of solar modules. There are three generations of solar cells, all of which promise a sustainable future: the 1st, 2nd, and 3rd generations. These cells come with advantages as well as disadvantages and are all useful technologies for the advancement of renewable energy production. It is even possible to combine different types of materials to create tandem solar cells, which lead to higher efficiencies. Undoubtedly, these high-efficiency solar systems provide effective technology solutions that satisfy the market requirements. Undeniably, the challenges of solar systems are a significant part of the decision-making stage when it comes to selecting the right kind of technology for building a high-efficiency system. Therefore, it is necessary to perform a complete assessment of the existing systems in the field, undertaking the achievements in the development of solar cell systems.

Keywords: Solar Cell, Efficiency, Multi-Junction.

1. INTRODUCTION

In today's world, it has become a necessity to generate energy in a way that does not damage nature or the environment [1]. For this aim, it is possible to use renewable energy sources such as wind, biomass, and the most promising one, solar. Solar energy helps create a sustainable planet by minimizing the negative impact on nature [2]. Consequently, the use of solar energy positively influences the protection of our environment and helps fight climate change. This type of energy generates electricity via solar cells.

Photovoltaics (PV) is the term for converting energy from sunlight into electrical energy. Devices with the use of semiconductors that can perform this process are known as solar cells and can be called photoconductive or photovoltaic cells depending on the physical processes of their application.

A photovoltaic cell uses a semiconductor such as silicon, which exhibits the photovoltaic effect. This effect occurs in semiconductors of p-type and n-type, which have positive (excess of holes) and negative (excess of electrons) charges respectively. As the electrons are released via the absorption of photons of sunlight, these free electrons are captured and create an electrical current [4]. This electric field is created as the electrons relocate to the p-side and holes move to the n-side [14]. This technology is by far one of the most efficient ways of harnessing energy from the sun [2].

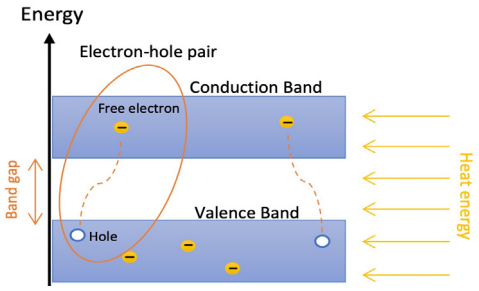

Figure 1. Energy diagram

This effect is illustrated in Figure 1, as the sunlight (heat energy) hits the solar cell modules, the electron-hole pairs are created. This happens as the photons (light particles) give energy to the electrons, which move up to the conduction band from the valence band, creating an electron-hole pair. The electron will then escape into the circuit the cell is connected to and charge the battery [5]. The band-gap indicated in the diagram is the minimum energy required for the excitation of an electron from the valence band to the conduction band, which is an important property of semiconductors. An ideal solar cell will have a band-gap of around 1.4 eV to absorb as much sunlight as possible.

Collectively, solar cells are classified into three generations. First-generation solar cells are mainly silicon-based wafers with efficiencies of 15 to 25%. They are the most commercialized type of solar cells due to their high efficiencies and abundance [1]. However, these cells have some disadvantages such as their costly manufacturing processes and long energy payback times [1]. Next, second-generation solar cells are made from materials such as amorphous silicon, CIGS and CdTe [5]. These cells are thin and flexible and have an efficiency of 1 to 22%, yet, they are not widely commercialized due to various factors such as scarcity of the elements used in them [5].

Finally, we have the very fast-growing third generation of solar cells, which includes a variety of cells, such as organic solar cells. The most exciting one of them all is the perovskite solar cell with a 26-27% efficiency. These cells offer flexibility, low cost, and easy manufacturing among other benefits. The catch here is that they are highly unstable as they are easily affected by their surroundings. Additionally, tandem (multi-junction) cells are a very interesting and fairly new technology that combines the advantages of at least two generations of solar cells, increasing their efficiency. In this paper, the highest efficiency systems of these different types of solar cells are explored.

2. HIGH EFFICIENCY SOLAR CELL SYSTEMS

As introduced before, there are various types of solar cells with a wide range of efficiencies. The efficiency of a solar cell, better known as power conversion efficiency (PCE), determines how much of the light incident is converted into output energy. This definition is simply explained by the following equation:

$$PCE = \frac{P_{in}}{P_{out}} \quad (1)$$

where, P_{in} and P_{out} are the input power and the output power respectively. When one talks about how efficient a solar cell is, they are referring to its PCE, i.e., how much energy is generated.

Let us compare the PCEs of silicon (first generation), thin-film (second generation), perovskite (a type of third-generation solar cell) and tandem solar cells. In Figure 2, we can see various efficiencies recorded by different institutions of these three types of systems. The blue lines represent the first generation, green lines show the second generation, orange is the perovskite, and purple is the multijunction (tandem) solar cells.

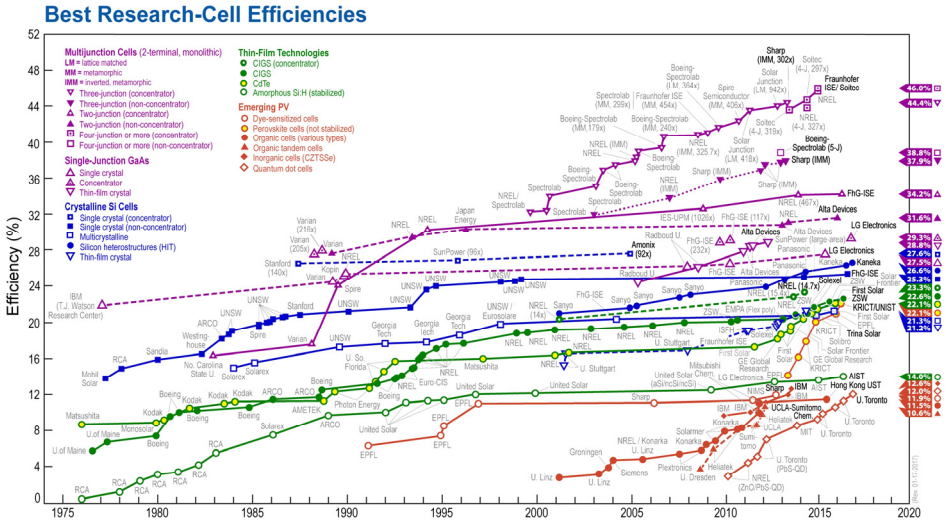

Figure 2. NREL solar cell efficiency table [15]

As seen in Figure 2, the highest silicon solar cell recorded is the Crystalline Silicon by Kaneka at a PCE of 27.6%. As for thin-film solar cells, the world records are 14%, 22.1% and 22.6% for amorphous silicon, cadmium telluride and CIGS cells, respectively. This clearly shows the difference in efficiency and commercialization of silicon and thin-film systems. Next, in orange, under "emerging PV", the efficiencies of various third-generation solar cells are available. The perovskite-silicon tandem solar cells have a high efficiency of 31.3%, while perovskite cells have 26.1%. It can also be seen that four- and three-junction systems lead to the highest efficiencies. It is important to note that all these systems offer different advantages, in addition to their efficiencies, such as flexibility and abundance.

2.1. First Generation, Silicon Solar Cells

Silicon solar cells are currently leading the market due to their high PCEs which are around 26.7% and stability [8]. These photovoltaic cells absorb light and generate electron-hole pairs, then separate charge carriers of opposite types of extracted to an external circuit [5].

Even though silicon solar cells offer high efficiencies, have the optimal band-gap for PV conversion, and are abundant, they still have limitations on the theoretical side - the Shockley-Queisser limit [16]. This limit refers to the peak theoretical efficiency of a solar cell made up of a single p-n junction. It can be calculated by evaluating the electrical energy extracted by each incident photon [17]. Using the AM1.5 spectrum and a bandgap of 1.4 eV, for a single p-n junction, the limit is around 33%. For silicon, taking into consideration other limitations such as the sensitivity of the efficiency to the temperature and environmental factors, assumptions of perfect solar absorption and no losses due to non-radioactive charge-carrier recombination condition of the atmosphere, the limit comes down to 29% [17].

Another drawback of silicon is that it is a semiconductor with an indirect band-gap, meaning that the maximum energy of the valence band falls to a different value of momentum than the minimum energy of the conduction band [21]. This leads to a much slower rate of the process compared to the direct band-gap materials, where the base of the conduction band and the top of the valence band take place at same value of momentum [21].

The different types of silicon-based photovoltaic cells are monocrystalline silicon (mono-Si), polycrystalline silicon (poly-Si) and thin-film amorphous silicon (a-Si) [11]. The main difference between these kinds of solar cells of the same material is their manufacturing processes. In the production process, silica is formed into metallurgical grade silicon, to a 98% level of purity, which is then refined into a polysilicon raw material with a 99.999% purity level [5]. This allows for mono-Si and poly-Si production, where the former shows a slightly higher efficiency of up to 27% and the latter around 17% to 22 % [5].

However, poly-Si has the advantage of lower cost in production. This is because the mono-Si are made from a single crystal of silicon, whereas the poly-Si are fabricated from many silicon ingots melted together. Also because of this long manufacturing process, polycrystalline silicon solar cells have high energy payback times, and time needed to generate the amount of energy used while creating the solar modules. In contrast, the duration for monocrystalline silicon photovoltaic cells is more reasonable. The third type, amorphous silicon cells, includes a thin uncrystallized layer of silicon that is attached to the substrate, making it very thin [11]. The mono-Si and poly-Si are considered first-generation solar cells, while the amorphous is a second-generation cell due to their thin-film structure.

Overall, silicon solar cells, specifically poly-Si, are currently leading the market, but research on other kinds of photovoltaics is going on due to their disadvantages such as cost and high energy payback times [5]. Nevertheless, they are the most commercialized type of cells due to their abundance and efficiency.

2.2. Second Generation - Thin Film Solar Cells

Second-generation solar cells consist of one or more layers of films of photovoltaic material on a substrate. They use direct band-gap materials unlike silicon systems, which allow them to have thin absorbing layers, of a few nanometers to tens of micrometers [5]. This allows for flexible, light cells which can be integrated into many different uses such as small appliances. The main thin-film cells are copper indium gallium selenide (CIGS), cadmium telluride (CdTe) and amorphous silicon(a-Si). Since these cells use fewer semiconductors, their efficiencies are lower compared to first-generation solar cells, and they occupy around 20% of the PV market [11].

2.2.1. Copper Indium Gallium Selenide (CIGS)

The CIGS cells are the highest efficiency of the three thin-film technologies mentioned, with a record PCE of 22.6% [11]. These cells have a structure that consists of a heterojunction system, one with different crystalline semiconductors. Due to its direct bandgap material, its thin layers can easily absorb light. The semiconductor layer is the p-doped CIGS which includes copper, indium, gallium, and selenium with the formula $CuIn_xGa_{(1-x)}Se_2$. The value of x can vary from 0 to 1, and the bandgap changes from 1.0 eV to 1.7 eV [5].

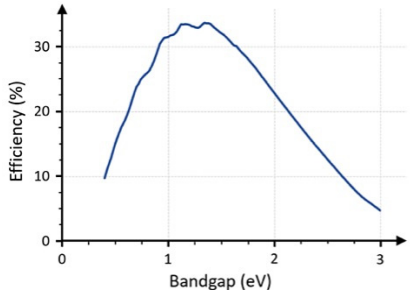

Figure 3. Shockley-Quessier limit [5]

As seen in Figure 3, the band gap range for CIGS cells is ideal for the Shockley-Queisser limit, reaching a PCE over 20%. Although they have high efficiencies and low energy payback times, these elements are very scarce, making it difficult to build many solar panels with them.

2.2.2. Cadmium Telluride (CdTe)

Cadmium Telluride, CdTe, is a direct band-gap material with a big absorption coefficient [12]. This way, it is possible to manufacture thin-film high-efficiency CdTe solar cells, like CIGS. One of the benefits of these cells is their low manufacturing costs, by producing modules from input materials in just a few hours [13]. They are again similar to CIGS in the sense that they also reach a PCE of a little over 20% which is considered good, and have a low energy payback time. Yet, they also have a serious scarcity problem and thus are not widely utilized.

2.2.3. Amorphous Silicon (a-Si)

Amorphous silicon, a-Si, is the form of silicon that is non-crystalline, unlike the first-generation poly-Si and mono-Si. [18]. Due to its high absorption capacity, it can be used in photovoltaic cells with very thin layers, which saves on material cost and time, leading to a low energy payback time. Thanks to their small layers, they are flexible and can be deposited onto various structures such as grass and plastic [18]. The downside of these cells is that they are comparatively lower in efficiency than other types of silicon cells, with a PCE of around 14%. Furthermore, they are highly unstable, and thus unsuitable for large solar power generation sites.

2.3. Third Generation, Emerging PV

Third-generation solar cells are cells that can overcome the Shockley-Queisser and are used to generate electricity from the Sun. This advancing technology is particularly convenient for the use of solar energy as these cells are flexible and have low material costs [5]. The biggest disadvantage regarding these cells is their instability problem; they are not stable when exposed to heat and other factors. Some emerging types are dye-sensitized, quantum dot, and the most promising one, perovskite solar cells (PSC). This paper will look at the latter as an example to explain these emerging PV solar cells.

2.3.1. Perovskite

Perovskite solar cells (PSC), named after Russian mineralogist L.A. Perovski, are a type of third generation solar cell which include organic polymers that absorb light

and produce photovoltaic effects by charge carriers [6]. This type of solar cell is especially exciting for the industry, as its PCE increased from 3.8% in 2009 to 22.1% in 2016, which is a large development in a short period of time [19]. Currently, the efficiency of the perovskite cell reaches approximately 27%.

Perovskite is a type of compound of the form ABX_3, where A and B are the cations and X is the anion [7]. X is a halide and can be elements such as O, Cl, Br, I and S [8]. The bigger cation A can be organic or inorganic molecules, such as methylammonium ($CH_3NH_3^+$) or cesium (Cs_3^+), while the cation B can be lead (Pb^{2+}) [7].

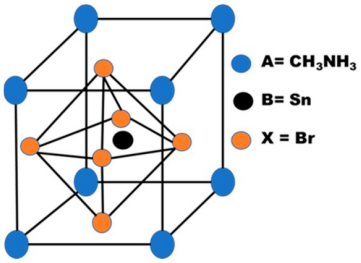

Figure 4. structure of a tin-based perovskite [54]

In Figure 4, the crystal structure of a cubic perovskite can be seen. Due to perovskite's structural distortion characteristics, researchers have been focusing on Tin-based PSC, where lead is substituted by Sn^{2+} (tin). The advantage of these cells would be that they are lead-free, as lead is harmful to the environment. These different material combinations determine the properties of the perovskite, some of which are band-gap and mobility [7].

PSCs have exceptional photoelectric properties and high optical absorption coefficients [19]. The perovskite light-absorbing layer can absorb solar energy well and the electron-hole pairs are efficiently and simultaneously transmitted and collected [19]. They have a layered structure consisting of a TCO-coated glass substrate, an electron-transport layer (n-type semiconductor), a perovskite absorber layer, a hole-transport layer (p-type semiconductor) and a back contact (metal/TCO/carbon) [20]. This structure is illustrated below in Figure 5.

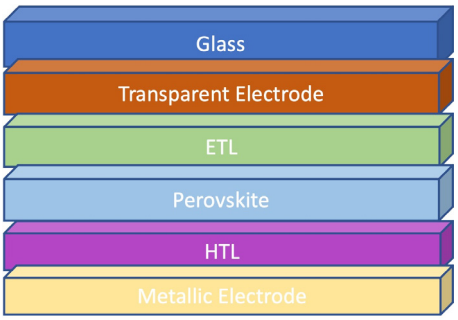

Figure 5. Structure of Perovskite Solar Cells

Presently, the biggest challenge perovskite solar cells face is the long-term stability of modules [20]. This problem is caused by the instability of the perovskite layer when in contact with moisture and heat.

This is due to the intrinsic stability, one that is caused by the crystalline structure of the perovskite, as well as the extrinsic stability, which are external factors, such as interaction with water [22]. There have been various methods implemented to solve this degradation problem, such as adding a protective layer to the perovskite material. However, a fully effective, long-lasting solution is yet to be found. It is necessary to continue this research to solve this issue permanently and commercialize perovskite solar cells.

2.4. Tandem (Multi-Junction) Solar Cells

There are many techniques for growing the efficiency of solar cells, and tandems are one of them. In literature, a few layers of different materials with different band-gap energies stacked together are more likely to have higher efficiencies, as single-junction cells are limited by the Shockley-Queisser limit. Yet, predictably, this will require a higher manufacturing cost than a regular single-junction cell.

A popular tandem solar cell is the perovskite-silicon system. Silicon solar cells on their own are the most commercialized solar cells. It is easy to find silicon on Earth and they have competitive efficiencies. Perovskites are a great match for silicon, as they can cover the wavelength area silicon cannot on its own. Perovskites can absorb high-energy photons, while lower-energy light particles are absorbed by the silicon layer, thus increasing the efficiency of the cell. For instance, when a high-energy photon is illuminated on silicon, it might cause a lot of heat, leading to a lot of loss. If a perovskite layer is placed on top of silicon, it will reduce this heat, preventing a large amount of heat loss, and the efficiency will go up.

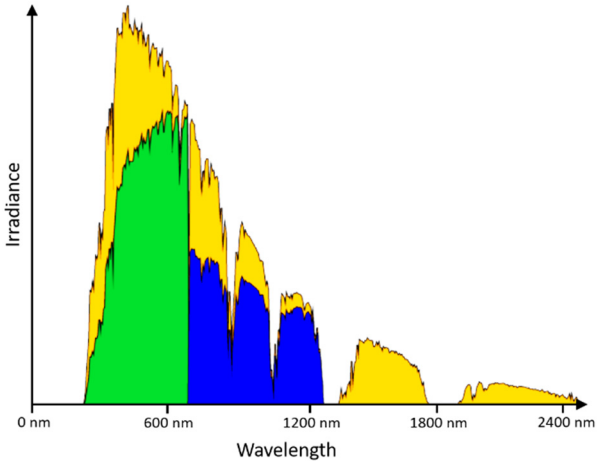

Figure 6. Spectral usage for a stacked tandem solar cell [5]

In Figure 6 above, the utilization of the spectrum (yellow) is illustrated. The top layer (green) has a larger band gap than the lower layer (blue), and both shorter and longer wavelengths can be absorbed. An example of a commercialized perovskite-silicon tandem solar cell is from Oxford PV [10] with an efficiency that could reach up to 30%. This tandem solution offers higher performance and consequently reduces the cost as less area is needed for more power, compared to their regular silicon solar cells at around 22%.

3. CONCLUSION

The three generations of solar cells presented all promise various characteristics for a sustainable future. We can conclude that silicon solar cells are leading the market, although their development has almost ended, as the current silicon solar cells are already very close to the Shockley-Queisser limit. The second and third-generation cells bring hope for the future with their increasing PCEs and features such as flexibility. Many scientists are continuing their research regarding these cells to improve their efficiencies and stabilities. More, tandem (multi-junction) solar cells offer a unique technology by combining more than one generation of solar cell materials to absorb a wider range of wavelengths, increasing the efficiency, and decreasing the energy payback time of modules. These new advanced technologies promise a bright future.

REFERENCES

[1] G. Yilmaz, C. Ozkok, "Perovskite Solar Cells and Instability Problems", Journal of Mehmet Akif Ersoy University of Science and Technology, Issue 1, Vol. 9, pp. 297-304, Duzce, Turkey, 2019.
[2] A. Waeli, H.A. Ali, "A Review of Photovoltaic Thermal Systems: Achievements and Applications", International Journal of Energy Research, Issue 2, Vol. 45, pp. 1269-1308, Bangi, Malaysia, 2021.
[3] K. Ranabhat, L. Patrikeev, A.A. Revina, K. Andrianov, V. Lapshinsky, E. Sofronova, "An Introduction to Solar Cell Technology", Journal of Applied Eng. Science, Issue 4, Vol. 14, pp. 481-491, Moscow, Russia, 2016.
[4] B.J. Feldman, "An Introduction to Solar Cells", The Physics Teacher, Issue 5, Vol. 48, pp. 306-308, St Louise, USA, April 2010.
[5] M.V. Madsen, A.S. Gertsen, "Introduction to Solar Cells", Technical University of Denmark, Coursera, Lyngby, Denmark, 2021.
[6] M.V. Dambhare, B. Butey, S.V. Moharil, "Solar Photovoltaic Technology: A Review of Different Types of Solar Cells and Its Future Trends", Journal of Physics: Conference Series, Vol. 1913, No. 1, pp. 1742-6596, IOP Publishing, Nagpur, India, 2021.
[7] A. Gomez, J. Pablo, "Charge Transport and Recombination Layers for Perovskite Solar Cells", pp. 10-15, Valencia, Spain, 2020.
[8] F. Zhimin, "Perovskite-Based Tandem Solar Cells", Science Bulletin, Issue 6, Vol. 66, pp. 621-636, Hefei, China, 2021.
[9] R.A. Deshpande, "Advances in Solar Cell Technology: An Overview", J. Sci. Res., Issue 65, pp. 72-75, Varanasi, India, 2021.
[10] "Leaders in Perovskite Solar Technology", Oxford PV, UK, 2022.
[11] T. Zhang, M. Wang, H. Yang, "A Review of the Energy Performance & Life-Cycle Assessment of Building-Integrated Photovoltaic (BIPV) Systems", Energies, Issue 11, Vol. 11, No. 3157, pp. 1-5, Hong Kong, 2018.
[12] T.D. Lee, A.U. Ebong, "A Review of Thin Film Solar cell Technologies and Challenges", Renewable and Sustainable Energy Reviews, Issue 70, pp. 1286-1297, Durham, USA, 2017.
[13] Office of Energy Efficiency and Renewable Energy, "Cadmium Telluride", Energy.gov, USA, 2022.
[14] J. Hanania, K. Stenhouse, J. Donev, "Photovoltaic Effect - Energy Education", energyeducation.ca, Canada, 2015.
[15] NREL, "Best Research-Cell Efficiency Chart", Photovoltaic Research, USA, 2022.
[16] L.C. Andreani, "Silicon Solar Cells: Toward the Efficiency Limits", Advances in Physics, Issue 4, Vol. 1, pp. 1-5, Pavia, Italy, 2019.
[17] W. Shockley, H.J. Queisser, "Detailed Balance Limit of Efficiency of p-n Junction Solar Cells", J. of Applied Physics, Vol. 32, pp. 510-519, Palo Alto, USA, 1961.
[18] D. de Rooij, "Amorphous Silicon Cells: Structure and Applications", Sinovoltaics, Hong Kong, April 2022.
[19] D. Zhou, T. Zhou, Y. Tian, X. Zhu, Y. Tu, "Perovskite-Based Solar Cells: Materials, Methods, and Future Perspectives", Jianghan University, Journal of Nanomaterials, Vol. 2018, Wuhan, China, 2018.
[20] Y. Rong, "Challenges for Commercializing Perovskite Solar Cells", Issue 361, No. 6408, pp. 1-18, Toronto, Canada, 2018.
[21] "Direct and Indirect Bandgap of Semiconductors", The University of Cambridge, Cambridge, UK, 2022.

BIOGRAPHIES

Sevim Zeynep Celik was born in Istanbul, Turkey on Jan 13, 1999. She studied Physics & Astronomy at York University in Canada and is furthering her education at Rovira i Virgili University, Toronto, Canada studying a master's in Energy Conversion Systems and Technologies. She worked as a math & science instructor for 3 years and as an application scientist for 8 months. She currently works as a technical customer support & business development specialist at a company that provides solar data & consultancy services for the advancement and optimization of solar power plants.

Rustam B. Rustamov was born in Ali Bayramli, Azerbaijan, on May 25, 1955. He is an independent expert on Space Science and Technology. In the past, he was in charge of the Azerbaijan National Aerospace Agency's activities as an Acting Director-General. He has mainly specialized in space instrumentation and remote sensing and GIS technology. Rustam B. Rustamov graduated Ph.D. at the Russian Physical-Technical Institute, S. Petersburg, Russia. He has invited the work at the European Space Agency within the Framework of the United Nations Program on Space Applications at the European Space Research and Technology Center, The Netherlands. Rustam B. Rustamov has been appointed to the United Nations Office for Outer Space Affairs Action Teams (member, Vienna, Austria), United Nations Economic and Social Commission for Asia and the Pacific (national focal point, Thailand), International Astronautically Federation (Federation's contact, Paris, France), Recent Advances in Space Technologies International Conference Program Committee (member, Turkey). He is the author of 18 books published by European and United States famous publishers and more than 130 scientific papers.

The 18th International Conference on
"Technical and Physical Problems of Engineering"
30 October 2022
International Organization of IOTPE

ICTPE Conference
www.iotpe.com
ictpe@iotpe.com
ictpe0@gmail.com

ICTPE-2022 Number 21 Code 06RES03 Pages 104-110

SOME ISSUES OF USE AND SIMULATION OF ELECTROMAGNETIC BRAKE IN WIND POWER PLANT

N.A. Aliyev E.N. Ahmadov S.A. Khanahmedova

Azerbaijan State Oil and Industry University, Baku, Azerbaijan
nadir.alili.52@mail.ru, elbrusahmed@gmail.com, samira1009@mail.ru

Abstract- The article considers the problem of modeling an electromagnetic brake, which is proposed to be used in a wind power plant as a stabilizing and damping element when the wind speed fluctuates, by considering it as an object with lumped parameters. As a model for calculating the electromagnetic moment, an equivalent circuit is proposed, which clearly depicts the structure of the object and its operation in dynamic modes. To take into account saturation, it is proposed to use expanded equivalent circuits, in which magnetic couplings between different circuits are replaced by complex electrical resistances, which make it relatively easy to determine the degree of saturation. Using equivalent circuits, a program based on MATLAB was compiled, and the results of the calculation are presented in the form of graphs.

Keywords: Wind Turbine, Electromagnetic Brake, Magnetic Circuit Saturation, Extended Equivalent Circuit.

1. INTRODUCTION

Due to the high cost of electricity and traditional energy carriers, there is a shortage of electricity in homes and farms, which encourages the use of renewable energy sources (RES). The development of RES has now become one of the fundamental postulates of the global new energy strategy [1, 2]. At the same time, it has become a topic of official policy in many nations. Solidly funded state programs in this area have appeared. In a number of countries, regulatory and legislative acts in the field of RES use were adopted, which formed the legal, economic, and organizational basis for this area of technical development. The economic justification is boiled down to policies that encourage the use of renewable energy, which is essential during the energy market's development, design, and adaptation phases.

The basis of RES, as you know, is sources that convert the energy of the sun and wind. These renewable energy sources have both advantages and disadvantages in comparison with traditional energy. The main advantages include the ubiquity of most of their species, environmental friendliness, and low operating costs, since the energy from these sources is free.

The main disadvantages of RES are the low density of the energy flow (specific power per unit area) and the variability in time of most types of RES. The first situation necessitates the construction of extensive power plant regions (the receiving surfaces of solar installations, the area of a wind wheel, etc.). Due to their high material consumption, these devices require more particular capital inputs than conventional power plants do. Lower operating costs eventually make up for the higher capital expenditure.

The most significant issues are connected to the temporal fluctuation of energy sources such solar radiation, wind, tides, runoff from minor rivers, and weather temperatures. The process of the entrance of solar energy has a major element of chance linked with weather conditions even if it is normally regular. For instance, if the change in energy of the tides is precisely cyclical. Even more erratic and fickle is wind energy.

The variability of electricity generation over time RES requires the creation of storage devices, as a rule, their function is performed by batteries. A sufficiently powerful power system, which also includes wind power plants (WPP) and solar power plants, can compensate for changes in the power of these plants. However, at the same time, in order to avoid changes in the parameters of the power system (primarily frequency), the share of unregulated power plants should not exceed 15% in terms of capacity. In general, the use of RES in the world has acquired a tangible scale and a steady upward trend. In some countries, the share of renewable energy in the energy balance is a few percent. According to various forecast estimates, which are currently not lacking, this share will reach or exceed 10% by 2020 in many states.

As can be seen from the above, one of the most accessible sources of renewable energy is wind energy. The use of wind energy in recent years has become even more relevant, following hydropower. The development of technologies and accumulated experience allow us to determine the main directions and methods of development. An analysis of the work carried out in this area allows us to conclude that the main problem of wind energy is obtaining electricity of the required quality. This, in turn, requires the integration of theoretical knowledge of aerodynamics and electromechanics.

There is a wide variety of electromechanical converters used in wind power plants. In terms of their energy performance, a special place among them is occupied by a synchronous generator with excitation from permanent magnets [3, 4]. However, their dynamic performance leaves much to be desired. Wind gusts causing significant oscillations of the wind turbine shaft and, accordingly, the synchronous generator leads to oscillations of electromagnetic power. As you can see, the reaction of a synchronous generator to gusts of wind is very strong, which often leads to it falling out of synchronism. The inability to influence this process through the excitation of the generator exacerbates this disadvantage.

The most important energy characteristic of the wind is its speed. It is known that the speed and direction of the wind change according to a random law, and the kinetic energy is proportional to the cube of its speed. Another major disadvantage of wind is its instability. Switching between low and high speeds is frequently required to maximize the effectiveness of the utilization of wind turbines due to the fluctuation of the wind speed. Wind generators must maintain the established parameters of the generated energy under any energy impact. Therefore, solving the problem of stabilizing the energy output is always an urgent task.

2. FORMULATION OF THE PROBLEM

Electromagnetic brakes (EMB) or electromagnetic slip clutches (EMS) are widely used in industry. In lifting and lifting equipment, EMTs provide a smooth descent of loads at the required speed, controlled by changing the excitation current of electromagnets [5, 6]. In various tests of engines and other propulsion systems, EMBs are used as a load, creating the necessary adjustable load moment. In the electric power industry, EMB has not yet found its application. However, its potential advantages give grounds for using it as a means of improving the conditions for dynamic and static stability of the electric power system (EPS), including WPPs.

The principle of operation of the EMB (Figure 1) is based on the occurrence of eddy currents in a massive metal disk when an alternating electromagnetic field is created in the EMB. The electromagnetic field penetrating the disk is created by DC electromagnets. When the shaft of the generating unit rotates, an alternating electromagnetic field is induced in the EMT disk, which causes eddy currents in the steel of the disk, the direction of which prevents a change in the flux of the magnetic induction vector. The interaction of the magnetic field and eddy currents leads to the appearance of a braking torque. When eddy currents flow through a disk with a finite resistance value, energy losses occur, which is accompanied by heat release in the EMB disk. Thus, the kinetic energy of the mechanical work of the EMB metal disk is transformed into thermal energy [3].

The EMB has a low inertia and directly affects the balance of moments on the shaft of the generating unit, and its parameters do not depend on the parameters of the WPPs mode and network. In addition, the EMB control system can have an independent power source (accumulator battery; generator integrated into the EMB), which makes it possible to provide an autonomous power supply to the EMB excitation system [3].

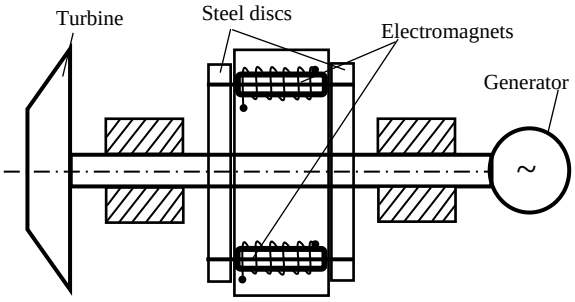

Figure 1. Electromagnetic brake device

Such advantages of EMB as speed, impact directly on the balance of moments on the shaft of the generating unit, independence of operation from the parameters of the external electrical network, give reason to believe that EMB can be used as a means of improving the conditions for the dynamic stability of wind farms and damping undamped and weakly damped oscillations of transient processes by intersystem connections caused both by emergency events and by the operation of automatic control systems for WPPs elements.

The task of controlling electromechanical processes is to ensure the static and dynamic stability of the WPPs, as well as the required quality of attenuation of transient processes. Management in emergency mode is provided mainly by relay protection and automation devices. The control of the WPPs mode with the help of EMB can be attributed to the prevention of violation of the stability of the system.

One of the main tasks standing in the way of using EMB in EPS is the search for EMB power control. To control the braking power of the EMB, it is necessary to control the excitation current of the EMB. The WPPs' behavior is described by a system of non-linear differential equations. The task of synthesizing the EMB control law is complicated due to the unipolar characteristic of the EMB torque (it develops only a braking torque, regardless of the direction of the current in the excitation winding). Despite the fact that, at present, there are many methods for synthesizing the control laws of nonlinear systems, taking into account various limitations, there are no universal methods.

3. PROBLEM SOLUTIONS

One of the distinguishing features of the use of EMB is its unipolar action - the device creates only a load moment, despite the fact that in the initial state the moment it develops is zero. This, in turn, means a sharply nonlinear dependence of the EMB power on time. The study of the static stability of the system is usually carried out using the method of "*small deviations*", which implies the linearization of the original system of nonlinear differential equations in the vicinity of the equilibrium point.

Linearization describes the properties of the system in a certain neighborhood with respect to the steady value of the parameters. However, considering the EMB as part of the power system, the linearization of the system of equations will, in turn, mean that the unidirectional action of the EMB is not taken into account. Thus, the use of standard methods for studying the static stability of wind farms, taking into account the operation of the EMB, is impossible. Therefore, the analysis of nonlinear equations was used as a research method.

Some questions about the possibility of using an electro-magnetic brake in a wind power plant are considered in [7, 8]. This is a relatively new approach to the application of special electrical machines in this field with competitive advantages. For example, at maximum wind speed, it is possible to regulate the work process. With an increase in the load on the blades of wind turbines, the speed of rotation of the wind wheel decreases, and the torque increases. Switching to the electromagnetic brake mode, it is possible to slow down and prevent an accident in case of an accidental gust of wind and ensure the safe operation of wind farms.

During the operation of the EMB, the dynamic stability of the wind farm is preserved and the attenuation of the transient process is ensured. A short circuit leads to acceleration of the rotor of the generating unit. As a perturbation causing a negative imbalance and, accordingly, braking of the rotor of the generating unit immediately after the application of the perturbation, one of the four generators in the presented scheme was switched off.

The results of calculations of transient processes are presented in Figure 2 [4]. As can be seen, the EMB does not work at the moment of the occurrence of a disturbance, switching on occurs only when the generator rotor accelerates. An analysis of the calculation results shows that the inclusion of EMB in operation allows improving the conditions for the flow of the transient process in the power system with a given disturbance. The operation of the EMB according to the principle of operation is similar to the operation of the speed controller of the generating unit. The difference is that the speed controller acts on both braking and acceleration, i.e., it has a bipolar action. The unipolar action of the EMB reduces the effectiveness of the influence on transients during disturbances, the EMB can only create a braking torque [9].

It follows from the above that the dynamic moment on the wind generator shaft changes periodically. If we add here the issues of starting and braking, as well as increasing reliability, it goes without saying that a wind turbine is a complex object. One way to dampen dynamic processes in such a system is to use an electromagnetic slip clutch. As shown above, structurally, EMB consists of a massive cylindrical armature and a salient-pole inductor with a massive core. Design features in the field of application of these machines are diverse [10, 11].

When developing electric drives such as wind turbines, it is often necessary to provide specific characteristics and properties of machines intended for these drives. One of the main characteristics of EMB is its mechanical characteristics - the dependence of the electromagnetic torque on slip ($M=f(s)$). Electric drives with EMB having rigid mechanical characteristics can ensure reliable operation of wind turbine mechanisms without the use of complex automatic control systems and limit overloads in the case of wind gusts. It is known that the design and study of EMB operating modes, taking into account changes in magnetic permeability, electrical resistivity of steel, edge effect, hysteresis losses, taking into account saturation, etc., are fraught with great difficulties.

The foregoing indicates the relevance of modeling and research methods for calculating the electromagnetic moment in the dynamic modes of operation of the EMB or electromagnetic slip. EMB used in wind turbines must have characteristics that ensured the possibility of its operation in the specified mode. Depending on the speed of the wind oscillation, the electromagnetic moment of the leading part varies over a wide range. In order to stably maintain the torque of the driven part, it is necessary to change the magnitude of the excitation current. In this case, many variants with highly saturated magnetic circuits are possible. The possibilities of computer technology make it possible to use the methodology of a computational experiment to study various modes of operation of the EMB in wind turbines. Given the initial data, it is possible to conduct a fairly accurate numerical analysis of the mathematical model.

4. MATHEMATICAL MODEL

Simplification of the method for calculating the electromagnetic moment without leading to significant errors is important. In addition to the painstaking analytical calculation of mechanical characteristics, we will use the method of constructing these characteristics according to equivalent circuits for EMS with a massive magnetic core. Such equivalent circuits clearly depict the structure of the object and allow you to effectively investigate the parameters and characteristics. To draw up equivalent circuits, consider the voltage balance equations in the circuits of a massive armature along the longitudinal and transverse axes for the steady state [12]:

$$r_b i_b = U_b \quad (1)$$

$$r_d i_d + \omega L_q i_q = 0 \quad (2)$$

$$r_q i_q - \omega M i_b - \omega L_d i_d = 0 \quad (3)$$

where, r_b is the ohmic resistance of the coupling excitation winding; i_b is the excitation current of the coupling; U_b is voltage of the winding excitation of the coupling; r_d is active resistance along the longitudinal axis of the massive armature; i_d is current along the longitudinal axis of the massive armature; ω is angular rotation frequency; L_q is transverse axis inductance; i_q is transverse axis current; r_q is active resistance along the transverse axis; i_d is current along the transverse axis; and L_d is longitudinal inductance

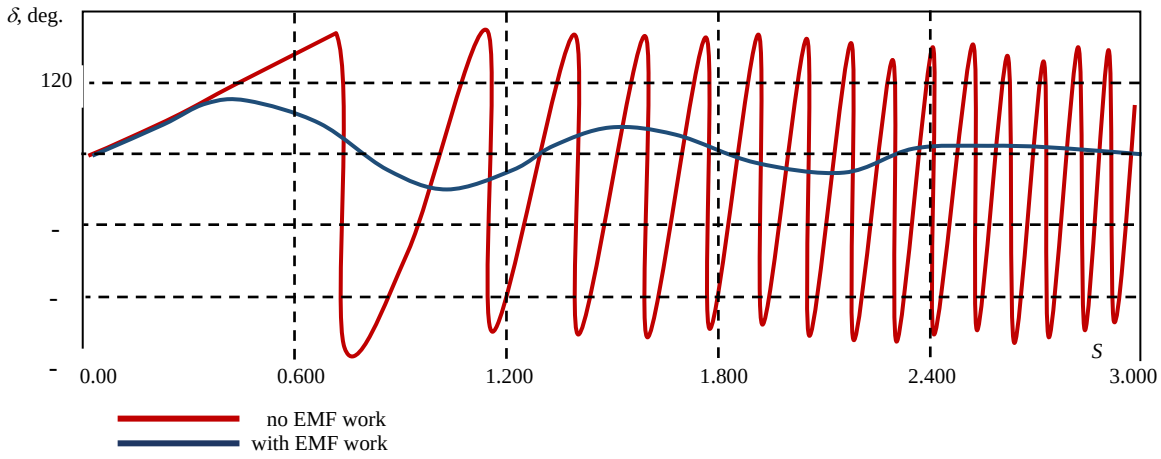

Figure 2. Dynamic stability of the electric power system

It is known that the equivalent circuit exists when the matrix of coefficients of the equation is symmetric. By symmetrizing the matrix of coefficients of Equation (2), we obtain [11, 12]:

$$\frac{r_q}{S} i_d + \omega_0 L_q \frac{r_q}{r_d} i_q = 0 \tag{4}$$

$$-\omega_0 L_d i_d + \frac{r_q}{S} i_q = \omega_0 M i_b \tag{5}$$

where, M is mutual inductance; $\omega = \omega_0 S$, ω_0 and S respectively, the angular frequency of idle and slip. Equation (5) corresponds to the equivalent circuit shown in Figure 3 [4].

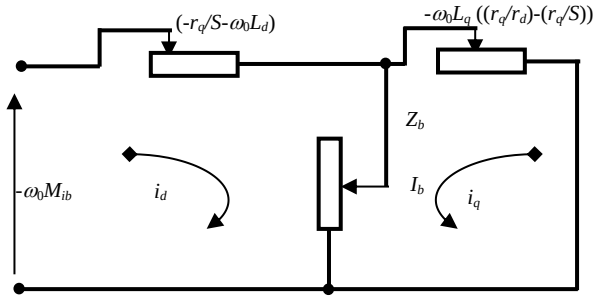

Figure 3. Synchronous generator equivalent circuit

Considering that the electromagnetic moment is defined as the Equation (6),

$$M = \frac{i_d^2 r_d + i_q^2 r_q}{\omega} \tag{6}$$

To calculate it, you need to determine the currents in the circuits d and q of the massive armature. Solving the system of Equation (5) for i_d and qd, we get Equations (7) and (8) [12]:

$$i_d = i_b \frac{\omega_0^2 M L_q r_q}{r_d \left[\left(\frac{r_q}{S} \right)^2 + \omega_0^2 L_d L_q \frac{r_q}{r_d} \right]} \tag{7}$$

$$i_q = i_b \frac{\omega_0^2 M r_q}{S \left[\left(\frac{r_q}{S} \right)^2 + \omega_0^2 L_d L_q \frac{r_q}{r_d} \right]} \tag{8}$$

Multiplying the numerator and denominators of Equations (7) and (8), respectively, by the value $\frac{L_d S^2}{r_q^2 r_d}$ and $\frac{S^2}{i_q}$ after a series of transformations we get Equation (9) [11]:

$$i_d = i_b \frac{\omega_0^2 T_d T_q M}{L_d \left(1 + \omega_0^2 T_d T_q\right)} \tag{9}$$

where, T_d and T_q are the time constants of the longitudinal and transverse axes, respectively. Thus, knowing all the EMS parameters, it is possible to calculate and build the mechanical characteristic $M = f(s)$ at various values of the excitation current. It should be noted that the equivalent circuit (Figure 3) was drawn up when considering EMS from the side of the excitation winding and when applying the theory of synchronous machines. Under normal operating conditions, the coupling flux is non-linear. This circumstance sharply complicates the calculation of characteristics taking into account saturation. Disregarding saturation leads to large errors. The operating modes of EMS and EMB with saturated magnetic circuits cannot be considered fully investigated until now [12].

To solve this issue, we will use expanded equivalent circuits with saturated armature and inductor cores as a mathematical model, which is one of the most convenient and intuitive methods. The essence of the method lies in the fact that when drawing up equivalent circuits, magnetic connections between different circuits are replaced by electrical connections, that is, by various electrical circuits with complex electrical resistances.

To establish a connection between complex magnetic and electrical resistances, the known relations are used [7]:

$$z = jk\frac{1}{z};\ \ \mathrm{Z} = \frac{\mathrm{F}}{\Phi} \tag{10}$$

where, $k = 4pf\left(w1kw1\right)2/p$ is the reduction coefficient, z and Z are the complex electrical and magnetic resistances of equivalent circuits, F and magnetic dynamic force and magnetic flux, respectively. Considering the similarity of the EMS magnetic circuits and an induction machine with a massive rotor, it is possible to make a magnetic circuit and, accordingly, an equivalent electrical circuit for the coupling shown in Figures 4 and 5 show the computed equivalent circuit [3, 4].

The following parameters apply to the comparable circuit in Figure 4 [3]:
where, z is complex resistance, including active and leakage inductive reactance of the excitation winding x_{1S}; x_μ is inductive resistance of the core of the field winding inductor; Z_d is complex resistance of the air gap; r_{20} is active resistance equivalent to magnetic losses in the massive armature; and x_{20} is the inductive resistance of the massive armature.

Thus, in the equivalent circuit, the saturated sections of the magnetic circuit are taken into account by nonlinear resistances, the characteristics of which can be approximated by expressions as a function of voltages and currents. The calculation of the circuit is carried out at a given value of the excitation voltage U_b of the coupling and functional dependences of nonlinear resistances $Z_1 = f\left(\dot{I}_1\right);\ \ Z_2 = f\left(\dot{I}_2\right);\ \ Z_3 = f\left(\dot{I}_3\right);$ $Z_4 = f\left(\dot{I}_4\right).$

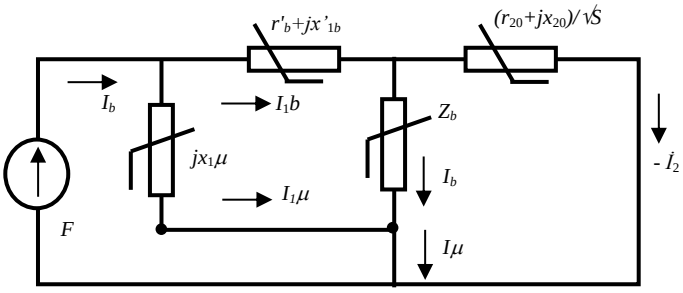

Figure 4. Expanded equivalent circuit with salient pole inductance

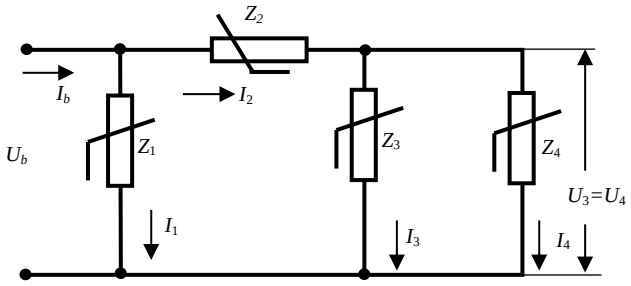

Figure 5. Calculated equivalent circuit of the coupling

The main ratios for the calculation are as Equations (11), (12), (13), (14) and (15):

$$\dot{I}_1 = Y_e U;\ \dot{I}_1 = \dot{I}_B\frac{Y_2}{Y_E};\ \dot{I}_2 = \dot{I}_B - \dot{I}_1 \tag{11}$$

$$\dot{I}_3 = \dot{I}_2\frac{Y_3}{Y_{e1}};\ \dot{I}_4 = \dot{I}_2\frac{Y_4}{Y_{e1}} \tag{12}$$

$$U_2 = \dot{I}_2 z_2;\ U_3 = U_4 = U_1 \tag{13}$$

$$Y_e = \frac{z_1z_3 + z_1z_4 + z_2z_3 + z_2z_4}{z_1z_2z_3 + z_1z_2z_4} \tag{14}$$

$$Y_{e1} = \frac{z_3 + z_4}{z_3z_4};\ \ Y_3 = \frac{1}{z_3};\ Y_4 = \frac{1}{z_4} \tag{15}$$

Based on the developed analysis, it is possible to create programs for calculating in MATLAB. At the same time, the use of a system of relative units makes it possible to simplify and generalize the results obtained and build an array current hodograph to study the effect of saturation on parameters that are suitable for a wide range of clutches and brakes of various capacities.

Figure 6 displays current hodographs for various coupling excitation current values. A comparison of the current hodographs allows us to conclude that with an increase in the excitation current, in the case of a saturated armature, it increases much more at large slips.

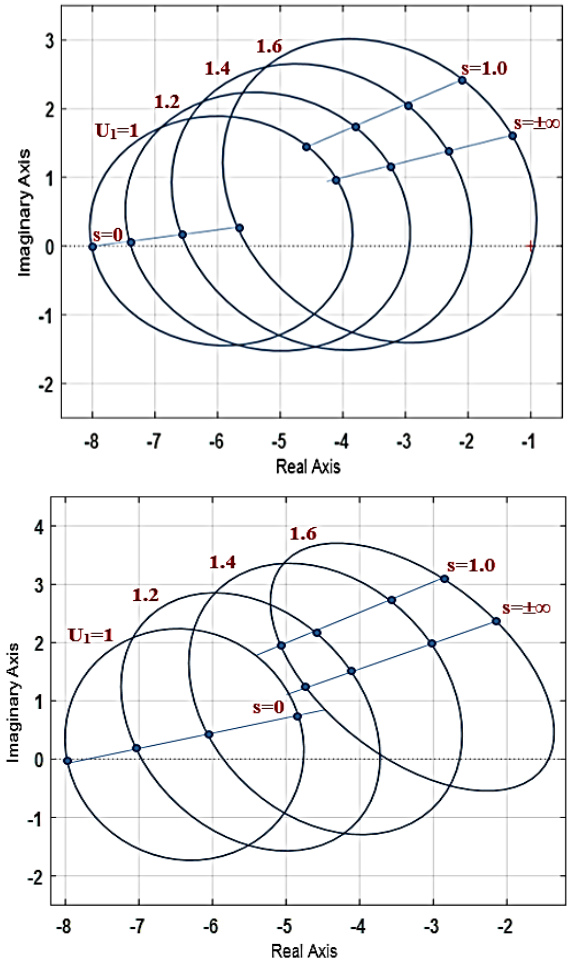

Figure 6. Hodographs of currents for various values of currents of coupling excitation

5. CONCLUSIONS

It is proposed to use an electromagnetic brake in a wind power plant as a damping and stabilizing element in case of sharp fluctuations in wind speed. A generalized mathematical model of an electromagnetic brake is defined in the form of equivalent circuits with a saturated magnetic circuit. A computational algorithm and a program have been developed to study various modes of clutch operation in order to select the main parameters that can provide the necessary characteristics under given conditions.

REFERENCES

[1] M.A. Bhuiyan, Q. Zhang, V. Khare, A. Mikhaylov, G. Pinter, X. Huang, "Renewable Energy Consumption and Economic Growth Nexus-A Systematic Literature Review", Systematic Review Article, Frontiers in Environmental Science, pp. 1-21, 29 April 2022.

[2] D. Gielen, F. Boshell, D. Saygin, M.D. Bazilian, N. Wagner, R. Gorini, "The Role of Renewable Energy in the Global Energy Transformation", Energy Strategy Reviews, Vol. 24, pp. 38-50, April 2019.

[3] R.N. Mustafaev, L.G. Gasanova, "Comparative Evaluation of the Efficiency of the Functioning of Modern Wind Power Plants", Journal Electromechanics, Izv. Universities, No. 4, pp. 57-60, Novocherkassk, Russia, 2008.

[4] A.I. Abdulkadyrov, N.A. Aliyev, "On the Use of an Electromagnetic Slip Coupling in a Wind Power Plant", International Scientific and Practical Conference on Development of Technical Sciences in the Modern World, pp. 76-96, Voronezh, Russia, 2016.

[5] M. Harun, R. Molla, N. Al Nahian Rahat, M. Alam, M.K. Uddin, "Construction and Experimental Analysis of an Electromagnetic Braking Clutch", The International Conference on Mechanical Engineering and Renewable Energy (ICMERE 2019), pp. 11-13, Chittagong, Bangladesh, December 2019.

[6] N. Fernando, "A Field Modulated Electromagnetic Clutch with Slip Control", IEEE 2nd Annual Southern Power Electronics Conference (SPEC), December 2016.

[7] D.M.M.S. Regis Prabha, "Development of Utilizing Magnetic Brake in Small Wind Turbine Speed Control using Fuzzy Logic Controller", Indian Journal of Science and Technology, No. 9, Vol. 13, pp. 1-13, Indian, April 2016.

[8] E.A. Sirotkin, A.S. Martyanov, E.V. Solomin, S.V. Kozlov, "Emergency Braking System for the Wind Turbine", The 2nd International Conference on Industrial Engineering, Applications and Manufacturing, May 2016.

[9] B.T. Polyak, O.N. Kuznetsov, V.V. Chumachenko, "Investigation of the Stability of a Power System with a Unipolar Electromagnetic Brake", Automation and Telemechanics, No. 9, Vol. 77, pp. 1557-1566, Moscow, Russia, 2016.

[10] N. Goudarzi, W.D. Zhu. "Studying the Potential of a Novel Multiple Generator Drivetrain in Wind Energy Conversion Systems", IMECO, pp. 15-21, San Diego, California, USA, November 2013.

[11] F.G. Huseynov, N.A. Aliyev, "Optimization of Geometry, Parameters and Characteristics of Electromagnetic Sliding Clutches and Brakes with a Massive Magnetic Core", Izv. Universities, Electromechanics, No. 10, pp. 75-78, Novocherkassk, Russia, 1983.

[12] V.M. Kutsevalov, "Analysis of Equivalent Circuits of Alternating Current Electric Machines", Journal Energy and Transport, No. 5, pp.98-103, Moskow, Russia, 1985.

BIOGRAPHIES

Nadir Abdulrakhman Aliyev was born in in Gakh, Azerbaijan on June 19, 1952. In 1969-1974, he studied at Energy Faculty, Azerbaijan State University of Petroleum and Chemistry, Baku, Azerbaijan majoring in Electrical Machines and Apparatuses, and received the Master degree. In 1974-1976, he worked as engineer, chief foreman of Baku plant of household air conditioners. In 1977-1979, he entered in graduate school. In 1980-1989, he was an assistant at the Department of Electric Machines and Apparatuses. Since 1990, he was an Associate Professor of Department of Electrical Equipment and Automation of Industrial Installations. He was a Candidate of Technical Sciences at Department of Electromechanics, Azerbaijan State University of Oil and Industry, Baku, Azerbaijan since 20116. His research interests are electric machines with a massive magnetic conductor and wind power, and modeling and research of special types of electromechanical converters. He published 65 scientific works, including 44 articles, 12 abstracts, 6 textbooks, 2 textbooks and 1 monograph.

Elbrus Nasi Ahmadov Was born in Shikhly Agdash, Azerbaijan on June 20, 1964. In 1982-1989, he studied at Faculty of Electromechanics, Azerbaijan Institute of Petroleum and Chemistry (State University of Petroleum and Industry), Baku, Azerbaijan and received the Master degree. In 1992-1996, he studied at Azerbaijan State Oil Academy, Baku, Azerbaijan. In 2003, he received the degree of Candidate of Physical and Mathematical Sciences. Since 2016, he worked as Head of Department of Electromechanics. His research interests are electrophysics, the effect of electric fields on substances, and protection of high-voltage electrical equipment from overvoltage. He is the author of 51 scientific works, including 32 articles, 8 these, 2 guidelines, 5 textbooks and 4 patents.

Samira Alkhadi Khanahmedova was born in Baku, Azerbaijan on 9 October, 1967. She received Master degree in electrical engineering in 1990. He hired as a senior laboratory assistant at Department of Electrical Equipment and Automation of Industrial Installations in 2004. She was a dissertation student at Azerbaijan State Oil and Industry University, Baku, Azerbaijan in 2007-2012. She defended her Ph.D. dissertation in the field of "Design and research of electromechanical elements on board autonomy moving objects" in 2014. She has worked as an assistant at Department of Electrical Equipment and Automation of Industrial Installations since 2015. She worked as an Associate Professor at Department of Electromechanics of the same university since 2016. Her research interests are control of asynchronous electric drives, the use of alternative energy sources, and management of various technological processes using programmable logic controllers. She is the author of 54 scientific articles, and 14 publications.

The 18th International Conference on
"Technical and Physical Problems of Engineering"
30 October 2022
International Organization of IOTPE

ICTPE Conference
www.iotpe.com
ictpe@iotpe.com
ictpe0@gmail.com

ICTPE-2022 Number 22 Code 07TAP01 Pages 111-118

APPLICATION OF ARTIFICIAL INTELLIGENCE IN SATELLITE DATA PROCESSING PROGRESSES AND CHALLENGES

J.H. Huseynov [1] H.J. Huseynov [2] R.B. Rustamov [2]

1. Baku High School, Baku, Azerbaijan, jalil.h.huseynov@gmail.com
2. Institute of Physics, Azerbaijan National Academy of Sciences, Baku, Azerbaijan
huseyn-1978@mail.ru, r_rustamov@hotmail.com

Abstract- Today Artificial Intelligence (AI) takes a vital place in the space community, particularly in Machine Learning (ML), as significant segment of AI. It is important to note that ML algorithms find number of applications for instance in navigation systems, such sensitive area as satellite image processing, spacecraft technical condition monitoring and satellite constellations operational management. The fact is that a large number of surveys on the applications of AI in space technology applications can be classified into two categories.

- No doubt that the first category doesn't meet today requirements being able to satisfy demands of data processing. It relates such subjects as Deep Learning (DL) and bioinspired AI algorithms; and
- The second category is related to the detailed presentation of development and application of space technology of AI techniques or algorithms.

It is needed to be undertaken all limitations indicated above whose interests are related in platforms of space technology applications and existing challenges of AI. This paper has been covers a large area of review for the use of advances of the AI in a wide aspects of space technology applications. In the meantime, several AI algorithms also have been demonstrated as a tool for application as a way of diversification.

Keywords: Artificial Intelligence, Satellite Image, Satellite Image Processing, Machine Learning, Algorithms, Deep Learning.

1. INTRODUCTION

AI has started to be interesting instrument of use and application in space technology for the Earth monitoring and observation. It has been developed as called Information Processing Language (IPL-11) as the first AI application in language. The fact is that AI and Space Exploration were continued to develop as the independent directions of research activities with further being a part of rover project implementation. It is important to note that AI currently actively uses in satellite operations systems, particularly in operational support apparatus of satellite constellations and rovers [1]. Computer Vision (CV) techniques remain one of the important instruments in application of satellite imagery processing based on the use of AI in the space technology area.

AI more convenient in application of advances in space robotics as indicated below two main factors:

- Thanks to development of advance technology in hardware,
- Running sophisticated algorithms thanks to improvement of computational capacity being possible to process big volume of data [2].

For the time being one of the great problems in the space technology exploration is to use appropriate processing with appropriate capacity for achievement of expected results of data generated from space. From this point of view, it is required to clarify questions:

- AI helps to be useful of use of satellite data processing;
- Solving challenges of satellite data processing with AI.

There is a need to updating sources related to the modern technology application in space research and studies such as the Deep Learning (DL) impact, Machine Learning (ML) and facility of AI. It concerns to the specific areas of remote sensing as well as Fault Detection Isolation and Recovery (FDIR), and Earth space exploration.

It has been related to the planning and functions of the Anomaly Detection (AD) and FDIR [3, 4]. It is identified that ML including DL and RL takes today vital place as the main technological instrument [5]. There are number of publications dedicated to the Al application in the area of the Earth remote sensing [6]. It opens an advantage of satellite data processing and makes possible the use of Al facilities in improvement of capacity of analyzing performance multichannel imagery. For the time being development of achievement in DL opens a big opportunity for reaching out high performance of remote sensing data processing. It has been dedicating number of research scientific papers to the DL facilities in remote sensing method use. It makes possible to evaluate and assess current situation and point out aspects needed to be undertaken for improvement [8].

It is necessary to indicate that the use of AI with further integration into Deep Neural Networks (DNNs) takes perspective place for achievement of expected results in high accuracy demonstration [9]. The fact is

that these advances open an opportunity to take benefits from use of such technology being able to get intended outcomes in satellite data processing. It can be recorded by analyzing scientific papers related to the current stage of publications. This paper, contrastingly, surveys up to date technology use for data collection and processing. It is focused on existing challenges and progresses of modern technology on the platform of new approach of algorithms development for achievement a high accuracy data processing.

2. MACHINE LEARNING AND SATELLITE DATA PROCESSING

There is no doubt that Artificial intelligence (AI) takes important place for processing of satellite information received from the method of remote sensing. It finds excellent performance with a high advance level of processing stage. The fact is that huge number of satellites which provide huge of information demand automatization and fast processing of a big volume of data with high accuracy. All above indicated circumstances make necessary a new approach of technology achievements of remote sensing method. In accordance with this situation facilities of ML required to be used and improved with further integration into the DL in order to reduce of existing limitation in data processing. There is one aspect needed pointed out that satellite data processing has to be successfully integrated into ML and DL in order to achieve expected results.

As it has been mentioned early satellites for Earth observation provide convenient environment for a best presentation of data. It makes possible to take part successfully in decision stage of the process. The line of stages has demonstrated in Figure 1. It demonstrates opportunities to select each segment of the processes with duly monitoring which is highly important for achievement of high accuracy results and making right decisions. It can be reflected three main stages of primary applications for implementation of the processes:

- Data classification i.e., systematization of collected similar pixels);
- Data segmentation related to the image for segmentation of the data undertaking with areal feature; a
- The final stage is to assessment of processed image [3].

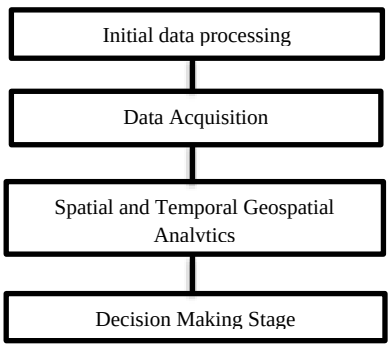

Figure 1. Satellite data processing stages

As it is the process of ML the next stage is to selection of learning algorithm with further trained data set which defines quality of data processing based on quality of trained data collection [10]. In conformity with this indication there is a highly need to control how correctly trained data is collected and selected. It demands to use methodology of unsupervised learning process for monitoring of condition of input data [11].

It is important to note that such approach of technology use makes possible to detect changes as well as monitoring of vegetation by use of land cover/land use methodology. No doubt that the list of application for similar use of technology can be enlarged which is needed to be considered in all the areas of application.

3. CLASSIFICATION OF SATELLITE IMAGE

The fact is that machine learning facility contents two categories:

- The first is supervised;
- The second is unsupervised.

It is necessary to mention that supervised category relates to the training data. In the other hand neural network [6] works and integrates successfully with satellite information as a convenient environment of spatial data processing. At the same time unsupervised learning opens environment for development and study of models for further classification of features of investigated objects.

The fact is that above indicated methods are working with spatial data. That means selected for investigation area is presented in the digital form for classification. For analyzing of situation there are identified for only selected application of the selected area for investigation covering all the period of time of analyzing process. Obviously in some applications, for instance climate change study indicated approach is becoming main tool for analyzing of processes.

It is necessary to point out that the change detection is one of the main aspects of application for definition and clarification of direction in data processing stage within the frame of the data processing time. Today one of the attractive instruments of space technology application is detecting any changes occurred in the monitored area. No doubt that it takes important place how effectively uses such technology for achievement high accuracy data processing. There are some approaches for effective use of methods in change detection case.

A multichannel imagery use for observation and detection of changes has been used with machine learning facilities for achievement of expected results [12]. For this purpose, has undertaken:

- Object correlation images (OCIs) method for change detection classification;
- Neighborhood correlation images (NCIs) method for change detection classification;
- No contextual features undertakings for change detection classification;
- NCI method use for change detection classification;
- bit format performance image information change detection classification.

As the traditional way of machine learning facility use has considered selection of tree as pone more instrument for efficient satellite data processing. It has been done comparison evaluation between the OCI and the NCI methods. At the same time change detection classification of the object-based category with incorporation of OCIs and the NCIs has demonstrated effective and high-performance accuracy which presents best application environment of change detection processes [13].

The use of change detection instrument in image transformation, rotation, or in any other correlations is indicating good results and performance [1]. Currently there are successfully other methods like neural networks and kernel methods are using for change detection as an important tool in Earth monitoring and observation processes.

4. KERNEL BASE EXTRACTION

The hyperspectral satellite images use is very complicated. The reason is a big volume of content of information. In the meantime, nonlinearity of the behavior of the data is another problem of use for the processing. No doubt that a big volume of content of information demands to spend a big time for data processing. In the meantime, existing band noises are the one more difficulty of use such information resources of data utilization. As far as obvious, modeling of the processes depends of the features of spectral wave range of the satellite data. the spectral bands represent the characteristics or features of the elements under consideration to model. There are number of approaches of selection of satellite image features. In this environment the use ML method in data processing can take priority place [15].

5. EXTRACTION ON THE BASE OF PURE PIXEL-BASED

An integration of image features of objects and materials discovered in the scene are defining by pixels of satellite images. It is necessary to extract automatically useful information from spectral bands being sure achievement expected accuracy of data processing. It can be developed by:

- Present of the NFINDER algorithm;
- Present of the VCA (vertex component algorithm);
- Present orthogonal subspace projection; and
- Present SVDD (support vector domain description) [1].

In order to achieve validation of processed data there is a need establishment relationship between processed and field data based on the models of prediction. It is common case to be sure of processed data how much reflects and merges actual condition of the process. It demands validation of the processing by use of ground measurements selected for sensitives areas. A comparison of both processing and field measurements are the sources for validation of conducted investigations. There are some weaknesses of parameters it is performed inaccurate results of data processing. Thanks to such circumstance it has discovered nonparametric and nonlinear regression techniques as it has called neural networks, support vector regression (SVR) [16], semi supervised SVM [17], relevance vector machines (RVM) [18], or Gaussian processes (GP) [19].

6. A NEW APPROACH

6.1. Learning Method

In order to extract nonlinear features of data it is necessary to use learning method. It covers a wide areas of computer science such as machine learning, image processing, etc. It opens opportunity to use and better select input data dividing into several lower dimensions of source which provides achievement better results of data processing. It is the way of performance for data visualization with high-dimensional. It makes possible to cover representation of data in a wide platform as a helpful tool for researches for overall data demonstration.

6.2. Manifold Learning

For manifold learning takes common position for selection and definition of data expected to be used for processing. It has been developed method for use of remote sensing data processing.

6.3. Remote Sensing

It is existing challenges to have updated land cover in order to be able to merge remote sensing data with selected for investigation area. For minimization of indicated problem impact into achievement of accurate data the methods NN and domain SVM (DASVM) can be used [1]. There is one more problem during classification of features on the land cover area is shifting of reference points selected spatial images. For solution this problem it has been decided to use kernel machines for minimizing of shifting impact of satellite images [20]. For the time being mainly uses by researches clustering margin system making successfully integrate land cover features.

6.4. Active Learning Method

It has been applied active learning method with selection of most relevant trained samples of ML. In general uses likelihood classification features with classification of object oriented [21]. The fact is that it is the same approach of use of active learning method for satellites with a high image resolution. It has been selected active learning approach with the computation of two stages classification based on trained data selection for achievement of a high accuracy data processing. It is important to mention that there is a big obstacles in selection information with a good quality making possible to use appropriate input data. In this case is most suitable way of problem solution is to consideration classification and localization methods. For this purpose, it has been proposed:

- Evaluation of the covertness of the objects and limitation of the frame; and
- Avoiding of stable detection from existing noises.

6.5. Multispectral Output Data

One more obstacle of classification, and prediction of data processing stage is using of multispectral output data. It faces with organized learning and trained data which can be helpful for prediction of process. A scaling of a big data takes a place effectively for multispectral image classification. It is efficiently work in hierarchical spectral image classification [22].

For minimizing above mentioned impact of negatively influencing into the methods of classification of satellite images can be achieved by use of the multilayer options. It can be useful for automatically protection signatures of trained data. In the other hand it is required to big memory tool architecture for data processing. For this reason, researchers have decided to select the areas which are easily would be applied as deep learning. It limits human impact and innervation for minimizing of features impacting to achieve expected results. At the same time, it opens an opportunity to receive reliable and best instrument for solving enough complicated tasks of classification within the satellite information processing stage.

6.6. Deep Learning

Deep learning contents is used in many layers. In general, it takes deep more than four or five with reflection of non-linear transformation. It is necessary to indicate that unsupervised behavior of learning format of the method makes significantly interesting instrument in particular in the field of remote sensing satellite data processing for Earth features observation classification. There is no doubt that Deep neural network (DNN) is the best methodology and instrument for satellite image classification opening the opportunity selection elimination of noises and data of synthetic aperture SAR [23].

Deep learning advances are using successfully for change detection with achievement of a high accuracy satellite data processing thanks to advances of the technology as it mentioned above circumstances.

6.7. Application of the Convolutional Neural Network (CNN)

No doubt that CNN is the network of the deep learning successfully using for data processing with high accuracy. The content of the CNN is:

- convolutional layer;
- nonlinear layer;
- pooling layer.

CNN operates based on transformation input data into output prediction throughout hierarchically recognition. There is some approaches for operation of CNN with formation of use of cascade analyses of the main component for study of filters with multilayer stages. It makes possible to induction and integration of layers for achievement of precise outcomes of processing [24]. The fact is that it has been considered use of CNN for classification of the hyperspectral images. In the meantime, supervised CNN has been undertaken for satellite image classification as one of the successful tools for these purposes.

There is limitation of common neural networks due to the ability of acceptance of input data only size of fixed vector and given output data for a fixed size vector. It makes possible to define only probability of classification. In the meantime, it is using fixed quantity of calculation steps in such of model, for instance quantity of layers in the model. It is important to mention that recurrent neural networks take unique place from the point of view of input sequences of vector, output as well as in many cases both of them. There are sources demonstrating a new approach of prediction of ocean and weather. Recurrent convolutional network is using for study of level in meteorological model of data processing. Such of system successfully works for tracking number of objects with existing circumstances [25].

It is necessary to point out that recursive neural network functions in the structure of hierarchy with opening an opportunity to achieve high results in the process of satellite data processing [25].

7. THE METHOD OF REMOTE SENSING

For the time being the method of remote sensing finds application for study of Earth features. It bases on information received from distance by use of air or satellite images. It makes possible to classify of electromagnetic wavelengths by means of specifically developed instruments for receiving and processing of data [26]. There is no doubt that this method has technological limitations during all the stage of applications. So, it takes to consider number of circumstances along all the processes starting from data collection with further image processing. Oner of the main obstacles of data achievement is noises during the use of remote sensing data gathering. It is important to use appropriate technology advances for minimizing such noises like clouds, devices impact and etc.

In the meantime, it is necessary to undertake challenges for transformation row data from remotely achieved systems. In this case DL can be successfully operate for limitation of transformation information problems by initially use of selection processes for reducing of data collection volume. It opens opportunity to consider needed for processing information.

7.1. Satellite Image Processing Systems Based on ML

There are always highly needs to improve data processing stage. It demands effective approach of processing in all line of the processes. For these purposes it has to be used algorithms for efficiently performing processing stage and visualization of the data for end users. In general, there are two algorithms are using for image interpretation as called Particle Swarm Optimization (PSO) and GA.

The fact is that for some reasons it happens loses of information makes limitation of effectively use such of interpretation system. How to solve existing problem? For location of this limitation, it is required to integrate variety of methods opportunities for minimizing of impact of negative consequences of data loses [27]. It has been suggested a new approach of development as called modified algorithm of evaluation for enhancement of brightness of image in stage of information interpretation.

7.2. Image Classification and Interpretation

As the general way it can be undertaken image classification and interpretation as processing each content of image pixels gathered remotely from any available sources such as air or satellite system. Parameters of representation use for classification of needed for processing data where is applying available known classified pixels. As general definition it calls as clusters.

There is a key advantage of the method. An s opportunity of the use of method is to application even in the case of no existing of sites. However, classification and identification of satellite images depends of the type if satellite images. It creates an environment for the next stage of data processing like reducing noises, segmentation which provides to achieve a best data processing. In general, the use of algorithms for classification and interpretation of images includes fuzzy algorithms. In this environment it can be achieved most sustainability of noises. Most probably the reason of such advantage is possible for a large number of turned parameters using for classification and interpretation.

7.3. Existing Problems of Remote Sensing

A challenge existing in satellite data processing have been undertaken in number of research works. It has been reflected a large of number reasons of image processing complexity such as satellite image size, no expected impact of factors, in some cases negative contribution of background of satellite data. In the meantime, different variation of satellite devices such as radiometric resolution, spectrum and spatial resolution of satellite as well as changing of observation point are contribution negatively for representation satellite information. This circumstance can be rejected by use of integrated of methods for minimization of contribution of each segment being able to achieve expected result in satellite data processing.

7.4. Data Volume

It is always common problem that the volume of satellite information is bigger than expert can be able to analyze and process for any pending needs. It is increasing more and more making important to find out solution of existing problem in satellite data processing for classification and interpretation. It demands to use CV methodology for possible effective solution of challenges of data processing. It is regrettable that up-to-date technology of AI is not optimized for satellite image.

For the time being there are variety of methods exist for satellite data classification and interpretation. But it is very difficult to find out method which could be acceptable for application for overall satellite information classification and interpretation. The fact is that SAR systems are successfully using as an alternative satellite information sources of remote sensing method. One more advantage of such system is no limitation existing in use of traditional optical sensors in remote sensing. There are a variety of colors and variations of texture opening a wide opportunity for visualization of data, making possible to observe a large-scale area within a day or at night at any weather condition no depending on condition of atmosphere. No doubt that SAR systems are demonstrating an advantage over existing traditional methods of remote sensing use it is also very complicated to apply easily of this system for satellite data classification and interpretation.

A circumstance of existing challenge needed to be solved and researchers have found a way of use advances of ML/DL methods for the SAR data. It has been dedicated application of DL for inversive task in visualization. It is demonstrated advantages and application of this approach in reconstruction of SAR system [28]. As an initial approach one layer of NN has used for study of features of SAR images. Nowadays, DL facility uses by different space technology communities as the perspective tool for satellite image classification and interpretation.

7.5. Image Classification and Interpretation Challenges

There are models for traditional satellite image processing operates on the statistical analyze:

- Linear Discriminant Analysis (LDA);
- Maximum Likelihood Estimation (MLE);
- PCA;
- Other regression-based models.

It is regrettable that many of traditional algorithms do not meet requirements and luck of logical system. In this case ML is very good tool for covering existing gap achieved based on dynamical progress into the traditional models. But there are also complexity and challenges due to the over complexity of calculation of the method of ML where required to be selected appropriate trained data. One more challenge is not sufficient data related to the ground truth data. In order to solve the problem, there is highly need limitation of trained data preparation. It can be achieved with help of noncontrolled method of training. At the same time accuracy of classification and interpretation controlled or in controlled can be improved with use of hybridization. In the parallel of this for data processing can be used for improvement of the speed of calculation with higher level processor ability [29].

The main challenges of statistical data are the permanent fluctuation of structures of data which makes ineffective in prediction of processing stage. From this point of view ML becomes very effective due to the experience during the process of trained data modeling of data classification and interpretation. This approach has been tested in some number research works and found best results and data validation of data classification and interpretation.

In conformity with comparative control of results conducted with use of data validation from appropriate reference data monitoring system it has been demonstrated that CNN application provides might accuracy outcomes as a whole then statistical data analyses and processing. Taking into account advantages of ML achieving prediction models hybridization different ML methods and integration of statistical

methods can be effectively contributed for achievement of expected results. It has been suggested combination of neuro and statistical algorithms in the simple phase of design in order to be able to select each of algorithms. Actually, each of them takes a vital place in solution fixed problem and no one of them evidenced as the best one for application.

At the same time for achievement best classification and interpretation of images of remote sensing is implementing combination of controlled an uncontrolled method of observation and pixel method. In the meantime, it integrates active method of training with reducing of fixed data for classification and interpretation.

8. SATELLITE DATA PROCESSING ALGORITHMS

There is standard requirement needed to be considered in algorithm accuracy and reliability which can be presented by evaluation performance of the system. It makes possible to discover advantages and weaknesses of algorithms. It opens an opportunity to develop spatial model of the investigated area with use of advances of remote sensing method with further geographical information system development. Evidence for assessment of algorithms is understanding of behavior during the work with different category of satellite images or support in assessment best parameters for different applications. For instance, digital elevation model (DEM) is one of the best instruments for study of natural disaster in particular river flood, coastal line change detection and many others [29].

There are number of technological possibilities which can be used for satellite image classification and interpretation. But it is complicated to find out common method for use of the all-satellite images as a whole. It depends of variety of colors and variation tessiture of satellite images. It is very difficult task to assist productivity of any algorithm in stage of image processing due to the diversity of nature of number of factors infusing to the productivity such as:

- algorithm itself;
- evaluation parameters of algorithm;
- algorithm evaluation method;
- algorithm performance nature of satellite images.

It has been studies and analyzed in number of scientific works different tips of metrics for assessment general efficiency of discussed methods of processing. [30, 31]. The fact is that for quantitate assessment indicated method is necessary to calculate some of parameters in order to be able to compare with existing methods to be sure of usefulness and reliability of application of selected method. It has been identified and analyzed four parameters of calculation such as:

- Index of Feature Similarity;
- Index of Structural Similarity;
- Accuracy;
- Call back

It is necessary to point out that Index of Feature Similarity and Index of Structural Similarity is needed to be considered in processing of images.

In this both stages are indicated features between input and final images. There are six typical indicators of effectiveness presented as below:

- Small features changes algorithm's response sensitivity indicator;
- Various condition capacity of algorithms;
- Reference performance for best algorithm accuracy;
- Image variability with integration of algorithm adaptability;
- Repeatability of data with use the same data and achievement of the result of algorithm presenting the reliability;
- Actual viability of the algorithm performing efficiency with regard time and space.

9. CONCLUSIONS

It is common approach of use of artificial intelligence with content of integration of neural network, deep learning, machine learning and any other algorithms make possible to use up to date computer technology with highly complexity of software development. In conformity with use of traditional methods it can be effectively and simple achievement of data processing. There is a big obstacle to use existing technology of satellite image processing are facing number of problems to meet requirements of data processing. It demands to consider application of deep learning methods as well as big data technology. In the other hand it makes necessary to undertake of problem solution of big data processing including archiving of satellite row data and its classification and interpretation.

It has been reviewed big number of AI algorithms where achievements are using for solving of number of problems. It is successful platform for processing of satellite images. There are number of limitations as type of data, detectors systems, and many others building negative environment of best use of processing. It is needed to find out common platform being use without any limitations and can be process data with partially or no participation of human. An extension of machine learning and deep learning capacity for technology of a big data in integration of cloud calculations still not clear for application and needed to be enhanced of knowledge and capability in use of up-to-date technology for satellite image classification and interpretation.

REFERENCES

[1] R. Alami, R. Chatila, S. Fleury, M. Ghallab, F. Ingrand, "An Architecture for Autonomy", The International Journal of Robotics Research, Vol. 17, 04 Januar 1998;

[2] L. Quan, Z.X. She, L. Peng, L. Shaomin, "Anomaly Detection and Fault Diagnosis Technology of Spacecraft Based on Telemetry-Mining", The 3rd International Symposium on Systems and Control in Aeronautics and Astronautics, No. 8, Vol. 10, pp. 233-236, 2010.

[3] S. Ibrahim, A. Ahmed, M. Zeidan, I. Ziedan, "Machine Learning Techniques for Satellite Fault Diagnosis", Ain Shams Engineering Journal, Vol. 11, No. 1, pp. 45-56, 2019.

[4] A. Guiotto, A. Martelli, C. Paccagnini, "SMART-FDIR: Use of Artificial Intelligence in the implementation of a Satellite FDIR", European Space Agency, (Special Publication) ESA SP, Vol. 532, p. 71, January 2003.
[5] A. Wander, R. Forstner, "Innovative Fault Detection, Isolation and Recovery On-Board Spacecraft, Study and Implementation Using Cognitive Automation", Conference on Control and Fault-Tolerant Systems (SysTol), pp. 336-341, Nice, France, October 2013.
[6] L. Lawal, C. Chatwin, "Optimization of Mass Volume Ratio of Spacecraft Structure for Advanced and High-Powered Communication Satellites", The 10th IEEE International Information and Telecommunication Technologies I2TS Conference, Vol. XX, pp. 1-30, Florianopolis, Brazil, 2011.
[7] G. Yu, Y. Tianshe, X. Nan, X. Minqiang, "Fault Detection and Diagnosis for Spacecraft using Principal Component Analysis and Support Vector Machines", The 7th IEEE Conference on Industrial Electronics and Applications (ICIEA), pp. 1984-1988, 18-20 July 2012.
[8] T. Yairi, N. Takeishi, T. Oda, Y. Nakajima, N. Nishimura, N. Takata, "A Data-Driven Health Monitoring Method for Satellite Housekeeping Data Based on Probabilistic Clustering and Dimensionality Reduction", IEEE Transactions on Aerospace and Electronic Systems, Vol. 53, No. 3, pp. 1384-1401, 2017.
[9] P. Robinson, M. Shirley, D. Fletcher, R. Alena, D. Duncavage, C. Lee, "Applying Model-Based Reasoning to the FDIR of the Command and Data Handling Subsystem of the International Space Station", Intelligent and Converged Networks, Issue 2, Vol. 3, pp. 213-244, 2003.
[10] M. Schwabacher, "Machine Learning for Rocket Propulsion Health Monitoring", The ninth ACM SIGKDD International Conference on Knowledge Discovery and Data Mining, Vol. 10, No. 03, pp. 8-24, 2005.
[11] A. Fijany, F. Vatan, A. Barrett, M. James, C. Williams, R. Mackey, "A Novel Model-Based Diagnosis Engine: Theory and Applications", IEEE Aerospace Conference Proceedings, Vol. 2, No. 3, pp. 2901-2910, 2005.
[12] D. Iverson, "Data Mining Applications for Space Mission Operations System Health Monitoring", Computer Engineer, Vol. 05, No. 12, pp. 2008-3212, 2008.
[13] K. Hundman, V. Constantinou, C. Laporte, I. Colwell, T. Soderstrom, "Detecting Spacecraft Anomalies Using LSTMs and Nonparametric Dynamic Thresholding", Manuscript submitted to ACM, pp. 1-21, 2018.
[14] J. Cervantes, F. Garcia Lamont, L. Rodriguez Mazahua, A. Lopez, "A Comprehensive Survey on Support Vector Machine Classification: Applications, Challenges and Trends", Neurocomputing, Vol. 408, pp. 189-215, September 2020.
[15] S. Taburoglu, "A Survey on Anomaly Detection and Diagnosis Problem in the Space System Operation", Journal of Intelligent Systems Theory and Applications, Vol. 2, No. 1, p. 13-17, 2019.
[16] T. Yairi, N. Takeishi, T. Oda, Y. Nakajima, N. Nishimura, N. Takata, "A Data-Driven Health Monitoring Method for Satellite Housekeeping Data Based on Probabilistic Clustering and Dimensionality Reduction", The IEEE Transactions on Aerospace and Electronic Systems, Vol. 53, No. 3, pp. 1384-1401, 2017.
[17] J. Tian, D. Chen, "Evaluating Satellite-Based Measurements for Mapping Air Quality in Ontario, Canada", Journal of Environmental Informatics, Vol. 10, pp. 30-36, 2017.
[18] F. Padula, J. MacDonough, D. Bondy, M. Cook, "Automated Supervised Land Use Classification and Change Detection: An Image Fusion-Based Approach", The IEEE International Geoscience and Remote Sensing Symposium, pp. 335-338, 25-30 July 2010.
[19] R.J. Aroma, K. Raimond, "A Review on Availability of Remote Sensing Data", The IEEE Technological Innovation in ICT for Agriculture and Rural Development (TIAR), pp. 150-155, 10-12 July 2015.
[20] V. Komissarov, "AI Applications for Satellite Imagery and Satellite Data", Emerj Artificial Intelligence Research, May 17, 2020.
[21] C. Schwegmann, W. Kleynhans, B. Salmon, "The Development of Deep Learning in Synthetic Aperture Radar Imagery", International Workshop on Remote Sensing with Intelligent Processing (RSIP), pp. 1-2, 18-21 May 2017.
[22] C. Schwegmann, W. Kleynhans, B. Salmon, "Manifold Adaptation for Constant False Alarm Rate Ship Detection in South African Oceans", The IEEE Journal of Selected Topics in Applied Earth Observations and Remote Sensing, Vol. 8, No. 7, pp. 3329-3337, 2015.
[23] D.R. Sowmya, P. Deepa, K. Venugopal, "Remote Sensing Satellite Image Processing Techniques for Image Classification: A Comprehensive Survey", International Journal of Computer Applications, Vol. 161, pp. 24-37, 2017.
[24] A. Schmidt, F. Lafarge, C. Brenner, F. Rottensteiner, C. Heipke, "Forest Point Processes for the Automatic Extraction of Networks in Raster Data", The ISPRS Journal of Photogrammetry and Remote Sensing, Vol. 126, pp. 38-55, 2017.
[25] J. Jeppesen, R. Jacobsen, F. Inceoglu, T. Toftegaard, "A Cloud Detection Algorithm for Satellite Imagery Based on Deep Learning", Remote Sensing of Environment, Vol. 229, pp. 247-259, 2019.
[26] R. Navalgund, P. Roy, "Remote Sensing Applications: An Overview", Current Science, Vol. 93, pp. 12-25, 2007.
[27] A. Asokan, J. Anitha, "Machine Learning Based Image Processing Techniques for Satellite Image Analysis -A Survey", International Conference on Machine Learning Big Data Cloud and Parallel Computing, pp. 119-124, 14-16 February 2019.
[28] S. Suresh, S. Lal, "Modified Differential Evolution Algorithm for Contrast and Brightness Enhancement of Satellite Images", Applied Soft Computing, Vol. 61, p. 622, 2017.

[29] W. Chen, Z. Jia, J. Yang, N.K. Kasabov, "Multispectral Image Enhancement Based on the Dark Channel Prior and Bilateral Fractional Differential Model", Journal Remote Sensing, Vol, 14, Issue 1, p. 1-25, 2022.
[30] M. Tipaldi, B. Bruenjes, "Survey on Fault Detection, Isolation, and Recovery Strategies in the Space Domain", Journal of Aerospace Information Systems, Vol. 12, No. 02, pp. 1-22, 2015.
[31] D. Atkinson, M. James, R. Martin, "SHARP - Automated Monitoring of Spacecraft Health and Status", IEEE, Vol. 02, No. 01, pp.1-6, 1990.

BIOGRAPHIES

Jalil H. Huseynov was born in Baku, Azerbaijan on March 15, 2006. Currently, he is a 10th high school student of Physics-Mathematical and Information Technology Lyceum. He has demonstrated outstanding achievements during his graduation as: The 3rd National subject contests - Silver medal, The 4th National subject contests - Gold medal, The 3rd Lofti Zadeh inter-schoolchildren logic Olympiad (2018) - Gold medal, American Mathematics Competition (2019) - The first place, National subject Olympiad (2020) - Bronze medal, The 24th Junior Balkan Mathematical Olympiad (2020) - Bronze medal, The 6th Caucasus mathematical Olympiad (2021) - Gold medal, National subject Olympiad (2021) - Gold medal, The 25th Junior Balkan Mathematical Olympiad (2021) - Gold medal, American Mathematics Competition 10 (2021) - The first place, The 1st International Lofti Zadeh Olympiad (2021) - Silver medal, The 18th International Zhautykov Olympiad (2022) - Bronze medal, International STEM Olympiad (2022) - Digital Silver medal, "European Mathematical Cup" (2022) - The second prize.

Huseyn J. Huseynov was born in Azerbaijan on December 20, 1978. He has received the B.Sc. and M.Sc. degrees from Department of Power Engineering, Azerbaijan State Oil Academy, and Baku, Azerbaijan in 1999 and 2002, respectively. Currently, he is a Scientific Researcher at the Laboratory of High Voltage Physics and Engineering, Institute of Physics, Azerbaijan National Academy of Sciences, Baku, Azerbaijan. His areas of expertise are in various types of heaters, including industrial carbon, butyl rubber, electric heater and clean water.

Rustam B. Rustamov was born in 1955, Ali-Bayramli district, Azerbaijan. is an independent expert on Space Science and Technology. In the past, he was in charging of the Azerbaijan National Aerospace Agency activities as an Acting Director General. He has mainly specialized in space instrumentation and remote sensing and GIS technology. Rustam B. Rustamov has graduated Ph.D. at the Russian Physical-Technical Institute, S. Petersburg, Russia. He was invited for the work at the European Space Agency within the Framework of the United Nations Program on Space Applications at the European Space Research and Technology Center, The Netherlands. Rustam B. Rustamov has appointed for the United Nations Office for Outer Space Affairs Action Teams (member, Vienna, Austria), United Nations Economical and Social Commission for Asia and the Pacific (national focal point, Thailand), International Astronautically Federation (Federation's contact, Paris, France), Resent Advances in Space Technologies International Conference Program Committee (member, Turkey). He is an author of 18 books published by the European and United States famous publishers and more than 135 scientific papers.

The 18th International Conference on
"Technical and Physical Problems of Engineering"
30 October 2022
International Organization of IOTPE

ICTPE Conference
www.iotpe.com
ictpe@iotpe.com
ictpe0@gmail.com

ICTPE-2022 Number 23 Code 07TAP02 Pages 119-123

APPLICATION OF EMISSION SPECTRA TO STUDY CHARACTERISTICS OF A BARRIER DISCHARGE

S.V. Rzayeva N.A. Ganiyeva

Department of Electromechanics, Faculty of Engineering, Azerbaijan State Oil and Industry University, Baku, Azerbaijan, sona.rzayeva@asoiu.edu.az, nigar.atakisiyeva75@mail.ru

Abstract- In this article, studies of the emission spectra of a pulsed barrier discharge in an air-water medium are considered. The main short-lived active particles formed in the plasma discharge were determined and its main characteristics were evaluated. The purpose of this work is to identify the main short-lived particles formed during the electric discharge treatment of water, as well as to estimate the discharge parameters by the method of emission spectroscopy. The results obtained can be directly used to elucidate the processes occurring in an electric discharge, and also as initial data in mathematical modeling of the physical pattern and chemical transformations in a barrier discharge.

Keywords: Water-Air Environment, Emission Spectrum, Spectral Region, Emission Bands, Micro Discharge.

1. INTRODUCTION

Electric discharge is widely used for the production of ozone in water purification technologies [1]. An increase in the efficiency of water purification compared to traditional ozonation is possible with the combined use of ozone and other active particles, as well as ultraviolet radiation generated in the discharge. From this standpoint, the discharge in moist air and water-air environment is of interest. In this case, the products of electric discharge treatment are ozone, hydrogen peroxide, and various kinds of radicals: OH, $O(^3P)$, $O(^1D)$, $O_2(b^1\Sigma_g^+)$, O_2^+, O^-, nitrogen-containing, and some other particles [2-5]. Under the influence of active particles, most of the impurities contained in the water are oxidized. Organic substances are oxidized up to complete mineralization (CO_2 and H_2O), or to the formation of less toxic products.

Studies by a number of authors [2-4] point to the possibility of increasing the efficiency of processing when switching to pulsed discharges. Thus, it was shown in [2] that a barrier discharge powered by nanosecond pulses has advantages in the purification of moist air from a number of organic impurities and ammonia, which is associated with a higher uniformity of this discharge. At the same time, it is noted that the active radicals formed during the processing have many times greater reactivity than ozone and ultraviolet radiation.

In [3], the effect of a pulsed corona discharge on aqueous solutions of phenol was considered. It is shown that in the case of a corona discharge above the water surface, the efficiency of electric discharge treatment is close to the efficiency of water ozonation. At the same time, the generated amount of ozone is significantly less than in the ozonation technology. The authors explain the high purification efficiency by the action of short-lived active particles, in particular, OH hydroxyl radicals. At the same time, it should be noted the relatively high complexity of installations based on a pulsed corona discharge and, accordingly, limited practical applicability.

One of the most promising and practically easy to implement electric discharge methods of water purification is the use of a pulsed barrier discharge in a water-air flow [4]. The installation, in which the principle of barrier discharge is implemented, has a high efficiency in water purification from organic impurities (in particular, phenol and trichloroethylene), as well as iron and manganese compounds, which are often found in groundwater. At the same time, the flow mechanism and the main acting factors of the discharge in a water-air medium have not been sufficiently studied due to the high degree of non-equilibrium of the discharge plasma, as well as high rate of elementary processes in discharge.

2. EXPERIMENTAL METHODOLOGY

It is known that a barrier discharge is a discharge in a gas that occurs under the influence of a voltage applied to the electrodes, if at least one of the electrodes is covered with a dielectric [5]. In such a discharge, charge transfer occurs in separate channels, called micro discharges, which are distributed over the entire volume of the interelectrode gap.

The discrete structure of the barrier discharge and the short lifetime of the discharge products make it difficult to study the main processes in the discharge plasma. One of the main research methods in this case is the spectral method. The study of the spectra of the barrier discharge is complicated by the low intensity of the glow, as well as the significant non-stationarity of the discharge when water drops are introduced into the discharge gap.

Therefore, a much smaller number of works are devoted to the study of radiation in this type of discharge than, for example, to spectral studies of a glow discharge or arc.

The measurements were carried out by the method of emission spectroscopy. The method of emission spectroscopy can provide not only reliable information on the presence of particles, for which the discharge energy is sufficient, but also allows one to estimate a number of the most important plasma parameters, such as the average electron energy, plasma temperature, and electric field strength.

2.1. Installation for the Study of Emission Spectra

The scheme of the discharge chamber used in the experiments is shown in Figure 1a. Water was sprayed into drops about 3 mm in diameter and fed to the electrode system. The discharge was created between wire electrodes 2 mm in diameter enclosed in quartz glass tubes with a wall thickness of 1.5 mm (Figure 1b). The width of the air gap between them was 3 mm. Air was pumped through the electrode system in the direction opposite to the water flow at a rate of 5-10 l/min. A quartz window was used to observe discharge radiation.

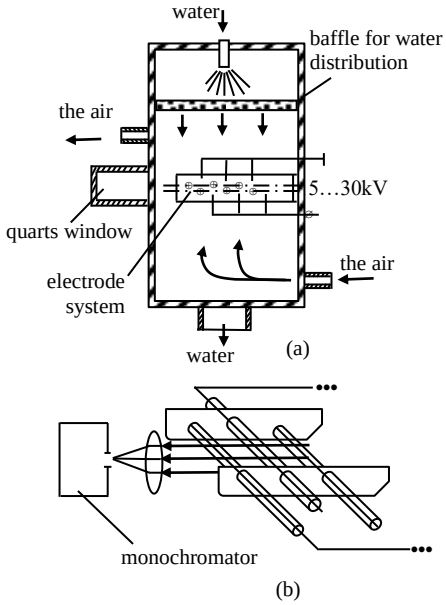

Figure 1. (a) Discharge chamber for observing the spectral characteristics of the discharge, and (b) the design of the electrode system used in the experiments

The emission spectra were recorded using an MDR-2 monochromator (Figure 2a). To record the spectra, photoelectronic multipliers tubes (PEMs) were used, the sensitivity range of which lies in the band from 200 to 650 nm and from 400 to 800 nm. Before the experiments, the PEM was calibrated using reference radiation sources. The PMT signal was amplified by a V6-9 selective amplifier and fed to the input of a storage oscilloscope (C9-8, Tektronix TDS-220). Thus, the setup made it possible to study the radiation spectrum of the barrier discharge in the wave lengths range (200-800 nm).

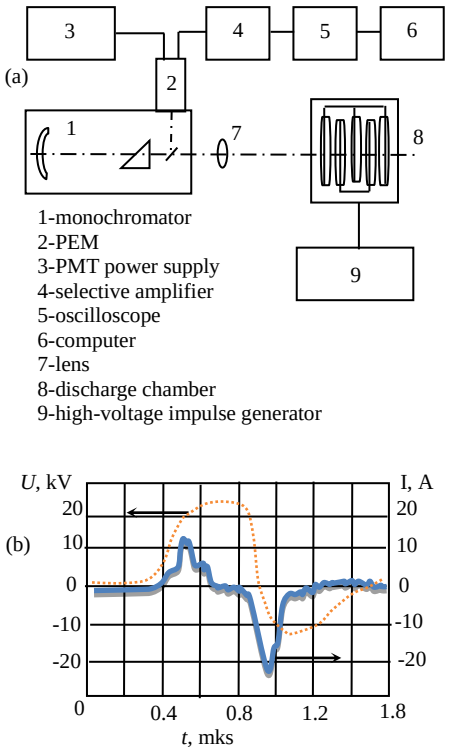

Figure 2. (a) Installation scheme for observing the spectral characteristics of the discharge, and (b) oscillograms of the current and voltage in the discharge

To power the electrode system, we used a nanosecond pulse generator consisting of a low-voltage thyristor unit and high-voltage magnetic compression links that form the output pulse [6]. The output capacitance of the generator was 150 pF. A pulsed voltage with an amplitude of 15-30 kV, a pulse duration of 500...600 ns, and a repetition rate of 1 kHz was applied to the electrodes. In the experiments, the electrical parameters of the installation were controlled - current, voltage, and output power. Measurements were made using a resistive divider, a low inductance current shunt, and a Tektronix TDS220 oscilloscope with up to 100 MHz bandwidth. Figure 2(b) shows the I and U waveforms on the electrode system.

The oscillograms were used to determine the barrier discharge ignition voltage, which was about 16.5 kV for the electrode system used in the experiments. At this voltage, the appearance of appreciable ozone concentrations at the output of the setup was recorded, and the glow of the discharge gap also arose. When the discharge ignition voltage was reached, the current in the circuit increased sharply. The energy input into the discharge gap at a voltage U=25 kV, calculated by integrating current and voltage oscillograms, was 45 mJ/pulse.

3. RESULTS

The barrier discharge in dry air and in air saturated with water vapor consisted of many micro discharges. The introduction of water drops led to a noticeable change in the electrical characteristics of the system: a decrease in the discharge ignition voltage, as well as an increase in the discharge current within 20%.

The emission spectrum of the barrier discharge plasma was studied in the wave lengths range (200...800 nm). Figure 3 shows the discharge spectrum in a water-air environment at atmospheric pressure.

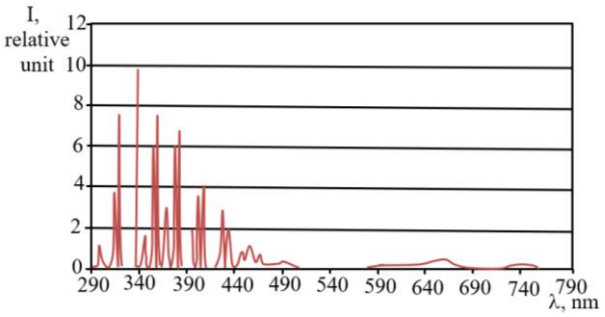

Figure 3. Emission spectrum of the air/water system in a barrier discharge

It can be seen from the Figure that the largest number of emission bands of different intensities lies in the wavelength region from 290 to 460 nm. In the region of the spectrum where the wave length is 500...800 nm, broad low-intensity emission bands are recorded. Spectral region 280...320 nm. In this region of the spectrum, three broad emission bands are recorded with maxima at 297.5 nm, 313.75 nm, and 316.0 nm (Figures 3 and 4). Mathematical processing of the spectra revealed the presence of a fine structure of the emission bands. So, in the wavelength range of 292-299 nm, 4 bands are visible with maxima at 292.5, 293.5, 296.25 and 297.5 nm (Figure 4), and in the wavelength range of 310...316 nm, 5 emission bands - 310.8, 312.3, 313.4, 315.5, 316 nm. Of these bands, only the 313.7 and 316.0 nm lines are narrow.

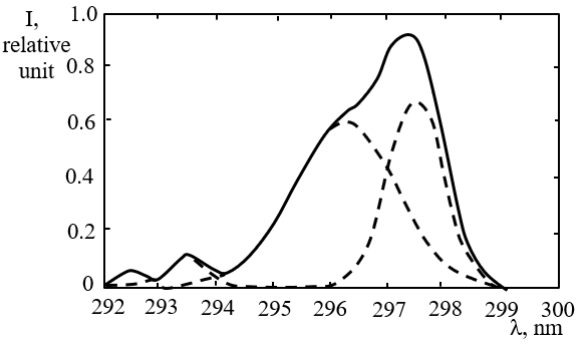

Figure 4. Emission spectrum of OH-radicals. Experimental observations (—) and results of mathematical processing (- -)

According to the literature data [7], the studied regions contain emission lines of OH radicals, as well as electronic-vibrational transitions of the molecular nitrogen of the 2^+ system. The broad emission bands are responsible for the electronic-vibrational transitions OH (A-X; 0-0). 310.8 nm OH (A-X; 0-0); 312.3 nm OH (A-X; 0-0); 315.5 nm OH (A-X; 1-1) and 296.25 nm OH (A-X; 1-0), 294.00 nm OH (A-X; 2-0), 292.5 nm OH (A-X; 2-0) [13]. The bands we studied, which are responsible for the hydroxyl radical (OH), are significantly shifted to the region of spectral long waves. The authors of [8], in a He/H_2O mixture in the study of glow discharge plasma, found a similar shift of OH-radical emission lines to the long-wavelength region and explained this by the presence of cluster molecules $(OH)_n^*$, which are formed when two or more OH radicals collide. One of the OH radicals is in an excited state. The presence of hydroxyl radicals of the barrier discharge is also confirmed by a weak band in the region of 660-670 nm.

The intensity of these emission bands increases as the concentration of water vapor in the air increases. At a humidity of 60%, saturation occurs, which is consistent with the results obtained in [9]. At the same time, the intensity of the band is directly proportional to the current density and increases without saturation. This behavior indirectly indicates that the formation of OH radicals can occur due to direct electronic processes of water excitation [10]:

$$e + H_2O \rightarrow e + H + OH,\ \varepsilon \geq 5.1\ \text{eV}$$

and/or by transferring the excitation of the excited oxygen atom $O(^1D)$ to water (2.3) [10]:

$$O_2 + e \rightarrow O\left(^1D\right) + O\left(^3P\right),\ \varepsilon \geq 6\ \text{eV}$$

$$O\left(^1D\right) + H_2O \rightarrow 2OH$$

The wavelength range is 320-600 nm. As can be seen from Figure 3, in this region of the spectrum, a number of intense emission lines are observed, which belong to the electronic-vibrational transitions N_2. In the emission spectra of the discharge, the band of molecular nitrogen 337.1 nm of the 2^+ system of nitrogen is well identified: the transition $N_2\left(C^3\Pi_u, v\right) \rightarrow N_2\left(B^3\Pi_g, v\right)$, as well as the bands of the 2^+ system of nitrogen N_2 (λ=380.75 nm and 400.25 nm).

When the voltage on the electrodes is increased to 23 kV, a weak nitrogen ion line appears (1^-- nitrogen system: transition $N_2^+\left(B^2\Sigma_u^+, v\right) \rightarrow N_2^+\left(X^2\Sigma_g^+, v\right)$ $\lambda = 391.4\,\text{nm}$, but its intensity is approximately 100 times less than the linear 337.1 nm. At voltages on the electrodes above 26 kV, weak emission bands appear in the wavelength region of 236.3 and 237.0 nm, which are related to electronically excited NO molecules (transition $0 \rightarrow 1$ of the γ- system of nitric oxide). In the spectral region 425-490 nm, several lines of low intensity are observed. It is not possible to identify all the lines, however, we believe that the weak bands at 434.0 nm and 486.1 nm are responsible for the emission of hydrogen atoms of series H_γ and H_β, respectively.

4. DISCUSSION OF RESULTS

Excitation of nitrogen. Of particular interest are the emission bands $N_2(C^3\Pi_u \rightarrow B^3\Pi_g)$ and $N_2^+\left(B^2\Sigma_u^+ \rightarrow X^2\Sigma_g^+\right)$. From the emission spectrum of the barrier discharge (Figure 3) that these emission lines do not overlap with each other, and the electron energies required to generate particles $N_2(C^3\Pi_u)$ and

$N_2^+\left(B^2\Sigma_u^+\right)$ are different and amount to 11.0 and 18.7 eV, respectively. Due to the large difference in the energies of the electrons required for the formation of these particles, the ratio of intensity $I\left(N_2^+\right)/I\left(N_2\right)$ depends significantly on the average electron energy in the discharge and electric field intensity and can be used to calculate these parameters [11, 12]. Using the dependences proposed by the authors [11], we estimated the electric field strength and the average electron energy, which amounted to about 100 kV/sm and 6 eV, respectively, which is an order of magnitude higher than the breakdown voltages during a discharge in air at atmospheric pressure.

In our case, when a voltage with an amplitude of 20 kV or less was applied to the electrodes, the emission band at 391.4 nm was not recorded. Considering that an energy of 18.7 eV is required to excite $N_2^+\left(B^2\Sigma_u^+\right)$, it can be assumed that there are no electrons with such an energy in the plasma. This allows you to determine the requirements for the supply voltage to reduce the production of nitrogen oxides in water treatment process.

Estimation of temperature of gas molecules. The average gas temperature in the discharge chamber, measured with a thermometer, was 300±1 K, which is 2–3 degrees higher than the air temperature at the installation inlet. Measuring the local gas temperature in the discharge gap is a more serious problem. The exact value of the temperature of heavy particles in the discharge can be determined from the rotational temperature of the state $N_2(C^3\Pi_{u\,v=0})$ with a wavelength λ=337.1 nm [5]. The small width of this line indirectly indicates a low plasma temperature, which practically does not differ much from 300K. Estimates have shown that the plasma temperature does not exceed 350 K. This value, apparently, corresponds to the plasma temperature inside the micro discharge. Determination of dissociation constants of possible oxygen decomposition reactions. Using the obtained values of the $E_{\max}$ in the discharge gap $E\approx$100 kV/sm, the rate constants of molecular oxygen dissociation were determined by expressions [10]:

$$O_2 + e = O\left(^3P\right) + O\left(^3P\right) + e$$

$$O_2 + e = O\left(^3P\right) + O\left(^1D\right) + e$$

$$O_2 + e = O\left(^3P\right) + O\left(^1S\right) + e$$

$$lgk = -7.9 - 13.4/E$$

$$lgk = -8.0 - 16.9/E$$

$$lgk = -8.8 - 11.9/E$$

$$k = 1.13\times10^{-8}\ \text{cm}^3\text{s}^{-1}$$

$$k = 8.78\times10^{-9}\ \text{cm}^3\text{s}^{-1}$$

$$k = 1.45\times10^{-9}\ \text{cm}^3\text{s}^{-1}$$

The results obtained are in good agreement with the corresponding reaction constants given in the literature [5]. Using *k*, one can determine the oxygen dissociation rate [10]:

$$v_{dis} = [O_2]n_e k = 6\times10^{18}\times2\times10^{7}\times1.13\times10^{-8} = 1.32\times10^{18}\ \text{cm}^{-3}\text{s}^{-1}$$

In this case, the lifetime of excited oxygen atoms lies within 10^{-4} s. The resulting atomic oxygen interacts with impurity particles and molecules of the surrounding gas. According to [1], the main ways of spending atomic oxygen in the absence of impurities are determined by the following expressions [1]:

$$O + O_2 + M \rightarrow O_3 + M,\ k = 5.4\times10^{-34}\ \text{cm}^6\text{s}^{-1}$$

$$O + OH \rightarrow H + O_2,\ k = 3.232\times10^{-11}\ \text{cm}^6\text{s}^{-1}$$

$$O + HO_2 \rightarrow OH + O_2,\ k = 5.69\times10^{-11}\ \text{cm}^6\text{s}^{-1}$$

$$O\left(^1D\right) + H_2O \rightarrow 2OH,\ k = 3.5\times10^{-10}\ \text{cm}^3\text{s}^{-1}$$

$$O\left(^1D\right) + O_3 \rightarrow 2O_2,\ k = 2.5\times10^{-10}\ \text{cm}^3\text{s}^{-1}$$

$$O + O_3 \rightarrow 2O_2,\ k = 8.9\times10^{-15}\ \text{cm}^3\text{s}^{-1}$$

$$O\left(^3P\right) + O_3 \rightarrow 2O_2,\ k = 8.0\times10^{-15}\ \text{cm}^3\text{s}^{-1}$$

The results obtained when considering the mechanism of chemical processes, taking into account the above reactions, can later be used in modeling the processes of water purification in a barrier discharge plasma. An adequate description of the mechanism of water purification requires knowledge of the main characteristics of the discharge, as well as taking into account all the main reactions occurring in the discharge gap. Obviously, spectral studies and theoretical modeling should be confirmed by chemical studies of the initial and final products of electric discharge processing. Therefore, they should be considered in combination with other methods for studying the processes occurring during water purification in a pulsed discharge.

5. CONCLUSION

1) Investigations of the emission spectrum of a pulsed barrier discharge in an air-water medium were carried out. It is shown that the main primary products of the action of a nanosecond pulsed barrier discharge on an air-water mixture, according to emission spectroscopy data, are OH radicals and excited oxygen atoms.

2) Based on the emission spectra of a barrier discharge in an air-water medium the electric field strength and the average energy of accelerated electrons are estimated, which are 100 kV/cm and 6 eV, as well as the temperature of molecules and ions in the discharge, which turned out to be close to 300 K.

3) The average energy of electrons in the discharge under study is below the threshold energy necessary for excitation of elementary reactions of formation of nitrogen oxides. Therefore, when treating water in a pulsed barrier discharge at voltages below 26 kV, nitrogen-containing products are absent.

REFERENCES

[1] V.V. Lunin, M.P. Popovich, S.N. Tkachenko, "Physical Chemistry of Ozone", Textbook, MGU, p. 480, Moscow, Russia, 1998.

[2] V.M. Zlatopolsky, T.S. Smolenskaya, "Transformation of Organic Compounds in Barrier

Discharge Plasma", Khnmiya High Energy, Vol. 30, No. 3, pp. 211-213, Moscow, Russia, 1996.
[3] W.F.L.M. Hoeben, "Pulsed Corona-Induced DEGRADATION of Organic Materials in Water", Ph.D. Thesis, Technical University Eindhoven, p. 164, Netherlands, 2000.
[4] S.G. Boev, V.M. Muratov, N.P. Polyakov, N.A. Yavorovsky, "Patent 2136600 RF MKI^6 C02F 1/46, 7/00, Reactor and Method of Water Purification", Bull., No. 23, p. 4, Moscow, Russia, 1999.
[5] V.I. Samoylovich, K.V. Gibalov, V.K. Kozlov, Russ. "Physical Chemistry of Barrier Discharge", Moscow State University, p. 176, Moscow, Russia, 1989.
[6] N.A. Yavorovsky, S.S. Peltsman, M.V. Khaskelberg, J.I. Komev, "Pulsed Bapiei Discharge Application for Water Treatment", International Conference of Pulsed Power Applications, pp. 192-198, Gelsenkirchen, Germany, 2001.
[7] A.R. Striganov, G.A. Odintsova, "Tables of Spectral Lines of Atoms and Ions", Energoatomizdat, Reference Book, p. 280, 1982.
[8] A.K. Shuaibov, L.L. Dashchenko, I.V. Shevera, "Optical Characteristics of Glow Discharge Plasma in He/H_2O Mixture", Plasma Phys., Vol. 27, No. 10, pp. 931-954, Moscow, Russia, 2001.
[9] D.N. Shin, C.W. Park, J.W. Hahn, "Detection of OH(A_2S^+) and O(^{1}D) Emission Spectrum Generated in a Pulsed Corona Plasma", Vol. 21, No. 2, pp. 228-232, Korean, 2000.
[10] V.M. Zlatopolsky, "Mechanisms for the Transformation of Harmful Impurities in the Barrier Discharge Zone", Ecological Systems and Devices, No. 1, pp. 36-42, Moscow, Russia, 2000.
[11] Y.H. Kim, P.H. Hong, M.S. Cha, Y.Y. Song, S.J. Kim, "Measurements of Electron Energy by Emission Spectroscopy in Pulsed Corona and Dielectric Barrier Discharges", Non-Thermal Plasma Technology for Pollution Control (ISNPT-3), The 3rd International Symposium, pp. 142-146, Seogwipo-si, South Korea, 2001.
[12] Y.L. Creighton "Pulsed Positive Corona Discharges, Fundamental Study and Application to Flue Gas Treatment", Ph.D. Thesis, Technical University Eindhoven, p. 239, Netherlands, 1994.
[13] A.K. Shuaibov, L.L. Shimon, A.I. Dashchenko, I.V. Shevera, "Optical Characteristics of the Plasma of a Glow Discharge in a He/H_2O Mixture", Plasma Physics Reports, 2001.

BIOGRAPHIES

Sona Vagif Rzayeva was born in Baku, Azerbaijan on October 14, 1976. In 1994, she entered the Energy Department, Azerbaijan State of Oil and Industry University, Baku, Azerbaijan. She received her Bachelor's degree in 1998 and the Master's degree in 2006. Since 2003, she has been working at Department of Electromechanics, Azerbaijan State of Oil and Industry University. She is the author of 25 scientific papers, 2 of which are textbooks.

Nigar Akif Ganiyeva was born in Baku, Azerbaijan on November 19, 1975. In 1996, she entered Energy Department, Azerbaijan State University of Oil and Industry, Baku, Azerbaijan. She received her Bachelor's degree in 2000 and the Master's degree in 2015. Since 2000, she has been working at Department of Electromechanics, Azerbaijan State University of Oil and Industry. She is the author of 17 scientific papers.

The 18th International Conference on
"Technical and Physical Problems of Engineering"
30 October 2022
International Organization of IOTPE

ICTPE Conference
www.iotpe.com
ictpe@iotpe.com
ictpe0@gmail.com

ICTPE-2022 Number 24 Code 07TAP03 Pages 124-130

EXPERIMENTAL RESEARCHES OF THE RANDOM CUTS-CRACKS INFLUENCE TO DESTROY OF CYLINDRICAL SHELL UNDER EXPANSION

A.P. Dzyuba [1] P.A. Dzyuba [1] R.A. Iskanderov [2]

1. Oles Honchar Dnipro National University, Ukraine, dzb@ua.fm, avatarrr@ua.fm
2. Azerbaijan University of Architecture and Construction, Azerbaijan, r.iskanderov@gmail.com

Abstract- The results of an experimental researches of the destruction of circular cylindrical shells under loading by an axial tensile force, the lateral surface of which is damaged by random straight through cuts-cracks, are presented. The location coordinates and the angle of inclination of the cuts to the generatrix of the shell were chosen according to the law of uniform distribution of random variables. Dependences of breaking loads on the number of accidental damages are given. The features of constructing a finite element simulation of the stress state of a shell with a rectilinear through cuts of the side surface located at different angles to the generatrix of the shell are considered. The results are presented in the form of graphs and pictures of the shell destruction.

Keywords: Cylindrical Shells, Experimental Studies, Longitudinal Stretching, Destruction, Random Cross Cuts-Cracks.

1. INTRODUCTION

Researching the bearing capacity of power elements of shell structures and, in particular, cylindrical shells widely used in many branches of mechanical engineering, is one of the important tasks of mechanics. These tasks become especially difficult in the case of predicting the strength and stability of such objects in the presence of damage of various nature, in particular, holes, cutouts, surface and through cracks of the side surface, the appearance of which in the shell can be caused by a fairly wide range of external influences. The presence and accumulation of such stress concentrators of various origins leads to significant disturbances in the stress-strain state and is often the cause of the destruction of structures and buildings [1-6].

Theoretical research of the bearing capacity of such structural elements with stress concentrators is connected with the need to solve rather complex mathematical problems. Thus, the method of researching the stress-strain state in orthotropic shells of arbitrary Gaussian curvature with cuts, holes, and other stress concentrators, which was developed in works [7-9], is based on the use of the theory of generalized functions of the two-dimensional Fourier transform, the integral representation of displacements and internal force factors and fundamental solutions of the statics equations of shallow shells. The references [4, 5, 10] are devoted to the research of significantly nonlinear mathematical models of behavior, loss of stability, and destruction of thin-walled shells with holes and cracks. Asymptotic research methods in the nonlinear mechanics of the destruction of bodies with cracks are used in [11].

The research of the stress-strain state in shells near holes, cracks, or cuts, as well as the behavior of the crack itself, its influence on the stress state, loss of stability of thin-walled structural elements, and subsequent destruction in the crack zone are presented in articles [2, 3, 12, 13]. The processes of damage accumulation in structural elements were studied in [14, 15], and the maximum permissible defects were studied in [16, 17]. Works [10, 18] are devoted to the experimental study of the behavior and load-bearing capacity of shell structures with damage in the form of through holes of various shapes under longitudinal tension, internal pressure, bending, and combined loading, and [19] to the torsional stability of cylindrical shells with a system of circular holes. Engineering methods for calculating structural elements with cracks within the framework of linear fracture mechanics are summarized in [6].

The complexity of the task of researching the load-bearing capacity of thin-walled shell elements increases significantly when the size and location of damage, in particular, in the form of circular holes or through cracks, is random, and the amount of damage accumulates during operation. One of these problems is the problem of predicting the strength of shells with randomly located cracks under axial expand tensile force loading.

The presented article is devoted to conducting an experimental study of the process of destruction of circular cylindrical shells loaded with an axial tensile force, weakened by a different number of rectilinear cross-sections, the coordinates of the location and the angle of inclination of which to the generatrix shell are random values, with the aim of obtaining results that could provide reliable real information about the behavior and the value of the bearing capacity of the shell structure under the conditions of damage accumulation and would serve as a reliable scientific and methodological basis for the development of adequate calculation schemes and corresponding theoretical calculation methods.

2. PREPARING MODELS AND EXPERIMENT TECHNOLOGY

When conducting experimental studies, the problem of manufacturing high-tech, nominally identical, high-quality models of shells is one of the most important for reducing the dispersion of experimental results. Models should be such that the difference in critical loads for different nominally identical samples is smaller than the difference associated with a change in the studied parameter [20]. Moreover, taking into account the random nature of the location of the damage, the statistical number of tested models should be quite significant. It is obvious that this requires a reduction in labor costs and the cost of manufacturing technology of nominally identical models.

In the presented article, special paper was used for the mass production of models of cylindrical shells. For the first time, the possibility of effectively using paper to study the behavior of thin-walled shells was shown in [21], and later in [22]. The rationale and results of an extensive approbation of the effective use of paper as a material for manufacturing shell models intended for experimental research are given in [19]. The main mechanical characteristics of the selected orthotropic material of the models were determined according to the results of the "σ-ε" diagrams of separate specially conducted experiments of tensile tests of samples and are: modulus of elasticity $E_x = 6.9\times10^3$ MPa, $E_y = 3.45\times10^3$ MPa, Poisson's ratios $\nu_x = 0.3$; $\nu_y = 0.15$ (here the indices x, y correspond to the main directions of orthotropy of the paper sheet). Sheet thickness $h = 0.23\times10^{-3}$ m.

As shown by experimental studies of mechanical properties, for the specified material, the ratio of the conditional yield strength σ_T to the modulus of elasticity E_x in the longitudinal direction is $\sigma_T/E_x \approx 3.6\times10^{-3}$. Of the sheet metals, this parameter is of the greatest importance for the thin tempered stainless steel of the X18H9H brand, which is widely used in experimental studies, for which $\sigma_T/E \approx 4.0\text{-}4.5\times10^{-3}$.

Thus, it turns out that, despite the low absolute values of the elastic characteristics of the selected material compared to metals, the ratio of its yield strength to the modulus of elasticity is higher than that of most other materials, including metals, and almost reaches these indicators for high-strength (high-alloy stainless) steel. This makes it possible to have fairly wide limits for conducting an experiment at the elastic stage of deformation.

The most important property of this material is its high ability to process, which leads to fairly simple manufacturing technologies of high-quality, practically identical samples and their preparation for testing without significant material costs. The specified properties of the selected material for the manufacture of shell models allow conducting large-scale systematic experimental studies of the influence of the accumulation of randomly damage on the value of the critical force of the loss of bearing capacity.

To make shells, rectangular sweeps were cut from a standard sheet of paper so that their sides were parallel to the main directions of orthotropy. The direction of E_x always coincided with the direction of the forming shell, and E_y - with its direction guiding. Strips with a width of 0.02 m remained along the long sides of the model blank, which were later used for gluing to the cylindrical ends in the circumferential direction. A strip with a width of 0.005 m was also left in the longitudinal direction for gluing the model.

On the scan of the shell, damage was created in the form of through straight cuts. To obtain their random location on the side surface of the shell (coordinate (x_i, y_i) of the middle of the section in the circumferential and longitudinal direction and the angle φ_i, i of its inclination to the generating line $i = \overline{1,n}$) a special computer program was developed, which made it possible to obtain random values (based on a uniform distribution) to determine the specified parameters and create a general picture of the scan of the shell with randomly damage for each number of n cuts. This picture in the appropriate scale was printed on a separate sheet of paper and superimposed on the scan of the shell (Figure 1), which made it possible to make cuts on each of the blanks with fairly high accuracy. Next, the ends of the sections were pricked on the sweep with the help of a drawing gauge to ensure the identity of their shape. Through cuts were made with the help of a sharp tool under the ruler.

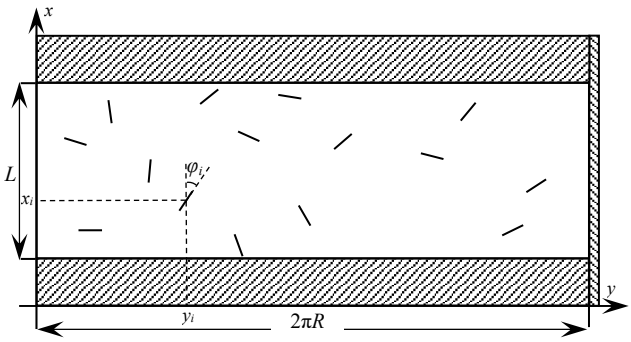

Figure 1. The scan of the side surface of the shell with damage

To give a cylindrical shape, each workpiece was superimposed on a steel cylinder, the diameter of which was $R = 0.0375$ m, and then was glued. The width of the adhesive joint was 5×10^{-3} m, and the working length of the shell was $L = 0.075$ m. The workpiece was held on the cylinder with the help of an elastic rubber band until the glue was completely polymerized. After that, the shell was removed from the cylinder and glued to the end devices, which ensured a rigid clamping of the ends and uniform transmission of longitudinal forces to the curvilinear edges of the shell.

The tests were carried out on the MP-0.5-1 kinematic press, the scheme of which is shown in Figure 2. The lower end of the shell (1) was rigidly attached to the movable massive part of the press (3) with a screw (4) using an end device (2). The upper end (5) was connected to the MP-0.5-2 dynamometer (10) by means of a screw

(6) and a suspension (7), which was rigidly connected to the upper part of the installation. A horizontal rod (8) was also attached to the upper end for the purpose of measuring the amount of tension with clock-type indicators (9), which were placed on the moving part of the press.

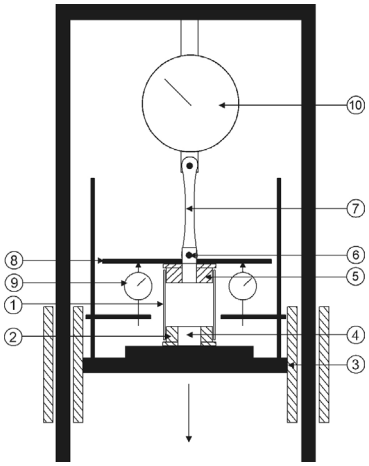

Figure 2. Loading scheme

The external tensile force always coincided with the axis of the shell. For shells with slits, this pattern of loads to a certain extent corresponded to off-center tension, since the slits were placed irregularly on the surface of the shell. The readings of the dynamometer and the indicator of longitudinal movement were recorded through equal intervals of the load values, which changed monotonically. On average, 15 load levels and measurements were obtained for each test. When the load reached a certain value, the shell ruptured. This load was considered the maximum that the shell can withstand.

3. NUMERICAL SIMULATION

As is known [23, 24], in the tasks of calculating the stress-strain state using the finite element method, the method of division into finite elements, the correct selection of the grid step, and the type and size of the finite element are of particular importance. It is especially important to correctly solve these issues in the presence of a stress concentrator, since theoretical solutions [7, 8, 12] imply the hypothetical possibility of "infinite" stress values at these "special" points. It is obvious that in this case it is advisable to reduce the mesh size of the elements near the cuts-cracks of the lateral surface, although it is obvious that this technique cannot fully reproduce the real state of the object. In addition, the difference in the sizes of the elements obtained in this way can also lead to a decrease in the accuracy of the calculation. Therefore, these issues require additional attention when applying the finite element approach to solving these problems, and if possible, experimental verification.

In the presented article, within the selected test scheme, the dependence of the maximum critical tensile load on the angle of random inclination of the cuts-cracks line φ_i to the generatrix of shell (Figure 1) was experimentally investigated and relevant comparisons were made. At the same time, the shell models had one section with a length of $l = 0.01$ m, located in the average cross-section of the shell at an angle $\varphi_i = 0°$, 15°, 30°, 45°, 60°, 75°, 90° to the generatrix of shell.

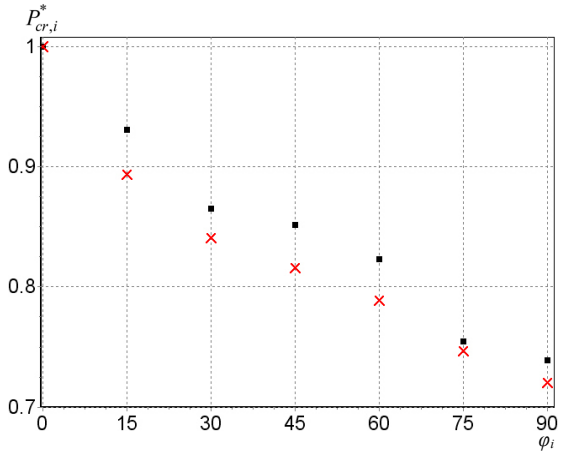

Figure 3. Dependence of critical loads on the angle of inclination of the cuts-cracks

Results of an experimental researches in the form of the dependence of the destructive load (marked - ■) from the angle of inclination slits are presented in Figure 3. From which it can be seen that the longitudinal section ($\varphi_i = 0°$) does not actually reduce the critical load, at the value of the angle $\varphi_i = 45°$ a certain transitional process is observed, and in general the largest decrease in the strength of the shell with a horizontal ($\varphi_i = 90°$) location of the section is almost 25%, as the result of reducing its "full" section by the length of the section. To increase the reliability of the finite-element calculation, a numerical experiment was conducted to select such parameters of the problem as the type of finite element, grid step, as well as the shape and width of the slit concentrator.

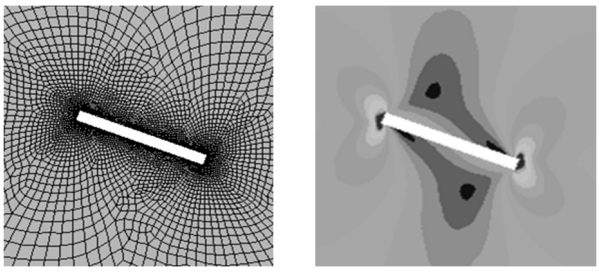

(a) (b)

Figure 4. Results of numerical calculations

A series of calculations was carried out for models with rectangular damage of different widths and a variable grid step (Figure 4a). This made it possible to establish that when the grid step increases, the spread of σ_{max} values increases, at the same time, when the step decreases below a certain value (10^{-3}), the spread of stress values σ_{max} also increases, which is associated with the accumulation of calculation error, because in places of concentration the stress rather large values took Based on

the results of numerical modeling using the obtained diagrams in the form of "slits width-average deviation" dependences, the optimal grid step and the width of the slit-concentrator were found, for which the spread of $\sigma_{\max}$ values was the smallest.

The pattern of stress distribution around the damage for a shell with one cut is shown in Figure 4b. The results of calculations for different φ_i in Figure 3 are marked with ×.

The calculated values were lower than the experimental values (with a deviation of up to 5%). This is explained by the fact that at the end of the crack there was a sharp increase in stresses, while the criterion of destruction failure in the calculations take into account the achievement of a certain calculated critical value σ_{cr} by the maximum stress, which corresponded to a certain experimentally determined destructive force for the shell without damage during axial stretching.

It should be noted that the correct determination of σ_{kr} for the calculation in the case of a complex stress-strain state in the presence of slits, which would correspond to the real destructive load, is possible only with the joint use of experimental and calculated data.

Due to the random nature of the location, the slits in the experiment could intersect, branch out, accumulate in separate zones, etc. Therefore, the finite-element calculation of all experimentally tested shell models leads to more significant differences between the calculation results and the test data. This is due to the need to take into account the mutual influence of stress concentrators and is a separate problem for research [9].

4. RESULTS OF EXPERIMENTAL RESEARCHES

In the course of the experiment, the value of the critical load, longitudinal displacements and images of destruction of the shells were recorded. A total of 288 models of 11 series of shells were tested, each of which had its own location of a different number of n randomly located and oriented rectilinear damages. The length of slits on all shells was the same and was 0.01 m. The number of slits varied from n = 0 (solid shell) to n = 50.

Data from experimental studies are presented in Table 1, where n is the number of damages; k is the number of tested models of each series; P_{cr} is experimental values of averaged destructive loads.

Table 1. Data of numerical calculations and experimental tests

n, *um*	0	1	3	5	10	15	20	25	30	40	50
k, *um*	6	8	8	42	32	32	32	32	32	32	32
P_{cr}, *H*	2316	1726	1619	1494	1349	1172	1172	1116	1036	909	811

The dependence of the relative critical load P_{cr}^{*} on the number of cuts is shown in Figure 5.

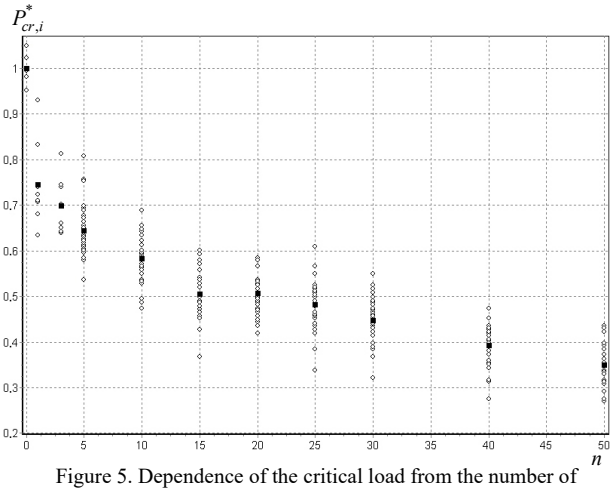

Figure 5. Dependence of the critical load from the number of damages

Here, P_{cr}^{*} is the ratio of destructive (rupturing) loads for the shell with damage and without damage; the symbol "○" shows the values $P_{cr,i}^{*}$ for each of the k tests of all 288 models depending on the number n of damage to the side surface, and their averaged values are indicated by the symbol "■".

Statistical analysis of the obtained experimental data was carried out to assess the influence of the random nature of the location of the coordinates of the middle of the through rectilinear slits and the angles of their inclination to the generatrix on the side surface of each of the shells on the scatter of the experimental data based on the results of the tests.

To construct the histogram, the test results of all 288 shells models of the specified 11 series were taken with the fixed number of damages (n = 0, 1; 3; 5; 10; 15; 20; 25; 30; 40; 50 pieces), for each of which was tested for k shell models, and for each of the 288 models had a different arrangement of slits. The values of the relative critical force $P_{cr,i}$ of the loss of stability were reductioned to the corresponding samplings which were normalized according to the Equation (1) [25]

$$z_i = \left(P_{cr,i} - P_{cr}^{*}\right) \Big/ S \tag{1}$$

where, $S^2 = \frac{1}{k-1}\sum_{i=1}^{k}\left(P_{cr,i} - P_{cr}^{*}\right)^2$, $P_{cr,i}$ and P_{cr}^{*} are the relative critical forces of the ith test and their average value, respectively; and k is the total number of trials.

Next, a normal distribution was restored for each of the samples [25]. Density histograms and theoretical density functions $g(z)$ for the reconstructed distribution of the random value of the relative critical force of the loss of stability for the results of test specified data sets are shown in Figure 6. Despite the random nature of the placement of slits, the deviation of the values $P_{cr,i}$ from the average P_{cr}^{*} does not exceed 20%.

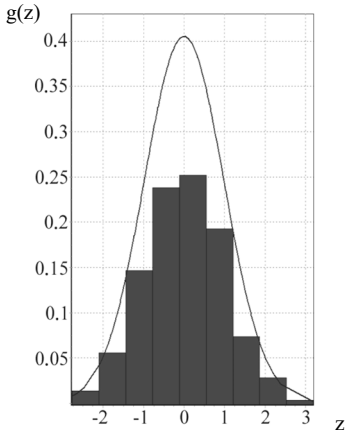

Figure 6. Histogram and density function of the restored distribution of the critical force

Among the features of the behavior of the shell models during the tests, it should be noted a significant drop in the bursting load of the shell (by almost 25%) at the very beginning of the graph (Figure 5), which means that even one damage already significantly reduces the strength of the shells. Further, the rate of reduction of the bearing capacity decreases, and the entire dependence has an uneven character. In particular, an increase in the number of damages in the interval n = 15-25, practically does not affect the decrease in P_{cr}^{*}.

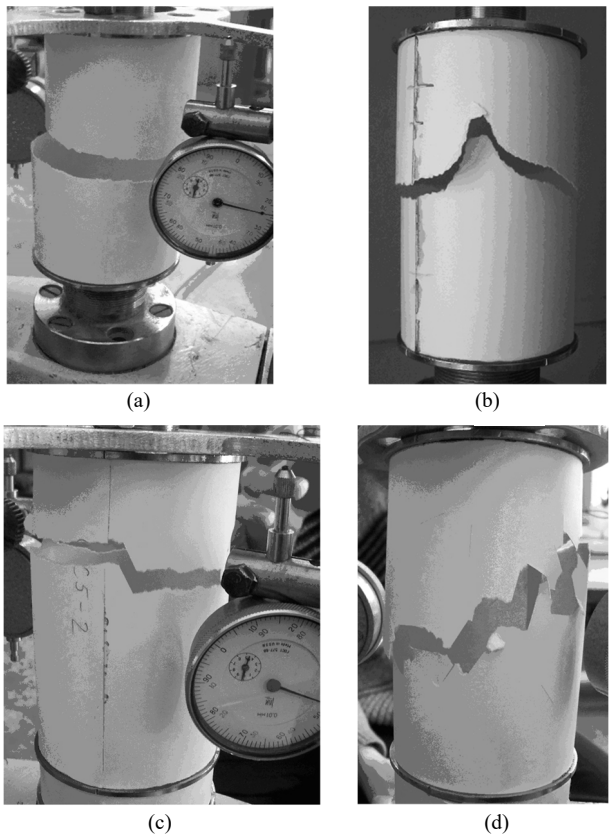

(a) (b) (c) (d)

Figure 7. Pictures of shell destructions with randomly n slits (a) n = 0; (b) n = 3; (c) n = 5; (d) n = 30, in longitudinal tension

Photographs of the tested shells with n = 0, 3, 5, 30 damages are shown in Figure 7. The shell without damage destruction along a circular contour, almost along the cross section (Figure 7a). For a small amount (n=1, 3 damages), a "tab" appears on the side opposite to the accumulation of damages during the rupture. And this is natural, since the shell distracted first, along some weakened generatrix line, and then, after skewing, the break line takes the form of a "tongue".

For $n \geq 5$ (Figure 7. b), this phenomenon is not observed, because the damages are already sufficient not to provoke such destruction. At the same time, it becomes more difficult to describe the process and predict the path of shell rupture. From the observations, it can only be noted that this "live cross-section" path is the shortest by which the cross-section of the shell could be covered. The shorter this path, the lower the bearing capacity of the shell.

It should be noted that, for example, with n = 20, the total length of the slits actually reaches the length of the perimeter of the shell. At the same time, its bearing capacity remains at the level of 50% of the undamaged shell (Figure 5). In general, the most dangerous are transverse damages and the accumulation of a collection of damages, in which a certain part of the shell is actually "removed" from the process of ensuring the load-bearing capacity of the shell.

5. CONCLUSIONS

The article proposes a sufficiently effective experimental method for studying the influence of randomly located damage in the form of rectilinear cuts-cracks of the side surface on the strength of a cylindrical shell loaded with an axial tensile force, due to the successful choice of material, models manufacturing technology, as well as possibility the mass nature of the tests. The experimental data are presented in the form of pictures of the destruction of shells and dependencies destructive loads from the number of randomly damages. Despite the random nature of the location the slits on surface of shells, the deviation of the critical loads from their averaged values does not exceed 20%.

The peculiarities of the finite element modeling of the stress-strain state of the shell with rectilinear slits were studied. The convergence of numerical and experimental data for the case of one slit does not exceed 5%. The specified difference is caused both by errors in the measurement of forces, displacements and the determination of the mechanical characteristics of the material, as well as by the peculiarities of the preparation of the finite-element calculation scheme in the tasks of calculating shells with cuts-cracks. The obtained results can be useful for predicting the strength of cylindrical shells when damage to their surface accumulates in the form of slits, and the results of the experimental studies are a reliable basis for ensuring reliability in the construction of appropriate mathematical models.

REFERENCES

[1] V.Z. Parton, "Fracture Mechanics: from Theory to Practice", M. Nauka, p. 240, 1990.
[2] A.N. Guz, M.S. Dyshel, "Destruction and penetration of Thin Bodies with Clippings in Stretching (Review)", Applied Mechanics, Vol. 26, No. 11, pp. 3-24. 1990.
[3] A.N. Guz, M.M. Dyshel, G.G. Kuliev, O.B. Milovanova, "Fracture and Stability of Thin Bodies with Cracks", Naukova Dumka, p. 184, Kiev, Ukraine, 1981.
[4] V.I. Mossakovsky, N.I. Obodan, E.F. Prokopalo, "Influence of Geometric Nonlinearity on Fracture of Thin-Walled Structures with Cracks", DAN USSR, Vol. 308, No. 5, pp. 1079-1081, 1988.
[5] N.I. Obodan, V.Y. Adlutsky, "Stability Loss of a Cylindrical Shell with a Crack as a Cause of Destruction", Bulletin of Dniprovsky University, Series: Mechanics, No. 10, Vol. 2, pp. 116-122, 2005.
[6] N.M. Borodachev, "Calculation of Structural Elements with Cracks", Engineering, p. 191, Moscow, Russia, 1992.
[7] V.C. Khizhnyak, V.P. Shevchenko, K.M. Dovbnya, "Stress State of Crack-Weakened Orthotropic Shells", Mat. Methods and Phys.-Mec. Fields, Vol. 44, VIP. 1, pp. 100-110, 2001.
[8] E.N. Dovbnya, V.P. Shevchenko, "Stressed State of Orthotropic Shells with a Rectilinear Cut", Teoret. and Appl. Mechanics, Vol. 18, pp. 63-65, 1987.
[9] E.N. Dovbnya, V.P. Shevchenko, "On the Evaluation of the Mutual Influence of a System of Cuts in Shallow Orthotropic Shells", Appl. Mechanics, Vol. 23, No. 7, pp. 50-55, 1987.
[10] N.I. Obodan, G.G. Sherstyuk, "Behavior of Thin-Walled Shells with Damages under Combined Loading", Problems of Computer Mechanics and Mechanical Strength of Structures, No. 4, pp. 112-121, 1998.
[11] L.V. Stepanova, E.M. Adulina, "Asymptotic Methods of Nonlinear Fracture Mechanics: Results, Contemporary State and Perspectives", Bulletin of the Samara State Technical University, Series: Phys.-Math, Science, No. 2, Vol. 31, p. 168, 2013.
[12] V.A. Osadchuk, "Stress-strain State and Limit Equilibrium of Shells with Cuts", K., p. 224, 1985.
[13] M.M. Dyshel, "Tension of a Cylindrical Shell with a Cut", Applied Mechanics, Vol. 20, No. 10, pp. 64-69, 1984.
[14] L.E. Stepanova, "Computer Simulation of Damage Accumulation Processes in Solids with Cracks using the User Procedure UMat of the Simulia Abaqus Computer Complex", Bulletin of the Perm National Research Polytechnic University, Series: Mechanics, No. 3, pp. 72-86, 2018.
[15] C. Sih, "Crack Tip Mechanics Based on Progressive Damage of Arrow: Hierarchy of Singularities and Multiscale Segment", J. Theoret. Appl. Fract. Mech. Vol. 51, No. 1, pp. 11-32, 2009.
[16] E.V. Kuznetsova, G.L. Kolmogorov, "Maximum-Permissible Defects in Cylindrical Shells Under the Action of Internal Pressure", Building l Mechanics of Engineering Structures and Structures, No. 2. pp. 63-69, 2013.
[17] M.I. Machorkin, M.M. Nykolyshun, "Limit Equilibrium of Cylindrical Shell with Longitudinal Crack with Regard for the Inertia of Material", J. Math. Sci., Vol. 249, No. 3, pp. 462-477, 2020.
[18] N.I. Obodan, G.G. Sherstyuk "Experimental Research of the Survivability of Damaged Shells" Problems of Strength", No. 11, pp. 96-100, 1989.
[19] A. Dzyuba, E. Prokopalo, P. Dzyuba, "Experimental Investigation on the Torsional Stability of Cylindrical Shells Weakened be Circular Holes", Journal Strength of Materials, Vol. 49, No. 6, pp. 829-837, 2017.
[20] W.D. Bebkok, "Experiments on the Stability of Shells", Thin-Walled Shell Structures, pp. 355-379, 1980.
[21] R.V. Rhode, E.E. Lundquist, "Strength Tests on Paper Cylinders in Compression Bending and Shear", NASA, Techn. Notc., No. 370, 1931.
[22] V.M. Chebanov "Investigation of the Stability of Thin-Walled Shells Using Paper Models", Engineering Collection, Institute of Mechanics of the Academy of Sciences, USSR, Vol. XXII, pp. 68-73, 1955.
[23] O. Zenkevich, "Finite Element Method in Engineering", Mir, p. 540, Moscow, Russia, 1975.
[24] S. Moaveni, "Finite Element Analysis, Theory and Application with ANSYS", Prentice-Hall, p. 526, New Jersey, USA, 1999.
[25] E.S. Pereverzev, O.F. Daniev, "Probability Distributions and their Application: Monograph", Dnenpropetrovsk National University, p. 416, Dnipro, Ukraine, 2004.

BIOGRAPHIES

Anatoliy Petrovych Dzyuba was born in Romny, Ukraine on November, 30, 1948. He graduated from Dnepropetrovsk State University, Dnipro, Ukraine, with a degree in Mechanics, in 1971. He received Doctorate degree of Technical Science in Deformed Solid Mechanics, in 2004. He received a Professor's degree in 2006. He was the Head of Calculating Mechanics and Structural Strength Department in 1994-2016. He was a Professor of Theoretical and Computational Mechanics Department, chief of Problematic Research Laboratory of Strength and Reliability of Constructions, Dnipro National University, Dnipro, Ukraine since 2016. He has 390 scientific publications, among which 189 articles, 12 monographs, 27 patents and certificates of inventions. He is Honored Worker of Science and Engendering of Ukraine.

Petr Anatolyevych Dzyuba was born in Dnipro, Ukraine on January 22, 1982. He received his Master of Science degree from Dnipro National University, Dnipro, Ukraine in 2004. He also received his Ph.D. degree in Mechanics in 2012. Since 2015, he worked as an Associate Professor at Computer Technologies Department, Applied Mathematics Faculty, Dnipro National University. He published 27 articles, and one monograph. His research interests include solid mechanics, thin-walled shell structures, computer technology.

Ramiz Aziz Iskanderov was born in Krasnoselo, Armenia on July 7, 1955. He received the M.Sc. degree in Mathematics-Mechanics from Azerbaijan (Baku) State University, Baku, Azerbaijan, in 1977. He also received the Ph.D. degree in Mathematics-Mechanics from Azerbaijan University of Architecture and Construction, Baku, Azerbaijan, in 1983. Since 2014, he has been a Doctor of Sciences in Mathematics, Professor of Mechanics Department, Azerbaijan University of Architecture and Civil Engineering, Baku, Azerbaijan. He has published 90 articles and three books. His research interests are theoretical mechanics, solid mechanics and mechanics of composite materials.

The 18th International Conference on
"Technical and Physical Problems of Engineering"
30 October 2022
International Organization of IOTPE

ICTPE Conference
www.iotpe.com
ictpe@iotpe.com
ictpe0@gmail.com

ICTPE-2022 Number 25 Code 07TAP04 Pages 131-135

ANALYSIS OF SUBSTATION COMPONENTS MODERNIZATION AND SUBSTATION DESIGN INTERFACE DEVELOPMENT

B. Celik [1] L.V. Krivova [2]

1. Rosatom State Nuclear Energy Corporation, Akkuyu Nuclear Power Plant, Mersin, Turkey
burakceliktwo@gmail.com
2. Higher School of High Voltage Engineering, Peter the Great Saint Petersburg Polytechnic University, Saint Petersburg, Russia, krivova.milla@gmail.com

Abstract- The paper devoted to the analysis of optimal ways for substation modernization taking into account the requirements for electrical installations, carbon dioxide emission, and costs. The best up-to-date solutions in Russia and some other countries were examined. The key points affecting the effectiveness of the 500 kV switchgear retrofitting by installing the disconnecting circuit breakers and fiber optic sensors are highlighted. Corresponding to the purpose of the research, the high voltage switchgear of a conventional 500/220 kV substation was investigated within the scope of equipment cost analyses, digital substation technologies, future of the substation industry, and modernization applications. As the subject of the research, possible ways of modernizing the switchgear with different calculation methods are compared. The developed web page interface for online substation design is represented. According to the report generated from the interface, proper values for the equipment selection are defined and possible equipment for modernization are selected. The accuracy of the interface and the commercial structure of the web page are underlined.

Keywords: Substation, Switchgear, Disconnecting Circuit Breaker, Current Transformer, Voltage Transformer, Fiber Optic sensors, Web Design.

1. INTRODUCTION

The future of power engineering is shaped according to some main factors, such as: the unstoppable population of the world, globalizing technology, increasing energy demands, growing industrial needs, and the aidless planet trying to provide all important elements while carrying all the pollution that is created meantime. Between each of those factors, there is a complicated net of connections that may light the way of possible improvements to lead the design and development procedure more efficiently. Nowadays, the increased energy consumption and generation consequently, the greenhouse gas emissions followed and governments have started to initiate the reduction of carbon footprint, with the encouragements about a series of policy measures to stop the climate change.

The share of renewable energy production worldwide recorded the fastest in the last decade. And the trend for the development of green energy is spreading to an increasing number of countries. Over the past five years, the part of renewables in total energy sources was estimated about 60% of the rapid growth in global production, while the use of wind and solar energy has more than doubled [1]. The installed capacity of renewables in the total energy production of the world increased significantly. Not only but also, grid businesses, the core business of the electricity industry, actively respond to climate change, establish energy conservation and emission reduction efforts, and promote the development for decrease in carbon footprint economy in the power industry [2-4]. Thanks to the policies that encourage a levelling of the net load curve, electricity costs and greenhouse gas emissions may be reduced by maximizing the use of variable renewable energy sources. Such policies can also optimize and modernize existing generation, transmission, and distribution capacity, easing grid reinforcement [5]. Despite the rapid share of electricity generation by renewables, the annually increased power demand caused by population growth and technological progress, may not be covered without burning fossil fuels for now. The modernizing of existing generation, transmission, and distribution systems equipment is the way to reduce the impact of oil, gas and coal as a source of power.

Digitalization of power industry and decarbonization are the most important goals of today's energy sector. Achieving the great results in this direction is possible by complete modernization or retrofitting the existing electrical installations. Political and economic issues influence to fulfilling ambitious plans for making the power engineering eco-friendly, more efficient, and with extremely high indexes of availability and reliability.

According to scientific studies of IEA, modernizing grids offers a great and sensible possibility to renovate the elements simultaneously. During the 2020-2030 years, the fifths part of global electric grids is expected to be updated, 16 million km of distribution lines and 1.5 million km of overhead lines approximately. Since electrical substations

are the key nodes of electrical power systems arranging the connections between primary source of power, it is clear that further improvements and best technological solutions integration will satisfy the power objects according to the 21st century standards [6].

2. MODERNIZATION ANALYSIS

The usage of technologies in electrical installations creates a significant improvement, in terms of increasing reliability, safety, operational flexibility, and finally economic efficiency. Nevertheless, when using cutting-edge equipment in the design of switching devices, instrument transformers, and conductors, the expected effect involves huge economical costs. The planning a substation to been build or modernize with non-conventional equipment creates significantly useful results. Especially, considering the less footprint of the non-conventional instrument transformers (IT) and disconnecting circuit breakers (which may be up to 90%), the price of land allocation for the substation can be decreased successfully as a major part of investments. The decreased footprint will lead the design or modernization process to more advantages. The amount of the reduction for construction and installation will reach up to 25% of total construction costs for conventional substation components.

During the designing of a new substation, the greatest costs are associated with the transporting and mounting of equipment. Moreover, for air-insulated substations with a high level of voltage like 500 kV, the construction cost will be about 63% of the total cost. For indoor substations, the percentage will be even higher, reaching 68%. Considering the switchyard of 500 kV substation only, the share of equipment cost is defined as about 72%. The resting 28% percentage of the cost comprises only the construction cost. By comparing this value with the erection percentages of the total substation and considering the first or previous construction expenses of the conventional substation as an evident loss, modernization of the switchyard only will become an affordable, sensible, and leading option. That, leading the investments to cover the equipment itself firstly, will keep the price-performance ratio of the modernization at a sensible level. Therefore, to increase the efficiency and reliability of existing substations, it is advisable to modernize the facility, besides building a new one.

On the other hand, the economic analysis findings outlined that, in some cases, the construction of a new substation may be more profitable than updating an existing one. According to various estimates, the deterioration of the equipment of Russian substations today averages 50%. Considering the total expenses, rebuilding the substation might create more reliable and sustainable results. Whereas, a partial reconstruction of the existing substation with a moderate degree of deterioration in general, is more than appropriate in the current economic conditions. Also, since the replacement of technically and physically obsolete equipment is necessary during each reconstruction, the increase in the reliability and the continuity of the power supply, make the procedure certainly preferable. In the light of the given information and findings, besides comparing rebuilding and modernizing, focusing on the modernization costing analysis might help define the details of future plans for substations.

As a primary goal of power systems, all inlets, outlets, and intermediate steps of a substation should be operated according to the limitations defined according to the policies, demand expectations, capacity characteristics, and the system's physical situation. Furthermore, as well as all common forms of industrial energy, electricity might be dangerous in case of running out of control. Even with an optimistic view, any possible failure may interrupt the system and create indirect problems. Each failure should be predicted and compensated precisely to prevent an accident or interruption. Such as all power systems, to keep the substation safe and under control, the design of secondary systems such as measuring and controlling systems requires significant attention. The industry of IT as a fundamental member of measuring and controlling systems provides the safe, reliable, and inventive solutions for modern needs. Nevertheless, considering the costings and estimating the share of IT in all substation investments will be defined as 1-3%. Surprisingly, besides the high costs of other equipment with the higher technology, new generation IT provides new technology at less cost.

In addition, the modern technology of non-conventional equipment will make the process more sensible based on reduced costs for maintenance, minimizing of utilization costs, refusing the copper cables, elimination of the analogue-digital converters, and modernized controls over the system's working factors. Taking into account aforesaid, the possibility to increase the speed of operation of protective relaying will be higher and the differential protection will operate with higher level of sensitivity.

As in all engineering fields, the cost-performance relationship should be kept at a reasonable level in the design or modernization of the substation. Fortunately, there is serious competition among manufacturers and it is possible to find better solutions in the purchasing process. Because especially for the secondary equipment such as fiber optic cables, optical sensors, and data cables, more items will be needed. For example, for a 500 kV switchyard three fiber optic cables will be required in general. These will be for protective relaying, backup protection, commercial accounting, and other measurements.

Up-to-date and rather obsolete technologies may bring some risks due to practical experiments or fatigue. However, with new technology, it is much easier to define and solve possible problems. For example, at the "Tobol" 500 kV substation there are 10 SF6 circuit breakers and 25 free-standing center break disconnectors. Changing them for DCB may be sensible but the mentioned parameters about costing and performance should be considered deeply and following the certain policies in its modernization processes.

According to the Russian Power Grids Company "Rosseti" requirements, one of the largest electricity grid

companies in the world, the payback period for digitalization is recommended to be limited by 10 years. At the same time, despite their higher costs, pursuing eco-friendly solutions, provides better results for nature because SF6 IT is not environmentally friendly for sure. Also, the operating costs of monitoring gas leakage, the danger of opening secondary circuits at the current transformers, maintenance, utilization costs, construction costs, the need for an analogue digital converter for compliance with the IEC61850 standard, large weight, and size make them less efficient than non-conventional IT [7].

Initially, the 500 kV switchyard was arranged according to a scheme with two circuit breakers per three connections. Six single-phase autotransformers AODCTN-167000/500/220 and six transmission lines are connected to the switchyard. Air blast circuit breakers VVBK-500-50, disconnectors RNDZ-500/3200U1, measuring transformers of current TFZM-500B-1 and voltage NKF-500-78U1 are installed in the scheme. Having applied the cutting-edge equipment and solutions, the switchgear scheme was changed with enriched reliability, availability and less footprint (about 35% reduction) [8].

3. ONLINE SUBSTATION DESIGN INTERFACE

According to the details described above, it is possible to say that substation design and modernization is of great importance. Especially, the future potential of digital substation applications supports the predictions in this regard. According to the report published by Global Market Insights in 2020, Digital Substation commercial volume, which was 96 billion USD in 2020, is expected to exceed 130 billion USD in 7 years. This 7-year increase expectation paves the way for digitalization in the substation market. The CAGR (compound annual growth rate) is over 6% to such an extent. Additionally, government regulatory policies and updates to conventional power system components for energy companies and customers will contribute the positive economic prospects. The energy research and development sector are expected to experience a significant increase due to the increasing demand for efficient transmission and distribution control systems. In the absence of efficient power grids in developing countries, efforts to expand existing infrastructure are increasing at a level that meets expectations.

The positive trend of today's consumers towards substation installation to provide reliable source of power and the increase in power grid operation time, availability, efficiency will force the energy industry and influence to the new breakthrough technologies design. In addition to the report, when the worldwide pandemic in 2019 is taken into account, it can be understood that the expected increases in the use of renewable energy resources and in the substation, market are in a mutualistic relationship and web design of many technological processes are crucial [9]. Based on this potential, a world-wide web-based interface was created which leads the users to enter the initial data of the electrical power system, to see the basic principles of substation design or modernization, to define the required values for each element, to choose the elements according to the required values, to define the approximate cost, lifetime, efficiency, reliability and scheme layout, to compare and analyze the different effects of the combinations of the elements, and to generate the report that includes all useful information regarding the design or modernization procedure [10].

The interface welcomes the user to the form in Table 1 with checkboxes showing that it is possible to choose one to three sources and one or two loads while entering the initial data of the system.

Table 1. Example of entering the initials to the interface [10]

Voltage Value (UHV)		500	kV
Sources			
● S 1 ● S 2 ○ S 3	Source1	Source2	
Apparent Power	8000	9500	MVA
Reactance	0.8	0.9	Per Unit
OHL Length	240	80	km
Please define the power demand qualifications.			
Loads			
● L 1 ● L 2	Load1	Load2	
Voltage	220	10	kV
Active Power Demand	360	56	MW
r_sim	0.87	0.8	-
Power Factor	0.92	0.9	-
Operating Hours	7500	5000	Hours
Please define the ratio of transformer load by consumer category.			
Consumer Categories	Range	Value	3-ph PT
● 1st Category	0.65 - 0.70	0.70	≥ 2
○ 2nd Category	0.70 - 0.80	0.80	2
○ 3rd Category	0.90 - 0.95	0.95	1 or 2
○ Design Preference	Enter here…		
Please define the network qualifications.			
S Basis		1000	MVA
Number of Transformers		2	-
Please define the voltage value for the periodical current at zero time.			
Voltage Value (USC)		500	kV

Especially in this part, the backend development of the interface was created with several arrangements to let the interface answer different options such as:
- single source - single load,
- single source - two loads.

If all the required values are entered into the system according to the definitions, the submission button leads the user to the following part as Table 2, which gives a chance to the user to check and verify the entered values.

Table 2. Checking the initial parameters [10]

Voltage Value (UHV)		500	kV
Sources	Source1	Source2	
Apparent Power	8000	9500	MVA
Reactance	0.8	0.9	Per Unit
OHL Length	240	80	km
Loads	Load1	Load2	
Voltage	220	10	kV
Active Power Demand	360	56	MW
r_sim	0.87	0.8	-
Power Factor	0.92	0.9	-
Operating Hours	7500	5000	Hours
Network Initials			
Transformer Load Ratio		0.7	-
S Basis		1000	MVA
U Mid-rated		515	kV
Number of Transformers		2	-
Specific Resistance		0.30	ohm/km

Edit Initial Data

In Tables 3 and 4 it is possible to generate the primary or detailed report with one click and achieve all the useful information as results of the calculations and algorithms.

The web design part consists of different layers such as frontend (visible) and backend (hidden) development and completely satisfies the requirements for ergonomic usage. HTML frameworks were used to accelerate the backend of the interface and to create a clean, sensible, and efficient look at the frontend of the interface.

Table 3. Primary results of the interface [10]

Medium Voltage Power Demand (MV PD)			
MV_P	313.2	MW	Active PD at MV
MV_S	340.43478260	MVA	Apparent PD at MV
MV_Q	133.42264129	Mvar	Reactive PD at MV
Low Voltage Power Demand			
LV_P	44.8	MW	Active PD at LV
LV_S	49.777777777	MVA	Apparent PD at LV
LV_Q	21.697630296	Mvar	Reactive PD at LV
Total Active Power Demand			
MV_P	313.2	MW	Active PD at MV
LV_P	44.8	MW	Active PD at LV
HV_P	358	MW	Active PD at HV
Total Reactive Power Demand			
MV_Q	133.42264129	Mvar	Reactive PD at MV
LV_Q	21.697630296	Mvar	Reactive PD at LV
HV_Q	155.12027159	Mvar	Reactive PD at HV
Total Power Demand at HV			
HV_P	358	MW	Total Active PD at HV
HV_Q	155.12027159	Mvar	Total Reactive PD at HV
HV_S	390.16188775	MVA	Total Apparent PD at HV

Table 4. Detailed results of the interface [10]

Transformer Selection Parameters			
I Installed	0.2252600709	kA	Installed Current
Minimum Rated Apparent Power of Power Transformer at HV			
S_Rated	273.11332143	MVA	1 Power Transformer (Three phase)
S_R. (3p)	91.037773810	MVA	3 Power Transformers (single-phase)
Network Calculations			
S BASIS	1000	MVA	Accepted Basis Apparent Power
U Midrated	515	kV	Basis Voltage Level at s/c Point
I BASIS	1.1210684838	kA	Basis Current at s/c Point
Per Unit Specific Reactance			
XSP	0.30	Per Unit	Midrange Specific Reactance of Transmission Line
Source1 Reactance Values			
XS1 PU	0.1	Per Unit	Reactance of Source 1
XL1 PU	0.1357338109	Per Unit	Reactance of OHL 1
X1	0.2357338109	Per Unit	Equivalent Reactance 1
Source2 Reactance Values			
XS2 PU	0.0947368421	Per Unit	Reactance of Source 2
XL2 PU	0.0452446036	Per Unit	Reactance of OHL 2
X2	0.1399814457	Per Unit	Equivalent Reactance 2
Total Reactance			
XK1 PU	0.0878281067	Per Unit	Equivalent scheme reactance for s/c point 1
Periodical Current at Zero Time			
USC	500	kV	Voltage at s/c Point
UPU	1	Per Unit	Voltage Per Unit at s/c Point
IK1P0	12.764347605	kA	Periodical Current at Zero Time
Calculated Values for Switchyard Equipment Selection			
Parameter	Value	Unit	Explanation
U Ins	500	kV	Installed - Rated Voltage
I Ins	0.2252600709	kA	Installed - Rated Current
I B0	12.764347605	kA	Breaking Current
I Peak	33.395299972	kA	Making Current

Circuit Breaker Timing Options

According to circuit breaker timing preferences and catalogue data it is possible to calculate the thermal withstanding below.

t_CB / CB Opening Time (from the catalogue)	0.02	sec.
t_PR_min / Minimal Time of Protective Relaying	0.01	sec.
t_AR / Auto-reclosure time	0.21	sec.

Calculate S/c Thermal Withstanding 48.878570938 kA^2 * s

In this regard, it was one of the challenging parts to show the possibilities of the interface to the user. At this point, JavaScript was used to animate some parts of the interface providing ergonomic usage with collapsible elements, alerts and warnings. At the same time PHP coding was effective and sensible while creating the calculations and tables during backend development.

4. CONCLUSIONS

Currently, the issue of modernization of electric power facilities is of great importance, because the deterioration of equipment at some electrical installations is 50% or more. In addition, the digitalization of the industry and compliance with the IEC 61850 standard is the exclusion of leaving the situation in its current position. The modernization of 500 kV switchyard was fulfilled by the online substation design. The interface that was created, meets user expectations and provide ease of application. In this regard, the results of the Excel calculations which form the basis of the coded web-based interface, manual calculations, and the calculations of the web-based interface, were compared and the accuracy rates are extremely high.

Developed web design is expected to be in the nearest future as the tool to:

- Create a connection between manufacturers of substation elements and the substation builders such as companies and/or engineers,
- Clarify the calculation methods of the substation design procedures for some engineers, students, etc.
- Minimize the possible errors and defining better results by calculating all the values according to the algorithm based on scientific formulations and accurate database parameters,
- Generate the primary and detailed results reports with numerical values of required scheme parameters, scientific graphs, costings and analytics.

REFERENCES

[1] BP Energy, "Statistical Review of World Energy Globally Consistent Data on World Energy Markets and Authoritative Publications in the Field of Energy", BP Energy Outlook, Vol. 70, pp. 8-20, 2021.
[2] M. Junxia, J. Linmin, X. Erfeng, L. Dunnan, "Study on Greenhouse Gas Emission Source Identification and Emission Calculation Method for Power Grid Enterprises", The 8th Int. Conf. Power Energy Syst. (ICPES 2018), pp. 289-292, 2019.
[3] IEA (2021), Global Energy Review, "CO_2 Emissions in 2020", IEA, Paris, 2020, www.iea.org/articles/global-energy-review-co2-emissions-in-2020.
[4] E.E. Novruzova, "Newest Innovative Technologies in Electric Power Industry", International Journal on Technical and Physical Problems of Engineering (IJTPE), Issue 42, Vol. 12, No. 1, pp. 6-9, March 2020.
[5] C. Schneider, "Energy efficiency," Chem. Eng. News, Vol. 66, No. 46, p. 5, 1988.
[6] R.E. Dickson, "The 21st Century Substation Design", J. Japan Soc. Nurs. Res., Vol. 22, No. 3, pp. 3-66, 1999.
[7] General Electrics, "Digital Substations - GE Grid Solutions", www.gegridsolutions.com/landing/digital-substation/.
[8] B. Celik, L.V. Krivova, "The Modernization Analysis of 500 kV Switchyard at an Electrical Substation", International Conference on Power Engineering Today and Tomorrow, pp. 6-8, Kursk, Russia, 30 March 2022.
[9] A. Kalwar, R. Ajmera, A. Gill, "ARQI: Model for Developing Web Application", International Journal on Technical and Physical Problems of Engineering (IJTPE), Issue 47, Vol. 13, No. 2, pp. 7-13, June 2021.
[10] www.substationdesigner.com.

BIOGRAPHIES

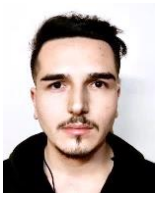

Burak Celik was born in Konya, Turkey on November 6, 1994. He graduated as a media artist from Anadolu University, Turkey in 2016 and as a mechatronics engineer from Erciyes University, Turkey in 2019. In 2018, he was granted by a scholarship and an internship of the European Union in the field of Promotion Management and Business Intelligence in Poznan, Poland. As a technical design engineer, he completed more than 30 projects for Konya Science Museum, Turkey. He received the M.Sc. degree as Rosatom's granted student in Electrical Power Engineering at Saint Petersburg Polytechnic University, Russia in 2022. Currently, he is an Electrical Engineer at Akkuyu Nuclear Power Plant, Mersin, Turkey. His research interests are in the areas of stage arts, business management, web design, energy efficiency and substation engineering.

Lyudmila Krivova was born in Voroshilovgrad, Russia on August 12, 1974. She graduated from Department of Power Plants, Tomsk Polytechnic University, Russia as engineer and received the Ph.D. degree in Power Plants and Power Systems from Novosibirsk State Technical University, Russia in 2003. Currently, she is an Associate Professor of Higher School of High Voltage Engineering, Peter the Great Saint Petersburg Polytechnic University, Russia. She was awarded by the ING-PAED-IGIP diploma and included in the list of International Engineering High School Lecturers. Her research interests are in the area of power plants design, structural and functional reliability of power plants, pedagogy and some aspects of linguistics. She is author and coauthor of more than 40 scientific journal publications and conference proceedings in field of power engineering and pedagogy, one monography.

The 18th International Conference on
"Technical and Physical Problems of Engineering"
30 October 2022
International Organization of IOTPE

ICTPE Conference
www.iotpe.com
ictpe@iotpe.com
ictpe0@gmail.com

ICTPE-2022 Number 26 Code 07TAP05 Pages 136-139

ANALYSIS OF PHOTOBIOLOGICAL PROCESSES OF THE EMISSION SPECTRUM OF LED LAMPS AND LUMINAIRES FOR INDOOR LIGHTING

S.A. Baghirov [1] S.S. Baghirova [2]

1. Department of Electrical Engineering, Azerbaijan Technical University, Baku, Azerbaijan, sabir.bagirov.61@mail.ru
2. Department of Automation and Control, Azerbaijan Technical University, Baku, Azerbaijan, selale.bagirova@mail.ru

Abstract- The article deals with the influence of the radiation of light-emitting diode (LED) light sources on the photobiological hazard for the retina. It has been shown that LED lamps with a directional diffuser coating and luminaires with diffuser and directional diffuser diffusers generally do not exceed the zero risk group (RG0) blue light hazard limits. The specified light sources at brightness not higher than 10^4 kd/m^2 for any values of the correlated color temperature (CCT) in the range of 2700-6500 K refer only to RG0. Most LED lamps and luminaires for indoor lighting are safe for the retina in terms of the photobiological hazard of blue light.

Keywords: Light, LED Lamps, Correlated Color Temperature, Blue Light Photobiological Hazard, Brightness.

1. INTRODUCTION

It is known that optical radiation (OR) in the tissues of living organisms can cause negative biological reactions, which are determined by the processes of energy conversion at the molecular level [1]. OR is well absorbed by the tissues of the human body, and its penetration depth is small and depends on the radiation spectrum with a wavelength from several micrometers in the ultraviolet region to several millimeters in the near infrared region of the spectrum.

The main processes of OR impact on the tissues of the human body is thermal (OR conversion into heat) and photochemical (OR conversion into energy of chemical reactions) processes. Thermal damage mainly depends on the heat transfer of the irradiated tissue, the depth of penetration of OR and the energy illuminance of the irradiated area. Exceeding the corresponding limit values results in bodily injury - local burns. Due to thermal conduction processes, i.e., diffusion of heat from the volume where OR is absorbed, the limit values for bodily injury depend on the size of the radiation area. Photochemical processes are characterized by action and depend on the energy exposure.

The values for safe energy exposure limits are set by the International Commission on Non-Ionizing Radiation Protection (ICNIRP) and standardized in [2]. This document regulates the limit of dangerous actinic ultraviolet radiation for the skin and eyes, the limit for irradiation of the retina of the eye with blue light and the limit for the danger to the retina of thermal radiation.

Blue radiation risk assessment and classification methods have been developed by the International Commission on Illumination (ICI) jointly with the International Electrotechnical Commission (IEC) [3, 4]. The danger of blue light is classified into four risk groups and is determined by the amount of energy that enters the retina through the pupil of the eye [3]. Hazard parameters for a given exposure time can be represented both as the maximum value of radiance L_B (for light sources with angular dimensions greater than 11 mrad) and as irradiance E_B (for light sources with angular dimensions less than 11 mrad).

The physiological basis for the hazard classification of the zero risk group (RG0) is that when the light source does not pose a danger to the retina for 10000 s. Low risk group (RG1) - the source does not pose a danger (when the limit values RG0 are exceeded) for 100 s. Medium risk group (RG2) - the light source does not pose a danger due to glare or discomfort, which are created by sources of high brightness for 0.25 s. High risk group (RG3) - the source is dangerous even with short-term exposure (at t<0.25 s). Exposure time and limit values of energy brightness L_B weighted by the blue light hazard function $B(\lambda)$ and energy illuminance E_B for different risk groups are shown in Table 1 [3].

Table 1. Limit values of energy brightness L_B, energy illuminance E_B and exposure time t [3]

Exposure time t, s	Maximum energy brightness L_B, W/m^2.sr	Maximum energy illuminance E_B, W/m^2	Risk group
$t \geq 10000$	100	0.01	RG0 (no risk)
$100 \leq t < 10000$	10^4	1.0	RG1 (low risk)
$0.25 \leq t < 100$	4×10^6	400	RG2 (medium risk)
$t < 0.25$	$> 4\times10^6$	> 400	RG3 (high risk)

To determine the danger of blue light, it is necessary to take into account the irradiance of the retina by the image of the light source. With instantaneous exposure, the image on the retina has the same angular size as that of the source. As the exposure time increases, the image spreads more and more over the area of the retina (due to the saccades of the eyes), which reduces its irradiance.

Therefore, it is necessary to determine the dependence of the angular size of the image for the exposure time from 0.25 s to 10000 s in the range of angles from 1.7 mrad (the smallest size on the retina) to 110 mrad [5]. The minimum value of 1.7 mrad is set for an exposure time of 0.25 s (limit between RG2/RG3); 11 mrad for 100 s exposure time (limit between RG1/RG2); 110 mrad for 10000 s exposure time (limit between RG0/RG1).

To date, all the positive and potentially negative aspects of the impact of artificial lighting on human safety have not been fully studied, but a number of important consequences of exposure to radiation have been studied sufficiently and standards have been developed that provide recommendations for improving the photobiological safety of lamps and lamp systems.

The most vulnerable organs that can be adversely affected by OR are the skin and eyes. The risks of photochemical damage to the retina that can occur with violet and blue light exposure are often associated with LED light sources, although the proportion of blue light in LED sources at the same CCT is about the same as that of light from other sources, such as luminescent lamps (LL) [6]. A number of studies have shown that there is no matter which source of light is generated, an incandescent lamp (IL), LL or LED lamp, the spectrum and brightness of the radiation are important (Figures 1, 2, 3) [3, 4, 7].

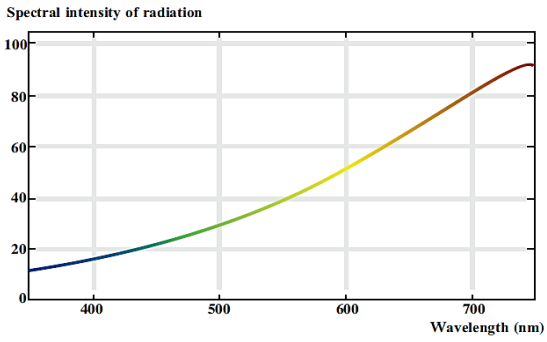

Figure 1. Emission spectrum of IL [7]

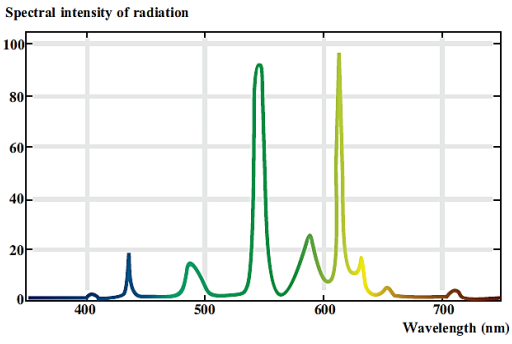

Figure 2. Emission spectrum of LL [7]

Before the advent of bright LEDs, the photobiological safety of lamps and lighting systems was focused on limiting ultraviolet radiation. After the use of white bright LEDs for illumination, the question of the safety of the retina of the blue light arose.

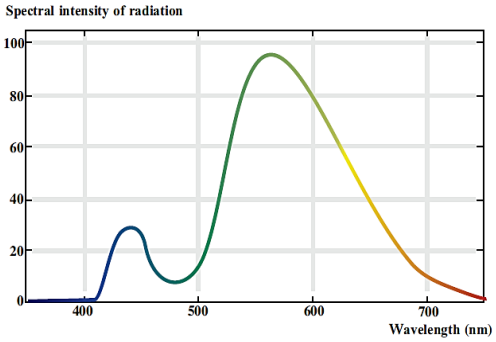

Figure 3. Emission spectrum of LED lamps [7]

According to [8], it must be taken into account when the observer directly looks at the light source, while overcoming the natural desire to avoid bright light. The ICI in [9] clarified the term "blue light hazard". It should only be used when considering the photochemical risk of damage to the retina (photo maculopathy) associated with fixation of sight on bright light sources. The risk of photochemical damage to the retina by blue light depends on the wavelength (with a maximum around 435-440 nm). Looking directly at a bright LED source from a close distance, even for a short period, can be dangerous in terms of photobiological damage.

An analysis of the results of a safety study of OR of LED lamps and luminaires obtained in a number of works [10-13] shows that most of them belong to RG0 of the complete absence of the risk of blue radiation hazard, a small part refers to RG1 and only individual LED lamps and luminaires with high CCT (more than 6000 K) may refer to RG2. The actual photobiological hazard in practice depends on the duration of exposure and is based on the perception response to bright light. The maximum exposure time in RG2 can be changed from 100 to 0.25 s.

If technical solutions are not used to distribute LED light over an area exceeding the area of the emitting crystal, then LEDs may be inferior in photobiological safety, for example, IL with frosted flasks or LL. However, LED lamps and luminaires without optical elements are usually not used. As with traditional lamps and luminaires, various optical devices are used to redistribute the light in such a way as to ensure that the specified requirements are met. Optical systems make it possible to distribute light over large areas and make LEDs suitable for general lighting.

For the further development of LED lighting, the issues of assessing the safety of light are relevant. The transition to LED lighting can be hampered by the fact that inaccurate information is often provided about LED lamps and luminaires. The statement that switching to LED lighting in everyday life threatens health is incorrect. It is also emphasized that LED lighting requires a completely new luminance detection system, since the existing system was designed for conditions not typical for LED. The aim of the work is to study the photobiological hazard of LED lamps and indoor lighting luminaires.

2. DISCUSSION OF THE RESEARCH METHOD AND BASIC MATERIAL

Studies of the levels of photobiological hazard of commercial samples of LED lamps and luminaires for indoor lighting of office and domestic premises were carried out. The measurements were carried out using the OST-300 optical radiation test system. The Spectro radiometric system of the complex contains monochromators, a photometric detector, a system for measuring the spectral density of radiation and the dimensions of light sources, as well as an eye simulator in the field of view of 1.7, 11 and 110 mrad, apertures for limiting the field of view, and reference light sources.

The processing of the measurement results is carried out by a computer with software based on spectral measurements and allows you to calculate the blue light energy brightness L_B, energy illuminance E_B, CCT, brightness L_V, illuminance E_V at a distance at which the photobiological hazard of light is determined. Light intensity curves and luminous flux are measured using a GO 2000 goniophotometer. The measurement error of lighting parameters on an OST 300 setup and a GO 2000 goniophotometer does not exceed 5%. The energy brightness L_B is determined using the Equation (1) [2]:

$$L_B = \sum_{300}^{700} L_\lambda B(\lambda)\Delta\lambda \le 100\ ,\ t > 10^4\ \text{s} \qquad (1)$$

where, L_λ is spectral energy brightness, $w \cdot m^{-2} \cdot sr^{-1} \cdot nm^{-1}$; $B(\lambda)$ is the spectral weighting function of the blue light hazard, in relevant units; $\Delta\lambda$ is the wavelength range in nanometers; and t is the exposure duration in seconds.

The measurement was carried out in accordance with the recommendations of the standards [3, 4] at a distance of 200 mm in a field of view angle of 11 mrad. We measured LED lamps in flasks with a directionally scattering coating and luminaires for indoor lighting with various types of diffusers - with diffuse and directionally scattering transmission. The results of the study of the energy and light characteristics of LED lamps and luminaires are shown in Tables 2 and 3. As can be seen from the obtained results, the blue light hazard of LED lamps with a directional diffuse surface, luminaires with a directional diffuse and diffuse transmission refers to RG0.

The assessment of the photobiological hazard of LED lamps and luminaires shows that in the vast majority of lamps belong to RG0 and are safe for indoor lighting.

Table 2. Parameters of LED spotlights for general lighting

Lamp characteristics	Lamp numbers	CCT, K	*Lv*, $W/m^2.sr$	RG
Bulb type A with directional diffusing surface	1	3729	22.1	0
	2	3748	21.6	0
	3	3788	18.7	0
	4	3793	7.2	0
	5	3796	46.1	0
	6	3816	23.1	0
	7	3857	27.1	0
	8	3883	1.5	0
	9	3910	27.3	0
	10	3929	33.2	0
	11	3935	27.4	0
	12	5707	42.7	0

For illumination of rooms in which the photobiological hazard of blue light should not exceed RG0 for any CCT, the brightness of the emitting surface should not exceed 10^4 kd/m^2.

Table 3. Parameters of LED luminaires designed to illuminate office and retail premises, educational and children's institutions, household premises

Luminaire characteristics	Lamp numbers	CCT, K	L_e, $W/m^2 \cdot sr$	L_v, kd/m^2	RG
With directional scattering transmission	1	3720	7.4	17090	0
	2	3905	23.2	47230	0
	3	4590	36.2	59250	0
	4	2852	30.4	104000	0
	5	2883	43.3	136000	0
	6	3377	44.6	139200	0
	7	3706	21.1	51010	0
	8	3742	25.3	56880	0
	9	3780	9.4	21300	0
	10	3938	379.8	802200	0
	11	5130	7.2	9156	0
With diffuse transmission	12	3652	2.9	7326	0
	13	3689	1.3	3182	0
	14	3714	1.7	4186	0
	15	3736	2.2	5300	0
	16	3770	2.0	4694	0
	17	3920	2.7	5989	0
	18	3925	6.5	13230	0
	19	3932	1.5	3342	0
	20	4739	6.9	11670	0

3. RESULTS

1) The photobiological hazard of blue light depends on the energy brightness, the angular size of the light source, the CCT, the distance to the observer;

2) Directional LED lamps, diffuse and directional transmittance luminaires generally do not exceed the RG0 blue light hazard limits. At brightness's not higher than 10^4 kd/m^2 for any CCT values in the range of 2700-6500 K, they refer only to RG0. LED lamps and luminaires for indoor lighting in terms of blue light photobiological hazard are safe for most applications;

3) Photobiological processes significantly depend on the emission spectrum, exposure time, and to some extent on the geometry of lighting devices, therefore it is important when implementing energy efficient lighting projects to use lamps and luminaires that meet the requirements of photobiological safety standards and recommendations regarding the safe conditions for the use of these products. These should be mandatory conditions for LED lighting.

NOMENCLATURES

1. Acronyms

LED: Light-Emitting Diode
CCT: Correlated Color Temperature
OR: Optical Radiation
IEC: International Electrotechnical Commission
ICI: International Commission on Illumination
LL: Luminescent Lamp
IL: Incandescent Lamp

2. Symbols / Parameters

L_B: Energy brightness
E_B: Energy illuminance
t: Exposure duration
$B(\lambda)$: Spectral weighting function of blue light hazard
L_V: Brightness
E_V: Illuminance
$L(\lambda)$: Spectral energy brightness

REFERENCES

[1] S.A. Baghirov, S.S. Baghirova, S.H. Kyslytsia, H.M. Kozhushko, S.Z. Mammadzada, "Circad Efficiency of Light-Emitting Diode Radiation for General Lighting", International Journal on Technical and Physical Problems of Engineering (IJTPE), Issue 50, Vol. 14, No. 1, pp. 172-176, March 2022.

[2] IEC 62471. "Photobiological Safety of Lamps and Lamp Systems", 2006.

[3] IEC/TR 62778, "Application of IEC 62471 for the Assessment of Blue Light Hazard to Light Sources and Luminaires", pp. 27-37, June 2014.

[4] IEC/TR 62471-2. "Photobiological Safety of Lamps and Lamp Systems, Part 2: Guidance on Manufacturing Requirements Relating to Non-Laser Optical Radiation Safety", p. 45, 2009.

[5] L. Lyons. "IEC Publishes Blue Light Hazard Assessment Guidelines", Semiconductor Lighting Engineering, No. 4, pp. 64-67, 2014.

[6] S.V. Shpak, L.N. Guba, Y.A. Basova, S.A. Baghirov, H.M. Kozhushko, "Research of the Quality of Color Rendering of LED Lamps and Luminaries", Scientific Bulletin, No. 1, Vol. 91, pp. 105-116, Poltava, Ukraine, November 2019.

[7] www.comsol.ru/blogs/calculating-the-emission-spectra-from-common-light-sources/.

[8] D.X. Slayn, "The Impact of new Lighting Products on Human Health and Safety", Lighting Engineering, No. 3, pp. 49-50, 2010.

[9] ICNIRP "Guidelines on limits of exposure to incoherent visible and infrared radiation", No. 105, Issue 1, pp. 74-96, 2013.

[10] F.B. Cohen, C. Martinsons, F. Vienot, G. Zissis, A.B. Sals, J.P. Cesarini, O. Enouf, M. Garcia, S. Picaud, D. Attia, "Light-Emitting Diodes (LED) for Domestic Lighting: Any Risks for the Eye?", Progress in Retinal and Eye Research, Vol. 30, pp. 239-257, 2011.

[11] S.V. Shpak, H.M. Kozhushko, S.H. Kyslytsia, T.V. Sakhno, O.S. Pitiakov, "Research of the Photobiological Safety of LED Lamps and Luminaires for General Lighting", Ukrainian Metrological Journal, No. 4, pp. 29-35, Kharkov, Ukraine, 2020.

[12] C. Martinsons, "Light Emitting Diodes (LEDs) and the Blue Light Risk", The International Review of Ophthalmic Optics, p. 7, May 2013.

[13] W.H. Guo, S.D. Yuan, T. Zhang, "Research on Blue Light Hazard Measurement Method Based on Actual Light Environment", Conference Proceeding by Commission International Lighting, pp. 1173-1180, 23 October 2017.

BIOGRAPHIES

Sabir Aghabaghir Baghirov was born in Jalilabad, Azerbaijan in 1961. In 1978, he entered Kharkov Civil Engineering Institute. In 1983-1987, he continued his career at Baku Electric Lamps Plant, Azerbaijan. In 1987, he entered Kharkov Civil Engineering Institute, Ukraine for a full-time postgraduate program on the specialty of lighting engineering and light sources. During his postgraduate studies, he worked as a junior researcher in Scientific Research Sector of the Institute. In 1990, he successfully completed his postgraduate studies and was appointed chief technologist at Baku Electric Lamps Plant, Azerbaijan. In 1993, he defended his dissertation on "The development and improvement of methods for dosing and mass determination of mercury in luminescent lamps" at Kharkov Institute of Municipal Engineers, Ukraine and received degree of Candidate of Technical Sciences. From 1993, he worked as a bureau chief, engineer-technologist of the 1st category in Technical Department, Baku Electric Lamps Plant. In 2013-2018, he worked as head of teaching laboratory at Azerbaijan Technical University, Baku, Azerbaijan. In 2016-2018 as Deputy Dean for Educational Affairs at Faculty of Electrical Engineering and Energy. In 2018, he was elected as a senior lecturer at the department. He is currently working on his doctoral dissertation on "Improving safety and energy efficiency in lighting systems" in higher education and research institutions of Ukraine. During his scientific activity he is the author of 39 articles, 9 inventions, 5 patents, 17 study textbooks.

Shalala Sabir Baghirova was born in Baku, Azerbaijan in 1998. In 2020, she graduated from Faculty of Energy, Electrical Engineering and Automation, Azerbaijan Technical University, Baku, Azerbaijan with a Bachelor's degree in electrical engineering. In 2020, she entered Master's degree in Energy Management at Azerbaijan Technical University. She continues his scientific research to save electricity in lighting equipment and improve the quality of lighting. She is a participant of national and international scientific conferences and the author of a number of articles.

The 18th International Conference on
"Technical and Physical Problems of Engineering"
30 October 2022
International Organization of IOTPE

ICTPE Conference
www.iotpe.com
ictpe@iotpe.com
ictpe0@gmail.com

ICTPE-2022 Number 27 Code 07TAP06 Pages 140-144

INVESTIGATION OF DEVELOPMENT FEATURES OF PHYSICAL PROCESSES UNDER INFLUENCE OF STRONG ELECTRIC FIELDS AND DISCHARGES OF VARIOUS DURATIONS ON SOLID DIELECTRICS

A.M. Hashimov [1] E.J. Gurbanov [2] K.B. Gurbanov [1]

1. Institute of Physics, Azerbaijan National Academy of Sciences, Baku, Azerbaijan
director@physics.ab.az, ahashimov@azerenerji.gov.az
2. Baku Engineering University, Baku, Azerbaijan, elqurbanov@beu.edu.az

Abstract- The study of changes in electro-physical properties of dielectric materials under influence of electric discharges has been studied for a long time. Electrical discharge activation of the surface of materials is of particular interest compared to mechanical, chemical, and temperature modification due to its application to materials with severe temperature limitations, exclusion of the use of toxic and explosive substances, and also in obtaining results, that are unattainable using traditional methods. In recent decades, great attention has also been paid to the development of short-duration high-voltage pulse technology for the implementation of various goals, both research and applied [1]. The interest are the processes, that initiate pulsed breakdown of dielectrics. Thus, this article will consider the development features of the physical processes, when solid dielectrics are exposed to strong electric fields and discharges of various durations, which is very important to consider, when choosing insulation, designing it, as well as during its production to prevent their breakdown when used in power systems.

Keywords: Short-Duration, Discharge, Electric Field, Pulse, Breakdown, Solid Dielectric, Nanosecond Duration, Runaway Electron, Treatment, Glass Fiber, Adhesion, Glow, Flame, Barrier, Crown.

1. INTRODUCTION

For dielectric materials, it is advisable to use activation by low-temperature non-equilibrium electric discharges - crown, glow, barrier, flame, the common property of which is a low energy consumption for heating the material. The higher the degree of non-equilibrium, that is, the difference in temperatures of electrons, ions and neutral particles, the less energy is spent on heating the gas, that is, all the energy received by "hot" electrons from the electric field is spent on ionization processes, excitation and dissociation of gas molecules or atoms surface layer of materials. It should be noted, that non-equilibrium discharges develop in high strength fields.

As is known, during operation, insulating structures can be exposed to strong electric fields and discharges of various durations. For example, when dielectric structures are exposed to fields and discharges of nanosecond duration, the development of breakdown processes proceeds differently than is customary in the classical version. Both in gaseous and condensed dielectrics, the main mechanism of these processes is associated with the effect of runaway electrons. The latter, as is well known, is associated with the violation of the electron energy distribution function in strong electric fields and the appearance of fast electrons capable of effecting impact ionization.

2. EXPERIMENTAL TECHNIQUE PART

In our researches, both various types of non-equilibrium electric discharges (crown, barrier, flame) and pulsed discharges of nanosecond duration were used. So, crown discharge is usually used as a charge generator [2]. For surface treatment, it is ineffective due to concentration near the electrode with a small radius of curvature.

Barrier discharges are widely used in technological processes of polymer film surface activation. A barrier discharge develops in thin gas gaps, bounded on one or both sides by dielectric barrier. Distances between the electrodes are 0.5-3 mm, and the voltage frequency is 50 Hz - 20 kHz. Electric field in the gap is homogeneous or weakly inhomogeneous. Physically, barrier discharge is a multi-avalanche process, that develops in fields with high intensity from 30 kV/cm to 70 kV/cm, and electron energies in crown sheath and in barrier discharge range from 2 eV to 15-20 eV, which corresponds to electron temperatures (25×10^3-250×10^3) [3]. Barrier discharge activation was carried out in various gases: air, nitrogen, oxygen, carbon dioxide, ammonia, and inert gases.

Surface treatment in oxygen-containing gases is more effective due to formation of atomic oxygen and ozone [4], including negative ions, which, under the action of electrostatic forces, immediately after formation adhere to dielectric surface.

Flame discharge, in contrast to barrier and crown discharges, covers large volumes of gas and the entire interelectrode gap. Physically, it is a flow of positive streamers, directed to cathode and is realized at distances between electrodes of 2-20 cm. Particularly, promising is the treatment of materials in dispersed form, for example, in the form of fibers or powders. The advantage of treatment in flame discharge in air is simplicity of its implementation (without use of chambers and pumping means).

To prepare the surface, a glow discharge is used, which is created in chamber at a gas pressure of 1-15 Pa and a voltage of several kV. Treatment of products in a glow discharge is carried out in oxygen, residual air or inert [5-7] and fluorine-containing gases [8]. It is shown, that the main parameters of a glow discharge, that affect the degree of treatment, are pressure, current density, and treatment time.

In [9], it was indicated, that there is a maximum in dependence of activation degree on the discharge current. With an increase in treatment time, the surface activity increases, and then either does not change or decreases, which may be associated with destruction of the surface layer. Adhesive properties remain from several days to several years. In a glow discharge, samples of C43-2 glasses and ST50-1 glass-ceramics were treated in oxygen, residual air, and inert gases. The increase in adhesion work in residual air was slightly lower, than in oxygen. In an inert gas, it was significantly lower, than in oxygen and air. Modifying effect of this type of discharge is associated with two mechanisms: first, it is the cleaning of the surface from adsorbed layers, which, during the subsequent deposition of coatings, create a weakly bound interfacial boundary; secondly, it is ion implantation. Technologically, the use of a glow discharge is associated with applying of pumping devices and sealing of reactors, which is not always acceptable (especially in the mass production of relatively large-sized products).

The use of barrier and flame discharges in relation to glass fibers leads to significant activation of the surface of bundles and an improvement in adhesion of glass fibers to epoxy resin. During production of glass fibers, a paraffin or polyterpene lubricant is applied to them, containing inert substances, that protect the glass fibers from mechanical damage and moisture. Lubricant greatly reduces the wettability and adhesion at the interface of the glass fiber-binder [10].

Physico-chemical activation of the surface layer of glass fibers depends on their location in bundle relative to the active zone of discharge, the contact time, and the physical mechanisms of interaction between the discharge and substance of the surface layer. In active discharge zone, charge carriers, that is, ions of both signs and electrons, are deposited on the fibers surface under action of fields (surface is charged) [11]. Calculations of charges and field strengths for fibers with a diameter of 13 μm give the value of limiting charge per unit length of the fiber [11]:

$$Q_{lim} = \frac{\pi\varepsilon_0\varepsilon \times rE}{1+(\varepsilon-1)\chi_\alpha} = 1\times10^{-10}\ \frac{\text{Cl}}{\text{m}} \qquad (1)$$

where, r is the fiber radius; E is the field strength (for streamer front $E=5\times10^6$ V/m); χ_a is depolarization coefficient, equal to the ratio of external field strength and self-charge field (for dielectrics, when charge is close to limit, $\chi_a = 1$).

With charges Q_{lim}, the electrostatic forces are quite sufficient to repel the fibers from each other (calculated accelerations $a = F/m$ give values of 0.1-1 m/s^2, which is enough to push apart from each other, if there is no sticking due to lubricants). The time constant for charging glass fibers is 10^{-4}-10^{-8} s, depending on conditions of charge flow, determined by resistivity of the surface layer, humidity, etc. Thus, after a short time, the fibers acquire charges sufficient to push them apart in the bundle from each other, which leads to fluffing of the bundle [12]. This phenomenon was observed visually in the flame discharge. The oscillatory motion of the fibers in discharge zone was observed both, when bundle was drawn through it and in a static position.

The integral effect of activation by flame and barrier discharges is established by measuring some parameters of finished products. Activation of the surface of glass fibers immediately before their impregnation with an epoxy binder, followed by polymerization, leads to two effects: more complete wetting of the glass fiber surface with the binder and higher adhesion at the fiber-binder interface [13]. In this regard, in oriented fiberglass plastics, for example, rods with a longitudinal by the arrangement of the fibers, the probability of the formation of longitudinal capillaries along the fiber-binder boundary decreases. This effect leads to decrease in water absorption and an increase in electrical strength in the longitudinal direction.

And now let's consider the features of physical processes, when exposed to strong electric fields and short-duration discharges on solid dielectrics. It has been shown in many articles [14, 15], that the Townsend ionization mechanism is valid even for very strong fields, when the distance to the cathode is large and the field strength exceeds the critical value, at which ionization friction of electrons on the gas can be neglected. In this case, to determine the average energy W_{av}, it is necessary to take into account the change in the number of electrons at $E > E_{av}$ as shown in Equations (2), (3) and (4) [14, 15]:

$$\frac{d\left(N_e W_{av}\right)}{dx} = eEN_e - F\left(W_{av}\right)N_e \qquad (2)$$

$$\frac{dN_e}{dx} = \alpha_i N_e \qquad (3)$$

$$\frac{dW_{av}}{dx} = eE - F\left(W_{av}\right) - \alpha_i W_{av} \qquad (4)$$

where, α_i is the impact ionization coefficient; N_e is the electron concentration in avalanche; W_{av} is the average electron energy. It can be seen from Equation (4), that even if deceleration of electrons by gas is completely neglected ($F[W_{av}]=0$), the average energy of electrons is limited [14]:

$$W_{av} < W_{av.\max} = \frac{eE}{\alpha} \qquad (5)$$

and at very large interelectrode gaps the Townsend ionization mechanism takes place (there are no runaway electrons) and electrons reaching the anode have low energies $W_{av} << eU$ **.**

At small distances between the electrodes $d < \frac{1}{\alpha_i}$, the electron multiplication differs radically from the Townsend one, and runaway electrons with maximum energy $eU = eEd$ predominate in the electron spectrum, and the lower point on the Paschen curve $\left(pd_{\min}\right)$ corresponds to ($\max\alpha_i$). In this case, the Paschen curve itself can be divided into three zones: the upper left branch of the curve corresponds to the electron runaway region, the region between the left and right branches corresponds to the electron multiplication region, and the zone below the right branch corresponds to the drift region of electrons that did not have time to multiply. Experiments [15] were carried out in uniform and nonuniform electric fields at elevated pressures in various gases (nitrogen, air, helium, neon, argon, krypton) without a preionization source.

In an inhomogeneous field under atmospheric conditions in air and nanosecond pulse durations, high specific energy inputs up to 1 J/cm^3 and an electron beam with a record current amplitude of ~70 A in air and ~200A in helium were obtained. In this case, a high-current beam at high pressure is formed due to runaway electrons. In a uniform field at the front of the voltage pulse, a volume charge is observed in the form of jets with plasma bunches on the cathode. With a decrease in the interelectrode distance, the diffuse discharge transforms into a contracted spark discharge. The magnitude and duration of the discharge current during a volumetric discharge depend on the parameters of the generator, interelectrode distance, pressure, and type of gas. With a volume discharge duration of 3 ns, the current density at the anode reaches 3 kA/cm^2, the specific energy input is ~1 J/cm^3, and the specific energy input power is ~400 MW/cm^3. In this case, the voltage across the gap is maximum in the quasi-stationary stage of the discharge, i.e., at the pulse front, when the number of fast electrons is large, and the propagation velocity of the avalanches, generated by these electrons, is $V_e \approx 10^8 \ \frac{\text{cm}}{\text{s}}$ (due to the preionization of the gap and which form a volume discharge).

Until recently, the runaway effect of conduction electrons in solid dielectrics was assigned a role similar to that realized in a discharge in gases. In this case, the mechanism of violation of the electrical strength of condensed dielectrics, especially solid ones, in the case of an electronic form of breakdown was considered similar to that of gaseous dielectrics.

When solid dielectrics are exposed to high-voltage pulses of nanosecond duration, it is already necessary to take into account the propagation velocity of the discharge channel, parameters of plasma state in discharge channel, its geometric dimensions, etc. It is not enough to know only the parameters of discharge gap (d, distance between the electrodes) and the high voltage pulse (U_0, discharge initiation voltage). By direct measurement of the propagation velocity of discharge channels by electron-optical chronography, it was found, that the speed of sound is the limit for propagation velocity of the discharge channel from the cathode and anode (i.e., $V_k < C_0 < V_a$, where V_k is the velocity of the discharge channel from cathode, V_a is from anode, C_0 is the sound speed. Mechanism of transition from subsonic primary channel to supersonic one requires special study. The speed V_a is determined mainly by voltage U_0 and corresponding instantaneous value dU/dt, while the speed V_k depends solely on U_0. Influence of the distance between the electrodes (d) and dU/dt on V_k is absent [16].

This may be due to the instability of the phase boundary of solid dielectric with its own melt. Supersonic rate of change in the curvature of this boundary under influence of super strong fields leads to appearance of a shock wave, which is consequence of the rapid energy release due to the injection of electrons from the valence band into conduction band and formation of the "shock wave + energy release zone" complex, called as electron detonation. As a result, a dense non-ideal high-pressure plasma arises, the destruction of which releases energy. Ionization degree of injected electrons will be determined as [17]:

$$\chi_e = \omega \frac{\Delta}{V} \tag{6}$$

where, $\omega = n / N$ is ionization probability, s^{-1}, n is number of electron-hole pairs; N is number of valence electrons); Δ is the length of shock compression zone; and V is the velocity of electron-detonation wave. In turn, ω depends on band gap and is defined as [17]:

$$\omega = \frac{n}{N} = \frac{\left(eEd^*\right)^2}{2\pi h E_d^*} \exp\left(\frac{E_d^*}{eEd^*} \ln\frac{1}{\alpha}\right) \tag{7}$$

where, α is the ratio of the width of valence band to the width of conduction band; E_d^* and d^* are, respectively, the effective value of band gap and the lattice constant under shock compression; and E is the field strength.

When solids are compressed, the band gap thickness varies linearly with pressure [17]:

$$E_d^* = E_{d0} - \alpha_p . p \tag{8}$$

where, $\alpha_p = \gamma . k$ is the pressure coefficient (J/Pa^{-1}), k is the compressibility factor, γ is the proportionality factor); E_d^* is the band gap after compression; and E_{d0} is the initial band gap.

These expressions make it possible to quantify in dielectrics the dependence of pressure P, the ionization probability ω, and the value E_d^* on the velocity of electron-detonation wave, to use the concepts and methods of high energy density physics to describe the dynamics and parameters of the matter state in discharge channel at the transition front at subsonic and supersonic velocities of its distribution [18].

Obviously, the rate of this process in various dielectric media and its "starting" parameters (U_0, dU/dt) are of particular interest. To correctly quantitatively take into account the influence of compressibility on the process of electron injection in solid dielectrics, it is necessary to carry out a number of experiments and theoretical studies. First of all, this applies to the study of influence of pressure α_p on electronic structure of wide-gap dielectrics. This will make it possible to more strictly determine the values of baric coefficients. We can say, that in this case this dependence will be nonlinear in a wide range of pressures.

3. CONCLUSIONS

Thus, this review summarizes the results of recent studies of the physics of high-voltage (alternating) electric discharges and pulsed discharges of nanosecond duration and their effect on solid dielectrics. The activation mechanism of the surface layer of solid dielectrics under influence of various types of non-equilibrium electric discharges at alternating voltage and breakdown of dielectrics under influence of high-voltage pulses of nanosecond duration is considered.

The results of the analysis showed, that among the known activation mechanisms under action of non-equilibrium electric discharges, the main role in increase in surface energy upon activation belongs to charging of components and formation of polar groups in substances, that form the surface layer of inhomogeneous dielectrics. In this case, activation of substances based on paraffin and polyterpenoid compounds, is associated with appearance of polar groups in oxidative reactions, initiated by dissociation products of molecules by electron impact under conditions of strong discharge non-equilibrium.

Breakdown mechanism of solid dielectrics under the action of nanosecond high-voltage pulses was also considered, and a quantitative interdependence between the electrical parameters of the process, thermodynamic parameters of substances, and physical properties of a solid dielectric was established. Results of the analysis showed, that taking into account this influence can lead to correction of existing and identification of new, previously not taken into account, phenomena, occurring in solid dielectrics. The development features of physical processes under influence of strong electric fields and discharges of various durations on solid dielectrics are studied.

REFERENCES

[1] E.J. Gurbanov, A.M. Hashimov, K.B. Gurbanov, "Study of the Most Energy-Efficient Modes of Generation of High-Voltage Nanosecond Pulses and Chemically Active Discharge Products for Active Disinfection of Fluid Food Products", International Journal on Technical and Physical Problems of Engineering (IJTPE), Issue 38, Vol. 11, No. 1, pp. 35-41, March 2019.

[2] C.M. Dzhuvarly, Y.V. Gorin, R.N. Mehtizade, "Crown Discharge in Electronegative Gases", Elm, p. 144, Baku, Azerbaijan, 1988.

[3] C.M. Dzhuvarly, G.V. Vechkhaizer, P.V. Leonov, "Electric Discharge in Gas Inclusions of High-Voltage Insulation", Elm, p. 193, Baku, Azerbaijan, 1983.

[4] I.L. Roikh, A.I. Fainshtein, "Mechanism of Surface Activation During Glow Discharge Processing", Physics and Chemistry of Materials Processing, No. 5, pp. 82-84, 1984.

[5] E.H. Voseen, "The Preparation of Substrates for Film Deposition Using Glow Discharge Techniques", J. Phys, E. Sci. Inst., Vol. 12, pp. 159-167, 1979.

[6] V.E. Kovalenko, S.A. Varchenya, "Influence of Glow Discharge Plasma on the Adhesion of Metal Condensates to Silicon Dioxide and Materials Based on it", Physics and Chemistry of Materials Processing, No. 1, pp. 63-68, 1988.

[7] B.A. Zharov, O.N. Solovieva, "Features of the Impact of a Glow Discharge on the Surface of Polymers", Electronic Processing of Materials, No. 5, pp. 49-51, 1988.

[8] Y.V. Gorin, F.K. Kulakhmetov, "On the Interaction of Electrical Discharges with Glasses", Electronic Processing of Materials, No. 2, pp. 28-30, 1992.

[9] I.L. Roikh, L.N. Koltunova, S.N. Fedosov, "Deposition of Protective Coatings in Vacuum", Mashinostroenie, p. 358, Moscow, Russia, 1976.

[10] Y.S. Lipatov, "Physical Chemistry of Filled Polymers", M. Chemistry, p. 304, 1977.

[11] B.I. Popkov, M.I. Glazev, "Kinetics of Charging and Dynamics of Fibers in an Electric Field", M, Nauka, 1976.

[12] E.D. Gurbanov, R.N. Mehtizade, I.N. Rahimov, K.K. Jalalov, "Influence of Dielectric Fibers on the Characteristics of the Flame Discharge", Reports of Academy of Sciences of Azerbaijan, Vol. 50, No. 10-12, pp. 10-15, 1994.

[13] Y.V. Gorin, F.K. Kulakhmetov, E.D. Gurbanov, "Effect of Dielectric Fibers on the Characteristics of a Barrier Discharge", Electronic Processing of Materials, No. 6, pp. 24-26, 1993.

[14] A.M. Tkachev, S.I. Yakovlenko, "Townsend Coefficient and Runaway Characteristics of Electrons in Nitrogen", Letters to ZhTF, Vol. 30, No.7, p. 14, 2004.

[15] I.D. Kostyria, V.S. Skakun, V.F. Tarasenko, A.M. Tkachev, S.I. Yakovlenko, "The Role of Fast Electrons in the Formation of a Volumetric Pulsed Discharge at Elevated Pressures", Letters to ZhTF, Issue 10, Vol. 30, p. 31, 2004.

[16] Y.N. Vershinin, "Correlation between the Rates of Electric Discharge and Sounds in a Solid Dielectric", JTF, Issue 2, Vol. 59, pp. 158-160, 1989.

[17] YN. Vershinin, D.S. Il'ichev, "Electronic Detonation in Solid Dielectrics", DAN, Vol. 365, No. 5, p. 197, 1999.

[18] Y.N. Vershinin, D.S. Il'ichev, P.A. Morozov, "Influence of shock Compression of Solid Dielectrics on the Injection of Valence Electrons in Strong Electric Fields", JTF, Issue 1, Vol. 70, 2000.

BIOGRAPHIES

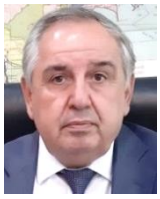

Arif Mamed Hashimov was born in Shahbuz, Nakhichevan, Azerbaijan on September 28, 1949. He is a Professor of Power Engineering (1993); Chief Editor of Scientific Journal of "Power Engineering Problems" from 2000; Director of Institute of Physics of Azerbaijan National Academy of Sciences (Baku, Azerbaijan) from 2002 up to 2009; and Academician and the First Vice-President of Azerbaijan National Academy of Sciences from 2007 up to 2013; and Director of Azerbaijan Research Institute of Energetics and Energy Design from 2014 up to 2020. From 2021 up to now he is Director of Institute of Physics of Azerbaijan National Academy of Sciences (Baku, Azerbaijan). He is laureate of Azerbaijan State Prize (1978); Honored Scientist of Azerbaijan (2005); Cochairman of International Conferences on "Technical and Physical Problems of Power Engineering" (ICTPE) and Editor in Chief of International Journal on "Technical and Physical Problems of Engineeing" (IJTPE). Now he is a High Consultant in "Azerenerji" JSC, Baku, Azerbaijan. His research areas are theory of non-linear electrical Networks with distributed parameters, neutral earthing and ferroresonant processes, alternative energy sources, high voltage physics and techniques, electrical physics. His publications are 350 articles and patents and 5 monographs.

Elchin Jalal Gurbanov was born in 1963. In 1986, he graduated from Electronics Faculty, Moscow Power Engineering Institute, Russia. In 1986-2006, he worked at Institute of Physics, Azerbaijan National Academy of Sciences, Baku, Azerbaijan as a leading scientific officer at Laboratory of "Physics and technique of high voltage". In 1995, he defended thesis on "Interaction of High Voltage Low Temperature Electric Gas Discharges with Components of Composite Materials" and awarded degree of Ph.D. in Physics. In 2006-2010, he studied at High Voltage Techniques and Electro Physics Department, Moscow Power Engineering Institute, National Research University and worked as a senior researcher. In 2018, he defended doctoral thesis on "Development of scientific and technological bases of effects of short-term high-electric pulses and gas discharges on different dielectric mediums" and awarded degree of doctor in technological sciences. At present, he works as an Assistant Professor at Department of Automation, Telecommunications and Energy, Baku Engineering University, Baku, Azerbaijan. He is the author of more than 100 scientific articles, have 3 patents and 1 certificate of authorship.

Kamil Bakhtiyar Gurbanov was born in Agdam, Azerbaijan on December 9, 1942. He is Candidate of Physical-Mathematical Sciences in the field of "physical mathematical sciences of polymers". He defended his dissertation at the Scientific Council of Institute of High Molecular Compounds, Academy of Sciences of RF, St-Petersburg, Russia in 1974. He is a Leading Researcher of the Institute on Physics, Azerbaijan National Academy of Sciences, Baku, Azerbaijan. He is a specialist on investigation of the physical-chemical processes in the conditions of action of the electrical discharges. Under his supervision the investigations on study of the processes of oxidation and modification of materials with the use of actions of the electrical discharges are carried out and also the high effective methods of solution of the ecological problems are developed.

The 18th International Conference on
"Technical and Physical Problems of Engineering"
30 October 2022
International Organization of IOTPE

ICTPE Conference
www.iotpe.com
ictpe@iotpe.com
ictpe0@gmail.com

ICTPE-2022 Number 28 Code 07TAP07 Pages 145-150

PARTIAL ANALYSIS OF THE MAGNETICALLY COUPLED RESONANT CIRCUITS UTILIZED IN A TYPICAL TESLA COIL WITH THE USE OF SECOND ORDER DIFFERENTIAL EQUATIONS

Nikan Mahdavi Tabatabaei

Department of Electrical and Computer Engineering, Aarhus University, Aarhus, Denmark
n.mahdavi.tabatabaei@gmail.com

Abstract- In this article we are going to be looking at the theory of operation of a typical Tesla coil, trying to understand this outstanding phenomenon and having a look at the essence of the presence of the RLC coupled resonant circuits in the Tesla coil and its consequences on the voltage gain of the system. We will then later in the article analyze these circuits mathematically by using second order differential equations and explain the wave functions for both of these circuits and try to come up with a technical and physical explanation for the theoretical outcomes. We are hypothetically going to witness that the first and the second circuits are in great harmony with each other, since they have the same resonant frequency, delivering their own energy to the other circuit and vice versa harmonically. This fascinating and mesmerizing system has a lot of remarkable mathematics and physics operating behind it, which are without a doubt worth analyzing.

Keywords: Tesla Coil, Resonant Frequency, RLC-Circuits, Second Order Differential Equation, Primary and Secondary Circuits, Magnetic Coupling, Transformer, Wave Functions, Quenching.

1. INTRODUCTION

The Tesla coil is without a doubt one of the best-known inventions of the great inventor Nikola Tesla. The Tesla coil, or as he called it "Apparatus for transmitting electrical energy" on his submitted patent in the year 1914, consists of two resonant RLC-circuits, though theoretically only containing capacitors and inductors, which are tuned in a way that both of the circuits have the same resonant frequencies, and thereby achieve highly efficient energy transformation between these circuits.

When you look at a standard Tesla coil, you may think that it looks like a huge transformer, just stepping up the voltage and achieving some voltage gain, but the theory of operation of these two devices are completely different and absolutely divergent. A usual transformer uses magnetic induction to step up the voltage, while a Tesla coil mainly uses resonant amplification between its two circuits to achieve the desired voltage gain.

We will prove that these two mentioned methods are just as effective when it comes to achieving voltage gain through the coils, but at very high frequencies, in which the Tesla coil operates, resonant amplification is just the better option when it comes to energy efficiency, and that is why Nikola Tesla chose to integrate the RLC-arrangement into his design instead of a standard transformer. Though a transformer is normally used in a Tesla coil to step up the low frequency voltage from our alternating current generator source to feed the primary circuit, which is shown in Figure 1 [4].

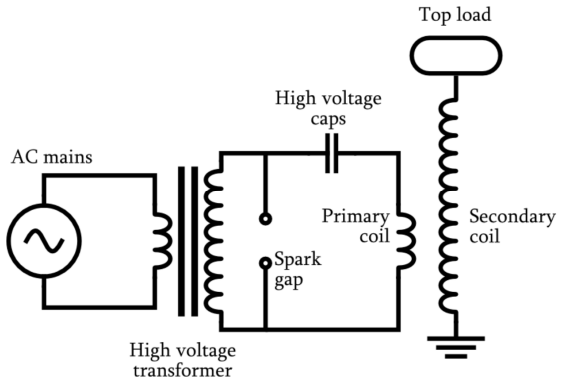

Figure 1. The circuit diagram for a conventional Tesla coil [2]

The Tesla coil continues to produce high voltages of up to hundreds of kilovolts and generate the gigantic sparks that everybody loves to see. In the following article we will be looking at the theory of operation of this fascinating device and the mathematical miracle that lay behind these physical phenomena in this design. Let us though for now get into the theory of operation of this intriguing and unique device. [7]

2. THEORY OF OPERATION

After stepping up the voltage with the help of the primary transformer we move forward to analyzing the primary and the secondary circuits' main characteristics. The main source's frequency is typically at 50 Hz, and so is the voltage fed to the primary circuit by the installed

transformer. The capacitance of the primary capacitor is deliberately chosen so that it almost is fully charged at 1/100 of the second. The spark gap is made so that the air breakdown happens exactly at the voltage peak of the capacitor.

Thus, when the voltage reaches its peak value, the spark gap fires, and the adjacent circuit "opens". Now we have an RLC-circuit, in which the current begins oscillating with the circuit's resonant frequency, if the resistances of the circuits are not too big, which they are not in this case. Since the secondary circuit is magnetically coupled with the primary circuit and is tuned to have the same resonant frequency as the latter, a voltage with the same frequency is induced in the secondary circuit. This mentioned resonant frequency is usually much higher than the main source's frequency, being typically between 50 kHz and 400 kHz, which is anywhere from 1,000 to 80,000 times higher than the main source's frequency. As the time goes on, the energy in the primary circuit is steadily transferred over to the secondary circuit. As this happens, the amplitudes of the oscillations in the primary circuit decrease sinusoidally, while the amplitudes of the oscillations in the secondary circuit increase also sinusoidally. When all the energy is stored in the secondary circuit this energy is then magnetically induced back in to the first circuit, and the cycle repeats again and again. Since the constant of magnetic coupling is intentionally kept low at around 0.05 to 0.2, several oscillations are required to achieve total energy transfer from one circuit to another.

Now that we know how a Tesla Coil operates, you might wonder how the secondary circuit magnetically induces a voltage in the primary circuit, when the voltage amplitude across the primary circuit is equal to zero, and thereby the spark gap is not excited. Is not the circuit open? The thing is that the spark gap has not had enough time to "quench" yet and the air between the spark gap is still ionized, and so the spark gap is technically still excited. This is how this procedure can keep going and duplicate itself repeatedly even at much lower voltage amplitudes [1, 2, 5].

At the end when the voltage in the secondary circuit has reached its peak value due to resonant rise, sparks will be fired from the top load, since the air around the top load has also been ionized during the process due to the high voltage and the masses of charges now stored at the top load.

3. THE SECONDARY CAPACITOR

In a normal Tesla coil the resonant frequency of the primary and the secondary circuits must be exactly the same, in order to have maximized voltage gain. This situation is also analogous to numerous mechanical phenomena like the harmonic oscillation of a spring or even that of atoms, when we are discussing quantum mechanics. This resonant frequency is hereby equal to:

$$f_{res} = \frac{\omega_{res}}{2\pi} = \frac{1}{2\pi\sqrt{L_p C_p}} = \frac{1}{2\pi\sqrt{L_s C_s}}.$$

The magnitude of the inductances of both coils in both circuits can easily be calculated, since the inductance of such a solenoid is equivalent to $L = \frac{\mu N^2 A}{l}$ where l is the length of the solenoid, A is the cross-sectional area of the solenoid, N is the number of turns of the coil, and the Greek mu indicates the permeability of the coil [6].

The capacitance of the capacitor in the first circuit can easily be found, but the capacitance of the second circuit is usually very hard to calculate, since there are so many different contributions to this magnitude. Therefore, it is always a good idea to replace the conventional capacitor in the first circuit with a variable capacitor, so that we always are able to tune the capacitor to the exact capacitance, where there is a mutual resonant frequency between the two circuits.

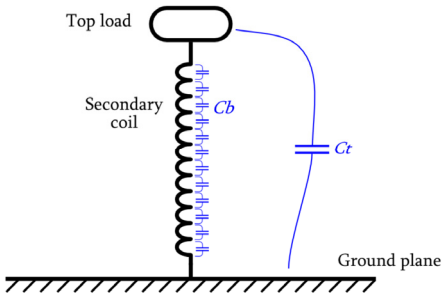

Figure 2. A sketch of some of the contributions to the diminutive capacitance of the secondary circuit [2]

The capacitance appearing in the second circuit can either be due to the contributions from the capacitance between the top load and the ground, the relative capacitance of coil turns, or other factors. There is a clear capacitance between the top load and the ground, where the medium/dielectric in this rather "unnormal" capacitor is simply air. Even though the top load and ground are also connected through the secondary coil, the coil's impedance is too high for it to be a part of this "capacitor".

Since the wires used in the secondary coil are not ideal superconductors, the wires in the coil themselves have resistances, and since these resistances (and also the inductances) of the coil are distributed all along the length of the wire, there is a slight amount of voltage drop off between the two adjacent turns of the coil. There are also potential differences between nonadjacent turns in the coil, but because of the presence of a longer distance these contributions are quite negligible. As shown in Figure 2, there are thousands of these tiny contributions in the secondary circuit, which make up a part of this secondary capacitance.

There may be all other kinds of contributions to the secondary circuit's capacitance. As an example, when sparks occur from the top load, there is a minor contribution to the secondary capacitance. There are furthermore environmental factors that can play a role in this aforementioned capacitance.

As it is observable in Figure 2, each of these discussed forms of capacitances are in parallel with each other, thus the total capacitance of the second circuit is the sum of all

these minor contributions. This capacitance is extremely small, and since $L_pC_p = L_sC_s$ is the case, due to the identical resonant frequency of the circuits, the secondary circuit's inductance must be tremendously larger than the first one's. This is usually achieved by utilizing a large number of windings in the secondary coil [1, 2].

4. THEORETICAL VOLTAGE GAIN

Let us now try to estimate the amount of voltage gained in such a system. The following derivation is based on the conservation of energy theorem; that is there is no ohmic or nonohmic resistors or other non-conservational devices that contribute to dissipation of energy in the two circuits.

Since the energy is first transferred from the primary circuit to the other, the maximal energy in the first circuit is equal to the maximal energy in the second circuit, that is when the capacitors are fully charged in each circuit; thereby we have that: $\frac{1}{2}C_pV_p{}^2 = \frac{1}{2}C_sV_s{}^2$. The V_p indicates the rms-value of the primary voltage and the V_s indicates the rms-value of the secondary voltage. Rewriting gives $\frac{V_s}{V_p} = \sqrt{\frac{C_p}{C_s}}$, and inserting $L_pC_p = L_sC_s$ into the equation gives $gain = \frac{V_s}{V_p} = \sqrt{\frac{L_s}{L_p}}$.

Now since the magnitude of the inductance of the secondary circuit is significantly larger than the magnitude of the inductance of the primary circuit, due to the opposite capacitor ratios, the voltage gain is also tremendously high. We are talking about output voltages of up to 10^6 orders of volts. Hence in a nutshell, this is how a Tesla coil is able to produce such high output voltages. You could argue that a normal transformer tends to step up the voltage with $gain = \frac{V_s}{V_p} = \frac{N_s}{N_p}$, which you might think is higher than the voltage gain achieved by resonant amplification. You are not exactly right. Because as said the inductance of a solenoid is equal to $L = \frac{\mu N^2 A}{l}$, which means that the voltage gain of a Tesla coil is also proportional to the winding ratio $gain = \frac{V_s}{V_p} \propto \frac{N_s}{N_p}$. Though since we tend to make the secondary coil longer and thinner and the primary coil shorter and thicker, the voltage gain might be very slightly less than a conventional transformer, but that's another discussion.

The actual problem with a transformer is the fact that you are forced to use an iron core in order to achieve great coupling and thereby highly efficient energy transformations, but when an iron core is used at very high frequencies it acts as much more of a resistor rather than a serving assistant, and since we here are working with very high frequencies and voltages resonant amplification with very low magnetic coupling constant is quite desirable and definitely the best way forward [1, 2, 3, 4].

5. EVENTUAL SOURCES OF ERROR

In this derivation we have not accounted for potential internal resistances of the circuits, which may contribute to energy loss throughout the circuits. We have used energy conservation, but we know for the matter of fact that this is practically not the case in the real world.

There are obviously numerous distinct ways, in which energy losses can occur in systems like this. As an example, we can discuss the fact that since there usually are several hundred meters of wire used in a Tesla coil, there is a tremendously large resistance present in each of the two circuit, contributing to energy loss whitin the circuits with the rate of $P = RI^2$ if they are ohmic, and if they are non-ohmic (as they ordinarily are) the resistance is a function of the temperature (and therefore so is the power P).

Furthermore, the impacts of the skin effect are easily perceptible on the resistance of the circuits on such high frequencies; that is when the current flows predominantly near the surface of the wire, which occurs at significantly high frequencies and thereby increases the resistance of the circuit entirely.

The spark gap itself acts kind of like a resistor, when the circuit through it is closed, thus dissipating a huge amount of energy in the form of light, heat and sound through each spark.

The dielectric itself inside the capacitor of the primary circuit, depending on the type of dielectric used and the operation frequency, dissipates a relatively small though accountable proportion of the energy when such an alternating current is applied to its junctions.

Moreover, when operating on such high frequencies, energy loss due to emission of electromagnetic waves is practically inevitable. Another energy loss contribution is from the top load, which is trying to ionize the air around itself to be capable of generating sparks.

6. QUENCHING

Quenching is the act of cooling down of the air, which occurs when the air stops being under breakdown and is not ionized anymore. In practice we want to achieve this quenching act for the spark gap between the cycles, that is when the primary circuit has delivered all its energy to the secondary circuit and the primary circuit is "resting". But the thing is, that if quenching happens at that exact moment the secondary circuit would not be able to magnetically induce the energy back to the primary circuit in the first half-cycle until the voltage reaches its peak value and thereby no energy is dissipated through the spark gap in the primary circuit during the first half-cycle, and thus more energy is transferred to the secondary circuit in total without dissipation.

Quenching is achieved by having a small magnetic coupling constant between the two coils of the two circuits. Having weak coupling between the circuits gives enough time for the spark gap to quench, though the problem with having weak coupling, in other words spacing the coils further apart from each other, is that it takes several oscillations for the energy to be transferred from the primary circuit to the secondary circuit, which in turn leads

to huge energy dissipation in the primary circuit is because of the spark gap. The problem with high coupling is that even though energy is transferred relatively quickly, the spark gap does not have enough time to achieve quenching, which means energy is dissipated through the spark gap in the primary circuit during the whole cycle instead, which in turn is quite the contrary to the latter. Having the ideal coupling constant helps us attain both of these good traits, that is being able to quench and transfer the energy fast between the circuits at the same time. This is crucial for building an ideal Tesla Coil. This ultimately ideal magnetic coupling constant tends to be around 0.05 to 0.2 [3].

7. DISCOVERING THE WAVEFUNCTIONS

We are now going to analyze a supposedly ideal Tesla coil, which contains two magnetically coupled resonant circuits as shown in Figure 3.

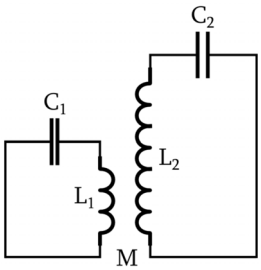

Figure 3. The schematic diagram for the magnetically coupled ideal LC-circuits of the Tesla coil [2]

Applying Kirchhoff's loop rule to both circuits, we obtain the Equations (1).

$$\begin{cases} L_1 \dfrac{d^2}{dt^2} q_1(t) + M \dfrac{d^2}{dt^2} q_2(t) + \dfrac{1}{C_1} q_1(t) = 0 \\ L_2 \dfrac{d^2}{dt^2} q_2(t) + M \dfrac{d^2}{dt^2} q_1(t) + \dfrac{1}{C_2} q_2(t) = 0 \end{cases} \quad (1)$$

Since these two circuits are in perfect resonance, we know that the operating frequency of both these circuits are the same, as suggested by Equation (2).

$$\omega_1 = \omega_2 = \omega_{res} \quad (2)$$

$$q_1(t) = \frac{Q}{4}\left(\cos\left(\frac{\omega_{res}}{\sqrt{1+k}}t\right) + \cos\left(\frac{\omega_{res}}{\sqrt{k-1}}t\right)\right) \quad (3)$$

$$q_2(t) = \frac{Qk}{4C_1\omega_{res}^2}\left(\cos\left(\frac{\omega_{res}}{\sqrt{1+k}}t\right) - \cos\left(\frac{\omega_{res}}{\sqrt{k-1}}t\right)\right) \quad (4)$$

where, k stands for the constant of magnetic coupling between the coils and is under the circumstances $0 < k < 1$. Notice that the formulas can be expressed in both the cartesian and the polar forms, though we have used Euler's formula to expand the expressions [1, 2].

We, furthermore, consider the following initial conditions for the system:

$$\begin{cases} q_1(0) = Q \\ \dfrac{d}{dt} q_1(0) = 0 \end{cases}, \quad \begin{cases} q_2(0) = 0 \\ \dfrac{d}{dt} q_2(0) = 0 \end{cases} \quad (5)$$

By sketching the graphs for these functions, we obtain the results shown in Figure 4 [1, 2].

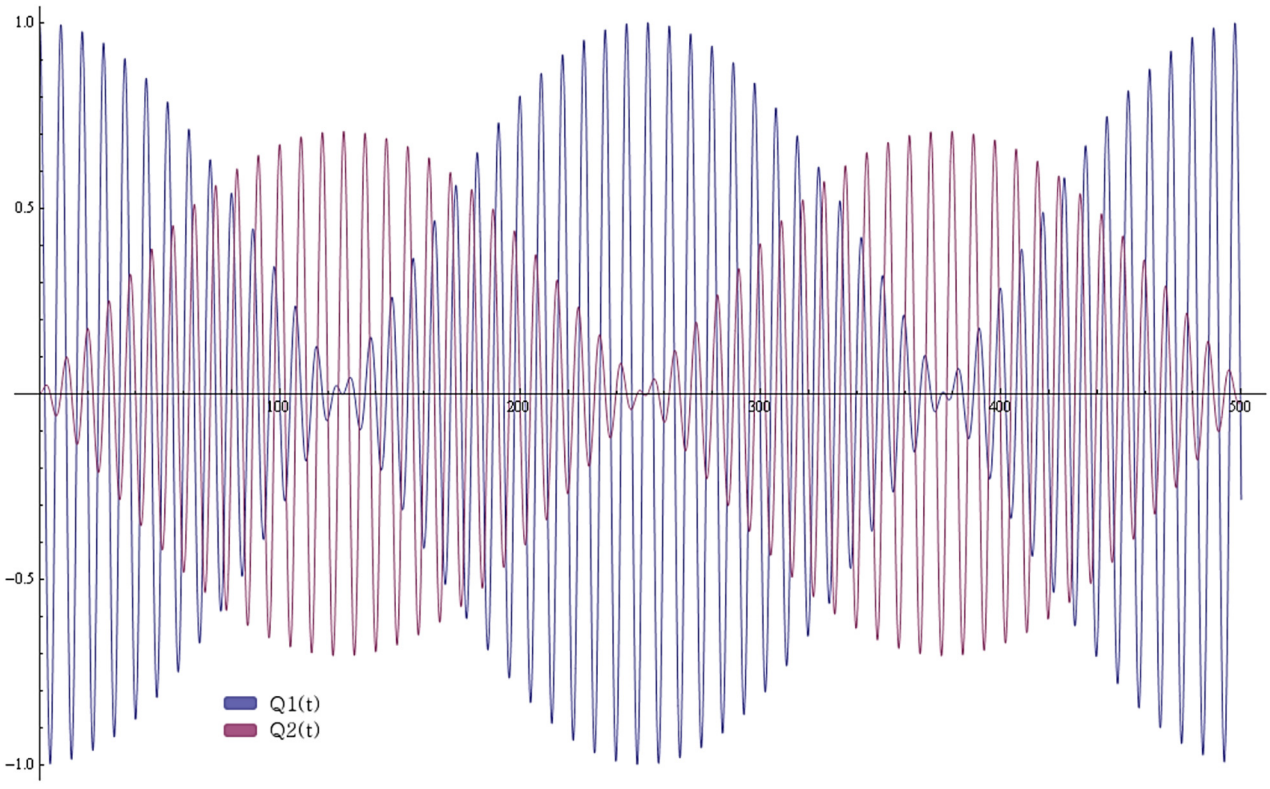

Figure 4. The graphs for the charges in both circuits relative to the time, according to Equations (3) and (4) [2]

Now it is time to look at the same circuits, but this time with additional resistances in series with each circuit, representing the sum of the contributions to the internal resistances of the two circuits as shown in Figure 5.

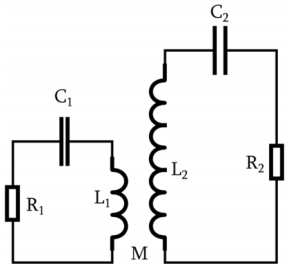

Figure 5. The schematic diagram for the magnetically coupled more realistic RLC-circuits of the Tesla coil [2]

Applying Kirchhoff's loop rule to the new circuits we obtain Equations (6) as follows:

$$L_1\frac{d^2}{dt^2}q_1(t)+M\frac{d^2}{dt^2}q_2(t)+R_1\frac{d}{dt}q_1(t)+\frac{1}{C_1}q_1(t)=0$$
$$L_2\frac{d^2}{dt^2}q_2(t)+M\frac{d^2}{dt^2}q_1(t)+R_2\frac{d}{dt}q_2(t)+\frac{1}{C_2}q_2(t)=0 \quad (6)$$

We again consider the two operating frequencies to be equal to the circuits' resonant frequency. There is actually no analytical solution for the differential equations given by Equation (6). These equations must be solved numerically. Implementing this system in a computing software and using the same initial conditions as the previous system, given by Equation (5), we obtain the following results as shown in Figure 6 [1, 2].

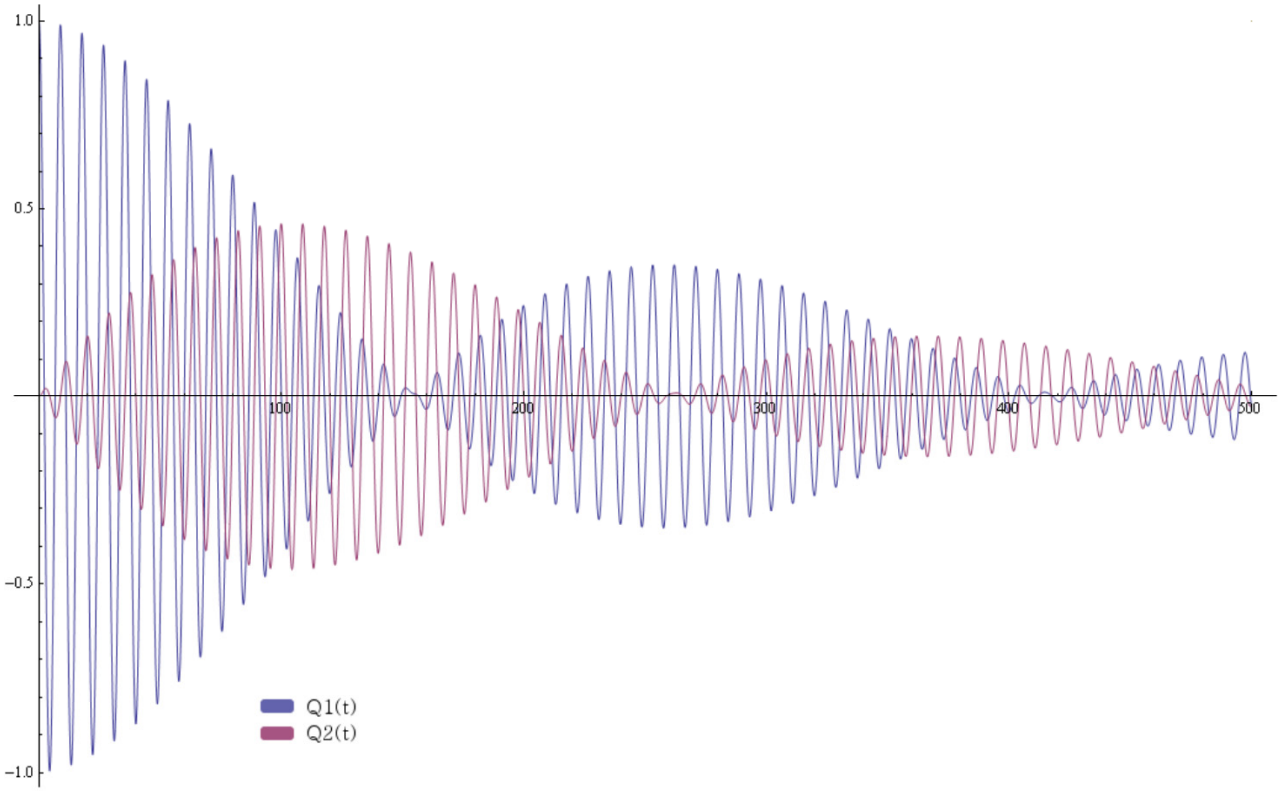

Figure 6. The graphs for the charges in both circuits relative to the time, acquired by solving Equation (13) numerically [2]

8. CONCLUSION

The graphs shown in Figures 4 and 6 correspond well to our theories. The energies get transferred harmonically from one of the circuits to the other and vice versa. There are though shifts in the frequencies of the two induced voltages in Figure 6, since there are resistances present in both of the circuits that manipulate the resonant frequency and thereby the operating frequency. The shifts are not homogenous since the resistance of the secondary circuit is considerably larger than the resistance of the primary circuit, which has been accounted for in our calculations [1, 2]. Now we understand why the Tesla coil is so significantly unique and very different from a conventional transformer and why it is so efficient when it comes to energy transformation at such high frequencies compared to a conventional transformer.

This astonishing invention by Nikola Tesla is only one of the few remarkable inventions of his. Tesla continues to invent the first radio (even before Marconi), the first ex-ray and the first AC motor in the history of mankind. These are still only a few examples of his great work. Tesla is definitely the inventor of the future.

REFERENCES

[1] C. Gerekos, "The Zeus Tesla Coil", Hazardous Physics, September 2011, http://hazardousphysics.christophergerekos.eu/main/zeus/The_Zeus_Tesla_Coil_2.html#theory-cycle.

[2] C. Gerekos, "The Tesla Coil", Free University of Brussels, 2011-2012, http://hazardousphysics.christophergerekos.eu/main/zeus/TheTeslaCoil-en.pdf.

[3] R. Burnett, "Quenching", Richie's Tesla Coil Webpage, http://www.richieburnett.co.uk/tesla.shtml.
[4] "How to Design a Tesla Coil", EDN Asia, December 9, 2019, https://www.ednasia.com/designing-a-tesla-coil/.
[5] K. Wilson "Tesla Coil Design, Construction and Operation Guide", www.teslacoildesign.com/design.html.
[6] "Self inductance of a long solenoid", Khan Academy, YouTube, 2017, www.youtube.com/watch?v=OhHcE9zLA7E.
[7] Nikan M. Tabatabaei, "Understanding RLC-Circuits Using Differential Equations and Phasor Diagrams", Ringkobing Gymnasium, Denmark, March 2022.

BIOGRAPHY

Nikan Mahdavi Tabatabaei was born in Tabriz, Iran, on October 1, 2003. He graduated from Ringkobing Gymnasium (High School), Denmark in the year 2022. He is currently studying Electrical Engineering at the Department of Electrical and Computer Engineering, Aarhus University, Aarhus, Denmark. He was a part of the Danish National Physics Olympiad Team in 2022 and was one of the winners of the Danish Mathematics Olympiad in 2022. He is a student member of the International Organization on Technical and Physical Problems of Engineering (IOTPE). His research interests regarding Electrical Engineering are particularly in the area of Advanced Controls in Power Electronics Systems.

The 18th International Conference on
"Technical and Physical Problems of Engineering"
30 October 2022
International Organization of IOTPE

ICTPE Conference
www.iotpe.com
ictpe@iotpe.com
ictpe0@gmail.com

ICTPE-2022 Number 29 Code 08ELM01 Pages 151-155

IMPACT OF THE PROFESSIONAL TRAINING IN ENGLISH DISCIPLINE ON LIFELONG LEARNING FOR FUTURE POWER ENGINEERS

L.V. Krivova

Higher School of High Voltage Engineering, Peter the Great Saint Petersburg Polytechnic University, Saint Petersburg, Russia, krivova.milla@gmail.com

Abstract- In the paper author represents the influence of mastering the professional disciplines in English for the future specialists' competences in power engineering, the impact of the special subject courses in non-native language for lifelong learning. The bachelor and master degree student curriculum are analyzed according to share of disciplines contact hours. The results of integrating the new engineering tasks of the top levels of Bloom's taxonomy are described in details. Anonymous survey of undergraduate and graduate respondents illustrates the successfulness of the designed class structure. The recently developed tasks for laboratory works are granted and possible scenarios for their adoption in the educational process are illustrated.

Keywords: Lifelong Learning, Curriculum, Fundamental Discipline, Professional Discipline, Hard Skills, Soft Skills, Power Engineer, Bloom's Taxonomy.

1. INTRODUCTION

Nowadays, the processes of science and technology are characterized by amazing rate, everything is changing very quickly being developed and improved. Modern engineer as well as a high school graduate should be able to acquire information, apply the relevant achievements of science and technology, and interact with colleagues abroad. Moreover, innovative solutions of professional problems require an approach beyond the traditional limits. Obviously, polytechnic universities all around the world should focus on the professional training in English by implementing modern educational technologies.

It is evident that the higher education institutions should focus on the modernization of the training path of future specialists. In this context, the new ways in the educational process gives to the engineering schools an opportunity to meet the requirements of the industry. New challenges and possibilities for academic staff and students require upgrading of educational programs. The combination of hard (professional disciplines) and soft (English proficiency, for instance) skills requires:

1) authentic materials as the educational resources (for lectures, seminars, etc.);
2) a new approach for outcomes assessment;
3) modern technologies for effective educational process arrangement.

Progress in power engineering equipment, design, and technologies lead to rapid "aging" of graduates' knowledge. Therefore, most of obtained knowledge may become irrelevant within 10-15 years in average. In this case the crucial goal of modern education - is to develop sustainable hard and soft skills and to motivate to lifelong learning [1, 2]. For example, the South Korea priorities the e-learning as an instrument for enduring study and have founded few cyber universities with electronic educational services that are focused on conception of professional knowledge and competences growth. The lack of natural resources of the country are substituted by the human resources and new breakthrough in science and technology. Graduating the university all students are taking the English exam as very important soft skill for future engineers.

Solving the modern engineering challenges requires to take into account not only sophisticated devices choice but also economic, environmental aspects, footprint of designed installation [3]. Therefore, the once obtained knowledge educational way is replaced by the process of progressive self-education. Teachers' responsibility in this case consists in:

- To apply the innovative professional information, up-to-date technologies in educational process,
- To structure the authentic materials and design assignments and projects according the Bloom's taxonomy,
- To synchronize the course materials with initial English level.

Contemporary professional competences are formed by taking into account the regular amendment of the disciplines content. Thus, it becomes visible that the modern teachers and students should be ready for continuous adapting to a constantly changing world [4]. Assuredly, the Bloom's taxonomy may be applied to course design and lectures, practical training and labs planning as an effective tool.

2. CURRICULUM ANALYSIS

For analysis, the curriculum for bachelor and master degree students training of the Tomsk Polytechnic University, Russia was chosen, the specialty is "Automation of Power Plants and Power Systems".

2.1. Bachelor Degree Curriculum

Entering the university for bachelor training, students are firstly study the fundamental (general) disciplines that are the basis for professional knowledge. From semester to semester the general or fundamental disciplines quantity is reduced while the professional disciplines are becoming predominant (Figure 1).

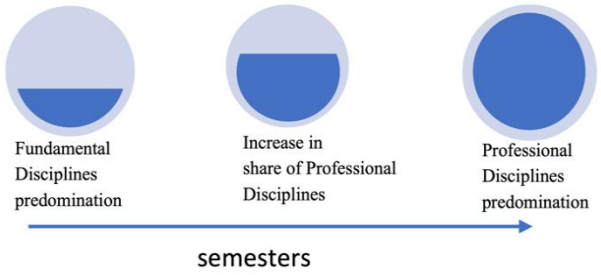

Figure 1. Distribution of the disciplines through semesters [5, 6]

In bachelor degree curriculum:

- "General English" discipline - 432 hours in total (were included in general/fundamental disciplines). Students are trained by linguistic teachers.
- "Professional Training in English" - 288 hours (were included in professional disciplines (Figure 2). These disciplines are delivered by professors of engineering departments. Requirements to language and pedagogical skills of such instructors are considered as ultimately high [5].

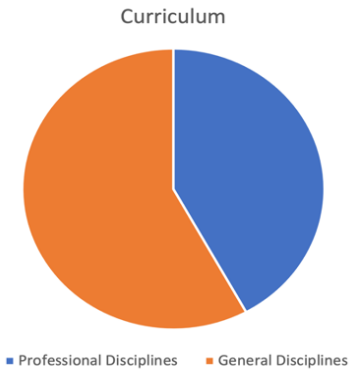

Figure 2. Share of general and professional disciplines for the B.Sc. curriculum [5]

General English is delivered at first two years of education and on the learning outcomes the next foreign language training is based. Traditionally, students are prepared for passing equivalent of Cambridge exam in the end of the eight semesters. From fifth to eight semesters scholars study the special subjects in English. Professors of the Institute of Power Engineering are involved in delivering classes on "Professional Training in English". Therefore, the classes content is focused on materials related to the future specialty of students.

2.2. Master Degree Curriculum

The "Professional Training in English" discipline, 216 hours in total, were included in share of professional disciplines (Figure 3) [6].

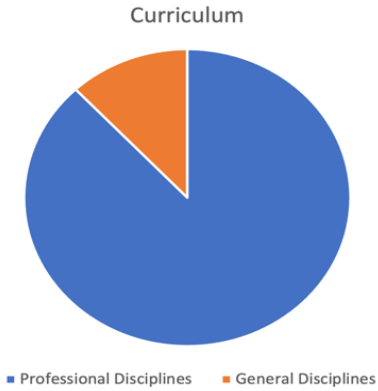

Figure 3. Share of general and professional disciplines for the M.Sc. curriculum [6]

Achieving the learning outcomes is provided by authentic literature (textbooks, scientific papers) or video resources of equipment manufacturers (Alstom, Siemens, General Electric, Prefetch, etc.), catalogs of power equipment of world well-known companies, reference books, schemes of the electrical connection of power plants and part of power systems, labs, conferences, presentations, online course in LMS Moodle [7, 8]. The final task is to write one chapter of master degree thesis in English. Optionally all the thesis may be completely fulfilled and defended in English. Obviously, the language knowledge of student is expected to be extremely high in this case.

For analysis, students survey was conducted between bachelor and master degree students of the Tomsk polytechnic university at the entering and before graduating the course "Professional Training in English" [9, 10]. Students were asked to assess their ability and readiness (from 0% to 100%) to be involved in various tasks that were used for achieving the learning outcomes (Table 1). The percentage in the chart indicates:

- Tasks focused on memorizing the information are the most suitable for starting the professional course in non-native language,
- Paper based assignments are psychologically more comfortable than listening and speaking tasks,
- Creative tasks are challenging for most students at the entering the course.

It should be noticed that master students have no obligation to use traditional solution for project tasks. Freedom in solving engineering tasks inspired them to find creative solution and overcome language barrier, be more familiar with nameplate parameters of equipment in English, be able to find appropriate information for project and for the master thesis chapter written in English consequently.

Table 1. Survey of B.Sc. and M.Sc. students

Participants / Tasks	Bachelor students		Master students	
	before %	after %	before %	after %
1. authentic texts (reading, translating, fill in the gaps, reconstruction)	58	94	78	99
2. tests, quizzes	55	93	67	98
3. authentic video (to watch, to answer the questions, to fill in the gaps)	33	79	63	86
4. labs (topics are not new)	64	91	70	99
5. individual projects	28	88	36	92
6. presentation (individual topic)	21	77	40	91
7. conferences, discussions	8	52	35	69

3. CREATIVE PROFESSIONAL TASKS

Taking into account few years' experiences of delivering professional topics in English and relying on deep analysis of some scientific papers devoted to the Bloom's taxonomy application to designing courses for future engineers tasks are recommended to be formed in accordance with cognitive levels (Figure 4), from the terms repeating at the very beginning to the analysis of the calculation results, proposing the better technical solution, and finally evaluating the chosen in the project equipment [11].

Figure 4. Bloom's taxonomy cognitive levels [11]

Choosing the proper materials for master students trained by the "Professional Training in English" discipline is obligatory to analyze the next initial information:

– Students' background on professional disciplines,
– Students' English language level,
– Hours for face-to-face classes,
– Declared in syllabus the learning outcomes after graduating the course.

In average, master degree students have the intermediate or even upper intermediate English level, what is enough for future success in professional activity and readiness for self-mastering new information connected with progress in power industry. For master students the creative tasks are more practical, interesting and effective.

3.1. Switching Procedure Simulation

Last year the new lab assignment was developed and involved in the educational process. The main idea is to focus more on switching procedure instead of English (Figure 5). Scholars were very enthusiastic at implementing simulation of switching procedure for the scheme with two work buses and transfer bus, traditionally used for 110 and 220 kV switchyards in Russia. This scheme was chosen for lab as the widely used in the course project "Power Plants and Substation Design", delivered in Russian. Listeners were asked to explain the procedure of circuit breaker repair with no power supply interruption. Errors are alarmed in visual and sound way with comments of load lost, for example. Having fulfilled the procedure, students overcome some inconvenience in using English for professional tasks and also noticed the better terms memorization.

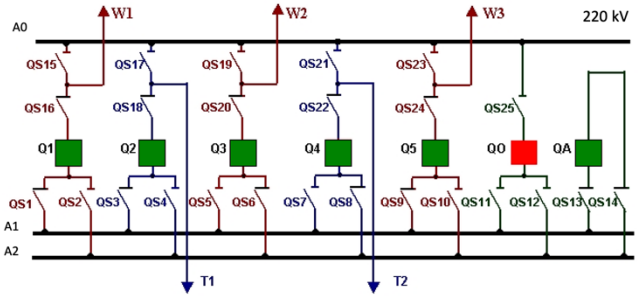

Figure 5. Simulation of the switching procedure [8]

3.2. Switchyard Modernization Analysis

In the discipline "Power Plants Design" that is delivered in Russian, students have to complete the individual course project. Traditionally, the main scheme solutions and chosen equipment are characterized by conventional approach and rather obsolete design. For the same course delivered in English it was proposed to retrofit the high voltage switchyard from the design power station with the replacement of:

- Air blast circuit breakers and free-standing horizontal center break disconnectors with modern disconnecting circuit breakers (DCB),
- Measuring oil-filled current and voltage transformers with modern optical current and voltage sensors,
- Reduce the switchyard footprint as one of the contemporary demands.

Students were asked to find solutions beyond their previous educational experience. There were only two requirements, modern solution and authentic literature as the sources of information.

The one of the variants of final 500 kV switchgear scheme layout by applying the catalogues of world leaders in power industry manufacturers and ABB-Hitachi simulation is represented at the Figure 6 [12]. The footprint reduction approximately 90% by using DCB and ring bus scheme and about 35% only for breaker and a half scheme layout.

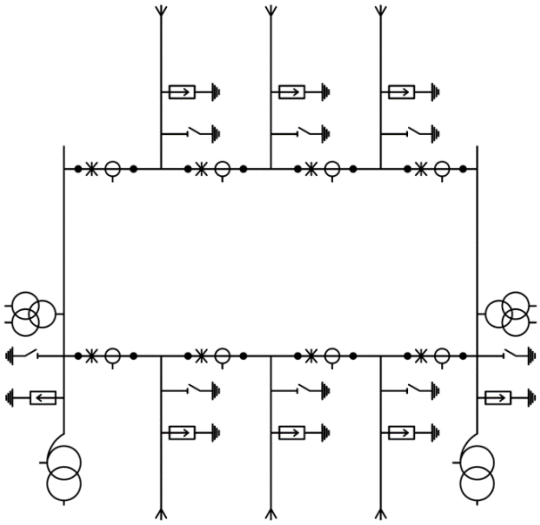

Figure 6. The principal scheme of modernized 500 kV power plant switchyard [12]

3.3. Online Substation Design

Based on the course project task and with support of educational aid the web page for online substation design was developed by master degree student. At the current stage the HV switchyard parameters in normal and abnormal conditions for further scheme components selection are available [13]. Students are able to choose the voltage level, consumer category, other important parameters of the electric installation as a part of power system. For high voltage substation design was chosen the scheme with two power systems and two autotransformers connecting three switchgears. The initial parameters that are obligatory for online substation design are:

- Voltage levels of sources and loads,
- Systems apparent power in MVA and per unit reactance,
- Length of transmission lines entering the switchyards,
- Quantity and capacity of load connections at medium and low voltage levels,
- Ratio of load simultaneously,
- Power factor magnitudes,
- Maximum operating hours for loads,
- Consumer categories.

The list of switchyards for 220-750 kV according to the last recommendations of Russian Ministry of Power Engineering is available with comments about quantity of bays and voltage level. The online procedure completely satisfies the requirements to modern substation design and form the new competences, hard and soft skills of future specialist in power engineering, like:

- Ability to apply new technology for labs or problems solving,
- To analyze initial data, to assess calculated parameters and to find the best engineering solution for the substation project,
- To be able to use English in the professional activity (active vocabulary is formed rapidly compare to the traditional approach of terms learning by heart, for example).

At labs the scholars follow the individual variants of input data for HV substation switchyard design and download the report with data:

- Power demands at medium and low voltage levels,
- Total power demand for three windings transformer or autotransformer sizing choice,
- Rated current in normal mode,
- Equivalent reactance of the scheme according to the place of short circuit,
- Periodic current at zero time of short circuit,
- Aperiodic current of short circuit,
- Peak current of short circuit,
- Short circuit thermal withstanding magnitude.

For correct report result the timing of circuit breaker contacts opening, minimal time of protective relaying and auto reclosure time have to be analyzed and selected.

After receiving the online report with calculated scheme parameters their task is to select the circuit breakers, disconnectors, instrument transformers, scheme layout. It is a non-verbal part. Improving speaking skills is accomplished at the defending the completely designed modern switchgear by answering the instructor question or group discussion. In the future the medium and low voltage level parameters calculation, catalogues of different manufacturers with nameplate parameters of modern equipment will be developed and include in the appendixes of web page.

4. LIFELONG LEARNING COMPETENCES FORMATION

Creative tasks in the course design are the crucial motivational tools, which have to be implemented in the educational process for outstanding learning outcomes. Independent learning and motivation to lifelong learning of power engineers in the future could be considered as the general idea of 21st century education. The simulation of professional tasks in English by integrating in educational process is a unique method that will provoke students for:

- Adopting, adapting, applying best international achievements in science and technology, like stat-of-the art-equipment,
- Using materials, data, parameters in both, native language and English,
- Studying all their life.

Having delivered the classes on "Professional Training in English" for about ten years, conducting annual students survey, analyzing the learning outcomes achievements it is possible to declare that combination of professional and English skills is the best tool for modern engineers training and their lifelong learning motivation.

The lifelong learning competences formation of cutting-edge engineers may be described as the result of overlapping the professional and fundamental disciplines, general and professional English (Figure 7). Outstanding learning outcomes maybe achieved by integrating creative tasks in English close to real engineering practice at electrical installations.

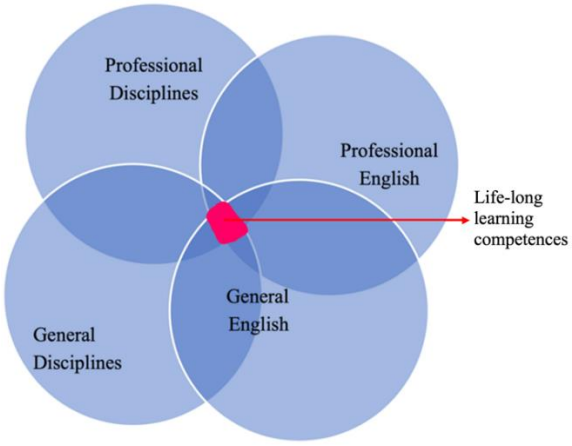

Figure 7. Lifelong learning competences formation [2]

5. CONCLUSIONS

The lifelong learning is a topical issue for new specialists training in the field of power engineering at a current moment. Updating requirements to power industry oblige engineers to find new technological solution both for existed objects (for retrofitting) and for new mounting electric installations. Forming the professional competences demanded by the 21st century power objects is not possible to fulfill without integrating English in the curriculum of bachelor and master degree students training as non-native speakers. Language knowledge as soft skill is crucial and an integral part for further self-studying success, motivating for cutting edge equipment application with decreased level of human errors connected by some misunderstanding.

Real practice provided by the manuals and authentic text translation by specialists in linguistics do not reflect the correctness of technical terms which are of paramount importance for making the right decisions in the field of design and operation. Supporting the professional disciplines in English by special software, simulations, other new technologies is really significant. Extremely important that all the means and devices for labs are designed with maximum similarity to the actual operating conditions of electrical installations that future specialists will face upon graduation the university.

ACKNOWLEDGEMENTS

The work of Mr. Burak Celik that was a part of the Master degree thesis was a great help with developing materials for the course mentioned in this paper. I also would like to thank Prof. Vladimir Kopjev for the valuable support in designing engineering task on switching procedure.

REFERENCES

[1] C.M. Mediano, S. Lord, "Lifelong Learning Competencies Program for Engineers", International Journal of Engineering Education, Vol. 28, No. 1, pp. 130-143, January 2012.

[2] L. Krivova, O. Imas, E. Moldovanova, P.J. Mitchell, V. Sulaymanova, K. Zolnikov, "Towards Smart Education and Lifelong Learning in Russia, In Smart Innovation, Systems and Technologies", Springer Science and Business Media Deutschland GmbH, Vol. 70, pp. 357-383, 2018.

[3] A.M. Hashimov, E.E. Novruzova, "New Technologies in Energy Sector and Automated Energy Accounting Systems and Their Main Factors of Influence on Ecology", International Journal on Technical and Physical Problems of Engineering (IJTPE), Issue 42, Vol. 12, No. 1, pp. 53-57, March 2020.

[4] Y. Mnaoui, A. Najoua, H. Ouajji, "Analysis of the Effect of Nonverbal Communication on English Performance: Case Study – Air Traffic Controller of Training Engineering", International Journal on Technical and Physical Problems of Engineering (IJTPE), Issue 49, Vol. 13, No. 4, pp. 57-62, December 2021.

[5] https://up.tpu.ru/view/detali.html?id=23907.

[6] https://up.tpu.ru/view/detali.html?id=25820.

[7] https://stud.lms.tpu.ru/course/view.php?id=2623.

[8] https://stud.lms.tpu.ru/course/view.php?id=4588.

[9] L.V. Krivova, V.Y. Ushakov, "Professional Training in English" - Discipline for Master Degree Students of "Digital Technologies in Power Engineering" Program", International Journal on Technical and Physical Problems of Engineering (IJTPE), Issue 45, Vol. 12, No. 4, pp. 97-102, December 2020.

[10] National Research Council, "Discipline-Based Education Research: Understanding and Improving Learning in Undergraduate Science and Engineering", The National Academies Press, Washington, DC, USA, 2012.

[11] R. Britto and M. Usman, "Bloom's Taxonomy in Software Engineering Education: A Systematic Mapping Study", IEEE Frontiers in Education Conference (FIE), pp. 1-8, 2015.

[12] dcbsubstations.com.

[13] http://substationdesigner.com.

BIOGRAPHY

Lyudmila Krivova was born in Voroshilovgrad, Russia on August 12, 1974. She graduated from Department of Power Plants, Tomsk Polytechnic University, Russia as engineer and received the Ph.D. degree in Power Plants and Power Systems from Novosibirsk State Technical University, Russia in 2003. Currently, she is an Associate Professor of Higher School of High Voltage Engineering, Peter the Great Saint Petersburg Polytechnic University, Russia. She was awarded by the ING-PAED-IGIP diploma and included in the list of International Engineering High School Lecturers. Her research interests are in the area of power plants design, structural and functional reliability of power plants, pedagogy and some aspects of linguistics. She is author and coauthor of more than 40 scientific journal publications and conference proceedings in field of power engineering and pedagogy, one monography.

The 18th International Conference on
"Technical and Physical Problems of Engineering"
30 October 2022
International Organization of IOTPE

ICTPE Conference
www.iotpe.com
ictpe@iotpe.com
ictpe0@gmail.com

ICTPE-2022 Number 30 Code 08ELM02 Pages 156-160

EDUCATION AND SUSTAINABLE DEVELOPMENT GOALS BY MEANS OF URBAN GARDENS

J. Bilbao E. Bravo O. Garcia C. Rebollar

Applied Mathematics Department, University of the Basque Country (UPV/EHU), Bilbao, Spain
javier.bilbao@ehu.eus, eugenio.bravo@ehu.eus, olatz.garcia@ehu.eus, carolina.rebollar@ehu.eus

Abstract- Monitoring systems have spread worldwide in recent years, both in industry and in services and home automation systems. One of the main reasons is the growth of IoT technologies. In turn, the transfer of knowledge from universities to society, through students, is nowadays part of the education system. At our university, a project related to sustainability and student practice has been launched. Within this framework, we want to apply the ideas of monitoring through IoT applications. One of the ideas is the measurement of certain environmental factors that occur both in an urban garden and in a composting process. In addition, only open hardware-based devices have been used. By means of the monitoring system, the environmental factors of a small urban garden, and also of a composting box, which are located at the university, can be measured. The factors to be measured are the following: air temperature, air humidity, soil moisture, ultraviolet radiation and the amount of light (brightness) received in the urban garden; and temperature and humidity in the composting process. To create this whole system, different alternatives have been considered and the best elements have been chosen, based on sustainability criteria, for each section of the project.

Keywords: IoT Technologies, Education, Engineering, Sustainability, Urban Garden.

1. INTRODUCTION

The measurement of environmental factors is an action that humans have always carried out, both in ancient times and today, because knowing the values of the different factors contributes to obtain better yields in different fields. For example, in agriculture it is important to know the amount of light a plant receives or the degree of humidity of the soil in order to irrigate at the optimum moment, so that water is not wasted and there is no risk of the plant drowning.

On the other hand, through composting, in addition to recycling organic waste, natural fertilizer can be produced both for personal gardens and to feed the soil of an agricultural land. Composting helps to reduce the pollution generated through waste and, therefore, to preserve the environment. In addition, on the emergence of IoT (Internet of Things) systems, there are many companies and individual users who use these factors to measure, install monitoring systems in different locations and collect data. This has several advantages, since the remote control and visualization of the data allows to know the nature of the elements to be controlled anywhere and at any time.

This project will therefore be carried out taking into account the relevant aspects in terms of sustainability. For this, it is intended to measure five environmental factors (temperature, air humidity, ground humidity, ultraviolet radiation and luminosity) of a small orchard located at the university, measure the temperature and humidity factors that occur in a compost box that will be next to it, collect them through free hardware components, store them and visualize them through an internet platform.

In addition, to do all this is intended, deepening in the field of sustainability, to feed a free hardware board that will be used and its sensors through an autonomous power supply system. In this way, taking advantage of the benefits offered by renewable energies and free hardware, it is intended to access the world of IoT systems and control the activity of environmental conditions and composting of an orchard through the monitoring system to be developed. Therefore, the results of this project and the generated system can be further developed in future projects.

2. DATA ACQUISITION SYSTEMS

In the same way that humans can sense environmental conditions through senses, electronic systems can receive this environmental information through DAQ (Data Acquisition) systems. Information from these electronic systems can be used by humans for other purposes.

Nowadays, they have become a fundamental part of human life and we can observe them in any type of activity, such as the control of industrial processes, cars, airplanes, medical equipment, household appliances, etc. In the field of agriculture, the situation is not much more unequal, since the use of sensors to control different factors and applications is increasing. Among these applications, for example, would be automatic irrigation, which is based on the right time to irrigate by controlling soil moisture. Other applications would be: control of the

internal conditions of the greenhouses, control of luminosity, temperature, ventilation, humidity, etc., control of the level of ultraviolet radiation, etc. This would lead some studies to consider sensor networks as one of the 10 technologies that would change the world for the better [1].

In order to understand the information received through the sensors, a processor is needed to translate the electrical or physical phenomena received from the sensors (change of voltage, current, temperature, pressure) into understandable data. Therefore, DAQ systems are used to carry out this process. These DAQ systems consist of sensors, a data acquisition hardware and a PC with programmable software. Compared to traditional measurement systems, these new PC-based systems offer greater processing, productivity, visualization and connectivity possibilities, thus making measurement systems more efficient, powerful and cost-effective [2].

If each of the sections of these systems is analyzed, the following can be said:

- Sensors: Sensors, also known as transducers, are responsible for reading a physical quantity, such as temperature, and converting this reading into an electrical signal that can then be measurable and communicable.
- DAQ devices: This device is the one that allows the interaction between the computer and the user's sensors. Its main function is to digitize the data it receives from the sensors so that it can be understood by the computer. To carry out this function, they have a circuit to adapt the signals received to a communication protocol, a converter to be able to pass the signals from analog to digital and finally a bus to communicate with the computer. This communication can be of several types: Ethernet, Wi-Fi, ModBus or others. There are DAQ devices that have a viewer to view the collected data, but often they do not, and, in these cases, we can only see it when the information reaches the computer.

Among this type of devices, we can find those known as process loggers or dataloggers, which are usually based on microcontrollers. These systems usually have internal memory, which gives them autonomy for data collection, allowing the data received from the sensors to be stored there. Therefore, they are very useful as a data collection system. This function is very useful, since if at any time the communication with the computer was interrupted, the system would have been able to store the data in the internal memory and not lose information. Therefore, the biggest advantage that these dataloggers have would be their ability to function even without the need for a computer. Because of this advantage, in many projects these types of DAQ systems are used as data collection systems.

Data loggers can be of various types. Some are capable of interpreting only one sensor, being very cheap, but others can have hundreds of inputs and have a great power in both software and hardware. For this project we will use a data collection system of this type, as it allows us to cover many different applications for the agricultural sector.

- PC with Inspection Software: Finally, to carry out the whole system, there would be a PC with all the software possibilities. This computer allows the interaction between the end user and the system. In addition, it enables to visualize, collect the information received, process it freely and perform the necessary calculations. The computer can also be used to control the configuration and operation of the entire system.

On the other hand, it should be noted that the use of these systems has greatly increased in areas such as industry and mining, which offer many advantages. For example, they facilitate data analysis and help make information more accessible, especially when dealing with large volumes of data. In addition, they offer a better level of data security, since as soon as data is received it can be sent and saved to different devices so that it is not lost. On the other hand, they offer great facilities and support for monitoring processes, allowing sensor networks to be physically located in different places and having the capacity to cover large areas. In this way, these systems are capable of capturing and monitoring at all times data from an infinite number of different parameters in large areas. Finally, since each of the above components can be modified or upgraded independently, cost savings are achieved.

3. CAMPUS BIZIA LAB AND SERVICE-LEARNING

The Campus Bizia Lab (CBL) program is an initiative derived from the Erasmus University Educators for Sustainable Development Project in which the University of the Basque Country (UPV/EHU) participated between 2013-2016. It aims to trigger a collaborative process between faculty, administration and services staff and students (transdisciplinary approach) in order to respond to sustainability challenges within the University itself. The main objective of Campus Bizia Lab is the implementation of any research to develop a high impact practice among students. That is, it consists of actions for transdisciplinary learning of students based on challenges that are based on sustainability. These actions involve both students and faculty and are usually materialized by means of the Final Degree Project (FDP) and the Final Master's Project (FMP).

The main objective of the program is to respond to the SDGs proposed by UNESCO within the university itself, through the FDPs and FMPs of different degrees. At the same time, it seeks to articulate transdisciplinary communities where different figures working specifically in the field of education for sustainability are involved in a cooperative manner: students, faculty and other staff of the university, such as technicians. In this way, the different projects that make up the CBL create synergies focused on the resolution of challenges and problems of unsustainability that are detected in the university campuses themselves, generating multilevel sustainable practices. The transdisciplinary nature of the program means that the learning processes linked to the design, development and evaluation of the projects have a high curricular impact on the students.

Service-Learning (SL) is a methodology based on practical and reflective experiences in which students are involved in a context with real problems, thus developing content and professional skills [3, 4]. One of the characteristics of SL is that the real needs of the community are detected, or at least some of them, normally related to the academic area being taught, in such a way that the link between educational institutions is promoted. Thus, university students can improve their training by connecting directly with the social reality [5]. Another advantage mentioned about service-learning is that it also creates and strengthens bridges of coordination between the university and the educational community [6-10]. Typically, projects are based on the following concepts:

- Experience,
- Active participation,
- Interdisciplinarity, and
- Teamwork.

Among the possible actions that can be carried out at the university, one of the most complete is the development of a Final Degree Project (FDP). The FDP is a project, report or study, which is carried out at the end of undergraduate studies. In Spain, in all undergraduate degrees, and after the university reform that was implemented at the end of the first decade of the 21st century (Bologna process), the development and presentation of an FDP is mandatory for all students. At the UPV/EHU, this methodology fits within its IKD framework of cooperative and dynamic learning (the university's own methodology) and within the application of the SDGs through initiatives such as the aforementioned Campus Bizia Lab.

4. OPEN HARDWARE

Open hardware is born from the ideology of open-source software. The latter appeared [11] as early as 1980. The software at that time was mostly proprietary and in order to modify it, several programmers began to encourage the trend to create free software programs. Thus, over the years, Operating Systems based on free software were also created, such as GNU, and it has been an idea that has been evolving up to the present day.

Free software defends four fundamental ideas: freedom of use, freedom of learning and change, freedom of distribution and dissemination of improvements. However, sharing hardware designs is not as easy as sharing software, since the hardware has to be physically the same to work exactly the same, and when copying the design, manufacturing costs have to be taken into account, and finally, it is necessary to make sure that the materials for product we want to develop are available.

However, overcoming these problems, the idea of open hardware is very important to create a competitive market. Many people have good ideas, but the materials needed to implement them can be very expensive or they lack the information about the products they want to use to understand how they work. Open hardware corrects these problems relatively well, bringing product prices down and making designs available to anyone.

In addition, products based on this idea, when the product is known to be faulty, offer the possibility of fixing it by themselves without having to take it to the store and pay a fortune. In the world of open hardware, you can find many different products, but the best known are Raspberry Pi and Arduino. In this project we will use the latter to create the monitoring system, so we will focus on it.

Arduino is one of the pioneers and most popular open hardware products [12]. It consists of an open hardware board and a microcontroller that provides an environment for developments. It has several analog and digital inputs, where sensors or switches can be connected, and several outputs, to connect motors or switches. All the ingredients are cheap and the user himself can assemble an Arduino board, buy the ingredients and see the plans; but you can also buy the board itself assembled and use this option to develop the project. It is, in short, a small and cheap computer, but in which you can replace the usual inputs (keyboard, mouse) or outputs of the computer (screen, printer) by sensors or motors that the user wants.

Thus, by connecting the necessary sensors and devices to be measured, and writing a program through the development environment, a complete monitoring system can be created, as will be done in this project. Moreover, since you can also find useful modules for the creation of stand-alone projects, it will be highly recommended for the development of the stand-alone product you intend to create.

On the other hand, on the Arduino website you can find numerous helps shared by the community, as well as a lot of developed codes and examples. For all these reasons, we have opted for the use of open hardware in this project, taking advantage of the benefits offered by the Arduino boards and with the idea of developing the project further in the future, leaving both the design and the codes in the hands of anyone:

5. PROJECT RESULTS

The results obtained after the complete configuration and development of the monitoring system will be shown below. First, a simple communication between both stations, configured by means of NRF24L01 modules, will be carried out to guarantee the connection and the correct communication. Then, with the complete code developed, the data will be sent from the remote station to the base station and from there some of the data collected in the Ubidots platform will be shown through the WiFi configuration.

It must be said that this project will not analyze in depth the values of the results obtained, i.e., it will not analyze how the values obtained affect the plantation, nor will it measure the conditions that occur in the composting box throughout the process. In addition, it would be necessary to implement liners and protections to be able to place them outdoors during adverse weather conditions.

Some of the results provided by the system can be seen in the Figures 1 and 2.

• Light level intensity (Lux):

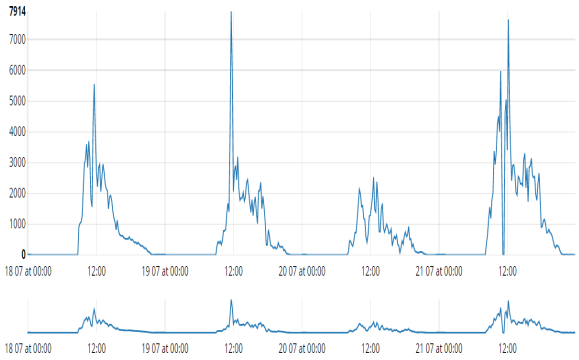

Figure 1. Light level intensity in the urban garden during some days

• Air humidity (%):

Figure 2. Air humidity in the urban garden during some days

Looking at the graphs, it can be said that the values are well collected and make sense, they are also shown in an easy-to-understand way and the data of the days of the different sections can be seen.

6. CONCLUSIONS

The main objective of this project is to develop a monitoring system to measure some environmental factors and the ins and outs of a composting process, using open hardware for this purpose and electrically powered by an autonomous system. To achieve this goal, hardware and software analysis has been carried out, with different options. A complete design of the autonomous power system has also been carried out and an efficient way of wireless communication has been designed. Once the methods and components to be used were selected, we proceeded to the system assembly and code creation section.

To fulfill all these functions, it has been proposed to develop a topology with 2 boards, in which one would work as a base station collecting the data by wireless connection and sending them to the IoT platform via WiFi, and also saving them locally on the SD card. The other would work as a remote station, connecting to it both the orchard and the compost monitoring sensors, collecting data from them and sending them to the base station through a module that allows radio communication. By having to face real situations and to respond and learn to adapt to different educational situations, the university students have also acquired engineering skills.

ACKNOWLEDGEMENTS

We are grateful to Jon Bilbao for his collaboration in the development and implementation of the project. We also thank the Sustainability Directorate of the University of the Basque Country (UPV/EHU) for its support and the grant that have made possible this research. We thank the support of the laboratory of the Applied Mathematics Department of the University of the Basque Country, UPV/EHU, and the collaboration of G. Ros in the development of the study.

REFERENCES

[1] N. Siddique, S.F. Hasan, S.M.S. Zabir, "Opportunistic Networking: Vehicular, D2D and Cognitive Radio Networks", CRC Press, 2017.
[2] National Instruments, Data Acquisition (DAQ), www.ni.com/es-es/shop/data-acquisition.html.
[3] J. Abellan, "Service-Learning and its Effect on Attitudes Towards Inclusion in Future Physical Education Teachers", Educational Contexts, Education Magazine, Vol. 27, pp. 83-98, 2021.
[4] M. Franco Sola, S. Figueras Comas, J. Campos Rius, E. Sebastiani Obrador, "Perceptions About the Contributions of Service-Learning to University Teaching and Learning in the Field of Physical Education: An Autobiographical Perspective from the Crossed Stories of Teachers", Educational Contexts, Vol. 27, pp. 65-81, 2021.
[5] J.M. Puig, M.J. Martin, L. Rubio, "How to Evaluate Service-Learning Projects?", Voices of Education, Vol. 2, Issue 4, pp. 122-132, 2017.
[6] S.H. Billig, "Support for K-12 Service-Learning Practice: A Brief Review of the Research", Educational Horizons, Vol. 80, pp. 184-189, 2002.
[7] A. Furco, "Service-Learning: A Balanced Approach to Experiential Education", International Journal on Research in Global and Development Education, pp. 64-70, 2011.
[8] V. Lorenzo, B. Matellanes, "Development and Evaluation of Psychosocial Skills in University Students Through a Service-Learning Program", International Journal of Education for Social Justice, Vol. 2, Issue 2, pp. 155-176, 2013.
[9] D. Mayor, A.M. Lopez, M.G. Solis, "Service-Learning as a Training Scenario and its Influence on Different Socio-educational Agents. Participant Perception", International Journal of Sociology of Education, Vol. 8, Issue 2, pp. 153-172, 2019. https://doi.org/10.17583/rise.2019.4071.
[10] M. Rodriguez Gallego, "Service-Learning as a Methodological Strategy at the University", Complutense Journal of Education, Vol. 25, No. 1, pp. 95-113, 2013.
[11] Ecured, Article About GNU www.ecured.cu/GNU/Linux
[12] Arduino, https://arduinodhtics.weebly.com.

BIOGRAPHIES

Javier Bilbao obtained the degree in Electrical Engineering from University of the Basque Country, Spain, in 1991. At present he is Ph.D. in Applied Mathematics and professor at the department of Applied Mathematics of that university. He has been General Chairman of some conferences of WSEAS organization. Current and previous research interests are: Distribution overhead electrical lines compensation, Optimization of series capacitor batteries in electrical lines, Modulization of a leakage flux transformer, Losses in the electric distribution Networks, Artificial Neural Networks, Modulization of fishing trawls, E-learning, Noise of electrical wind turbines, Light pollution, Health risk of radiofrequencies. He is the General Chairman of the International Conferences on Engineering and Mathematics (ENMA) and member of the committees of International Conferences on Technical and Physical Problems of Power Engineering (ICTPE).

Eugenio Bravo obtained the degree in Electrical Engineering from University of the Basque Country, Spain, in 1991. At present he is Ph.D. in Applied Mathematics and professor at the department of Applied Mathematics of that u niversity. Current and previous research interests are distribution overhead electrical lines compensation, optimization of series capacitor batteries in electrical lines, modulization of a leakage flux transformer, losses in the electric distribution networks, artificial neural networks, modulization of fishing trawls, e-learning, noise of electrical wind turbines.

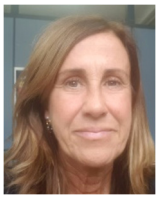

Olatz Garcia obtained the degree in Mathematics from University of the Basque Country, Spain, in 1989. At present she is Ph.D. in Applied Mathematics and professor at the department of Applied Mathematics of that university. Her current and previous research interests are e-learning, optimization of series capacitor batteries in electrical lines, Noise of electrical wind turbines.

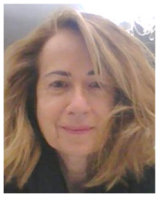

Carolina Rebollar obtained the degree in Mathematics from University of the Basque Country, Spain, in 1986. At present she is Ph.D. in Applied Mathematics and professor at the department of Applied Mathematics of that university. She is Academic Secretary at the Faculty of Engineering Bilbao (University of the Basque Country) and Director of the "Aula Company ZIV", where projects are developed annually for the electric company "ZIV I+D Smart Energy Networks", participating teachers and students.

The 18th International Conference on
"Technical and Physical Problems of Engineering"
30 October 2022
International Organization of IOTPE

ICTPE Conference
www.iotpe.com
ictpe@iotpe.com
ictpe0@gmail.com

ICTPE-2022 Number 31 Code 10MCE01 Pages 161-168

INVESTIGATION ON THE BEHAVIOR OF NUMERICAL MODELING OF THE STEEL JOINTS EQUIPPED WITH CURVED DAMPERS AGAINST HEAT

Z. Zamanzadeh [1] M. Tapdigli [2] R. Nuraliyev [3]

1. Faculty of Civil Engineering, Khazar University, Baku, Azerbaijan, z.zamanzadeh@khazar.org
2. CONCO JCSC, Baku, Azerbaijan, m.tapdiqli@conco.az
3. Azerbaijan State Oil and Industry University, Baku Azerbaijan, rnuraliyev@gmail.com

Abstract- Recently, controlling the response of the structures through input energy absorption and dissipation in times of earthquake has been detected. One of the common energy absorption systems are the metal dampers used to improve the earthquake performance of the structures. These dampers behave based on flow property. Whenever pressures generated in damper are greater than the yield stress of the metal materials, the metal damper flows. This way, a fraction of the input energy is dissipated on the curved damper and the resulting damage in the members of the frame structures is reduced. In this paper, a type flowing metal dampers named curved metal dampers have been studied. These dampers have simple geometry and are fabricated by cutting steel sheets. These dampers dissipate the input energy to the structure through bending yield. The curved metal dampers are modeled using finite component software, Abaqus. Then, the effect of various geometric parameters of the curved metal dampers on their performance under heat loading is studied. Results show that by increasing the length of the curved metal dampers, the values associated with initial hardness, resistance and energy dissipation capacity of the dampers are reduced. In average, these parameters are reduced 31.45%, 24.2%, and 34.1%, respectively. As the depth and the thickness of the curved metal dampers increases, their behavior improved and the values associated with initial hardness, resistance and energy dissipation capacity are increased. In average, these parameters are increased 50.4%, 47.61%, and 31.25%, respectively.

Keywords: Steel Joints, Curved Damper, Heat Loading.

1. INTRODUCTION

Considering their proper plasticity, steel bending frames are usually used in seismic design of the structures. However, these structural systems have low hardness that may result in irreparable damage to them because of large displacements of the structure. Also, investigating the damages in the bending frames after strong earthquakes reveals breakdown and rupture in beam to column joint followed by damage to the main elements of the structure [1].

One of the approaches in modern seismic design of the structures is increasing their damping to dissipate input energy and reduce seismic response of the building. As a new seismic design method of the structures, using the same dampers as energy dissipation systems could be mentioned [2]. These systems can concentrate energy dissipation in predefined regions and reduce the nonlinear behavior of the main structural members of the frame which deal with gravity bearing task. So, the possibility of damage in the main structural members is reduced, too. Now, utilizing passive energy dissipation in the structures is known as an effective and fairly non-expensive method to reduce earthquake damages. This dissipation could be based on different mechanisms; inelastic deformation of plastic metals like steel in metal dampers, friction slips in friction dampers [3], fluid passing through narrow apertures in viscose dampers, deformation of the viscoelastic materials in viscoelastic dampers could be mention as some examples.

To achieve an economic seismic resistant design, the energy absorption and dissipation of the structures must be considered. In recent years, many researchers have proposed various techniques to increase the energy dissipation capacity of the structures based on the flow property of the metals. Metal dampers are considered one of the most common energy dissipation systems. They are used to control and reduce seismic response of the structures in times of earthquakes. These dampers operated based on flow property of the metals. Whenever applied forces on a damper are greater than its capacity, metal damper flows. This way by plastic deformation, the damper absorbs the input energy to the structure and prevents damage to the main members of the frame [4].

The choice of design parameters for this type of dampers has considerable effect on nonlinear behavior of the structures. As the metal dampers do not require complicated technology for fabrication, they have lower implementation and maintenance cost in comparison to other systems.

Also, lower impact of the environmental conditions (like temperature, humidity, and etc.) on their mechanical, they are of much importance in seismic design of the structures by improving the existing building. Considering the aforementioned reasons, in regions with potential seismic construction such as Iran, studying the performance of the energy absorption systems like the metal dampers is very important. Fire resistance of beam to column joints is very important in the design of steel bending frames. Quantifying the effect of heat loads on beam buckling, displacement, rotation, hardness of the joint, and anchor-of-rotation behavior for temperatures from 20 to 900 degrees centigrade is performed. Results show good performance for screw end sheet joint in terms of high resistance and low breakdown in comparison with three other joint types [5].

Previous studies in recent decades have investigated fire behavior of the typical screw joints. However, few studies have investigated the behavior of screw joints with high resistance screws exposed to fire. This study includes a series of numeric analyses to investigate the behavior of two screw joints types, i.e., expanded screw end sheet joints and beam to column screw sheet exposed to fire with and without preloading. Different parameters like the thickness of the joint sheet will be investigated. Also, this study investigates a numeric method for damage index parameters using an explicit dynamic solver and breakdown modes, deflection along the aperture, displacement of the beam, and the axial forces resulting from the fire in details. Results show that preloading on screws has no substantial impact on the response of the end joint sheet exposed to fire, and the behavior of beam to column joint sheet exposed to fire depends on the thickness [6].

A numeric analysis is evaluated using Abaqus, on high resistance metal end sheet joints exposed to fire. Results of numeric modeling by using anchor-rotation equation, breakdown mode, and the pattern of yield line of the joint show acceptable accuracy compared to experimental results. It provided an efficient, economic, and accurate tool to study the performance of the high fire resistance steel joints. Hence, this numeric analysis method can be used with high reliability for predicting the behavior of high fire resistance steel joints with maximum anchor under different fire conditions and various environment temperatures [7].

In 2017, Hsu and Halim proposed and designed a novel metal damper called the curved metal damper. They equipped several one-floor frames and a metal aperture with the curved metal dampers, and tested under cyclic loading. These dampers were installed in beam to column joint region of the steel frames. After adding the curved metal dampers to the steel frames, their performance was improved [8]. In their next experimental study in 2018, the curved metal dampers were used in the bracing metal frames [9].

Structural fire resistance is defined as the characteristic of a building for fire resistance and protection [10]. There are two issues to define fire resistance.

The first issue is the ability of a member to maintain structural strength and stability when exposed to the fire. The second one is for some members such as walls and ceilings that prevent the spread of fire. Fire resistance is typically achieved by placing a sample under a standard test [10]. The result of the test called the degree of durability against fire in hours. It is obtained based on the time that takes for the sample to meet the accepted criteria in the experiment.

The degree of fire resistance required for different components of the building is given in the regulations, which depends on the type of use, number of floors and floor area. Regarding the standard test is a comparative test and not a predictor of actual behavior, the degree of resistance to laboratory fire to estimate how long a member cannot be destroyed in a real fire cannot be used. In general, the degree of fire resistance of a structural member is a function of:

- The volume of applied heaviness to the part
- Type of part (beam - column, etc.)
- Dimensions of the part and support situations
- The heat current from the fire around the part
- Type of substantial (steel concrete, etc.)
- The effect of growing the temperature of a structural part on the mechanical properties of its component.

The behavior of a structural member in a fire depends on the mechanical and thermal characteristics of that member. As the temperature increases, the resistance of the member to a certain deformation decreases the coefficient of elasticity and stiffness [10].

The curved metal damper investigated in this research is one of the different types of submersible metal damper. The reason for naming these dampers is the geometry with the curvature of their steel piece. These attenuators dissipate the energy entering the structure by absorbing energy and performing inelastic deformations. There is no need for advanced technology to make curved metal dampers because these dampers have a simple geometry and are made by cutting steel sheets according to the required dimensions. So, the speed of manufacturing and installing curved metal dampers is high. Curved metal dampers can be used in the seismic design of steel structures by reinforcing existing buildings.

The geometric details of the curved metal damper are shown in Figure 1. As shown in the figure, there is a gap between the direction of application of the axial load $(P\Delta)$ and the damping center, which is called the decentralization (Δ). Due to the effective geometric structure of curved metal dampers, when these dampers are subjected to axial force, due to the deviation of the axial force from the center of the curved metal dampers, an additional bending anchor is created in them.

According to the above, the behavioral mechanism of curved metal dampers is of the bending yield type. In other words, when they are subjected to reciprocating loading, the receiver behaves flexible and the curved metal dampers are compressed and stretched. These dampers can be installed at the connection of the beam to the column.

By predicting the concentration of noise in curved dampers, they actually act as a fuse in the building and reduce the nonlinear behavior of the main members of the frame by deforming the plastic. If the connection of the curved metal damper to the structure is of the screw type, after the earthquake, in case of failure, they can be repaired or replaced at a lower cost.

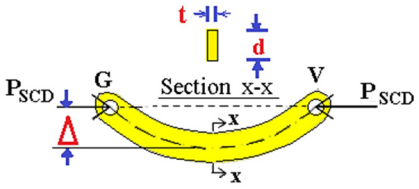

Figure 1. Details of the Geometry of the Curved Metal Damper [9]

2. METHODOLOGY

To evaluate the effectiveness of curved metal dampers on the improvement of the performance of steel connections, a steel connection of single-span, single-story rigid connection was modeled in the environment of Abaqus software. In the steel connection of the beam and column sections, a box with box 300×10 mm specifications have been selected from the box sections.

The angle L15×150×10 mm was used for the connection of beam-to-column. The studied models include a steel connection with rigid connections without any damper and one steel connection with rigid connections with a curved metal damper. Both connections have a length of span and a height of 2000 mm. Figure 2 presents the dimensional characteristics of steel connections. It should be noted that the solid element in Abaqus software has been used to model the beam, column and curved damper.

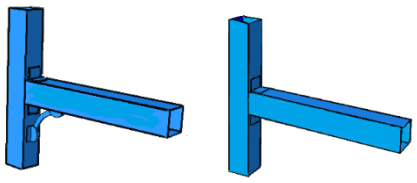

Figure 2. The dimensional characteristics of steel connection with curved metal damper [11]

The length of curved metal dampers in this study is equal to 400 mm. The depth and thickness of the curved metal dampers were selected equal to 80 mm and 30 mm, respectively. The angle between the two ends of the curved damper was also equal to 90 degrees. The names of models were selected according to the selected geometric parameters for the curved dampers. All the curved metal dampers were modeled using finite element software Abaqus and were analyzed under thermal loading. Steal ST37 with the yield stress of 240 MP and the ultimate stress of 370 MP was used in the modeling of the curved dampers. Also, the elasticity module was selected equal to 210 GP and the Poisson ratio equal to 0.3. The protocol of the thermal loading applied to the dampers can be observed in Figure 3.

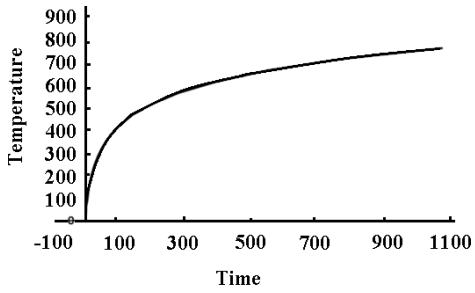

Figure 3. Thermal loading applied to the curved dampers [11]

The tie will be used to connect or weld the damper to the connection plate, and the load of gravity in the first step and the heat load in the second step will be used for loading. The details of loading and how to introduce the interaction between different parts of the connection are given in Figure 4.

The meshing has been performed individually for each segment and we use "structure" mesh for the meshing of the intended model due to its meshing accuracy and "C3D8R" mesh for the elements of the model. The size of meshes for beam, column, and joints is 4 cm. The size of mesh for the modeling of curved dampers was considered equal to 2 cm due to its sensitivity. The details for the meshing of the intended joints are shown in Figure 5.

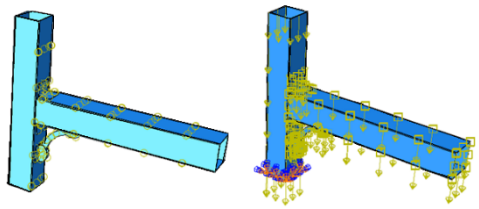

Figure 4. Introducing the loading and interaction between different parts of the connection [11]

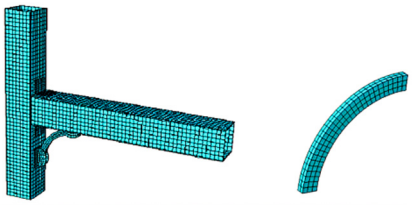

Figure 5. Meshing of the intended joint [11]

2.1. Confirmation

For validation, the article of Navid Siahploo, et al., Who investigated the behavior of heat-treated steel joints in 2014, has been used. The model consists of a vertical column and a planar beam and the height of the column is 2.85 meters and the length of the beam is 2.7 meters.

The cross section of the connection beam is IPE300 and the cross section of the connection column is 300 HEA. Figure 7 shows the cross section of the beam and column that is used. The screw connection specifications with the end plate are shown in Figure 8. The Figure 9 shows a comparison between deformations created in junction region for the laboratory sample and finite element model of paper and simulated finite element model.

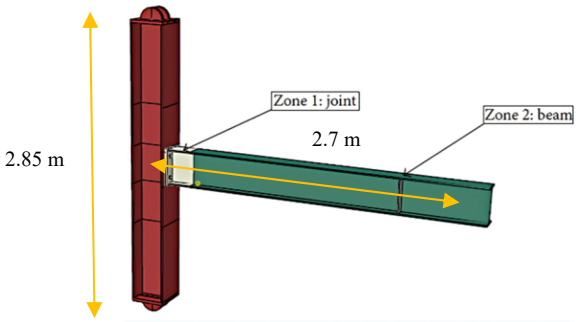

Figure 6. General and specifications of the reference sample [11]

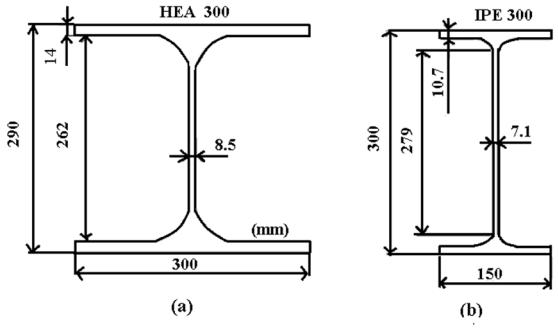

Figure 7. Geometric characteristics of beams and columns, (a) cross section of beam and (b) cross section of column [11]

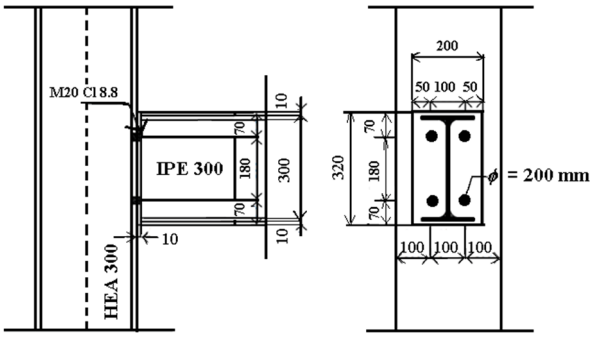

Figure 8. Screw connection specifications with the end plate [11]

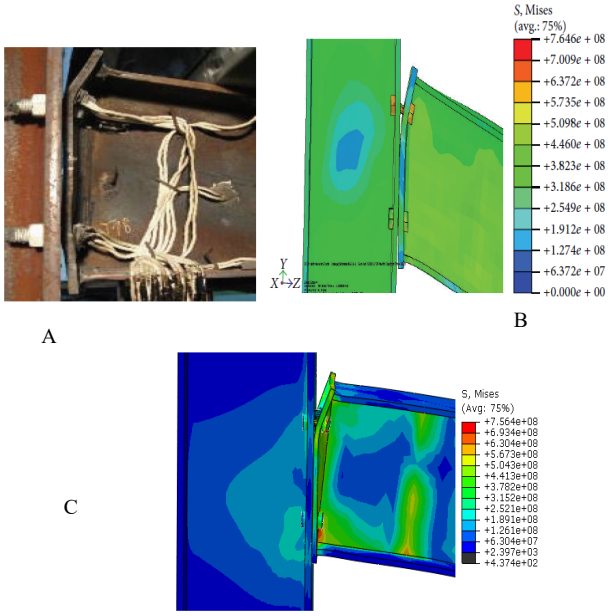

Figure 9. Correspondence of results related to stresses and location of failure in connection: (A) Reference laboratory sample; (B) the finite element model of the reference paper; (C) finite element model [11]

Figure 10 compares laboratory results and numerical analysis of displacement diagrams over time. It is observed that the displacement-time curve for connection corresponds well with the test results in the elastic and plastic range.

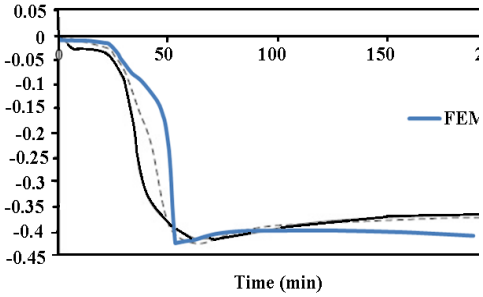

Figure 10. Comparison of laboratory results and numerical analysis of displacement diagrams over time [11]

3. RESULTS AND DISCUSSION

3.1. Stress Distribution in Curved Damper

After the analysis of curved damper models in ABAQUS software, the results are extractable numerically and graphically. Figure 5 shows the way of stress distribution during the thermal loading process. It is worth noting that the stress distribution is according to von Mises yielding criterion. As it can be observed in the figure, the yielding area gets bigger by increasing the displacement applied to the damper. It was specified by investigating the results that the area in the middle of the damper has reached yielding, which shows its bending performance due to the effective curved geometry of the damper. The maximum stress appeared in the center of the interior curve of the curved damper, which is consistent with the way of elastic stress distribution from the total axial force and bending moment stresses.

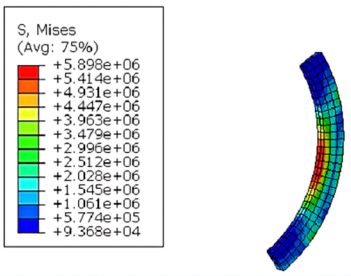

Figure 11. Stress distribution in the curved damper during the loading process [11]

3.2. Stress Distribution in Steel Connection

Stress distribution in the area of steel connection without damper and with curved damper is compared with each other in the figure. As it can be observed, after adding the curved metal damper to the steel frame, the stress in the connection of beam to column is reduced such that no segment of the lower flange of beam reached yielding. It was also specified that during the loading process, first the curved metal damper yields and then by the increase of relative connection displacement, a small part of the upper flange of beam was yielded in the area

of connection to column, which shows the effectiveness of the curved damper in improving the performance of steel connection. The level of yielded area in the curved metal damper is also representing its high potential in absorbing and damping the incoming energy to the frame.

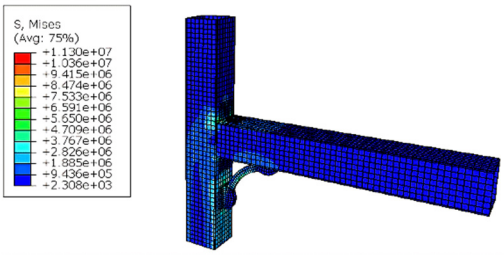

Figure 12. Stress distribution in the connection area of a steel structure with a curved damper [11]

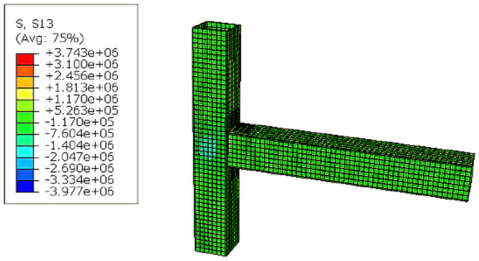

Figure 13. Shear pressure distribution in the joint area of a steel structure without a curved damper [11]

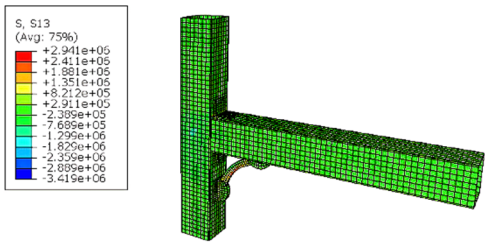

Figure 14. Stress distribution in the connection area of a steel structure with a curved damper [11]

3.3. Pressure Distribution in Steel Joints under Different Thermal Loads

The distribution of stress in the steel joint area equipped with a curved damper under the effect of different thermal loads in Figures 11 and 12 are compared. The curved current shows the effectiveness of the curved damper in improving the performance of the steel joint. The amount of area flowing in the curved metal damper also indicates its high capacity in absorbing and dissipating the input energy to the joint due to increased heat load.

The connection of a steel structure with a curved damper under the heat load of 765 °C provides 20.67% less displacement than a connection without a damper. Figure 18 shows the time displacement diagram of both types of connections without dampers and equipped with curved dampers.

As the connection temperature of steel structure with the curved damper increases from 765 °C to 1530 °C, the displacement of the connection increases from 35 cm to 44 cm. The dampers are under different heat effects.

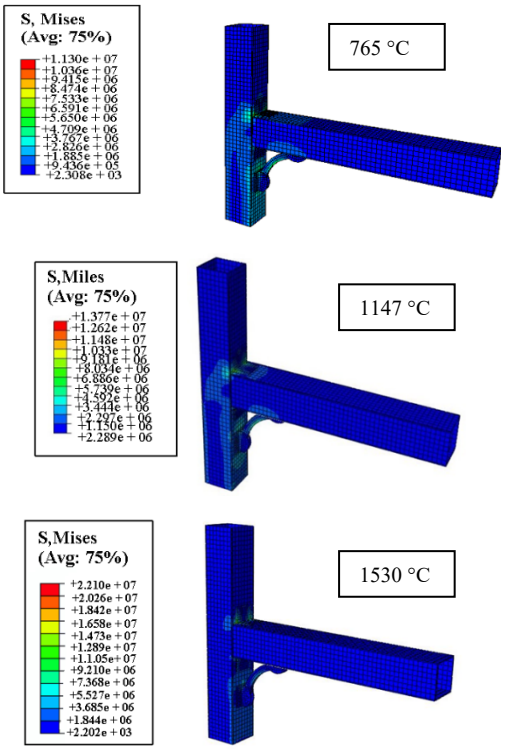

Figure 15. Comparison of stress distribution in the connection area of steel structure with curved shape damper under different thermal load [11]

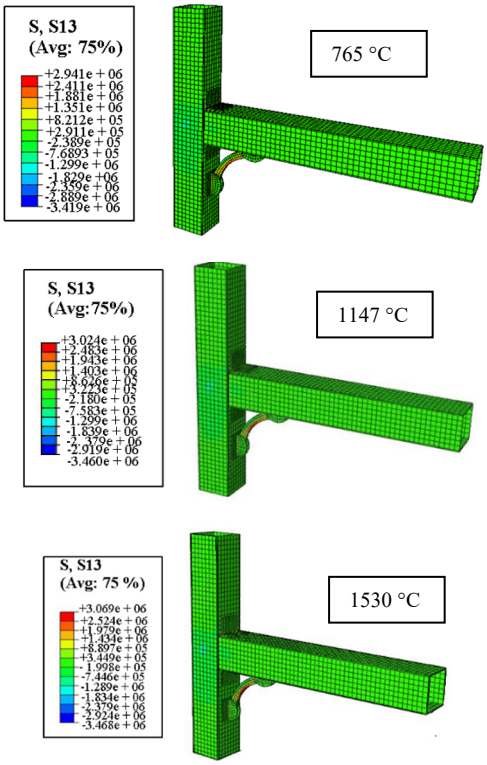

Figure 16. Comparison of shear stress distribution in the connection area of steel structure with curved shape damper under different heat load [11]

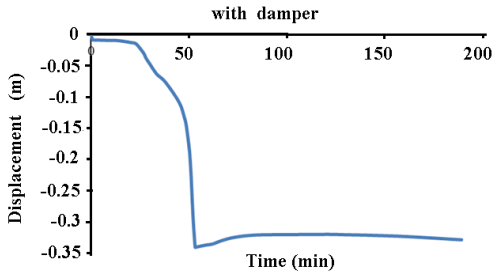

Displacement of connection time with damper

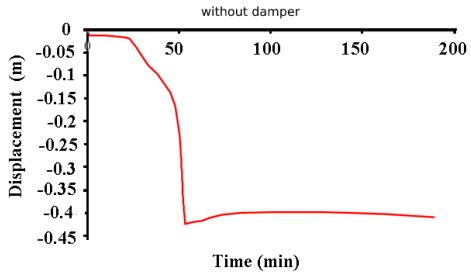

Displacement of connection time without damper

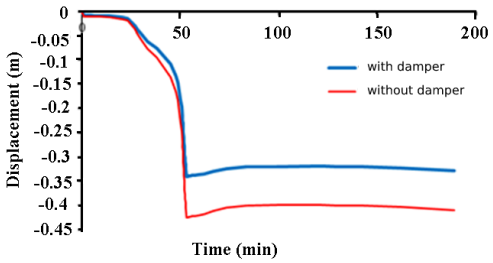

Figure 17. Comparison of displacement diagram of connection time with and without damper [11]

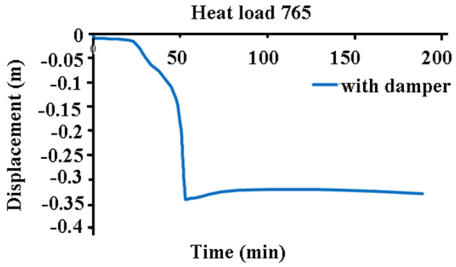

Displacement diagram of damper connection time under the effect of heat load 1147

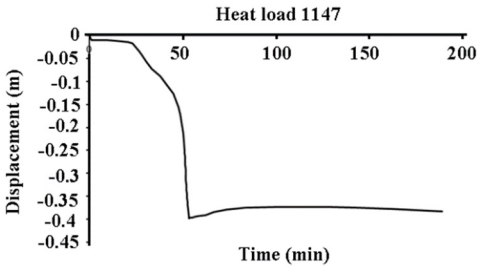

Displacement diagram of the connection time of the eggplant under the effect of heat load 765

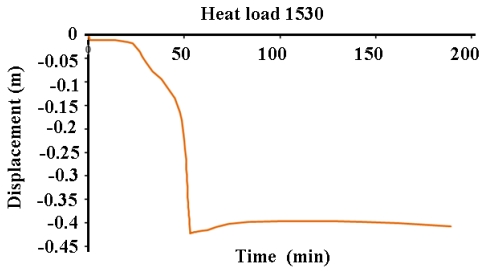

Displacement diagram of the connection time of the eggplant under the effect of heat load 1530

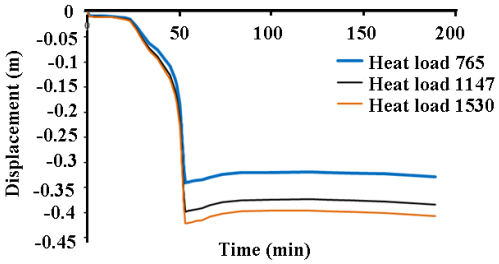

Figure 18. Displacement diagram of the connection time of the eggplant under the effect of different thermal loads [11]

By reducing the damper angle from 120° to 60° when the connection was subjected to a heat load of 765 °C, the energy loss increased and the maximum value was 60° (1854 KN.m) using the damper and the minimum was 30° (1770 KN) using the damper. m) was obtained. In fact, if you use a 30-degree damper, less energy loss occurs compared to a 60-degree damper (Figure 19).

By reducing the damper angle from 120° to 60° when the connection was subjected to a heat load of 1147° C, the energy loss increased and the maximum value was 60° (2298.96 KN.m) and the minimum was 30° (2194.8). KN.m) was obtained. In fact, if you use a 30-degree damper, less energy loss occurs compared to a 60-degree damper (Figure 20).

By reducing the damper angle from 120° to 60° when the connection was subjected to a heat load of 1530°C, the energy loss increased and the maximum value was 60° (3379. 47KN.m) using the damper and the minimum was 30° (3226.356 KN.m) In fact, if a 30-degree damper is used, less energy loss occurs at 4.52 compared to a 60-degree damper (Figure 21).

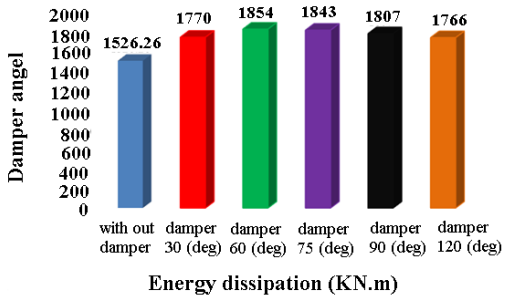

Figure 19. Comparison of the effect of curved damping angle on steel joint energy dissipation under heat load of 765 °C [11]

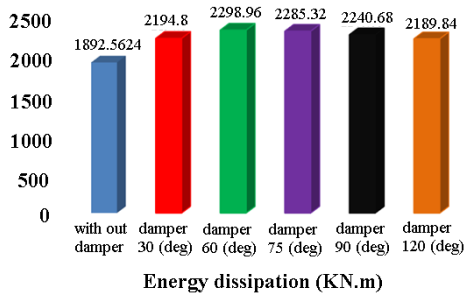

Figure 20. Comparison of the effect of curved damping angle on the energy dissipation of steel joint under heat load of 1147 °C [11]

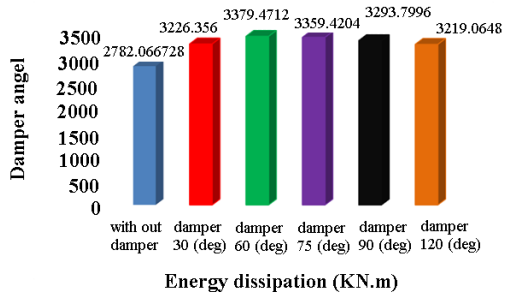

Figure 21. Comparison of the effect of curved shape damping angle on the energy dissipation of steel joint under heat load of 1530 °C [11]

4. CONCLUSIONS

In this paper, the effect of using curved metal dampers in improving the behavior of steel joints under the effect of heat load in Abaqus software was investigated. From all the issues raised, the following can be mentioned

- Examining the stress distribution in the curved metal damper, it was found that the maximum stress and the flowing area of the damper occur in its middle part, which indicates the effective geometry of the damper and its flexural performance. Also, a significant part of the curved damper has reached the delivery stage, which indicates the optimal use of the damper capacity in energy consumption.
- By increasing the length of the curved metal dampers, the values related to the initialhardness parameters, resistance and energy dissipation capacity of the dampers decreased. So that the mentioned parameters decreased on average about 31.45%, 24.2% and 34.1%, respectively.
- As the depth and thickness of the curved metal dampers increased, their behavior improved and the values related to the initial hardness parameters, strength and energy dissipation capacity of the dampers increased. The mentioned parameters increased on average about 50،4%, 61,47% and 31،25%, respectively.
- A steel joint with a curved metal damper performed better than a damper without a damper. Which shows the effectiveness of curved metal dampers on improving the response of steel joints.
- The distribution of stress in the steel joint area equipped with a curved damper under the effect of different thermal loads in the figure is compared. The curved current shows the effectiveness of the curved damper in improving the performance of the steel joint. The amount of area flowing in the curved metal damper also indicates its high capacity in absorbing and dissipating the input energy to the joint due to increased heat load.

NOMENCLATURES

1. Symbols / Parameters

$P\Delta$: Axial Load

Δ : Decentralization

REFERENCES

[1] H. Saffari, A.A. Hedayat, M.P. Nejad, "Post-Northridge Connections with Slit Dampers to Enhance Strength and Ductility", Journal of Constructional Steel Research, No. 80, pp. 138-152, 2013.

[2] A. Ghabussi, J. Asgari, M. Mohammad, S. Rohanimanesh, "Improving Seismic Performance of Portal Frame Structures with Steel Curved Dampers Author Links Open Overlay Panel", Structures, No. 24, pp. 27-40, 2020.

[3] A. Shirkhani, I.H. Mualla, N. Shabakhty, S.R. Mousavi, "Behavior of Steel Frames with Rotational Friction Dampers by Endurance Time Method", Journal of Constructional Steel Research, No. 107, pp. 211-222, 2015.

[4] F. Saeedi, N. Shabakhty, S.R. Mousavi, "Seismic Assessment of Steel Frames with Triangular-Plate added Damping and Stiffness Devices", Journal of Constructional Steel Research, No. 125, pp. 15-25, 2016.

[5] R. Rahnavard, R.J. Thomas, "Numerical Evaluation of the Effects of Fire on Steel Connections", Part1: Simulation Techniques", Case Studies in Thermal Engineering, No. 12, pp. 445-453, 2018.

[6] Z. Guo, N. Lu, F. Zhu, R. Gao, "Effect of Preloading in High-Strength Bolts on Bolted-Connections Exposed to Fire", Fire Safety Journal, No. 90, pp. 112-122, 2017.

[7] X. Qiang, F.S. Bijlaard, H. Kolstein, X. Jiang, "Behavior of Beam-to-Column High Strength Steel Endplate Connections under Fire Conditions-Part 1: Experimental Study", Engineering Structures, No. 64, pp. 23-38, 2014.

[8] H.L. Hsu, H. Halim, "Improving Seismic Performance of Framed Structures with Steel Curved Dampers", Engineering Structures, N. 130, pp. 99-111, 2017.

[9] H.L. Hsu, H. Halim, "Brace Performance with Steel Curved Dampers and Amplified Deformation Mechanisms", Engineering Structures, No. 175, pp. 628-644, 2018.

[10] Standard (ASTM2001a) Office of Development and Promotion of National Building Regulations, American Society for Testing and Materials, West Conshohocken, PA, USA, 1898.

[11] Abaqus, "Modeling and Results Obtained from FEM Software", Abaqus 6.9, Khazar University, 1978.

BIOGRAPHIES

Ziaaddin Zamanzadeh was born in Tabriz, Iran on September 20, 1981. He received the B.Sc. degree from Tabriz University, Tabriz, Iran and the M.Sc. degree from Tabriz Branch, Islamic Azad University, Tabriz, Iran and the Ph.D. degree from University of Minho, Braga, Portugal, all in Civil Engineering, in 2005, 2008, and 2017, respectively. Currently, he is a Professor of Civil Engineering at Khazar University, Baku, Azerbaijan. He is also an academic member at the same university and teaches structural analysis, finite element method, mechanics of materials, and steel structures, reinforced concrete structures. His research interests are in the area of structural engineering particularly shear strengthening of RC beams and estimation of statically equivalent seismic forces of single layer reticular domes. He is a member of the International Journal of Civil Engineering and Journal of Engineering Research and Reports.

Murad Tapdigli was born in Gadabay, Azerbaijan on January 5, 1996. He received the B.Sc. degree in Civil Engineering from Khazar University, Baku, Azerbaijan with honor diploma. During his bachelor, he gained profound academic knowledge and software skills directly related with civil engineering. Currently, he is working as a senior Site Engineer CONCO JCSC, Baku, Azerbaijan. His research interests are in the area of civil engineering with especially of structural engineering.

Rashad Nuraliyev was born in Baku, Azerbaijan on February 17, 1987. He received the B.Sc. degree from Azerbaijan Architecture and Construction University, Baku, Azerbaijan and the M.Sc. degree from University of Naples Federico II, Naples, Italy and the Ph.D. degree from University of Montpellier, Montpellier, France (Dual Program) and Azerbaijan Architecture and Construction University, all in Civil Engineering, in 2009, 2014, and 2017, respectively. Currently, he is an instructor at Azerbaijan State Oil and Industrial University, Baku, Azerbaijan and project engineering in SOCAR Oil and Gas construction trust, Baku, Azerbaijan. His research interests are in the areas of structural and geotechnical engineering.

The 18th International Conference on
"Technical and Physical Problems of Engineering"
30 October 2022
International Organization of IOTPE

ICTPE Conference
www.iotpe.com
ictpe@iotpe.com
ictpe0@gmail.com

ICTPE-2022 Number 32 Code 10MCE02 Pages 169-175

VIBRATIONS OF A HOMOGENEOUS LONGITUDINALLY STIFFENED CYLINDRICAL SHELLS WITH VISCOUS-ELASTIC MEDIUM

J.M. Tabatabaei

Department of Civil Engineering, Faculty of Engineering and Architecture, Istanbul Rumeli University, Istanbul, Turkey, nadermt@gmail.com

Abstract- The development of modern technology and technologies imposes new theoretical and applied requirements to the mechanics of deformable solids, as well as to all branches of science. These requirements are imposed on the properties (physical, mechanical, anisotropic, inhomogeneous, viscoelastic, etc.) of materials selected to accurately determine the boundaries of working resources, structural elements and devices in general. To consider its properties and clarify the equations interpreting the tense-deformation state. On the other hand, in addition to the external influences to which objects and structural elements are exposed, taking into account the effects of the environment in which they are located is also an integral part of the requirements for certain models. The presented article is devoted to a very complex field of the theory of reinforced cylindrical shells, which is widely used in practice. In the article, a cylindrical shell is chosen as the design. The shell is reinforced with rectilinear rods along the axis. It is assumed that the coating material is not homogeneous, that is, the axis passing through the middle surface of the shell and the perpendicular to this axis change the elastic modulus linearly in both (one of which is circular) directions. Since there is a viscoelastic medium inside the structure under study, its influence, in addition to the hydrostatic action of one medium, also takes into account the friction between the medium and the coating (Pasternak model). When solving the problem, the condition of stationery of the Hamilton-Ostrogradsky variation principle is used, which refers to the integral principle of mechanics. With this condition, all parameters of the oscillation of the structure are determined.

Keywords: Shell, Medium, Pasternak Model, Variation Principle, Heterogeneity, The Frequency Equation.

1. INTRODUCTION

The article [1] is devoted to the topic "Oscillation of a reinforced inhomogeneous cylindrical shell with various media", proposed by the author's supervisor, which is the initial part when it is not complicated. In this article, it was assumed that the shell material consists of a composite (fiberglass) material, and in this article, it is also accepted that the inhomogeneity depends on three coordinates, that is, the displacement of the shell points linearly depends on all three coordinates. The problem posed in the article was solved to the end, the energy method (the principle of variation) was chosen as the solution method, the resulting equation for determining the natural frequency of vibrations of the structure was solved numerically and characteristic curves were constructed. The results were analyzed.

In the article [2], the tense-deformation state of a cylindrical shell made of orthotropic material was investigated if the structure is reinforced externally with rectilinear rods parallel to its axis. The density of the structural material, taking into account the axis directed in the direction of the normal of the shell surface and the modulus of elasticity, is chosen as a linear function of coordinates (in the special case, parabolic), varying in this direction. The tense-deformation state of the structure under consideration was studied in the case of free oscillatory motion during the movement of a liquid medium inside it. In accordance with the requirement of the oscillation theory, an intrinsic frequency oscillation equation was constructed, the resulting equation was solved numerically, and the results are presented in the form of graphs and widely analyzed.

In the article [3], the stress-strain state of the structural element was investigated with a relatively complex formulation. The complexity of the problem lies in the fact that the expression between deformation and displacement is geometrically nonlinear. On the other hand, the structure in question is reinforced with ribs forming an orthogonal network, while the structure is exposed to a viscoelastic medium from the outside and pressure from the inside. The influence of the external environment was taken into account in the case of simultaneous application of hydrostatic pressure and friction force. Parametric vibrations of the structure are considered here.

In the article [4], the problem of nonlinear formulation was considered, which is a more complex area of deformable solid mechanics. In the question, a cylindrical shell made of viscoelastic material was chosen and the refined Timoshenko theory was applied. This theory mainly takes into account the sliding deformation, the force of inertia of rotation and geometric nonlinearity.

The solution of the problem under consideration is reduced to a system of integro-differential nonlinear relaxation equations with a singular kernel. The Bubnov-Galerkin method was chosen as a solution in combination with the numerical method using quadrature formulas, and the convergence of the result was verified. The influence of viscoelasticity on nonlinear oscillations of the cylindrical shell and dynamic stability is analyzed.

In the paper [5] based on V.Z. Vlasov moment less theory, a problem of dynamical stability of an isotropic cylindrical shell variable along the generatrix of thickness and density under the action of symmetric external pressure variable along the generatrix under different boundary conditions was considered. The exact solution was obtained at one ratio of change in thickness, pressure and density. Structural elements of long and medium shells with variable thickness of materials are used in different fields of machine-building and aero cosmic engineering for mass optimization.

In the case of five boundary value problems minimum values of the excitation coefficients were obtained in relation to the possible arise of nongaming vibrations for the first and second instability domains that have great importance for engineering practice. The assessment of the accuracy of the WKB method was performed for the considered boundary value problems and laws of changes in thickness and density.

The results of experimental studies of frequencies and the forms of natural vibrations of heterogeneous cylindrical shells with holes were given in [6]. The study was performed by the method of holographic interferometry. Influence of holes and other constructional features on the main dynamical characteristics of shells was established. The procedure for conducting the experiment was described. Experimental data were compared with numerical results obtained by the finite elements method.

The review of the works given in the paper shows that the vibrations of a strengthened, viscous-elastic medium contacting cylindrical shell whose material is heterogenous along the thickness in the direction of generatrix and annular directions were not studied. In the article [1] a similar problem was solved; reinforcement was done with rings. The shell material is heterogeneous (depends on all three coordinates), inside the liquid medium and the ring materials are also homogeneous.

2. PROBLEM STATEMENT

The design under consideration is a closed cylindrical shell, inside of which there is a viscoelastic fluid, the body of which is mutually orthogonal to all three coordinate axes with a density varying in the direction and Young's modulus, reinforced from the outside by rectilinear rods parallel to the central axis (Figure 1.).

Consider a three-dimensional functional that takes into account the heterogeneity of the coating material depending on stress, relative deformation and density, as follows:

$$V=\frac{1}{2}\iint\int_{-\frac{h}{2}}^{\frac{h}{2}}\left(\sigma_{11}\varepsilon_{11}+\sigma_{22}\varepsilon_{22}+\sigma_{12}\varepsilon_{12}+\right.$$
$$\left.+\rho\left(\left(\frac{\partial u}{\partial t}\right)^2+\left(\frac{\partial \vartheta}{\partial t}\right)^2+\left(\frac{\partial w}{\partial t}\right)^2\right)dx\,dy\,dz \quad (1)$$

Constants included in the equations expressing the stress-strain states of structures whose material is inhomogeneous (Young's modulus, density, etc.). They should be replaced with variables [8]. In order not to complicate the solution of the problem under consideration too much, the Poisson's ratio is assumed to be constant.

The relationship between the stresses and relative deformations of the coating points, the question of which is considered in the oscillation, can be chosen as follows:

$$\sigma_{11}=\frac{E(x,\theta,z)}{1-\nu^2}(\varepsilon_{11}+\nu\,\varepsilon_{22});$$
$$\sigma_{22}=\frac{E(x,\theta,z)}{1-\nu^2}(\varepsilon_{22}+\nu\,\varepsilon_{11}); \quad (2)$$
$$\sigma_{12}=G(x,\theta,z)\,\varepsilon_{12}$$

$$\varepsilon_{11}=\frac{\partial u}{\partial x};\ \varepsilon_{22}=\frac{\partial \vartheta}{\partial y}+\frac{w}{R};\ \varepsilon_{12}=\frac{\partial u}{\partial y}+\frac{\partial \vartheta}{\partial x} \quad (3)$$

For the shell material, we take the modulus of elasticity and density as follows:

$$E(x,\theta,z)=E_0 f_1(z)\,f_2(x)\,f_3(\theta);$$
$$\rho(z,x)=\rho_0 f_1(z)\,f_2(x)\,f_3(\theta) \quad (4)$$

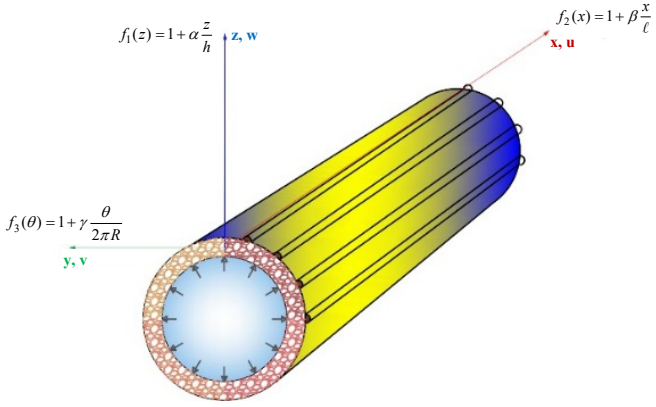

Figure 1. Longitudinally stiffened inhomogeneous cylindrical shell (general view)

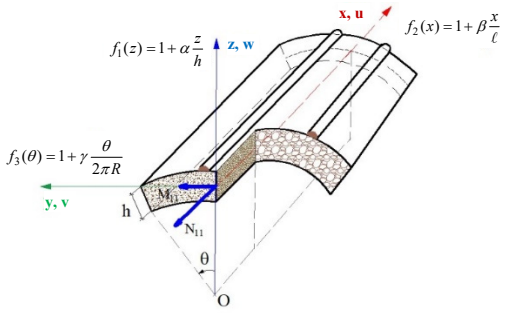

Figure 2. Working scheme of the construction

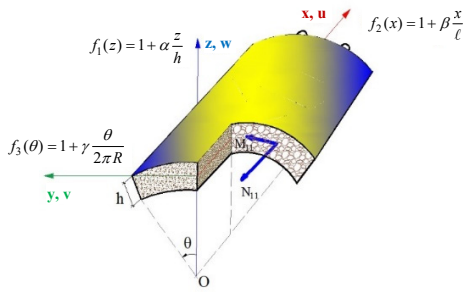

Figure 3. Body of the construction

Taking into account (4) in (2), we obtain:

$$\sigma_{11} = \frac{E_0}{1-\nu^2}(\varepsilon_{11} + \nu\,\varepsilon_{22}) f_1(z)\, f_2(x)\, f_3(\theta)$$
$$\sigma_{22} = \frac{E_0}{1-\nu^2}(\varepsilon_{22} + \nu\,\varepsilon_{11}) f_1(z)\, f_2(x)\, f_3(\theta) \qquad (5)$$
$$\sigma_{12} = G\,\varepsilon_{12} = \frac{E_0}{2(1+\nu)}\,\varepsilon_{12}\, f_1(z)\, f_2(x)\, f_3(\theta)$$

where, E_0 is an elasticity modulus of the heterogeneous material of the shell, ρ_0 is the density of the homogeneous shell material (Figure 3). Allowing for (5) the functional of the total energy of the cylindrical shell is of the form [8]:

$$V = \frac{R E_0}{2(1-\nu^2)} \int_{-\frac{h}{2}}^{\frac{h}{2}} f_1(z)\,dz \times \iint \{\varepsilon_{11}^2 + 2(1-\nu)\varepsilon_{11}\varepsilon_{22} +$$
$$+\varepsilon_{22}^2 + \varepsilon_{12}^2\} \times f_2(x) f_3(\theta)\,dx\,d\theta + \int_{-\frac{h}{2}}^{\frac{h}{2}} f_1(z)\,dz \times \qquad (6)$$
$$\times \iint \rho_0 \left(\left(\frac{\partial u}{\partial t}\right)^2 + \left(\frac{\partial \vartheta}{\partial t}\right)^2 + \left(\frac{\partial w}{\partial t}\right)^2 \right) f_2(x)\, f_3(\theta)\, R\,dx\,d\theta$$

The expression for the potential energy of elastic deformation of the *i*th longitudinal rib is:

$$\Pi_i = \frac{1}{2}\int_0^l \left[\tilde{E}_i F_i \left(\frac{\partial u_i}{\partial x}\right)^2 + \tilde{E}_i J_{yi} \left(\frac{\partial^2 w_i}{\partial x^2}\right)^2 + \right.$$
$$\left. + \tilde{E}_i J_{zi} \left(\frac{\partial^2 \vartheta_i}{\partial x^2}\right)^2 + \tilde{G}_i J_{kpi} \left(\frac{\partial \phi_{kpi}}{\partial x^2}\right)^2 \right] dx \qquad (7)$$

Kinetic energy of ribs is written as follows:

$$K_i = \rho_i F_i \int_0^l \left[\left(\frac{\partial u_i}{\partial t}\right)^2 + \left(\frac{\partial \vartheta_i}{\partial t}\right)^2 + \right.$$
$$\left. + \left(\frac{\partial w_i}{\partial t}\right)^2 + \frac{J_{kpi}}{F_i} \left(\frac{\partial \phi_{kpi}}{\partial t}\right)^2 \right] dx \qquad (8)$$

Equations (7) and (8) are written depending on the kinetic and potential energy of the *i*th rod on the geometric and physical parameters of the rod. They are called as follows: u_i, ϑ_i, w_i corresponding displacements in the direction of the coordinate axes of the points of contact of the *i*th rod with the coating (so that there are no repetitions, the designations refer to the *i*th rod), F_i the cross-sectional area of the rod in the direction generating the coating, $\tilde{E}_i$ the elastic modulus of the rod in tension, J_{yi}, J_{zi} are the moment of inertia of the *y* axis, *z* in the plane of the shaft cross-section, J_{kpi} is the moment of inertia during torsion, ρ_i is the density, *t* is the time, respectively, the angles of rotation and torsion. Let's write down the expressions of the torsion and rotation angles:

$$\phi_{kpi}(x) = \phi_2(x, y_i) = -\left(\frac{\partial w}{\partial y} + \frac{\vartheta}{R}\right)\Bigg|_{y=y_i} \quad \phi_i(x) =$$
$$= \phi_1(x, y_i) = -\frac{\partial w}{\partial x}\Bigg|_{y=y_i}$$

Since potential energy is work performed with the opposite sign, the work performed under the action of an elastic medium on the coating as an external force can be written as follows:

$$A_0 = -R \int_0^l \int_0^{2\pi} q_r\, w\,dx\,d\theta \qquad (9)$$

Let's write down the total energy of the structure in question: when recording the total energy, it is necessary to consider the structure in question as a mechanical system and take into account the energy of each element included in it (shell, k_i ribs, the influence of the medium):

$$J = V + \sum_{i=1}^{k} (\Pi_i + k_i) + A_0 \qquad (10)$$

Accounting for the influence of external q_r forces by various models is given in the scientific literature. Since the vibrations of the reinforced cylindrical shell are studied in this issue, it is necessary to take into account the friction force. In this case, the Pasternak model is considered more suitable:

$$q_r = \mu w - \int_{-\infty}^{t} \Gamma(t-\tau)\, w(\tau)\, d\tau \qquad (11)$$

where, these quantities μ, Γ, $\Gamma(t-\tau) = Ae^{-\lambda(t-\tau)}$, A, λ were interpreted in [1].

Rigid contact conditions between the shell and the rods must be rigid, which means that deformations cannot occur in a jump:

$$u_i(x) = u(x, y_i) + h_i \phi_1(x, y_i)$$
$$\vartheta_i(x) = \vartheta(x, y_i) + h_i \phi_2(x, y_i)$$
$$w_i(x) = w(x, y_i),\ \phi_i(x) = \phi_1(x, y_i) \qquad (12)$$
$$\phi_{kpi}(x) = \phi_2(x, y_i), h_i = 0.5\,h + H_i^1$$

where, H_i^1 and h_i are the linear dimensions of the rod.

The boundary (Navier) conditions of the considered construction can be written as follows if $x = 0$ and $x = l$:

$$\vartheta = 0,\ w = 0,\ N_{11} = 0,\ M_{11} = 0 \qquad (13)$$

where, the values T_{11}, M_{11} are the internal forces arising in the shell of length *l* (Figures 2 and 3).

The solution of the issue considered in the article implies finding the frequency of its oscillation. To do this, you first need to get the frequency equation. The simplest and most reliable method of obtaining the frequency equation is the principle of variation [1]:

$$\delta W = 0 \tag{14}$$

the integral expression w is shown in [1].

A mathematical apparatus has already been obtained for studying and completing the proper vibrations of the structure under consideration. In the design under consideration, it is assumed that the shell body is inhomogeneous in three directions, the rods are homogeneous, a viscoelastic medium moves inside the shell. In the design under consideration, it is assumed that the shell body is inhomogeneous in three directions, the rods are homogeneous, a viscoelastic medium moves inside the shell. To determine the stress-strain state of the described structure (in particular, its own oscillatory movements), it is possible to integrate the total energy (10) of the system in question into (12), (13) boundary and contact conditions and obtain the desired results.

3. PROBLEM SOLUTION

The values *u*, *ϑ*, *w*, included in the full energy expression of the system (10), contains inside the desired frequency *ω*, as well as unknown constants $u_i, \vartheta_i, w_i\ (i=0,1,2,3)$ and wave numbers *k, n,* it can be expressed by trigonometric functions as follows.

$$\begin{aligned} u &= (u_0 + u_1 x + u_2 R\theta + u_3 z)\cos kx \cos n\theta \sin \omega t \\ \vartheta &= (\vartheta_0 + \vartheta_1 x + \vartheta_2 R\theta + \vartheta_3 z)\sin kx \sin n\theta \sin \omega t \\ w &= (w_0 + w_1 x + w_2 R\theta + w_3 z)\sin kx \cos n\theta \sin \omega t \end{aligned} \tag{15}$$

Applying (15), we can calculate the work (9):

$$\begin{aligned} A_0 = {} & \frac{\pi^2 h l}{4\omega}\left(\mu - \frac{A\beta}{\omega^2+\beta^2}\right)\times\Big[w_0^2 + l w_0 w_1 + \\ & + \left(\frac{l^2}{3} - \frac{1}{2k^2}\right) w_1^2 + 2R w_0 w_2 + \pi l R w_1 w_2 + \\ & + \frac{R^2 l}{2}\left(\frac{4\pi^2}{3} + \frac{1}{n}\right) w_2^2 + \frac{h^3}{12} w_3^2 \Big] \end{aligned} \tag{16}$$

Simplifying (10), the following dependences were accepted (Figure 2) [7]:

$$f_i(x\cdot y\cdot\theta) = \delta_i^j \begin{cases} 1+\alpha\dfrac{z}{h} & z\ ,\ i=1 \\ 1+\beta\dfrac{x}{l}\ , & x\ ,\ i=2 \\ 1+\gamma\dfrac{\theta}{2\pi R} & \theta\ \ ,\ i=3 \end{cases} \tag{17}$$

$(i = 0,1,2,3;\ j = 1,\ 2,\ 3).$

where, is the $\delta_i^j = \begin{cases} 1\ , i=j \\ 0\ , i\neq j \end{cases}$ Kronecker symbol, *α*, *β*, *γ* are constant coefficients and are indicators of the change in the inhomogeneity of the shell in the direction of the corresponding coordinates;

$x \in [0,1]$, $y \in [0, 2\pi]$ and $t \in [0, \pi/\omega]$

Finally, if we integrate the variables *x*, *y*, *t* in the appropriate bounds, we can write the Lagrange function J depending on the desired quantities $u_i, \vartheta_i, w_i\ (i = 0,1,2,3)$:

$$\begin{aligned} J = {} & t_0 a_1 + \sum_{i=2}^{39} t_i a_i + \rho_0 \omega^2 [(u_0^2 + \vartheta_0^2 + w_0^2)C_1 + \\ & + 2(u_0 u_1 + \vartheta_0\vartheta_1 + w_0 w_1)C_2 + u_1^2 C_3 + (\vartheta_1^2 + w_1^2)C_4 + \\ & + 2(u_0 u_2 R + w_0 w_2)C_5 + 2\vartheta_0\vartheta_2 R C_6 + \\ & + 2(u_0 u_3 + \vartheta_0\vartheta_3 + w_0 w_3)C_7 + u_1 u_2 R C_8 + R(\vartheta_1\vartheta_2 + w_1 w_2)C_9 + \\ & + u_1 u_3 C_{10} + (\vartheta_1\vartheta_3 + w_1 w_3)C_{11} + (u_2^2 + w_2^2)C_{12} + \vartheta_2^2 C_{13} + u_2 u_3 C_{14} + \\ & + (\vartheta_2\vartheta_3 + w_2 w_3)C_{15} + (u_3^2 + \vartheta_3^2 + w_3^2)C_{16} + \\ & + \frac{1}{2}\sum_{i=1}^{k_1}(E_i F_i + \rho_i F_i \omega^2)\frac{k^2 l}{2}\left(H_i - \frac{h}{2}\right)\cdot[u_0^2 + \\ & + u_0 u_1 l + u_1^2\left(\frac{l^2}{3} - \frac{1}{2k^2}\right) + 2R u_0 u_2 \theta_i + u_0 u_3\left(H_i + \frac{h}{2}\right) + \\ & + 2R u_1 u_2 l\theta_i + u_1 u_3 l\left(H_i + \frac{h}{2}\right) + R^2 u_2^2\theta_i^2 + R u_2 u_3\theta_i\left(H_i + \frac{h}{2}\right) + \\ & + \frac{1}{3}u_3^2\left(H_i + \frac{H_i h}{2} + \frac{h^2}{4}\right)\Big]\cos^2 n\theta_i + \\ & + \frac{1}{2}\sum_{i=1}^{k_1}\left[E_i J_{yi}\frac{k^2 l}{2}\left(H_i - \frac{h}{2}\right) + \omega^2\rho_i F_i\right]\cdot[w_0^2 + w_0 u_1 l + \\ & + w_1^2\left(\frac{l^2}{3} - \frac{1}{2k^2}\right) + 2R w_0 w_2\theta_i + w_0 w_3\left(H_i + \frac{h}{2}\right) + \\ & + R w_1 w_2 l\theta_i + w_1 w_3 l\left(H_i + \frac{h}{2}\right) + R^2 w_2^2\theta_i^2 + R w_2 w_3\theta_i\left(H_i + \frac{h}{2}\right) + \\ & + \frac{1}{3}w_3^2\left(H_i^2 + \frac{H_i h}{2} + \frac{h^2}{4}\right)\Big]\cos^2 n\theta_i + \\ & + \frac{1}{2}\sum_{i=1}^{k_1}\left[E_i J_{zi}\frac{k^2 l}{2}\left(H_i - \frac{h}{2}\right) + \omega^2\rho_i F_i\right]\cdot[\vartheta_0^2 + \vartheta_0\vartheta_1 l + \\ & + \vartheta_1^2\left(\frac{l^2}{3} - \frac{1}{2k^2}\right) + 2R\vartheta_0\vartheta_2\theta_i + \vartheta_0\vartheta_3\left(H_i + \frac{h}{2}\right) + R\vartheta_1\vartheta_2 l\theta_i + \\ & + \vartheta_1\vartheta_2 l\left(H_i + \frac{h}{2}\right) + R^2\vartheta_2^2\theta_i^2 + R\vartheta_2\vartheta_3\theta_i\left(H_i + \frac{h}{2}\right) + \\ & + \frac{1}{3}\vartheta_3^2\left(H_i^2 + \frac{H_i h}{2} + \frac{h^2}{4}\right)\Big]\sin^2 n\theta_i + \\ & + \frac{1}{2}\sum_{i=1}^{k_1}\left[\frac{l}{2R^2}\left(H_i - \frac{h}{2}\right)G_i J_{kpi} + \omega^2\rho_i F_i\right]\cdot\{[(\vartheta_0 - n w_0)^2 + \\ & + l(\vartheta_0 - n w_0)(\vartheta_1 - n w_1) + (\vartheta_1 - n w_1)^2 + \\ & + 2R(\vartheta_0 - n w_0)(\vartheta_2 - n w_2)\theta_i + \\ & + (\vartheta_0 - n w_0)(\vartheta_3 - n w_3)\left(H_i + \frac{h}{2}\right) + Rl(\vartheta_1 - n w_1)(\vartheta_2 - n w_2)\theta_i + \\ & + (\vartheta_1 - n w_1)(\vartheta_3 - n w_3)\frac{l}{2}\left(H_i + \frac{h}{2}\right) + R^2(\vartheta_2 - n w_2)\theta_i^2 + \end{aligned}$$

$$+\frac{R}{2}(\vartheta_2-nw_2)(\vartheta_3-nw_3)\left(H_i+\frac{h}{2}\right)\theta_i+\frac{1}{3}(\vartheta_3-nw_3)^2\cdot$$
$$\cdot\left(H_i^2+\frac{H_i h}{2}+\frac{h^2}{4}\right)\Bigg]\sin^2 n\theta_i-\left[\frac{n}{R}\omega_2(\vartheta_0-mw_0)+\frac{l}{2}(\vartheta_1-mw_1)+\right.$$
$$+R(\vartheta_2-nw_2)\theta_i+\frac{l}{2}(\vartheta_3-nw_3)\left(H_i+\frac{h}{2}\right)\Bigg]\sin 2n\theta_i+$$
$$+n^2w_2^2\cos^2 n\theta_i\}+\frac{\pi^2 hl}{4\omega}\left(\mu-\frac{AB}{\omega^2+\beta^2}\right)[w_0^2+lw_0w_1+$$
$$+\left(\frac{l^2}{3}-\frac{1}{2k^2}\right)w_1^2+2Rw_0w_2+\pi l R\, w_1w_2+$$
$$+\frac{R^2 l}{2}\left(\frac{4\pi^2}{3}+\frac{1}{n}\right)w_2^2+\frac{h^3}{12}w_3^2\Bigg] \qquad (18)$$

$P_0=k\,u_1u_0;\ P_1=k\,u_1^2;\ P_2=k\,u_1u_2;$

$P_3=k\,u_1\,u_3;\ P_4=k^4\,u_0^2;\quad P_5=2k^2u_0u_1;\ P_6=P_1;$

$P_7=2k^2u_0u_2;\ P_8=2k^2u_0u_3;\quad P_9=2k^2u_1u_2;$

$P_{10}=2k^2u_1u_3;\ P_{11}=k^2u_2^2;\ P_{12}=k^2u_2u_3;\ P_{13}=u_3^2k^2$

$t_0=u_1^2+u_2^2;\ t_{1+i}=-P_i+\frac{1-\nu}{R}l_i\quad(i=0,1,2,3);$

$t_{i+5}=P_{i+4}+\frac{1}{R^2}T_i+l_{4+i}(i=0,1,2);$

$t_8=P_7+\frac{1}{R^2}T_4+l_8;\ t_9=P_8+\frac{1}{R^2}T_5+l_7;$

$t_{10}=P_9+\frac{1}{R^2}T_6+l_{11};\ t_{11}=P_{10}+\frac{1}{R^2}T_7+l_{12};$

$t_{12}=P_{11}+\frac{1}{R^2}T_3+l_9;\ t_{13}=P_{12}+\frac{1}{R^2}T_9+l_{13};$

$t_{14}=P_{13}+\frac{1}{R^2}T_7+l_{10};\ t_{15}=S_0R-\frac{1}{2}k\,R\,u_0\,\vartheta_2;$

$t_{16}=S_1R-\frac{1}{2}k\,R\,u_1\,u_2;\quad t_{17}=S_2R-\frac{1}{2}k\,R\,u_2\,\vartheta_2;$

$t_{18}=S_3R-\frac{1}{2}k\,R\,u_3\,\vartheta_2;\quad t_{19}=\frac{1}{R^2}\vartheta_2^2;\ t_{20}=u_0u_2;$

$t_{21}=u_1u_2;\quad t_{22}=u_2^2;\quad t_{23}=u_2\,u_3;$

$t_{24}=\frac{1}{2R}\vartheta_1u_2+\frac{1-\nu}{2}u_1\vartheta_2;\ t_{25}=\vartheta_2^2R;$

$t_{26}=n^2u_0^2+k^2\vartheta_0^2-2nku_0\vartheta_0;$

$t_{27}=2n^2u_0u_1+2k^2\vartheta_0\vartheta_1-2nku_0\vartheta_2-2nku_2\vartheta_0;$

$t_{28}=2n^2u_0u_2+2k^2\vartheta_0\vartheta_2-2nku_0\vartheta_2-2nku_2\vartheta_0;$

$t_{29}=2n^2u_0u_3+2k^2\vartheta_0\vartheta_3-2nku_0\vartheta_3-2nk\vartheta_0u_3;$

$t_{29+i}=n^2u_i^2+k^2\vartheta_i^2-2nku_i\vartheta_i\quad(i=1,2,3);$

$t_{33}=2n^2u_1u_2+2k^2\vartheta_1\vartheta_2-2nku_1\vartheta_2-2nku_2\vartheta_1;$

$t_{34}=2n^2u_1u_3+2k^2\vartheta_1\vartheta_3-2nku_1\vartheta_3-2nku_3\vartheta_1;$

$t_{35}=n^2u_2u_3+k^2\vartheta_2\vartheta_3-2nku_2\vartheta_3-2nku_3\vartheta_2;$

$t_{36+i}=-n\,u_i\vartheta_1+k\vartheta_1\vartheta_i\quad(i=0,1,2,3);$

$S_i=\vartheta_2(n\vartheta_i+w_i)\quad(i=0,1,2,3);$

$l_i=u_1(n\vartheta_i+w_i)\quad(i=0,1,2,3);$

$l_{4+i}=-n\,ku_0\vartheta_i-nk\vartheta_0\vartheta_i-ku_0w_i-kw_0u_i\quad(i=1,2,3);$

$l_{7+i}=-knu_i\vartheta_i-ku_iw_i\quad(i=1,2,3);$

$l_{11}=-knu_1\vartheta_2-nku_2\vartheta_1-ku_1w_2-ku_2w_1;$

$l_{12}=-knu_1\vartheta_3-nku_3\vartheta_1-ku_1w_3-ku_3w_1;$

$l_{13}=-knu_2\vartheta_3-nku_3\vartheta_2-ku_2w_3-ku_3w_2;$

$T_0=n^2\vartheta_0^2+2nw_0\vartheta_0+w_0^2;$

$T_i=2n^2\vartheta_0\vartheta_i+2n\vartheta_0w_i+2n\,w_0\vartheta_i+2w_0w_i\quad(i=1,2,3);$

$T_{3+i}=n^2\vartheta_i^2+2n\omega_i\vartheta_i+w_i^2\quad(i=1,2,3);$

$T_7=2n^2\vartheta_1\vartheta_2+2nw_2\vartheta_1+2n\,w_1\vartheta_2+2w_1w_2;$

$T_8=2n^2\vartheta_1\vartheta_3+2nw_3\vartheta_1+2n\,w_1\vartheta_3+2w_1w_3;$

$T_9=2n^2\vartheta_2\vartheta_3+2nw_3\vartheta_2+2n\,w_2\vartheta_3+w_2w_3;$

$a_1=\frac{h\pi l}{2}\left(1+\frac{\gamma}{2}+\frac{\beta}{2}+\frac{\beta\gamma}{4}\right);$

$a_2=\frac{h\pi l}{2}\left(1+\frac{\gamma}{2}+\frac{\beta}{2}+\frac{\beta\gamma}{4}\right);$

$a_3=\frac{R\,\beta}{2k}\left[\pi^2+\frac{\gamma\,l}{2\pi^2}\left(\frac{8\pi^3}{3}-\frac{\pi}{2n^2}\right)\right];$

$a_4=\frac{\pi\alpha\beta h^2}{24k}\left(l+\frac{\gamma}{2}\right);$

$a_5=\frac{\pi lh}{2n}\left(1+\frac{\gamma}{2}+\frac{\beta}{2}+\frac{\beta\gamma}{8l}\right);$

$a_6=\frac{\pi h}{2}\left[\frac{l^2}{2}+\frac{\gamma\,l^3}{4}+\pi h\beta\left(\frac{l^3}{3}+\frac{1}{2k^2}\right)+\frac{\beta\gamma}{2}\left(\frac{l^2}{3}+\frac{1}{2k^2}\right)\right];$

$a_7=\frac{\pi l}{2}\left[\frac{l^2}{3}+\frac{1}{2k^2}+\frac{\gamma h}{2}\left(\frac{l^2}{3}+\frac{1}{2k^2}\right)+\frac{\beta\gamma h}{8}\left(l^2-\frac{3}{k^2}\right)\right];$

$a_8=\frac{hlR}{2}\left[\pi^2+\frac{\gamma}{2}\left(\frac{8\pi^2}{3}-\frac{1}{2n^2}\right)+\frac{\beta\pi^2}{2}+\frac{\beta\gamma}{4}\left(\frac{8\pi^2}{3}-\frac{1}{2n^2}\right)\right];$

$a_9=\frac{\pi h^2\alpha}{3}\left(\frac{1}{l}+\frac{\gamma\,l}{2}+\frac{\beta\,l}{2}+\frac{\beta\,\gamma\,l}{4}\right);$

$a_{10}=hR\left[\frac{\pi^2l^2}{4}+\frac{\gamma hl^2}{8}\left(\frac{8\pi^2}{3}-\frac{1}{2n^2}\right)+\beta h\pi^2\left(\frac{l^2}{6}+\frac{1}{4k^2}\right)\right]+$
$+\frac{\beta\gamma h}{2}\left(\frac{l^2}{6}+\frac{1}{4k^2}\right)\left(\frac{8\pi^2}{3}-\frac{1}{2n^2}\right)\Bigg];$

$a_{11}=\alpha h^2\left(\frac{\pi l^2}{6}+\frac{\pi\gamma\,l^2}{12}-\frac{\beta}{k}-\frac{\pi\beta\gamma}{6k}\right);$

$a_{12}=\frac{\pi\,h\,lR^2}{2}\left[\frac{8\pi^2}{3}-\frac{1}{2n^2}+\frac{\beta}{2}\left(\frac{8\pi^2}{3}-\frac{1}{2n^2}\right)+\right.$
$\left.+\gamma\left(\pi^2+\frac{2}{n^2}\right)+\frac{\beta\,\gamma}{2}\left(\pi^2+\frac{1}{n^2}\right)\right];$

$$a_{13}=\frac{Rh^2l\alpha}{24}\left[\pi^2+\frac{\gamma}{2}\left(\frac{8\pi^2}{3}-\frac{1}{2n^2}\right)+\right.$$
$$\left.+\frac{\pi^2\beta}{2}+\frac{\beta\gamma}{4}\left(\frac{8\pi^2}{3}-\frac{1}{2n^2}\right)\right];$$
$$a_{14}=\frac{\pi lh^3}{24}\left(1+\frac{\alpha}{2}+\frac{\beta}{2}+\frac{\beta\gamma}{4}\right);\ a_{15}=-\frac{\gamma hl}{2}\left(1+\frac{\beta}{2}\right);$$
$$a_{16}=\frac{\gamma h}{4}\left[l^2+\beta\left(\frac{l^2}{9}+\frac{1}{k^2}\right)\right];$$
$$a_{17}=-\pi hlR\left(1+\frac{\gamma}{2n}+\frac{\beta}{2}+\frac{\beta\gamma}{4n}\right);\ a_{18}=-\frac{\alpha\gamma h^2l}{24}\left(1+\frac{\beta}{2}\right);$$
$$a_{19}=-\frac{\pi l}{2}\left(1+\frac{\gamma h}{2}+\frac{\beta h}{2}+\frac{\beta\gamma h}{4}\right);\ a_{20}=-\frac{\gamma hl}{2}\left(1+\frac{\beta}{2}\right)=a_{15};$$
$$a_{21}=-\gamma h\left[\frac{l^2}{4}-\frac{\beta}{2}\left(\frac{l^3}{3}-\frac{1}{2k^2}\right)\right];$$
$$a_{22}=-\pi hR\left(\frac{1}{l}+\frac{\gamma l}{2n}+\frac{\beta l}{2}+\frac{\beta\gamma l}{4n}\right);$$
$$a_{23}=-\frac{\alpha\gamma h^2l}{24}\left(1+\frac{\beta}{2}\right)=a_{18};\quad a_{24}=-\frac{\beta\gamma h}{2k};$$
$$a_{25}=-\frac{h\pi l}{2}\left(1+\frac{\pi\gamma}{24}+\frac{\beta}{2}+\frac{\beta\gamma}{4}\right)=b_7;$$
$$a_{26}=-\frac{\pi hl}{2R^2}\left(1+\frac{\pi\gamma}{24}+\frac{\beta}{2}+\frac{\beta\gamma}{4}\right);$$
$$a_{28}=\frac{\pi^2hl}{2R}\left[1+\frac{\pi\gamma}{18}+\frac{\beta}{2}+\frac{\beta\gamma}{3}\right];$$
$$a_{27}=\frac{\pi h}{R^2}\left[\frac{l^2}{4}+\frac{\pi\gamma l^2}{96}+\beta\left(\frac{l^2}{9}+\frac{1}{4k^2}\right)+\frac{\pi\beta\gamma}{2}\left(\frac{l^2}{9}+\frac{1}{4k^2}\right)\right];$$
$$a_{29}=-\frac{\pi h^2l\alpha}{24R^2}\left(1+\frac{\pi\gamma}{18}+\frac{\beta}{2}+\frac{\beta\gamma}{3}\right);$$
$$a_{30}=\frac{1}{R^2}\left(\pi h+\frac{\gamma h}{2}\right)\left[\frac{l^8}{6}+\frac{l}{4k^2}+\beta\left(\frac{l^2}{8}+\frac{3l}{8k^2}\right)\right];$$
$$a_{31}=\pi\left(\frac{hl}{2}+\frac{\beta h}{2}\right)\left[\frac{4\pi^2}{3}+\left(\gamma+\frac{\beta\gamma}{l}\right)\left(\pi^2-\frac{2}{n^2}\right)\right];$$
$$a_{32}=\frac{\pi h^3l}{24R^2}\left[1+\frac{\gamma}{2}+\frac{\beta}{2}+\frac{\beta\gamma}{4}\right];$$
$$a_{33}=\frac{h\pi^2}{R}\left[\frac{l^2}{4}+\beta\left(\frac{l^2}{6}+\frac{1}{4k^2}\right)+\frac{\gamma l^2}{6}+\frac{2\beta\gamma}{3}\left(\frac{l^2}{6}+\frac{1}{4k^2}\right)\right];$$
$$a_{34}=\frac{\pi h^2}{12R^2}\left[\frac{\alpha l^2}{4}+\alpha\beta\left(\frac{l^2}{6}+\frac{1}{4k^2}\right)+\frac{\alpha\gamma l^2}{8}+\frac{\alpha\beta\gamma}{2}\left(\frac{l^2}{6}+\frac{1}{4k^2}\right)\right];$$
$$a_{35}=\frac{\pi^2alh^2}{24R}\left[1+\frac{\beta}{2}+\frac{2\gamma}{3}+\frac{\beta\gamma}{3}\right];\quad a_{36}=\frac{\pi\beta h}{2kR^2}\left(1+\frac{\gamma}{2}\right);$$
$$a_{37}=\frac{\pi^2alh^2}{24R}\left[l-\beta+\frac{\gamma l}{2}-\frac{\beta\gamma}{2}\right];$$
$$a_{38}=\frac{\pi^2\beta h}{Rk}\left(\frac{1}{2}+\frac{\gamma}{3}\right);\quad a_{39}=\frac{\pi\alpha\beta h^2}{24\,kR^2}\left(1+\frac{\gamma}{2}\right);$$
$$c_1=\frac{\pi hl}{2}\left[1+\frac{\gamma}{2}+\frac{\beta}{2}+\frac{\beta\gamma}{4}\right];$$
$$c_2=\frac{\pi h}{2}\left[\frac{l^2}{2}+\frac{\gamma l^2}{4}+\beta\left(\frac{l^2}{3}+\frac{1}{2k^2}\right)+\frac{\gamma l}{2}\left(\frac{l^2}{3}+\frac{1}{2k^2}\right)\right];$$
$$c_3=\pi h\left[\left(\frac{l^2}{6}+\frac{1}{4k^2}\right)l\left(1+\frac{\gamma}{2}\right)+\left(\frac{l^2}{8}+\frac{3}{8k^2}\right)l\beta\left(1+\frac{\gamma}{2}\right)\right];$$
$$c_4=\pi h\left[\left(\frac{l^2}{6}-\frac{1}{4k^2}\right)l\left(1+\frac{\gamma}{2}\right)+\left(\frac{l^2}{8}-\frac{3}{8k^2}\right)l\beta\left(1+\frac{\gamma}{2}\right)\right];$$
$$c_5=h\left[\frac{\pi^2l}{2}+\left(\frac{4\pi^2}{3}+\frac{1}{n}\right)\left(\frac{\gamma l}{2}+\frac{\beta\gamma}{4}\right)+\frac{\pi^2\beta}{2}\right];$$
$$c_6=h\left[\frac{\pi^2R}{2}+\left(\frac{4\pi^2}{3}+\frac{1}{n}\right)\left(\frac{\gamma l}{4}+\frac{\beta\gamma}{4}\right)+\frac{\pi^2\beta}{2}\right];$$
$$c_7=\frac{\pi\alpha h^2}{24}\left(1+\frac{\gamma l}{2}+\frac{\beta l}{2}+3\beta\gamma l\right);$$
$$c_8=\pi R\left[\frac{l^2}{2}+\frac{\gamma l^2}{4}+\left(\frac{l^2}{3}+\frac{1}{2k^2}\right)\left(\beta+\frac{\beta\gamma}{2}\right)\right];$$
$$c_9=\pi R\left[\frac{l^2}{2}+\frac{\gamma l^2}{4}+\left(\frac{l^2}{3}-\frac{1}{2k^2}\right)\left(\beta+\frac{\beta\gamma}{2}\right)\right];$$
$$c_{10}=\frac{\alpha h^2}{12R}c_8;\quad c_{11}=\frac{\alpha h^2}{12R}c_9;$$
$$c_{12}=\frac{\pi^2R}{2}\left[(l+\beta)\left(\frac{4\pi^2}{3}+\frac{1}{n}\right)+(\gamma l+\beta\gamma)\left(\pi^2+\frac{1}{n^2}\right)\right];$$
$$c_{13}=\frac{\pi^2R}{2}\left[(l+\beta)\left(\frac{4\pi^2}{3}-\frac{1}{n}\right)+(\gamma l+\beta\gamma)\left(\pi^2-\frac{1}{n^2}\right)\right];$$
$$c_{14}=\frac{R\alpha h^2l}{12}\left[\pi^2\left(1+\frac{\beta}{2}\right)+\left(\frac{\gamma}{2}+\frac{\beta\gamma}{4}\right)\left(\frac{4\pi^2}{3}+\frac{1}{n}\right)\right];$$
$$c_{15}=\frac{\alpha h^2lR}{12}\left[\pi^2\left(1-\frac{\beta}{2}\right)+\left(\frac{\gamma}{2}+\frac{\beta\gamma}{4}\right)\left(\frac{4\pi^2}{3}-\frac{1}{n}\right)\right];\ c_{16}=\frac{h^2}{12}c_1$$

4. CONCLUSIONS

For the construction under consideration (18), we vary the expression of the total energy and obtain a system of algebraic Equations based on the coefficients of independent variations u_i, ϑ_i, w_i $(i=0,1,2,3)$. By making the main determinant of the resulting system of equations equal to zero, we obtain its solution. This equation will be the frequency equation of the system, and this equation can be solved by taking the following geometric, physical and mechanical quantities.

$$\rho_0=\rho_j=1850\ \frac{\text{kg}}{\text{m}^3};\ \tilde{E}_i=6.67\times10^9\ \frac{\text{N}}{\text{m}^2};\ m=1;\ n=8;$$
$$h_i=0,45;\ R=160\,\text{cm};\ n=8;\ \mu=10^6\ \frac{\text{N}}{\text{m}^2};\ h_i=0.45\,\text{mm};$$

$\nu = 0.35$; $\frac{l}{R} = 3$, $\frac{h}{R} = \frac{1}{6}$, $\alpha = 0.4$; $R = 160\,\text{cm}$;

$F_i = 5.2\,\text{mm}^2$; $I_{kp,i} = 0.23\,\text{mm}^4$; $I_i = 5.1\,\text{mm}^4$;

$I_{zi} = 1.3\,\text{mm}^4$; $\lambda = 0.005$; $A = 0.1615$.

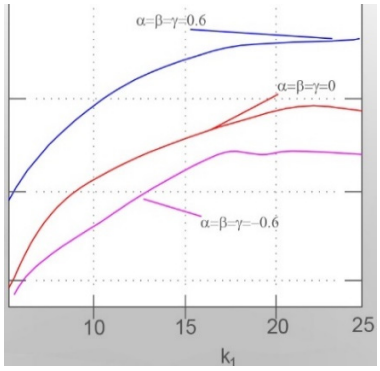

Figure 4. Dependence of the frequency parameter on k_1

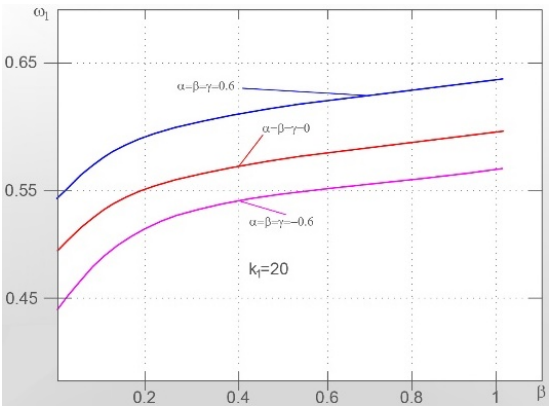

Figure 5. Dependence of the frequency parameter on β

Numerical calculations have been completed and the results are described in two graphs. The graphs are constructed of the frequency parameter of the coating $\omega_1 = (\rho_0 R^2 \omega^2 / b_{11})^{1/2}$ depending on the number of longitudinally reinforcing rods k_1 and on the parameter β of inhomogeneity in the direction of the coordinate axis x. When the number of rods directed in the longitudinal direction changes, the frequency of the structure also changes, which after reaching the highest value, it begins to decrease. Increasing the number of rods creates the effect of inertia in the oscillatory motion. In the problem under consideration, the change in the value of β, which is a parameter of inhomogeneity only in the direction of the forming shell, was taken into account in the calculation. Here it was observed that with increasing positive values of the inhomogeneity parameter of the system (Figure 5) the frequency of the system increases.

REFERENCES

[1] R.A. Iskanderov, J.M. Tabatabaei, "Vibrations of Fluid-Filled Inhomogeneous Cylindrical Shells Strengthened with Lateral Ribs", International Journal on Technical and Physical Problems of Engineering (IJTPE), Issue 42, Vol. 12, No.1, pp. 121-125, March 2020.

[2] F.S. Latifov, R.N. Aghayev, "Oscillations of Longitudinally Reinforced Heterogeneous Orthotropic Cylindrical Shell with Flowing Liquid", The 13th International Conference on Technical and Physical Problems of Electrical Engineering (ICTPE-2017), pp. 301-305, Van, Turkey, 21-23 September 2017.

[3] M.A. Mekhtiev, "Nonlinear Parametric Vibrations of a Stiffened Cylindrical Shell with Viscous-Elastic Filler", Machine Mechanics, Mechanism I Materials, No. 3, Vol. 16, p. 28-30, Minsk, Belarus, 2011.

[4] B.K. Eshmatov, "Nonlinear Vibrations and Dynamic Stability of a Viscous-Elastic Cylindrical Shell with Regard to Shift Deformation and Rotation Inertia", Izv. University of Russian AS, Solid Mechanics, No. 3, pp. 36-41, Moscow, Russia, 2009.

[5] A.A. Mochalin, "Parametric Vibrations of a Heterogeneous Annular Cylindrical Shell of Variable Density under Various Boundary Conditions", Saratov State University, Ser. Math. Mech. Informatics, No. 15, Issue 2, pp. 211-215, 2015.

[6] A.S. Kairov, L.A. Latenskaya, V.A. Kairov, "Experimental Study of Resonance Vibrations of Heterogeneous Cylindrical Shells with Holes by the Holographic Interferometry Method", No. 2, Vol. 32, pp. 40-49, 2020.

[7] V.A. Lomakin, "The Theory of Inhomogeneous Bodies", MGU, Moscow, 1975.

[8] I.Y. Amiro, V.A. Zarutskiy "Studies in the Field on Dynamics of Ribbed Shells", Appl. Mechanics, Vol. 17, JS II, pp. 3-20, 1981.

BIOGRAPHIES

Javad Mahdavi Tabatabaei was born in Tabriz, Iran, on July 06, 1981. He received the B.Sc. degree from Mahabad Branch, Islamic Azad University, Iran and the M.Sc. degree from Azerbaijan Architecture and Construction University, Baku, Azerbaijan, both in Civil Engineering in 2003 and 2009, respectively. He is studying in Ph.D. in Civil Engineering at Azerbaijan Architecture and Construction University. Currently, he is an Academic Member in Department of Civil Engineering, Faculty of Engineering and Architecture, Istanbul Rumeli University, Istanbul, Turkey. He is also Director of International Relations Office at the same university. He has published 15 papers in international conferences and journals. His scientific interests are construction with suitable energy managing, optimum architecture, energy efficiency and saving in buildings, and sustainable energies-based buildings.

AUTHOR INDEX

Supported, Held and Published by:

International Organization on "Technical and Physical Problems of Engineering" (IOTPE)
www.iotpe.com